



Università
Ca' Foscari
Venezia

**Scuola Dottorale di Ateneo
Graduate School**

**Dottorato di ricerca
in Scienze chimiche
Ciclo XXVI
Anno di discussione 2012-2013**

***Study of innovative water repellent systems for the
preservation and restoration of artificial stone
materials***

***Studio di nuovi sistemi idrorepellenti per il risanamento e
il recupero di materiali lapidei artificiali***

**SETTORE SCIENTIFICO DISCIPLINARE DI AFFERENZA: CHIM/12
Tesi di Dottorato di Laura Falchi, matricola 955842**

Coordinatore del Dottorato

Prof. Maurizio Selva

Tutore del Dottorando

Prof.ssa Elisabetta Zendri

*“Sic Maiores voluerunt solemniter declarari
Quanta debet esse inter doctos
Concordia non quidem opinionum
Sed animorum et studiorum
Ad veritatem indagandam
et propugnandam”*

Abstract

Water represents one of the most significant degradation factor for a wide typology of historical or contemporary building materials, like plasters, mortars, concretes, bricks and natural stones. Water can act both directly and indirectly by transporting pollutants and soluble salts, affecting the materials stability and causing serious damages. Nowadays, the protection of the stone materials from the action of water is, therefore, a major challenge for the construction, and is assuming an increasing importance as a consequence of the intensification of precipitations and world climate changes. The protection of the stone materials is, however, a complex problem, which should take into account different points such as: the chemical-physical and structural compatibility with the other materials present; the environmental sustainability beside the productive processes and costs; the suitability and specificity of the developed solutions and their effectiveness and durability.

Many solutions have been developed to aim the problem of the protection of architectonic surfaces from the degradation processes linked to the water action. Up to now, the attention has been focused on water-repellent dispersions in water and/or organic solvents to apply by impregnation. Despite the consolidate use of these systems during the years, the penetration depth of the impregnation treatments is limited and their distribution is not always homogeneous. This might cause degradation phenomena in restricted areas at the interfaces. Furthermore, the protection given by them is limited to the external surface, and is not maintained in presence of cracks, fissures, of powdering of the treated surface. For these reasons, in the last years, it has been studied a new approach based on the development of water-repellent renders and cement mortars made with water-repellent admixtures. These systems can be used as renders also in restoration and act as protective barriers against the penetration of water.

The lack of data regarding these new systems makes it difficult to evaluate the effects and the chemical-physical interactions between the water-repellent admixtures and the different components of mortars and concretes. Furthermore, few information are available and additional investigations are demanded to enlarge the knowledge on the effectiveness and compatibility at long term in different environmental situations. The aim of this research is the study of the behavior of different binder systems, e.g. limestone cement, natural hydraulic lime, and pozzolana-lime, admixed with water repellent siloxanes, metal soaps and vinyl polymers.

A complete methodology based on a micro-to-macro approach was adopted in order to evaluate the behaviour and the effectiveness of the different systems by considering their chemical, physical, structural properties. The starting point was the study of the water-repellents in water and in alkaline solutions, followed by the study of the interactions and the influence of the water-repellent admixtures on the hydration reactions of the binders. Then, the effectiveness

and the durability of the mortars was evaluated in different environmental conditions (exposure to UV light, rain and salt crystallization). At last, the mortar mixtures with better effectiveness and durability were applied on models of salty masonries, evaluating their behaviour in a realistic situation.

Each point was studied with suitable techniques. XRF spectroscopy, FT-IR spectrometry, XRD analysis, thermogravimetric techniques as TGA-DSC and scanning electron microscopy (SEM-EDX) allowed to evaluate the influence of the water-repellent admixtures on the binders hydration, the interactions between admixtures and mortars, and the effects due to salt crystallization processes. Tests according to the European normative were used, together with thermographic imaging, porosimetric and ultrasonic measurements, in order to characterize the mechanical, physical and structural properties of the different mortar mixtures and to evaluate the influence due to the water-repellent admixtures. To discuss the data, a tentative multivariate statistical approach is proposed too.

The results highlighted that the water-repellent admixtures influenced to a different extent the hydration of the binders, causing a delay in the reaction kinetics, in particular when metal soaps, such as zinc stearates, were used. The admixtures studied had high effectiveness and allowed to obtain durable water-repellent mortar mixtures. In particular, the siloxanes demonstrated long-lasting effects also after the exposure to UV-light, artificial rain, and salt solutions. However, the application of the mixtures on salty masonries, showed that not always the water-repellent mixtures had longer durability in comparison to the mortars without admixtures. This was due also to the hydration delay caused by the water-repellent admixtures and to the subsequent lower mechanical properties of the applied mortars.

The different behaviour and durability of water-repellent mixtures exposed to salt solutions or applied on models of salty masonries indicates that field observations must complete the laboratory results.

Keywords: water-repellent admixtures, metal soaps, siloxanes, limestone cement, natural hydraulic lime, pozzolana-lime, mortars, restoration, salty masonry, microstructure, hydration.

Sommario

L'acqua rappresenta uno dei principali fattori di degrado per un'ampia tipologia di materiali dell'edilizia storica e contemporanea quali malte, intonaci, calcestruzzi, mattoni e pietre naturali. L'acqua può esercitare un'azione diretta o può comportare il trasporto di inquinanti e Sali solubili, causando effetti evidenti sulla stabilità del materiale e danni di notevole entità. La protezione dei materiali lapidei dall'azione di degrado dell'acqua è, ad oggi, una delle maggiori sfide nel campo della prevenzione del degrado e della manutenzione delle superfici architettoniche, anche a causa dei cambiamenti climatici mondiali che hanno portato in molti casi all'aumento di fenomeni meteorologici anche di notevole violenza. La protezione dei materiali lapidei è, tuttavia, un problema complesso, che deve tenere in conto aspetti quali la compatibilità chimico-fisica e strutturale con gli altri materiali presenti e con l'ambiente circostante, la sostenibilità in termini ambientali oltre che economico-produttivi, la flessibilità e specificità d'uso dei sistemi sviluppati, la loro efficacia e la durabilità nel tempo.

Innumerevoli soluzioni sono state sviluppate per affrontare il problema della protezione dall'azione dell'acqua. La maggior parte dei sistemi sviluppati per la protezione dei materiali lapidei si basa su interventi d'impregnazione delle strutture con liquidi idrorepellenti di diversa natura. Nonostante l'ampio utilizzo, questi sistemi applicati per impregnazione presentano alcuni limiti: la profondità di penetrazione è limitata e la distribuzione nel materiale non è sempre omogenea, questo crea situazioni di interfaccia tra la parte trattata e non all'interno del materiale che possono portare a fenomeni di degrado localizzato. Inoltre il tipo di protezione fornita è solo superficiale e non è garantita in caso di formazione di crepe, fessure, o polverizzazioni della superficie trattata. Per questi motivi si è sviluppato negli ultimi anni un approccio diverso per quanto riguarda gli intonaci di finitura e le malte solitamente a base cementizia, che prevede l'idrofobizzazione del materiale attraverso l'additivazione di composti idrofobici in massa. Questi sistemi possono essere impiegati per la stesura o il rifacimento di finiture e agiscono come barriera protettiva rispetto alla penetrazione d'acqua dall'esterno.

La mancanza di dati riguardante questi nuovi sistemi rende tuttavia difficile la valutazione degli effetti e delle interazioni chimico-fisiche dei composti idrorepellenti con i diversi componenti delle malte. Inoltre si hanno ancora scarse informazioni circa l'efficacia di tali sistemi idrorepellenti nel tempo e in condizioni ambientali diverse. L'obiettivo di questa ricerca è lo studio del comportamento di diversi sistemi leganti, cemento al calcare, calce idraulica naturale e calce pozzolanica, additivati con idrorepellenti a base di silossani, saponi metallici e polimeri vinilici

Si è scelta una metodologia di ricerca integrata, basata su un approccio micro-to-macro, per poter valutare il comportamento e l'efficacia dei diversi sistemi alla luce delle loro proprietà chimiche, fisiche e strutturali. Si è partiti dallo studio dei composti idrorepellenti in ambiente acquoso e basico, proseguendo con lo studio delle interazioni e dell'influenza degli additivi sulle reazioni di idratazione dei leganti in esame. È stata quindi valutata l'efficacia e la durabilità delle

malte prodotte utilizzando i leganti e gli idrofobizzanti in studio, considerando diverse situazioni ambientali d'impiego. Infine, gli impasti che hanno dimostrato migliore efficacia e durabilità sono stati applicati su macromodelli di murature soggette a processi di risalita capillare di soluzioni saline, valutando quindi il comportamento di questi impasti in una condizione molto più simile a quella reale

Per ogni fase della ricerca sono state utilizzate diverse tecniche analitiche. Spettrometria FT-IR e XRF, termogravimetria, calorimetria differenziale a scansione, microscopia elettronica a scansione e diffrazione a raggi X hanno permesso di valutare l'influenza degli additivi sull'idratazione dei leganti, le interazioni tra additivi e malte, e gli effetti prodotti dai processi di cristallizzazione salina. Test normati insieme a misurazioni di diverso tipo, tra le quali anche misure porosimetriche, ultrasoniche e termografiche, sono stati necessari per caratterizzare i diversi sistemi, le loro proprietà fisico-meccaniche e strutturali e comprendere gli effetti della presenza degli additivi idrorepellenti. Infine viene proposto un approccio statistico multivariato per la discussione di alcuni dei dati ottenuti.

I risultati hanno messo in evidenza che gli additivi idrorepellenti studiati influenzano in varia misura i processi di idratazione e dei leganti, provocando un rallentamento delle reazioni, particolarmente critico nel caso dell'utilizzo di saponi metallici e dello stearato di zinco in particolare. Gli additivi studiati risultano efficaci nel conferire idrorepellenza agli impasti, anche se intonaci con additivi silossanici dimostrano una maggiore durabilità e mantengono le proprietà idrorepellenti anche dopo esposizione a pioggia, luce UV e a soluzioni saline. L'applicazione di tali impasti su murature soggette a processi di risalita capillare e dalla presenza di sali solubili ha tuttavia dimostrato che gli intonaci idrorepellenti non sempre hanno durabilità maggiore di quelli non additivati. Questo è dovuto anche all'influenza degli additivi sul processo di idratazione del sistema legante e sullo sviluppo conseguente delle proprietà meccaniche. La differenza di comportamento e di durabilità degli impasti sottoposti a test normati di esposizione a soluzioni saline rispetto agli stessi impasti applicati su modelli di muratura indica che i test di laboratorio necessitano di ulteriori verifiche in campo.

Parole chiave: additivi idrorepellenti, saponi metallici, silos sani, cemento al calcare, calce idraulica naturale, calce pozzolanica, intonaci, restauro, murature affette da cristallizzazione di sali solubili, microstruttura, idratazione.

Acknowledgments

This is the part of the Thesis I prefer, where I can remember and thank all the people that I have met and that have helped me in this long, but satisfying Journey. I would like to thank all the people and institution that have helped me to conceive, design and develop this research. I pray, excuse me if I forget somebody. You are in my heart if not in my present mind.

I would like to thank Prof. Elisabetta Zendri, my tutor for her supervision of my work, always giving me interesting suggestions but allowing me to freely choice and develop my research. Many thanks to Prof. Pietro Riello, who kindly read and corrected this long and huge thesis.

I would thank Prof. Guido Biscontin who believed in me and helped me to undertake this Journey and who told me “Just buy that sand and start!”, and all the people of Volteco S.p.A., in particular Marco Ruzzier and Nicoletta Vesco, for introducing me to the use of integral water-repellent admixtures.

I would like to thank all the “Chemistry for Restoration” team of Ca’ Foscari: Francesca Izzo, Eleonora Balliana, Manuela Sgobbi, Marta Melchiorre De crescenzo Laura Agostinetto. We have endured a lot of difficulties together, and have had a lot of fun.

Sincere thanks to Guido Driussi of Arcadia S.r.l., and all the “arcadian guys” : Mauro Tonon, Zeno Matteo Morabito, Alessandro Mazzuccato, and Antonella Sanguin. You have taught me how to prepare a mortar, how to analyse it and take care of me at Bressanone.

Thank to the expert technician in Venice: Tiziano Finotto and Loris Bertoldo, who have been watched over me for three years and fixed for me a lot of broken things, and Davide Cristofori, who taught me how to use our SEM-EDX and to appreciate Jazz music.

Many thanks to the BAM institute of Berlin and in particular to my German tutors Dr. Urs Müller and Dr. Patrick Fontana and to the Chefin Dr. Birgit Meng. You have kindly host me, setting me in the lab, taught me a lot of things and made XRD, XRF, MIP, FT-IR, TG-DSC, QUV-spray chamber, available to me during my stay at Berlin. Thanks to the whole staff of the 7 division of BAM and in particular to the expert technicians and colleagues Andrée Gardei, Elgin Rother, Christian Lehman, and Dr. Lorenzo Miccoli.

I thank all the other colleagues and friend who have shared with me lunches, problems, troubles, fun, parties but most of all *lunches*, here in Via Torino (Alvise, Paolo, Nicolò, Marco, Gabriele, Gloria, Riccardo, Chandrashekar, etc) or in Berlin (Monika, Sasha, Susan, Sophie, Evelyn, Milena, Andrea, Lorenzo, Christopher, Carlo etc).

Thanks to my wonderful students Marco Piovesan and Nicolò Mengardo and to my lovable students Irene Griffante and Eleonora Capovilla, I am proud of the work we have done together.

Thanks to all the suppliers of the starting Materials, in particular to Gabriele Fortunati of Neuchem and to the staff of Villaga Calce S.p.a.

Thanks to the Colorificio San Marco group S.p.a., and to its technical staff, especially Umberto Dainese, for allowing me to perform ATR-FT-IR mapping with their instrument.

Thank to dr. Cristiano Varin and Giuseppa Toscano for helping me with the PCA analysis.

Thanks to all the colleagues I met in the different Conferences I participated.

Un grazie special alla mia famiglia che mi ha supportato e sopportato per tre anni, a mamma e papà e alle rispettive tribù Falchi e Biancon.

Grazie a Luca, perchè nothing else matters...

Table of Contents

Abstract	I
Sommario	II
Acknowledgments	V
Table of contents	VII
Glossary	XI
Chapter 1. Introduction	1
<i>1.1. Background</i>	1
<i>1.2. Objective and Innovations</i>	2
<i>1.3. Synopsis of the thesis</i>	3
<i>1.4. State of the Art</i>	4
1.4.1. Ancient and modern hydraulic binders	4
1.4.1.1. Hydraulic binders in the Conservation of Cultural Heritage	5
1.4.2. Chemical and physical aspects of hydraulic binders	6
1.4.2.1. Cement	7
1.4.2.2. Natural hydraulic lime	11
1.4.2.3. Pozzolana-lime	12
1.4.3. Deterioration of porous building materials	13
1.4.3.1. Moisture in porous mortars and stones	14
1.4.3.2. Moisture and salts in mortars and stones	16
1.4.3.3. Salty masonries: the case of Venice	18
1.4.4. Water repellent systems	20
1.4.4.1. Metal soaps	21
1.4.4.2. Silane /siloxanes	24
1.4.4.3. Organic polymers	28
Chapter 2. Research strategy	31
<i>2.1. Starting materials</i>	33
2.1.1. Binder systems	33
2.1.2. Aggregates	33
2.1.3. Water-repellent admixtures	33
<i>2.2. Casting procedure and exposure condition</i>	34
2.2.1. Water-repellent binder pastes	35
2.2.2. Water-repellent mortars	37
2.2.1. Exposure/weathering condition of water-repellent mortars	37
2.2.1.1. Artificial ageing conditions	37
2.2.1.2. Resistance to salt crystallization	37
2.2.2. Water-repellent mortars on salty masonry	38

<i>2.2. Investigations techniques</i>	40
2.2.1.X-ray fluorescence analysis	40
2.2.2.X-ray diffraction	40
2.2.3.Differential scanning calorimetry/ Thermogravimetric Analysis	40
2.2.4.Fourier Transform Infrared Spectroscopy	40
2.2.5.Optical microscopy (OM)	41
2.2.6.Scanning electron microscopy coupled with energy dispersive X-ray probe	41
2.2.7.Isothermal calorimetry	41
2.2.8.BET analysis	41
2.2.9.Colorimetric measurements	41
2.2.10.Consistence and density of the fresh mortar mixtures	42
2.2.11.Density, microstructure (MIP) and ultrasonic measurements (US)	42
2.2.12.Mechanical properties of the mortars	43
2.2.13.Capillary water absorption	44
2.2.14.Contact angle measurements	44
2.2.15.Water vapour permeability	45
2.2.16.Conductivity measurements	45
2.2.17.Mid IR Infrared Thermography	45
Chapter 3. Results	47
<i>3.1. Analysis and Characteristics of the Starting Materials</i>	<i>47</i>
3.1.1.Limestone cement	47
3.1.2.Natural hydraulic lime	48
3.1.3.Pozzolana-Lime	48
3.1.4.Aggregates	49
3.1.5.Water repellent admixtures	54
3.1.5.1. Silanes/siloxanes	54
3.1.5.2. Stearates	55
3.1.5.3. Organic polymer	56
3.1.6.Weathering of water repellent admixtures	60
3.1.6.1. Water-repellents in water	60
3.1.6.2. Water-repellents in Ca(OH) ₂ saturated solution	60
3.1.6.3. Water-repellents in oven at 55°C	61
<i>3.2 Study of the hydration of binder pastes</i>	<i>63</i>
3.2.1 Limestone cement pastes with water-repellents	64
3.2.1.1 XRD Study of limestone cement pastes with water repellents during the hydration	64
3.2.1.2 TG-DSC Study of limestone cement pastes	67
3.2.1.3 FT-IR study of limestone cement pastes	70
3.2.1.4 SEM observations of limestone cement pastes	73
3.2.1.5 Isocalorimetric measurements	77
3.2.2Natural hydraulic lime pastes with water-repellents	78
3.2.2.1 XRD Study of natural hydraulic lime pastes	78
3.2.2.2 TG-DSC Study of natural hydraulic lime pastes	80
3.2.2.3 FT-IR study of natural hydraulic lime pastes	84
3.2.2.4 SEM observations of natural hydraulic lime pastes	86
3.2.3Hydraulic pozzolana-lime pastes with water-repellents	89
3.2.3.1 XRD Study of hydraulic pozzolana-lime pastes	89
3.2.3.2 TG-DSC Study of hydraulic pozzolana- lime pastes	91
3.2.3.3 FT-IR study of hydraulic pozzolana- lime pastes	95
3.2.3.4 SEM observations of pozzolana-lime pastes	97
3.2.3.5 Isocalorimetric measurements	101
3.2.4Distribution of the water repellents inside the binder matrixes	102

3.3 Chemical and physical properties of Mortars with water- repellent admixtures	106
3.3.1 Limestone cement mortars with water-repellents	106
3.3.1.1 Mix design, composition and properties of fresh mortars	106
3.3.1.2 Properties of 28 days aged limestone cement hardened mortars	107
3.3.2 Natural hydraulic lime mortars with water repellents	120
3.3.2.1 Mix design, composition and properties of fresh mortars	120
3.3.2.2 Properties of 28 days aged natural hydraulic lime mortars	120
3.3.3Pozzolana-lime mortars with water repellents	130
3.3.3.1 Mix design, composition and properties of fresh mortars	130
3.3.3.2 Properties of 28 days aged natural hydraulic lime mortars	130
3.4 Artificial weathering of mortar specimens	140
3.4.1. Artificial weathering of limestone cement mortars	140
3.4.1. Artificial weathering of natural hydraulic lime mortars	144
3.4.2. Artificial weathering of pozzolana-lime mortars	147
3.5 Resistance to salt crystallization	152
3.5.1. Salt weathering of water-repellent limestone cement mortars	153
3.5.1.1. Resistance to salt crystallization and external appearance of water repellent limestone cement mortars after the exposure	153
3.5.1.2. Composition, microstructure and salt distribution in limestone cement mortars after the exposure	158
3.5.1.3. Capillary water absorption and compressive strength after the exposure	161
3.5.2. Salt weathering of water-repellent natural-hydraulic-lime mortars	163
3.5.2.1. Resistance to salt crystallization and external appearance of natural hydraulic lime mortars after the exposure	163
3.5.2.2. Composition, microstructure and salt distribution in natural hydraulic lime mortars after the exposure	168
3.5.2.3. Capillary water absorption and compressive strength after the exposure	172
3.5.3. Salt weathering of water-repellent pozzolana-lime mortars	173
3.5.3.1. Resistance to salt crystallization and external appearance of pozzolana-lime mortars after the exposure	173
3.5.3.2. Composition, microstructure and salt distribution in pozzolana-lime mortars after the exposure	178
3.5.3.3. Capillary water absorption and compressive strength after the exposure	180
3.5.4. XRD analysis of different mortar mixes after the salt weathering	181
3.6. Water-repellent mortars applied on salty masonry	184
3.6.1. Mortar mixtures	184
3.6.2. Observation during the capillary rise of salt solutions	185
3.6.3. Chemical-physical properties of the mortars before and after one moths of exposure to capillary rise of salt solution	190
3.6.3.1. Chemical composition	190
3.6.3.2. Mechanical strength, capillary water absorption, microstructure and salt distribution	191
Chapter 4. Discussion, conclusions and perspectives	201
4.1 Discussing the results of Chapter 3.2:	202
4.1.1 Hydration reactions of Limestone Cement Pastes without and with water-repellents	202
4.1.2 Hydration reactions in natural hydraulic lime pastes without and with water-repellents	206
4.1.3 Hydration reactions of pozzolana-lime pastes without and with water-repellents	207

Table of contents

<i>4.2 Discussing the results of Chapter 3.3</i>	209
<i>4.3 Discussing the results of Chapter 3.4</i>	214
<i>4.4 Discussing the results of Chapter 3.5</i>	215
<i>4.5 Discussing the results of Chapter 3.6</i>	217
<i>4.6 Correlation of physical properties of water-repellent mortars: a multivariate approach</i>	220
4.6.1 PCA analysis of water-repellent mortars	220
4.6.2 PCA analysis of water-repellent mortars before and after the exposure to the action of saline solutions	225
<i>4.7 Conclusions</i>	230
4.7.1 Main Results	231
<i>4.8 Perspectives</i>	232
References	233
Appendix 1 Materials information	247
Estratto per riassunto della tesi di dottorato	

Glossary

CEMENT NOTATIONS AND ABBREVIATIONS

The commonly used cement chemical nomenclature will be used in the thesis together with orthodox chemical notation. The following scheme summarizes the abbreviation used¹:

Cement chemical nomenclature

C= CaO	S= SiO₂	A=Al₂O₃	F=Fe₂O₃
H=H₂O	Ĉ=CO₂	Ŝ=SO₃	K= K₂O
N= Na₂O	M=MgO	P=P₂O₅	T=TiO₂
C₃S=	Tricalcium silicate (3CaO.SiO ₂) <i>alite, impure form of C₃S found in commercial Portland clinker</i>		
C₂S=	Dicalcium silicate (2CaO.SiO ₂) <i>Belite or larnite, impure form of C₂S found in commercial Portland clinker</i>		
C₃A=	Tricalcium aluminate (3CaO.Al ₂ O ₃)		
C₄AF=	Ferrite (4CaO. Al ₂ O ₃) <i>Solid solution between C₂F and C₂A</i>		
CH=	Calcium hydroxide (Ca(OH) ₂) <i>Portlandite, hexagonal phase</i>		
C-S-H=	Calcium silicate hydrate <i>XRD-amorphous phase of non-stoichiometric composition, close to jennite and tobermorite structures</i>		
Afm=	Alumino ferrite monosubstituted- monosulfoaluminate/ monocarbonate (C ₃ A.CĈ/Ŝ.12H= Ca ₄ Al ₂ (SO ₄)(OH) ₁₂ .5H ₂ O) <i>Usually with substitution of Al by Fe</i>		
Aft=	Alumino ferrite trisubstituted- ettringite (C ₃ A.3ĈŜ.H ₃₂ = Ca ₆ Al ₂ (SO ₄) ₃ (OH) ₁₂ .26H ₂ O) <i>Usually with substitution of Al by Fe</i>		
PC=	Portland Cement Commercial cement of type I of 95-100 _{wt} -% clinker; often described as OPC-ordinary Portland cement. Which is a specific pure composition of 100 _{wt} -% clinker		
w/c or w/b=	Mass ratio of water to cement or water to binder		

Other Abbreviations

XRF	X-ray fluorescence analysis
XRD	X-ray diffraction
TG-DSC	Thermogravimetric analysis- differential scanning calorimetry
FT-IR	Fourier Transform Infrared Spectroscopy
OM	Optical microscopy
SEM-EDX	Scanning electron microscopy with energy dispersive X-ray probe
MIP	Mercury intrusion porosimetry
US	Ultrasonic measurements

¹ Taylor, H.F.W. 1990

CEMENT VOCABULARY²

Admixtures	a material other than water, aggregates, hydraulic cement, and fiber reinforcement, used as an ingredient of a cementitious mixture to modify its freshly mixed, setting, or hardened properties and that is added to the batch before or during its mixing
Admixture, air-entraining	An admixture that causes the development of a system of microscopic air bubbles in concrete, mortar, or cement paste during mixing.
Admixture, retarding	An admixture that causes a decrease in the rate of hydration of the hydraulic cement and lengthens the time of setting.
Air content	The total volume of air voids in cement paste, mortar, or concrete, exclusive of pore space in aggregate particles, usually expressed as a percentage of volume of the paste, mortar, or concrete.
Aggregate	Granular material usually derived from natural rock, crushed stone, or sand. Hardened binder paste binds fine aggregates to form a mortar and coarse aggregates to form a concrete.
Binder capillarity	material forming the matrix of concretes, mortars, and sanded grouts the movement of a liquid in the interstices of concrete, soil, or other finely porous material due to surface tension (also called capillary rise, capillary action, or capillary suction).
Carbonation.	— (1) reaction between carbon dioxide and a hydroxide or oxide to form a carbonate, especially in cement paste, mortar, or concrete; (2) the reaction with calcium compounds to produce calcium carbonate
Cement (Portland cement)	a hydraulic cement produced by pulverizing portland-cement clinker and usually with addition of calcium sulfate to control setting.
Chemically bound water	Water in the interlayer spaces of C-S-H that is bound by molecular bonds
Clinker	a partially fused product of a kiln that is ground to make cement
Curing	action taken to maintain moisture and temperature conditions in a freshly placed cementitious mixture to allow hydraulic cement hydration and (if applicable) pozzolanic reactions to occur so that the potential properties of the mixture may develop.
Dry mix	(1) a concrete, mortar, or plaster mixture, commonly sold in bags, containing all components except water; (2) a concrete of near-zero slump.
Durability	the ability of a material to resist weathering action, chemical attack, abrasion, and other conditions of service.
Ettringite	(1) a mineral, high-sulfate calcium sulfoaluminate ($3\text{CaO}\cdot\text{Al}_2\text{O}_3\cdot 3\text{CaSO}_4\cdot 30\text{-}32\text{H}_2\text{O}$), occurring in nature or formed by sulfate attack on mortar and concrete; (2) the product of the principal expansion producing reaction in expansive cements.
Gypsum	calcium sulfate dihydrate ($\text{CaSO}_4\cdot 2\text{H}_2\text{O}$).
Hardening	gain of strength and other properties of a cementitious mixture as a result of hydration after final setting
Hemicarboaluminate	Calcium aluminate carbonate hydrate ($\text{Ca}_4\text{Al}_2(\text{CO}_3)_{0.5}(\text{OH})_{13.5}\cdot 5.5(\text{H}_2\text{O})$) <i>Carbonate bearing Afm</i>
Hydrate or slaked lime	$\text{Ca}(\text{OH})_2$. Prepared by reacting quicklime with water, a process called slaking.
Hydraulic cement	a binding material that sets and hardens by chemical reaction with water and is capable of doing so underwater. For example, portland cement and slag cement are hydraulic cements.
Hydraulic hydrated	the hydrated dry cementitious product obtained by calcining a limestone

² Definitions of the American Concrete Institute: ACI CT-13, 2013

lime	containing silica and alumina to a temperature short of incipient fusion so as to form sufficient free calcium oxide to permit hydration and at the same time leaving unhydrated sufficient calcium silicates to give the dry powder its hydraulic properties.
Hydrophobicity	Repelling, tending not to combine with, or incapable of dissolving in water
Limestone	a sedimentary rock consisting primarily of calcium carbonate.
Mirabilite	hydrous sodium sulfate mineral $\text{Na}_2\text{SO}_4 \cdot 10\text{H}_2\text{O}$
Monocarboaluminate	Calcium aluminate carbonate hydrate ($\text{C}_3\text{A} \cdot \text{C}\hat{\text{C}} \cdot 12\text{H} = \text{Ca}_4\text{Al}_2(\text{CO}_3)(\text{OH})_{12} \cdot 5\text{H}_2\text{O}$) <i>Carbonate bearing Afm</i>
Monosulfoaluminate	See "AFm"
Mortar	a mixture of cement paste and fine aggregate; in fresh concrete, the material occupying the interstices among particles of coarse aggregate; in masonry construction, joint mortar may contain masonry cement, or may contain hydraulic cement with lime (and possibly other admixtures) to afford greater plasticity and workability than are attainable with standard portland cement mortar
Natural hydraulic lime	Hydraulic lime produced by heating calcining limestone that contains clay and other impurities
Paste	a mixture of hydraulic binder and water.
Pozzolan	a siliceous or silico-aluminous material that will, in finely divided form and in the presence of moisture, chemically react with calcium hydroxide at ordinary temperatures to form compounds having cementitious properties (there are both natural and artificial pozzolans).
Quicklime or free lime	calcium oxide (CaO) (as in clinker and cement) that has not combined with SiO_2 , Al_2O_3 , or Fe_2O_3 during the burning process, usually because of underburning, insufficient grinding of the raw mixture, or the presence of traces of inhibitors.
Sulfate attack—	The chemical reaction that occurs between sulfates usually in soil or groundwater and concrete or mortar; the chemical reaction is primarily with calcium aluminate hydrates in the cement-paste matrix, often causing deterioration.
Thaumasite	Calcium sulphate carbonate hydrate ($\text{Ca}_3[\text{Si}(\text{OH})_6]\text{CO}_3 \cdot \text{SO}_4 \cdot 12\text{H}_2\text{O}$) <i>Typical product of sulphate attack</i>
Thenardite	anhydrous sodium sulfate mineral Na_2SO_4
Setting	a chemical process that results in a gradual development of rigidity of a cementitious mixture, adhesive, or resin.
Waterproof	— an idealized property of a material indicating imperviousness to water in either liquid or vapor state. Note: because nothing can be completely impervious to water under infinite pressure over infinite time, this term should not be used.
Water repellent	property of a surface that resists wetting (by matter in either liquid or vapor state) but permits passage of water when hydrostatic pressure occurs

1. Introduction

1.1. Background

Water represents one of the most important degradation factors for a wide typology of materials like plasters, mortars, concretes, bricks and natural stones. The architecture degradation processes due to the water action is a long time problem with an increasing importance in the last years, as a consequence of the intensification of precipitations and world climate changes. The damages caused by water to buildings and architectures are often serious with high maintenance costs for the reparation of materials and structures not well protected.

Many research have been developed for the characterization and formulation of water-repellent systems for reducing and minimizing the degradation processes linked to the water action. Up to now, the attention has been focused on water-repellent dispersions in water and/or organic solvents to apply by impregnation to the buildings. Despite the consolidate use of these systems during the years, the protection given by them is limited to the external surface of the materials. For this reason, a different approach based on bulk water-repellent materials has also been developed and pulled for by companies for the applications on building industry.

Different hydrophobic compounds have been used during the years to obtain mortars with water repellence properties. However, few information are available about the chemical-physical characteristics, compatibility and interaction between the mortar matrix and these hydrophobic materials. Different studies focalized mostly on the measurements of the mechanical characteristics and on the evaluation of the water repellence performances in cement based mortars. Besides, most of the commercial water-repellent additives have been tested and are recommended only for Portland cement mortars.

In specific fields of construction, such as in the architectonical restoration field, has grown, in the last years a new awareness of the limits of Portland cement. The requirement of reliable, durable solutions, able to repair ancient architectures without cause new damages, leads to rethink at the use of Portland cement mortars and to prefer adopting more compatible solution, such as natural hydraulic limes mortars or artificial hydraulic limes mortars made with pozzolana. These kinds of mortars demonstrate chemical, mechanical and microstructural characteristics compatible with different traditional building materials and historical mortars. In more recent buildings (19th and 20th centuries) cement based mortars might have been used as original materials, in these cases the use of cement mortars for the restoration works should be favoured, in particular special kinds of cement might be used, instead of pure Portland cement. Moreover, the production and use of hydraulic binders such as natural hydraulic lime, pozzolana-lime, or special kind of cement (e.g. limestone cements) involve less employ of energy and a lower production of CO₂ (cement production releases an estimated 0.7–0.9 t CO₂/t cement while natural hydraulic lime NHL3.5 releases around 0.6 t CO₂/t cement and during its carbonation around 0.3 t CO₂/t cement is reabsorbed)¹.

¹ WBCSD; 2009

1.2. Objective and Innovations

The aim of this research was to design and study hydraulic mortars with water-repellent properties. The integral water-repellent mortars were designed in order to be compatible for restoration application, i.e. suitable for the restoration of historical and ancient buildings to protect them from the damaging action of water. The compatibility criteria include the physical, chemical and mechanical properties which should be defined based on the traditional mortars characteristics and on the quality and the performance of the repair mortar after application on masonry, in order to assure the durability on the long term².

In this work, the water-repellent hydraulic mortars have been prepared with different binder systems: natural hydraulic lime, pozzolana-lime and limestone cement. The water-repellent properties were obtained adding to the mortar mixtures suitable hydrophobic compounds of different nature. The hydrophobic materials selected were of different nature; some of them (calcium and zinc stearates or silane water-based emulsions) are already well known and commonly used to obtain water repellent cement mortars, while other are of more recent production such as powder silanes, i.e. silanes supported on inorganic carriers (calcium carbonate or silica powder).

Considering the lack of data regarding the use of hydrophobic compounds in mortars made using limestone cement, natural hydraulic limes or pozzolana-lime as binder systems, and considering the peculiar importance of developing and testing new compatible solution for the restoration of historic buildings, the objectives of this work are multiple:

- to define a suitable mix design for the preparation of water repellent hydraulic mortars based on different hydraulic binders such as limestone cement, natural hydraulic lime, pozzolana-lime;
- to study the chemical-physical interaction of the water-repellent admixtures and the mortar matrixes, in particular the influence of the additives on the hydration reactions of the binders;
- to study the physical characteristics, the structures, the mechanical properties and the water repellence performances of water-repellent mortars and evaluate if the mortar mixtures are compatible with a possible employment in restorations works;
- to study the behavior of the mortars which undergoes artificial weathering test (UV-Light and artificial rain) or rising damp cycle with sodium sulfates solutions
- to study the performances of integral water-repellent mortars applied on salty brick masonry.

The innovation of the thesis regards:

- the selection and development of compatible and more eco-friendly materials, such as traditional lime based mortars and limestone cement with reduced clinker to cement ratio;
- the adoption of an integral and complete approach from the micro to the macro scale;
- the study of systems and mechanism not well-known yet, such as the influence of several water-repellents admixtures on peculiar mortar binders.

To obtain a good knowledge of the systems an approach based both on the macro and micro scale was chosen. Several macroscopic characteristics were measured on mortar specimens in laboratory conditions, such as mechanical behavior, water-repellence properties, water vapor permeability. These characterization was compared and completed with the results obtained

² Schueremans, L. et al., 2011.

from the study of the mortars microstructure and of the hydration mechanism of the binders admixed with hydrophobic compounds. Furthermore, the transversal study from the micro to macro proceeded on water-repellent mortars applied on salty masonries.

The use of instrumental techniques and different tests to evaluate mechanical and physical properties of the mortars gave the possibility to study the different water-repellent systems, the influence of the additives on the systems properties, and the system ageing processes.

1.3. Synopsis of the thesis

In order to answer the defined objectives, the thesis is organised around six chapters.

Chapter 1. Introduction: presents the objectives of the thesis. Summarizes the state of the art regarding chemical and physical properties of binders and mortars similar to the ones studied, the damage caused by the action of water and salt solutions on porous building materials and the methods used to preventing it.

Chapter 2. Research Strategy: presents the materials and describes the methodology. Lists The analytical techniques and methods adopted.

Chapter 3. Results: exposes the analytical results obtained by the measurements done. It is a technical part which consider all the analytical results obtained. This chapter, in turn, is divided into six major parts which:

- 3.1 investigate the chemical and physical properties of the starting materials;
- 3.2 reports the results of the different analytical techniques used to follow the hydration reaction of the different binders in presence of water-repellent admixtures;
- 3.3 reports the chemical and physical properties of integral water-repellent mortars;
- 3.4 shows the behaviour and the measurements done on specimens during and after artificial weathering under UV-Light and rain;
- 3.5 reports on the resistance of the water-repellent mortars to the crystallization of damaging salts;
- 3.6 evaluate the performance of some of the mixtures studied when applied on walls which undergoes rising damp phenomena with salt solution.

Chapter 4. Discussion, Conclusions and Perspectives:

- correlates and discusses the results presented in Chapter 3, proposing a chemical mechanism for the binders hydration, evaluating the physical properties of the water-repellent mortars, and analysing the damage processes due to artificial weathering under UV-Light and rain or to salt solution exposure;
- proposes a multivariate statistical approach (Principal Component Analysis of the data) for a further discussion of some of the data;
- concludes summarizing the results on the influence of water-repellent admixtures on chemical and physical properties of the binders and evaluating if the mixtures might be suitable for restoration works. Introduces direct perspectives of the work and future investigations.

1.4. State of the Art

1.4.1. ANCIENT AND MODERN HYDRAULIC BINDERS

Inorganic binders and the mixtures made with them, e.g. plasters, mortars and concretes, are the most important materials in the constructions field.

Binders are mainly composed by fine powders able to form plastic mixtures when mixed with water which undergoing chemical –physical reactions are able to set and hardened forming a resistant and hard materials. Binders may be define as adhesive substances able to join fragments or masses of solid matter in a compact whole³.

Unlike aerial limes mortars, which set through carbonation reaction of lime with CO₂ and water in air, hydraulic mortars are defined as mortars capable of setting and hardening by chemical reaction with water in humid and wet environment or under water.

The hydraulic properties of mixtures of lime and crushed fired bricks (“cocciopesto” mortars) was known since antiquity. The first use of volcanic sands in mortars seems to date back to the X century B.C., when Phoenician and Israelites mixed natural pozzolana in waterworks, ports, water tanks⁴. The Greeks also used to added some volcanic pozzolana from Cantorini¹ to their mortars, but it is thanks to the Romans that the use of pozzolana in mortars became a common and well-regulated practice. Vitruvio in the V books of “De Architectura” described the construction of ports advising to use pozzolan from Cuma (Naples) for the mortars:

“...Eae autem structurae, quae in aqua sunt futurae, videntur sic esse faciendae, uti portetur pulvis a regionibus, quae sunt a Cumis continuatae ad promunturium Minervae, isque misceatur, uti in mortario duo ad unum respondeant. ...”⁵

The use of volcanic ashes from the Rhine near Koblenz known as Trass, was also introduced likely during that time.

A gradual decline in the quality of the mortar used in buildings set in after the Roman times; throughout the Middle Ages, the knowledge and skills regarding the use of pozzolana-lime mortars were lost, and rediscovered at the beginning of the Renaissance.

An hydraulic effect similar to the pozzolana-lime binders could be obtained also by substituting ordinary sand with ground-fired clay (chamotte) or finely ground bricks or tiles (cocciopesto), this techniques, known already by the Romans, was commonly used in Venice since the XIV century for rendering mortars, plasters, mosaics, frescoes and floors in “terrazzo alla Veneziana” style, thanks to the good resistance of these mixes in the wet climate of the lagoon⁶.

The use of slaked lime and natural or artificial pozzolana remained during a long time as the unique material for the production of mortars and concrete with hydraulic properties. Only In the late 1700s it was recognized that limestone containing clay minerals fired at higher temperatures (up to 1250°C) could produce limes with hydraulic properties. The forerunner of these investigations was John Smeaton, but for several years the old mixtures of lime and pozzolana retained its supremacy. However, the researches went on and in 1796, under the name of Roman cement, was patented an hydraulic cement made by calcining nodules of

³ Lea, M. 1997

⁴ Ellison, P.T. 1998

⁵ Marco Vitruvio Pollione, 15 B.C

⁶ Piana, M., E.Danzi, 2002; E., Armani 1984

argillaceous limestone. In 1812 Louis Vicat prepared an artificial hydraulic lime calcining mixtures of limestone and clays. Vicat made also a clear distinction between artificial and natural hydraulic lime: the former prepared calcining mixtures of limestone and clays, the latter calcining argillaceous limestone till 1100-1200°C.

Artificial and Natural hydraulic lime constituted a link with the modern hydraulic binder developed in the mid-19th century: Portland cement, a cement made from a blend of clay materials and limestone fired at a temperature of around 1450°C. The use of cement spread rapidly at the end of the 19th century to assume a position of absolute predominance in the 20th century displacing the natural cements⁷.

Nowadays cement is the most used binder and only in 2011 (even considering the negative effect of the economical crisis) the European production of cement was around 201 million Tons (2% more than in 2010)⁸. However, the production of cement can cause environmental impact at all stage of the process⁹ and its production required a great expenditure of energy (3.8 GWh of electrical energy and 2.5 million Tons of coal in Italy in 2011).

From the beginning of the 21th century, new concepts as Environmental Sustainability, Ecological Architecture, Conservation of the Cultural Heritage became central themes of the international discussion, with an increasing awareness that the respect of the environmental sustainability is not only a responsibility of the entire community but also a territorial and economic development factor. Sustainability is defined as a continuous process, a necessity of combine economic needs, environmental and social equilibria.

One of the most discussed theme in 2011 was the CO₂ emissions deriving from the cement production. At this regard, it is interesting to notice that the production of different mixed cement evolved in comparison to pure Portland cement, in the last decades. In order to reduce the production costs, the energies involved in the production, the CO₂ emissions, and to improve the re-use and the immobilization of wastes¹⁰, mixed cement of different types¹¹ were mainly produced such as limestone cements (CEMII), pozzolanic cements (CEMIV), composite cements (CEMV). In particular the most produced cement in Italy in 2011, was limestone cement (CEMII) (66.3% of the total national production)⁶.

1.4.1.1. Hydraulic binders in the Conservation of Cultural Heritage

In the frame of the conservation of Cultural Heritage cement repair materials have been widely used during the last century also in restoration works of historical buildings. Cement was considered an optimal binder due to the fast hardening and the good compressive strength. However, is nowadays accepted from the conservator scientist community that cement is not always the better solution for repairing and restoring ancient buildings¹². The mechanical properties of cement products, i.e. the compressive strength and the elasticity, differ often from the ones of the historical building materials. In particular, historical mortars display usually low

⁷ AA.VV. *Atti del Convegno di Scienza e Beni Culturali*, 1985; Lea, M. 1987 ; Callebaut, K., 2001; Taylor, H.F.W, 1990

⁸ AITEC, RELAZIONE ANNUALE 2010; AITEC, RELAZIONE ANNUALE 2011; in 2007 the European production pre-crisis was around 277 Ton

⁹ Struble, L., J. Godfrey, 2004

¹⁰ Alternative raw materials classified as waste are for example alumina dust, metallurgical slags, fly ashes, sludge. See also Kejin Wang (editor), 2004; WBCSD 2009

¹¹ In the following chapter a complete description of the cement type is given

¹² C. Sabbioni, A. Bonazza, G. Zappia, 2002; F. Pacheco, et al. 2012; C. Sabbioni, et al. 2001

compressive strength values but good elasticity, while cement mortars present higher values of compressive strength but lower elasticity. The application of these material during past restoration works often led to stresses to the ancient, pre-existing materials, causing the formation of cracks and detachments. Also the microstructure characteristics of cement mortars are often not compatible with traditional building materials and techniques; the low water vapor permeability of cement mortars can lead to the stagnation of water inside the walls, detachments and formation of salts sub-efflorescences. Furthermore, damaging chemical processes can taken place in presence of cement material, which are rich in sulphates and alkali that can attack the original materials¹³.

For these reasons is nowadays accepted the idea of using traditional material and techniques to produce mortars compatible with the historical ones. The so called approach of the “reverse engineering¹⁴”, a concept borrowed from the design industry, can be used to describe this process of study of the ancient building materials, gaining knowledge of the material and techniques used and subsequent re-proposal/re-make of new compatible construction materials.

Possibly, in the re-make-stage, a new mix design of the material might be proposed, always checking the compatibility with the original material, in order to obtain materials with enhanced properties or specific characteristics which enable a better protection of the original parts.

With this in view, in the last years different studies have focused on the use and properties of pozzolans in hydraulic lime mortars or on natural hydraulic lime for the use in restoration works¹⁵.

1.4.2. CHEMICAL AND PHYSICAL ASPECTS OF HYDRAULIC BINDERS

Hydraulic lime have traditionally classified by the amount of reactive clay material they contain. Several classification were proposed to determine the hydraulicity of hydraulic lime.

One of the most known is the Vicat classification which is based on the definition of an Hydraulicity index:

$$I = (\text{SiO}_{2\text{total}} + \text{Al}_2\text{O}_3 + \text{Fe}_2\text{O}_3) / (\text{CaO}_{\text{total}})$$

Vicat attributed the hydraulicity to the clays impurities mixed to limestone during the heating process. He did not consider, however, that not all the SiO₂ is available to combine with the CaO and that CaCO₃ in the stone is not always completely converted in CaO during burning. Vicat formula is perfectly applicable to cement, but cannot be today adopted for hydraulic limes. The most reliable methods for natural hydraulic limes is to consider only the combined silica¹⁶. Other classification are based on the setting time or on the cementation index (it is supposed that combined silica is present only as tri-calcium silicate and this is not correct for natural hydraulic limes or pozzolana-lime mixtures).

¹³ Chabrelie, A. 2010

¹⁴ Karoglou, M., A. Bakolas, N. Kouloumbi, A. Moropoulou 2011

¹⁵ Gibbons, P. 1997; Liebig, E. 1997

¹⁶ Jan Elsen, et al. 2012; Stewart, J. D., A. Henry, 2011, p210

Considering the hydraulicity the following kind of hydraulic limes can be identified: feebly-hydraulic, moderately-hydraulic and eminently hydraulic. The last ones set quicker and are characterized by higher compressive strengths than the other.

Nowadays the hydraulic lime and hydraulic lime mortars are defined by European Standard EN 998-1, EN413, and EN 459-1, 2, 3. In the following paragraphs a description of the hydraulic binders and of the reactions occurring during heating is presented, together with a short description of the general processes of setting and hardening of Portland cement, natural hydraulic limes and pozzolana/lime mixtures.

1.4.2.1. Cement

Cements are the modern eminent hydraulic binder, whose mixtures set and hardened also under water developing resistant hydrated compounds and a firm solid structure. They constitute of Calcium- silicates, aluminates and ferro-aluminates anhydrous compounds able to react with water to form insoluble hydrated compounds.

Portland cement is made by heating a mixture of limestone and clay at around 1450°C. Minor corrective components (pirite/ iron, bauxite, sand) may be added to the mixture to increase the proportion of Fe_2O_3 , Al_2O_3 and SiO_2 .

The minerals extracted are ground and burnt in rotary kilns where the following reaction occur¹⁷:

- Below 120°C free water is evaporated, in clays compounds interlayer water is lost at 100-250°C while dehydroxylation begins at 300-400°C.
- 400 to 600 °C - clay-like minerals are decomposed into their constituent oxides; principally SiO_2 and Al_2O_3 . Dolomite ($\text{CaMg}(\text{CO}_3)_2$) decomposes to calcium carbonate, MgO and CO_2 .
- 650 to 900 °C – Calcium carbonate decompose to quicklime (CaO) together with the clay minerals. Quicklime react with quartz and clay mineral decomposition products to form belite (Ca_2SiO_4) (called also larnite).
- 900 to 1300 °C - the remaining calcium carbonate decomposes to CaO and new crystalline phases such as Al-Si spinel, cristobalite and, above 1100 °C mullite, are formed.
- 1300 to 1450 °C - partial (20–30%) melting takes place, and belite reacts with calcium oxide to produce alite ($\text{Ca}_3\text{O}\cdot\text{SiO}_4$) (or Hatrurite). The products nodulized and form the clinker.
- Reaction during cooling. The liquid crystallises giving aluminates and ferrite, polymorphic transition of alite and belite occur.

The clinker is mixed with a few per cent of gypsum to control the rate of set and finely ground to make the cement. The clinker composition is typically around 67%wt CaO , 22%wt SiO_2 , 5%wt Al_2O_3 , 3%wt Fe_2O_3 and 3%wt of other components and normally contains four major phases: alite C_3S (tricalcium silicate), belite $\beta\text{-C}_2\text{S}$ (dicalcium silicate), aluminate phase C_3A and ferrite phase C_4AF ¹³. This phases in contact with water are responsible of the setting and hardening of the cement¹⁸.

In particular alite and belite are responsible of the hardening (i.e. the significant development of the mechanical properties of Portland cement), while aluminate and ferrite phases are responsible of the setting (i.e. the stiffening without significant development of compressive

¹⁷ Taylor, H.F.W. 1997, the cement chemistry notation is used to express the reaction components, a summary of the cement notations and cement abbreviations is given in Glossary and Nomenclature

¹⁸ Odler, I, 2000

strength). The tendency of hydration of an ordinary Portland cement paste can be calculated for each clinker phase, and results similar to Figure 1. 1 can be obtained¹⁹, demonstrating the faster hydration of alite in comparison to belite (not completely consumed after 100 days).

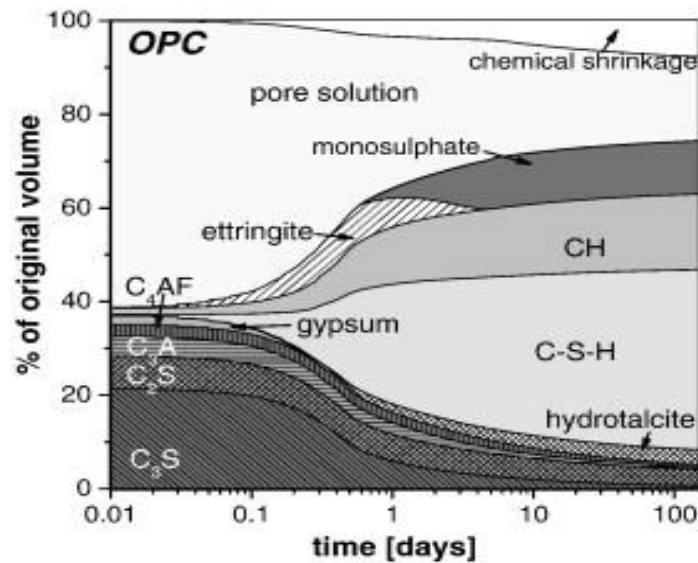
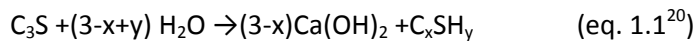
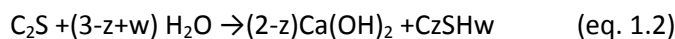


Figure 1. 1 The volume of the different cement phases as function of time in hydrating OPC cement pastes modelled by GEMS using the Parrot and Killoh equations¹⁶

Upon contact with water, tricalcium silicates (the main phase of cement) undergoes hydration, yielding an amorphous calcium silicate hydrate phase called the C-S-H phase and calcium hydroxide as products of hydration (eq. 1.1).



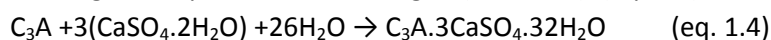
The C-S-H phase is an amorphous or nearly amorphous material structurally related to the crystalline phases 1.4 nm tobermorite and jennite on the nanometer scale, foreign ions may be incorporated in the C-S-H. On the micrometer scale the C-S-H appears either as a dense amorphous mass or a microcrystalline material with an acicular or platelet-like morphology. Dicalcium silicate in its most reactive modification β -C₂S (belite) undergoes similar hydration reaction (eq. 1.2) and produce identical C-S-H products, even if the reaction rate is more slowly.



Six Al₄O tetrahedra and Ca²⁺ ions form the structure of Tricalcium aluminate, which usually exist in its cubic form, however also orthorhombic or monoclinic modification might be found in the presence of increased amount of alkalis in the raw mix. The hydration of C₃A occur immediately upon contact with water producing metastable hexagonal calcium aluminates hydrates C₂AH₈ or C₄AH₁₉ (eq. 1.3), both belonging to the AFm phases. Subsequently, the hexagonal hydrates transform to stable cubic hydrate C₃AH₆ (hydrogarnet).



In order to retard the fast hydration of C₃A, which caused a fast initial setting, calcium sulphate (gypsum or hemihydrates) is added to the clinker. Gypsum and C₃A react in presence of water forming an AFt phase called ettringite (trisulfate). (eq. 1.4)



¹⁹ De Weerd, K. et al. 2011

²⁰ Collepardi, M. 1980

Ettringite exhibit crystals with acicular morphology. After exhaustion of the available calcium sulphate, the trisulfate phase may react with the remaining tricalcium aluminate and convert to tricalcium aluminate monosulfate hydrate ($C_3A \cdot \tilde{C}S \cdot 12H$) commonly called monosulfate, which crystallizes in thin hexagonal platelets.

The products formed in the hydration of the ferrite phase are similar to those formed in the hydration of C_3A , but the Fe^{3+} replaces Al^{3+} to a limited degree in the crystalline lattice.

From the kinetic point of view, the hydration of Portland cement involves several stages which starts immediately upon contact with water in the so called pre-induction period, when a rapid dissolution of ionic species occur²¹ and the formation of hydrates gets under way. In the induction period (or dormant period) the hydration rate slows down till the acceleration stage, when a rapid hydration of C_3S is associated with the formation of silicate hydrates and also the hydration of C_2S starts. In the post acceleration period the hydration slow down and the process become diffusion controlled. The silicate hydrates continued to be formed both from the C_3S and C_2S . The hydration of C_2S goes on for longer time. The aluminate phases C_3A and C_4AF hydrate faster than C_3S and C_2S in the induction and acceleration period.

Types of cement

Throughout the world different types of cement are designed for general construction use, the different types have various names in different countries, even if the specification with which such cements must comply are similar. In Europe the Standard EN 197-1:2011 defines and gives the specification of common cement products and their components (Table 1. 1). Specifications are based both on chemical composition and on physical properties such as specific surface area. Ordinary Portland cement is CEMI, but different addition are used to give specific properties to the cements, as it is possible to see from the table, silica fume, pozzolana, fly ash, limestone might be added to the cement mix.

Moreover the common cements are classified according to mechanical, physical and durability requirements, as listed in Table 1. 2 and Table 1. 3.

In the present research a particular type of cement was investigated, a Portland limestone cement CEMII-BL. Limestone cement are cement particularly common in Italy for the production of rendering and plasters, in fact CEMII was the most produced cement type in Italy in 2011 (66.3% of the total national production)⁶, while CEMII-B-L represent the 20% of the whole Italian production (6643tons). Limestone cement is characterized by a high calcium carbonate content (till 30%) which influence its physical structure and its hydration mechanism and kinetic²². Rendering mortars made with this binder are usually more compact and with higher mechanical strength in comparison to mortars made with CEMI thanks to the presence of fine calcium carbonate powder which acts as a filler between the aggregates, and presents a better resistance to sulphate attack in comparison to Ordinary Portland Cement CEMI.

²¹ Odler, I, 2000

²² Tsivilis, S. et al. 2002; Lothenbach, B. et al. 2008; S. Tsivilis, et al. 1998; Tsivilis, S., et al. 2003

EN 197-1:2000

Table 1- The 27 products in the family of common cements

Main types	Notation of the 27 products (types of common cement)		Composition [proportion by mass ¹⁾]										Minor additional constituents	
			Main constituents											
			Clinker K	Blastfurnace slag S	Silica fume D ²⁾	Pozzolana		Fly ash		Burnt shale T	Limestone*			
natural P	natural calcined Q	siliceous V				calcareous W	L	LL						
CEM I	Portland cement	CEM I	95-100	-	-	-	-	-	-	-	-	-	0-5	
CEM II	Portland-slag cement	CEM II/A-S	80-94	6-20	-	-	-	-	-	-	-	-	0-5	
		CEM II/B-S	65-79	21-35	-	-	-	-	-	-	-	-	0-5	
	Portland-silica fume cement	CEM II/A-D	90-94	-	6-10	-	-	-	-	-	-	-	0-5	
	Portland-pozzolana cement	CEM II/A-P	80-94	-	-	6-20	-	-	-	-	-	-	-	0-5
		CEM II/B-P	65-79	-	-	21-35	-	-	-	-	-	-	-	0-5
		CEM II/A-Q	80-94	-	-	-	6-20	-	-	-	-	-	-	0-5
		CEM II/B-Q	65-79	-	-	-	21-35	-	-	-	-	-	-	0-5
	Portland-fly ash cement	CEM II/A-V	80-94	-	-	-	-	6-20	-	-	-	-	-	0-5
		CEM II/B-V	65-79	-	-	-	-	21-35	-	-	-	-	-	0-5
		CEM II/A-W	80-94	-	-	-	-	-	6-20	-	-	-	-	0-5
		CEM II/B-W	65-79	-	-	-	-	-	21-35	-	-	-	-	0-5
	Portland-burnt shale cement	CEM II/A-T	80-94	-	-	-	-	-	-	6-20	-	-	-	0-5
		CEM II/B-T	65-79	-	-	-	-	-	-	21-35	-	-	-	0-5
	Portland-limestone cement	CEM II/A-L	80-94	-	-	-	-	-	-	-	6-20	-	-	0-5
		CEM II/B-L	65-79	-	-	-	-	-	-	-	21-35	-	-	0-5
		CEM II/A-LL	80-94	-	-	-	-	-	-	-	-	6-20	-	0-5
		CEM II/B-LL	65-79	-	-	-	-	-	-	-	-	-	21-35	0-5
	Portland-composite cement ³⁾	CEM II/A-M	80-94	←----- 6-20 -----→									0-5	
CEM II/B-M		65-79	←----- 21-35 -----→									0-5		
CEM III	Blastfurnace cement	CEM III/A	35-64	36-65	-	-	-	-	-	-	-	-	0-5	
		CEM III/B	20-34	66-80	-	-	-	-	-	-	-	-	0-5	
		CEM III/C	5-19	81-95	-	-	-	-	-	-	-	-	0-5	
CEM IV	Pozzolanic cement ³⁾	CEM IV/A	65-89	-	←----- 11-35 -----→					-	-	-	0-5	
		CEM IV/B	45-64	-	←----- 36-55 -----→					-	-	-	0-5	
CEM V	Composite cement ³⁾	CEM V/A	40-64	18-30	-	←----- 18-30 -----→			-	-	-	-	0-5	
		CEM V/B	20-38	31-50	-	←----- 31-50 -----→			-	-	-	-	0-5	

1) The values in the table refer to the sum of the main and minor additional constituents.

2) The proportion of silica fume is limited to 10%.

3) In Portland-composite cements CEM II/A-M and CEM II/B-M, in Pozzolanic cements CEM IV/A and CEM IV/B

and in Composite cements CEM V/A and CEM V/B the main constituents besides clinker shall be declared by designation of the cement.

* L : total organic carbon (TOC) shall not exceed 0.5% by mass; LL: TOC shall not exceed 0.20% by mass.

Table 1. 1 Classification of common cements.

Strength class	Compressive strength (MPa)			Initial setting time (min)	Soundness (expansion) (min)
	Early strength		Standard strength		
	2 days	7 days	28 days		
32.5 N	-	≥16.0	≥32.5	≥ 75	≤10
32.5 R	≥10.0	-			
42.5 N	≥10.0	-	≥42.5	≥ 60	
42.5 R	≥20.0	-			
52.5 N	≥20.0	-	≥52.5	≥ 45	
52.5 R	≥30.0	-			

Table 1. 2 Mechanical and physical requirements. The strength is determined in accordance with EN 196-1

Property	Test Reference	Cement type	Strength class	Requirements
Loss of ignition	EN196-2	CEMI; CEMII	All	≤5.0%
Insoluble residue	EN196-2	CEMI; CEMIII	All	≤5.0%
Sulphate content (as SO ₃)	EN196-2	CEMI; CEMII ^a ;	32.5 N; 32.5R; 42.5N;	≤3.5%
		CEMIV; CEMV; CEMIII	42.5R; 52.5N; 52.5 R	≤4.0%
Chloride content	EN196-21		All	≤0.10%
Pozzolanicity	EN196-5		All	Satisfies the test

A= cement types CEM IIB-T and CEMIII/C may contain up to 4.5% of sulphate

Table 1. 3 Chemical requirements in accordance to EN 197

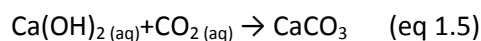
1.4.2.2. Natural hydraulic lime

Natural hydraulic lime are obtained burning a limestone containing silica, alumina and iron oxides, which above certain temperatures combine, totally or partially, with the Calcium Oxide²³. Traditional vertical kilns, similar to the ones used for aerial lime, heat the mixture to 1000°C-1200° C, below the sintering temperature. The reactions occurring upon heating are similar to cement:

- Below 120°C free water is evaporated, dehydroxylation of clays at 300-400°C.
- 400 to 600 °C - clay-like minerals are decomposed into oxides.
- 650 to 900 °C – Calcium carbonate decompose to quicklime (CaO) together with the clay minerals.
- 900 to 1200 °C - Quicklime react with quartz and clay mineral and form silicates and aluminates. Belite (Ca₂SiO₄) is formed.

The resulting mixture need to be slaked with enough water to convert quicklime (CaO) to lime hydrate (Ca(OH)₂), but not so much that a chemical set begins. A mixture of air-hardening (slaked lime) and hydraulic binders is obtained as a final product.

The setting and hardening of natural hydraulic lime is ensured by the hydration reactions of silicates, aluminates and calcium hydroxide. The same reactions described for cement materials occur (see above equation 1.2, 1.3, 1.4), even if the tri-calcium silicate is completely absent. Natural hydraulic lime hardened slowly with a slow formation of C-S-H due to the hydration of belite. Together with the hydration of silicates and aluminates, also some of the calcium hydroxide reacts and carbonates (eq. 1.5).



²³ Pellizzon Birelli, M., Ph.D thesis 2003

The natural hydraulic lime, as described by the EN 459-1, must fulfill particular requirements: they should be produced from clayey limestone, without the addition of pozzolana, gypsum, ash, or cement. Natural hydraulic lime are classified according to their compressive strength expressed in N/mm² (MPa) (Table 1. 4).

Lime type	CaO+MgO	MgO	CO ₂	SO ₃	Free Lime	Compressive strength 28 days
NHL2	-	-	-	≤3	≤15	2-7
NHL3.5	-	-	-	≤3	≤9	3.5-10
NHL5	-	-	-	≤3	≤3	5-15

Table 1. 4 Classification of natural hydraulic lime in accordance to EN 459

1.4.2.3. Pozzolana-lime

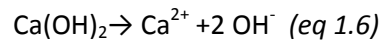
The mixture pozzolana-lime constitute an artificial hydraulic lime. Pozzolana components confer hydraulicity to the mixture. Natural Pozzolanas are of different natures and are described from the ASTM C618 as 'a siliceous or siliceous and aluminous material which, in itself, possesses little or no cementitious value but which will, in finely divided form in the presence of moisture, react chemically with calcium hydroxide at ordinary temperature to form compounds possessing cementitious properties'. Pozzolana are, therefore, latently hydraulic materials, able to react hydraulically only in presence of a suitable activator (such as an alkali hydroxide). The general terms of pozzolana includes different glassy or amorphous materials , which contains CaO, SiO₂ and Al₂O₃ as their main oxides. Pozzolana are usually material of volcanic origin, burnt clays or Trass (volcanic tuff-stone) that can be roughly divided into the categories listed below²⁴, according to their origin and properties:

- “natural, very finely divided, highly reactive materials of volcanic origin. These materials were formed from a combination of minerals, (mainly consisting of silica and alumina with smaller and variable quantities of other minerals containing calcium, magnesium, iron, potassium, and sodium), ejected from volcanoes in the form of very finely divided vitreous material. Well known sources include pozzolana from Pozzuoli in Italy, volcanic pozzolana from South-east France, Trass from the Rheinlands and tuff from the Aegean islands. Crushed pumice was also used.
- Low temperature calcined clay products in various forms. Pozzolanic additives derived from lightly fired and finely crushed clay products, such as clay tile or brick, were used already by the Romans.
- Heat activate clay or kaolin. Burning kaolin or other clay minerals, reactive polymorphs, thermodynamically unstable, can be formed, (e.g. metakaolin). These materials combine readily with calcium hydroxide to form calcium silicate hydrates and calcium aluminosilicate hydrates.
- Mineral slag and ashes of organic origin. Furnace slag is a vitrified material containing silica, alumina, lime and other minerals, it requires grinding to convert it into a reactive material. Coal ash is widely used, in the form of PFA (pulverised fuel ash) as an additive to cementitious mortars and in lime-based grouts.”²⁵

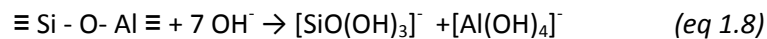
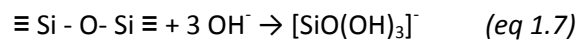
²⁴ Gibbons, P. 1997

²⁵ Gibbons, P. 1997

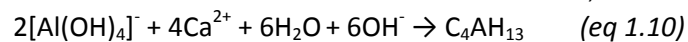
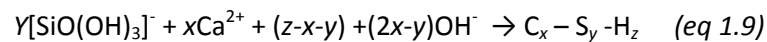
The mixture pozzolana-limes is able to set and form an hydraulic binders thanks to the pozzolanic reaction.²⁶ When water is added to the mix of lime and pozzolana the calcium hydroxide dissolve and a basic solution (pH ~12,5 at 20°C) of calcium hydroxide is formed (Eq. 1.6):



The network modifiers cations Ca^{2+} , K^+ , Na^+ , are removed from the minerals structures and the silicates and aluminosilicates networks are partially depolymerized because of the basic pH and the presence of OH^- in solution:



This dissolved monosilicates and aluminates species are able to react with the Ca^{2+} ions in solution to form silicates C-S-H and calcium aluminate hydrate C_4AH_{13} (eq 1.9, 1.10).



The dissolution of aluminosilicates glass determines the total reaction rate, because is the slowest step. After the precipitation of hydrated products on the outer surfaces of the pozzolan the reaction proceeds under diffusion control of OH^- and Ca^{2+} through the precipitated products and becomes a topochemical reaction. Rise in curing temperature leads to a faster hydration rate, but seems not to affect the process and the products.

Studies on hydraulic limes where pozzolans rich in metakaolin and kaolin were used, the formation of a poorly crystallized gel of calcium hydrosilicate, gehlenite C_4ASH_8 and hydrogarnets $\text{C}_3\text{ASzH}_{6-2z}$, such as katoite [$\text{C}_3\text{A}(\text{S})_{3-x}(\text{H})_{2x}$, (with $1.5 \leq x \leq 3$)] were observed²⁷.

1.4.3. DETERIORATION OF POROUS BUILDING MATERIALS

“Brick, mortar and porous stone undergo deterioration processes when exposed to the aggressive action of the environment. The rate and symptoms of such processes are influenced by a number of variables, partly depending upon the properties of the material itself and partly upon several environmental factors, acting separately or in various combination”²⁸.

The deterioration of porous building materials results by the combined action of chemical processes acting together with physical processes, such as mechanical stresses. This action involves not only the external surface of the porous materials but the entire bulk materials through its interlinked open porosity.

The porosity of a porous building materials can be seen as a favourite way of free access of the degradation factors inside the inner matrix. But what does open porosity means?

The total porosity is the volume of pore space in the material to its volume in per cent, while the open porosity, called also *effective porosity*, indicates the total pore volume determined by the mercury intrusion, therefore the total accessible porosity²⁹. Higher open porosity or strongly interlinked pores determine higher specific areas exposed to the degradation factors.

²⁶ Shi, C., R. L. Day, 2000

²⁷ Donchev, et al. 2010; Sepulcre-Aguilar A., et al. 2010; Gualtieri, A.F. et al. 2006

²⁸ Torraca, G. 1981, p1

²⁹ Winkler E.M., 1975 p28; Amoroso, G.,1983, p10-11

Among the various agents harmful for porous building materials, humidity of different origins is one of the most important and will be discussed in the following paragraphs.

1.4.3.1. Moisture in porous mortars and stones

The presence of water in historical and recent porous buildings material provokes serious degradation phenomena. The water is responsible for the fast proceeding of physical-chemical degradation processes as for direct action, i.e. rainfalls, as indirectly for transporting pollutants and soluble salts inside the porous structures of natural and artificial stones.

The porous structure of mortars is usually hydrophilic and highly permeable to water. Salts and pollutant dissolved in water have, therefore, easy access to the mortars insides³⁰.

The hydrophilic behaviour of mortars is easily explained considering its nature. In fact, mortars are mainly composed of inorganic mineral materials, and both water and minerals show a high polarity in their structures due to the differences in electro negativity between oxygen and the other elements participating in chemical bonds. Water is able to make hydrogen bonds with other water molecules and hydroxyl- or other polar groups present in minerals surfaces and to wet them³¹.

This wettability is also the base for moisture transport inside the mortars. Different moisture transport system can be distinguished; *gravity, capillary systems, diffusion, hydrostatic pressure* are some of the most important water transport systems, and often some of them are acting together³².

Every time meteoric waters flow over buildings surfaces because of *gravity* force, the rain runoff causes wash-out processes and erosion of the exposed surfaces. Rain wash-out can have, maybe, the positive aspect of cleaning the surfaces, but unfortunately, rain does not fall uniformly onto a building and its effect can be different on different building material. The surfaces are therefore wetted, weathered and damaged in different ways.

From the surfaces the water penetrates deeply into the porous materials through *capillary absorption*: the mortar joints and renders can be wetted and then water can be sucked by stone or bricks with smaller diameter of pores, or diffuse inside the walls. These drying-wetting cycles are anyway dangerous for the substrate, which can remain wet also for long periods.

What makes water enter the capillaries of porous building materials and even rise against gravity is the balance between cohesive forces within the liquid water, defined as its surface tension σ (dy/cm) and the adsorption forces of the polar mineral surfaces illustration of the difference between a hydrophilic and a hydrophobic material by the means of a contact angle: on top capillary pores and underneath a water droplet (Figure 1. 2)³³. The "attractivity" between water and solid, better defined as the wettability of the substrate, depends on the contact angle between water drops, surrounding air and the mortar surface (contact angle $<90^\circ$ defines hydrophilic surfaces). The contact angle correspond to the thermodynamic height which minimize the free surface energy and is described by Young- Dupré equation: $\gamma_{LG}\cos\theta = \gamma_{SG} - \gamma_{SL}$ (γ =surface tension; L=liquid; G=gas; S=solid; θ =contact angle).

³⁰ Hall, C., W.D.Hoff, 2002; Wendler, E, A.E: Charola, 2008, pp. 57-74; Winkler E.M., 1975 p 103

³¹ Torraca, G. 1981, p7-10

³² Verhoef, L.G.W, 2001, pp. 21-36 ; K.L. Mittal Editor,2003 in particular the contributions of Wayner, P.C p1-23, Zhang J. and D.Y. Kwok, p 96-116

³³ Houvenaghel, J. Carmeliet, 2001, pp. 191-200; Johansson, A. 2006

The capillary force F_c and the corresponding capillary tension p_c in a cylindrical pore can be expressed by :

$$\text{Capillary force } F_c = 2 r \pi \gamma_{\text{water}} \cos \theta \text{ (eq 1.11)}$$

$$\text{Capillary tension } p_c = 2 \gamma_{\text{water}} \cos \theta / r \text{ (eq 1.12)}$$

For materials with $\theta < 90^\circ$ adsorptive forces exceed cohesive forces resulting in capillary absorption. The maximum height that can be reached by vertical transport is given by the Jurin law:

$$H_{\text{max}} = 2 \gamma_{\text{water}} \cos \theta / r \rho g \text{ (eq 1.13)}$$

where ρ = density of water; g = gravity force; θ = contact angle; r = capillary radius

Smaller capillary give rise to higher capillary rise, while larger capillaries provide faster water absorption rate .

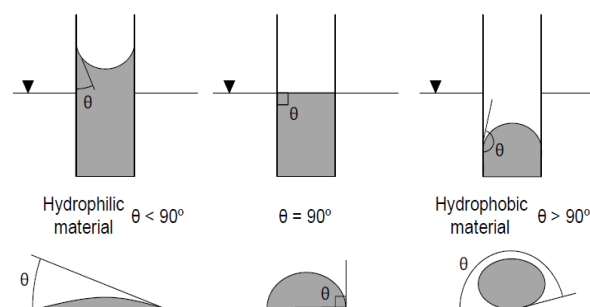


Figure 1. 2 illustration of the difference between a hydrophilic and a hydrophobic material by the means of a contact angle: on top capillary pores and underneath a water droplet (1)

In the reality the porous system of stone is further more complex and the pores have tortuous paths, but what is more important is that a deeply penetration of water inside the materials is possible from raining water but also from the soil through water absorption.

The role of water vapour and the *diffusion processes* of water vapour inside porous matrixes are of no less importance. Only in rare case the porous system of stone is completely dry or fully saturated with water, being in most cases liquid water and water vapour both present. Water vapour can come from the outside and enter in the pore structures, or originates by evaporation of liquid water inside the pores. The vapour is then transported inside the matrix through diffusion processes due to gradients of relative humidity and temperature.

Usually the relative humidity is lower outside a wet material and the water vapour can be transported outside the capillary pore system, in a drying process. However, the drying process is not linear: changes in parameter such as temperature and relative humidity influenced the water vapour pressure and the equilibrium between liquid water and vapour inside the porous matrix leading to complicated evaporation/condensation phenomena³⁴. These phenomena can be influenced by the geometry of the pores which generates different partial pressures, and by the presence of salts which can act as preferential condensation site. The adsorption of water vapour on the salts and on some building materials, such as clays, induce hygric dilatation and cause an additional stress on the surfaces.

Walls are complex systems which can be affected by all the form of transportation seen above. Water can wet the buildings during precipitations or penetrate the structure from the soil, and

³⁴ Hall, C., W.D.Hoff, 2002.

can diffuse inside the wall and water vapour can evaporate from the surfaces in different ways. It is therefore important to protect the buildings reducing the entrance of liquid water in the walls but also allowing them to dry fast thanks to a high permeability to water vapour. In fact, the presence and the stagnation of moisture between the masonry and the rendering mortars applied on the surfaces cause detachments and disaggregation of the mortars.

1.4.3.2. Moisture and salts in mortars and stones

The damages described above are worsened by the presence of salts or in presence of freeze-thaw cycles because the substrate structure undergoes mechanical stresses due to precipitation/crystallization and dissolution/melt processes.

Indeed, during freeze-thaw cycles the water molecules develop well ordered structures increasing in volume (the density changes from 1 Kg/m³ for liquid water to 0,917 Kg/m³ for ice at 4°C) that cause mechanical pressure on the pores walls³⁵.

Water soluble salts present in the materials or coming from the environment are one of the most damaging factors of mortars. The very complex capillary system of stone and mortars complicate the understanding of the mechanisms such as solution, salt migration, salt crystallization, salt hydration, thermal expansion of entrapped salts. However, the transport of salt solution within the porous structure is driven by capillary water absorption mechanisms.

Once inside the porous matrix, the evaporation of the water induces the precipitation and crystallization of the salts, developing strong crystallization pressures when the growing crystals encounter a pore wall, and leading to serious physical weathering³⁶.

The pressure developed by a growing crystal in an idealized porous system composed by two classes of communicating pores is described by eq 1.14 according to the thermodynamic approach of Everett³⁷. The crystallization pressure is inversely proportional to the pore radius and depend on the salt nature (γ).

$$P_r = 2 \gamma (1/r - 1/R) \quad (\text{eq 1.14})$$

where P_r = pressure by crystal growth; γ = surface tension of the salt; r and R = pore radius.

Different salts crystallized in lower density structures, but readily hydrate or dehydrate in response to changes in the temperature and relative humidity of the atmosphere. The salts change consequently also their dimensions and can develop further pressure on pore walls. For examples sodium sulphates are able to hydrate to mirabilite $\text{Na}_2\text{SO}_4 \cdot 10 \text{H}_2\text{O}$ and dehydrate to thenardite Na_2SO_4 also at room temperature (20°C) inside the pores³⁸. Furthermore, the presence of hygroscopic salts inside the pores might act as a driving force for water suction and the presence of salts choking partially the pores enhanced the capillary suction because the pore diameter decrease.

The most common soluble salts present in stone materials are sulphates, chlorides, nitrates and carbonates of alkali metals and magnesium. Besides the physical weathering due to the crystallization-hydration-dehydration, those salts are able to cause also chemical weathering of

³⁵ G.G., Litvan. 1980, pp. 455-463; Amoroso, G., 1983, p23-28

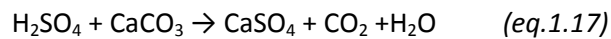
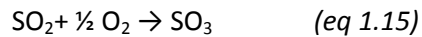
³⁶ Scherer, G.W. 2000; Rossi-Manaresi, R., A. Tucci, 1991; Benavente, D., et al. 2004

³⁷ Everett, D.H. 1961; Fitzner, B., R. Snethlage 1982, pp 13-24

³⁸ Rodriguez- Navarro C., E. Doehne, E. Sebastian 2000

mortars in presence of water. In fact, water which is able to dissolve different pollutants and salts such as sulfates, NO_x , CO_2 and to form acid solutions and salts solutions.

In presence of sulfur dioxide and water the following reactions can occur:



The volume of gypsum is 20% higher than calcium carbonate (gypsum $74.7 \text{ cm}^3/\text{mol}$; calcite $36.9 \text{ cm}^3/\text{mol}$ at 25°C) and this causes new stress to the mortar substrates. Furthermore gypsum is more soluble than calcium carbonate (gypsum 0.014 g/L , calcite 0.214 g/L in cold water) and can be easily washed out. The sulphate ions SO_4^{2-} can also interact with hydraulic lime or cement mortars structure to products damaging salts such as gypsum, ettringite and thaumasite³⁹ in the so called *sulfate attack* (Figure 1. 3).

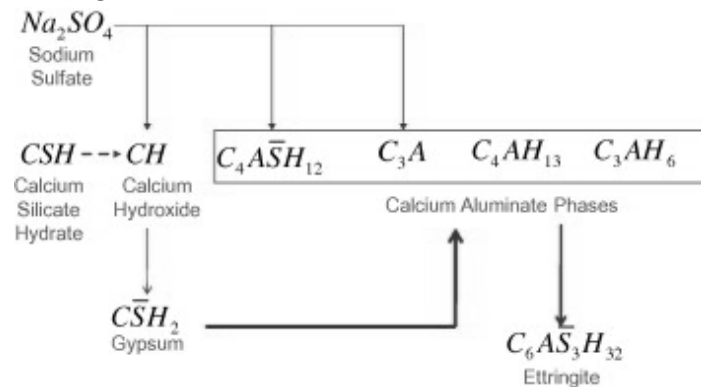
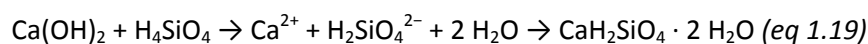


Figure 1. 3 Schematic diagram of the chemical reactions due to sulfate ingress³⁴

Also hydration reactions and alkali-silica reactions are possible in presence of water. This reaction is the same as the Pozzolanic reaction, and can be schematically represented as following:



This reaction causes the expansion of the altered aggregate by the formation of a swelling gel of Calcium Silicate Hydrate (C-S-H). This gel increases in volume with water and exerts an expansive pressure inside the material, causing spalling and loss of strength of the concrete, finally leading to its failure.

The entity of damages caused by the water and by salt crystallization depends on the exposure of mortars but also on the structure of the mortar itself. As we have seen above, the porosity of the mortar and its mechanical properties play an important role in determining the effects of the weathering. Mortars with high open porosity, low elasticity and fine pore radius are more prone to this kind of weathering, because phenomena as capillary rise/transport is enhanced with smaller diameter pores and eventual salt crystal growth is forced in smaller place.

Furthermore, the entire system wall-mortar have to be taken into account. When mortars with low water-vapour permeability are applied as rendering mortar on walls, act like a physical

³⁹ Sarkar, S. et al. 2010; Chabrele, A. 2010

barrier to water solutions inducing the evaporation of water and the precipitation of salt at the wall/mortar interface leading to sub-efflorescence formation and detachments.

The water and acid water solution can act also by preferential dissolution and leaching of several ions and compounds present in mortars and actively change the binder composition.

The presence of moisture in building materials increases significantly the thermal conductivity⁴⁰, decreasing the thermal isolation of the structures and resulting in power loss and unhealthy environments⁴¹, where bio-fouling and biological growths are favoured⁴². At last, also the anti-esthetical formation of humidity spots on building surfaces have to be taken in account when speaking of historical and artistic buildings, because can change the aspect of the surfaces (Figure 1. 4).



Figure 1. 4 examples of damage caused by water action and moisture on mortars, from left to right: detachments, spots and bio-fouling, powdering

During the last years, the problem of the degradation due to water action is of primary interest in force of the intensification of the meteorological events together with the air pollution and the dangerous atmospheric particulate, not any more limited to the urban areas. In force of these reasons, it is clear as the development of adequate water-repellent systems for constructions is a crucial point and an important step to considered already in the building construction project. The fast degradation of buildings involves not only loss for the economy but also for the history and society with a progressive loss of our cultural heritage. The intervention and maintenance costs of materials commonly used for building construction are often appreciable and the results of these interventions never give the possibility to reach the original materials state.

1.4.3.3. Salty masonries: the case of Venice

The city of Venice, as almost all the historical Italian cities, constitutes of historic building built principally with brick masonry. To obtain durable structures in the lagoon's environment, the citizens have developed peculiar technological solutions over the centuries. Starting from their foundations, the building of Venice show complex structures designed to face the problems due to a soft soil, the presence of salty water⁴³, and the marine aerosol⁴⁴.

⁴⁰ ISO 9869

⁴¹ United Nations Environment Programme 2007; An estimate of the European Environment Agency has shown that, if the current building methods are maintained, about 549 Mtoe will be consumed for housing and for the tertiary sector in 2020 European Environment Agency – EEA. Report No 05/2008 2008.; F. Barreca, C.R. Fichera 2013

⁴² C.A. Crispim, P.M. Gaylarde, C.C. Gaylarde 2003; C.C. Gaylarde, P.M. Gaylarde 2005

⁴³ Micheletti, C., et al. 2011

⁴⁴ O' Dowd, C. et al. 1996; Mcinnes, L.M., P.K. Quinn, 1995; Marengo, E. et al. 1995

The foundations of the buildings in Venice are based on a complex system composed of wood, water and soil⁴⁵(Figure 1. 5). Wood poles were driven into the terrain to pack the soft layers below, and a platform was laid over the poles. The foundation walls were then built with brick on this base. The walls directly on the banks were covered with a more compact material: *Istria Stone*, a limestone from the Istrian quarries to avoid capillary water absorption and penetration of salty water inside the structures. Bricks adobe were built over this base, outside the level of water, binding the bricks with hydraulic grouts made with *cocciopesto*.

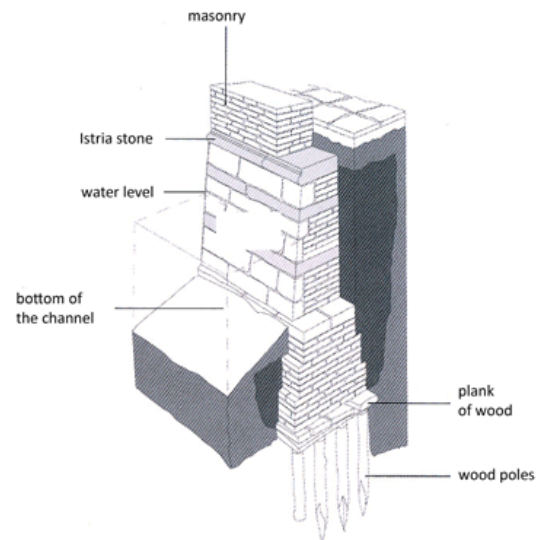


Figure 1. 5 The foundation of the buildings in Venice. (Stefano Zanovello from a drawings of Mario Piana)

Hydraulic rendering mortars and plasters were also used to protect the masonries from the marine aerosol.

These protection are, nowadays, not enough and the venetian historic brick masonries undergo serious decay, accelerated also by the intensified phenomena of the high tides.

According to the sea salt origin, a 'rising damp zone' and a 'sea spray zone' can be identified in brick walls exposed to marine environment⁴⁶, where different kind of degradation occur, blistering and salt efflorescences and sub-efflorescences in the former case, powdering in the latter case. The zone just above the ground, completely wet, usually show less deterioration than the zone above where there is the evaporation/drying front.

Considering several research studies regarding the distribution of the salts in venetian⁴⁷ or in other brick walls interested by rising damp, a model for rising damp and soluble salts can be proposed⁴⁸ as summarized in Figure 1. 6. The salt solution from the basement of the wall rise up by capillary forces. When the evaporation rate overcomes the rising damp rate the solution becomes more concentrated, if the oversaturation with respect to one saline phases is reached, that phases crystallize.

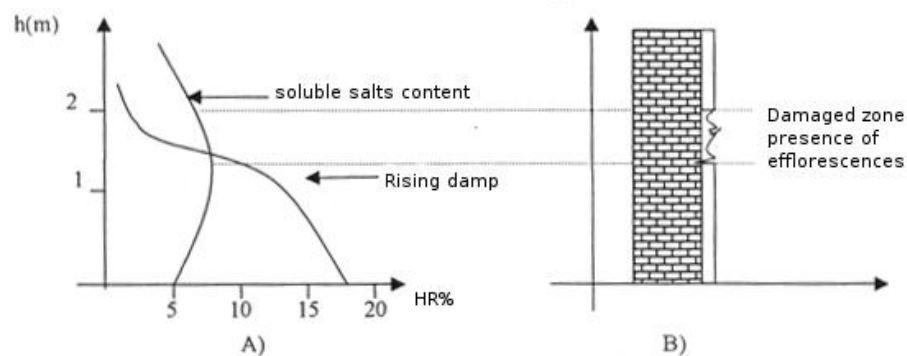


Figure 1. 6 A) relative humidity and distribution of soluble salts versus walls height. B) degradation zone relative to the evaporation front and to the curves of figure 1.4A

⁴⁵ Biscontin, G., F. Izzo, E. Rinaldi, 2009

⁴⁶ Lubelli, B. et al. 2004

⁴⁷ Fassina, V. et al. 2002; Bakolas, A., G. Biscontin, A. Moropoulou, E. Zendri, 1996; G. Biscontin 2001 Veniale, F. 2003; Biscontin, G.; Cattalini, 1980; Biscontin, G. et al. 1979; Driussi, G. et al. 1985

⁴⁸ Arnold, A. 1982

1.4.4. WATER REPELLENT SYSTEMS

The individuation of water-repellent protection systems, able to protect porous building material from the damaging action of water, was considered and developed in several researches⁴⁹.

The water protection of natural and artificial stone materials has been traditionally carried out via impregnation with hydrophobic chemicals. Oils, waxes, animal fats, egg yolks, cactus juices are some example of traditional water repellent applied on stone surfaces in the last centuries. They were gradually substituted, from the XX century, by acrylic and vinyl resins, silane-siloxane oligomer or polymer water dispersion or organic solution⁵⁰. These products are mainly used for surface building treatments, during which the liquid product have to penetrate the material and form a protective layers within the pore walls (Figure 1. 7).

The protection based on impregnation is the only possible treatment for finished buildings, but the success of this treatment is often critical and depends on various factors like the real deepness reached, the formation of a continuous layer, the risk of altered the water vapour permeability of the substrate, and the conservation of the water-repellent properties over the time. The protection is obviously compromised in presence of cracks, which become a preferential water entrances with the formation and acceleration of degradation processes.

Another possibility to obtain a good protection against the action of water is to obtain durable water-repellent material, thanks to a bulk hydrophobization of the materials. On this idea are based the traditional addiction of ox blood, vegetable oils, proteic materials, cactus juice in mortar mixtures and the more recent addiction of water-repellent additives such as organic polymers, silane-siloxane systems, metal soaps⁵¹.

One of the most important advantage of bulk hydrophobization is the total protection of the system since the construction moment, obtaining in this way a total water repellent structure and avoiding since the beginning the access of the water and the formation of degradation processes. Moreover, this protection is maintained even in presence of decohesion and cracks.

Actually some of the most used water-repellent additives are based on the use of metallic-soaps. Only few published paper relate about the behaviour of water-repellent mortars admixed with metal soaps, and focused mainly on the macroscopic properties such as the reduction of water absorption in cement and aerial lime mixtures doped with calcium, zinc and sodium stearate and oleate additives⁵². Despite the good results obtained thanks to the additives, there are not complete studies and it is not fully clear the action and interaction in the structure. Few are also the studies on mortars durability mixed with calcium and zinc stearates and sodium oleates processed to ageing cycles and artificial and natural degradation.

Other commonly used additives are silane-siloxane both as liquids (organic solutions or water-based emulsions) and in powder form. These modified systems added in small percentage to the mixture give good hydrophobicity and seems compatible with different mixture based on cement, lime and gypsum⁵³. The new powder silane additives are based on alkylsilane with

⁴⁹ Amoroso, G. 2002; Lazzarini, L., M.L. Tabasso 1986; Collepardi, M. 2010

⁵⁰ Maravelaki-Kalaitzaki, P. 2007; T. Stambolov, J.R.J. Van Aspered de Boer. 1972; L. Scueremans, et al. 2007

⁵¹ Martinola G. 2004

⁵² Lanzon M, Garcia-Ruiz PA. 2009;

⁵³ Jakobsmeier, L. 2000; Lanzon; PA Garcia-Ruiz. 2009; A. Izaguirre, J. Lanas. 2009

hydrophobic later groups or modified alkylsiloxane with lateral organic groups. The modified compounds can be attached to inorganic carrier like silica or calcium carbonate in order to obtain a product in powder easy to store, dose and mix. Alternatively, it is possible to add silane-siloxane water dispersions, similar to the one used for impregnation treatments, into the mixing water⁵⁴. However, only few studies are available on the interactions between powder silicone admixtures with the binders commonly present in the commercial mixture and problems like pH, reaction time and rheology of the compounds⁵⁵.

In Figure 1. 7 some of the possible actions of the water repellents and a corresponding list of the most common used substances can be seen: some products act developing an impermeable layer on the substrate surfaces (as in c), some others fill the porosity and occlude physical the pores (as in b). These kinds of treatments constitute a physical obstacle to the penetration of water inside the porous substrate but also block the moisture inside the material and stop the free circulation of water vapour and the evaporation from the substrate leading to the detachment phenomena.

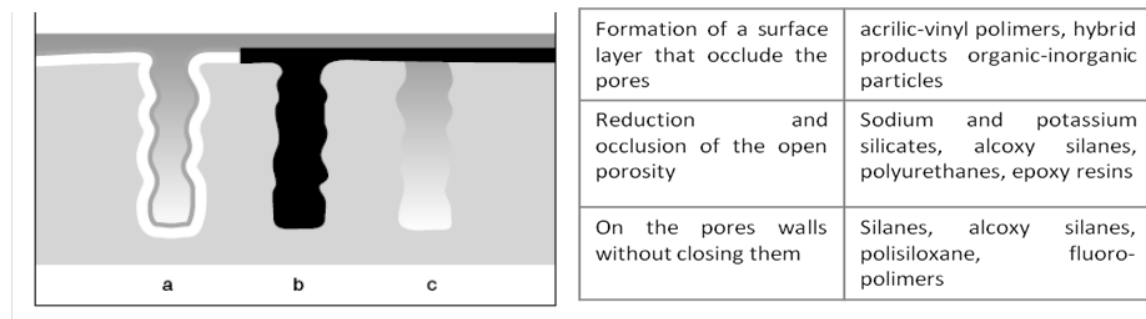


Figure 1. 7: Examples of different water-repellents systems applied by impregnation⁵⁶

Other water repellents are able to impregnate the substrates without blocking the pores. They distribute themselves on the pore walls and create an hydrophobic layer able to repulse water. The water absorption is inhibited from the presence on the substrate surfaces of hydrophobic groups which change the surface tension of the materials. These Hydrophobic groups can be of different natures, most of them are long apolar alkane chains, with low affinity with water. The same substances can be mixed in fresh mortars mixtures to obtain water repellent properties.

In the following paragraphs a short overview of the most important class of water-repellent admixtures for integral water-repellency of mortars and concretes is given.

1.4.4.1. Metal soaps

The term "Metal soaps" indicates different metallic soaps of fatty acids of vegetable origin, in particular fatty acids with a carbon-chain length of 14-18 carbons, such as stearates, palmitates and oleates (Figure 1. 8, Figure 1. 9). The most important, in terms of number of applications and quantities produced, are the metallic stearates of calcium, zinc, magnesium and aluminium. Depending on the nature of the fatty acid is possible to distinguish between saturated and unsaturated soaps. The most important representative of the first group are the stearates. In

⁵⁴ P. Zhang, et al. 2010; Aberlee, T., et al. 2010 P.Emmenegger, F. Vallee. New Approaches to Increase Water Resistance of Gypsum Based Building Materials. Proceedings of the conference "Drymix Mortar Yearbook 2010". 2010.

⁵⁵ Fabric, Wacker silicones SILRES® Lasting protection for Building. *www.Wacker.com*. [Online] 2011.

⁵⁶ elements-29-chemical-umbrella-for-buildings-2010

reality, being these metal soaps mainly produced from natural sources/oils, no pure stearates are commonly sold, but only mix of different chain-length soaps as C16 or C18. No big differences in the behavior are observed from one fatty acid to another. Regarding unsaturated metal soaps, as a consequence of the double bond, they have a lower melting point than the corresponding linear saturated soaps and their solubility is usually slightly improved. In the case of shorter acid, such as laureates, the properties are greatly influenced by the respective metal base.

What affects more the properties and the behaviour of these soaps is the metal part. Big difference in the chemical and physical behaviour can be observed in presence of different metals: salts of alkaline metals are soluble in water and act like surfactants, while alkaline earth metals and other bi- or trivalent metals form water insoluble, highly hydrophobic salts.

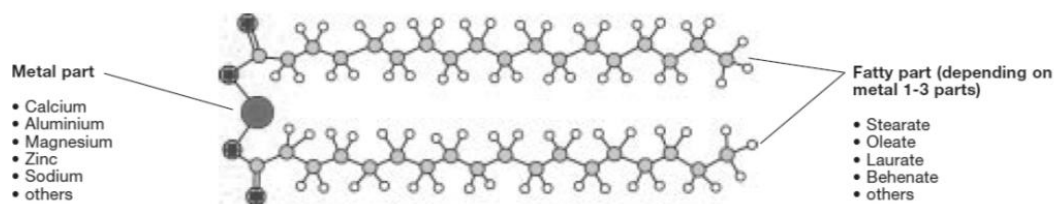


Figure 1. 8 Generic Metal Soap structure⁵⁷

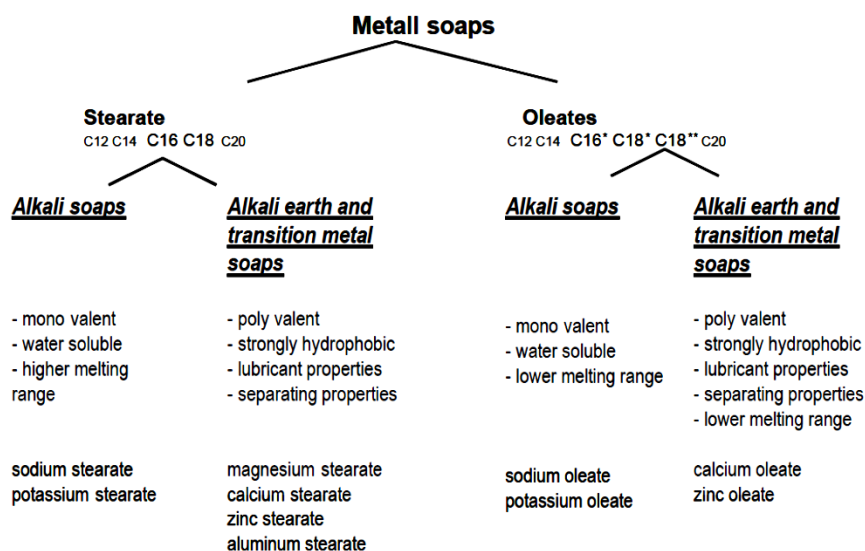


Figure 1. 9 Schema describing different Metal Soaps and their properties

Metal soaps are manufactured by using one of the following three processes: double decomposition (precipitation process), direct reaction of carboxylic acid with metal oxides, hydroxides and carbonates (fusion process), and direct reaction of metals with molten fatty acids⁵⁸.

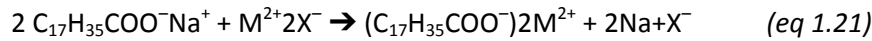
In the precipitation (or double composition) reaction the fatty acid is first saponified in heated water with an equimolar to a slight excess quantity of a strong alkali solution (sodium hydroxide, caustic potash solution, ammonia):



⁵⁷http://www.baerlocher.com/fileadmin/media/0.5_Service/0.5.1_brochures/0.5.1.3_product_brochures/metallic_stearates.pdf

⁵⁸ Golnen, M. et al. 2005; Golnen, Mehmet, 2010; Moreira, A. P. D. et al. 2009

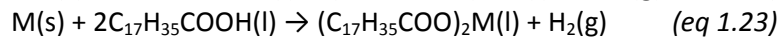
The resulting alkali stearate is soluble in water. The alkali stearates react then with a metal salt solution (e.g. calcium chloride solution, aluminium sulphate solution) to form the desired water-insoluble stearates that precipitate:



M = Zn^{2+} , Ca^{2+} or similar; X = Cl^- , $1/2 \text{SO}_4^{2-}$ or similar

The water-soluble salts obtained as by-products of the precipitation reaction, is removed by filtration and washing. Finally, the resulting wet cake must be dried and the product de-agglomerated or milled. This double-decomposition reaction typically produces very light, fine powders with a large surface area and a more platelet morphology.

Metal soaps are obtained also by the reaction of metal oxides, hydroxide, carbonate, or acetate with a molten fatty acid at temperatures sufficiently high to form metal soaps.



M = Zn^{2+} , Ca^{2+} or similar

Metal soaps are used for different purposes thanks to their properties, i.e. lubricating properties, separating properties, water repellence, gelling capacity, stabilising effect, foam inhibition, acid scavenger⁵⁹. Metal soaps are also the most commonly used additives in cement mortar production, in order to obtain water repellents properties and a diminished water capillary absorption.

The current researches about the use of metal soaps as water-repellent additive for mortars focalized on modified cement mortars and the water absorption coefficient, the wettability and the mechanical strength⁶⁰. The results are obtained pointed out that the water-repellent properties of the final mortars with increasing dosages, but higher than 2% by mass caused reduced mechanical properties, and that the addition of sodium oleates was particularly effective in comparison to calcium and zinc stearates.

The metal soaps are dispersed inside the mortar matrix and exercise their water repellent action modifying the surface tension of the mortar surfaces, and therefore the contact angle between water and the surfaces, thanks to the organic, long apolar chains. Inside the capillary pores the phenomena of the inverse meniscus is observed and the entrance of water prevented. Their structure allowed them to act also on the porosity of the mix, acting as mild air-entraining agents. They dispose themselves at the interface air bubbles/binder/water stabilizing the air bubbles. Due to their hydrophobic properties, is difficult to obtain a good dispersion and lumps are often formed⁶¹.

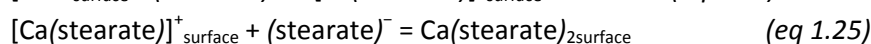
Few information are available regarding the interactions between metal soaps and construction materials such as binders or aggregates. Feeble physical interactions between the –OH of the

⁵⁹ Metallic stearates are used in the plastic industry, as acid scavengers, lubricants and release agents and in melt processing. In the pharmaceutical and cosmetic industry they are used due to their outstanding lubrication and release properties, their thixotropic effect and their capacity for gelation, for drugs preparation and tablet pressing and for creams as anti-caking agents. In the textile industry, metallic stearates are applied for dry impregnation and as antistatic agents. The printing ink industry utilises metallic stearates as swelling and suspension aids for other additives such as pigments.

⁶⁰ Riethmayer, S.A. 1961; A.T. Albayrak, et al. 2005

⁶¹ M. Lanzón, P.A. Garcia Ruiz. 2008

mortar matrix and the polar head of the soaps are usually considered to be responsible for the stabilization of the soap inside the matrix, while the apolar tail confers hydrophobic properties. Sodium stearates and oleates differ from the alkaline-metal soaps because of their solubility in water. This second kind of metal soaps is able to be easily dispersed in the mixing water. In contact with calcium hydroxide product during the hydration reactions of cement, or in presence of lime, or calcium carbonate, sodium soaps react to form a more stable precipitate of calcium soaps in the basic environment of the mortar⁶².



It was not investigated yet, if similar mechanism can happen also in the presence of other stearates, e.g. zinc stearates.

1.4.4.2. Silane /siloxanes

Silanes are saturated chemical compounds composed of hydrogen and silicon atoms. They are considered homologous of alkanes because silicon atoms can be linked to form chains of different length, where the number of silicon atoms in the chain defines the size. Hydrogen atoms can be substituted by side functional groups, e.g. alkyl chains, to obtain organosilanes or siloxane. Also -OH groups or halogen can be incorporated into a silane. The introduction of an alkoxy group, i.e. an alkyl group bonded to oxygen (R-O), produces the so-called alkoxy silanes, often used as water repellents.

Silanes are less thermally stable than alkanes and kinetically labile, and more prone to decompose if the silicon chain increases.

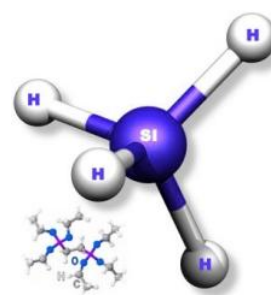
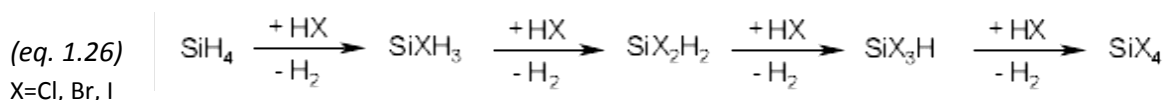


Figure 1. 10 chemical structure of monosilane

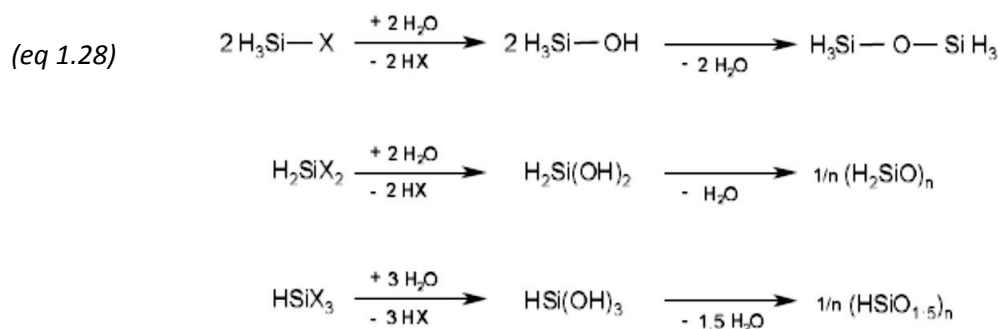
Silicon is able to bond itself to other silicon atoms and hydrogen to form a series of compounds with the general formula $\text{Si}_x\text{H}_{2x+2}$ that are known as silanes and can be distinguished in Mono-, Di-, Tri-, etc. silane. The silicon atoms can bond to 4 other atoms with a tetrahedral coordination and silicon chains and web structure can be formed.

The chemistry of silicon differs from the chemistry of carbon, because the electronegativity of silicon is lower than the hydrogen atoms, and polar Si-H bonds have a reverse polarity in comparison to the C-H bond and therefore a higher sensitivity to hydrolysis. If monosilane reacts with halogen atoms, the hydrogen can be substituted (eq. 1.26):



The reactivity of halogenosilanes to water is drastically enhanced. In presence of water a strong reaction of hydrolysis of the Si-X bond and the formation of silanols occur, these latter compounds are not stable and further react (condensation) to form siloxanes (eq. 27). The stability of the products increases with the dimension of the alkoxy group.

⁶² Lanzón, M., et al. 2011



Silicones are polymeric Siloxane with sides' alkyl-substituent with general formula R_2SiO (Figure 1. 11). The most important starting compounds for the synthesis of silicones is methylchlorosilane, which can be synthesized and further transformed to silicone compounds by the direct Rochow-Müller synthesis. Mono-, di- and tri-chlorosilanes are transformed in organosilicones compounds thanks to hydrolysis-condensation reaction.

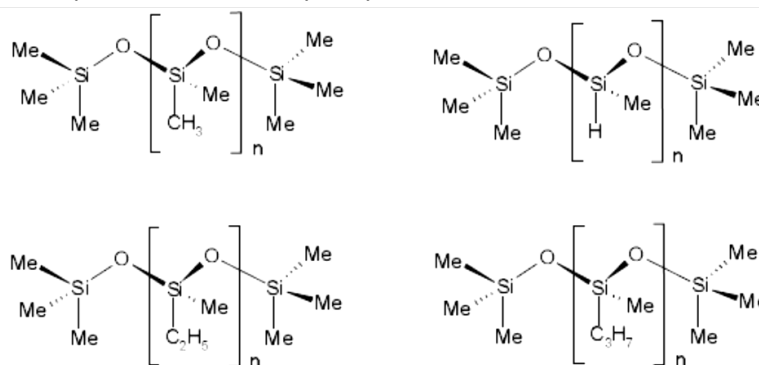
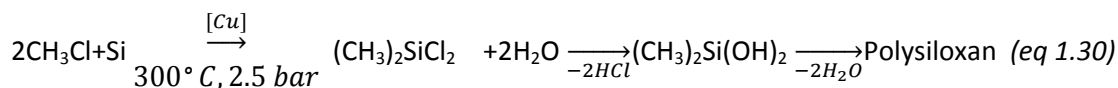


Figure 1. 11 Structure of some siloxanes, Me= alkyl group



In the silicon chemistry the siloxane units can be classified in four different structures, depending on the organic substituent or hydrogen bond to the central silicon unit mono-, di-, tri and tetrafunctional silicon atoms can be distinguished (Figure 1. 12).

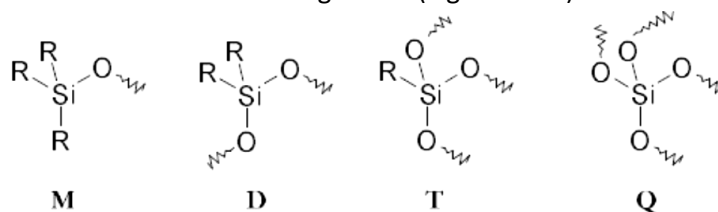


Figure 1. 12 Structures of siloxane Units

These groups of compounds are used for several industrial and medical applications. Siloxanes are versatile materials used in a wide range of applications including adhesion promoters, coupling agents, crosslinking agents, dispersing agents, and surface modifiers⁶³. Siloxanes can also be chosen to impart hydrophobic or oleophobic (oil and stain repellent) characteristics to surfaces. Siloxanes with alkyl groups (such as butyl and octyl) and aromatic groups (such as phenyl) and even some organofunctional groups (such as chloropropyl and methacrylate) are

⁶³ Witucki, G. L. A

hydrophobic. Similarly, silanes containing fluoroalkyl groups are oleophobic (oil repellent). Alkoxysilyl groups attached to these silanes allow them to actually penetrate, cure in and even bond to many inorganic substrates.

Alkyl siliconates, alkyl silanes, siloxanes, polysiloxanes and silicone resins are the ones of the most popular water repellent agents for impregnation protective treatments and in mass hydrophobization. These products belong to the family of alkyl silicones and are originated from the ethylsilicates developed by Ebelman around 1845. The German chemist Ladenburg synthesized the first silicone fluids by 1872, but it is only in 1912 that Stock was able to attach by Grignard reaction organic groups to silicon. In the

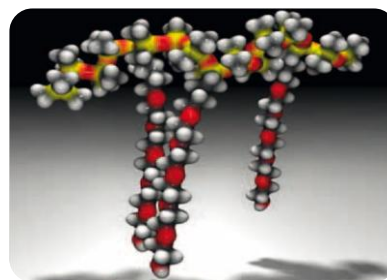


Figure 1. 13 Organo modified siloxane used as water repellent

'40es the Dow Corning Corporation started its production of silicones and ten years later this kind of water repellents were commercialized in Europe. In the '60es high molecular weight silicones were used dissolved in organic solvents, while in the 1970's oligomeric siloxanes in white sprits or alcohol were commercialized. More ecological and healthy formulations of water-based emulsion of silicones were developed at the end of the '80es (1998), cream formulations followed in 2000 for a better penetration depth in impregnation treatments. Around 2002 and 2005 products for dry-mix mortars system have been developed: silanes and modified siloxanes supported on inorganic carrier powders for in-bulk hydrophobization are nowadays available⁶⁴. Silanes and siloxanes perform their water- repellent action modifying the surface properties of the material on which they are applied. As Charola reported: "This surface modification serves also to reduce soiling and decay from environmental influences and biocolonization"⁶⁵.

Impregnation treatments

In protective treatments obtained by impregnation of stone substrates with siloxanes, the products are applied on the stone surface and penetrate through capillary suction inside the porous matrix. Thanks to basic catalysis the siloxanes are easily hydrolyzed. Then, while the solvent evaporates, condensation reactions between hydrolyzed silanes molecules and the -OH present on stone surfaces take place. A complete description of the reaction can be found in⁶⁶ Arkles, B. 1977. A schema of the reaction is shown in Figure 1.

Impregnation treatments of a porous substrate have to take in account different aspects such as the influence of the formulation, the influence of the alkyl group, the influence of the substrate, the application techniques, the durability of the water-repellence, and the influence of second treatments.

The formulation, the alkyl group, the substrate and the application techniques can influenced the penetration depth, which is a crucial parameter in determining the success of a protective treatment. The final water-repellent effect will depends on the penetration depth reached and on the alkyl substituents attached to the silicon backbone. Long alkyl side-chains assure a better water-repellent effect but commonly short alkyl side-chains are used, because more stable to further reactions, the longer chains used are n-octyl or iso-butyl groups.

⁶⁴ Roos, M., et. al. 2008

⁶⁵ E.Wendler, A.E: Charola, 2008

⁶⁶ Arkles, B. 1977

The nature of the stone determines the number of sites available for the polymerization of the silane on the surfaces but also eventually further chemical interactions, while the porosity regulates the capillary suction of the liquid silane inside the matrix and therefore the penetration depth.

The durability of the water-repellency is affected from the deposition of hydrophilic substances on the surface, from the physical-chemical degradation of the water repellent on the surface, but also from the formation of cracks and scaling. Furthermore, the impregnated area might acquire properties different in comparison to the non-impregnated parts, (such as higher mechanical resistance or lower permeability). These effects should be avoided.

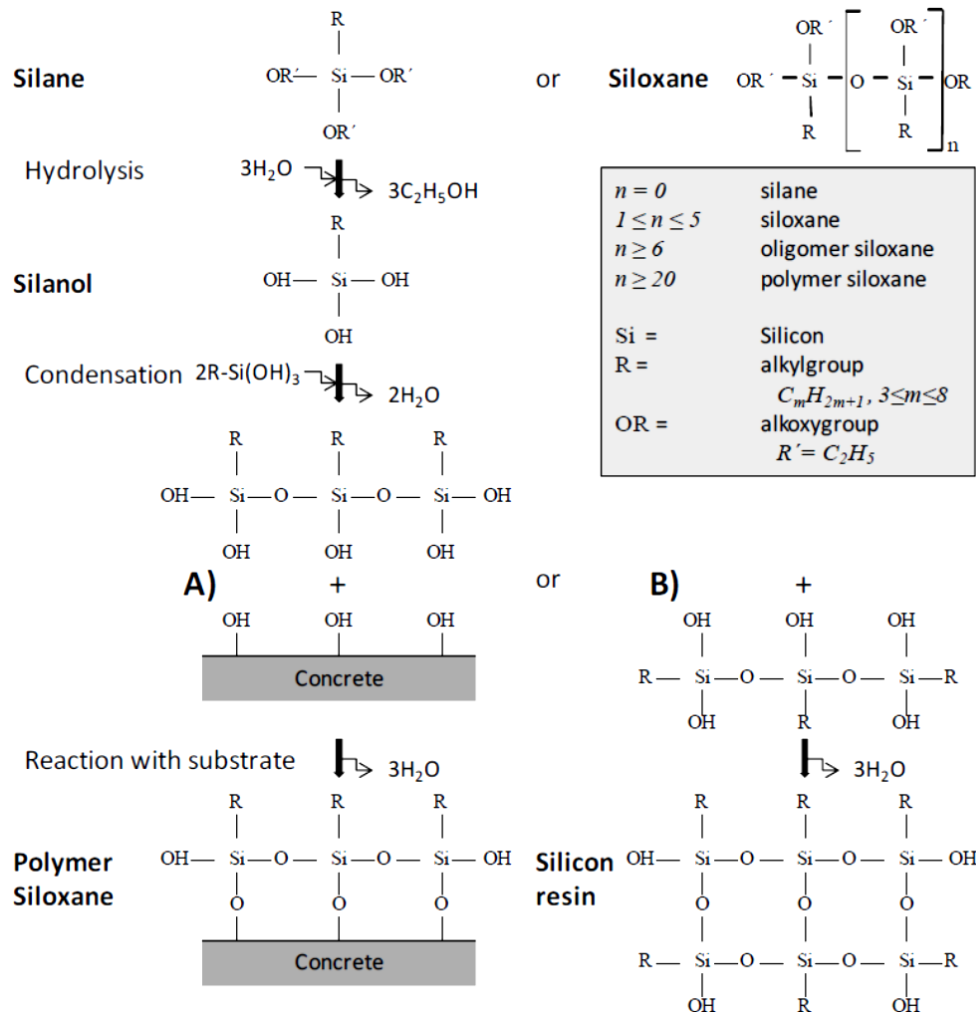


Figure 1 reaction of an organofunctional triethoxysilane with the concrete matrix, based on Arkles, B. 1977. Ethanol is liberated during the hydrolysis. A) and B) represent two different possibilities: a fine network of polymer siloxane on the pore walls (A) or a silicon resin (B) are formed.

Integral water-repellency

The addition of water repellent additives inside the formulation of mortars can help in overcoming the aforementioned problems regarding the penetration depth and the homogeneity of the resulting material. This solution is possible only with the production and application of new mortar mixtures but has remarkable advantages, such as the possibility of maintain water-repellence properties also in presence of cracks or scaling and to design mortar mixtures with the desired mechanical and permeability properties.

The availability of powder products containing water-repellent siloxanes, allowed also dry-mix formulations for modern and efficient construction works.

Alkylsiloxanes with hydrophobic side-chains are supported on inorganic carriers such as calcium carbonate or amorphous silica powders.

The use of this products or of emulsion silanes as admixtures of the mortars lead to integral water-repellent mortars. Interesting reduction of capillary water absorption was measured both on cement and lime mortars, and also on special mixing such as strain hardening cement-based composites⁶⁷.

The penetration of water inside these mortars has been studied with normal water absorption tests, evaluating the contact angles, and with neutron radiography also for cracked mortars. With the last technique was observed that the water is not normally able to penetrate in the substrate, but if the experiment is conducted in high relative humidity conditions water vapour can penetrate in the substrate and condense in the smaller capillary pores or wherever a non-hydrophobized surface is found. Therefore a good dispersion of the additives and the right dosage are necessary requirements in order to obtain a complete protection.

H-NMR and ²⁹Si-NMR analysis were conducted on some alkylsiloxane dispersed in calcium hydroxide solution to obtain information about the interaction and the possible chemical bonds that can occurs in mortars systems. The hydrolysis and then the condensation of the silanes with themselves and with the calcium hydroxide was observed. Also in presence of cement binders similar reactions occur. Therefore, the basic environment of the mortars can lead to the hydrolysis and preferential condensation of the silanoxanes with themselves, and to the formation of lumps of admixture inside the mixes, worsening the distribution.

1.4.4.3. Organic polymers

Different kind of organic polymers have been used for several years to treat and protect natural or artificial stone materials thanks to their water-repellent properties. Among the first products is possible to remember different natural waxes, oils, but also artificial microcrystalline waxes⁶⁸.

Also impregnation treatments of mortars with acrylic or vinyl polymers is well known and documented, even if not always these treatments led to satisfying results⁶⁹. These waxes and acrylic or vinyl polymers undergo degradation processes, which can affect their properties. The oxidative degradation of synthetic polymers is one of the major cause of the alteration of the mechanical (cracking), chemical (change of molecular weight), physical (reduction in adhesion, elasticity or wetting behaviour) properties.

The use of vinyl derivatives or acrylic resins also as mortar admixtures developed from the 1950es in order to obtain waterproof wall coatings of insulation with cement-polymer products⁷⁰. Polyvinyl acetates, acrylic resins and styrene-butadiene rubber are some of the most used admixtures⁷¹ in polymer-mortar products.

To overcome the problems due to the rigidity and the brittleness of aged polymer films or to enhance particular properties (such as water-repellence of the final mixtures), new copolymer product were developed. Among them copolymers of ethylene, vinyl laurate and vinyl chloride

⁶⁷ M. Lanzón, P.A. Garcia Ruiz, 2008; A. Izaguirre, J. Lanas 2009; P. Zhang, et al., 2010

⁶⁸ Amoroso, G., 1983

⁶⁹ Carretti, E., L. Dei, 2004; Milanese, C., et al., 2009; Cappitelli, F. 2007

⁷⁰ Wagner, H.B., 1965

⁷¹ Ramli, M., A. A. Tabassi, 2012; Brien, J. V., K.C. Mahboub, 2013; Van Gemert, D., et al., 2005

demonstrated good water-repellent properties thanks to the long organic chain of the vinyl-laurate, furthermore they showed improved adhesion, high flexural strength and deformability⁷². The formulation of these water-repellent copolymers can be also re-dispersible in order to be use in dry-mix formulation.

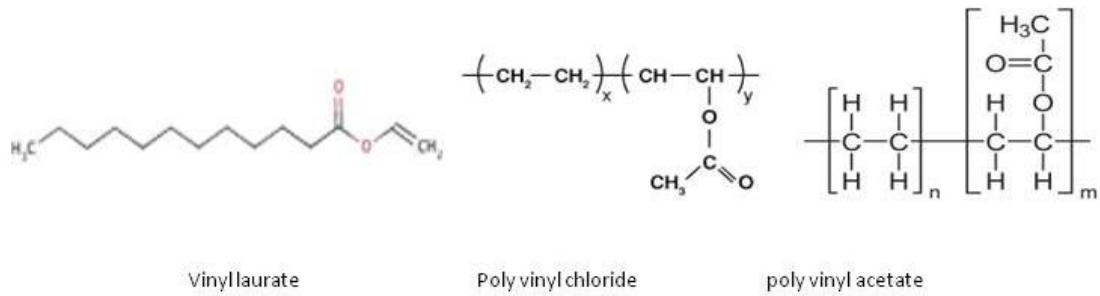


Figure 1. 14 chemical structure of vinyl laurate, poly vinyl chloride, poly vinyl acetate

⁷² VINNAPAS® 8031 H - Wacker Chemie AG

2. Research strategy

The methodology adopted in this thesis involved subsequent studies of different water-repellent mortar mixtures, involving a micro-to-macro approach.

The research strategy was developed in order to deal with the four principal topics described above in Chapter 1. Objective and innovations:

- the study of the hydration reactions and the microstructure of different hydraulic binders in presence of water-repellent admixtures;
- the study of the physical and chemical properties of several mortars with water-repellent admixtures.
- the study of the behaviour of the mixtures in different weathering condition, i.e. weathering under UV-Light and dousing with water, resistance to salt crystallization.
- the evaluation of water-repellent mortar mixtures applied on salty masonry.

For each topic different analytical techniques were used to obtain a deep knowledge of the involved phenomena.

Binder pastes of limestone cement, natural hydraulic lime or pozzolana-lime were prepared with and without water-repellent admixtures, sampled at different hydration time and analyzed with XRD, SEM-EDX, TG-DSC, FT-IR spectroscopy methods. The knowledge of the composition of the samples at different time allowed to describe the reaction mechanism and the influence of water-repellent admixtures on it.

Laboratory mortars specimens (standard 4X4X16 cm prisms or 4X4X4 cm cubes) with limestone cement, natural hydraulic lime or pozzolana-lime as binders were produced adding different water-repellents. Normalized test and analytical techniques were involved to understand the macro- and micro-structure of the specimens, the mechanical properties, the hygric properties and the behaviour in presence of water . The use of standard specimens and norms allowed easily comparison with existing data.

The specimens underwent two different kind of artificial weathering in laboratory condition, which allowed to test the resistance to UV-Light, rain and resistance to salt crystallization and gave indicative information/idea on the possible behaviour of the mortars applied in real outdoors environments. Evaluation of the damage of the mortars was assessed by visual control, measurements of physical properties such as mass loss, mechanical strength, microstructure, evaluation of the chemical composition with FT-IR spectroscopy , SEM-EDX or XRD analysis.

Being the water-repellent mortars designed for the protection of wall and historic masonry to the damaging action of water, and considering a possible application on historical buildings in the Venice area, some of the mortar mixtures were applied on models of salty masonry.

The mortar mixtures demonstrating better behaviour during the previously done were applied on mock up-walls made of traditional bricks. The walls was exposed to capillary absorption of aqueous solution of sodium sulphates for several weeks. The behaviour and effectiveness of the water-repellent mortar mixtures was assessed by visual observation, determination of the water uptake, study of the microstructure and of the composition by FT-IR and TG-DSC

measurements, study of the circulation of the water inside the structure also with infrared thermography (thermal imaging).

In Figure 2. 1 a graphical scheme of the methodology applied in this work is given.

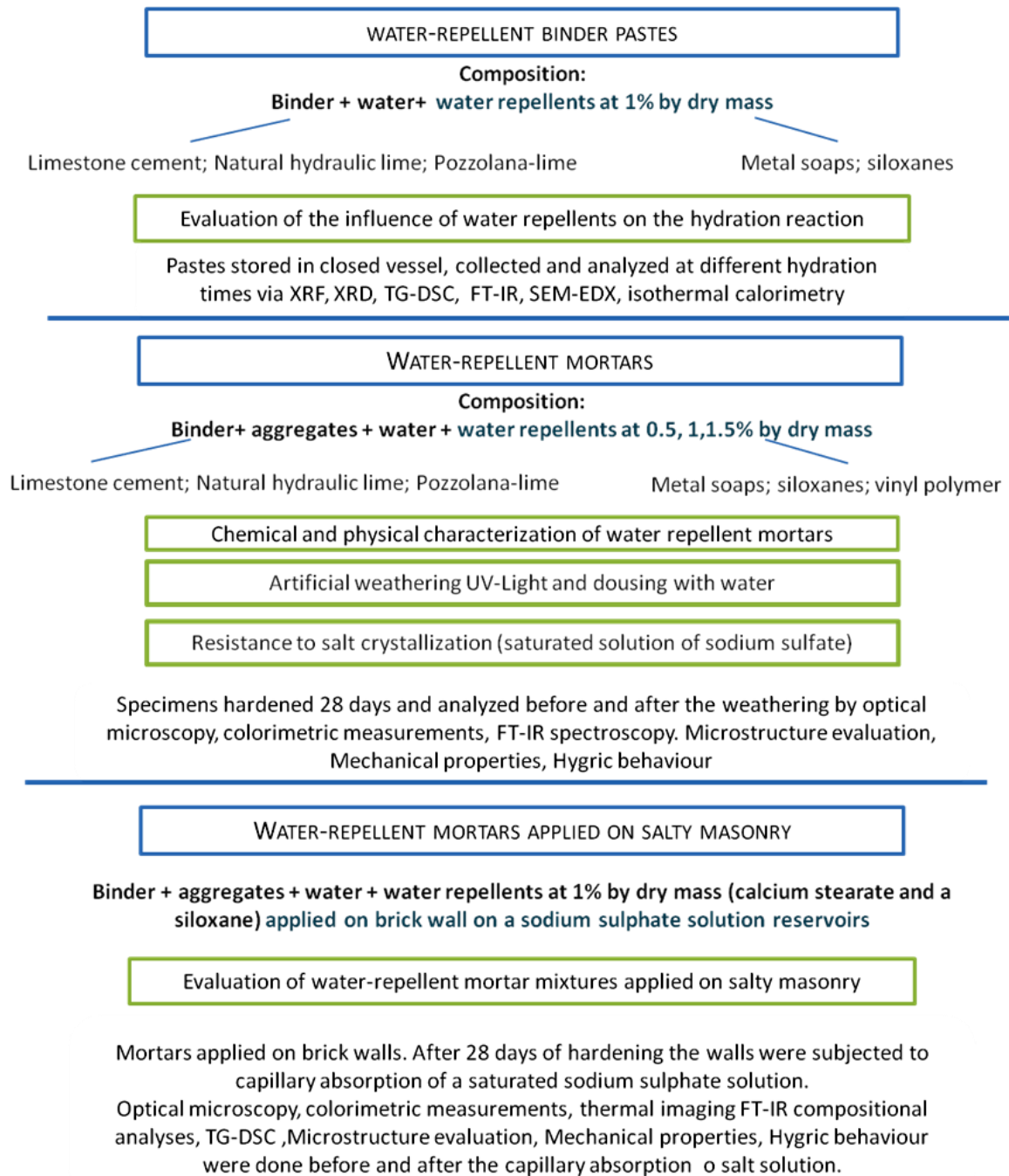


Figure 2. 1 Scheme summarizing the research strategy

2.1. Starting materials

2.1.1. BINDER SYSTEMS

Three different hydraulic binders were chosen in this study to design suitable mortars for restoration application:

1. limestone cement CEM II/B-L 32,5 R supplied by CementiRossi® (Pederobba, Italy) was used for the production of cement specimens;
2. natural hydraulic lime “Calce dei Berici” NHL3.5 (conform to the norm EN 459-1: 2002) supplied by Villaga SpA (Cerano di Dolcé Verona, Italy), produced with local marl heated to 1100°C in traditional lime kilns;
3. hydraulic lime based on a mix of 1:1 by mass of industrial lime hydrate supplied by BASF® (main component $\text{Ca}(\text{OH})_2$, traces: calcite) and the pozzolana of volcanic origin from Greece S&B μ -silica®, a buff colored volcanic ultrafine siliceous material with high glass content supplied by S&B Industrial Minerals.

2.1.2. AGGREGATES

With the limestone cement, the natural hydraulic lime and the pozzolana-lime binders different kinds of sands mix were used. Respectively:

1. carbonate-siliceous sand in Fuller granulometric size distribution with a size fraction of 0/ 1.5) was used for the production of cement specimens.
2. Carbonate-siliceous sand in Fuller granulometric size distribution with a size fraction of 0/ 1.2) was used for the production of cement specimens
3. Siliceous sand (conform to the norm EN 196-1) with a size fraction of 0/2.

2.1.3. WATER-REPELLENT ADMIXTURES

Different commercial water-repellent admixtures were used to prepare water-repellent hydraulic mortars. The additives were chosen among the classes of water-repellents: silane/siloxanes, metal soaps and organic polymer.

The additives chosen are:

1. Sitren P750 - EVONIK, triethoxysiloxane supported on amorphous silica powder;
2. Sitren P730- EVONIK, triethoxyoctylsiloxane supported on calcium carbonate powder;
3. Silres A - Wacker Chemie, siloxanes supported on silica powder;
4. Tegosivin HE 328 - EVONIK, organosiloxane/water microemulsion;
5. Calcium Stearate 82% pure- Sigma Aldrich, mixture of calcium stearates-palmitates and other fatty acids;
6. Zinc Stearates pure-Sigma Aldrich, mixture of zinc stearates-palmitates other fatty acids;
7. Socal U1S1-Solvay, ultrafine coated PCC (calcium carbonate particle), nanoparticles 40-130 nm of calcium carbonate covered by calcium stearate.
8. Vinnapas® 8031 H (Wacker) redispersible powder based on a terpolymer of ethylene, vinyl laurate and vinylchloride

The starting materials were characterized as pure materials analyzing them with X-ray fluorescence, X-ray diffraction, FT-IR spectroscopy, BET adsorption, Helium pycnometer. The instruments and the methodology used for the analyses will be further discussed in the next paragraphs. Further technical information and the technical datasheets of the starting materials are reported in Appendix I.

Artificial ageing of the water-repellent admixtures were performed In order to evaluate the stability of the pure water-repellents in different environmental conditions. In particular, were tested:

- the behaviour of the water-repellents in contact with water. The water repellents were put in vials with deionised water for one month and the solution was sampled at 30 minutes, 24 hours, 7 and 28 days, dried in oven at 40°C till constant mass and analysed through FT-IR spectrometry.
- The behaviour of water-repellents in alkaline environment similar to the one present in the mortars. The water repellents were mixed with a saturated solution of calcium hydroxide (pH~12), kept in closed vessel for 150 days and the solution was sampled at 30 minutes, 24 hours, 7, 14, 28, 90 and 150 days, dried in oven at 40°C and analysed through FT-IR spectrometry.
- The resistance to accelerated ageing. The water repellents were put in oven at 55±5°C for one year and analysed by FT-IR spectroscopy.

2.2. Casting procedure and exposure condition

2.2.1. WATER-REPELLENT BINDER PASTES

Binder pastes were prepared by mixing the chosen binders with water-repellent admixtures and water.

The water-repellent admixtures were added at 1% by mass of the binder and the dry powder were mixed with a stirrer for 5 minutes at low speed (145±10 rpm). The dosage of the water-repellent admixtures was chosen considering previous literature data and the necessity of having enough admixtures to observe possible effects¹. One paste for each binder was prepared without admixtures and was used as reference.

Water was added and the resulting mixture was stirred for three minutes at 285±10 rpm. The water to binder ratio (w/b) chosen was equal to the w/b used for mortars of standard consistence made with the same binder².

The mixtures were stored in closed PET vessels at 23°C and samples were collected at different hydration times (0, 2, 4 hours; 1, 2, 7, 14, 21, 28, 42, 56, 84, 140 days) and dried in a vacuum

¹Lanzon M, Garcia-Ruiz PA. 2009; Izaguirre, A., J., *et al.*, 2010; Zhang, P., FH. Wittmann, Tj Zhao ,2010

² The consistence of fresh mortars evaluated by flow table (EN 1015-3) was determined on standard mixtures made with the different binders, aggregates, water, but without water repellent admixtures. The w/b ratio was chosen in order to obtain a slump diameter of the mortars around 17±1 cm. The same w/b ratio was then used for the preparation of the binder pastes.

oven at 40°C and 40 mbar for 7 hours to stop the hydration processes. The samples were then stored under nitrogen atmosphere to avoid carbonation.

Table 2. 1 summarizes the names and the composition of the prepared binder pastes.

Table 2. 1 Composition and names of the prepared binder pastes. links to right: pastes made with limestone cement (CM), pastes made with natural hydraulic lime (NHL), pastes made with pozzolana+lime (HL)

Limestone cement Binder: CEMIIB-L 32.5			Natural hydraulic lime Binder: NHL3.5			Hydraulic lime Binder: pozzolan+lime		
Paste label	Water-repellent	w/b ratio	Paste label	Water-repellent	w/b ratio	Paste label	Water-repellent	w/b ratio
CPA	-	0.9	NHLA	-	0.7	HLP A	-	1.3
CP750	Sitren p750	0.9	NHL750	Sitren p750	0.7	HLP750	Sitren p750	1.3
CP730	Sitren p730	0.9	NHL730	Sitren p730	0.7	HLP730	Sitren p730	1.3
CPsil	SilresA	0.9	NHLsil	SilresA	0.7	HLPsil	SilresA	1.3
CPtes	Tegosivin HM	0.8	NHLcast	Ca Stearate	0.7	HLPtes	Tegosivin HM	1.3
CPcast	Ca Stearate	0.9	NHLznst	Zn stearate	0.7	HLPcast	Ca Stearate	1.3
CPznst	Zn stearate	0.9						

2.2.2. WATER-REPELLENT MORTARS

Water-repellent mortars were prepared mixing the binders with the correspondent aggregates in 1:3 ratio by volume, with the water-repellent admixtures chosen and with water. The water repellent admixtures were added at 0.5, 1, 1.5% of the total dry mortar's weight in order to evaluate the influence of different dosages. Reference mixtures without water repellent were also made.

Sample preparation (mixing, demoulding and curing) were done according to the European standard EN 196-1. In a first step, the binders, the aggregates and the water repellent admixtures were mixed as dry powder in a planetary mixer at low speed (145±10 rpm). In a second step, water was poured on the dry components and the obtained mixture was worked for 3 minutes (285±10 rpm). The w/b ratio was calculated in order to obtain a mortar slump of 170±10 mm measured by flow table test, according to the method EN 1015-3. Finally, the obtained mixture was poured in disposable container for obtaining prisms (40x40x160 mm). The obtained samples were stored at RH= 90% and T= 20±2 °C. Different hardening times were chosen for the different binders because the hydrations and the hardening depends on their composition (e.g. pozzolana-lime mortars needed longer hardening times). The limestone cement mortars were stored for 28 days, the natural hydraulic lime mortars for 60 days and the pozzolana-lime mortars for three months. After then some of the specimens were cut in order to obtain cubes (4X4X4 cm) or slices (2X4X4 cm). Table 2. 2 summarizes the different mixtures prepared and their names.

Table 2. 2 mix design of the water-repellent mortars mixtures, Limestone cement mortars (CM), natural hydraulic lime mortars (NM) and pozzolana-lime mortars (PM) were prepared. The table continues in the following page.

Mix label	Binder			Water repellent admixtures	
	Binder type	Binder/aggregate (by volume)	Water/binder	name	% by mass
CMA	CEMII/B-L	1:3	0.96	-	-
CM7500.5	CEMII/B-L	1:3	0.96	Sitren p750	0.5
CM7501	CEMII/B-L	1:3	0.96		1
CM7501.5	CEMII/B-L	1:3	0.96		1.5
CM7300.5	CEMII/B-L	1:3	0.96		0.5
CM7301	CEMII/B-L	1:3	0.96	Sitren p730	1
CM7301.5	CEMII/B-L	1:3	0.96		1.5
CMSil0.5	CEMII/B-L	1:3	0.96		Silres A
CMSil1	CEMII/B-L	1:3	0.96	1	
CMSil1.5	CEMII/B-L	1:3	0.96	1.5	
CMtes1	CEMII/B-L	1:3	0.96	Tegosivin HE	1
CMtes5	CEMII/B-L	1:3	0.96		5
CMcast0.5	CEMII/B-L	1:3	0.96	Ca Stearate	0.5
CMcast1	CEMII/B-L	1:3	0.96		1
CMcast1.5	CEMII/B-L	1:3	0.96		1.5
CMznst0.5	CEMII/B-L	1:3	0.96	Zn stearate	0.5
CMznst1	CEMII/B-L	1:3	0.96		1
CMznst1.5	CEMII/B-L	1:3	0.96		1.5
CMvin0.5	CEMII/B-L	1:3	0.96	Vinnapas 8031 H	0.5
CMvin1	CEMII/B-L	1:3	0.96		1
CMvin1.5	CEMII/B-L	1:3	0.96		1.5
NMA	NHL3,5	1:3	0.50	-	-
NM7500.5	NHL3,5	1:3	0.50	Sitren p750	0.5
NM7501	NHL3,5	1:3	0.50		1
NM7300.5	NHL3,5	1:3	0.50	Sitren p730	0.5
NM7301	NHL3,5	1:3	0.50		1
NMSil0.5	NHL3,5	1:3	0.50	Silres A	0.5
NMSil1	NHL3,5	1:3	0.50		1
NMcast0.5	NHL3,5	1:3	0.50	Ca Stearate	0.5
NMcast1	NHL3,5	1:3	0.50		1
NMznst0.5	NHL3,5	1:3	0.50	Zn stearate	0.5
NMznst1	NHL3,5	1:3	0.50		1
NMsoc0.5	NHL3,5	1:3	0.50	Socal	0.5
NMsoc1	NHL3,5	1:3	0.50		1
PMA	Lime+pozzolan	1:3	1.25	-	-
PM7501	Lime+pozzolan	1:3	1.29	Sitren p750	1
PM7301	Lime+pozzolan	1:3	1.29	Sitren p730	1
PMsil0.5	Lime+pozzolan	1:3	1.30	Silres A	0.5
PMsil1	Lime+pozzolan	1:3	1.19		1
PMsil1.5	Lime+pozzolan	1:3	1.24		1.5
PMtes1	Lime+pozzolan	1:3	1.14	Tegosivin HE	1
PMcast0.5	Lime+pozzolan	1:3	1.29	Ca Stearate	0.5
PMcast1	Lime+pozzolan	1:3	1.29		1
PMcast1.5	Lime+pozzolan	1:3	1.28		1.5
PMznst0.5	Lime+pozzolan	1:3	1.29	Zn stearate	0.5
PMznst1	Lime+pozzolan	1:3	1.29		1
PMznst1.5	Lime+pozzolan	1:3	1.30		1.5

2.1.1. EXPOSURE/WEATHERING CONDITION OF WATER- REPELLENT MORTARS

Water-repellent mortar specimens were exposed to two different artificial weathering conditions in order to evaluate their durability in different environmental conditions.

2.1.1.1. Artificial ageing conditions

Ageing tests were performed to simulate the processes caused by sunlight and water. The literature abounds of examples of different kinds of artificial ageing, and different assessment of the ageing tests would have been possible³. In order to standardize the method and lacking a specific norm, the indications of the EN 13687 standard "Products and systems for the protection and repair of concrete structures- Test Methods- determination of thermal compatibility- Part2 Thunder-shower cycling (thermal shock)" were followed. The ageing test described by the normative prescribes the succession of heating and raining cycles b (storage under radiant heat at 60 ± 5 °C for 5 hours and 45 minutes, dousing with water at 12 ± 3 °C for 15 minutes).

The ageing test was performed on 4X4X4 cm mortar specimens prepared. Four sides of each specimen were covered with epoxy resins, while the upper surface and the correspondent back side were not covered to allowed a free circulation of water vapor. Three specimens for each mix were put in a Global UV test GUT 200 (WEISS Technik) chamber and six hours cycles were performed alternating:

- 5 hours and 45 minutes → continuous irradiation of the samples with UV light in the range of 290nm-400nm and power E_e of 41 W/m^2 .
- 15 minutes → dousing with water at 15 °C, conductance $< 25 \mu\text{s/cm}$, dosing rate $40 \text{ Lmin}^{-1} \text{ m}^{-2}$ (correspondent to $\sim 960 \text{ ml}$ of water/sample every cycle considering a sample with 16 cm^2 of exposed surface).

Scans and photos of the specimens were done before, during and after the test visual observation. The contact angle and the capillary water absorption was measured before and after the test. Furthermore, observations with optical microscope, colour measurements and FT-IR analyses of the surfaces were performed.

2.1.1.2. Resistance to salt crystallization

The resistance to salt crystallization was evaluated according to EN 12370. The specimens were immersed in a saturated salt solution of sodium sulphate decahydrate for immersion cycles of two hours, followed by drying at 40 °C for 22 hours in the oven. The mass losses was measured after each cycle and visual observation were performed.

After the test macro- and micro- observations (also by SEM-EDX microscopy), colour measurements, FT-IR analyses and some XRD measurements were performed.

To evaluate the depth reached by the salts, after the test the degraded specimens were cut and samples collected every 0.5 cm from the outer layer to the inside of the specimen. The evaluation of the soluble salt content in each of these samples was considered measuring the conductivity of as described in the Normal 13/83.

³ Izaguirre A., J. Lanás, J. Álvarez 2010; M.A. Kargol, et al., 2011

The specimens were finally desalinated in deionised water to extract the salts, the water was replaced every day and the desalination process continued till the ionic conductivity of the water returned similar to the ionic conductivity of water in contact with not-weathered specimens.

Capillarity water absorption and compressive strength measurements were repeated on the degraded specimens after salt extraction/desalination in deionised water.

Microstructure investigation were performed on some mortar mixtures with mercury intrusion porosimeter MIP before the salt cycles, after the salt cycles and after the desalination of the samples.

2.1.2. WATER-REPELLENT MORTARS ON SALTY MASONRY

Water-repellent mortars were applied on models brick walls in laboratory condition to study the behaviour of the mortars applied on masonry and to evaluate the suitability of the mortar mixtures as repairing mortars for restoration of historical buildings. In particular the experimental conditions tried to simulate the difficult situation of most of the historical masonry of Venice⁴.

Two walls (50X75X25 cm) made of solid bricks and hold together by a lime-cement hydraulic grout were casted over a plastic reservoir (65X 35 X10 cm). The walls were covered by a first layer of rendering mortar (*rinzaffo*) made with the same composition of the grout (lime-cement mortar) in order to homogenize the surface on both sides of the walls. The walls were casted in advance and the reservoir was filled with saturated salt solutions of mixed sodium chloride and sodium sulphate for one year and then dried. Both the use of solid bricks and of the salt solutions was chosen in order to simulate rising damp phenomena similar to the ones present in the historical masonry of Venice.

A complete characterization of the rendering mortar layer was done before apply new layers. The determination of the rendering microstructure with MIP analysis and of the composition with FT-IR spectroscopy, TG-DSC analyses was done, together with the determination of the hardness with a Schmidt Hammer sclerometer⁵.

Some selected water-repellent mortar mixtures were applied as plasters (*intonachino*) on the render mortar on both sides of the walls. The mortar mixtures selected are listed in Table 2. 3

The mixtures were prepared as described above for the laboratory specimens, and then applied with a unique thick layer (1 cm) on the surfaces of the walls.

The walls were covered by plastic towels and maintained at a relative humidity of $80\pm 5\%$ HR and 20 ± 2 °C for 28 days.

The reservoirs were then filled with fresh saturated solution of sodium sulphates.

⁴ See also Chapter 1

⁵ See paragraph 2.2.12 Mechanical properties of the mortars pag. 13

Table 2. 3 mix design of water-repellent mortars mixtures applied on brick walls. Limestone cement mortars (WCM), natural hydraulic lime mortars (WNM) and pozzolana-lime mortars (WPM) were applied on brick walls.

Mix label	Binder			Water repellent admixtures	
	Binder type	Binder: aggregate (by volume)	Water/binder	name	% by mass
WCMA	CEMII/B-L	1:3	0.96	-	-
WCM7501	CEMII/B-L	1:3	0.96	Sitren p750	1
WCMcast1	CEMII/B-L	1:3	0.96	Calcium stearate	1
WNMA	NHL3,5	1:3	0.50	-	1
WNM7501	NHL3,5	1:3	0.50	Sitren p750	1
WNMcast1	NHL3,5	1:3	0.50	Calcium stearate	1
WPMA	Lime+ pozzolan	1:3	1.25	-	1
WPM7501	Lime+ pozzolan	1:3	1.29	Sitren p750	1
WPMcast1	Lime+ pozzolan	1:3	1.29	Calcium stearate	1

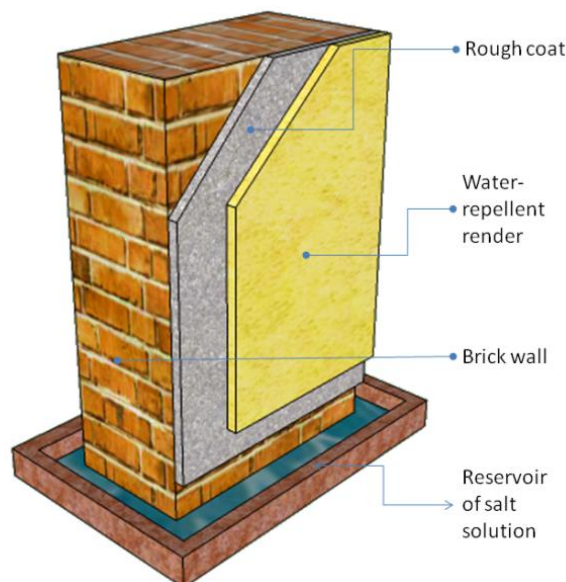


Figure 2. 2 Model of the salty wall (© L. Falchi 2013)

The behaviour of water repellent mortars applied on the walls was investigated using different techniques and methods *before, during and after* having filled the reservoirs with salt solutions. Samples collected from the hardened plaster layers were characterized by MIP analyses, FT-IR spectroscopy, TG-DSC analysis, ionic conductivity applied as described in the following paragraphs.

On the plaster were measured the hardness (by Schmidt Hammer sclerometer), the capillary water absorption (water absorption tube test ⁶), the colour, the visual appearance by macro and micro observations. Furthermore, the walls were monitored during the salt solution absorption by thermal imaging.

All these mentioned analyses and methods will be better described in the following paragraphs.

⁶ RILEM Test Method II.4

2.2. Investigations techniques

Several analytical techniques were employed to evaluate the hydraulic properties of the mortars and to characterize them. Moreover, different material testing were carried out following the norms of several European standards.

2.2.1. X-RAY FLUORESCENCE ANALYSIS

XRF analysis allowed to obtain qualitative and semi-quantitative information about the elemental composition of the samples. With this techniques the atoms with low atomic number could not be detected, and no speciation of the atoms is possible, but anyway the elemental information is useful to better understand other analysis such as XRD or FT-IR analysis.

The XRF analysis were carried out with a EDAX EAGLE III instruments, with an X-ray tube at 40W (Rh), 80mm² nitrogen cooled Lithium drifted Silicon crystal detector. EDAX Data Acquisition Module via PCI interface was used to get and elaborate the data.

2.2.2. X-RAY DIFFRACTION

X-ray powder diffraction was employed in order to recognize and define major and minor crystalline phases. Qualitative powder analysis was performed on dried and grinded samples with a Rigaku Ultima IV X-ray diffractometer, a 40KV and 40 mA Cu X-ray tube was used. The measurements ranged from 3°-63° 2θ with a 0,02° 2θ step size. The software PDXL was used for the data interpretation (BAM Institute-Berlin⁷). Some of the samples were analyzes with a Philips PW1050 diffractometer, a generator Philips PW1830, with a 40KV and 30mA Cu X-ray tube (Ca Foscari University- Venice⁸).

2.2.3. DIFFERENTIAL SCANNING CALORIMETRY/ THERMOGRAVIMETRIC ANALYSIS

This technique gives qualitative and quantitative information about the compounds present and their thermal stability. The thermal decomposition and dehydration of different compounds can be detected and quantified.

The analyses were performed on dried and ground samples. The samples were measured with a Netzsch STA 409/C instrument equipped with a differential scanning calorimeter and a thermogravimetric system. A heating program of 10°C /min from 20°C to 1000°C in N₂ atmosphere was used. Sample masses were about 25 mg and were packed into Pt/Rh crucibles. All curves were evaluated using the NETSCH TA3.5 software and further processed using Origin Pro8.5 software.

2.2.4. FOURIER TRANSFORM INFRARED SPECTROSCOPY

Further chemical-compositional information about the chemical groups present in the pastes and mortars were provided by FT-IR techniques. FT-IR spectroscopy analyses were performed using different instrumental set-ups.

⁷ XRD analyses were performed in collaboration with Dr.Eng. Urs Müller who is kindly acknowledged

⁸ XRD analyses were performed in collaboration with Prof. Pietro Riello and Tiziano Finotto who is kindly acknowledged

The characterization of the starting materials, pastes and mortars were carried out using a Nicolet Nexus 670/870 spectrometer in the mid- infrared region ($4000-400\text{ cm}^{-1}$) on pellets made by pressing a mixture of ground sample with KBr powder (1:100-wt%). Spectra were collected at 4 cm^{-1} resolution (32 scans) and processed with the Omnic 6.0 software and Origin 8.5 software. Micro attenuated total reflection (ATR- FT-IR) analysis and ATR-FT-IR mapping profiles of some binder pastes were obtained with a Nicolet* iN MX 10 Infrared Microscope equipped with a nitrogen cooled MCT detector (CdSe crystal), in the mid-infrared regione ($4000-400\text{cm}^{-1}$) at 2 cm^{-1} resolution and a spatial resolution down to $3\mu\text{m}$. The spectra were processed with the Omnic Picta software.

A Perkin Elmer Spectrum One FT-IR ATR with diamond cell was used to measured the trasmittance in the $400-4000\text{ cm}^{-1}$ range, with 4 cm^{-1} resolution on the mortars surfaces after the artificial weathering tests.

2.2.5. OPTICAL MICROSCOPY (OM)

Light and UV-Light observation of the samples were carried out with an Olympus SZ X9 microscope or with the digital optical microscope Dino-Lite AM4113/AD4113.

2.2.6. SCANNING ELECTRON MICROSCOPY COUPLED WITH ENERGY DISPERSIVE X-RAY PROBE

The observation of the sample through SEM-EDX allowed to study the microstructure, the phase morphology and the elemental composition of the samples. Different crystals and structures can be recognized.

Cracked surfaces of the samples or smooted surfaces were metalized with carbon or with gold to work in high vacuum conditions (20KV accelerating voltage) and observed with:

-Quanta 200FEI (Philips), with a Tungsten cathode and a Si(Li) Brucker 133 eV EDX detector (BAM institute Germany).

-SEM-EDS JEOL JSM 5600 LV with a OXFORD-Link Isis series 300 microanalysis system (Ca Foscari University- Venice)⁹

2.2.7. ISOTHERMAL CALORIMETRY

The isothermal calorimetry was used to evaluate the reactivity of the pozzolanic components. The release of heating during the hydration process of the pastes is measured. A Tam Air isothermal calorimeter was used to analyze fresh paste samples with 1% by mass of water repellent at 23°C . Two different samples for each mix were measured.

2.2.8. BET ANALYSIS

The specific surface area of raw materials was evaluated via BET analysis with the instrument Micromeritics tristar II Surface area and Porosity¹⁰.

2.2.9. COLORIMETRIC MEASUREMENTS

A CM2600d Konika Minolta portable spectrophotometer with a D65 illuminant (representing day light, colour Temperature 6504°K . three pulsed xenon lamps) and 10° standard observer was used to measure the colour of mortar samples as described by the NorMal 43/93. Mortar

⁹ SEM-EDX analyses were performed with the technical assistance of Dr. Davide Cristofori who is kindly acknowledged

¹⁰ BET analysis were performed by Eng. Elgin Rother who is kindly acknowledged

surfaces were quite rough and with aggregates of different colours, therefore the measures should be average results collected on larger area in order to obtain reliable colour values, a medium averaged spot size of 11 mm \varnothing was then considered and the average of nine measurements was calculated for each specimens. Simultaneous data with specular component included (SCI) or excluded (SCE) were collected. The reflectance spectra were collected in the 360-740 nm range, UV numerical adjustment with a 400nm cut filter. The data were processed by the Spectra Magic NX software which calculated the hue coordinates a^* , b^* and the Lightness L^* of the samples in the CIEL*a*b* colour space¹¹. The total colour difference (ΔE^*) was calculated:

$$\Delta E^* = \sqrt{\Delta L^{*2} + \Delta a^{*2} + \Delta b^{*2}} \quad \text{Eq 2.1}$$

2.2.10. CONSISTENCE AND DENSITY OF THE FRESH MORTAR MIXTURES

The workability of the fresh mortars was evaluated determining their consistence by flow table (EN 1015-3). The slump diameter of the mortars should be around 17 cm to obtain a good consistence and workability of the mortar. The apparent density of fresh mortars was measured following the UNI EN 1015-6. The fresh mortar mixtures were poured on a calibrated bowl and weighted, the apparent density is calculated dividing the mass to the geometrical volume.

2.2.11. DENSITY, MICROSTRUCTURE (MIP) AND ULTRASONIC MEASUREMENTS (US)

The bulk density of the mortars was calculate on dried prismatic specimens considering the mass and the geometric volume of the systems, while the real density was evaluated with Helium picnometer on grinded samples (powder diameter <63 μm).

Porosimetric analysis with mercury intrusion porosimetry MIP allowed investigating deeply the microstructure of the different mixtures, evaluating the bulk density, the total open porosity and the pores size distribution. MIP analysis were performed as described in the Normal 4/80 on samples collected with scalpel, dried and then analyzed with Pascal 140 and Pascal 240 Thermo Nicolet instruments (pressurization with automatic speed-up continuous adjustment logic), able to measure pores till 3,7 nm. The relation between the pore size and the applied pressure, assuming the pore is cylindrical, is expressed by the Washburn equation (eq. 2.2):

$$(eq\ 2.2) \quad r = (2\gamma\cos\theta)/p$$

where r =pore radius, γ =mercury surface tension, θ =contact angle, p =absolute applied pressure.

The results are an average of three samples at least.

Ultrasonic techniques can be used to provide information regarding the microstructure of composite materials¹². The analysis allowed a non-destructive evaluation (NDE) of building materials and in real cases allowed obtaining the quality and the degradation state of building materials. The most commonly used technique in ultrasonic characterization of cementitious materials is the ultrasonic pulse velocity (UPV), followed by acoustic wave attenuation and backscattering noise characterization. Ultrasonic measurements of the mortar specimens were carried out with a Controls 58-E4800 UPV with standard piezoelectric sensor at 45 Hz (cylinder 5cm \varnothing X5cm h), pulse rate 2 s, resolution 0.1 μs , with direct configuration of the measurements (transmitter and receiver at the opposite sides of the specimens).

¹¹ UNI 8941:1987

¹² Molero-Armenta, M., et al. 2009

Cross measures of prismatic specimens (4X4X16 cm) were performed along the prisms axes as shown in Figure 2. 3.

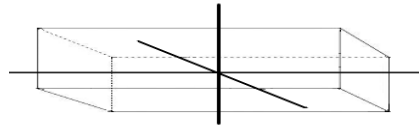


Figure 2. 3 scheme of the ultrasonic measurement directions (the sensor were put at each asses end)

2.2.12. MECHANICAL PROPERTIES OF THE MORTARS

The mechanical properties of the mortars specimens were evaluated with flexural and compression tests. Three specimens for each mix were tested following the 1015-11 1999, UNI EN 12390-3:2009 and UNI EN 12390-5:2009. A Zwick/Roell Z010 press was used with a pre-load of 10N and a loading rate of 5N/s for the flexural strength, and a pre-load of 20N and a loading rate of 50N/s for the compressive strength evaluation. The Testxpert II software was used to elaborate the data. The curves of load versus Strain were registered, the elastic modules was calculated with the tangential and the secant methods.

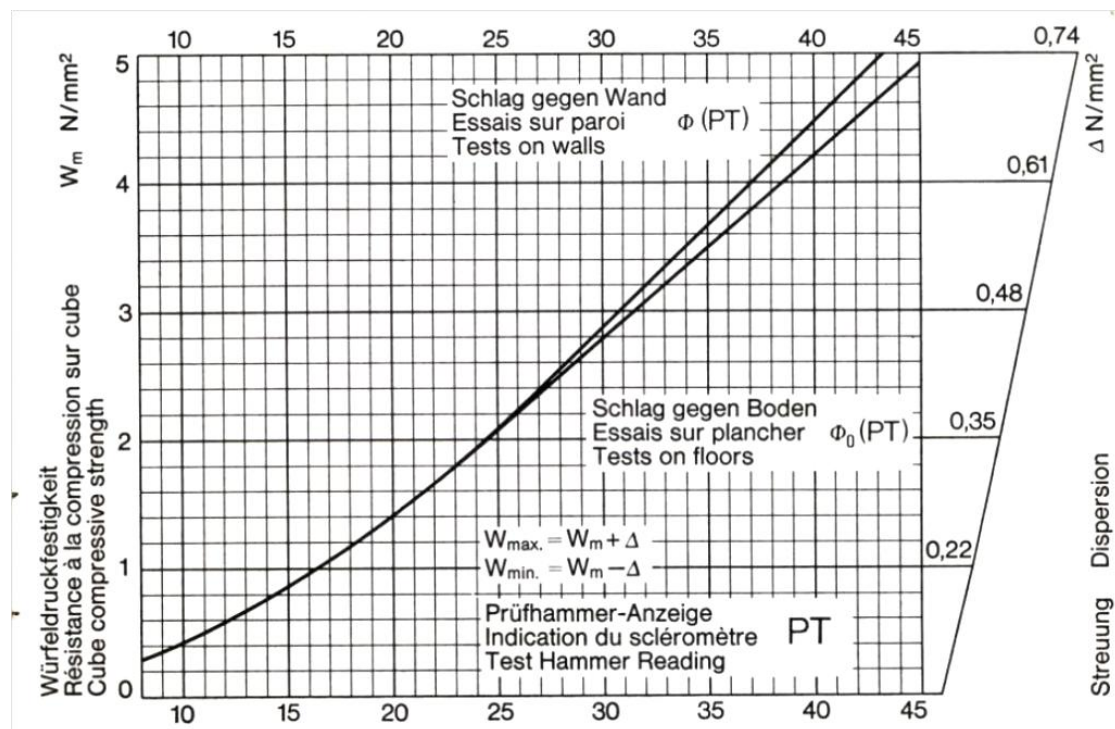


Figure 2. 4 Compression strength of cubic samples versus the hammer rebound of a PT sclerometer

The mechanical properties of the hardened mortars applied on walls was evaluated with a Schmidt Hammer PT sclerometer for soft materials (strength between 0.5 and 5 MPa, percussion energy: 0.88 J). The instrument allowed to determine the elastic properties and surface hardness of the mortars measuring the rebound of a ball for a particular force (0.88J) after impacting on the area under study. The rebound should be directly linked to the hardness of the surface and might be correlated with the compressive strength of concretes. Figure 2. 4 show a graph of the correlation between compressive strength and the Hammer rebound and was used to transofrme the data measured in mechanical strength expressed in N/mm². However when

measurements of composite structures are performed (such walls composed of different layers each one with a different hardness and compressive strength) the measurements might be more imprecise. For these reasons, in this study, both the hammer rebound found and the respective theoretical strength are considered. Nevertheless, this method allows also the identification of weak spots, which often correspond with underlying faults and was, therefore, a suitable method to evaluate also the damaging process due to rising damp and salt solution absorption on walls.

2.2.13. CAPILLARY WATER ABSORPTION

The normative EN 1015-18 1999 defines the method for the determination of the capillary water absorption on mortar specimens. The water absorbed by a porous material in contact with deionised water for surface and time unit and the calculation of the capillary water coefficient are therein described.

Prismatic dry specimens were measured in a climatic chamber at $(23 \pm 2)^\circ\text{C}$ with a scale accuracy of 1 mg. Both the absorption of the inner side and of the outer side of the specimens was measured, before and after weathering tests.

From the experimental data the water absorption is calculated:

$$(eq. 2.3) \quad Q_i = \frac{(m_i - m_0)}{A} \cdot 1000$$

in mg/cm²

with m_i = specimen mass (mg) at time t_i (vs); m_0 = mass of the dry specimen (mg); A = surface area of the wet side.

The capillary absorption coefficient, defined as the coefficient of the absorption curve in the first linear part, is calculated by linear interpolation of the experimental data. The average of three specimens was considered.

To evaluate the water absorption of the mortars applied on wall another testing method was used, described by the Norm 44/93 and by RILEM Test Method II.4 water absorption tube test. The equipment necessary for measuring water absorption under low pressure consists of a pipe-like apparatus designed for vertical surfaces. With a flat, circular brim (at the bottom end of the pipe) which can be fixed to the masonry surface by interposing a piece of putty. The water present in the apparatus when totally filled exerts a pressure around of 1170 pascals over the wall surface which corresponds to a dynamic wind pressure of 157.8 kilometers per hour (approximately 98.1 mph). The quantity of water absorbed by the material during a specified period of time is read directly from the graduated tube. The water absorption is calculated:

$$(eq. 2.4) \quad \frac{Q_{t_i} - Q_{t_{15}}}{S}$$

where Q_{t_i} = water adsorbed at time t_i (ml); $Q_{t_{15}}$ = water adsorbed after 5 minutes (ml); S = surface (cm²).

2.2.14. CONTACT ANGLE MEASUREMENTS

The water repellence of the mortar surfaces was verified also by contact angle measurements of water drops (Norm 33/89). A Data Phisic ETT/XL instrument was used to measure the contact angle, the water drop profile was extrapolated with ellipse fitting method, and the contact angle automatically defined by the software. For each surface at least 20 different

water drops were measured. This technique is strongly influenced by the surface roughness, therefore the outer and smoother sides of the mortar specimens were used.

2.2.15. WATER VAPOUR PERMEABILITY

The water vapour permeability was evaluated following the UNI EN 1015-19, DIN 52615 and DIN 52752. The measures were performed on 4X4X 2 cm specimens fixed and sealed with paraffin upon open vessels half-filled with sodium-carbonate saturated solution. The water vapour was transported by diffusion mechanism through the sample thanks to the water pressure gradient on the two sides of the sample. The sodium-carbonate saturated solution assures a partial water pressure of 93% inside the vessel, outside the pressure was 50% HR, everything was stabilized at 23°C. The closed system was weighted at different times and the mass loss allowed to calculate the evaporation rate. The water vapor permeance, the water vapour transmission and the water vapour resistance factor μ were calculated according to the norms UNI EN 1015-19, DIN 52615 and DIN 52752.

2.2.16. CONDUCTIVITY MEASUREMENTS

The evaluation of the soluble salt content in weathered and un-weathered mortars was evaluated measuring the ionic conductivity as described by the Normal 13/83. Ground and dried samples of mortars (95÷105 mg) were put in deionised water (100 ml) and the electrical conductivity of the measurements was measured with a Metrohm 644 conductometer.

2.2.17. MID IR INFRARED THERMOGRAPHY

Infrared Thermography is a non-invasive investigation methods already well known to engineers and architects which allowed to investigate and assess the condition of historic masonry in situ¹³. It is commonly used for the detection of building defects, such as thermal bridges, air leakage or moist spots, particularly in the context of energy conservation and might be particularly useful in detecting rising damp phenomena.

It measures thermal radiation emitted by the material and depicts the examined area as an image in colours corresponding to a predefined temperature scale.

The measurements were carried on using a Flir B400 Infrared Camera working in a spectral range of 7-13 μm , with an IR resolution of 320X240 pixels, thermal sensitivity of 0.05°C at +30° and a -20°C to +120°C temperature range with accuracy of $\pm 2\%$ of reading¹⁴.

¹³ Tavukçuoğlu, A., et al. 2005; E. Grinzato, et al. 2002; E. Grinzato, et al. 2000; Moropoulou, A., et al. 2013

¹⁴ The measurements were performed in collaboration with Prof. Piercarlo Romagnoni and Dr Massimiliano De Bei of IUAV university of Venice with their instrument. They are kindly acknowledged.

3. Results

As described in the Synopsis of the thesis (1.3 Synopsis of the thesis), this chapter regards the ponding and reports the analytical results and the measurement done. The discussion of the results and a summary of the main results are given in the following chapter (Chapter 4. Discussions, conclusions and perspectives).

In the present chapter, the results regarding the starting materials, the hydration of the binders with water-repellent admixtures, the properties of water-repellent mortars, the resistance of the mortars to artificial ageing, the resistance to the salt crystallization and the behaviour of water-repellent mortars applied on salty masonries are described in as many different sections.

Each section described in depth the results of each analytical techniques used for study the pastes or mortars made with different binders.

3.1. Analysis and Characteristics of the Starting Materials

This chapter describes the composition and some chemical-physical properties of the starting materials. The materials were analyzed through different analytical techniques such as XRF, XRD, TG-DSC, FT-IR spectrometry to characterize them. A complete description of the analysis performed on the binders, aggregates and water-repellent admixtures is given.

The last paragraph of this chapter (paragraph 3.1.6 Weathering of water repellent admixtures) reports the results regarding the behavior of the pure water-repellent admixtures in contact with water, or with calcium hydroxide saturated solutions, or exposed in oven at 40°C. The water-repellent admixtures resulted resistant to the different kind of weathering tested. The most interesting transformation was the ionic exchange of the zinc ions with calcium ions which occurred to the zinc stearates immersed in a saturated solution of calcium hydroxide.

3.1.1. LIMESTONE CEMENT

The anhydrous limestone cement CEM IIBL was characterized by XRD, FT-IR, TG-DSC and XRF techniques to determine its composition. The results are shown in Table 3.1 1.

XRD qualitative analysis allowed to detect the crystalline phases present. Hatrurite, a tricalcium silicate of general formula Ca_3SiO_5 ; larnite, a bicalcium silicate Ca_2SiO_4 ; calcite CaCO_3 ; gypsum $\text{CaSO}_4 \cdot 2\text{H}_2\text{O}$; and a slight presence of brownmillerite $\text{Ca}_2(\text{Al,Fe}^{3+})_2\text{O}_5$ (main peak at 12.15 2θ) were recognized from the XRD pattern. The XRF semiquantitative elemental analysis, showed high percentage of calcium due also to the presence of added calcite.

The FT-IR analysis of the anhydrous limestone cement confirmed the presence of a high content of calcium carbonate (the strong bands at 1428, 875 and 713 cm^{-1}), together with silicates (1100-900 cm^{-1}). It is also possible to observe small peaks due to the $-\text{OH}$ stretching in the 3700-

3000 cm^{-1} region related to a slight presence of gypsum and calcium hydroxide in the anhydrous cement. The presence of gypsum, calcium hydroxide and calcium carbonate were confirmed also by TG-DSC analysis. A first mass loss around 100-200°C was linked to the dehydration of coordination water, and also to the loss of water from gypsum. In the 400-500°C range the dehydration of calcium hydroxide and in the 650-750°C range the decarbonation of calcium carbonates occurred and it was possible to calculate the presence of a 1% of calcium hydroxide and a 23% of calcium carbonate in the sample.

3.1.2. NATURAL HYDRAULIC LIME

In the XRD pattern of the natural hydraulic lime (Table 3.1 2) a high presence of calcium hydroxide in the mineral form of portlandite was found, together with calcium carbonate as calcite. Quartz and calcium silicates (both tri and di calcium silicates) were also detected. The XRF analysis confirmed the presence of silicon, calcium and aluminium.

In the FT-IR spectrum (Table 3.1 2) the peaks relative to calcium carbonate and calcium hydroxide were found at 2971-2868, 1425, 875, 713 cm^{-1} and 3643 cm^{-1} , respectively. The peaks of asymmetric and symmetric stretching of O-Si-O bonds at 1095-912 cm^{-1} and the bending Si-O at 796 cm^{-1} were related to the presence of silicates. The TG/DSC curves collected for the natural hydraulic lime are shown in Table 3.1 2, the TG curve shows two major mass losses due to the dehydration of a 12% of calcium hydroxide and the decarbonation of a 32.10% of calcium carbonate.

3.1.3. POZZOLANA-LIME

The binder of a hydraulic lime is composed, usually, of an aerial lime and a silicate component. For the formulation of the pozzolanic mortars the following material were selected as binder:

- Calcium Hydroxide from BASF, main component $\text{Ca}(\text{OH})_2$, traces: calcite
- Greek Pozzolana S&B μ -silica[®] a volcanic ultrafine powder composed mainly of aluminium-silicates.

The results of the XRF, XRD, FT-IR, TG-DSC analysis are reported in Table 3.1 3.

The XRF analysis of the calcium hydroxide showed high percentage of calcium, low amounts of sodium, silicon and magnesium. The XRD analyses led us to recognize the presence of pure portlandite ($\text{Ca}(\text{OH})_2$) and a really little percentage of calcite (CaCO_3) due to a slight carbonation of the portlandite. The sharp FT-IR peak at 3643 cm^{-1} , related to the -OH stretching, is typical of calcium hydroxide, while the lower peaks at 1473 cm^{-1} and 874 cm^{-1} were due to a partial carbonation. The TG-DSC analysis of calcium hydroxide showed a unique mass loss due to the dehydration of a 85% of calcium hydroxide.

The Pozzolana was mainly composed of silicates (silicon content of 80%) and aluminates; Na, Mg, K around 3% were found. The XRD spectra showed a huge broad peak from 16 2θ to 32 2θ due to the presence of amorphous compounds such as amorphous silica. Quartz (SiO_2), and albite ($\text{NaAlSi}_3\text{O}_8$) were recognized as major crystalline phases. The peaks labelled as 1 in Table 3.1 4 indicated the presence of phyllosilicates, in particular muscovite ($\text{KAl}_2(\text{AlSi}_3\text{O}_{10})(\text{F},\text{OH})_2$), celadonite or glauconite¹, and the presence of an Aft phase such as halloysite $\text{Al}_2\text{Si}_2\text{O}_5(\text{OH})_4 \cdot 2\text{H}_2\text{O}$. In the FT-IR spectrum a broad peak of -OH stretching was due to water

¹ usually present in volcanic tuffs as solid solutions

adsorbed or linked to the silicates, while the strong peak at 1051 cm^{-1} together with the 791 cm^{-1} peak were related to the presence of silicates. The TG curve showed that the pozzolana had a unique constant and slight mass loss in the $150\text{-}450^\circ\text{C}$ range due to the loss of adsorbed and crystallized water from the silicates.

The apparent and specific surface of calcium hydroxide and of the pozzolana were measured with BET analysis, in order to evaluate the surface area.. The results are reported in Table 3.1 4. The calcium hydroxide and the pozzolana had a high surface area, the former was characterized by a lower density ($2,41\text{ g/cm}^3$) and a higher surface area ($10,89\text{ m}^2/\text{g}$) in comparison to the latter ($2,61\text{ g/cm}^3$ and $10,697\text{ m}^2/\text{g}$), while they presented a similar micro porosity with the average pore diameters around $25\text{-}30\text{ nm}$.

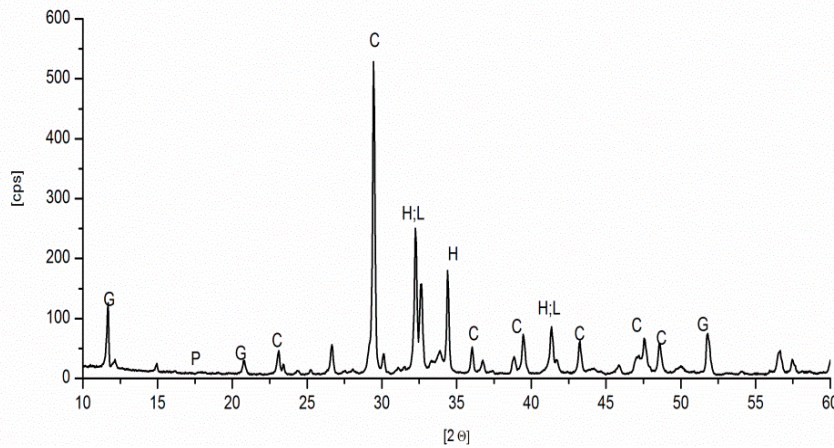
3.1.4. AGGREGATES

As aggregates different kind of sands were selected to be mixed with the different binders to obtain the different mortar mixes.

- A silicate-carbonate sand was chosen for the limestone cement. The aggregate used is composed of silicates and carbonate sands supplied by Epiù S.r.l. in a Fuller granulometric distribution from 0.0 to 1.2 mm .
- The commercial dry-mixed mortar Vimak BIO, produced and supplied by Villaga s.p.a., was chosen as basis for the water-repellent natural hydraulic lime mortars. The binder and the aggregates were also supplied separately to allowed the analysis of the different starting materials. Carbonate-silicate sands in Fueller granulometric distribution from 0.0 to 1.2 mm are used in the dry-mixed mortar Vimak BIO.
- For the pozzolana-lime binder a Normal Sand defined by the EN 196 normative was chosen. The Normal Sand is composed of silicate sand in Fueller granulometric distribution from $0,08\text{-}2\text{mm}$, sold in plastic bags of $1350\pm 5\text{ g}$. The use of the Normal Sand allows a good reproducibility of the experimental tests.

The normal sand has a standard composition defined by the normative EN 196 (only pure silicates), but the other two aggregates were analysed by FT-IR and TG-DSC analysis to better define their composition. The FT-IR of the two aggregates showed the presence of the same compounds: calcium carbonate and silicates (Table 3.1 5 Characterization of the aggregatesTable 3.1 5), but the relative presence of the silicates was higher for the aggregates used with limestone cement, while the Villaga aggregates (for the natural hydraulic lime mortars) were composed of almost pure calcium carbonate. The TG-DSC analysis confirmed the FT-IR analysis (Table 3.1 5) with almost a $5,21\%$ of calcium carbonate for the limestone cement aggregates and more than 95% of calcium carbonate for the NHL aggregates.

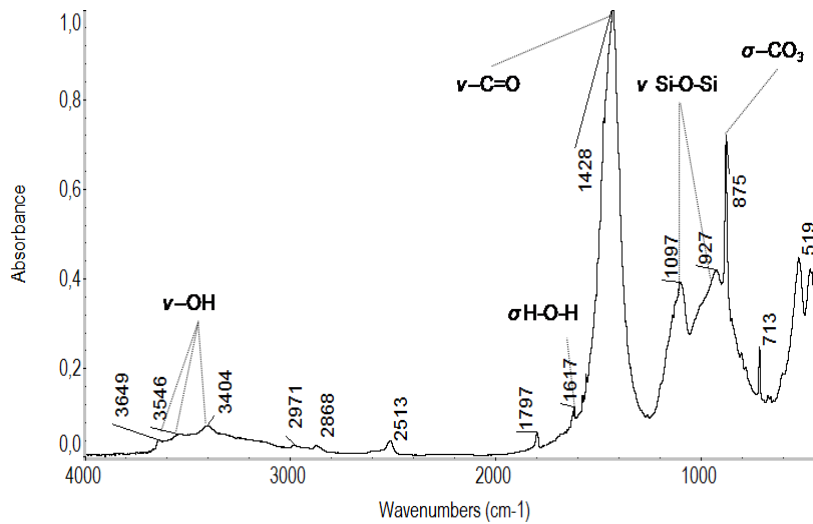
Table 3.1 1 Characterization of Limestone Cement



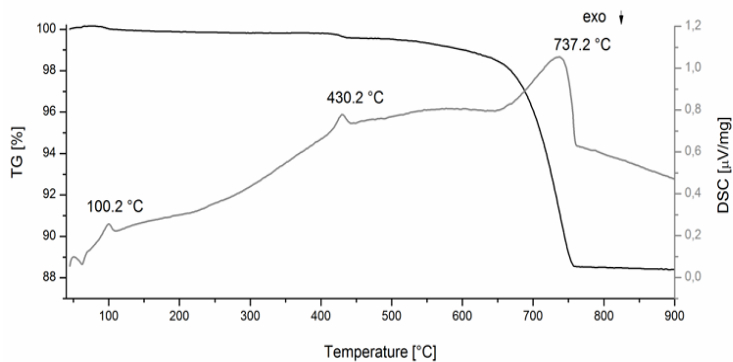
Element	At%
Mg	0.3
Al	2.6
Si	21.6
S	9.3
K	0.6
Ca	60.0
Fe	2.7

Chemical composition by XRF analysis. The precision of the technique are +/- 1-2%

XRD diffraction pattern of anhydrous limestone cement (Cementi Rossi s.p.a. CEMII B/L); C=calcite, G=gypsum, H=hatrurite, L= larnite



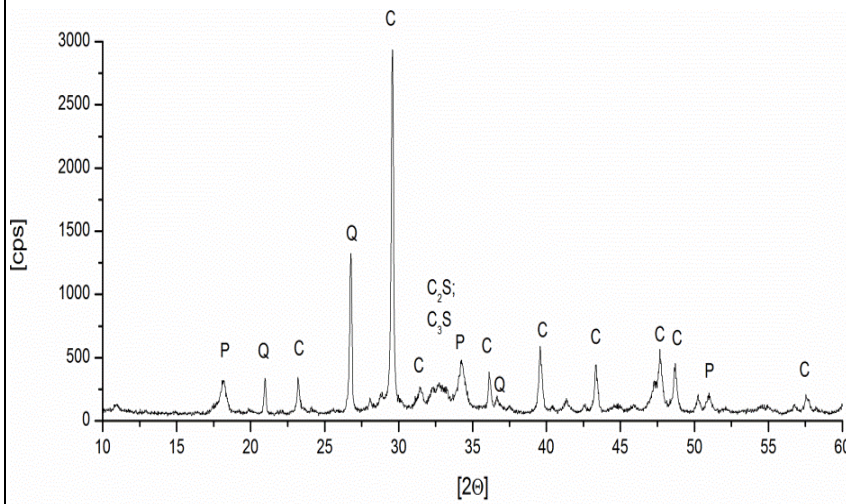
FT-IR spectrum of anhydrous limestone cement (Cementi Rossi s.p.a. CEMII B/L)



DSC peak °C	Mass Loss %	Transformation	Compound %
100.2	0,68	Loss of water	-
430.2	0,16	Dehydration of Ca(OH) ₂	0,66
737.2	10,02	Decarbonation of CaCO ₃	22,79

link: TG/DSC curves of limestone cement ,right: its chemical composition determined by TG-DSC analysis

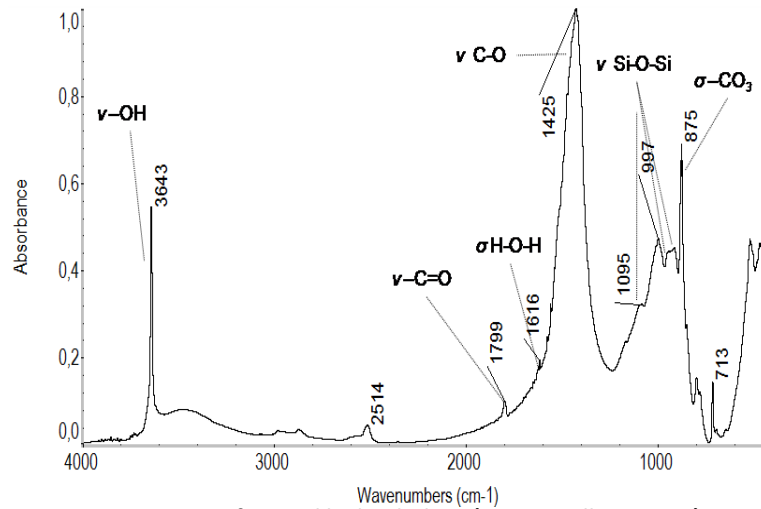
Table 3.1 2 Characterization of the natural hydraulic lime



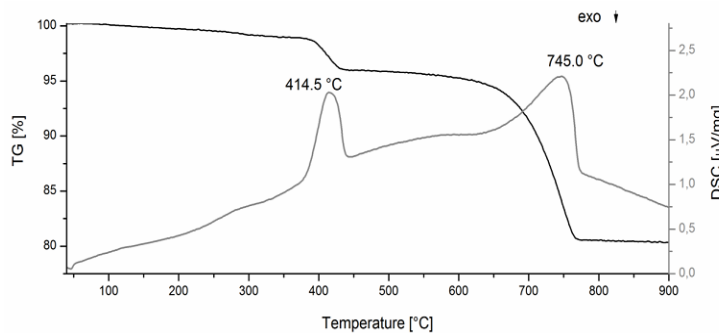
Element:	At%
Mg	0.3
Al	3.6
Si	21.2
S	1.1
K	0.8
Ca	56.5
Fe	2.6

Elemental composition by XRF analysis
 Chemical composition by XRF analysis. The precision of the technique are +/-2%

XRD diffraction pattern of the natural hydraulic lime (NHL 3.5 Villaga S.P.A.);
 P=portlandite, C=calcite, Q= quartz, C₂S= dicalcium silicatse, C₃S= tricalcium silicates



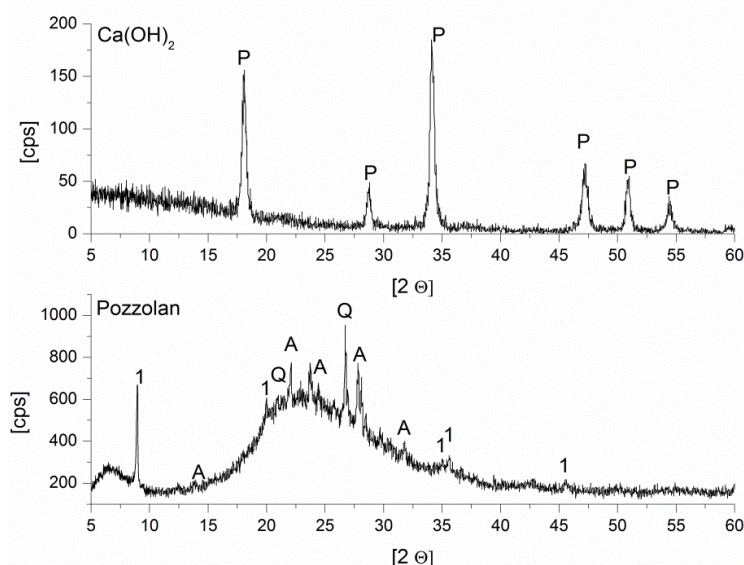
FT-IR spectrum of natural hydraulic lime (NHL 3.5 Villaga S.P.A.)



DSC peak °C	Mass Loss %	Transformation	Compound %
414.5	2.81	Dehydration of Ca(OH) ₂	11.56
745.0	14.11	Decarbonation of CaCO ₃	32.10

links: TG/DSC curves of natural hydraulic lime and right: its chemical composition determined by TG-DSC analysis

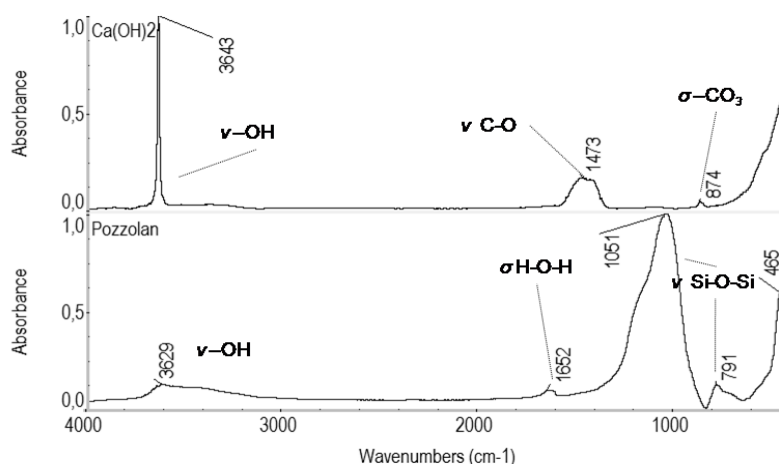
Table 3.1 3 Characterization of the pozzolana and lime



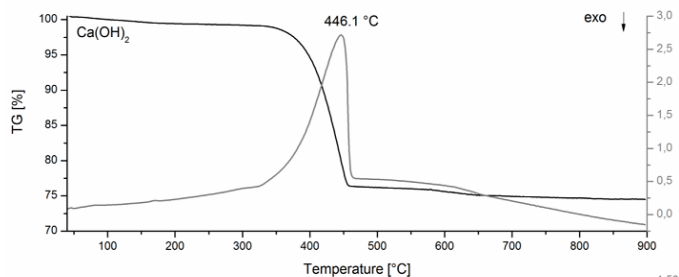
Element:	Ca(OH) ₂	Pozzolan
	At%	At%
Na	0.3	3.7
Mg	0.8	2.3
Al	0.1	8.9
Si	0.3	80.4
S	0.2	0.2
K	0.3	2.7
Ca	97.8	1.1
Fe	0.1	0.5

Elemental composition by XRF analysis Chemical composition by XRF analysis. The precision of the technique are +/-1-2%

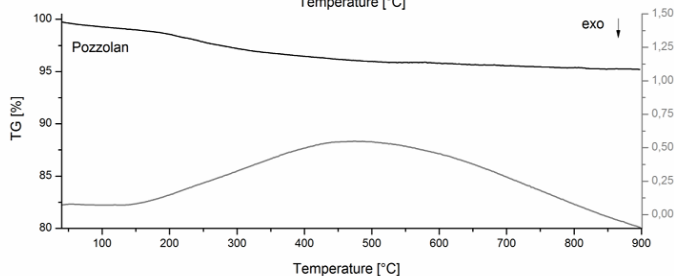
XRD diffraction pattern of the pozzolanic hydraulic lime (NHL 3.5 Villaga S.P.A.); P=portlandite, C=calcite, Q= quartz, A=albite 1= halloysite or muscovite



FT-IR spectra of calcium hydroxide (up) and pozzolan (down)



DSC peak °C	Mass Loss %	Transformation	Compound %
446.1	20.30	Dehydration of Ca(OH) ₂	83.52



DSC peak °C	Total Mass Loss %	Transformation	Compound %
400-500	4.38	Loss of water	-

TG-DSC curves of calcium hydroxide (up) and pozzolan (down); right: chemical transformation and quantification of the relative compounds (up: calcium hydroxide, down: pozzolan)

Table 3.1 4 apparent density and real surface area of the binder; Distribution of the pore diameter in relation to the cumulative volume and total Pores area obtained from BET measurements of the calcium hydroxide (links) and the pozzolan (right)

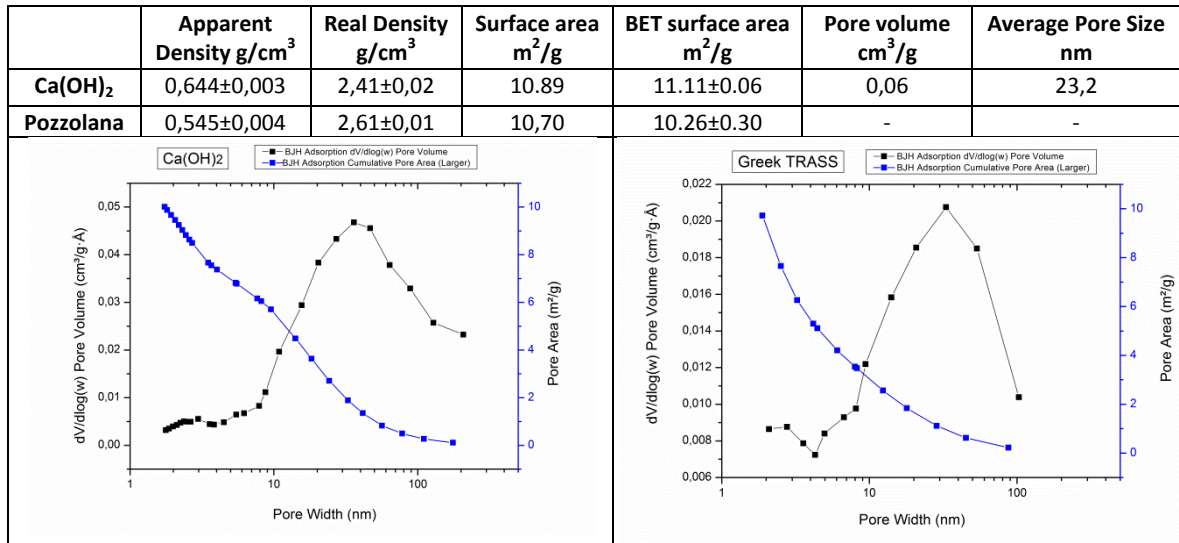
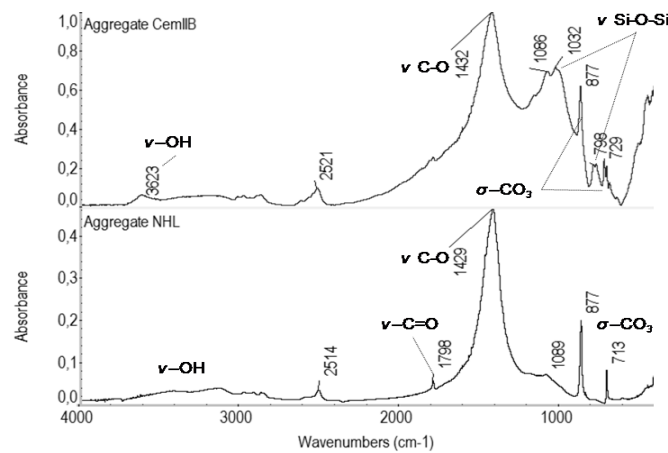
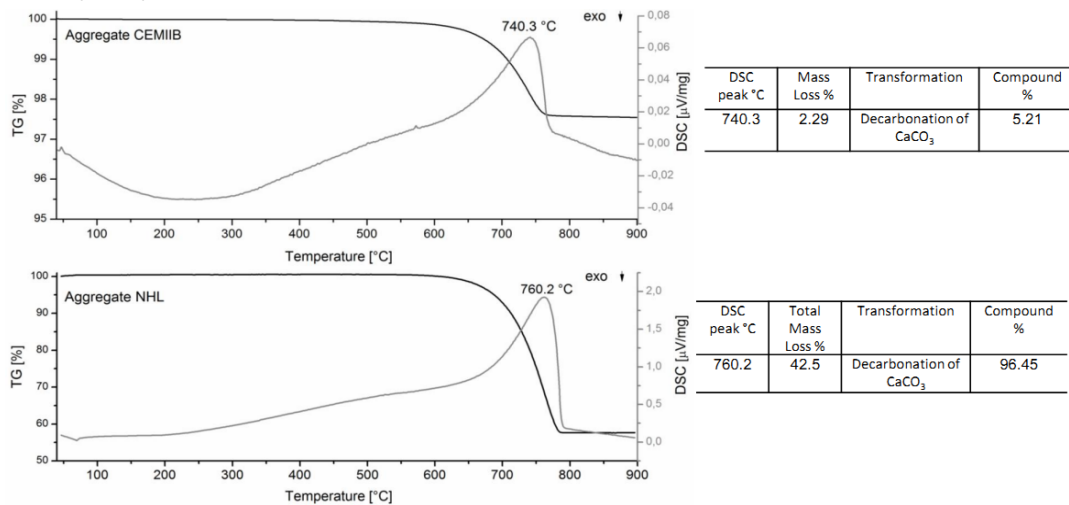


Table 3.1 5 Characterization of the aggregates



FT-IR spectra of the aggregates chosen for the limestone cement mortar (up) and the natural hydraulic lime mortars (down)



TG-DSC curves of the aggregates used with limestone cement (up) and with natural hydraulic lime (down), the relative calcium carbonate content is calculated from the mass loss in the 600-800 °C range (right)

3.1.5. WATER REPELLENT ADMIXTURES

The admixtures were chosen among different classes of water-repellents: silanes/siloxanes, metal soaps, water dispersible polymers as seen in Chapter 2.1.3. In this section the chemical-physical characterization of the water repellents is reported considering the different classes.

3.1.5.1. Silanes/siloxanes

The XRF analysis allowed to notice² (see Table 3.1 6) high presence of silicon in the silanes/siloxanes. The liquid silane Tegosivin HE showed the presence of sodium, probably due to the addition of sodium hydroxide as emulsion stabilizer³. The FT-IR analysis (Figure 3.1 1) allowed to obtain more information about the chemical composition. In each product, it was possible to observe the bands related to the silanes/siloxanes and the ones related to the inorganic carrier (when present).

The main absorptions related to silane-siloxanes compounds were:

- C-H aliphatic stretching absorptions around 2970 cm^{-1} ($\nu_{\text{as}}\text{ CH}_3$), 2930 cm^{-1} ($\nu_{\text{as}}\text{ CH}_2$), 2860 cm^{-1} ($\nu_{\text{s}}\text{ CH}_3$);
- Si-CH₃ and C-H bending absorption around 1260 cm^{-1} ($\sigma_{\text{sym}}\text{ CH}_3$);
- Si-O-Si stretching absorptions at 1096 cm^{-1} ($\nu_{\text{as}}\text{ Si-O-Si}$) and at 1020 cm^{-1} . Disiloxanes and small-ring cyclosiloxanes show a single Si-O-Si band. As the siloxane chains become longer or branched, the Si-O absorption becomes broader and more complex, showing two overlapping bands, typical also for poly dimethylsiloxanes⁴
- Small Si-OH stretching absorptions in the $958\text{--}810\text{ cm}^{-1}$ range;
- Si-O-Si and O-Si-CH₃ symmetric stretching absorptions at 802 cm^{-1} .

Other bands visible in the FT-IR spectra of the silanes/siloxanes were: Sitren P750[®] and Silres A[®] presented bands of Si-O-Si stretching absorptions at around 1100 cm^{-1} and the Si-O-Si bending absorptions at 472 cm^{-1} , due to the silica carrier; the presence of a calcium carbonate carrier in Sitren P730[®] was confirmed by the $1450, 873, 715\text{ cm}^{-1}$ absorptions confirmed also by the presence of calcite in the XRD analysis.

Different thermal degradation processes were observed for the different silanes (Figure 3.1 4 and Table 3.1 7). The thermogravimetric curve of Sitren P750[®] presented a first slight mass loss to $200\text{ }^\circ\text{C}$ due to the loss of water adsorbed or coordinated on the amorphous silica of the carrier. A major mass loss was seen around $400\text{--}500\text{ }^\circ\text{C}$ related to the decomposition of the organic part of the compound. The TG-DSC analysis of Sitren P730[®] showed two major transformation: a first one at $300\text{--}450\text{ }^\circ\text{C}$ due to the degradation of the organic silane, a second one at $650\text{--}750\text{ }^\circ\text{C}$ due to the endothermic decarbonation of calcium carbonate carrier. Silres A[®] had a TG curve similar to Sitren P750[®] but seemed less thermolabile: the mass loss related to the silane decomposition occurred only at $500\text{--}600\text{ }^\circ\text{C}$. The relative DSC analysis showed that an exothermic process occurred together with the mass loss. Tegosivin HE showed also TG-DSC curves similar to Sitren P750[®] but the mass loss at $400\text{--}550\text{ }^\circ\text{C}$ was high, around 95%, being this compounds composed mainly of silanes/siloxanes, without inorganic carriers.

² It should be reminded that the XRF give only semi quantitative results, and therefore the relative error on the measurement is around 1%.

³ See Appendix 1.

⁴ Bellamy, L.J. 1975

3.1.5.2. Stearates

XRF elemental analysis of the stearates highlighted the presence of a high percentage of the metal ion (calcium, zinc or sodium) (Table 3.1 6). The analysis of zinc stearate showed also a high percentage of sodium and chlorine: sodium chloride is commonly used in the zinc stearate production⁵. The metal stearates taken into account were not pure compounds, but composed of a mix of metal carboxylates with different chain lengths, moreover little percentages of different metal ions could have been present in the compounds.

The Ft-IR analysis allowed a first comparison of the different stearates⁶ (Figure 3.1 1). The main and common absorptions found were:

- C-H aliphatic stretching absorptions around 2950 cm^{-1} ($\nu_{\text{as}}\text{ CH}_3$), 2920 cm^{-1} ($\nu_{\text{as}}\text{ CH}_2$), 2850 cm^{-1} ($\nu_{\text{s}}\text{ CH}_3$);
- -COO^- antisymmetric stretching mode associated with the stretching vibration of the COO^- group around $1570\text{-}1540\text{ cm}^{-1}$, these bands exhibits multiplet structures depending on the mode of coordination of the COO^- group with the metal ion. It depends only on the metal ion and not on the chain length;
- -CH_2 scissoring deformation and -CH_3 antisymmetric bending at 1470 cm^{-1} ;
- -COO^- symmetric stretching mode at around 1420 cm^{-1} , a unique symmetric stretching mode is observed;
- -CH_2 bending absorptions or methylene progressive bands are visible at 1110 cm^{-1} and $725\text{-}690\text{ cm}^{-1}$.

Socal® is a commercial product where a calcium stearates is supported on nanoparticles of calcium carbonate. Its FT-IR spectrum showed, therefore, the bands due to the calcium carbonate at $1458, 879, 718\text{ cm}^{-1}$. The absorptions due to calcium stearate were small, probably only a low percentage of stearate was used.

FT-IR analysis was not able to differentiate carboxylates structure with slight different chain lengths, but only structures with a different coordination ions. XRD analysis was more effective in differentiate the different phase structure of the stearates (Figure 3.1 3). Both calcium and zinc stearates were crystalline and show complex XRD patterns, in which metallic stearates and palmitates were recognizable⁷.

The thermogravimetric analysis of calcium and zinc stearates showed a major decomposition step in the $350\text{-}500^\circ\text{C}$ range (Figure 3.1 4 and Table 3.1 7). The correspondent DSC curves showed that the decomposition took place with at least two different endothermic reactions. During the decomposition the bonds between metal ion and the fat acid chains broke and then carboxylic compounds of different chains length are formed and decomposed.

Also Socal® presented a little mass loss between $350\text{ }^\circ\text{C}$ and 500°C due to the decomposition of the calcium stearate present in the compounds, while a major mass loss occurred at $650^\circ\text{C}\text{-}750^\circ\text{C}$ correspondent to the endothermic decarbonation of the calcium carbonate present.

⁵ saponification of fatty oils with NaOH solutions and precipitation of the metal soaps with metal salts solutions as ZnCl_2 solutions

⁶ M.A.Mesubi, 1982

⁷ It was difficult to identify each peak because metal soaps deriving from different fatty acids generate complicate XRD spectra and they are not completely crystalline. Moreover, it was found by Granier and Gregoire, 1988 that the room temperature structures of these stearates are sensitive to purity and thermal treatments and that solid solution are possible for different carboxylates.

For calcium stearate another slight mass loss occurred at 115°C, this weight loss was due to one mole water of crystallization which was split off at this temperature with an endothermic process (as indicated by the relative DSC peak). The crystalline structure of the stearate changed as consequence of the water loss⁸. Also in the case of sodium stearate a similar behaviour was seen at 200,3°C with a slight mass loss correspondent to an endothermic transformation.

3.1.5.3. Organic polymer

VINNAPAS® 8031 H (VINNAPAS® RI 551 Z) is a terpolymer powder of ethylene, vinyl laurate and vinylchloride that is dispersible in water. The XRF analysis showed therefore a high presence of chloride together with calcium, silicon and aluminium due to the presence of an inorganic carrier/stabilizer (Table 3.1 6).

The FT- IR spectrum allowed to characterize the chemical structure (Figure 3.1 1):

- -OH stretching absorptions were visible at 3695cm⁻¹ and 360 cm⁻¹;
- C-H aliphatic stretching absorptions at 2942 cm⁻¹ (v_{as} CH₃), 2920 cm⁻¹ (v_{as} CH₂), 2858 cm⁻¹(v_s CH₃);
- C=O stretching band around 1737 cm⁻¹;
- -CH₂ symmetric stretching and -CO₃ stretching absorptions at 1435 cm⁻¹
- -C-Cl stretching mode at around 1265 cm⁻¹, due to vinylchloride;
- -CH₂ bending absorptions or methylene bands were visible at 1102 cm⁻¹ and 690 cm⁻¹;
- Small Si-O-Si stretching absorptions at 1100 cm⁻¹ (v_{as} Si-O-Si) and at 1033 cm⁻¹.

The TG-DSC analysis of Vinnapas 8031H (Figure 3.1 4 and Table 3.1 7) showed three major mass losses: the first two at 300-350 °C and 400-500 °C related to the thermal decomposition of the organic polymer, the third one at 700°C due to the decarbonation of calcium carbonate used as stabilizer/carrier.

Table 3.1 6 Elemental composition by XRF analysis Chemical composition by XRF analysis. The precision of the technique are +/-1-2%

Water repellent admixtures	XRF Analysis- Element At%								
	Na	Mg	Al	Si	S	Ca	Fe	Zn	Cl
Sitren P 750	2	1,5	0,8	94,9	0,6	-	-	-	-
Sitren P 730®	-	0,6	-	20,2	-	76,8	-	-	-
Silres A®	3,4	1,6	0,8	92,8	1,2	-	-	-	-
Tegosivin HE®	5	-	-	52,2	-	0,4	-	-	-
CaSt	6,2	1,7	-	9	-	82,1	0,1	-	-
ZnSt	24,6	2,7	0,4	0,5	-	0,5	-	67,2	4
NaSt	27	-	1	-	-	0,6	1	-	-
Socal	-	-	-	-	-	87,8	0,1	-	-
Vinnapas	-	-	2,7	1,8	-	30,6	0,1	64,8	

-- not found

⁸ Valor, A. et al. 2002

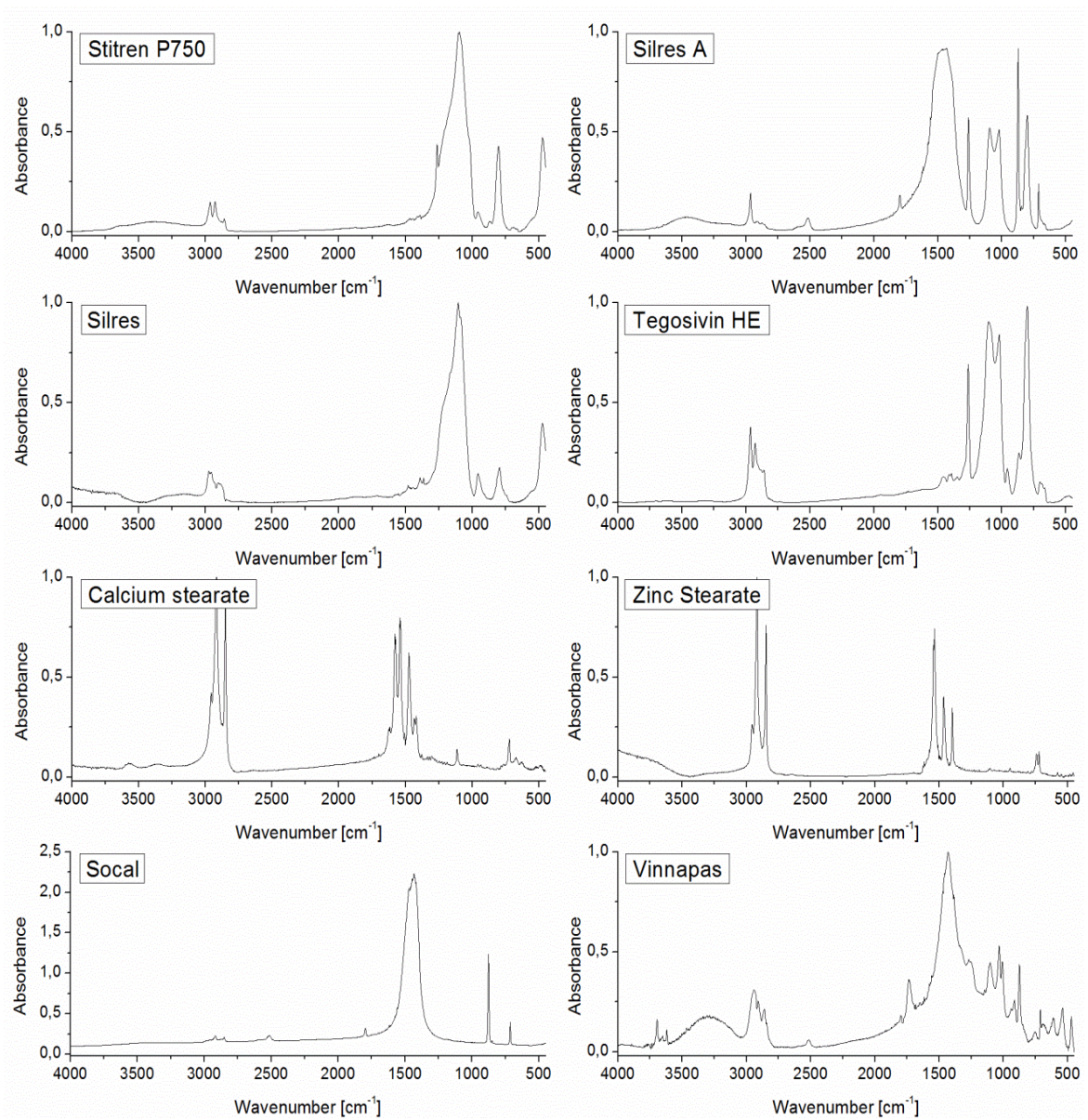


Figure 3.1 1 FT-IR spectra of the water-repellent admixtures

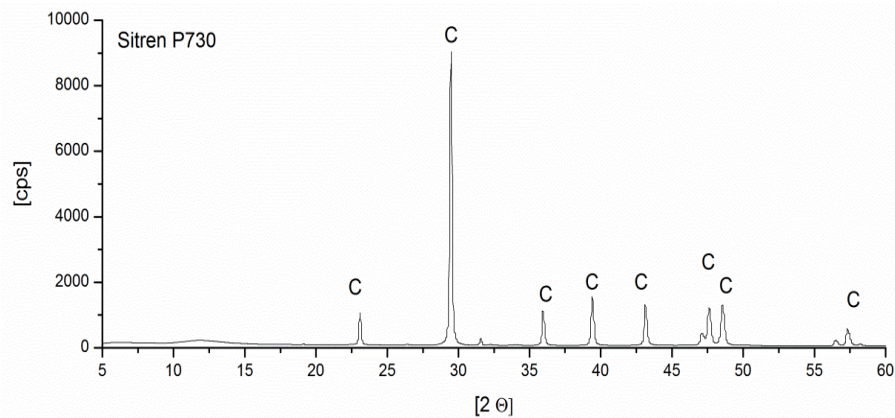


Figure 3.1 2 XRD pattern of Sitren P730

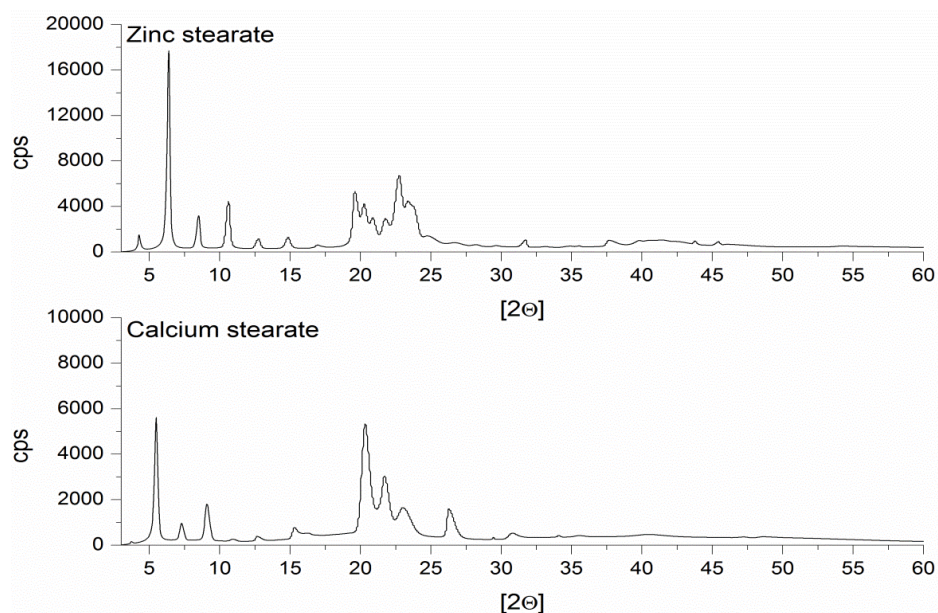


Figure 3.1 3 XRD pattern of Zinc stearates (above) and Calcium stearates (below) C=calcite

Table 3.1 7 TG-DSC analysis, mass losses -wt%

Sample	Mass Losses (%) and relative steps		Residual Mass (%)	Residues identification
Sitren P750®	2.84 (40÷200°C)	26.57 (350÷660 °C)	70.59	SiO ₂
Sitren P730®	0.57 (40÷200°C)	16,24 (300÷400 °C)	32.57 (400÷800 °C)	50.62 CaO
Silres A®	2.35 (40÷200°C)	6.89 (400÷600 °C)	90.76	SiO ₂
Tegosivin HE®	1.02 (40÷200°C)	89.89 (350÷600 °C)	9.11	-
Calcium St	2.78 (100÷150°C)	76.10 (400÷500 °C)	7.17 (650÷750 °C)	13.95 CaO
Zinc St	-	74.53 (350÷500 °C)	25.65	-
Sodium St	1.56 (40÷200°C)	73.69 (400÷500 °C)	24.75	-
Socal	-	2.04 (300÷450 °C)	41.15 (600÷800 °C)	56.81 CaO
Vinnapas	43.02 (250÷350 °C)	29.03 (350÷500 °C)	7.52 (650÷800)	20.43 CaO

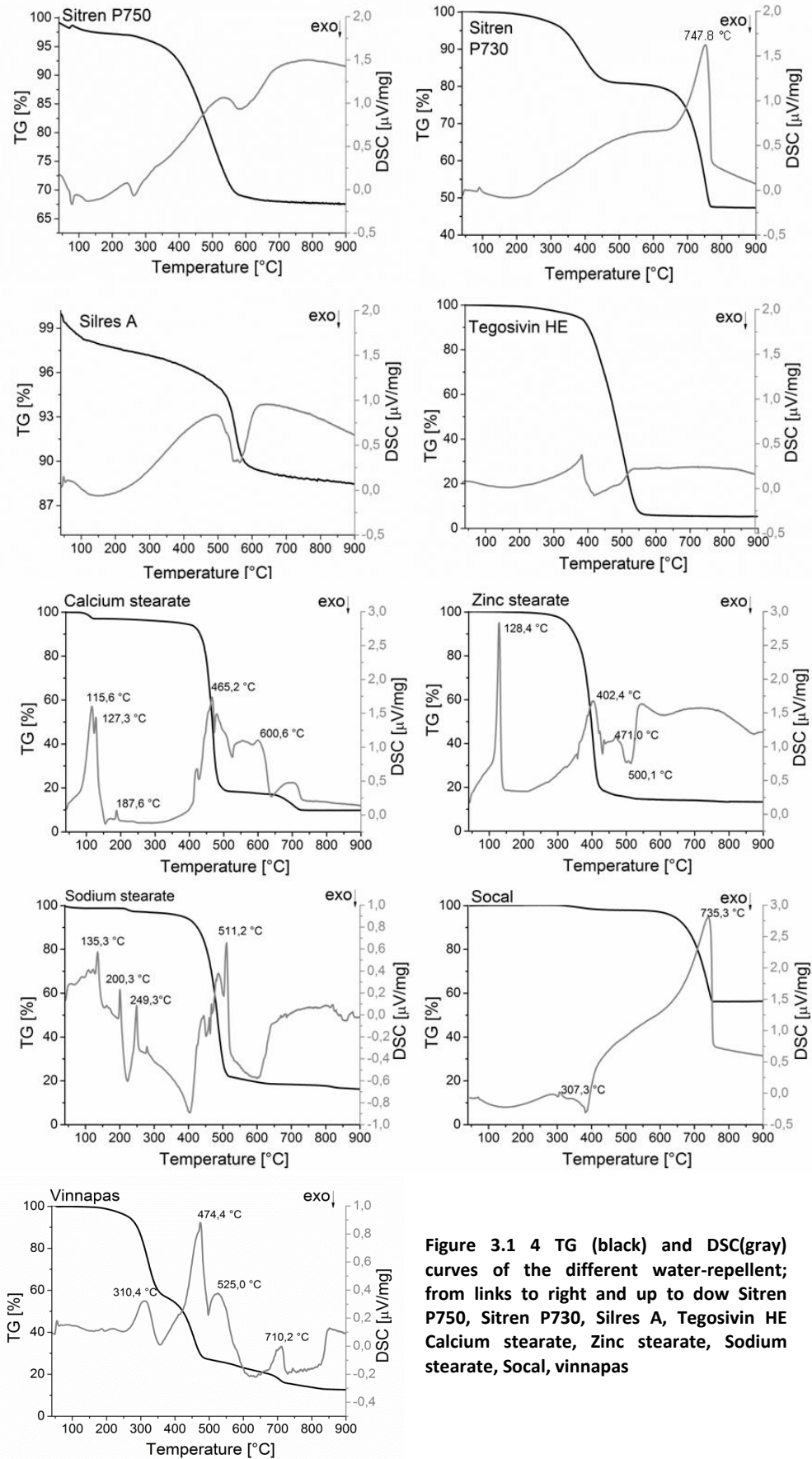


Figure 3.1 4 TG (black) and DSC(gray) curves of the different water-repellent; from links to right and up to dow Sitren P750, Sitren P730, Silres A, Tegosivin HE Calcium stearate, Zinc stearate, Sodium stearate, Social, vinnapas

3.1.6. WEATHERING OF WATER REPELLENT ADMIXTURES

The water-repellents were exposed to different environmental conditions in order to verify the behaviour and the stability of the compounds. In particular, the conditions were chosen to verify the water-repellents ability of maintaining their hydrophobic nature and to repulse water.

The water-repellents were put:

- in contact with pure water to observe possible changes of the compounds in a simple wet environment;
- in contact with calcium hydroxide saturated solution to observe changes in a basic environment similar to the one present in the mortars;
- in oven at $55\pm 5^\circ\text{C}$ to observe changes due to an accelerated ageing.

3.1.6.1. Water-repellents in water

The water-repellents Sitren P750[®], Sitren P730[®] and Silres A[®], calcium stearates, zinc stearates and the organic polymer Vinnapas[®] were put in contact with deionised water in closed vessel for one month and the water was sampled at 30 minutes, 24 hours, 7 and 28 days and analysed through FT-IR spectrometry. Figure 3.1 5 shows the collected spectra at 7 and 28 days are.

The powder silanes were hydrophobic and tended to remain at the interfaces air-water at the beginning but after one week and, even more, after one month tended to being partially dispersed in water. After one month it was possible to observe the presence of new peaks at 1380 cm^{-1} of Si-O(CH₃)₂ stretching and at around 620 cm^{-1} of Si-O bending, both on Sitren p750[®] and Silres A[®], silanes/siloxanes supported on amorphous silica, due probably to a partial hydration of the silica. The peaks related to the -CH stretching at $2980\text{-}2920\text{ cm}^{-1}$ were less visible, maybe a partial separation of the hydrophobic silane oil from the inorganic amorphous silica carrier occurred, and the silica tended to be disperse in water, while the silane migrated to the inter-phase air-water.

In the case of Sitren P730[®] a -OH stretching at 1630 cm^{-1} appeared at 7 day together with the Si-O absorptions at 620 cm^{-1} , furthermore the Si-O-Si stretching absorption at 1100 cm^{-1} of the amorphous silica increased in comparison to the Si-O-Si, Si-O-CH₃ stretching absorption at 1020 cm^{-1} , maybe a partial separation of the silicone oil from the calcium carbonate carrier occur.

Both the calcium and zinc stearates after remained completely separated from the liquid water. The organic dispersible polymer Vinnapas dispersed immediately in water forming a white latex, the FT-IR spectra showed that the calcium carbonate carrier was not visible in the latex (probably sediments on the bottom) while the organic part was clearly visible and that the product remained stable in pure water.

3.1.6.2. Water-repellents in Ca(OH)₂ saturated solution

The three silanes Sitren P750[®], Sitren P730[®] and Silres A[®], the calcium and zinc stearates and the organic polymer Vinnapas[®] were mixed with a saturated solution of calcium hydroxide (pH~12) in closed vessel for 150 days, to obtain an alkaline environment similar to the one present in the mortars. Samples dried in oven at 40°C were analysed through FT-IR spectrometry and with TG-DSC (Figure 3.1 6).

The silanes water-repellents in saturated calcium hydroxide solution tend to be dispersed earlier than in pure water, after three days some of the powder remain dispersed in solution. The FT-IR spectra remained similar to the original water-repellents . The peaks related to the presence of calcium hydroxide and calcium carbonate, due to a partial carbonation of the solution during the

drying step, appeared at around 1430, 870, 714 cm^{-1} . The Si-O-Si stretching absorption at around 1050 cm^{-1} broadened and covered the Si-O stretching at 950 cm^{-1} both in Sitren P750[®] and Silres A[®] spectra, and a small -OH absorption at 1620 cm^{-1} appeared. This suggest a partial hydration of the compounds and maybe a partial separation of the organosilane/siloxane from the silica carrier. The FT-IR spectra of sitren P730 remained unchanged.

The calcium stearates remained stable as confirmed by the FT-IR spectra. In the FT-IR spectra of zinc stearates collected after 28 and 150 days is interesting to notice the appearance of a little absorption at 1582 cm^{-1} near the major absorption at 1539 cm^{-1} . This new peak can be related to the -COO⁻ stretching of calcium stearate, due probably to a ionic exchange in the saturated calcium hydroxide solution. This ionic exchange of the zinc stearate was confirmed also by the TG-DSC analysis which showed the formation of a new DSC peaks at 115 $^{\circ}\text{C}$ typical of the endothermic process due to a mole of water of crystallization split off from calcium stearate ($\text{Zn}(\text{C}_{18}\text{H}_{36}\text{O}_2)_2 \rightarrow \text{Ca}(\text{C}_{18}\text{H}_{36}\text{O}_2)_2$).

The organic polymer vinnapas dispersed in solution, but the film obtained after collecting and drying the latex solution became more brittle over time. The FT-IR spectra showed the same absorptions of the additive in water, but the bands tend to broaden with the ageing time.

3.1.6.3. Water-repellents in oven at 55 $^{\circ}\text{C}$

Sitren P750[®], Sitren P730[®] and Silres A[®], calcium stearates, zinc stearates, Socal[®] and the organic polymer Vinnapas[®] were put in open vessel in oven for one year and analysed with FT-IR to observe possible changes. The spectra at the beginning and after one year in oven are shown in Figure 3.1 7. No big differences were detected in any case. Only for Sitren P750[®] and Silres A[®] was possible to notice the broadening of the O-Si stretching absorptions around 900-1100 cm^{-1} .

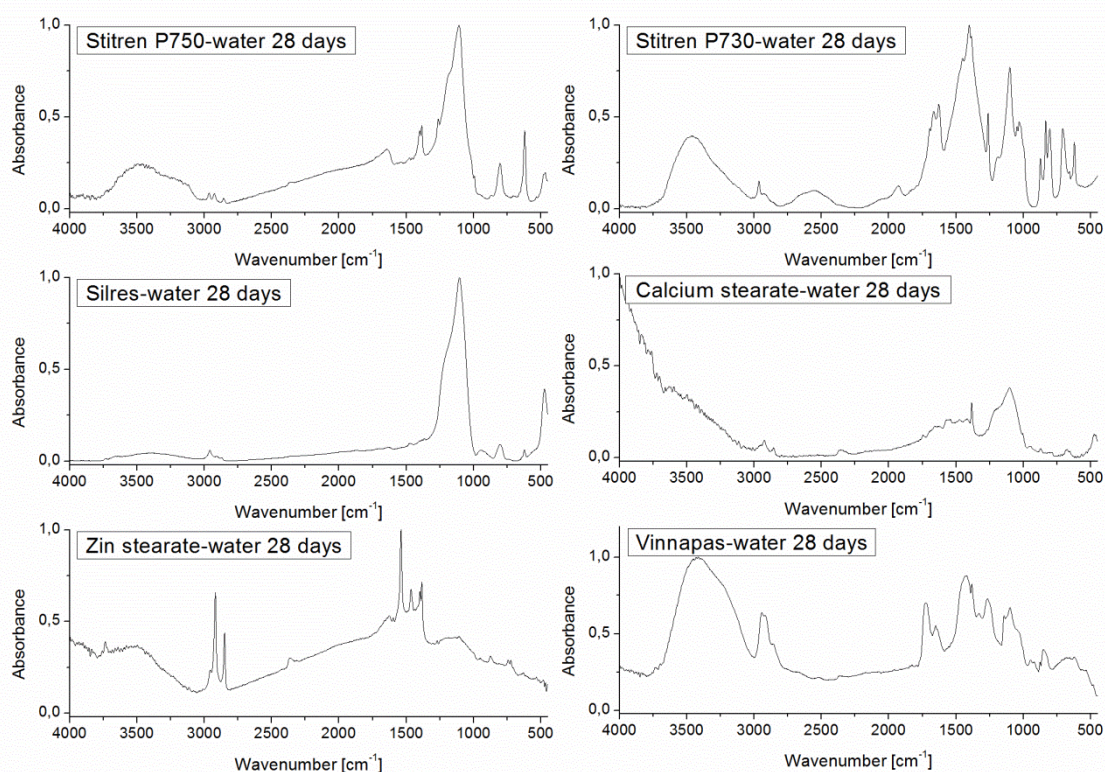


Figure 3.1 5 FT-IR spectra collected for the pure water-repellent admixtures in water for 7 and 28 days (7d and 28d, respectively)

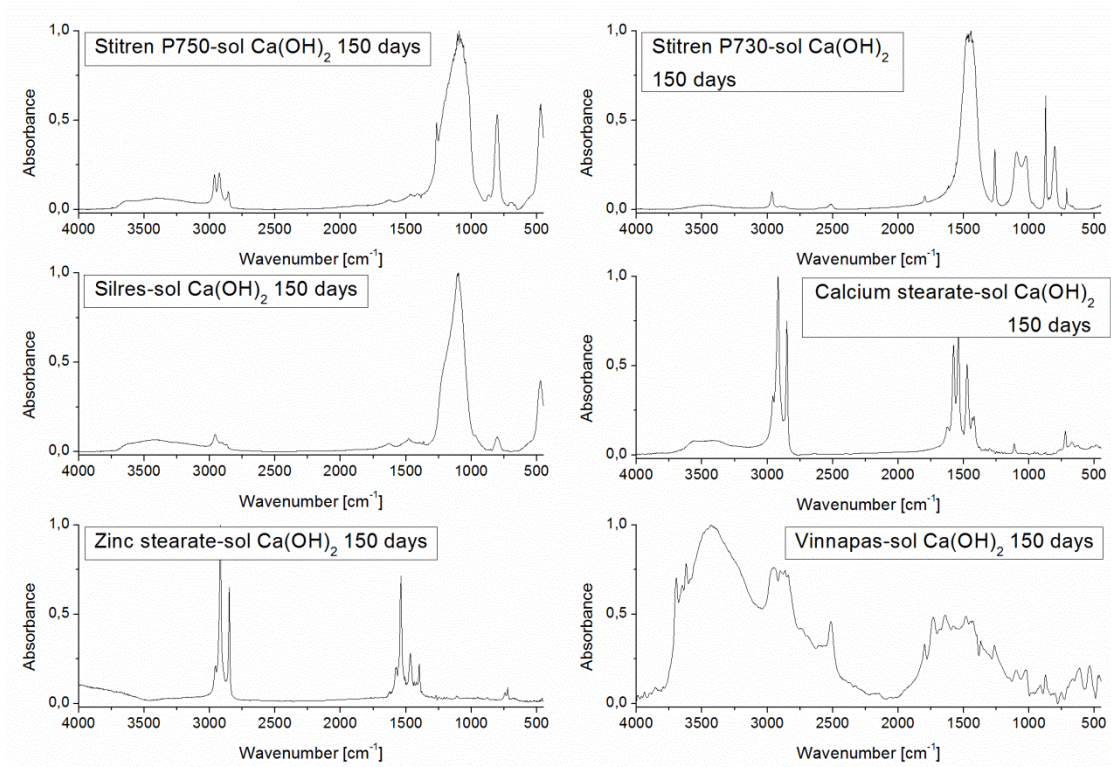


Figure 3.1 6 FT-IR spectra collected for the pure water-repellent admixtures in calcium hydroxide saturated solution for 150 days

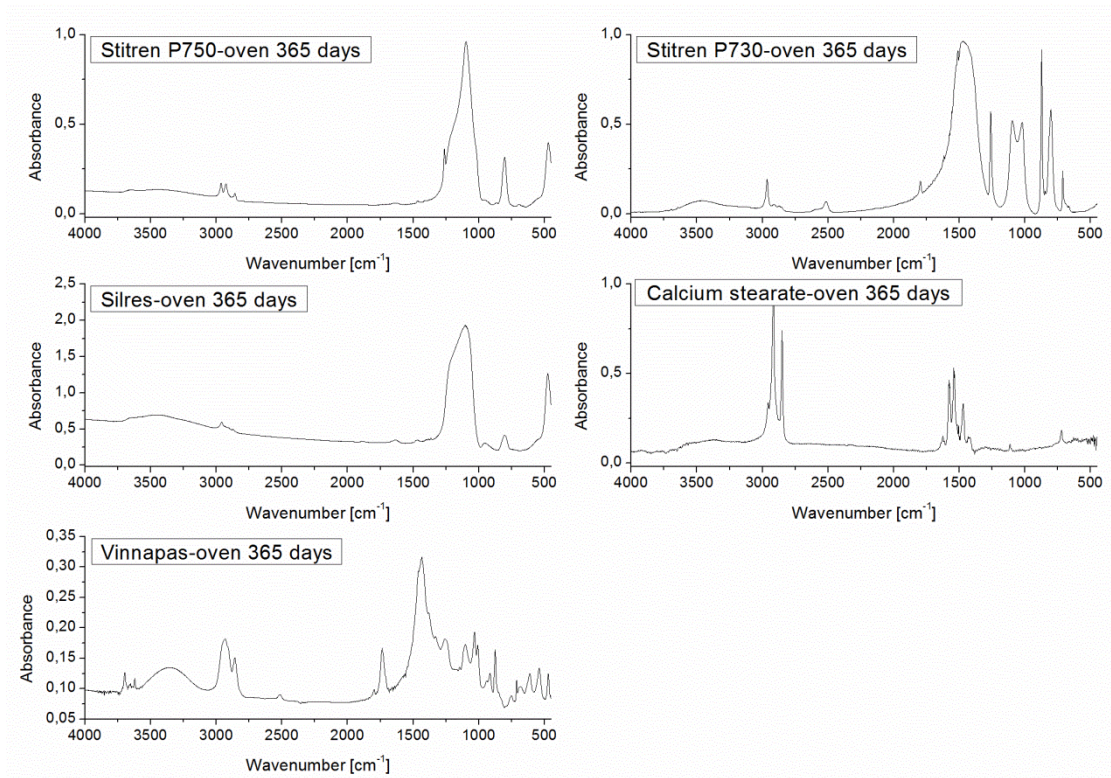


Figure 3.1 7 IR spectra of water repellents after 1 year in oven at 55°C

3.2 Study of the hydration of binder pastes

The present chapter relates on the study of the hydration reactions of binder pastes added with water-repellent admixtures, with the aim of observing the influence of the water repellents on the hydration reactions and hardening of different binders. Binder pastes composed of limestone cement, natural hydraulic lime or pozzolana-lime with water repellent admixtures were prepared, sampled at different hydration times and analyzed with different techniques such as XRD, FT-IR, TG-DSC, isocalorimetric analysis and SEM observation¹.

This hydration-study was also a preliminary study which allowed to collect information and knowledge in order to better understand the behaviour of mortars made of the same binders and added with water-repellent admixtures. Therefore it was chosen:

- to use a water-repellent concentration of 1% by dry weight of the pastes (which was used also by Zhao, T. Wittman, F.H² and will be used also for the preparation of water repellent mortars);
- a water-binder ratio equal to the water-binder ratio found and used for the preparation of water repellent mortars³;
- sampling times, chosen on the basis of preliminary tests, at 0, 4, 24, 48 hours, 7, 14, 21, 28 days, 2 months and also 3 months.

A summary of the prepared pastes is given at each subsection/paragraph of this chapter, together with complete report and description of the analytical results.

In the chapter 4.1 *Discussing the results of Chapter 3.2* the results will be interconnected and a complete description of the hydration mechanism and of the influence of the water-repellent admixtures is proposed.

To shortly summarize the main results described in this chapter:

- the presence of limestone caused a longer stability of the ettringite phase in limestone cement pastes;
- natural hydraulic limes showed an hydration similar to the cement but slower due to the absence of C₃S;
- pozzolana-lime pastes had slow hydration with evident formation of silico-alluminates phases and amorphous C-S-H only after 3 months;
- the presence of the admixtures caused delay of the hydrations, in particular when zinc stearate was used. Silane/siloxanes powder admixtures did not influenced strongly the hydration reactions.

¹ The commonly used cement chemical nomenclature will be used together with orthodox chemical notation. The following scheme summarizes the abbreviation used:

Cement chemical nomenclature and other abbreviations according to Taylor, H. F. W 1997			
C= CaO	S= SiO ₂	A=Al ₂ O ₃	F=Fe ₂ O ₃
H=H ₂ O	Ĉ=CO ₂	Ŝ=SO ₃	K= K ₂ O
N= Na ₂ O	M=MgO	P=P ₂ O ₅	T=TiO ₂
C-S-H= poorly crystalline or amorphous calcium silicate hydrate of unspecified composition			

² Zhao, T., Wittman, F.H 2011

³ The water-binder ratio may strongly influence the hydration and the behavior of the pastes and of the mortars and should be the same to compare the results. See also Chapter 3.3

3.2.1 LIMESTONE CEMENT PASTES WITH WATER-REPELLENTS

The composition of limestone cement pastes prepared and analyzed during their hydration are shown in Table 3.2 1. The paste names will be used in the tables and graphs to identify the different pastes.

Table 3.2 1 Mix design of Limestone cement pastes

Paste names	Binder	additive	additive class	Additive (%)	w/b ratio
CPA	Cem IIB	-	-	1	0.9
CP750	Cem IIB	Sitren p750	powder silane	1	0.9
CP730	Cem IIB	Sitren p730	powder silane	1	0.9
CPsil	Cem IIB	SilresA	powder silane	1	0.9
CPtes	Cem IIB	Tegosivin HM	emulsion silane	1	0.8
CPcast	Cem IIB	Ca Stearate	metal soap	1	0.9
CPznst	Cem IIB	Zn stearate	metal soap	1	0.9

3.2.1.1 XRD Study of limestone cement pastes with water repellents during the hydration

XRD qualitative analysis of limestone cement pastes without and with 1% by mass of water-repellent admixtures at different curing times allowed to recognize the crystalline phases present. The XRD patterns of the cement paste CPA, without water-repellent admixtures, are shown in Figure 3.2 1.

The XRD pattern of the fresh paste (CPA 0h), collected immediately after the addition of water, showed the peaks related to the presence of gypsum, calcite and the silicates phases hatrurite (C_3S) and larnite (C_2S). The same crystalline phases were found also in the anhydrous limestone cement. After 7 hours it was already possible to identify the formation of portlandite, due to the hydration of the silicates phases, and the formation of ettringite ($9.1^\circ 2\theta$) from gypsum and C_3A . The transformation of gypsum in ettringite was completed within 24 hours.

After 7 days a strong decrease of the peaks around $33-34^\circ 2\theta$ of the silicates phases occurred, mainly due to the fast hydration of hatrurite. After 7 days and then after one month new peaks at $10,8^\circ 2\theta$ and $11,7^\circ 2\theta$ were visible which could be related to the presence of AFm phases (aluminate, ferrite, sulphate, carbonate phases), and coexisted with the ettringite. Unlike normal Portland cement, where the formation of monosulphates or monosulphoalluminates is observed⁴, in limestone cement CEMIIB/L, the presence of calcium carbonate caused the preferential formation of AFmono- and hemi-carbonate phases from the reaction of calcite and calcium hydroxide with the remaining aluminates. This led also to the stabilization of AFt phases such as ettringite also after 56 days⁵. In particular, the peak at $10.8^\circ 2\theta$, visible after 7 days, can be related to the presence of solid solution of AFm carbonate and hemicarbonate phases which developed into monocarbonates after 21 days (Mc at $11.7^\circ 2\theta$). Calcium hydroxide was, therefore, consumed also during the formation of hemicarbonates.

⁴ Taylor, H. F. W 1997; Lea, M., 1997

⁵ Lothenbach, B., *et al.* 2008; Kakali, G. *et al.* 2000; De Weerd, K., *et al.* 2011;

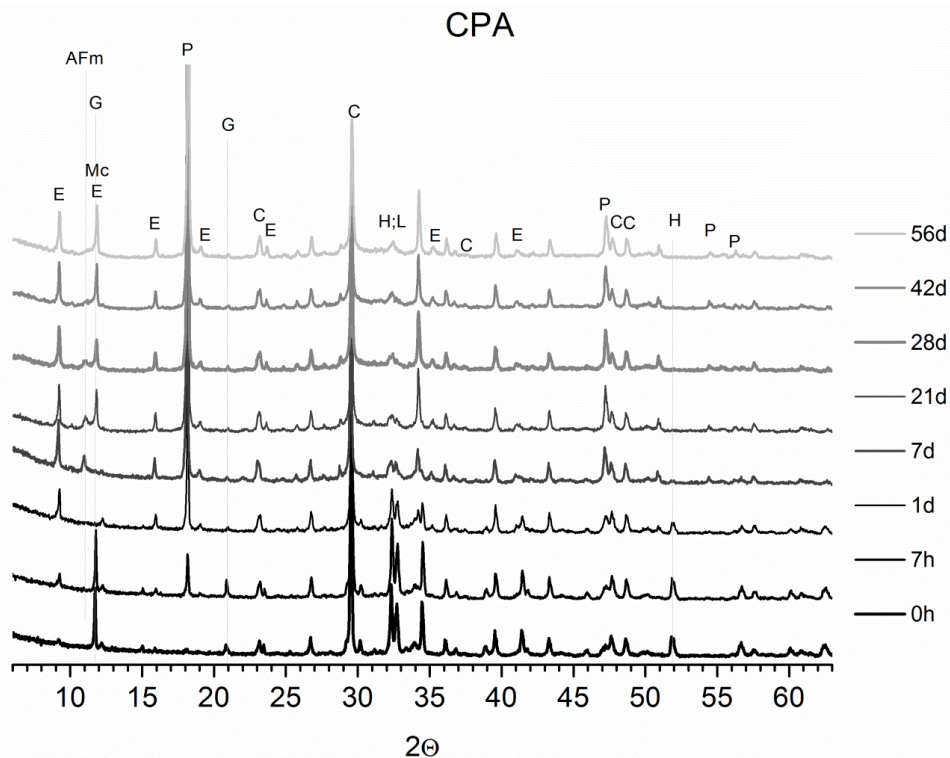


Figure 3.2 1 XRD patterns registered for the limestone cement paste without admixtures fresh and after 7 hours, 1, 7, 21, 28, 42, 56 days of hydration; E= ettringite; G=gypsum; Mc= monocarbonate; P=portlandite, C=calcite; H=Hatrurite; L=larnite; P=portlandite; E=ettringite

In order to study the different hydration products formed in limestone cement pastes with water repellents, the XRD patterns registered at different times were compared (Figure 3.2 2, Figure 3.2 3).

Only slightly differences were observed, mainly in the 8-22° 2θ and 29-37° 2θ range. In particular, it was possible to notice the formation of the same hydration products found in the pastes CPA(without water repellents), but differences in the hydration kinetic.

The presence of the silane/siloxanes Sitren P750, Sitren P730, Silres A, Tegosivin HE 328 modified the hydration kinetics, in particular it was observed:

- a slowdown in the formation of portlandite at early ages, whose peaks at 18° 2θ were visible after 7 hours instead of 4 hours;
- the inhibition of the transformation of hemicarbonates in monocarbonates (see the 7-14-28 days), but after 56 days only the monocarbonate peaks at 11,7° 2θ can be seen both in the paste PCA and with siloxane water-repellents;
- hydration of the silicates phases C₃S and C₂S similar to CPA (without admixtures).

The differences observed in presence of calcium and zinc stearates in comparison to PCA were:

- the coexistence of the hemicarbonates and monocarbonates peaks at 7 days due probably to a faster transformation of hemicarbonates into monocarbonates in comparison to the paste without water-repellents;
- a slowdown of the portlandite formation after 7 hours in the paste CPznst with zinc stearate;
- the presence of two distinct peaks at 32° and 33° 2θ after 28 days indicating a slower hydration of the C₃S and C₂S compounds.

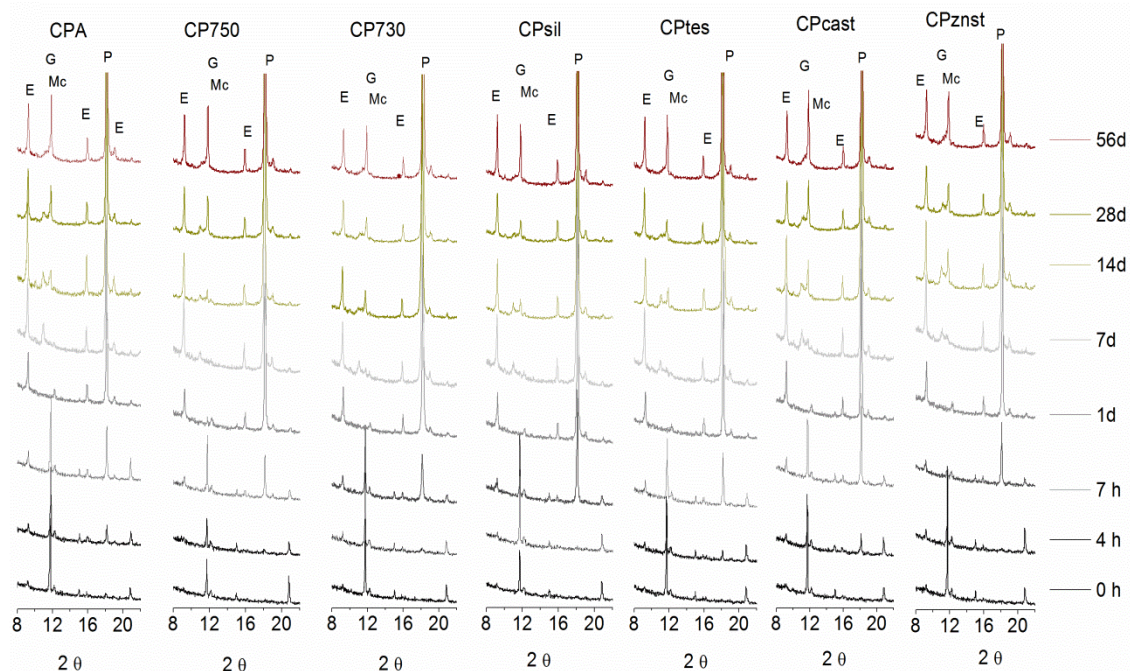


Figure 3.2.2 Comparison of the XRD patterns in the 8° - 22° 2θ range registered for the limestone cement paste without admixtures and with water-repellent admixtures fresh and after 4, 7 hours, 1, 7, 21, 28, 42, 56 days of hydration. E= ettringite; G=gypsum; Mc= monocarbonate; P=portlandite

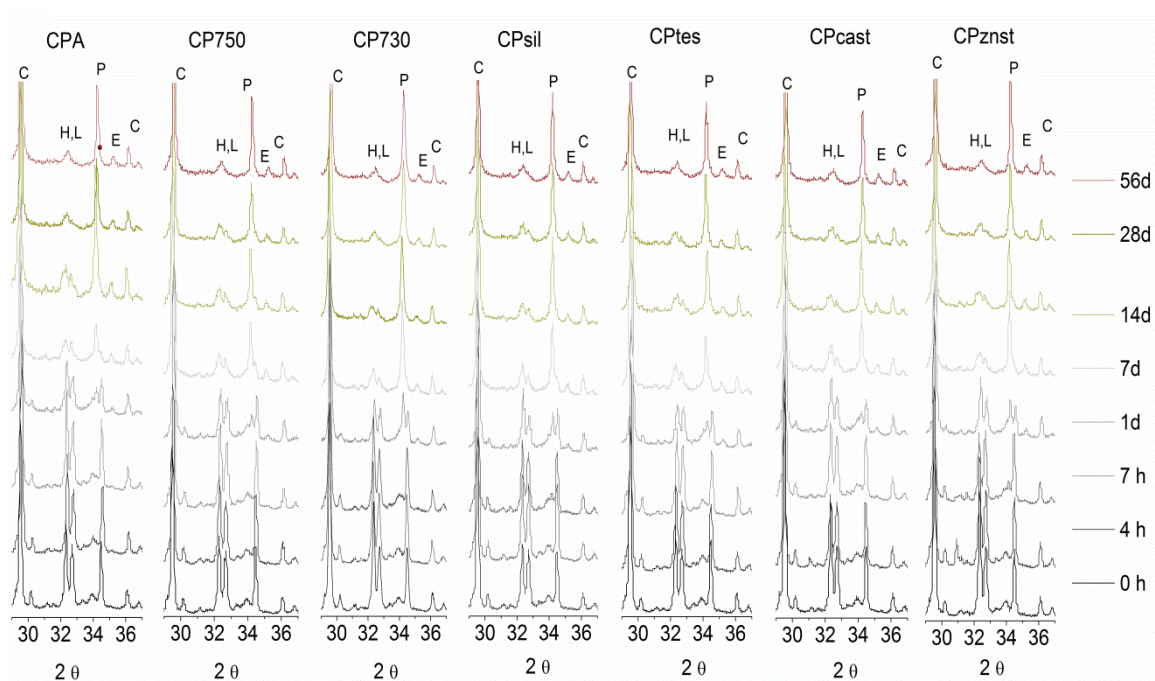


Figure 3.2.3 Comparison of the XRD patterns in the 29° - 37° 2θ range registered for the limestone cement paste without admixtures and with water-repellent admixtures fresh and after 4, 7 hours, 1, 7, 21, 28, 42, 56 days of hydration. C=calcite; H=Hatrurite; L=larnite; P=portlandite; E=ettringite

3.2.1.2 TG-DSC Study of limestone cement pastes

TG-DSC measurements were performed on samples collected after 1, 7, 28, 56 days of hydration. In Table 3.2 2, Table 3.2 3, and Table 3.2 4 the chemical composition and TG and DSC curves obtained on sample collected from the limestone cement pastes are shown.

Three principal mass losses (TG-curves) and correspondent thermal effects (DSC curves) were identify in all the samples:

- a first mass loss and correspondent endothermal transformations till 200 °C, due to the loss of absorbed and linked water;
- a second mass loss and another endothermal effect below 500°C, due to the dehydration Ca(OH)_2 ;
- a third mass loss and the correspondent peak between 650°C-800°C, due to the decomposition of calcium carbonate.

The first step was due to the loss of linked water and increased with the hydration time and the consequent formation of hydrated phases. Near the first endothermal effect, visible from the first day of hydration, other effects appeared between 150-180 °C after 7 days. The first effect was probably due mainly to the presence of ettringite while the second broad peak may be due to the convolution of the dehydration peaks of Afm phases and C-S-H⁶. Unfortunately, it is not possible to relate the enveloped peaks to specific dehydration reaction and only the total mass loss can be estimated (Table 3.2 2).

The second step increased with the time: the calcium hydroxide produced from the C_3S and C_2S increased while the hydration go further.

The third step was due to the decarbonation of calcium carbonate present in the limestone cement pastes and remain quite constant in all the sample analyzed.

The comparison between the TG and DSC curves of the pastes with water-repellent admixtures showed only slight differences. The DSC curves of CP750, CPsil and CPtes (with water repellent silanes) after seven days showed the presence of a second endothermic transformation in the 100-200°C range, due probably to the dehydration of Afm and C-S-H phases. This peak was visible only after 28 days in CPcast and CPznst curves. This could be linked to a delayed formation of hydrated C-S-H and Afm's in CPcast and CPznst pastes.

To understand the rate of hydration at different times, the amount of water loss, of calcium hydroxide and calcium carbonate was estimated considering the mass losses in the ranges 80-200°C, 350-500°C, 600-800°C, respectively. The results are listed in Table 3.2 2.

The comparison of the quantitative data allowed to better understand the effects due to the water-repellents. The total water TW content was similar for the mixtures at same ages. It was possible to observe a higher loss of water for the pastes with stearates (PCcast and PCznst) in the first month, while after 56 days the paste CPA (without water-repellents) had the major mass loss. If a siloxane was added (CP750, CP730, CPCsil, CPtes) the water mass loss and the hydration seemed delayed.

At early ages and till 7 day a strong increase of calcium hydroxide was observed for all the samples, after that, the lime production decreased and the carbonation became the major reaction, explaining why the amount of lime was lower after 56 days. Lower percentages of

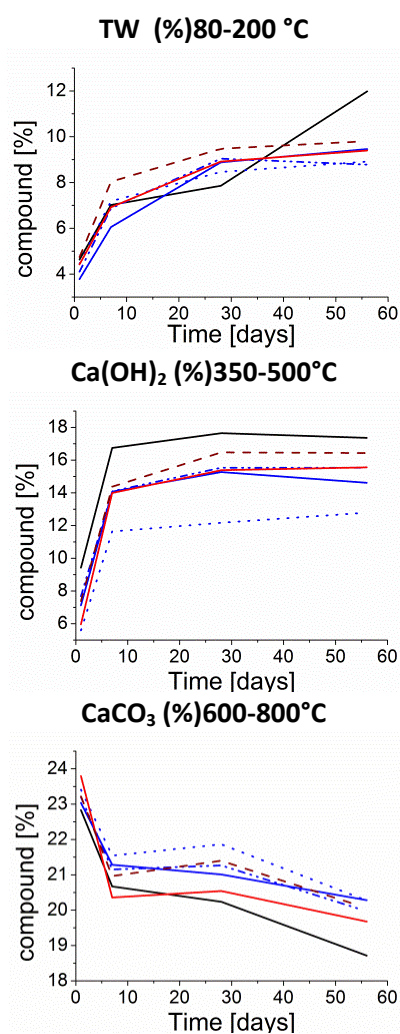
⁶ Ramachandran, V. S. 2003; Ramachandran, V. S. 1988; Ramachandran, V. S. 1969

calcium hydroxide were measured at every time in the admixed pastes in comparison to CPA (see Table 3.2 2). In presence of different water-repellents the amount of calcium hydroxide produced was similar, except in CPtes (liquid silane) which had a lower production of lime.

The calcium carbonate content decreased with the time, in order to explain this process it should be remembered that: i) calcium carbonate is partially involved in the hydration reaction to form alumina-carbonates phases, ii) the data indicate a relative percentage amount of the compounds in each specific samples and not an absolute quantity, when the relative percentage of a compound is increasing over time in one sample, the others decrease. In fact it was possible to observe that while the calcium hydroxide increased the calcium carbonate decreased.

Table 3.2 2 Amounts of water, calcium hydroxide, and calcium carbonate at 1, 7, 28, 56 days in the different limestone cement samples measured by TG-DSC.

sample name	TW (%)	Ca(OH) ₂ (%)	CaCO ₃ (%)
	80-200 °C	350-500°C	600-800°C
CPA1d	4,6	9,4	22,8
CPA 7d	7,0	16,7	20,7
CPA 28d	7,9	17,6	20,2
CPA 56d	12,0	17,4	18,7
CP750 1d	3,8	7,1	23,0
CP750 7d	6,1	14,1	21,3
CP750 28d	8,9	15,3	21,0
CP750 56d	9,5	14,6	20,3
CP730 1d	4,3	6,7	23,2
CP730 7d	6,6	13,2	20,1
CP73028d	8,9	13,8	21,0
CP73056	6,8	15,3	21,3
CPsil 1d	4,1	7,7	23,2
CPsil 7d	6,9	14,1	21,2
CPsil 28d	9,0	15,5	21,3
CPsil 56 d	8,8	15,5	20,0
CPtes 1d	4,5	5,6	23,4
CPtes 7d	7,2	11,6	21,5
CPtes 28d	8,5	12,2	21,9
CPtes 56d	8,9	12,8	20,3
CPcast 1d	4,4	6,0	23,8
CPcast 7d	6,9	14,0	20,4
CPcast28d	8,9	15,4	20,5
CPcast56d	9,4	15,6	19,7
CPznst 1d	4,7	7,4	23,2
CPznst 7d	8,0	14,4	21,0
CPznst 28d	9,5	16,5	21,4
CPznst 56d	9,8	16,4	20,1



— CPA
 — CP750 - - CP730 ···· CPsil
 ···· CPtes — CPcast - - CPznst

Table 3.2 3 TG-DSC curves of the limestone cement paste without admixtures after 1, 7, 28, 56 days of hydration

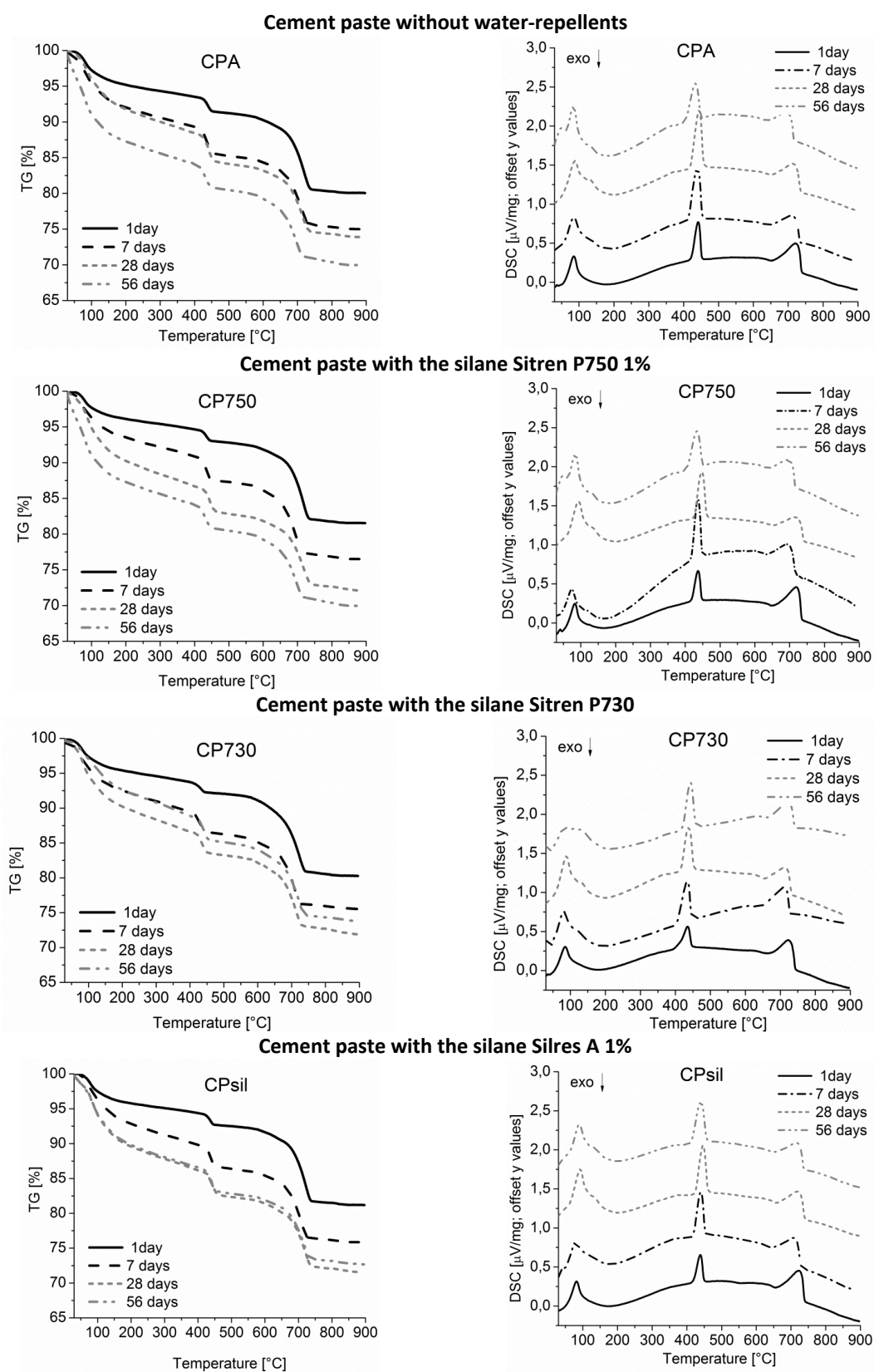
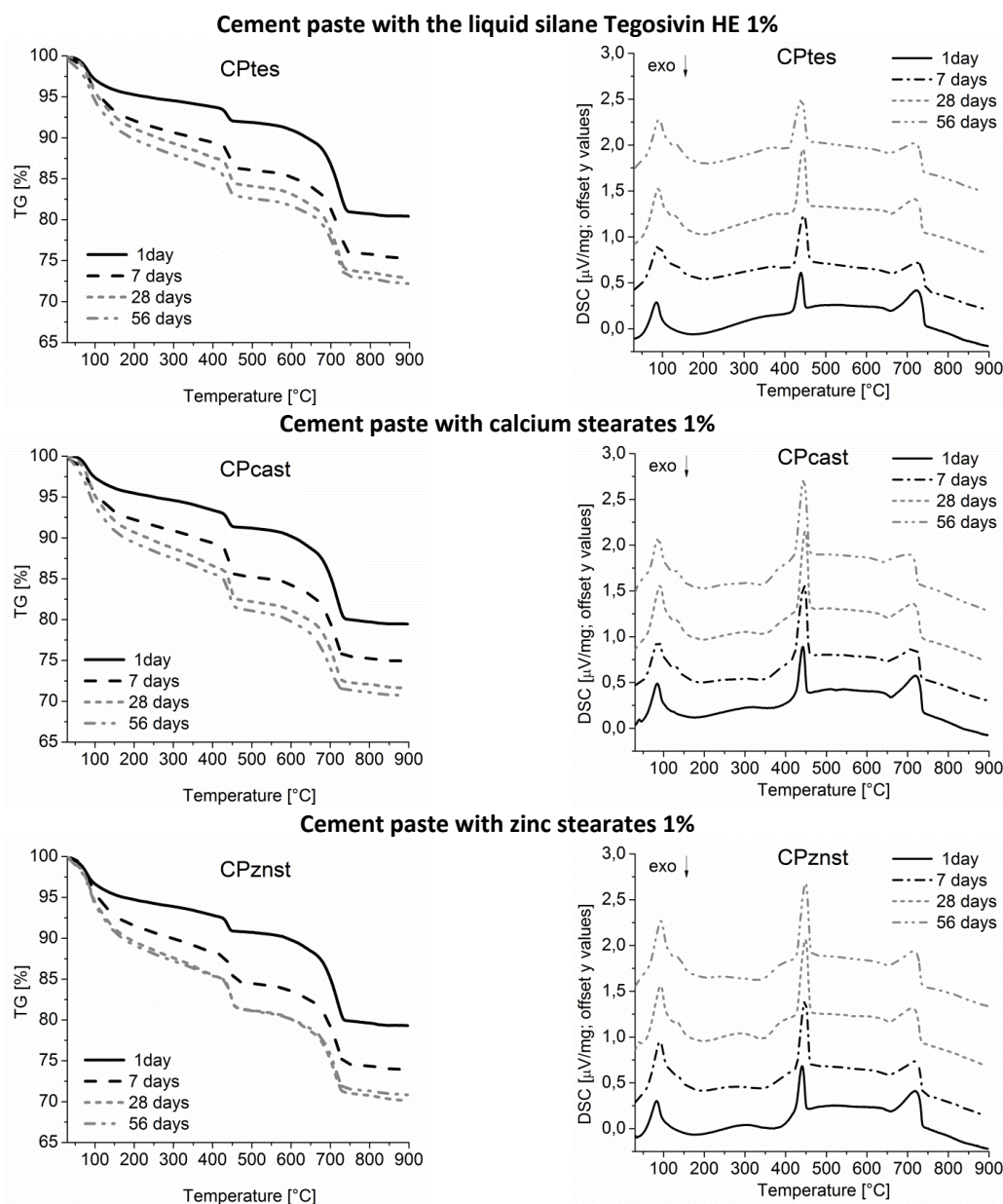


Table 3.2 4 TG-DSC curves of the limestone cement pastes after 1, 7, 28, 56 days of hydration



3.2.1.3 FT-IR study of limestone cement pastes

Table 3.2 5 lists the main absorption found while Figure 3.2 4 shows the FT-IR spectra of the limestone cement paste CPA (without water repellents) registered at different hydration times and Figure 3.2 5 shows the comparison of different spectra obtained after 0, 1, 7, 28, 42, 56 days in the $4000\text{--}2000\text{ cm}^{-1}$ and $1300\text{--}700\text{ cm}^{-1}$ ranges.

Calcium carbonate and silicates were present since the beginning.

The broad peaks of water at 3400 cm^{-1} and around 1600 cm^{-1} (due to the ν_2 frequency corresponding to H_2O typical of hydrated phases) increased after 7 days, during the hydration. After 1 days the presence of calcium hydroxide was detected. The other main feature of the hydrated PCA was the displacement of the stretching mode Si-O-Si from 915 cm^{-1} in the

anhydrous cement mix to around 1000 cm^{-1} in the samples collected after 24 hours, due to the production of silicate and aluminate hydrates⁷.

In the admixed samples the presence of calcium carbonate in all samples was confirmed by the strong bands at 1480 cm^{-1} , 875 cm^{-1} and 712 cm^{-1} , while the absorption bands at $1100\text{--}900\text{ cm}^{-1}$ were related to silicates. No peaks related to the presence of gypsum in the anhydrous cement or to ettringite in the hydrated cement were visible, probably they were covered by the stronger peaks of silicates⁸. PCcast and PCznst showed also sharp peaks of --CH_2 stretching at 2920 cm^{-1} and 2850 cm^{-1} which did not change during the hydration⁹.

In presence of different water repellent admixtures, the --OH stretching peak of calcium hydroxide and the peaks of the silicate hydrates appeared at different times and have different intensities. PCA showed a strong --OH stretching absorption after 28 days, while the pastes added with silane PC750, PCSil, PCTes and in particular PC730 showed a sharp --OH absorptions at 3645 cm^{-1} after 1 or 7 days. The pastes added with stearates PCcast and PCznst showed --OH absorptions similar to PCA.

The silicates peaks at 970 cm^{-1} grew in a similar way for all samples, with particular strong intensity for PCznst after 56 days.

Table 3.2 5 Main FT-IR absorptions observed during the hydration of limestone cement pastes

Frequency	Absorption	Compound	Observations
3640 cm^{-1}	$\nu\text{--OH s}$	Calcium hydroxide	The peak appeared after 1 day in PCA and increased during the hydration.
3400 cm^{-1}	$\nu\text{--OH br}$	Water	Increased during the hydration.
$2930;2850\text{ cm}^{-1}$	$\nu\text{--CH s}$	Aliphatic stretching	the peaks were visible only for the admixed pastes and were due to the organic chains of the water-repellent admixtures. The peak remained unchanged during the hydration.
1600 cm^{-1}	$\delta\text{--OH sh}$	Constitutive water	The peak increased with time due to the formation of hydrated compounds.
1436 cm^{-1}	$\nu\text{--CO}_3\text{ s}$, strong	Calcium carbonate	Calcium carbonate was present since the beginning and remained quite constant during the hydration in comparison to the other peaks.
$957; 812; 668; 537\text{ cm}^{-1}$	ν and δ Si-O-Si or Al-O	C-S-H C-A-H	In particular, the 957 cm^{-1} peak could be due to the Si-O-Si stretching or to the Al-O vibration (together with the peaks at 812 cm^{-1} , 668 cm^{-1} , 537 cm^{-1}) associated to hexagonal aluminate hydrates and ettringite
915	$\nu\text{ Si-O-Si s}$	C_3S	Decreased during the hydration.
875 cm^{-1}	$\delta\text{--CO}_3\text{ s}$	Calcium carbonate	See above 1436 cm^{-1} .
712 cm^{-1}	$\delta\text{--CO}_3\text{ s}$	Calcium carbonate	Increased during the hydration.

⁷ Trezza, M.A, A.E Lavat, 2001

⁸ Pajares, I., *et al*, 2003; Trezza, M.A, A.E Lavat, 2001

⁹ Adediran Mesubi, M. 1982, Pages 61-71

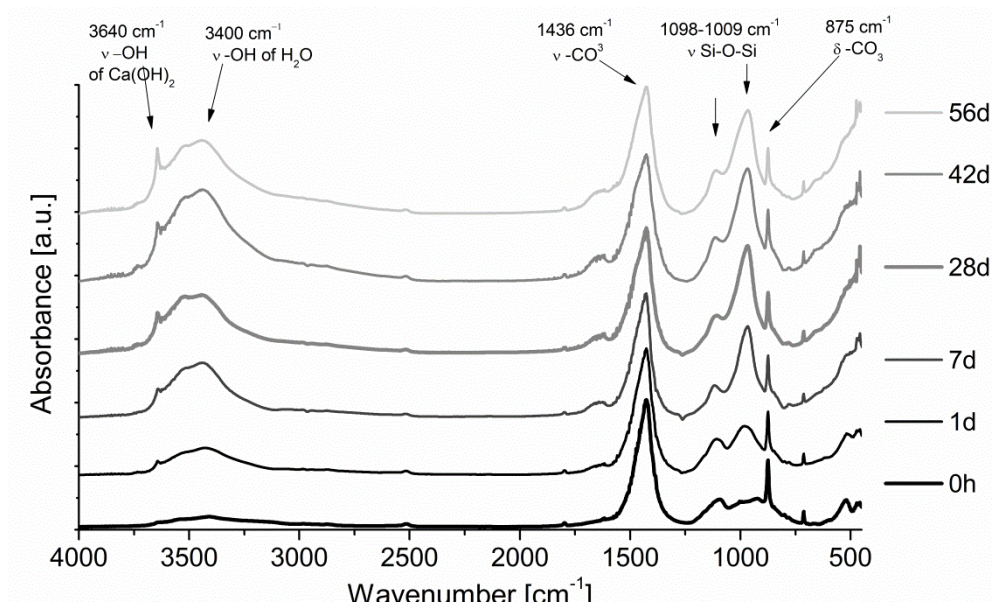


Figure 3.2 4 FT-IR spectra of CPA, without water-repellents after 0, 1, 7, 28, 42 and 56 days of hydration

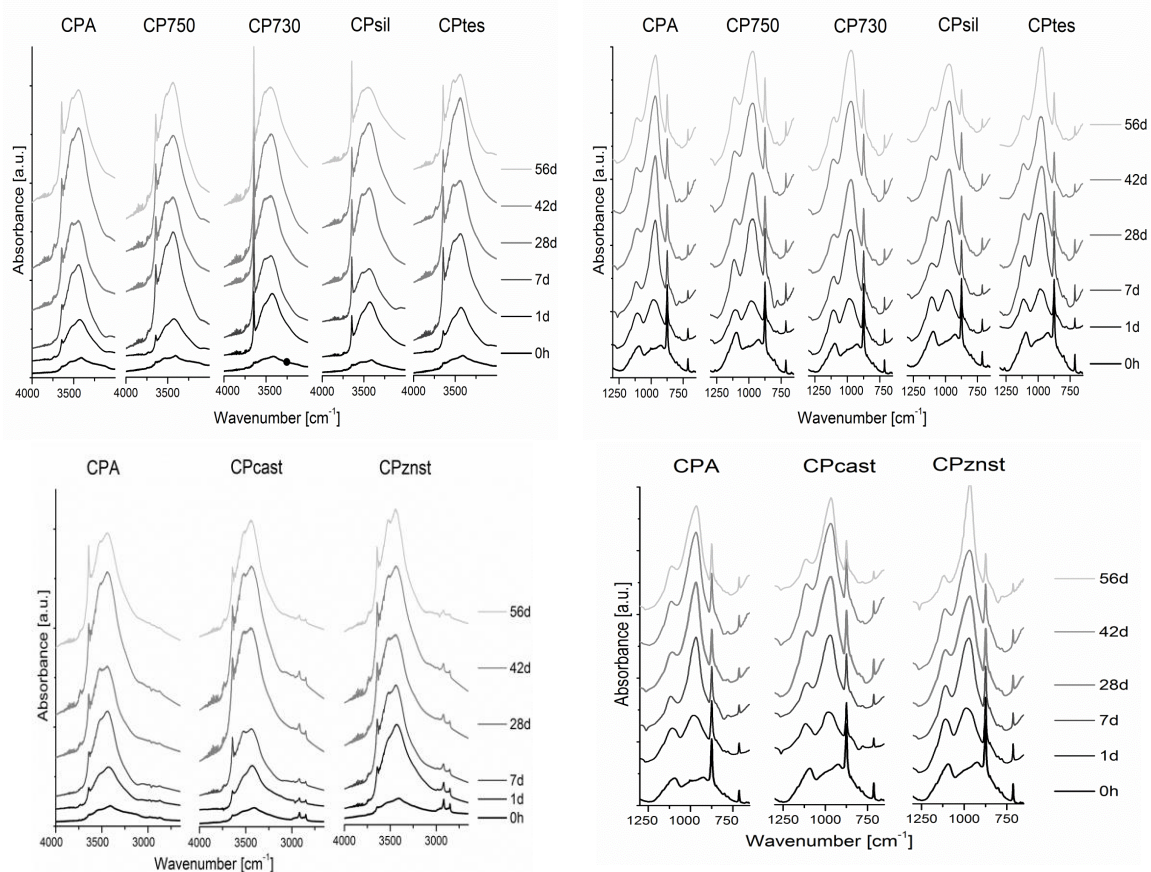


Figure 3.2 5 FT-IR spectra of the limestone cement pastes admixed with water-repellents, the figures show the comparison of different spectra obtained after 0, 1, 7, 28, 42, 56 days at 4000-2000 cm^{-1} (left) and 1300-700 cm^{-1} (right)

3.2.1.4 SEM observations of limestone cement pastes

The morphologies of cement paste samples can be studied thanks to SEM observation. This technique is commonly used to study the hydration reaction of cements. Different morphologies of C-S-H have been identified by the researcher thanks to SEM observations. Furthermore different crystal phases present in the pastes can be observed with SEM, such as ettringite or aluminate hydrates. Table 3.2 6 give a short description of the common morphology of the main hydration products of Portland cement¹⁰.

Table 3.2 6 CSH Morphologies observed by SEM observation as described by V.S. Ramachandran, 1997

	Product	Morphology
amorphous	C-S-H gel	Type I. Elongated or fibrous particles, occurs at early ages Type II. Honey-combed structure, does not normally occurs, unless it is formed in the presence of admixtures Type III. Equant or flattened particles (under 100nm in largest dimension) Type IV. Compact and dimpled, it is a late hydration products that form within the volume of the original cement grain
crystalline	CH	Thin hexagonal plates of size tens of micron across.
	Ettringite	Relatively long rods with parallel sides and no branching
	Monosulphate hydrate/ hexagonal calcium aluminate hydrate	Thin hexagonal plates (1000nm by 1000nm)

After 28 days of hydration the structures seemed similar for the different pastes at low magnifications (200X), but P750, PC730, PCSil had a more compact matrix and a higher presence of elongated grain and flat platelets. At higher magnification was possible to observe differences in the pastes structures (Table 3.2 7; Table 3.2 8).

- After 7 days the reference paste CPA was characterized by the presence of partially hydrated cement grains covered with acicular C-S-H of Type I (EDX analysis pointed out the presence of Si and Ca) and well shaped hexagonal portlandite crystals (only Ca, O and C were detected by EDX). Rods with parallel sides, recognizable as ettringite were also present (Si, Ca, S, Al were found in correspondence of the rods). The pastes with silanes CP750, CP730, CPSil and CPtes showed more complex structures with flat-layered structure due probably to a fast formation of aluminate hydrates, together with the acicular C-S-H gel and hexagonal crystal of CH. CPcast and CPznst were similar to CPA, but less portlandite crystals and more rods of ettringite were visible.
- After 28 days (Table 3.2 7) the structure of CPA became denser and compact, the C-S-H gel grew and covered the clinker grains completely. The mixes with silane siloxanes were still characterized by the presence of the aluminates and a high presence of C-S-H gel. When stearates were added (CPcast or CPznst) the structure was similar to CPA, with higher presence of ettringite also after 28 days.
- After 56 days (Table 3.2 8) CPA had a dense structure mainly composed of C-S-H acicular gel and the presence of flat sheets of aluminate hydrates was observed. CP750, CP730, CPznst showed an irregular structure where some of the flat platelets were still visible together with short C-S-H acicular structures. CPSil, CPtes, CPcast had also compact structure with highly interconnected C-S-H acicular gel.

¹⁰ Ramachandran V.S., 1997

Beside observing the proceeding of the hydration reactions, SEM observation allowed also to see the grains of carrier when a silane supported on an inorganic carrier was added to the paste (CP750, CP730, CPsil) (Figure 3.2 6). Some spherical grains of carrier (calcium carbonate) were visible in the paste CP730 after 7 days, but disappeared for longer times of hydration, probably the carrier was directly involved in the hydration reaction, maybe also in the formation of hemicarbonate and monocarbonate AFm phases. In CP750 and CPsil, after 56 days, the spherical grains of amorphous silica used as carrier were visible, but covered by hydration products¹¹. The presence and distribution of steirates inside the limestone cement pastes was more difficult to define, but thanks to EDX mapping was possible to observe a higher presence of carbon and zinc in correspondence of pore walls (Figure 3.2 7).

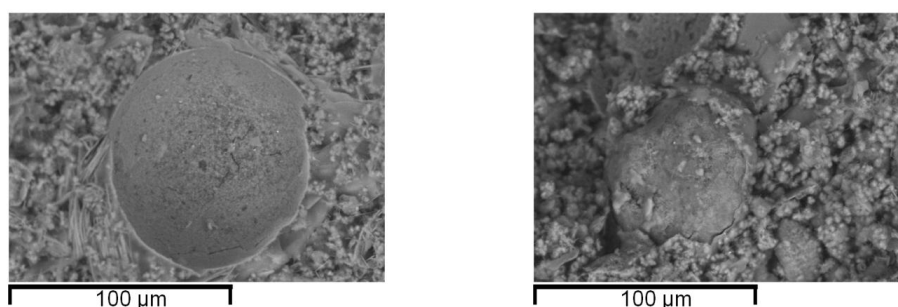


Figure 3.2 6 Grains of carrier in the cement pastes CP730 and CPsil after 7 days of hydration – Secondary electron images (1000X). Links CP730, right: CPsil

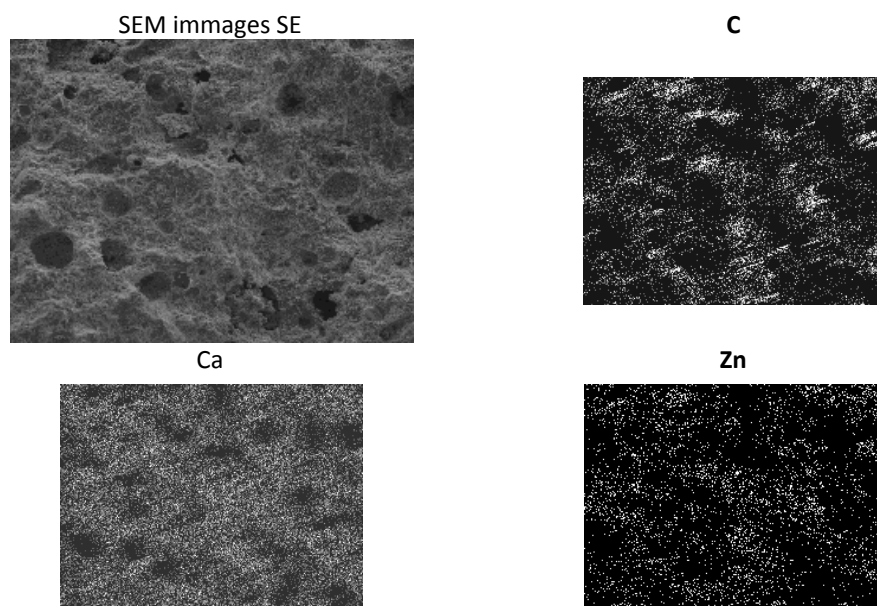


Figure 3.2 7 SEM images and relative EDX elemental mapping of PCznst (100X)

¹¹ Silica might have an effect similar to fly ashes, which are able to enhance the reactivity as inert filler (provision of additional nucleation sites on the surface of the filler; increase of the effective water to cement ratio) and as active pozzolanic material (change of particle packing). Deschner, F. *et al.* 2012; Shayan, A. *et al.*, 1996; Torii, K. *et al.* 1994; Fraay, A.L.A. *et al.* 1989; De Weerd, K. M. *et al.* 2011

**Table 3.2 7 Cement pastes after 28 days of hydration –Secondary electron images (5000X)
Without admixtures**

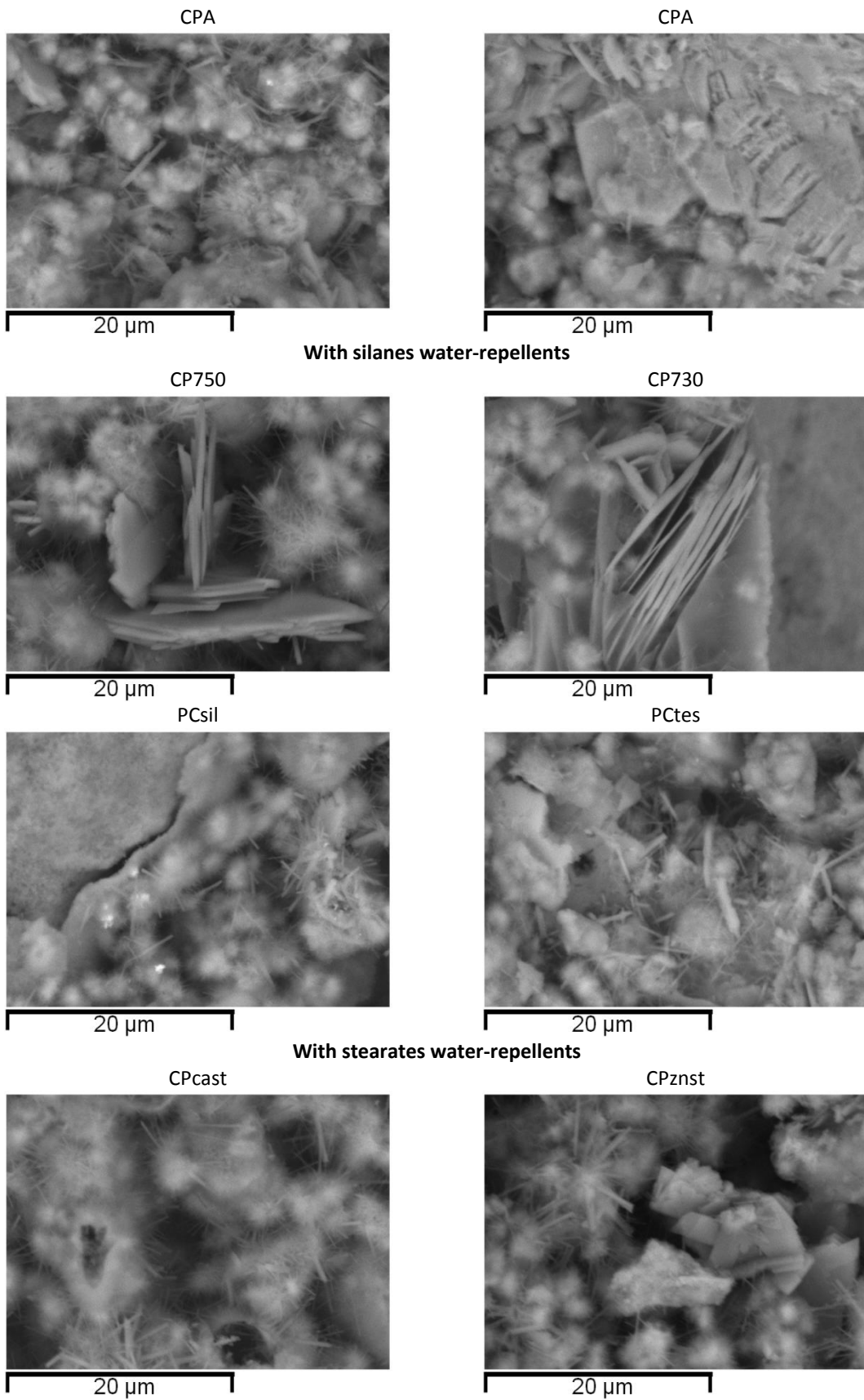
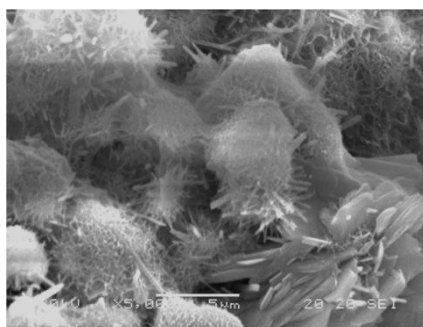


Table 3.2 8 Cement pastes after 56 days of hydration –Secondary electron images (5000X)
Without admixtures

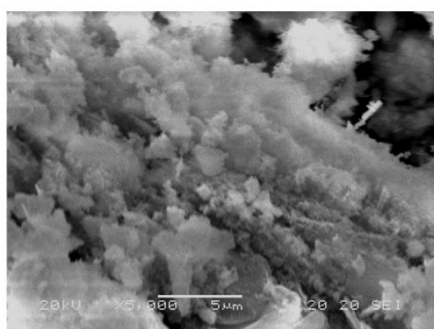
CPA



20 μm

With silanes water-repellents

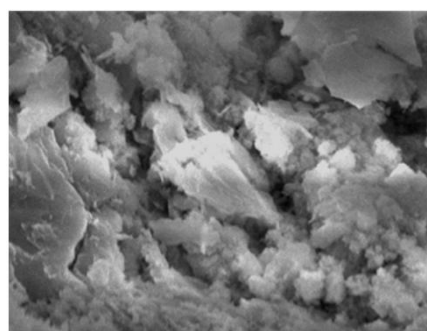
CP750



20 μm

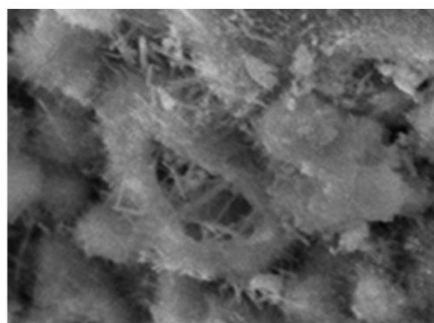
PCsil

CP730

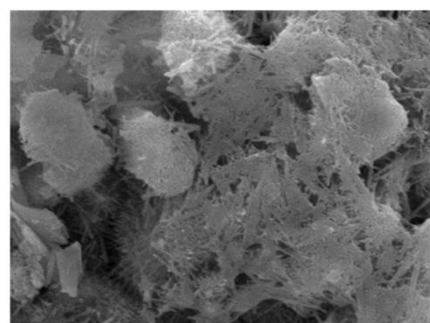


20 μm

PCtes



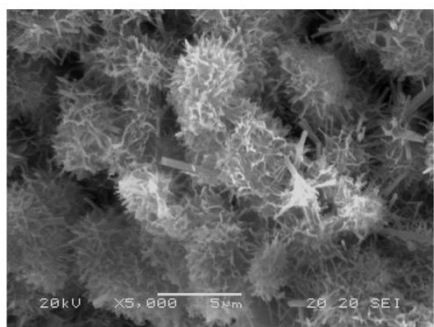
20 μm



20 μm

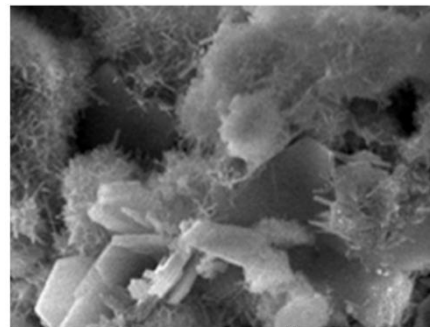
With stearates water-repellents

CPcast



20 μm

CPznst



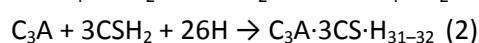
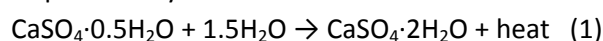
20 μm

3.2.1.5 Iso-calorimetric measurements

Some of the cement pastes were analyzed also with conduction calorimetry to better follow the setting process. The hydration and setting of limestone cements are exothermic processes: measurements of the total heat and rate of heat development provides information on the kinetics and mechanism of hydration. Figure 3.2 8 shows the typical variation of the rate of heat evolution (measured as thermal power) versus hydration time up to 50 hours obtained from the conduction calorimeter¹².

The initial reaction and the induction period last around 4 hours, after then the main peak of heat evolution and a period of deceleration was seen.

The initial reaction was due to the release of Ca^{2+} and OH^- ions, as soon as the cement came into contact with water and also to the hydration of calcium sulphate hemihydrates to calcium sulphate dihydrate and to the formation of ettringite (see equation 1 and 2).



The calorimetric curves of water repellent pastes differed in the acceleratory period, during which the rate of hydration should be controlled by the rate of C–S–H formation:

-PCA started the acceleration period after 4 hours and reach the maximum rate of heat after 16 hours;

-PCcast, PC750, PCtes showed a slightly faster acceleration;

-PCsil showed a slightly slow acceleration;

-PCznst began the acceleration period after 6 hours and reached the maximum heat-rate after 19 hours, showing a slow setting.

After 25-30 hours (after the main hydration peak) a weak and broad shoulder appeared before the end of the deceleration period. Ylmén¹³ observed a similar, but less distinct, shoulder in some Portland cements and attributed it to the dissolution of aluminate phases e.g. C_3A , which become reactive at this stage due to reduction in sulphate concentration in the pore solution. The sulphate concentration is higher and block aluminate dissolution, and then decrease and allows for C_3A dissolution and subsequent formation of ettringite.

The siloxanes might have a slight accelerating effect due to the presence of silanolic acid groups able to accelerate the hydration of the C-S-H phases. While calcium stearates might have an accelerating effect due to a higher calcium ions release in the pore solution, and to a shorter induction period and a faster crystallization of calcium hydroxide (responsible of the heat release during the acceleratory period).

The retarding effect due to the addition of zinc stearate is probably due to the presence of the heavy metal ions zinc, whose retarding effect is known and described in the literature¹⁴. The nucleation and growth of C-S-H gel determines the rate of early hydration of the alite present in Portland cement. In addition to C-S-H gel, crystalline portlandite, $\text{Ca}(\text{OH})_2$, is precipitated from a supersaturated solution containing Ca^{2+} and OH^- ions. The rate at which the relevant ionic species are made available at the surfaces of the alite grains controls the rate of reaction and hence the setting time of the cement. Heavy metal ions, such lead and zinc ions, cause

¹² Banfill, P., *et al.* 2007; Bensted J. 1980; Taylor H.F.W. 1997

¹³ Ylmén, R. *et al.* 2010

¹⁴ Weeks, C. *et al.* 2008. Further information about the influence of heavy metal ions on cement hydration will be given also in paragraph 3.2.5 Discussing the results: the reaction mechanisms

retardation of set either because they form insoluble zinc or lead hydroxides at high pH which coat the surface of the cement grains preventing their hydration, or because the formation of calcium hydroxy-zincate ($\text{CaZn}_2(\text{OH})_6 \cdot 2\text{H}_2\text{O}$) occur during the retardation period. This consumes both calcium and hydroxide ions, which would be removed from solution, thereby delaying the normal cement hydration process .

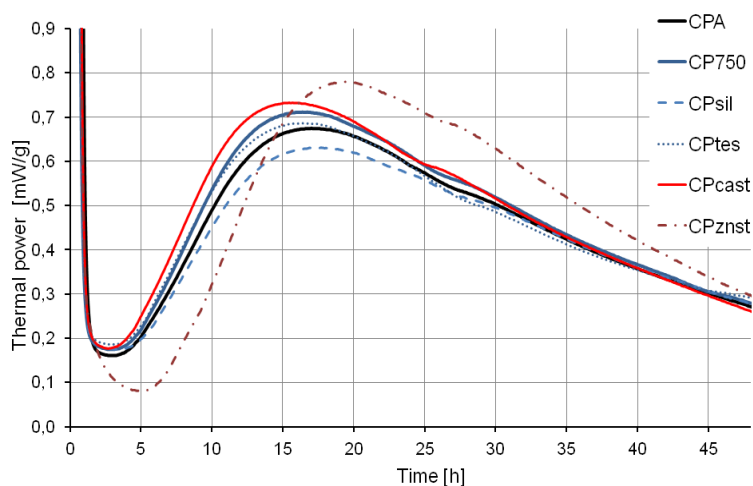


Figure 3.2 8 variation of the rate of heat evolution versus hydration time up to 50 hours for limestone cement pastes without (CPA) or with 1% of water repellent (CP750, CPsil, CPtes, CPcast, CPznst).

3.2.2 NATURAL HYDRAULIC LIME PASTES WITH WATER-REPELLENTS

Table 3.2 9 shows an overview of the pastes prepared with natural hydraulic lime as binder. NHLA can be considered as a reference paste because was prepared without water repellents.

Table 3.2 9 Mix design of natural hydraulic lime pastes

Paste names	Binder	additive	additive class	Additive (%)	w/b ratio
NHLA	NHL3,5	-	-	-	0.7
NHL750	NHL3,5	Sitren p750	powder silane	1	0.7
NHL730	NHL3,5	Sitren p730	powder silane	1	0.7
NHLsil	NHL3,5	SilresA	powder silane	1	0.7
NHLcast	NHL3,5	Ca Stearate	metal soap	1	0.7
NHLznst	NHL3,5	Zn stearate	metal soap	1	0.7

3.2.2.1 XRD Study of natural hydraulic lime pastes

XRD analysis of samples collected at different time from NHLA allowed to observe the hydration mechanism of the natural hydraulic lime binder (Figure 3.2 9). In this case the hydration was followed till three months (84 days) because natural hydraulic limes had usually higher percentages of Iarnite, i.e. di-calcium silicates and tend to have longer hydration times in comparison to cements¹⁵.

¹⁵ Gulotta, D. *et al.*,2013; Lanas, J. *et al.*,2004

After few minutes of hydration of NHLA, without admixtures, was possible to recognize calcite, portlandite, quartz, and di-calcium and tri-calcium silicates (0 h in Figure 3.2 9). In the natural hydraulic lime studied the high presence of portlandite and calcite, in comparison to larnite, led to suppose that the NHL was prepared at low temperature (less than 1200°C) or that part of the calcite have been added in a second moment as a filler.

During the hydration reaction of NHLA, C_2S and C_3S phases were consumed and their peaks in the 31-34° 2θ range diminished and almost disappeared after 56 and 84 days. A little presence of gehlenite (C_2AS), another typical phase component of NHLs have been identified (major peak at 23.8° 2θ) from the 21 days, but was not clearly visible and weak. Calcium aluminium-silicates similar in composition to gehlenite can also have been present but difficult to detect with XRD because poorly crystalline¹⁶. Instead, after 5 hours of hydration, NHLA showed a new strong peak at 11° 2θ identified as calcium aluminium oxide carbonate hydrate ($Ca_8Al_4O_{14}C O_{2.24}H_2O$) which is transformed at longer times (7-14 days) in Calcium aluminium hydroxide carbonate hydrate ($Ca_4Al_2(OH)_{12}(CO_3)(H_2O)_5$), identified by the major peak at 11,8° 2θ . The high presence of calcium carbonate in the system probably stabilized this kind of phases, instead of more common aluminium-silicates, such as gehlenite, that appear only after 21 days.

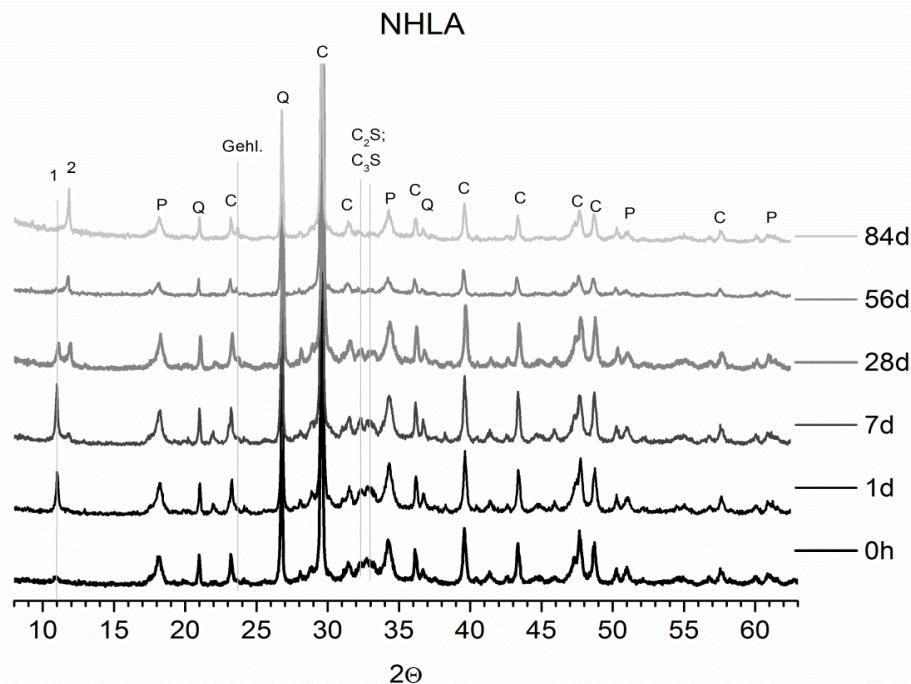


Figure 3.2 9 XRD patterns of samples collected from NHLA paste at 0, 1, 7, 28, 56, 84 days; 1= calcium aluminium oxide carbonate hydrate $Ca_4Al_2O_6 \cdot CO_3 \cdot 11H_2O$, 2=Calcium aluminium oxide hydroxide carbonate hydrate ($Ca_4Al_2(OH)_{12}(CO_3) \cdot 5H_2O$), Gehl= gehlenite; P=portlandite, Q=quartz, C=calcite, C_2S =larnite; C_3S =halite.

The XRD patterns of natural hydraulic lime pastes without and with water repellents are compared in the 10-25° 2θ , and slightly differences can be observed (Figure 3.2 9). No particular differences were seen in comparison to NHLA XRD spectra, and mainly related to the kinetic. It was possible to divide the pastes with siloxanes from the ones with stearates in order to observe common trends in each group:

¹⁶ See Chapter I, Paragraph 1.4.2. Chemical and physical aspects of hydraulic binders; and M.J. Varas, et al., 2005.

-when the siloxane Silres A was present the calcium aluminium oxide carbonate hydrate (labelled as 1 in the patterns) is formed after 1 days (instead of 5 hours as in NHLA) and was quickly transformed in calcium aluminium hydroxide carbonate hydrate, which prevailed at 14 days and remained alone at 56 days (in NHLA calcium aluminium oxide hydrate was still present after 56 days);

- both calcium and zinc stearates slightly slowdown the production of monocarbonates (calcium aluminium hydroxide carbonate hydrate) and the hydration of the silicates (larnite and halite); a higher presence of gehlenite ($\text{Ca}_2\text{Al}_2\text{SiO}_7$) instead of monocarbonates ($\text{Ca}_4\text{Al}_2(\text{OH})_{12}(\text{CO}_3)(\text{H}_2\text{O})_5$) was observed in NHLcast and NHLznst.

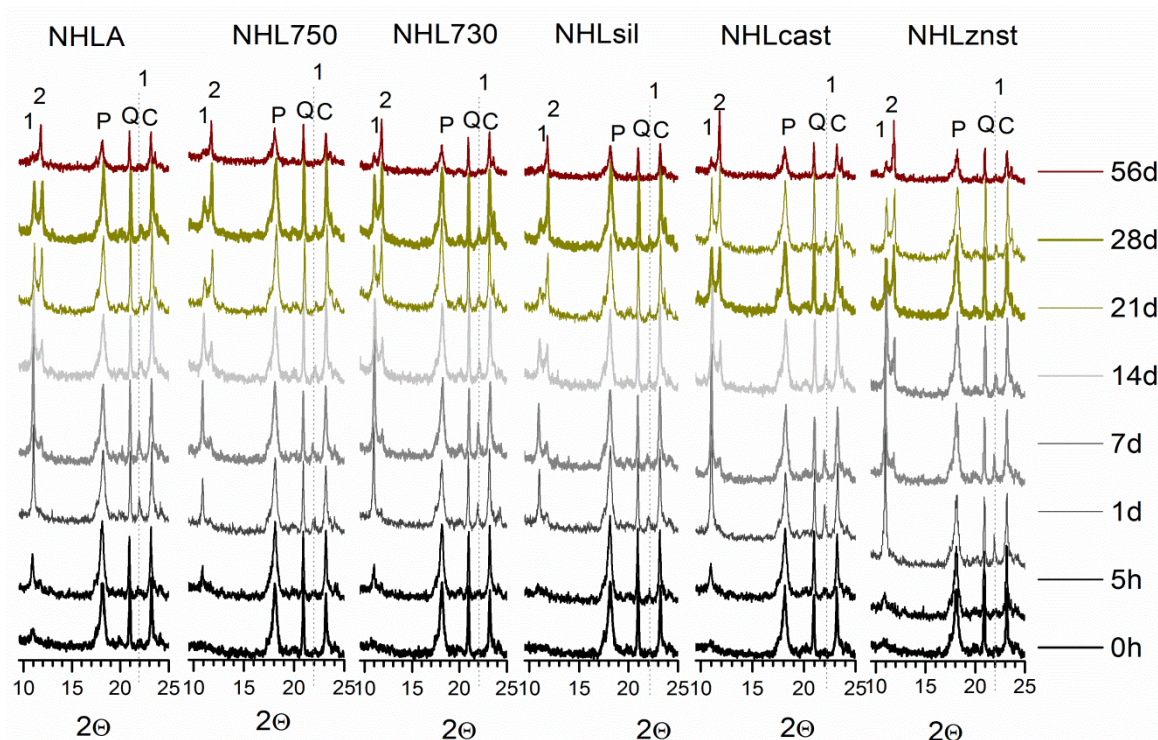


Figure 3.2.10 Comparison of the XRD patterns in the 9° - 13° 2θ range registered for the natural hydraulic lime pastes fresh and after 5 hours, 1, 7, 14, 21, 28, 56 days of hydration. 1= calcium aluminium oxide carbonate hydrate $\text{Ca}_4\text{Al}_2\text{O}_6\cdot\text{CO}_3\cdot 11\text{H}_2\text{O}$, 2=Calcium aluminium oxide carbonate hydroxide hydrate ($\text{Ca}_4\text{Al}_2\text{O}_6(\text{CO}_3)_{0.5}(\text{OH})\cdot 11.5\text{H}_2\text{O}$), Gehl= gehlenite; P=portlandite, Q=quartz, C=calcite.

3.2.2.2 TG-DSC Study of natural hydraulic lime pastes

The influence of water-repellent admixtures on the hydration reaction of natural hydraulic lime was further evaluated by TG-DSC analyses. The collected data at 0, 1, 7, 28 and 56 days are shown in Table 3.2.10 and Table 3.2.11.

As seen for cement pastes, also NHLs pastes were characterized by three major mass losses associated with endothermic transformations between 40 and 900°C. And also in this case the transformation were related to:

- the loss of absorbed and linked water, also from the hydrated compounds, till 200°C;
- the loss of water due to the dehydration of calcium hydroxide, from 350°C to 500°C, which was present from the beginning but increased further with the hydration in all pastes studied¹⁷;

¹⁷ The hydration of the C_3S and C_2S produce also calcium hydroxide which dehydrated at 380°-500°C

-the loss of carbon dioxide due to the de-carbonation of calcium carbonate, in the 600-800°C range and which remained quite constant during the hydration..

The first step, related to the loss of water absorbed and linked to different compound, was the result of different reactions, as suggested also by the different convoluted DSC peaks (see also Figure 3.2 11). The first part of the mass loss was due to moisture, while the second part, from 100°C to 200°C was due to the dehydration of silicate and aluminate hydrates. This second part increased with the hardening time and with the formation of hydrated compounds¹⁸, such as aluminium carbonates (DSC peak centred at 100°C), and silicate hydrates (DSC peak centred around 130°C). After 28 days, the peak of the silicates was already preponderant and covered the first one in NHLA, NHL750, NHLsil, NHLznst, while the two different peaks were both visible in NHL730 and NHLcast, due probably to a hydration delay.

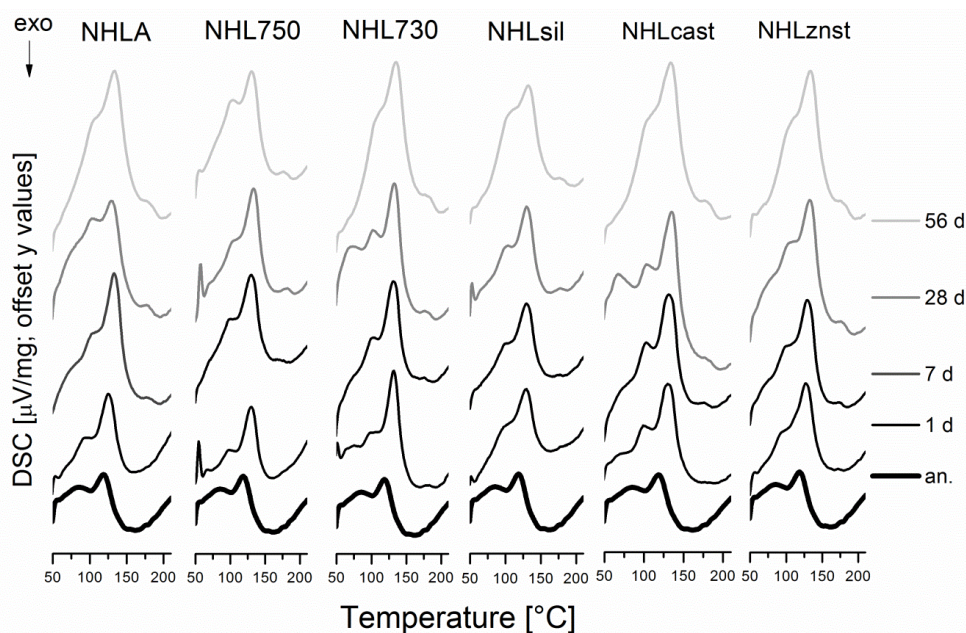


Figure 3.2 11 comparison of DSC curves of samples collected at 0, 1, 7, 28 and 56 days in the 50-200°C range

Three ranges, corresponding to the three reaction describe above, were considered for the quantitative calculation of the compounds: Loss of total water (TW) 80-200°C; dehydration of calcium hydroxide ($\text{Ca}(\text{OH})_2$) 350-500°C and de-carbonation of CaCO_3 (CaCO_3) 600-800°C (Table 3.2 10). The quantitative results are listed in Table 3.2 10.

The total water increased during the hydration because higher percentages of hydrated compound were formed. It was possible to notice that NHLA, paste without additives, had a high production of hydrate compounds in the first seven days (from 0.7% to 3.3%) after than lower amount of bound water were detected, even if the hydration was proceeding and the total amount still increased. The same trend have been observed for NHLA in the second range (350-500°C): while the hydration goes further di-calcium and tri-calcium silicates reacted producing $\text{Ca}(\text{OH})_2$. In the same ranges, the curves of the admixed pastes showed a lower but more constant increasing. At early ages and till 7 days a lower production of hydrated compounds and calcium hydroxide have been noticed (in particular NHL750 or NHLsil, NHLcast, NHLznst).

High amount of hydrated compound have been calculated only at 28 days for all the admixed paste, therefore the hydration was shifted and slowed down in comparison to NHLA. In

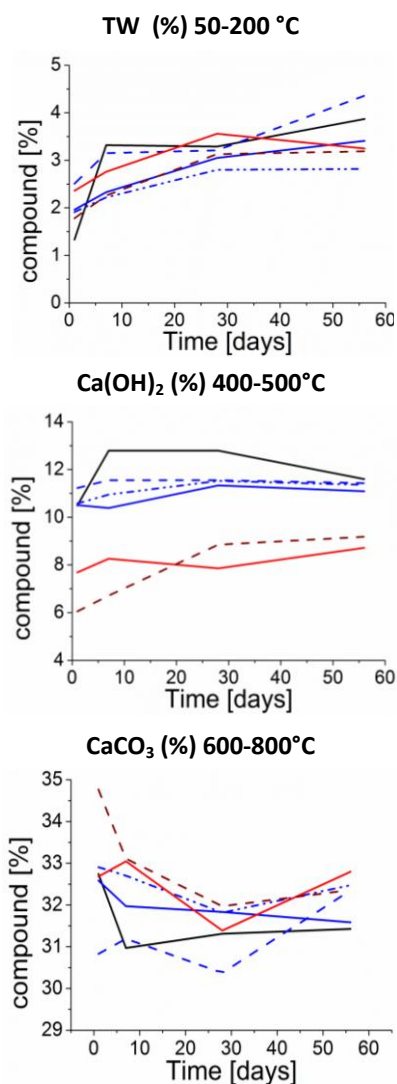
¹⁸ Ramachandran, V.S, 2003, pp 111

particular, when calcium or zinc stearate were added we observed also the inhibition of the formation of portlandite.

The amount of calcium carbonate remained quite stable for all the sample analysed with meaningless variation. It decreased in the first months while the hydrated products and calcium hydroxide increased, and increased at 56 days maybe due to a partial carbonation of the samples.

Table 3.2 10 Comparisons of the amount of water, calcium hydroxide, and calcium carbonate at 1, 7, 28, 56 days for the different natural hydraulic lime pastes.

sample name	Tbw (%)	Ca(OH) ₂ (%)	CaCO ₃ (%)
	90-200	350-500	600-800
NHLA0d	0,7	10,8	33,8
NHLA1d	1,3	10,5	32,7
NHLA 7d	3,3	12,8	31,0
NHLA 28d	3,3	12,8	31,3
NHLA 56d	3,9	11,6	31,4
NHL750 1d	2,0	10,5	32,6
NHL750 7d	2,3	10,4	32,0
NHL750 28d	3,1	11,3	31,8
NHL750 56d	3,4	11,1	31,6
NHL730 1d	2,5	11,2	30,8
NHL730 7d	3,2	11,6	31,2
NHL73028d	3,2	11,6	30,4
NHL73056	4,4	11,4	32,4
NHLsil 1d	1,9	10,6	32,9
NHLsil 7d	2,2	10,9	32,7
NHLsil 28d	2,8	11,5	31,8
NHLsil 56 d	2,8	11,4	32,5
NHLcast 1d	2,4	7,7	32,7
NHLcast 7d	2,8	8,3	33,0
NHLcast28d	3,6	7,9	31,4
NHLcast56	3,3	8,7	32,8
NHLznst 1d	1,8	6,1	34,8
NHLznst 7d	2,3	6,7	33,1
NHLznst 28d	3,1	8,9	32,0
NHLznst 56d	3,2	9,2	32,4



— A
 — P750 — P730 — silres — tegosivin
 — Cast — znst

Table 3.2 11 TG-DSC curves of natural hydraulic lime paste with water-repellent additives 1% by mass at different hydration times (0, 1, 7, 28, 56 days)

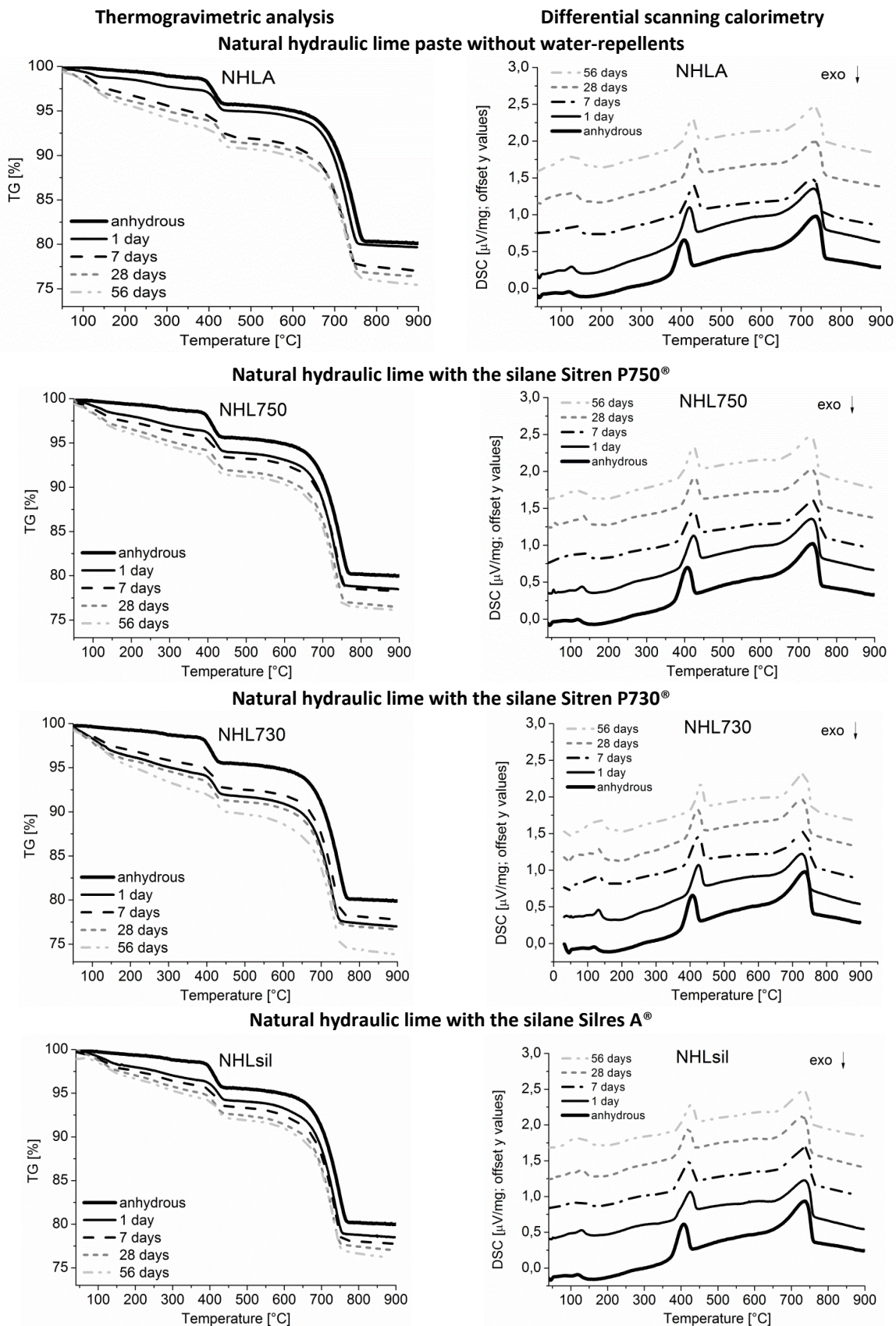
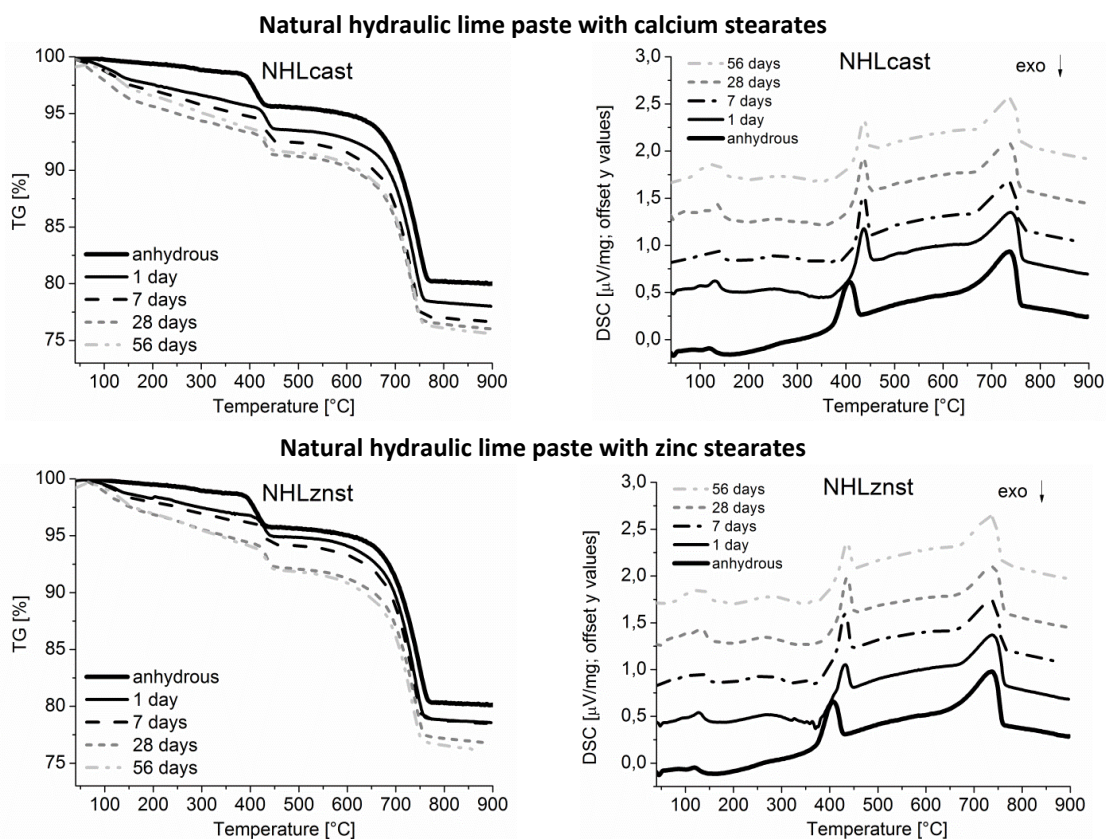


Table 3.2 12 (follow from the previous table) TG-DSC curves of natural hydraulic lime paste with water-repellent additives at different hydration times (0, 1, 7, 28, 56 days)

3.2.2.3 FT-IR study of natural hydraulic lime pastes

Table 3.2 13 summarize the major FT-IR absorptions observed in the samples and the relative compounds. The FT-IR analysis of the paste NHLA, without water repellents is shown in Figure 3.2 12, while Figure 3.2 13 shows the FT-IR spectra of the admixed pastes in the $1150\text{--}750\text{ cm}^{-1}$ range.

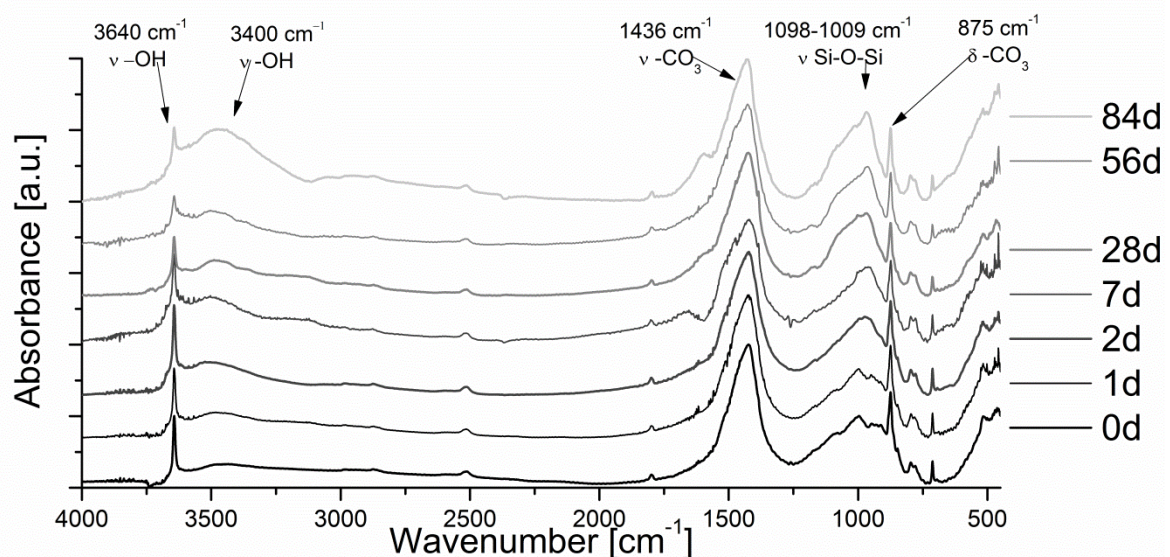
At early ages peaks calcium hydroxide, calcium carbonate and silicates were always present. While the hydration reactions went further the carbonates remained quite constant, confirming that no further carbonation occurred. But the major differences were seen in the $1150\text{--}750\text{ cm}^{-1}$ region where the silicates and aluminates absorbed: in NHLA samples after 7 days the absorptions due to the anhydrous silicates decreased and were covered by the stronger peaks of C-S-H. The shoulder at 1000 cm^{-1} , due to C_2S and still visible after 56 days, confirmed that the hydration of C_2S took place slowly¹⁹. Calcium silicates were also present as lower peaks in a secondary region in which carbon of calcite vibrates as well ($2930\text{--}2920\text{ cm}^{-1}$ and $2855\text{--}2850\text{ cm}^{-1}$) and are more visible after one month. When water-repellent admixtures were added minor differences can be seen in the peak intensity of the $1150\text{--}750\text{ cm}^{-1}$ region (Figure 3.2 13). –In NHL750 and NHLsil the absorption due to C-S-H (950 cm^{-1}) became higher than the absorption of C_2S only after 28 days, while the absorption at 1087 cm^{-1} was still visible after 7 days, indicating a slight slowdown of the hydration reactions.

¹⁹ Lanas, J., et al. 2004

- When Sitren P730® (silane supported on calcium carbonate) was added the peak at 950 cm^{-1} was higher in comparison to 998 cm^{-1} after 28 days due to an enhanced hydration.
- With calcium and zinc stearates a general slowdown of the hydration was observed: the absorption at 950 cm^{-1} remained low also after 56 and 84 days and the shoulder at 1100 cm^{-1} was still visible after 56 and 84 days. Moreover it was possible to observe a shoulder at 850 cm^{-1} after 28 and 56 days of hydration, due to the presence of anhydrous C_2S and gehelenite.

Table 3.2 13 Main FT-IR absorptions of natural hydraulic lime pastes

Frequency	Absorption	compound	Observations
3640 cm^{-1}	$\nu\text{-OH s}$	Calcium hydroxide	The peak increased during the hydration.
3400 cm^{-1}	$\nu\text{-OH br}$	Water	Increased during the hydration.
$2930;2850\text{ cm}^{-1}$	$\nu\text{-CH s}$	Aliphatic stretching	the peaks were visible only for the admixed pastes and were due to the organic chains of the water-repellent admixtures. The peak remained unchanged during the hydration.
1600 cm^{-1}	$\delta\text{-OH sh}$	Constitutive water	The peak increased with time due to the formation of hydrated compounds.
$1436\text{ cm}^{-1}; 875\text{ cm}^{-1}$	ν and $\delta\text{-CO}_3\text{ s}$, strong	Calcium carbonate	Calcium carbonate was present since the beginning and remained quite constant during the hydration in comparison to the other peaks.
$1087\text{ cm}^{-1}; 797;779\text{ cm}^{-1}$	ν and $\delta\text{ Si-O-Si br}$	Quartz	The broad peak centred at 1087 cm^{-1} and doublet visible at $797\text{-}779\text{ cm}^{-1}$ were typical of quartz (detected also by XRD analysis) and remained stable during the hydration ²⁰ .
$998; 850$ and $930; 908\text{ cm}^{-1}$	ν and $\delta\text{ Si-O-Si s}$	Anhydrous silicates	the bands at 850 and 998 cm^{-1} were attributed to anhydrous C_2S ; the bands at 930 cm^{-1} , 908 cm^{-1} were attributed to anhydrous C_3S ²¹ . These bands decreased and were covered by the C-S-H absorption peak during the hydration.
965 cm^{-1}	$\nu\text{ Si-O-Si br}$	C-S-H	The broad peak due to silicate and aluminate hydrates increased during the hydration.
850 cm^{-1}	$\delta\text{-Al-O}$		Appeared at 7 days of hydration in NHLA. Might be due to the presence of gehelenite and C_3A .

**Figure 3.2 12 FT-IR spectra of NHLA, without admixtures at different hydration times: 0, 1, 2, 7, 28, 56, 84, days**²⁰ Varas, M.J. M. Alvarez de Buergo, R. Fort, 2003²¹ Taylor, H.F.W. 1997

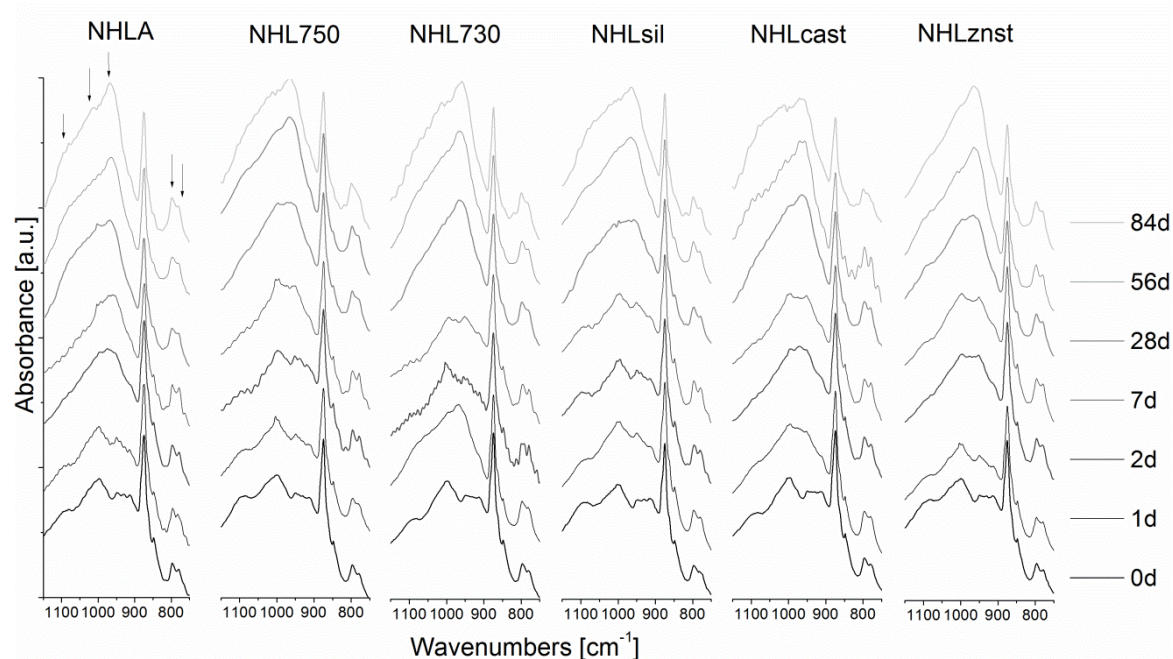


Figure 3.2 13 FT-IR spectra of natural hydraulic lime pastes without and with admixtures in the $1150\text{-}750\text{ cm}^{-1}$ range at different hydration times: 0, 1, 2, 7, 28, 56, 84, days. The arrows indicates the principal peaks which changes during the reaction

3.2.2.4 SEM observations of natural hydraulic lime pastes

After 28 days of hydration, SEM observations allowed to appreciate the different microstructures of NHL pastes. NHLA, NHL750, NHL730 had fine, compact and homogeneous structure, intercalated by narrow pores, while the microstructure of NHLsil seemed less coherent and powdery and large round pores were visible in NHLznst and NHLcast. The EDX elemental mapping of NHLznst confirmed that higher zinc percentages were observed around the pores. The porosity of NHLcast and NHLznst indicated that calcium and zinc stearates worked like air entraining agents behaving as surfactants inside the pastes.

The SEM observations of the hydration products at 28 and 56 days of hydration (Table 3.2 14; Table 3.2 15) allowed to see the presence of hydrated calcium silicate phases (C-S-H), although different morphologies were observed.

The paste NHLA presented sparse fibrous C-S-H (type I) after 28 days with shorts needle-like structure, while after 56 days it showed a typical network of fibrous C-S-H covering most of the aggregate grains, with clusters of long needle-shaped C-S-H.

The presence of sitren P750® and Silres® enhanced the hydration and already after 28 days a higher presence of long needle-like C-S-H was visible, a complex fibrous structure of hydrated products was seen also after 56 days when slag fragments were almost completely covered by the hydration products. Carrier grains of Sitren P750®, Silres®, Sitren P730® were visible within the pastes NHL750, NHL730, NHLsil but covered by hydration products.

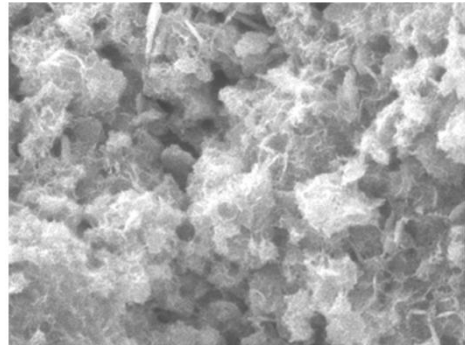
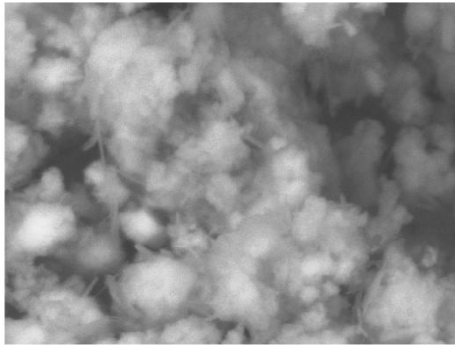
The stearates caused a delay of the formation of hydrated products visible after 28 days, while after 56 days globular C-S-H were cross-cut by a number of acicular, needle shaped particles and cluster.

After 28 days, portlandite crystals, recognizable as typical hexagonal plates, were embedded within the binder matrix in every paste analyzed.

Table 3.2 14 SEM images of natural hydraulic lime pastes, microstructure at 28 days

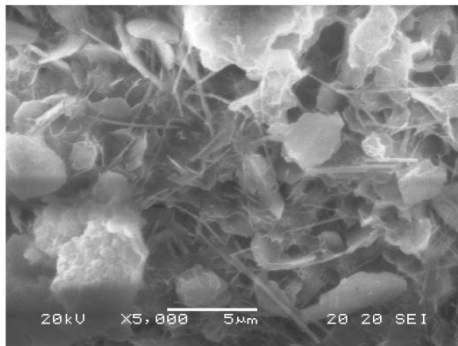
Natural hydraulic lime pastes after 28 days of hydration –Secondary electron images (5000 X)

NHLA without admixture

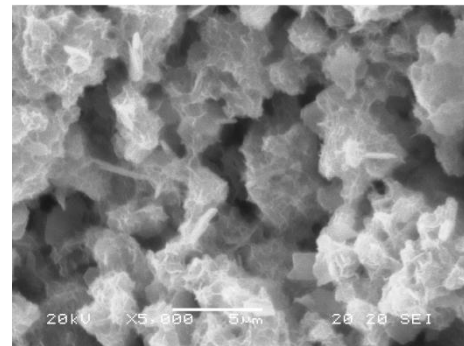


With silanes water-repellents

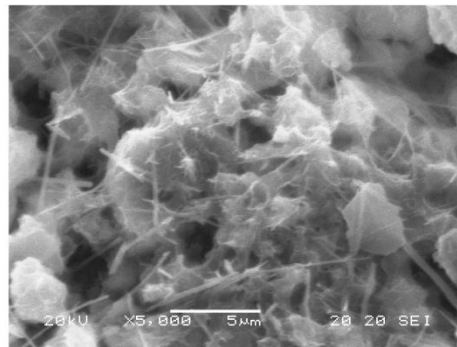
NHL 750



NHL730

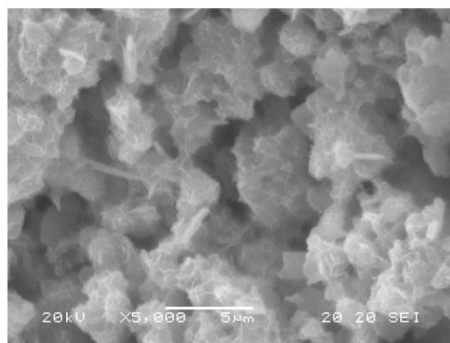


NHLsil



With stearates water-repellents

NHLcast



NHLznst

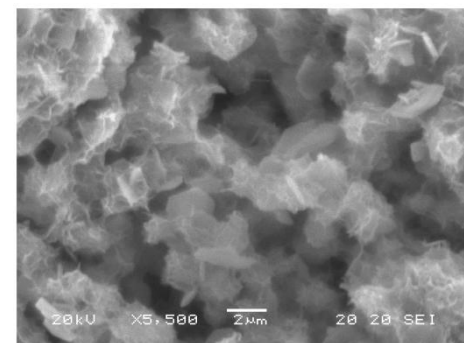
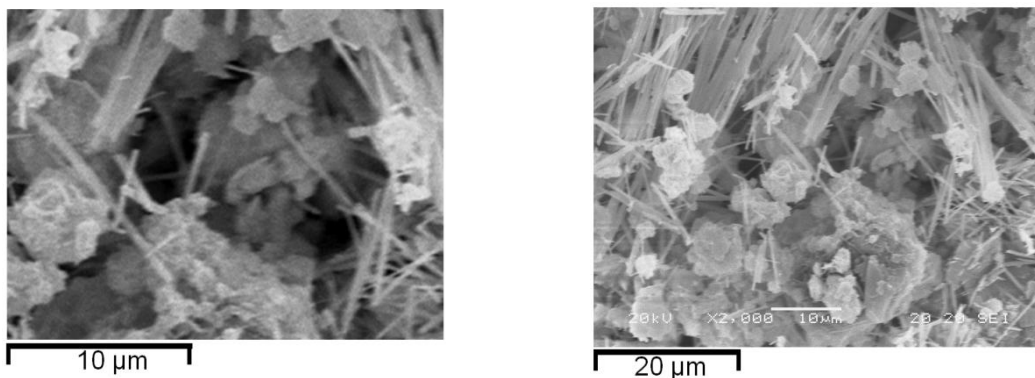


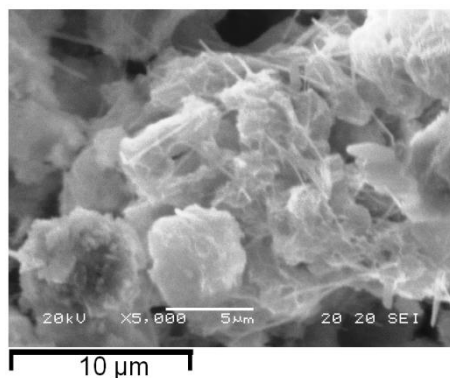
Table 3.2 15 SEM images of natural hydraulic lime pastes, microstructure after 56 days

Natural hydraulic lime pastes after 56 days of hydration –Secondary electron images
 NHLA without admixture (links 5000X, right 2000X)

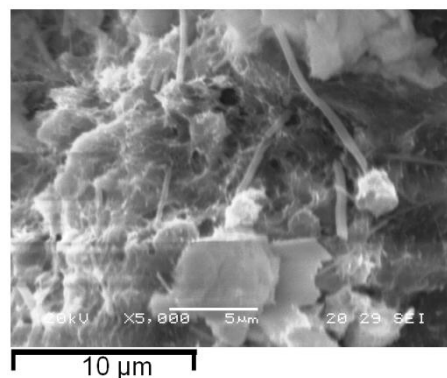


With silanes water-repellents (5000 X)

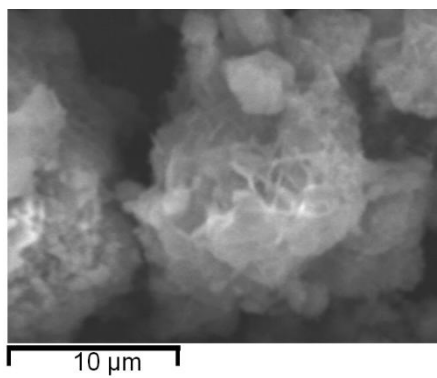
NHL 750



NHL730

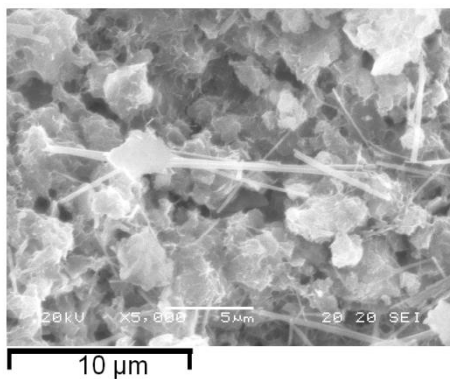


NHLsil

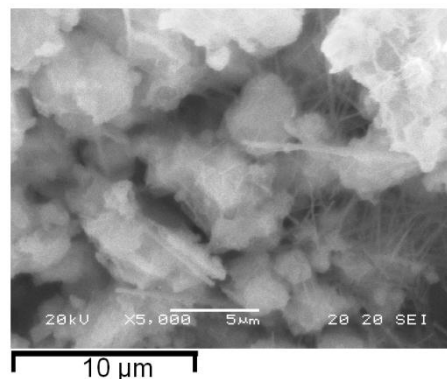


With stearates water-repellents (5000 X)

NHLcast



NHLznst



3.2.3 HYDRAULIC POZZOLANA-LIME PASTES WITH WATER-REPELLENTS

Table 3.2 16 summarized the different pastes prepared mixing equal part of greek pozzolana and calcium hydroxide with different water repellent admixtures and water. As usual a reference paste without admixtures was also prepared (HLA). The hydration of pozzolana-lime pastes was followed for 5 months because the reactions proceeded slower than the limestone cement and the natural hydraulic lime and required a longer study.

Table 3.2 16 Composition of the hydraulic pozzolana-lime pastes

Paste names	Binder	additive	additive class	Additive (%)	w/b ratio
HLA		-	-	-	1,25
HL750	Pozzolana Ca(OH) ₂ 1:1 by mass	Sitren p750	powder silane	1	1,3
HL730		Sitren p730	powder silane	1	1,3
HLsil		SilresA	powder silane	1	1,2
HLtes		Tegosivin HM	emulsion silane	1	1,14
HLcast		Ca Stearate	metal soap	1	1,3
HLznst		Zn stearate	metal soap	1	1,3

3.2.3.1 XRD Study of hydraulic pozzolana-lime pastes

Portlandite, quartz, albite present in the starting materials were easily recognized in the XRD pattern of the pastes during the whole hydration period considered (Figure 3.2 14). A slight percentage of calcite appeared (29.5 2 θ peak) while the hydration went further, probably due to a partial carbonation of calcium hydroxide.

During the hydration, the main differences in the XRD-patterns were observed at low angles, 8°-13° 2 θ , where the main peaks of AFm and Aft phases were found.

–At early ages the XRD-patterns of the paste HLA reflected the composition of calcium hydroxide and greek pozzolana, but only after 1 day of hydration, the peaks related to the halloysite $Al_2Si_2O_5(OH)_4 \cdot 2H_2O$ and muscovite, labelled as peak **1** at 8,9 2 θ in Figure 3.2 14, decreased and a new peak at 11.36 2 θ appeared (labelled as **2**) identified as an AFm monocarbonate solid solution: halloysite was consumed to form the monocarbonate solid solution.

–After 7-14 days instead of the AFm solid solution two different modification AFm-phases were identified by the main peaks at 11.2 2 θ and 11.42 2 θ (peaks **2** and **3** in Figure 3.2 14): Paraaluminumhydrocalcite $Ca Al_2(CO_3)_2(OH)_4 \cdot 6H_2O$ (nr **2**) and calcium aluminium oxide carbonate hydroxide hydrate $Ca_4Al_2O_6(CO_3)_{0,5}(OH) \cdot 11,5H_2O$ (nr **3**).

–After 5 months, it was possible to observe another little peak at 11.75 2 θ , identified as a calcium aluminium oxide carbonate hydrate ($Ca_4Al_2O_6 \cdot CO_3 \cdot 11H_2O$).

It may seem quite unusual to observe the formation of these aluminated phases instead of crystalline silicates hydrates such as gehlenite hydrate or hydrogarnet or even poorly crystallized gel of calcium hydrosilicate, commonly found in the pozzolanic reaction of kaolinite or other natural pozzolanas²². However, similar compounds have been previously found in aluminate cements and in studies regarding the hydration of C₃A phases in presence of CaCO₃²³.

²² Shi, C., R.L.Day, 2000; Donchev, I. *et al.*, 2010; Habert, G., *et al.*, 2007

²³ Lothenbach, B. *et al.*, 2008; Kakali, G. *et al.* 2000; Taylor, H. F. W. 1997; Lea, M. 1997.

Besides these crystalline phases it was observed the decreasing of the amorphous phases of the anhydrous pozzolana in the range 20-35 2θ during the curing and the increasing of a broad peak in the range 3-10 2θ due to the formation of new amorphous phases ²⁴.

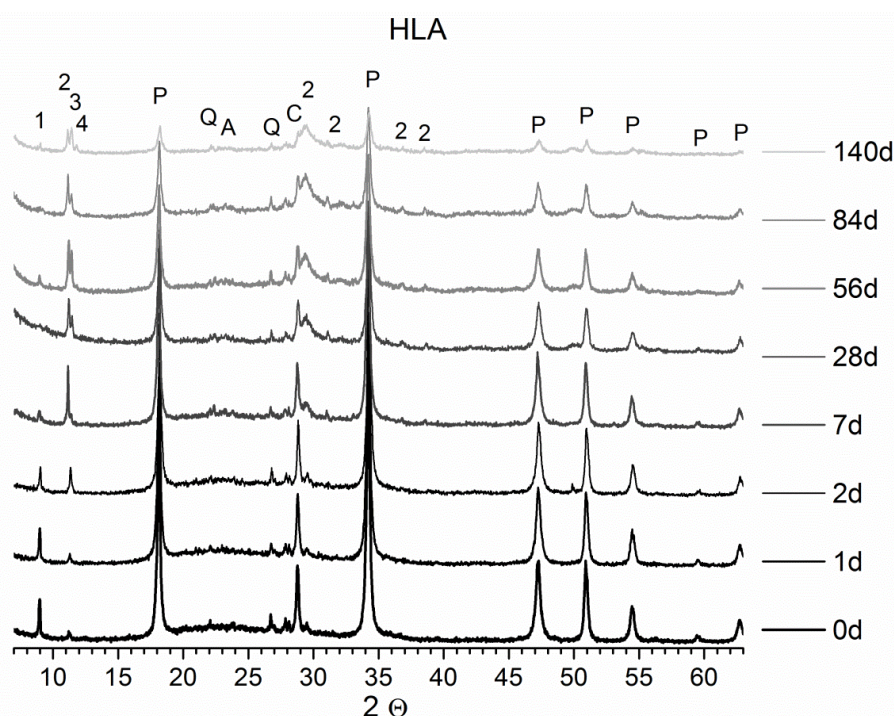


Figure 3.2 14 XRD patterns of HLA, without admixtures, registered after 0,1,2,7,28, 56, 84 (3 months), and 140 (5 months) days; P=portlandite, Q= quartz, C=calcite, A= albite, 1= Aft phases or calcium aluminum silicate (Halloysite), 2= Paraaluminumhydrocalcite $\text{Ca Al}_2(\text{CO}_3)_2(\text{OH})_4 \cdot 6\text{H}_2\text{O}$, 3= calcium aluminium oxide carbonate hydroxide hydrate $\text{Ca}_4\text{Al}_2\text{O}_6(\text{CO}_3)_{0,5}(\text{OH}) \cdot 11,5\text{H}_2\text{O}$, Calcium Oxide Carbonate Hydrate $3\text{CaO} \cdot \text{Al}_2\text{O}_3 \cdot \text{CaCO}_3 \cdot 11\text{H}_2\text{O}$

Figure 3.2 15 shows a comparison of the XRD pattern of pastes without and with water repellents in the most significant range: 8°-13° 2θ . When water repellent admixtures were added, reactions similar to HLA took place but slightly difference were observed regarding the reactions kinetic.

- For the pastes HL750 and Hlsil it was observed that: at two days the peak nr. **2** of AFm solid solution was broader and lower than in HLA; at 28 and 84 days the peak **3** was generally lower and broader; after 140 days the peak nr **4** (Calcium Oxide Carbonate Hydrate $3\text{CaO} \cdot \text{Al}_2\text{O}_3 \cdot \text{CaCO}_3 \cdot 11\text{H}_2\text{O}$) was not visible. Probably Sitren P750® or silres A®, both silane/siloxanes on amorphous silica, tended to stabilize the Paraaluminumhydrocalcite (nr **2**) and the calcium aluminium oxide hydroxide hydrate (nr. **3**) and slowed down the hydration process.
- On the other hand the use of sitren P730®, a silane supported on calcium carbonate, in HL730 seemed to positively quicken the hydration: a distinct double peak of the AFm phases was found around 11,5° 2θ already after 2 days; the peak nr. **3** was growing faster at 28 days; the peak nr. **4** was visible already after 84 days and not only after 5 months as in HLA.
- The mix HLtes (emulsion silanes/siloxanes) had a similar reaction rate to HLA and did not influence the hydration reaction.

²⁴ Donchev, I., *et al.*, 2010; Sepulcre-Aguilar, A. F.H. Olivares, 2010 ; Gualtieri, A.F., *et al.* , 2006

–When stearates were added in HLcast and HLznst it was observed: a slow formation of Paraaluminumhydrocalcite till 2 days of hydration; the presence of the peak 3 already after 2 days; -the stabilization of calcium aluminium oxide carbonate hydroxide hydrate (peak 3), instead of the formation of Calcium Oxide Carbonate Hydrate (peak 4), in particular when Calcium stearate was added.

The comparison of the 20° - $35^{\circ}2\theta$ range did not show particular differences for admixed and not admixed pastes, a general formation of hydrated and poorly crystalline silicate compounds CSH was seen together with the production of calcite.

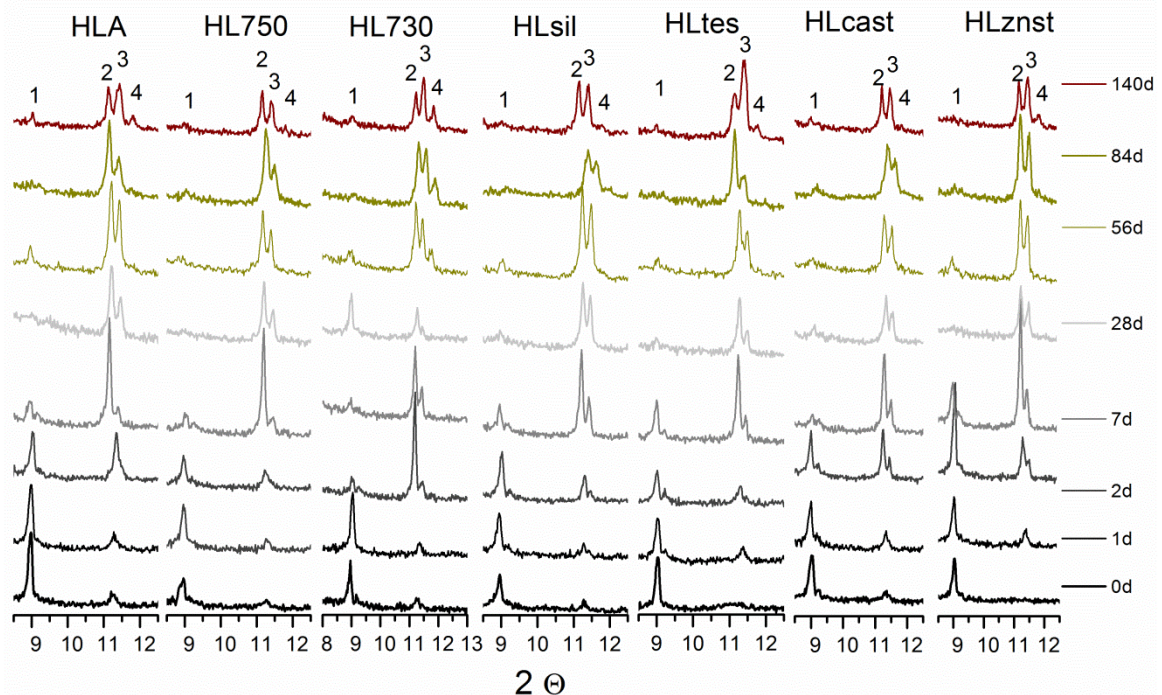


Figure 3.2 15 XRD patterns in the 8° - $13^{\circ} 2\theta$ range of pozzolana-lime pastes; 1= Aft phases or calcium aluminium silicate (Hallosite), 2= Paraaluminumhydrocalcite $\text{CaAl}_2(\text{CO}_3)_2(\text{OH})_4 \cdot 6\text{H}_2\text{O}$, 3= calcium aluminium oxide carbonate hydroxide hydrate $\text{Ca}_4\text{Al}_2\text{O}_6(\text{CO}_3)_{0,5}(\text{OH}) \cdot 11,5\text{H}_2\text{O}$, Calcium Oxide Carbonate Hydrate $3\text{CaO} \cdot \text{Al}_2\text{O}_3 \cdot \text{CaCO}_3 \cdot 11\text{H}_2\text{O}$

3.2.3.2 TG-DSC Study of hydraulic pozzolana- lime pastes

The TG and the DSC curves (Table 3.2 18, Table 3.2 19) registered for HL pastes showed the same mass losses and endothermic reaction seen also in limestone cement pastes and in natural hydraulic lime pastes: in the 80° - 200°C range the dehydration of hydrated compounds; from 350°C to 500°C the dehydroxylation of $\text{Ca}(\text{OH})_2$ took place; after 600°C decarbonation of CaCO_3 . The DSC curves of the samples at different hydration times showed an increasing of the endothermic peaks in the 80°C - 200°C range, as seen also for natural hydraulic lime and limestone pastes. However, the second range (350°C - 500°C) decreased showing that the calcium hydroxide diminished with the time: the lime was consumed during the reaction to form hydrated compounds detectable in the first range of TG and DSC curves. In particular, after 7 days was already possible to observe three peaks in the DSC curves: at 85°C , a small one at 115°C , and at 138°C (Figure 3.2 16), due to C-S-H, Aft phases and Afm phases, respectively²⁵.

²⁵ Ramachandran, V.S., Ralph M. Paroli, J. J. Beaudoin, A. H. Delgado, 2002; W Sha, G.B Pereira 2001; Manjit Singh, 2004

After 28 and 84 days the DSC peaks at 115°C and 136°C were strongly increased and at 84 days covered partially the peak at DSC 85°C of C-S-H.

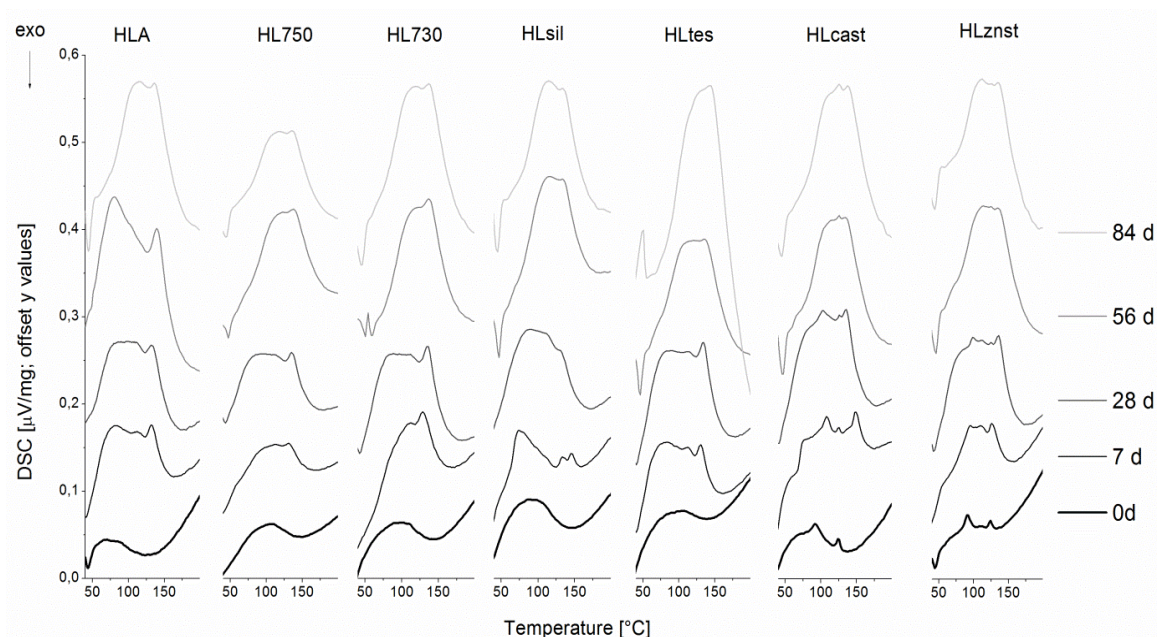


Figure 3.2 16 DSC curves of different pozzolana-lime pastes at 0,7, 28,56, 84 days ranging from 45°C to 200°C

The presence of different water repellents caused significant variation of the DSC curves in the first 300°C (Figure 3.2 16) because their shape reflected also the presence of the admixed water repellent. In particular, when a stearate was added peaks at 95°C and 125°C, due to dehydration and melting of stearates, were visible. Also the pastes with siloxanes (HL750, HLsil; HLtes) presented a peculiar profile till 7 days and lower peaks at 138°C.

Table 3.2 17 shows a easier and meaningful comparison of the effects of the water repellents on the pastes hydration done considering the quantitative composition calculated from the mass losses in the ranges: 80-200°C (water of hydration); 350°-500°C (calcium hydroxide); 650°-800°C (calcium carbonate). The mass loss at 80-200°C was due to different dehydration reaction and was not possible to clearly attribute one temperature range to a single reaction, but the percentage of total water lost is reported.

The total bound water TW due to hydrate compounds of HLA increased strongly in the first 7 days, then went slowly on till 84 days, when a decrease in the production rate occurred. The percentage of calcium hydroxide presented a symmetrical trend to the TW in HLA. A partial carbonation was observed at 84 days. A similar behaviour was seen also for HL750 even if the total production of hydrated compounds and the consume of calcium hydroxide was smaller. When other siloxanes or stearates are added the formation of new hydrated compounds slew down after 28 days, and then slightly increased after 84 days in HL730, HLsil, HLtes added with siloxanes. A higher consumption of calcium hydroxide was observed in presence of stearates correspondent, however, also to a higher carbonation of the samples HLcast and HLznst in comparison to the others.

Table 3.2 17 Quantitative determination of the compound present from the TG curves: the total bound water of hydrated phases (Tbw), calcium hydroxide and calcium carbonate content are considered

sample name	Tbw (%)	Ca(OH) ₂ (%)	CaCO ₃ (%)
	80-200 °C	350-500°C	600-800°C
HLA0d	0,9	35,5	14,1
HLA7d	2,6	20,5	22,4
HLA28d	3,6	24,5	10,6
HLA56d	4,9	20,8	7,0
HLA84d	4,4	19,7	8,9
HL750 0D	1,2	33,7	11,9
HL750 7d	2,5	23,2	17,2
HL750 28d	3,6	21,6	15,1
HL750 56d	4,4	17,9	10,2
HL750 84d	3,9	17,6	9,4
HL730 0D	1,0	38,2	9,8
HL730 7d	2,3	24,8	15,6
HL730 28d	3,4	23,3	12,9
HL730 56d	3,5	21,5	8,6
HL730 84d	4,1	20,1	7,1
HLsil 0d	1,3	39,8	11,1
HLsil 7d	1,9	15,7	31,2
HLsil 28d	2,7	25,2	15,9
HLsil 56d	2,8	23,8	10,1
HLsil 84d	3,7	17,3	15,1
HLtes 0d	1,0	35,9	10,2
HLtes 7d	2,3	18,5	23,1
HLtes 28d	3,2	23,6	9,3
HLtes 56d	3,8	17,1	9,0
HLtes 84d	4,6	18,0	9,4
HLcast 0d	0,8	29,3	16,5
HLcast 7d	2,5	10,7	28,2
HLcast 28d	3,8	14,8	19,2
HLcast 56d	3,5	12,2	14,3
HLcast 84d	3,7	13,7	11,9
HLznst 0d	1,3	32,4	14,1
HLznst 7d	2,1	16,3	27,4
HLznst 28d	3,3	18,7	16,7
HLznst 56d	3,2	15,1	14,1
HLznst 84d	3,6	14,9	12,8

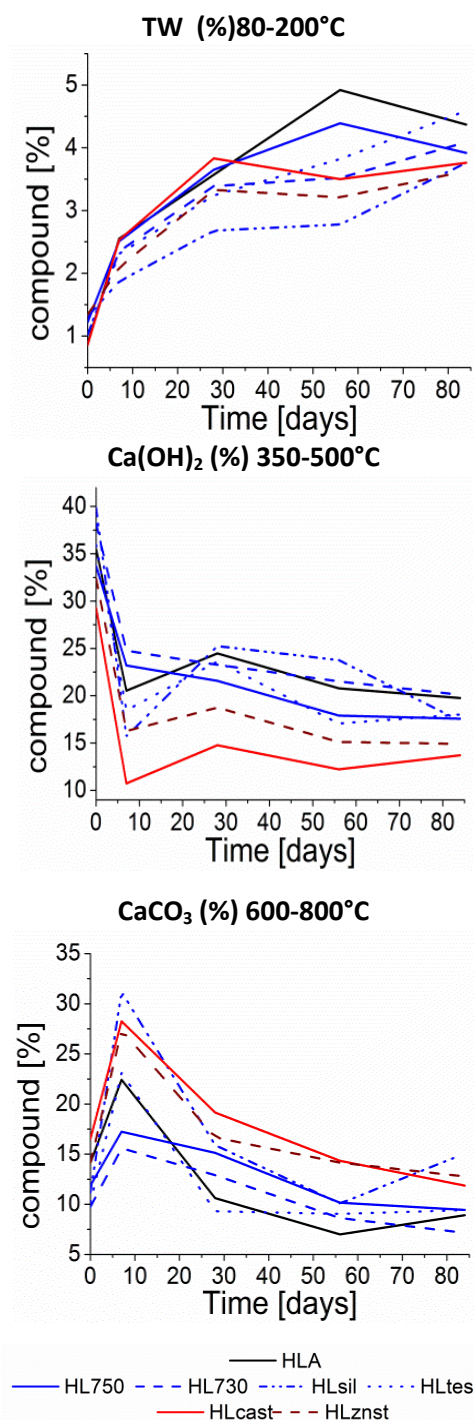


Table 3.2 18 TG-DSC curves of pozzolana lime paste with water-repellent additives 1% by mass at different hydration times (0, 1, 7, 28, 56, 84 days)

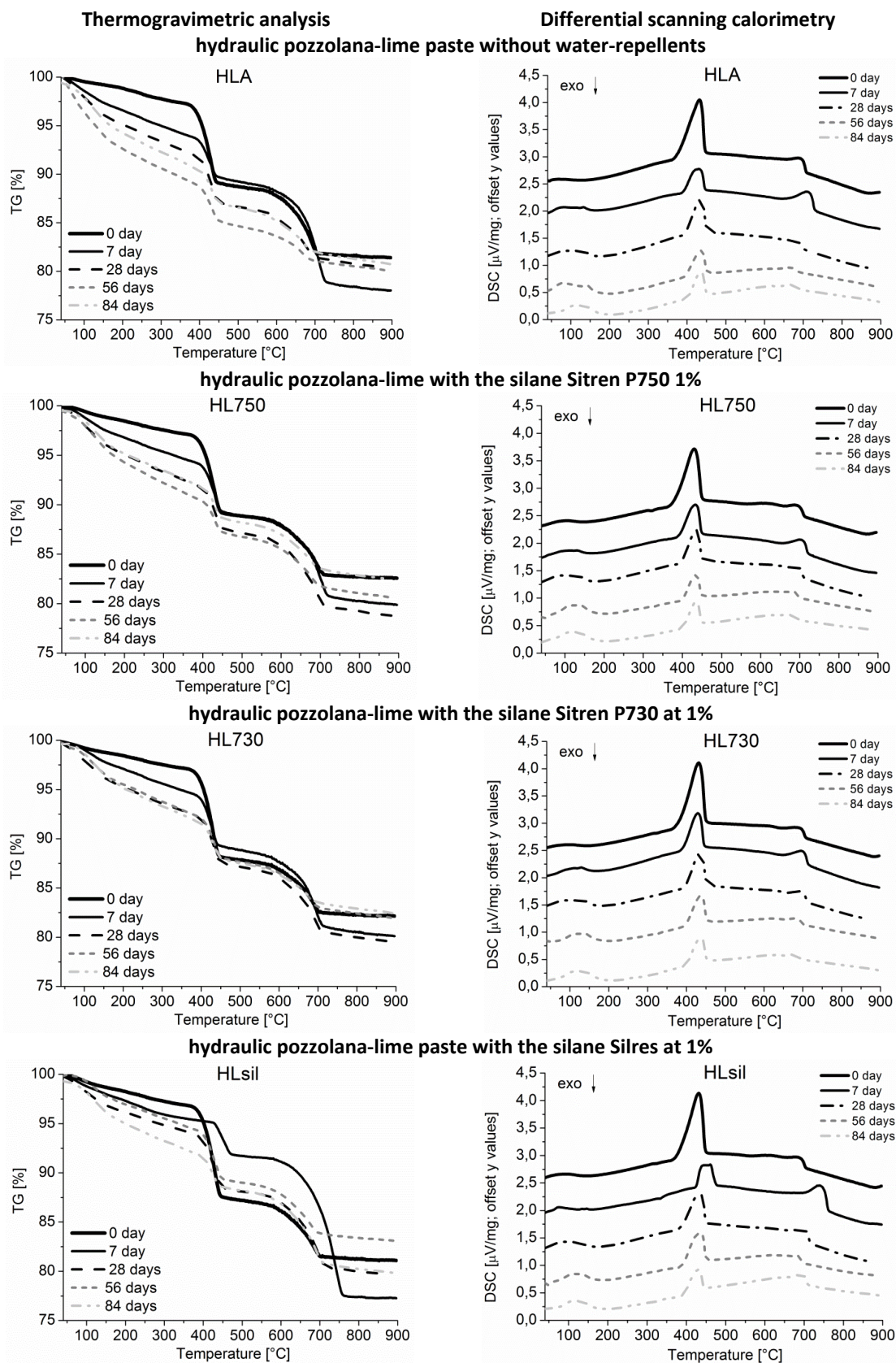
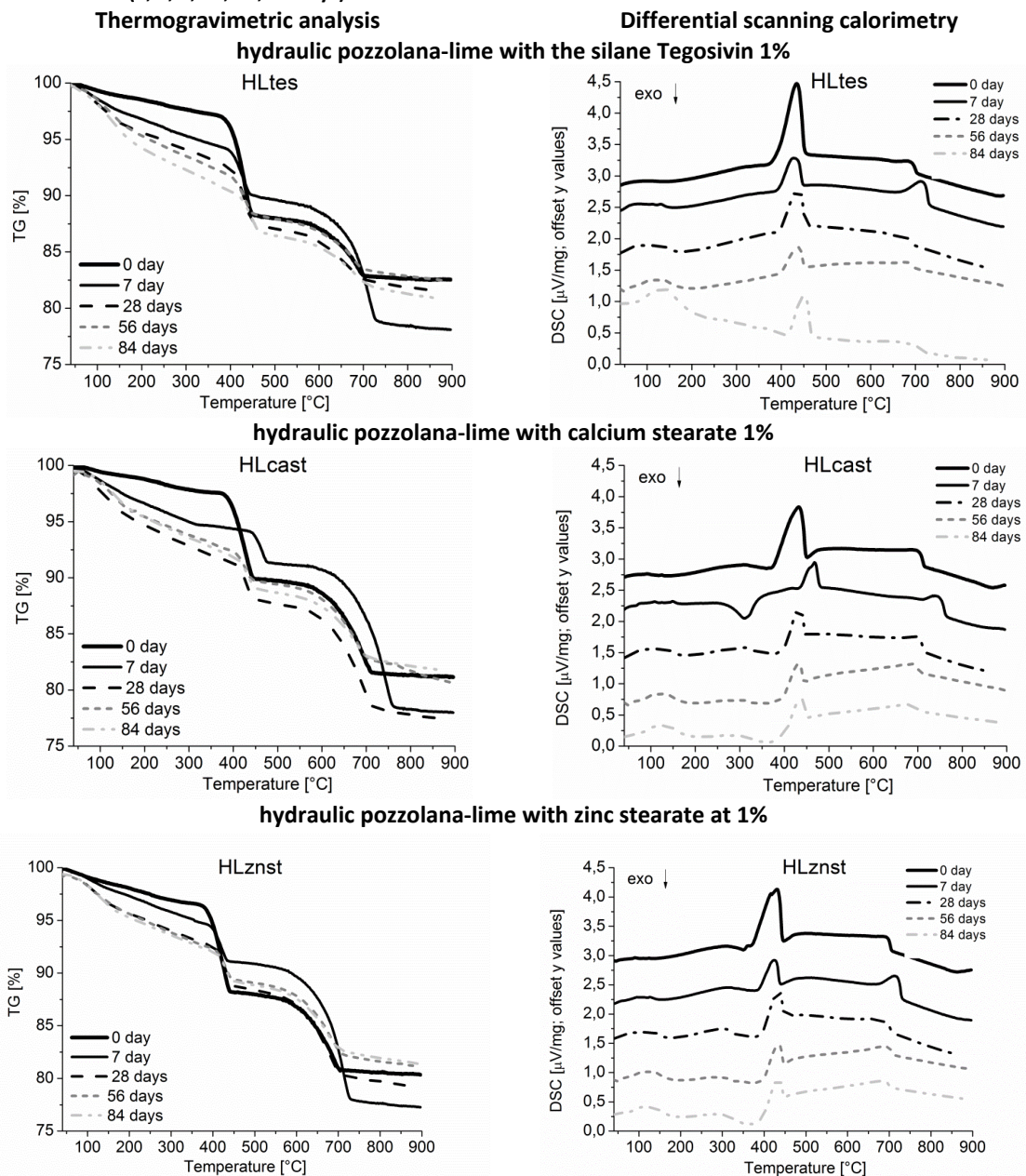


Table 3.2 19 TG-DSC curves of pozzolana lime paste with water-repellent additives 1% by mass at different hydration times (0, 1, 7, 28, 56, 84 days)



3.2.3.3 FT-IR study of hydraulic pozzolana- lime pastes

FT-IR measurements confirmed the composition of the samples at different times and allowed to observe also poor crystalline and amorphous C-S-H. The major peaks visible in the spectra (Figure 3.2 17) were due to the calcium hydroxide and to the silicates (Si-O-Si stretching at $1100\text{--}900\text{ cm}^{-1}$ but centred in 1020 cm^{-1}) present in the lime and in the pozzolana, respectively²⁶, furthermore a little presence of calcium carbonate was detected. The absorption bands of aliphatic stretching were seen in HLcast and HLznst samples, and due to the admixtures.

While the hydration proceeded, the calcium hydroxide peaks diminished due to its consumption in the reaction. Further differences were observed in the $1600\text{--}950\text{ cm}^{-1}$ range (Figure 3.2 18) where the silicates peaks changed shape due to the formation of new silicates hydrates. In particular, during the hydration (Figure 3.2 18) the C-S-H peak centred at $970\text{--}960\text{ cm}^{-1}$ increased

²⁶ See also Chapter 3. 1

with different speed in the different mixtures. The evolution of the C-S-H production was, therefore, followed considering the ratio $\text{Si-O-Si}^{970} / \text{Si-O-Si}^{1030}$. In HLA, after 7 or 28 days, was possible to distinguish a shoulder (around 955 cm^{-1}) on the right side of the first silicates peak (1040 cm^{-1}); after 84 days the convolution of peaks relative to silicates shifted to 968 cm^{-1} and after 9 months the peak due to hydrated silicates was clearly visible at 970 cm^{-1} . The latter peak confirmed that amorphous or poorly crystalline silicate hydrates are significant products of the hydration reaction. As the hydration went further, two convoluted peaks centred at 1480 cm^{-1} and at 1417 cm^{-1} were distinguished related, probably, to the formation of mono- and tri-carbonates phases, detected also by XRD. Spectra of HL750, HL730, HLtes were completely similar to HLA spectra (the C-S-H peak at 970 cm^{-1} overcame the silicates of the pozzolana at 1030 cm^{-1} after 84 days); on the contrary, HLSil, HLcast and HLznst after 84 days presented a weaker C-S-H peak clearly visible only after 5 months.

Table 3.2 20 Main FT-IR absorption detected in pozzolana-lime pastes during the hydration.

Frequency	Absorption	compound	Observations
3640 cm^{-1}	v -OH s	Calcium hydroxide	The peak decreased during the hydration.
3400 cm^{-1}	v -OH br	Water	Increased during the hydration.
$2930;2850 \text{ cm}^{-1}$	v -CH s	Aliphatic stretching	the peaks were visible only for the admixed pastes and were due to the organic chains of the water-repellent admixtures. The peak remained unchanged during the hydration.
1600 cm^{-1}	δ -OH sh	Constitutive water	The peak increased with time due to the formation of hydrated compounds.
$1436 \text{ cm}^{-1}; 875 \text{ cm}^{-1}$	v and δ - CO_3 s, strong	Calcium carbonate	Calcium carbonate was present since the beginning and remained quite constant during the hydration in comparison to the other peaks.
$1480-1417 \text{ cm}^{-1}$	v - CO_3	Carbonate hydrates	Convoluted peaks due to carbonates which were more visible after 56 days.
1020 cm^{-1}	v Si-O-Si br	Silicates	The stretching at $1100-900 \text{ cm}^{-1}$ but centred in 1020 cm^{-1} was due to the pozzolana and decreased during the hydration.
970 cm^{-1}	v Si-O-Si br	C-S-H	The broad peak due to silicate and aluminate hydrates increased during the hydration.

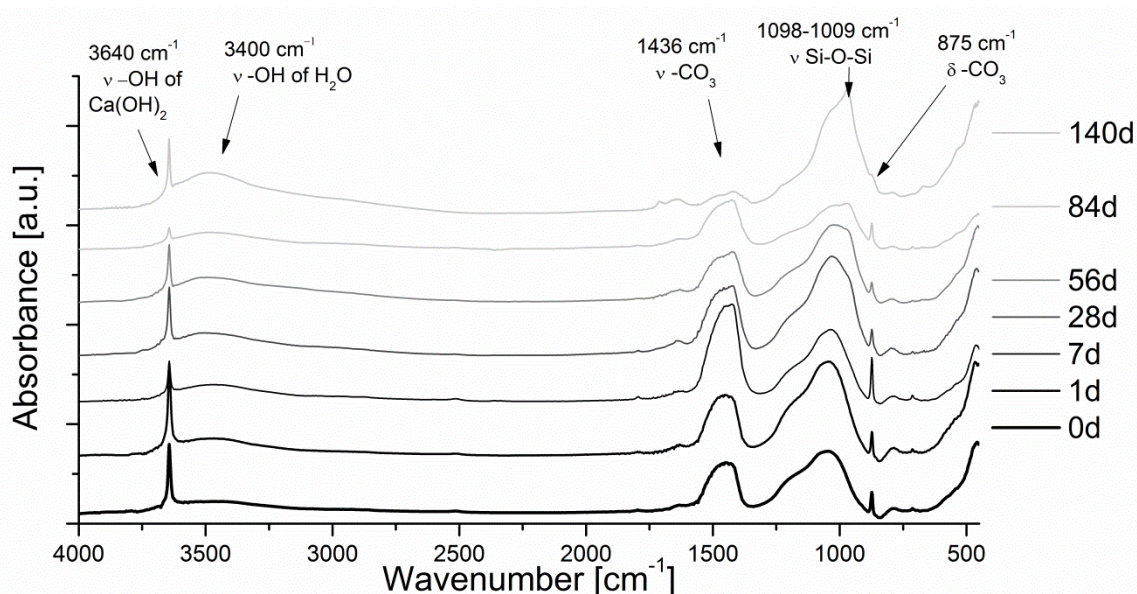


Figure 3.2 17 FT-IR spectra of pozzolana-lime paste without admixtures HLA at 0,1, 7, 28, 56, 84, 140 days

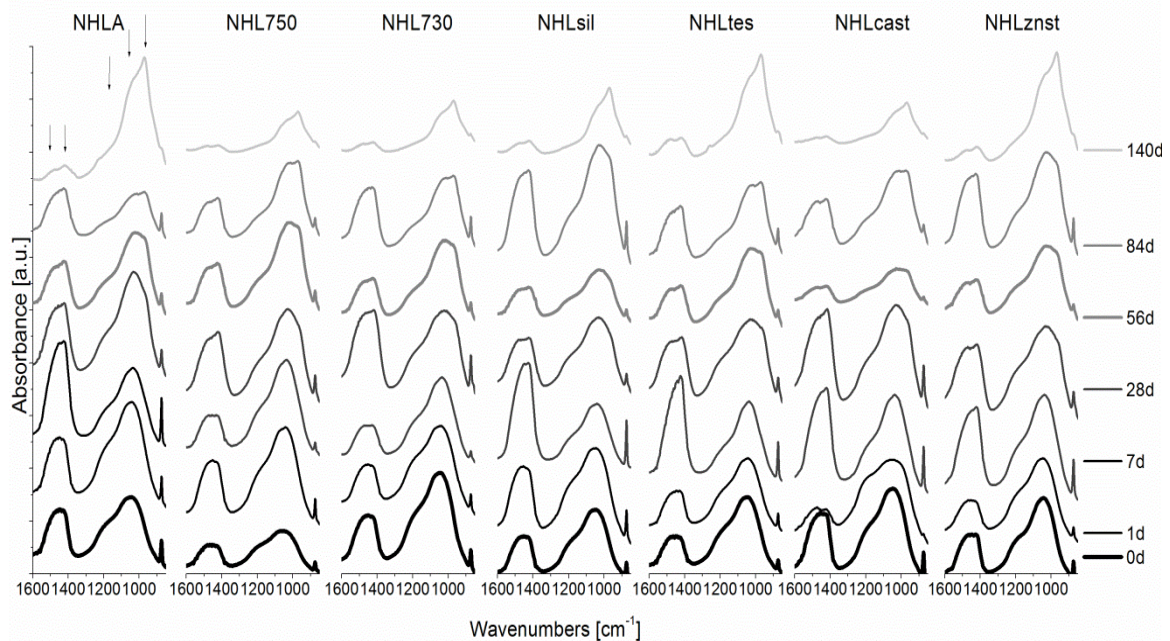


Figure 3.2 18 FT- IR spectra ranging from 1600 to 900 cm^{-1} of different pastes at different hydration times (0,1,7,28,56,84,140 days)

3.2.3.4 SEM observations of pozzolana-lime pastes

The variation of the morphology of pozzolana-lime pastes were monitored using Scanning Electron Microscopy (Figure 3.2 19, Table 3.2 21, Table 3.2 22). In the pastes after 7 days, big, round-shaped grains were surrounded by thinner, elongated fragments and a finer matrix. EDX analysis performed on the bigger grains showed the presence of silicon as main component, followed by calcium, probably due to a mixed calcium silicates compounds. The thinner and bright fragments were constituted of calcium and aluminium and were visible only at early hydration times, after then were covered by hydration products. The finer matrix was composed of fine quartz grains and calcium aluminates and silicates.

SEM observation of HLA, without admixtures after 7 days revealed a complex bulk matrix with only few and really fine acicular structures on the surfaces of some grains, while after 28 days the microstructure was more compact, with more acicular structures. The EDX analysis performed on a general area and on different points of HLA after 28 days allowed to identify a high presence of silicon in the elongated grains (point a Figure 3.2 19), silicon and calcium were found in point b and in similar small grains, while aluminium and calcium are predominant in the compact grains similar to point c. Only after 84 days a well formed binding network of acicular and film-like amorphous structures covered and joined the grains; underneath, some cubic calcite crystals as well as some elongated crystal of aluminates compounds can be recognized.

When silanes/siloxanes supported on silica carrier were added (HL750, HLsil) the amorphous silica grains used as carrier were recognizable and later covered by hydration products. The microstructure at 28 and 84 days seemed more compact and homogeneous in comparison to HLA (Table 3.2 21 and Table 3.2 22). Thin needle-like structures bound the matrix grains together with the gel-like layer. The formation of these structures indicates a slightly faster speed of hydration, influenced probably also by the presence of the admixture and the carrier.

HL730 after 84 days had the same bounded structure of HLA, where gel-layers seemed to be formed. The SEM-EDX analysis of HL730 after 84 days (Figure 3.2 19) evidenced the presence of flat hexagonal crystals of calcium aluminates (elements detected Ca, Al, Si, Cl, K)²⁷. The brighter round-shaped grains visible in HL730, mainly composed of calcium, were the carrier grain of Sitren P730®.

The microstructures of the pastes HLcast and HLznt were really similar to HLA, the formation of the same gel layer during the hydration was noticed. The EDX analysis on aggregates of fine and bright powder material showed calcium alone due probably to a non perfect dispersion of the water-repellent and the formation of lumps inside the matrix. For HLZnt was possible to perform an elemental mapping to detect the distribution of Zinc, due to the zinc stearate (Figure 3.2 20) which was found only on pore walls.

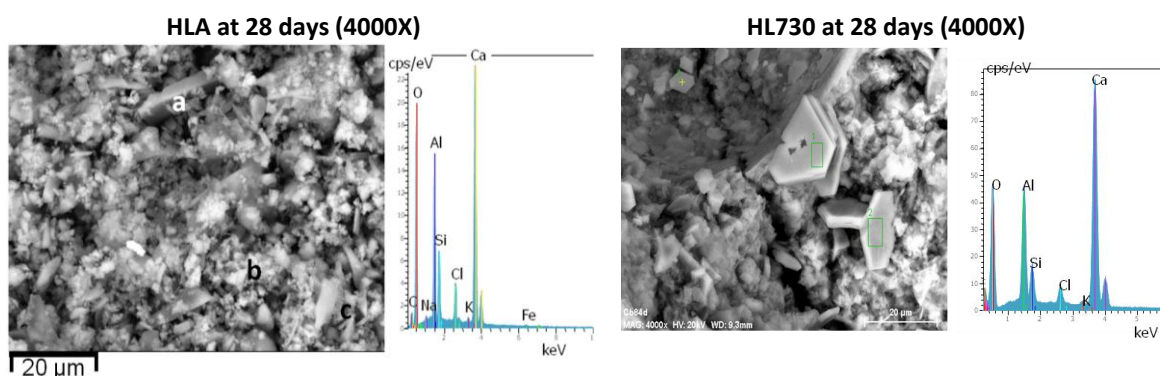


Figure 3.2 19 SEM images of HLA and HL730 at 28 days (4000X, scale bar= 20 µm) and correspondent EDX spectra. On points a, b, c further EDX spectra were collected

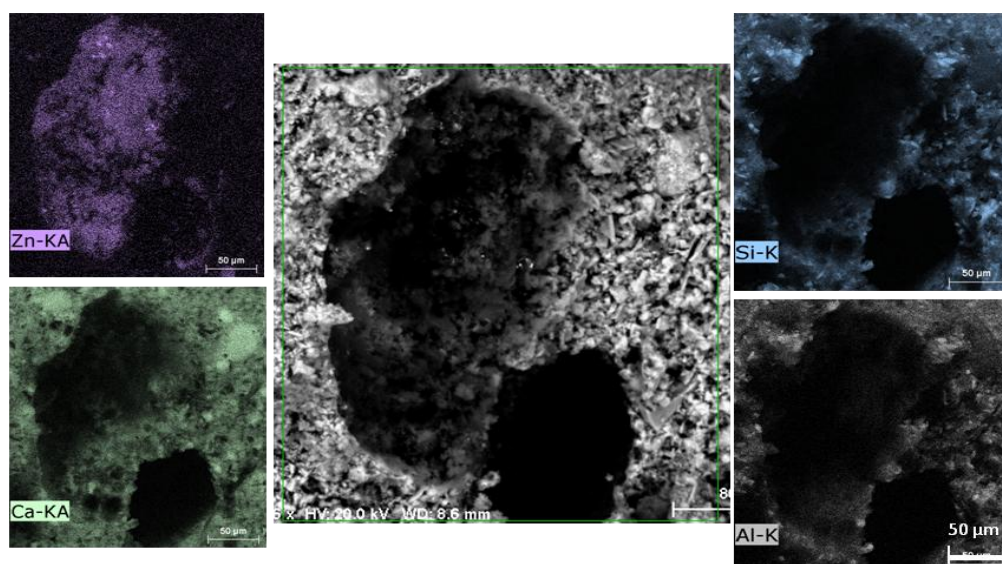


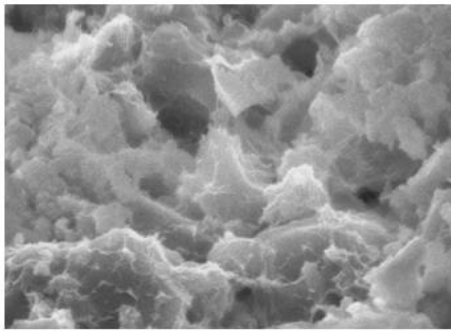
Figure 3.2 20 Elemental maps of HLznt after 84 days, zinc, silicon, calcium and aluminium were detected (scale bars=50 µm). It is possible to observe that zinc is present mainly on pore walls.

²⁷ García del Cura, P. G.; 1999

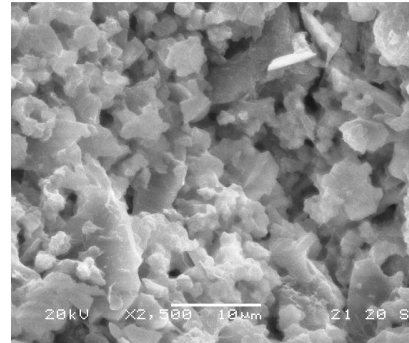
Table 3.2 21 SEM images of pozzolana-lime pastes without or with water repellents after 28 days (SEI 2500 X)

Hydraulic lime-pozzolana pastes after 28 days of hydration –Secondary electron images (2500X)

HLA without admixture



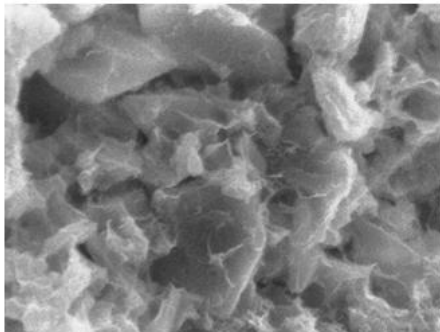
10 µm



20 µm

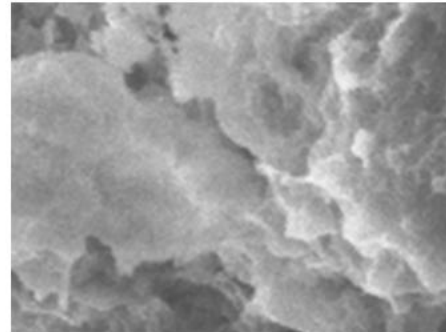
With silanes water-repellents

HL750



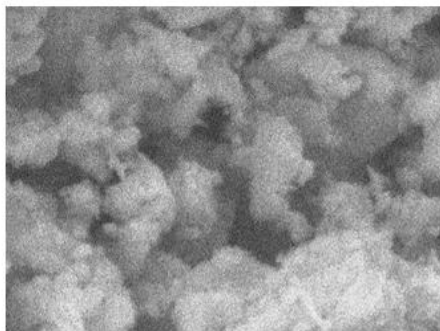
10 µm

HL730



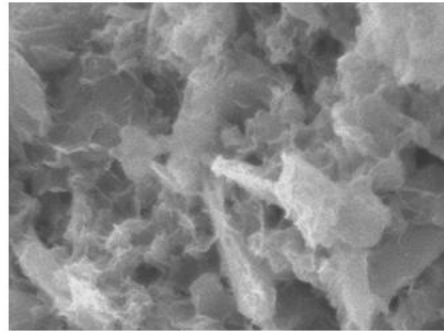
10 µm

HLsil



10 µm

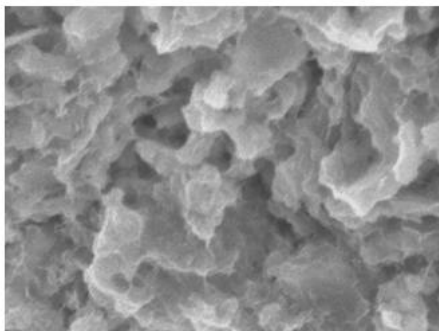
HLtes



10 µm

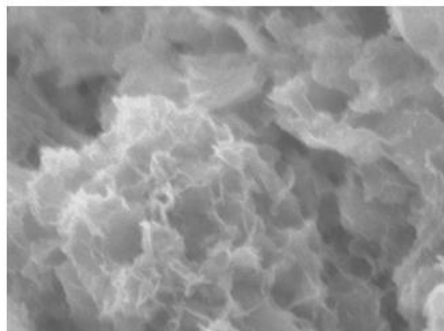
With stearates water-repellents

HLCast



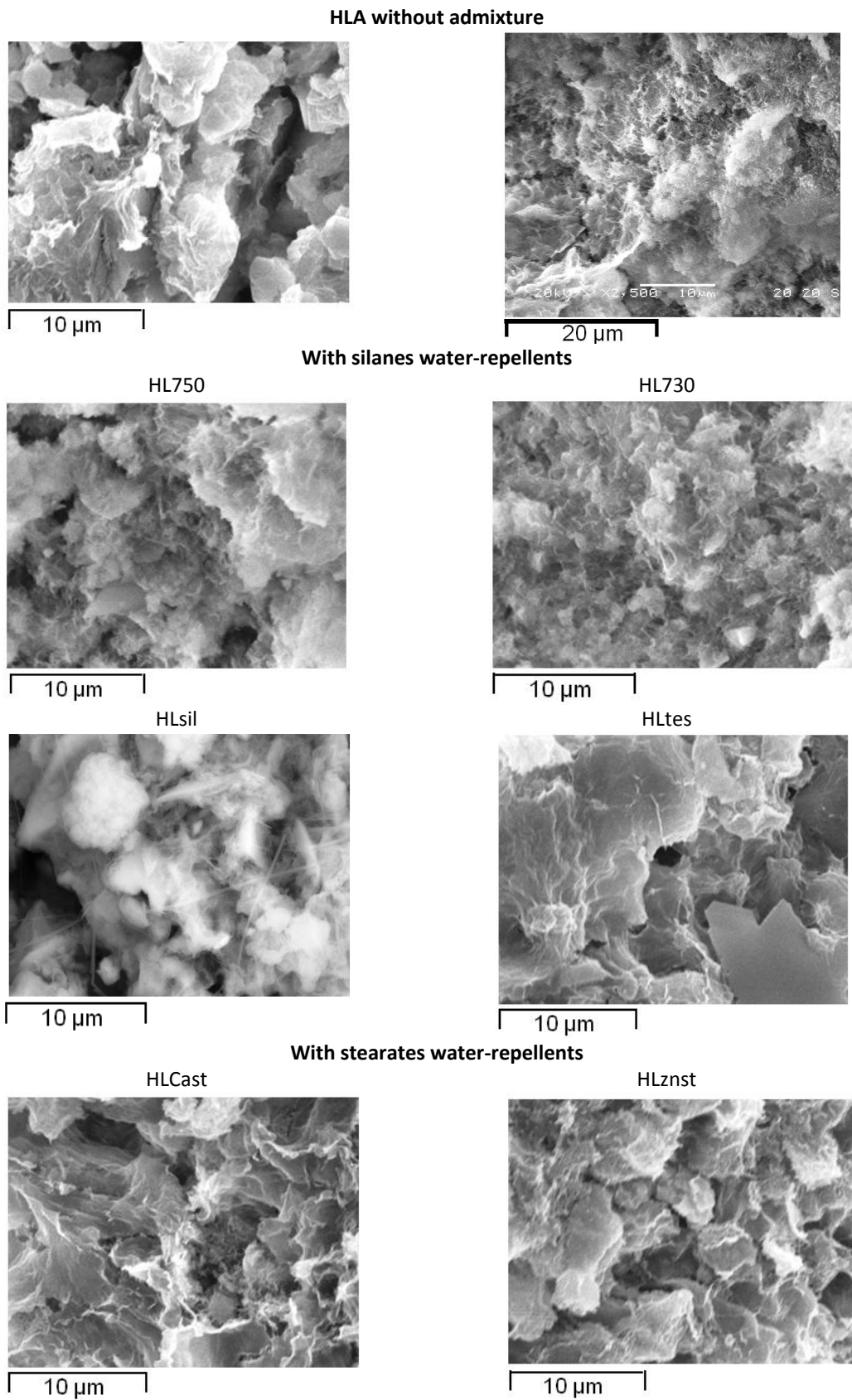
10 µm

HLznst 28g



10 µm

Table 3.2 22 SEM images of Hydraulic lime-pozzolana pastes after 84 days of hydration –SEI (2500X)



3.2.3.5 Isocalorimetric measurements

The heat of hydration of pozzolana-lime pastes was measured with isothermal induction calorimetry in order to gain further knowledge of the hydration kinetics²⁸. The rate of heat development versus hydration time curves and the cumulative evolved heat up to 60 hours and 24 hours are shown in Figure 3.2 21 and Figure 3.2 22, respectively.

The heat of hydration curves for all the pastes considered did not show the typical profile of the hydration reactions of a normal cement binder. All the samples, in fact, showed i) an intense exotherm peak immediately after mixing the pozzolana and portlandite powders with water and ii) a longer continuation of the initial exotherm. Only the paste without admixture showed a superimposed peak at approximately 4 hours of reaction, characterized by a relatively rapid increase in rate of heat evolution followed by a slower decrease, resulting in an asymmetric peak shape.

The first high exothermal peak should be related to contributing exothermal processes as water adsorption on the pozzolana, hydration and solvation of exchanged and dissolved metal cations, dissolution of portlandite²⁹. Snellings and Mertens explain the continuous rate of heat evolution or the presence of a second peak considering that the continuous rate: “can be related to the continuous pozzolanic reaction as evidenced by the formation of CSH, $C_4A\hat{C}_{0,5}H_x$ and $C_4A\hat{C}H_x$ reaction products by XRD and TG”²⁸, and in the latter case the dissolution of portlandite controlled the precipitation of C–S–H gel on the zeolite surface. The first cover of reaction products might be broken due to the changing solution environment, and the rupture might cause a second exothermal peak after approximately 3 hours of reaction.

The presence of different water repellents seems to influence the reactions slightly, with a slower but homogeneous production of CSH in comparison to HLA. Considering the total heat release (Figure 3.2 22), however, higher total heat release were observed in presence of water-repellent admixtures (in particular in HLSil, HLtes, HLcast).

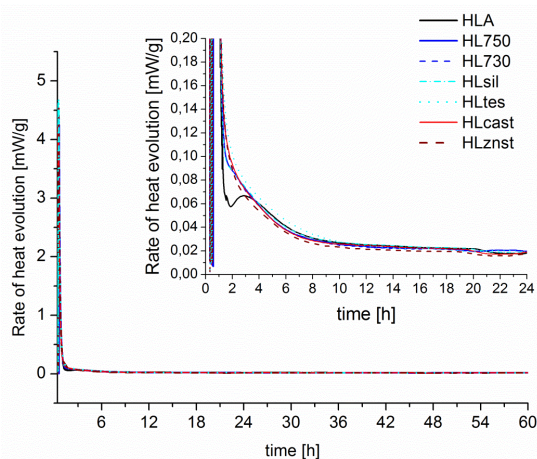


Figure 3.2 21 The rate of heat evolution of pozzolana-lime at 25°C of pastes without (HLPA) or with water repellent admixtures.

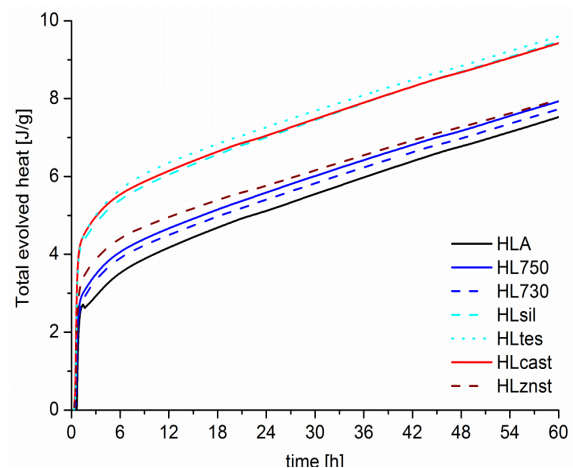


Figure 3.2 22 Patterns of cumulative evolved heat over time of the different pastes

²⁸ Two samples for each mix were analyzed, the instrument was calibrated in order to have the highest resolution.

²⁹ Snellings, R., *et al.* 2010

3.2.4 DISTRIBUTION OF THE WATER REPELLENTS INSIDE THE BINDER MATRIXES

A fundamental aspect to consider within the context of the characterization of water-repellent binder pastes is the study of the distribution of the admixtures. The distribution might influence both the hydration reactions of the binder and the morphological and physical chemical properties of mortars made with water-proofing agents.

It was not easy to individuate the particles of the water repellent: the similar chemical nature of some of the admixed water-repellents (the silicones first of all) and of the matrixes (mostly silicates) and the low percentages of admixtures used hinder a full recognition of the distribution. On the other side, an increased percentage of water-repellent in the matrix can influence also its distribution, therefore, we decided to analyze the prepared pastes with 1% of admixtures and to prepare new pastes with no more than 5% of admixed water-repellents.

The water-repellent admixtures showed similar distribution in the different binders, therefore the distribution in the different systems is here described together. The results will be considered for understanding the distribution of water repellents also in mortar matrixes.

In the attempt of finding out evidence of the distribution of the additives inside the binder matrixes techniques such as optical microscope MO and SEM observations and EDX elemental mapping and FT-IR-ATR micro measurements were used. Some of the SEM observation have been already displayed in the previous paragraphs. Here is shown a complete overview of the different situations found.

Three different groups can be distinguished including pastes added with: i) powder silanes and stearates supported on inorganic carriers; ii) calcium and zinc stearates powders; iii) the emulsion silane Tegosivin® and the redispersible polymer Vinnapas®.

Powder siloxanes

In this case grains of the carriers were found thanks to MO and SEM observations all over the pastes matrix (Table 3.2 23), but it was not possible to find out if the siloxanes remained linked to the powder surfaces or if there was a migration during the mixing or the hydration. Micro FT-IR-ATR spectroscopy was used to map cement paste samples to distinguish the siloxanes, but the samples porosity and surface roughness did not allow to obtain clear maps at the different wavelengths. However, the map relative to the Si-O-Si stretching absorption at 1057 cm^{-1} of cement pastes admixed with 5% of Sitren P750® was more defined than the others (see Table 3.2 23). Unfortunately, no particular evidences of the presence of the powder siloxane Sitren P750® were seen with this technique, only lower transmittance was detected in presence of pores (right part of the FT-IR map in Table 3.2 23).

The hypothesis that the hydrophobic siloxanes separate from their inorganic carriers is, however, suggested by the behaviour of the powder water-repellents in saturated calcium hydroxide solution (see Chapter 3.1). In that case the organo-siloxanes seemed to separate from the carrier after one month, the carrier decreased its hydrophobicity and dispersed itself inside the liquid. Furthermore, the carrier grains were covered by hydration products over time and partially involved and consumed in this reaction, while the presence of hydrophobic compounds over the grain surface should prevent this behaviour. Considering the hydrophobic nature of the siloxanes is possible that they slowly separate from the carrier and then dispose at the air-water interfaces.

Calcium and zinc stearates

Evidences of the distribution of calcium and zinc stearates inside the matrix were obtained both with EDX elemental maps and with micro FT-IR ATR spectroscopy. We have already seen above some examples of the distribution of stearates inside the binder matrix thanks to SEM-EDX analysis, and Table 3.2 24 summarizes the principal data and features related to the stearates distribution:

-Optical microscope and SEM images at low magnification evidenced a porous structure of binder pastes added with calcium or zinc stearates;

-EDX maps evidenced the presence of higher percentage of carbon in correspondence of the pore walls and on some spherical grains not visible in pastes without admixtures. In the same areas no Silicon or Aluminium were detected. In presence of zinc stearates, zinc and carbon were detected on the pore walls;

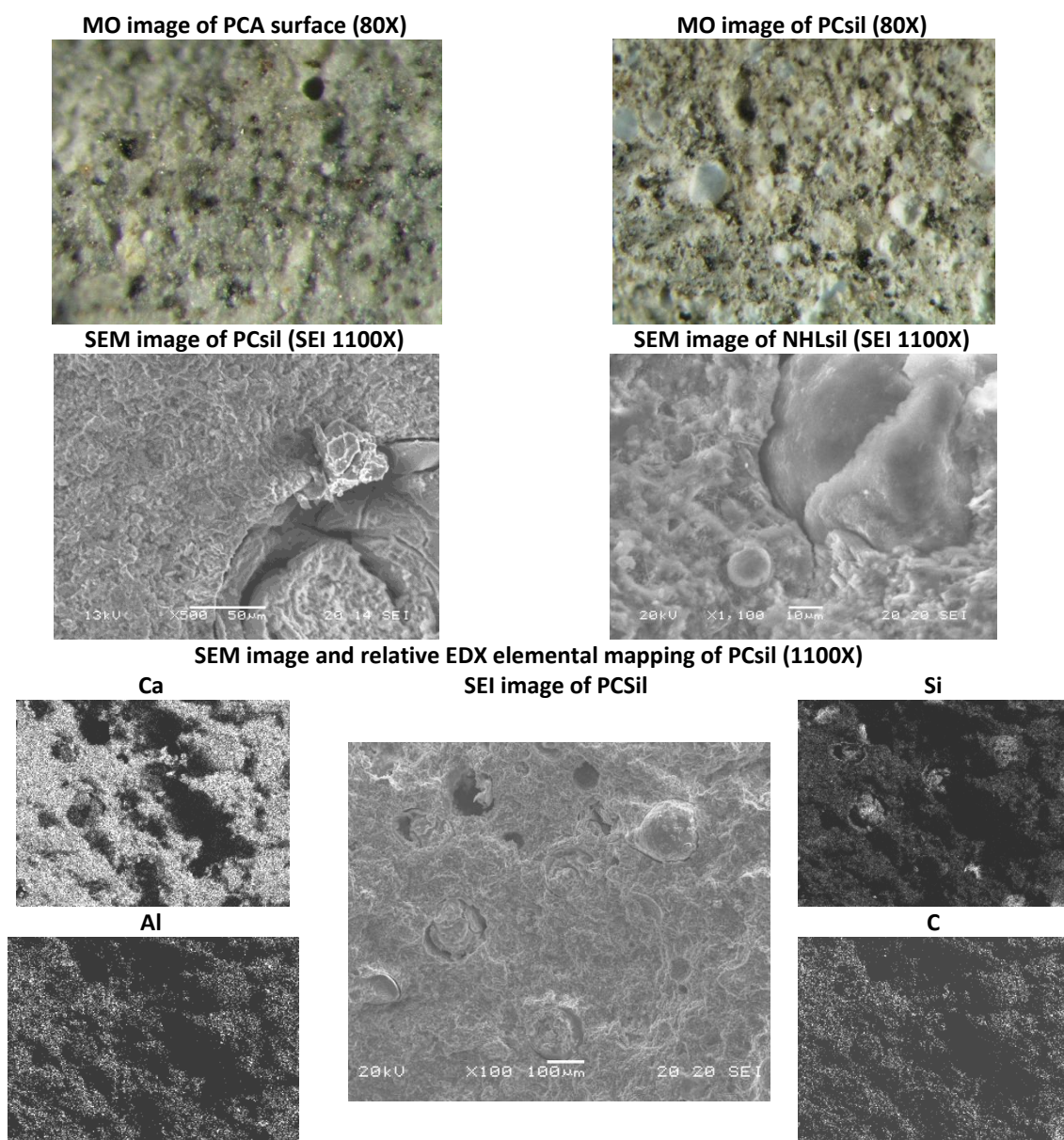
-In the FT-IR ATR maps of pastes with stearates the transmittance was generally lower over the pores (see Table 3.2 24 red area of the FT-IR maps), but the maps registered at 2917cm^{-1} and 2890cm^{-1} ($-\text{CH}_2$ stretching region typical of the organic admixture) were different from the others, showing a higher transmittance over the pore walls.

These data and their hydrophobic nature indicate that the metal soaps behaved like surfactants and remained at the interfaces water-air-binder. They can act as air entraining agents, stabilizing air bubbles, or forming oriented aggregates inside the matrix (micelles).

Emulsion silane and Vinnapas

The emulsion silane Tegosivin HE[®] and the polymer Vinnapas[®] were not clearly detectable with the analysis performed, no aggregates or lumps were found. However a general increase of the porosity was observed with MO and SEM, is possible therefore, that they acted as air entraining agents. The two admixtures distributed in an homogeneous way, having also surfactants in their formulation which assured a better compatibility with the liquid binder pastes allowing complete miscibility.

Table 3.2 23 Distribution of water repellents inside binder matrixes: 1- repellents on inorganic carriers. The grains of the carrier are clearly visible in comparison to the mixes without water-repellents (HLA)



μ FT-IR ATR mapping of PC750 with 5% of water repellent
 (links: MO image, pore are visible as dark holes, right: FT-IR map of the absorption at 1057 cm^{-1})

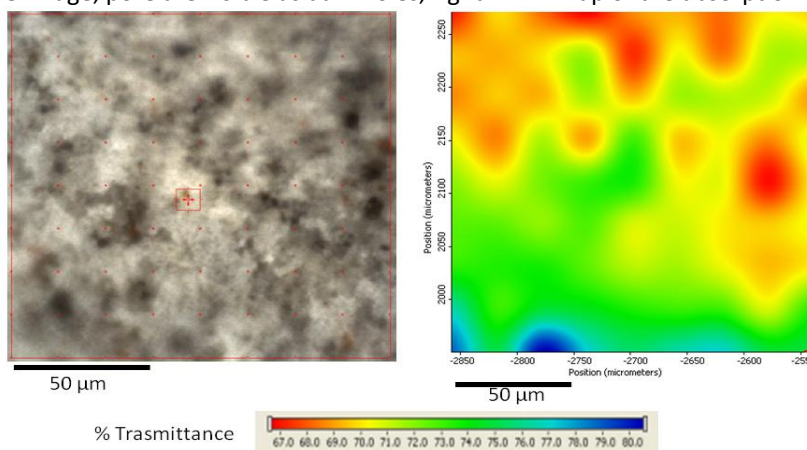
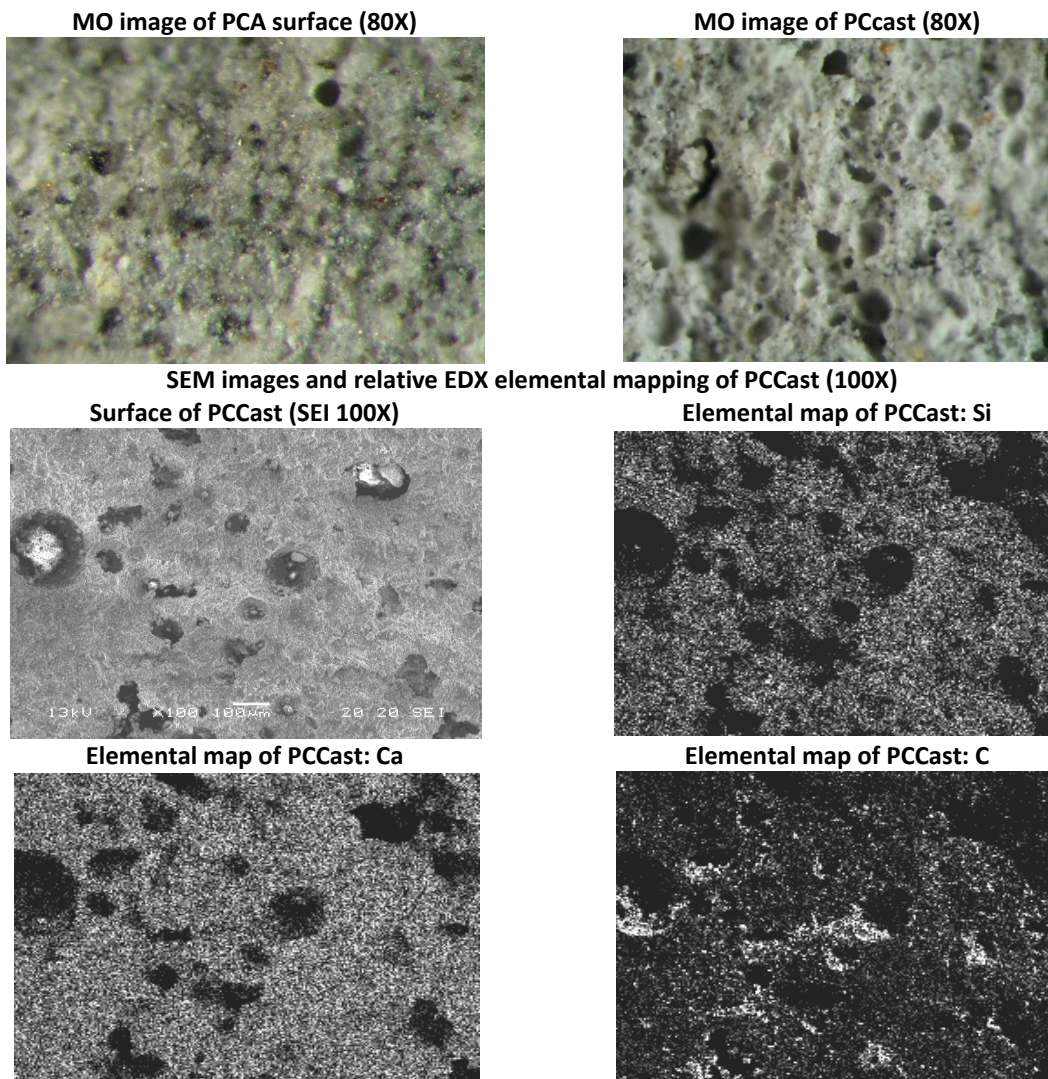
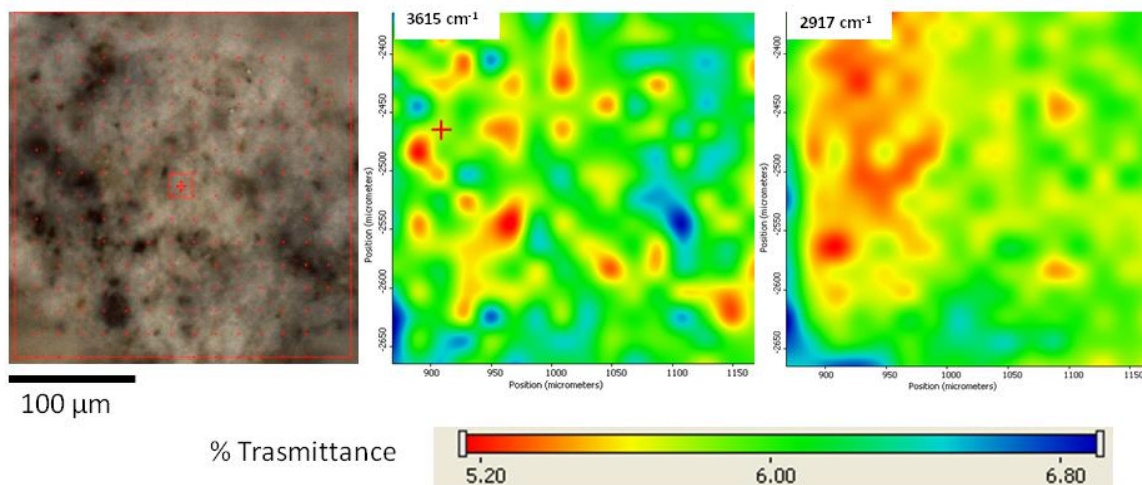


Table 3.2 24 MO,SEM-EDX and μ FT-IR analysis of some cement binder pastes with stearates giving evidences of the distribution of the admixtures inside the matrix



μ FT-IR ATR mapping of PCCast with 5% of water repellent

(links: MO image, pore are visible as dark holes, right: FT-IR maps of the absorptions at 3615, 2917 cm^{-1})



3.3 Chemical and physical properties of Mortars with water-repellent admixtures

This part of the thesis was undertaken with the aim to explore the physical and chemical properties of limestone cement mortars, natural hydraulic lime mortars, pozzolana-lime mortars, admixed with different water-repellents.

Different standard tests were carried out on admixed mortars specimens in order to evaluate the general properties of the mortars studied and, in particular, their behaviour in presence of water in laboratory conditions. The results are presented by considering the different mortar mixtures and on the basis of different binders.

The studies and tests done were addressed to the knowledge of two main topics/aspects:

- the physical properties of fresh and 28 days aged mortars such as density, workability, porosity and mechanical strength;
- the behaviour of admixed mortar specimens in respect of liquid water and water vapour.

The results concerning the different items will be compared and discussed in Chapter 4 Discussions.

3.3.1 LIMESTONE CEMENT MORTARS WITH WATER-REPELLENTS

3.3.1.1 Mix design, composition and properties of fresh mortars

Different limestone cement mortars were prepared by mixing limestone cement CEMII B/L with a silicate-carbonate sand, water and different water repellents³⁰. The water repellent admixtures added, their dosage and the water binder ratio (w/b) used are listed in Table 3.3 1. The mortar mix CMA, without water repellents, was prepared as reference and the water binder ratio w/b was fixed for all the mixes at 0.96. The water repellents were added as 0.5% ,1%, 1.5 % by mass of the dry binder and sand mix, as reported in previous similar studies³¹. The silanes/siloxanes Sitren P750[®], Sitren P730[®], Silres A[®], Tegosivin HM[®], calcium and zinc stearates and the polymer Vinnapas 8031H[®] were chosen as water repellent admixtures.

Beside the mixtures composition, Table 3.3 1 also shows the density and the slump diameter of the fresh mortars. The presence of water repellents has always caused a decrease of the mixture density except for CMsil1.5, with 1.5% of Silres A[®].

The presence of higher dosages of silane/siloxanes caused an increased density of the fresh mortars. The use of calcium or zinc stearates changed only slightly the density, while the use of Vinnapas 8031 H[®] caused a strong decrease of the density. The water repellents might act as air entraining agents (in particular in CMvin mixes).

The mixtures consistency, evaluated by considering the slump diameter, mainly depends on the nature of the water admixtures used. Silane/siloxanes caused a decreased workability in comparison to CMA. CMznst mixes presented decreased slump diameter and viscous and pasty consistence. A similar pasty consistence was observed also for CMcast0.5,1,1.5 mixes. The slump diameters of CMvin0.5, 1, 1.5 were greater than CMA ones, the addition of Vinnapas 8031H[®] resulted in a flower mix probably because the additive worked as a plasticizer³².

³⁰ See Chapter 3.1.4 Aggregates

³¹ P. Zhang, F.H. Wittmann, Tj Zhao, 2010 ; F.L. Maranhao, V.M John, 2008

³² Probably the long polymers chain increase the flowability of mortar disposing between the grains

Table 3.3 1 Limestone cement mortars composition; density and consistence of fresh mortar mixtures. W/b= water binder ratio by mass; Slump ϕ = diameter of the mortar slump according to EN 1015-3.

Mix name	Water-repellent admixture			w/b	Density g/cm ³	Slump ϕ cm
	name	class	% by mass			
CMA	-	-	-	0.96± 0.02	2,27± 0.02	17.5±0.3
CM7500.5	Sitren p750	silane with amorphous silica as carrier	0.5	0.96± 0.02	2.10± 0.02	16±0.3
CM7501			1	0.96± 0.02	2.11± 0.02	16.5±0.3
CM7501.5			1.5	0.96± 0.02	2.13± 0.02	16.2±0.3
CM7300.5	Sitren p730	Silane on CaCO ₃ carrier	0.5	0.96± 0.02	2.18± 0.02	16.8±0.3
CM7301			1	0.96± 0.02	2.21± 0.02	16.7±0.3
CM7301.5			1.5	0.96± 0.02	2.22± 0.02	17±0.3
CMSil0.5	Silres A	silane with amorphous silica as carrier	0.5	0.96± 0.02	2.15± 0.02	16.8±0.3
CMSil1			1	0.96± 0.02	2.10± 0.02	16.3±0.3
CMSil1.5			1.5	0.96± 0.02	2.8± 0.02	15.9±0.3
CMtes1	Tegosivin HM	emulsion silane	1	0.96± 0.02	2.04± 0.02	15.1±0.3
CMtes5			5	0.96± 0.02	2.05± 0.02	18±0.3
CMcast0.5	Ca Stearate	metal soap	0.5	0.96± 0.02	2.29± 0.02	17.5±0.3
CMcast1			1	0.96± 0.02	2.23± 0.02	17.3±0.3
CMcast1.5			1.5	0.96± 0.02	2.19± 0.02	17±0.3
CMznst0.5	Zn stearate	metal soap	0.5	0.96± 0.02	2.23± 0.02	15.5±0.3
CMznst1			1	0.96± 0.02	2.22± 0.02	15.2±0.3
CMznst1.5			1.5	0.96± 0.02	2.27± 0.02	14.7±0.3
CMvin0.5	Vinnapas 8031 H	terpolymer powder of ethylene. vinyl laurate and vinylchloride	0.5	0.96± 0.02	1.89± 0.02	20±0.3
CMvin1			1	0.96± 0.02	1.75± 0.02	20.5±0.3
CMvin1.5			1.5	0.96± 0.02	1.80± 0.02	21.3±0.3

3.3.1.2 Properties of 28 days aged limestone cement hardened mortars

FT-IR spectroscopy: characterization of limestone cement mortars after 28 days of hydration

The chemical composition of 28 days hardened mortars was investigated thanks to FT-IR ATR analysis on samples collected from the mortar bulks. Figure 3.3 1 shows the spectra collected for the mortars with 1.5% of water repellents added.

CMA spectrum, without water-repellents, showed: the absorption of -OH stretching at 3640 cm⁻¹ of calcium hydroxide formed during the clinker hydration; the broad -OH peak centred at 3400 cm⁻¹ due to hydrate compounds; the presence of calcium carbonate (-CO₃ stretching at 1436 cm⁻¹, -CO₃ bending at 875 cm⁻¹); different silicates peaks in the 900-1100 cm⁻¹ range. At 950 cm⁻¹ it is possible to distinguish the Si-O-Si absorption of hydrated silicates due to the formation of CSH during the hydration.

Similar spectra were registered on water-repellent mixtures. In the 3000-2800 cm⁻¹ range the absorptions of aliphatic -CH, -CH₂ can be seen for the mixtures CM7501.5, CMSil1.5, CMtes, CMcast1.5 and CMznst1.5. For the mixes CMtes1.5, CMznst1.5 and CMvin1.5, the absence of the -OH absorption at 3640 cm⁻¹ and the relative lower Si-O-Si stretching at 950 cm⁻¹ might suggest a *delayed hydration* of the C₃S and C₂S phases and a slower production of CSH and calcium hydroxide.

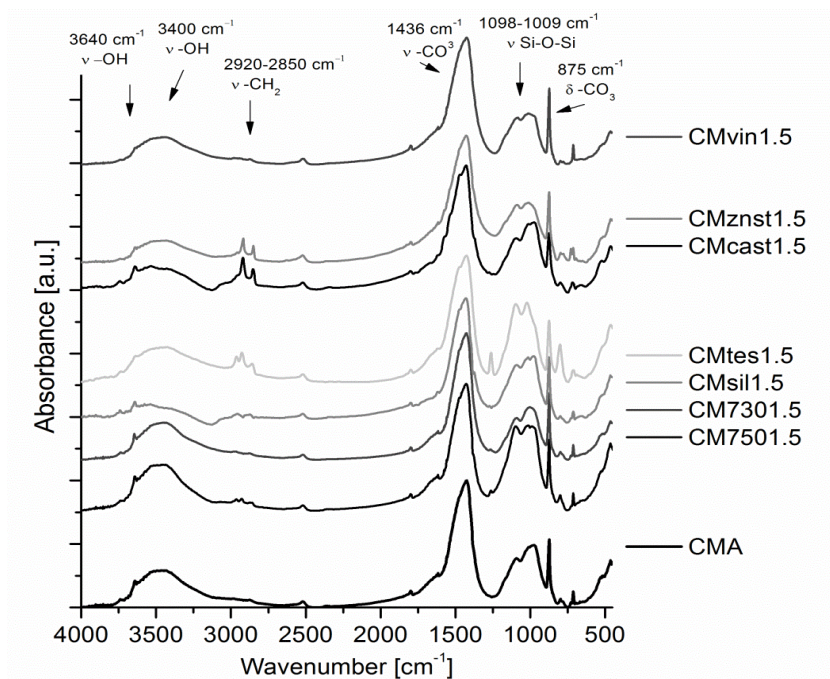


Figure 3.3 1 FT-IR ATR spectra of different limestone cement mortars without (CMA) or with water repellents added at 1.5% by dry weight, the correspondent mix names are listed next to each spectrum

Morphological and colour characterization

The visual observation of the hardened mortars did not allow to see differences (Table 3.3 2). Only CMZnst and CMtes mixtures showed slightly rougher surfaces and seemed to have higher porosity.

To further characterize the visual appearance of the samples, colorimetric measurements in the CIEL*a*b* colour space were performed. The colorimetric values reported in Table 3.3 3 were evaluated from reflectance spectra collected on the mortar mixes¹. The values collected including the specular component (SCI) or excluding it (SCE) are both reported, even if the variations between the two were negligible, pointing out that the mortars were opaque and did not have a glossy appearance.

All the analysed samples were light grey and presented similar L*, a*, b* values. The scale range was tight and the colour differences were quite negligible, also considering the natural dishomogeneity of the mortar textures. It was possible, however, to observe a slight increase of the yellow component, by adding a siloxane (CM750, CMsil, CMtes mixtures), while an increase of the blue one by adding a stearate (CMcast and CMznst mixtures). Furthermore, the addition of a stearate and its increasing dosage caused an increase of the L* component, i.e. the lightness.

¹ The measurements were taken in three different areas for each sample. A set of three spectra was acquired for each point, with final colorimetric values coming from an average of 9 acquisition (errors correspond to standard deviation).

Table 3.3 2 Images of CMA, CM7501, CMznst1; above. macro photos (1:1 scale) , below: optical microscope OM 7X observation of 28 days aged specimens

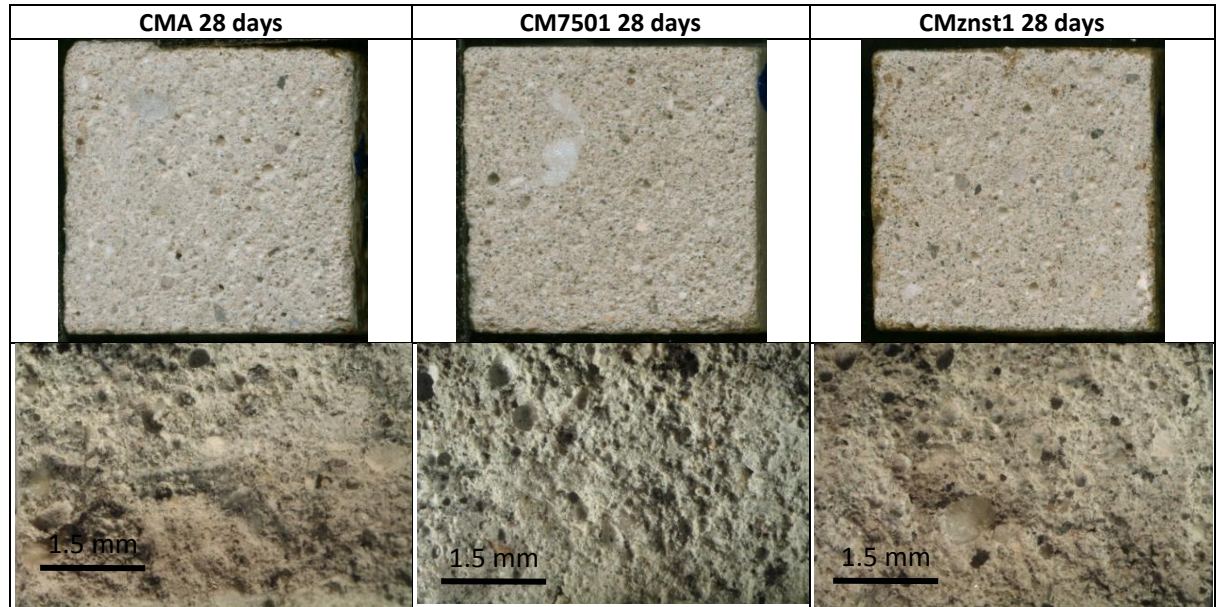
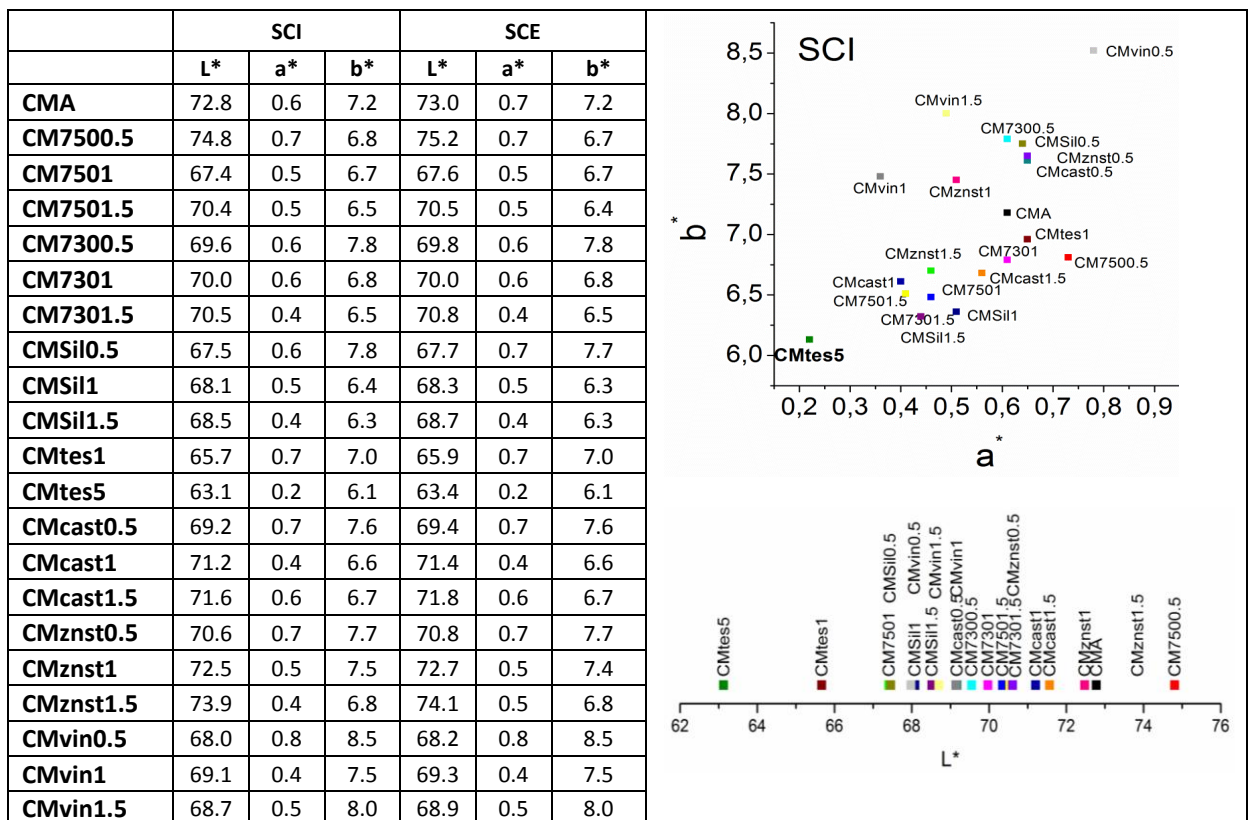


Table 3.3 3 Colorimetric data collected for limestone cement mortar mixes, the L*, a*, b* parameters listed regards the lightness, the red-green hue and the blue-yellow hue, respectively, (illuminant D65). The measurements are reported with specular component included (SCI) or with specular component escluded (SCE) . The graphs on the right show the colorimetric parameters L*, a*, b* in the CIEL*a*b* space when the specular component is included (SCI).



Density and porosity of limestone cement mortars

The structure and microstructure of the hardened mortars was investigated by considering the density and the porosity of the specimens, also with mercury intrusion porosimeter (Table 3.3 5, Table 3.3 4). In the following list the measures performed are summarized²:

- the *real density* was measured on dried, finely ground samples with Helium picnometer;
- the *bulk density* was measured by considering the ratio between the mass and the geometrical volume calculated on cube specimens (28 mm³) (the average of 5 samples was considered);
- the *bulk density MIP* was obtained from MIP analyses, it include the open porosity and exclude the porosity ≤ 4 nm (detection limit of MIP instrument);
- With the name *apparent density MIP* it was considered a measure which included the close porosity and the open porosity ≤ 4 nm;
- the *total porosity* was evaluated by considering the ratio between bulk density and real density;
- The *total open porosity MIP* was calculated by the MIP software from the total cumulative volume of mercury intruded inside the sample during the analysis; the *average pore radius* was also given by the MIP analyses;
- *Ultrasonic measurements* were performed on 16*4*4 cm prismatic specimens, the value is the average of three specimens for each mixture.

Negligible differences were observed between the real density of different mortar mixes, therefore a unique values was calculated: 2.73 g/cm³. On the other side, the different bulk density and the different porosity greatly depend on the water repellent admixture and on its dosage.

Generally speaking, the bulk density and porosity data calculated on the specimens agree with MIP results: lower bulk densities correspond to higher cumulative volumes of intruded mercury (total cumulative volume MIP) and, therefore, to higher open porosities (total open porosity MIP). This inverse correspondence implies that the close porosity did not change so much, while the open porosity increases more. Direct correspondence between bulk density and ultrasonic measurements was observed, probably because a denser matrix should be more compact and the ultrasonic wave travel faster inside the material.

To go into more details, CMA, without water repellents, presented a bulk density around 1.68 g/cm³ and a total porosity around 38.5%, of which 29.5% was open porosity. The % volume distribution and cumulative volume versus the pore radius (Table 3.3 4) evidenced that no pores larger than 5µm were present and that smaller pores were homogeneously distributed.

CM750 mixtures, added with Sitren P750®, were slightly denser at 0.5% of water repellent. The open porosities were also similar but their distribution changed for higher percentages of water repellent: the porosity in the 1-10 µm range increased in CM7501.5 in comparison to CM7501 and CMA.

CM730 mixtures showed lower porosity in the 1-10 µm range and higher open porosity in the 0.1-1 µm pore radius range in comparison to CMA.

CMsil mixtures were characterised by similar values of density, porosity and compactness to CMA.

Both uses of the emulsion silane Tegosivin HE and the polymer Vinnapas 8031H caused a remarkable change in the mortar structure with increased porosity. The strong differences

² see also Chapter 2.2.10. Density, microstructure (MIP) and ultrasonic measurements

between the total porosity and the open porosity values indicated that a high close porosity were present. The increasing of the admixtures percentages caused a further increase of the total porosity of CMtes and CMvin mixtures and larger pores were enhanced (1-10 μm range). Higher bulk densities, lower porosities and faster ultrasonic waves were detected by adding calcium or zinc stearates (CMcast and CMznst mixtures), the pore size distribution showed in both cases that at increasing water repellents percentages led to higher porosity in the 0.1-1 μm range and to a lower porosity in the 1-10 μm range.

Table 3.3 4 Distribution of the porosity and cumulative volume versus the pore radius of the different limestone cement mixtures

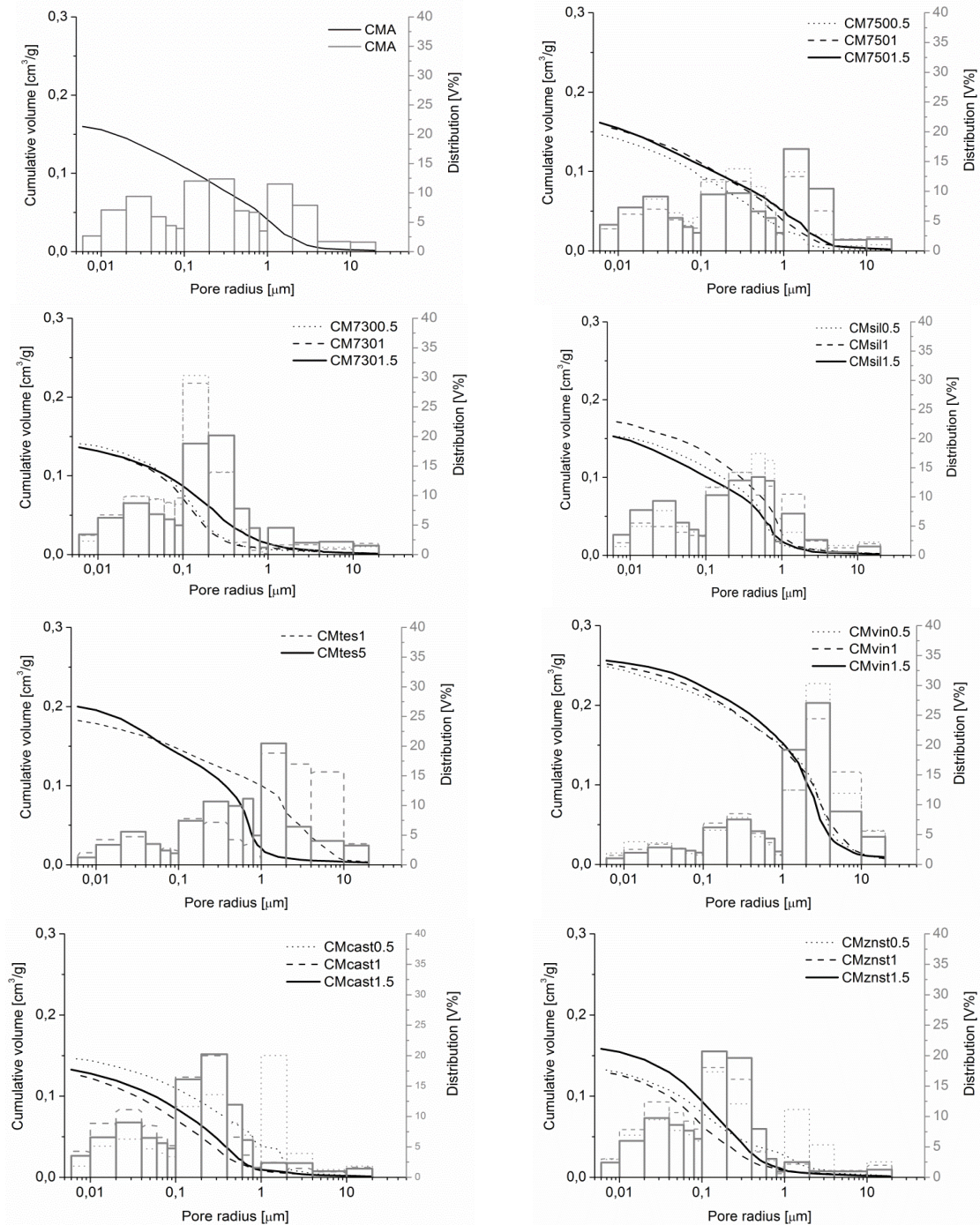


Table 3.3 5 Real density, apparent density and porosity data of mortars (the average of three measurements with their standard deviation is reported).

	Real density (g/cm ³)	Bulk density (g/cm ³)	Bulk density MIP (g/cm ³)	Apparent density MIP (g/cm ³)	Total porosity (%)	Total open porosity MIP (%)	Total cumulative volume MIP(mm ³ /g)	Average pore radius MIP(micron)	Ultrasonic measurements (m/s)
CMA	2.73±0.01	1.68±0.02	1.76±0.02	2.50±0.21	38.5±0.1	29.5±0.8	167±6	1.2±0.5	5397±158
CM7500.5	2.73±0.01	1.74±0.01	1.87±0.05	2.61±0.09	36.4±0.1	28.3±0.5	151±1	1.8±0.1	5397±158
CM7501	2.73±0.01	1.66±0.01	1.79±0.01	2.51±0.02	39.4±0.1	28.9±0.7	162±4	1.1±0.2	4594±86
CM7501.5	2.73±0.01	1.66±0.01	1.84±0.01	2.66±0.05	39.3±0.1	30.9±0.2	168±1	1.8±0.1	4398±114
CM7300.5	2.73±0.01	1.83±0.01	1.87±0.02	2.55±0.09	33.1±0.1	26.6±0.1	143±1	0.2±0.1	6129±113
CM7301	2.73±0.01	1.81±0.01	1.87±0.01	2.54±0.010	33.6±0.1	26.4±0.1	141±1	0.1±0.1	6821±80
CM7301.5	2.73±0.01	1.23±0.92	1.87±0.05	2.55±0.09	54.8±0.1	26.4±0.1	141±2	0.3±0.1	5899±168
CMSi0.5	2.73±0.01	1.69±0.01	1.81±0.06	2.52±0.15	38.0±0.1	28.0±0.2	155±1	0.6±0.1	4458±84
CMSi1	2.73±0.01	1.74±0.04	1.74±0.01	2.49±0.10	36.4±0.1	30.3±0.4	174±3	0.8±0.1	4172±80
CMSi1.5	2.73±0.01	1.61±0.02	1.84±0.02	2.59±0.09	41.0±0.1	28.9±0.5	157±1	0.7±0.1	4430±51
CMtes1	2.73±0.01	1.68±0.01	1.80±0.04	2.63±0.08	38.4±0.1	31.5±2.9	175±9	3.8±0.5	3224±233
CMtes5	2.73±0.01	1.63±0.02	1.86±0.09	2.73±0.09	40.5±0.1	31.7±3.0	170±1	0.8±0.2	2510±60
CMcast0.5	2.73±0.01	1.77±0.05	1.92±0.08	2.69±0.16	35.0±0.1	28.5±1.0	148±1	1.8±0.1	7008±152
CMcast1	2.73±0.01	1.78±0.03	1.92±0.04	2.71±0.07	34.7±0.1	28.7±4.2	149±19	1.4±1.0	6026±198
CMcast1.5	2.73±0.01	1.70±0.01	1.86±0.02	2.50±0.02	37.7±0.1	25.5±2.1	137±5	0.4±0.3	5423±92
CMznst0.5	2.73±0.01	1.73±0.01	1.91±0.01	2.58±0.20	36.6±0.1	26.0±0.3	136±1	0.1±0.1	6082±202
CMznst1	2.73±0.01	1.82±0.01	1.86±0.05	2.53±0.04	33.6±0.1	26.2±0.6	141±1	0.1±0.1	5996±140
CMznst1.5	2.73±0.01	1.65±0.02	1.78±0.03	2.50±0.04	39.5±0.1	28.6±0.9	161±2	0.3±0.2	4226±141
CMvin0.5	2.73±0.01	1.44±0.01	1.55±0.09	2.53±0.09	47.2±0.1	38.9±0.1	252±1	3.2±0.1	4949±176
CMvin1	2.73±0.01	1.44±0.01	1.54±0.01	2.55±0.08	47.2±0.1	39.4±0.2	255±1	3.2±0.8	4917±116
CMvin1.5	2.73±0.01	1.42±0.01	1.52±0.01	2.52±0.81	47.9±0.1	39.4±0.8	259±2	2.7±0.1	4593±133

Mechanical properties of the hardened limestone cement mortars

In order to evaluate the suitability of a mortar for a specific purpose/application, we cannot forget its mechanical behaviour. It is evident that, in order to find the correct application of a mortar, the compressive and flexural strengths should be known.

The mechanical properties usually depend on the macro and microstructure of the mortar but also on the hydration rate of the system. A faster hydration corresponds to the formation of an interconnected and compact matrix with usually higher mechanical performances.

The flexural and compressive strength of the different limestone cement mortars was measured according to the EN1015-11³. Table 3.3 6 and Table 3.3 7 lists the compressive and flexural strength data obtained from specimens aged 28 days and Table 3.3 8 shows the curves of compressive strength vs. percentage strain registered.

CMA had a flexural strength around 1.21 MPa and a compressive strength of 11.07 MPa. The uses limestone cement was a CEMII B 32.5: preparing the specimens in accordance to EN1015-2 with a normal sand it should developed a compressive strength around 32.5 MPa after 28 days of hydration. The found values were lower because a finer sand was used and the water binder ratio w/b was increased to reach the correct consistence of the fresh mix⁴.

The addition of water repellents influenced the mechanical behavior in different ways:

- The silanes supported on silica carrier Sitren P750[®] and Silres A[®] and the emulsion silane Tegosivin HE[®] caused a strong decrease of the flexural and compressive strength of CM7501, CMsil1, CMtes1 mixes, this might have been due to their microstructure, in particular CMtes1 had higher porosity and really low density. However, the loss of mechanical strength in CM750 and CMsil mixtures cannot be explained only by considering the increased porosity but also the hydration rate must be taken into account: the addition of the water-repellent admixtures were able to influence the hydration⁵, in comparison to CMA. The increasing of water repellent dosage caused the decreasing of compressive strength in CM750 and CMtes mixes, while an increase was noticed for CMsil mixes.
- The use of the silane Sitren P730[®] in CM730 mixes allowed to reach mechanical strengths higher than CMA, thanks to the higher bulk density and the positive influence on the hydration reactions (as seen in the chapter 3.2).
- Both CMcast and CMznt mixtures (added with metal soaps) reached higher compressive strengths and similar flexural strengths to CMA due to their higher bulk densities and lower porosity (see paragraph above). For higher water-repellent percentages the compressive strength even if the corresponding densities increased⁶. Probably the strong retarding effect of these metal soaps on the binder hydration, seen in Chapter 3.2 and suggested also by the FT-IR analyses reported above, slowed down the formation of a well interconnected matrix and therefore the development of high mechanical strengths.

³ See Chapter 2.2.11. Mechanical properties of the mortars.

⁴ High w/b ratios cause the increasing of the porosity and the formation of further capillary pores.

Furthermore no plasticizing agents were added to decrease the w/b ratio in order to evaluate only the influence of the water repellents on the mix.

⁵ See also the chapter 3.2 Study of the hydration of pastes

⁶ See also the previous paragraph on mortars density and microstructure

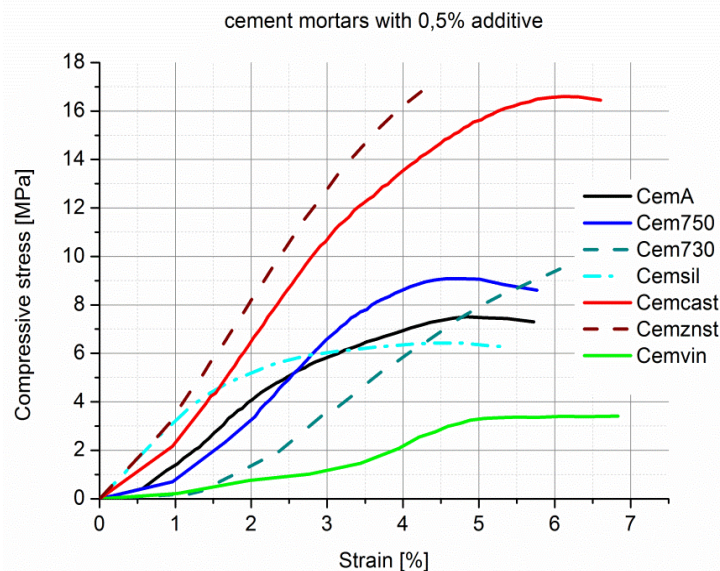
Table 3.3 6 Compressive strength and flexural strength of 28 days specimens without (CMA) or with 1% of water repellent added, the values are the average of three measurements, the standard deviation is given as error. The tangential and secant modulus are reported.

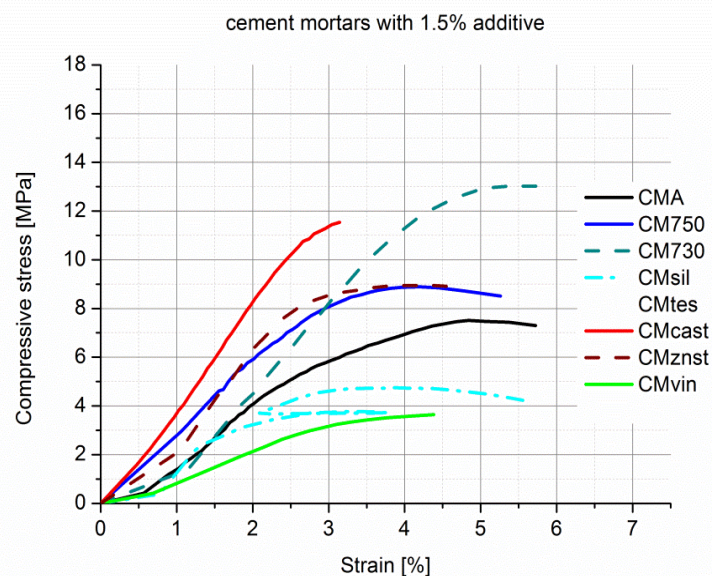
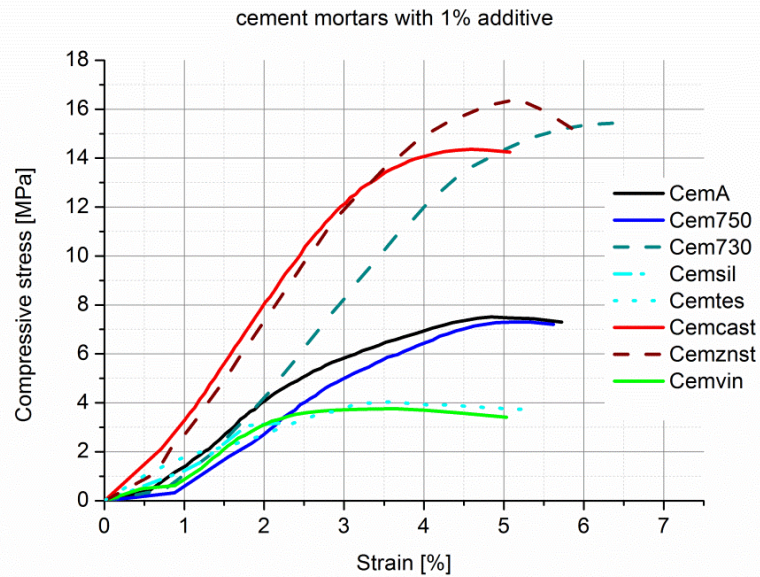
Mortar mix	Compressive strength			Flexural strength
Water repellent at 1%	σ_{max} (MPa)	E_{mod} tangential (MPa)	E_{mod} secant (MPa)	σ_{max} (MPa)
CMA	11.07±0.60	1.66±0.02	1.79±0.03	1.21±0.05
CM7501	8.25±0.35	1.23±0.05	1.37±0.04	1.09±0.03
CM7301	15.76±0.63	2.53±0.08	2.31±0.01	1.45±0.08
CMSIL1	4.55±1.78	1.22±0.02	1.24±0.05	0.98±0.07
CMtes1	5.34±0.64	1.86±0.04	1.84±0.15	1.23±0.12
CMcast1	14.56±1.30	3.91±0.05	3.51±0.09	1.07±0.08
CMznst1	17.08±0.97	3.59±0.02	3.42±0.51	1.11±0.12
CMvin1	3.77±0.89	1.30±0.09	1.06±0.16	1.14±0.03

Table 3.3 7 Compressive strengths values of the different mixes at different water repellents percentages: without (CMA), 0.5%, 1. 1.5% by weight.

Mix name	Water repellent	Compressive strength at different water repellent dosage		
		σ_{max} (MPa)		
CMA	-	11.07±0.60		
		0.5 %	1 %	1.5%
CM750	silicone	10.51±1.00	8.25±0.35	8.90±1.57
CM730	silicone	10.61±0.62	15.76±0.63	13.31±0.78
CMSIL	silicone	6.83±0.91	4.55±1.78	11.84±5.77
CMtes	silicone	-	5.34±0.64	5.00±0.32
CMcast	Ca stearate	16.80±0.13	14.56±1.30	12.23±0.93
CMznst	Zn stearate	18.30±0.38	17.08±0.97	9.27±0.75
CMvin	terpolymer	4.05±0.22	3.77±0.89	4.40±0.14

Table 3.3 8 Graphs of the compressive stress of limestone cement mortars vs. their percentage strain, mixes with different water repellents at 0.5% (below), 1%, 1.5% (in the following page).





Water vapour permeability of limestone cement mortars

The water vapour permeability is a key consideration for masonry applications, because it defines the "breathability" of the mortar, i.e. the possibility to have a free circulation of water vapour inside and outside the mortar. Cement mortars tend to have a consistent and 'closed' pore structure that traps water rather than allowing the building to breathe. Therefore, the measure of the water vapour permeability is important to fully understand the behaviour of our limestone cement mixtures in the presence of water.

One of the most used and simple indicator of the breathability of a porous substrate is the water vapour resistance factor μ , whose values are inversely proportional to the water vapour permeability. Cement mortars usually present μ values in the range of 15-35, while cement-free hydraulic mortars are characterized by a higher permeability and a vapour resistance factor that can vary in the range of 4-15⁷.

⁷ Izaguirre, A. et al., 2010; Maravelaki-Kalaitzaki, P., et al. 2007; Biscontin, G., L. Falchi, 2011

Figure 3.3 2 graphically shows the water vapour permeability results expressed as water vapour resistance μ , while Table 3.3 10 (see p. 119) lists the complete water vapour permeability results. The average of three specimens was considered with the relative standard deviation.

The μ value of CMA was lower than that of a normal cement, the permeability was, therefore, quite high. The addition of water repellents caused a general increase of the μ , except in CMvin mixtures where the high open porosity allowed to obtain a higher permeability.

Open porosity and permeability might be related, because a higher open porosity should allow a faster vapour transmission. Actually, water vapour transmission inside a porous matrix is regulated by complicated mechanisms, and can depend also on the chemical-physical interaction between the vapour and the material and on the complicate adsorption-diffusion-condensation-evaporation processes⁸. In the present study not always a higher water vapour permeability corresponded to a higher open porosity: CM750, CMSil and CMtes mixtures were characterized by high open porosity but their water vapour permeabilities were lower than CMA. Furthermore, to higher dosages of water-repellent admixtures corresponded lower permeability, even if the open porosity evaluated via MIP was high.

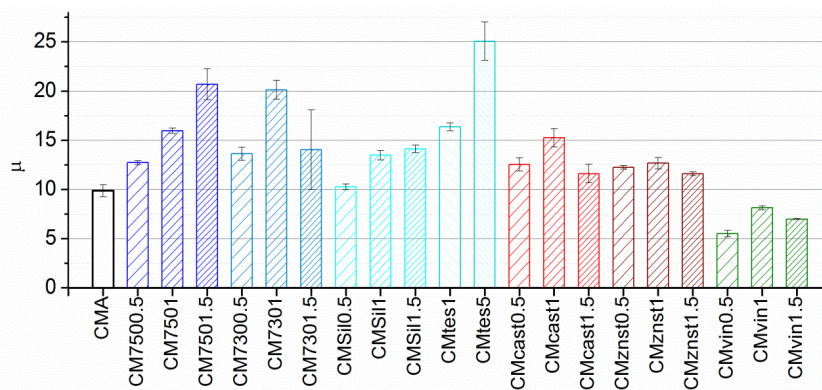


Figure 3.3 2 water vapour resistance factor μ of limestone cement mortars, Average of three measurements with standard deviation as error bars.

Capillary water absorption and contact angle measurements of limestone cement mortars

In previous published studies, it was observed that the water-repellent admixtures did not distribute themselves homogeneously and that often the outer surfaces presented lower absorption coefficient than the inner core⁹. This could be due i) to a preferential migration of the additive to the outer surface of the mortar; ii) to a lower porosity of the outer layers, more prone to a fast carbonation. Therefore, in this study both water absorption coefficients of the inner core and of the outer side of the specimens were considered, measuring the water absorption and putting either the cut- inner surfaces or the external surfaces in contact with water. Moreover, other studies pointed out that a wash-out of the water repellents might occur with time and that the water repellence diminished with few absorption cycles¹⁰. For these reasons the absorption tests were repeated several times.

⁸ Hall, C., Hoff W., 2002, p61-93

⁹ Li, W., et al. 2011, Wittmann, F.H., et al. 2011

¹⁰ Quadrelli M., et al. 2007

Figure 3.3 3 and 3.3.4 show the water absorption coefficients on the inner and outer surfaces values and the water absorption coefficients of repeated water absorption cycles¹¹.

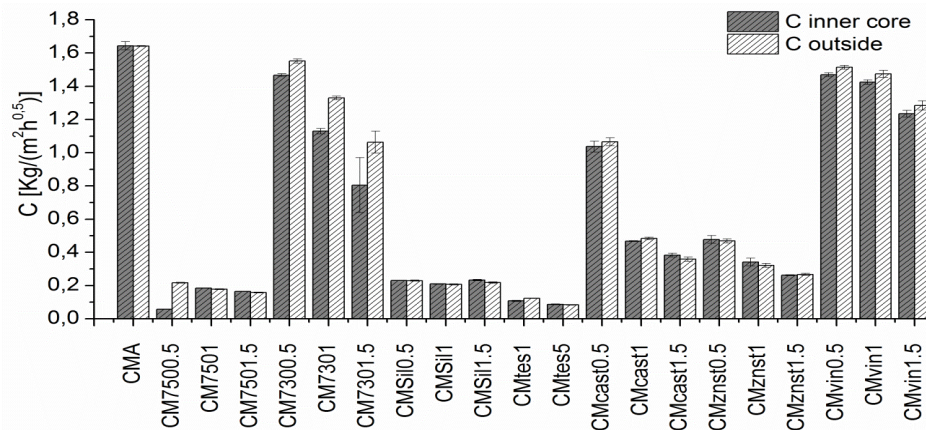
Table 3.3 9 shows the absorption curves obtained. The capillary water absorption coefficients and the contact angle of water drops are reported in Table 3.3 10. The average of three specimens is reported with their standard deviation as error.

Only slight and homogeneous differences between the water absorption of the inner core and the outside surfaces were observed for each mortar mix: every water repellent seems able to distribute quite homogeneously in the mortar bulk.

The total water repellent effect depended more on the used admixtures and on the dosage. Higher water repellent percentages corresponded always to lower water absorption, while the different water-repellents influenced the repellence behaviour in the following ways:

- silane/siloxanes Sitren P750®, Silres A®, Tegosivin HM® strongly decreased the water absorption and reached a complete hydrophobization with contact angle higher than 90°;
- CM730 and CMvin¹² had slightly lower water absorption in comparison to CMA
- the stearates decreased the absorption of CMcast and CMznst mixes only at higher percentages and had always contact angles inferior to 90°.

By repeating the absorption tests several times it was observed that the water absorption of CMA, CM750, CMSil, CMtes proportionally decreased, probably because a further hydration of the samples occurred in presence of water and water vapour, which caused the increase of the matrix compactness. The water absorption of CM730, CMcast0.5 and CMcast1, CMznst0.5 CMvin mixtures increased with repeated cycles, probably a wash-out effect of the water repellent. It is interesting that the water repellence diminished more for lower water-repellents percentages. Higher water-repellents percentages seemed to assure a more durable water-repellence effect.



¹¹ The table with a complete list of the water absorption coefficients at repeated cycles is reported in Appendix

¹² Sitren P730® presents lower active principle (less silane) over the carrier grains in comparison to Sitren P750® as declared by the supplier

Figure 3.3 3 Histograms of the water absorption coefficients of the inner core and external surfaces. The average of three measurements with their standard deviation is reported. Average of three measurements with standard deviation as error bars.

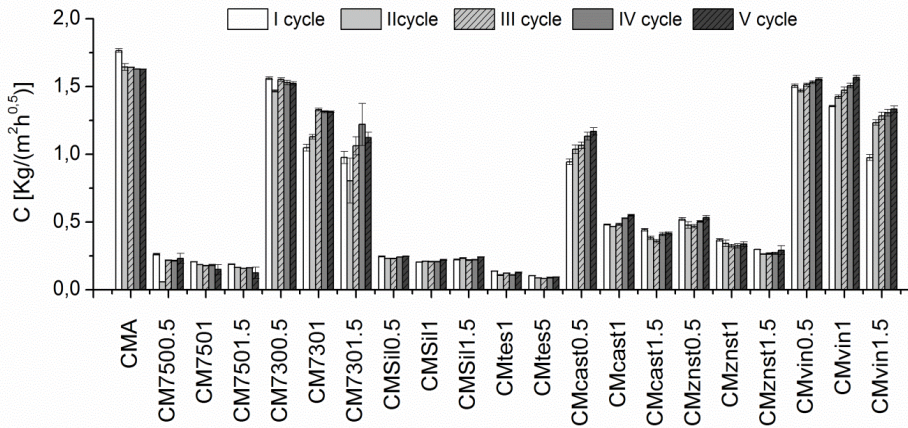
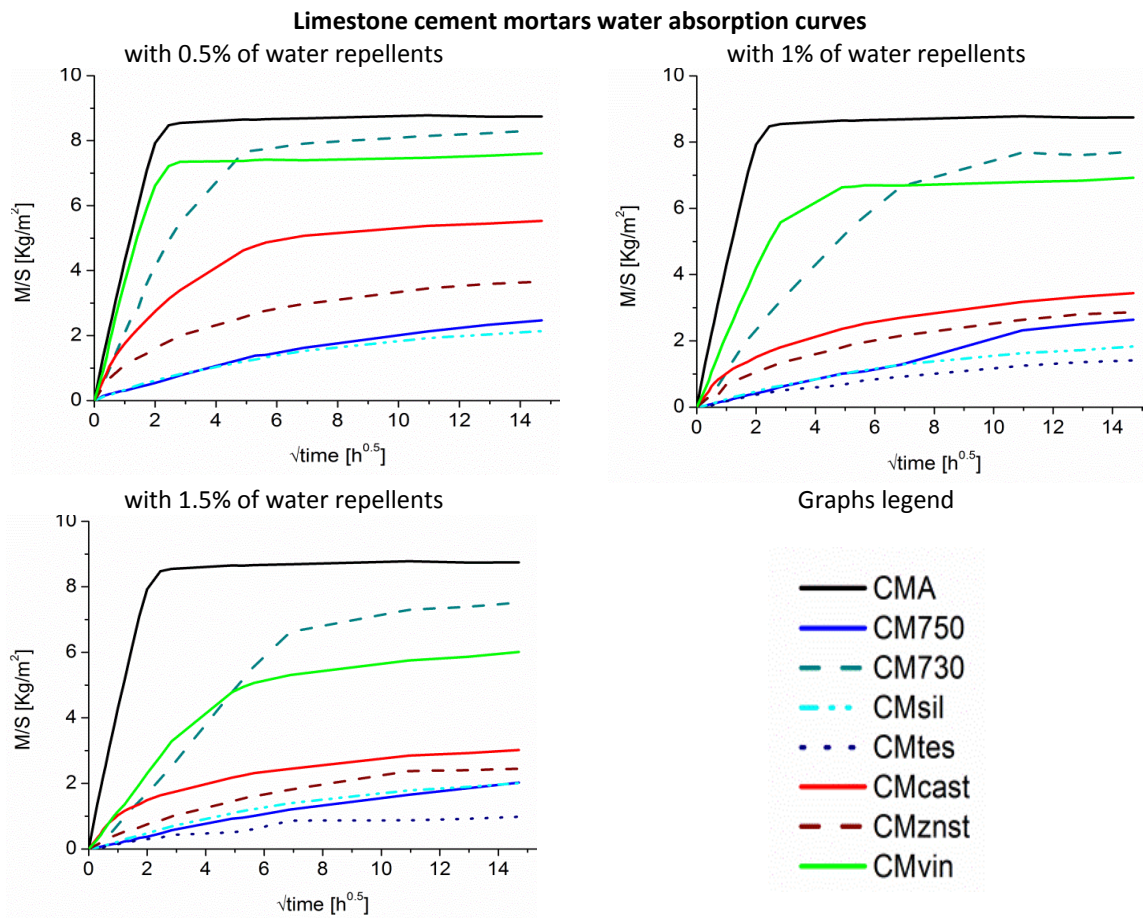


Figure 3.3 4 Histogram of the water absorption coefficients of the different mixes after several water absorption cycles. every cycle included a water absorption test lasted 72 hours and the drying to constant weight in oven at 40°C. Average of three measurements with standard deviation as error bars.

Table 3.3 9 Capillary water absorption curves of the inner core of limestone cement mortars without or with water repellents at 0.5%, 1%, 1.5% , first water absorption



3.3 Chemical-physical properties of water-repellent mortars

Table 3.3 10 water vapour permeability expressed with similar parameters: Permeability $\text{kg}/(\text{m}^2\cdot\text{s})$; WDD (wasserdampfdurchlässigkeit) $\text{g}/(\text{m}^2\cdot 24\text{h})$; water vapour resistance μ ; equivalent air layer sd of limestone cement mortars without (CMA) and with water repellents added at 0.5%, 1%, 1.5%. Water absorption coefficients of the inner core of the specimens and of the outside surfaces and contact angle measured on the specimens surfaces. The average of three measurements with their standard deviation is reported.

sample mix	Water vapour permeability				Capillary water absorption		wettability
	Permeability $\text{kg}/(\text{m}^2\cdot\text{s})$	WDD $\text{g}/(\text{m}^2\cdot 24\text{h})$	μ	sd (m)	Inner core in contact with water C ($\text{kg}/(\text{m}^2\cdot\text{h}^{0.5})$)	Outside surface in contact with water C ($\text{kg}/(\text{m}^2\cdot\text{h}^{0.5})$)	Contact angle θ (°)
CMA	$1.37\cdot 10^{-6}\pm 0.1\cdot 10^{-6}$	118±14	9.9±1.2	0.20±0.02	1.77±0.03	1.64±0.05	W*
CM7500.5	$1.03\cdot 10^{-6}\pm 0.04\cdot 10^{-6}$	89±3	12.7±0.4	0.25±0.01	0.26±0.01	0.06±0.00	89±12
CM7501	$0.84\cdot 10^{-6}\pm 0.03\cdot 10^{-6}$	72±2	16.0±0.5	0.32±0.01	0.21±0.00	0.18±0.00	98±7
CM7501.5	$0.65\cdot 10^{-6}\pm 0.11\cdot 10^{-6}$	56±9	20.7±3.2	0.41±0.06	0.19±0.01	0.16±0.00	113±4
CM7300.5	$0.97\cdot 10^{-6}\pm 0.10\cdot 10^{-6}$	84±9	13.6±1.3	0.27±0.03	1.56±0.02	1.47±0.02	35±1
CM7301	$0.67\cdot 10^{-6}\pm 0.06\cdot 10^{-6}$	58±5	20.1±1.9	0.40±0.04	1.05±0.05	1.13±0.03	61±6
CM7301.5	$1.34\cdot 10^{-6}\pm 0.9\cdot 10^{-6}$	116±96	14.0±8.1	0.28±0.16	0.98±0.09	0.81±0.33	86±8
CMSil0.5	$1.28\cdot 10^{-6}\pm 0.07\cdot 10^{-6}$	111±6	10.3±0.6	0.21±0.01	0.25±0.01	0.23±0.00	115±2
CMSil1	$0.96\cdot 10^{-6}\pm 0.07\cdot 10^{-6}$	82±6	13.5±1.0	0.27±0.02	0.20±0.00	0.21±0.00	108±6
CMSil1.5	$0.90\cdot 10^{-6}\pm 0.05\cdot 10^{-6}$	78±4	14.1±0.8	0.28±0.02	0.22±0.01	0.23±0.01	113±2
CMtes1	$0.79\cdot 10^{-6}\pm 0.04\cdot 10^{-6}$	68±3	16.4±0.8	0.33±0.02	0.14±0.00	0.11±0.01	118±9
CMtes5	$0.54\cdot 10^{-6}\pm 0.08\cdot 10^{-6}$	47±7	25.1±3.9	0.50±0.08	0.10±0.00	0.09±0.01	114±3
CMcast0.5	$0.97\cdot 10^{-6}\pm 0.09\cdot 10^{-6}$	84±10	12.5±1.4	0.25±0.03	0.94±0.04	1.04±0.06	65±9
CMcast1	$0.87\cdot 10^{-6}\pm 0.09\cdot 10^{-6}$	75±10	15.3±1.9	0.31±0.04	0.48±0.01	0.47±0.01	89±5
CMcast1.5	$1.08\cdot 10^{-6}\pm 0.21\cdot 10^{-6}$	93±18	11.6±1.9	0.23±0.04	0.44±0.02	0.38±0.02	86±12
CMznst0.5	$1.01\cdot 10^{-6}\pm 0.03\cdot 10^{-6}$	88±3	12.3±0.4	0.25±0.01	0.52±0.02	0.48±0.05	66±6
CMznst1	$1.02\cdot 10^{-6}\pm 0.09\cdot 10^{-6}$	88±8	12.7±1.2	0.25±0.02	0.37±0.02	0.34±0.05	80±4
CMznst1.5	$1.09\cdot 10^{-6}\pm 0.04\cdot 10^{-6}$	94±3	11.6±0.4	0.23±0.01	0.30±0.01	0.26±0.01	97±6
CMvin0.5	$2.33\cdot 10^{-6}\pm 0.29\cdot 10^{-6}$	201±25	5.5±0.6	0.11±0.01	1.51±0.03	1.47±0.02	49±4
CMvin1	$1.61\cdot 10^{-6}\pm 0.08\cdot 10^{-6}$	139±7	8.1±0.4	0.16±0.01	1.35±0.01	1.42±0.03	82±13
CMvin1.5	$1.81\cdot 10^{-6}\pm 0.02\cdot 10^{-6}$	157±2	7.0±0.1	0.14±0.00	0.98±0.05	1.23±0.04	74±8

*W= completely wettable

3.3.2 NATURAL HYDRAULIC LIME MORTARS WITH WATER-REPELLENTS

3.3.2.2 Mix design, composition and properties of fresh mortars

Table 3.3 11 reports the composition of water repellent mortars prepared using the dry mix product Vimak BIO, with natural hydraulic lime as binder. The mortar used, Vimak BIO, is a commercial dry mix mortar: admixtures such as plasticizers and air entraining agents are present in its composition, which regulates the density and workability of the fresh mortar. In fact the w/b ratio required (Table 3.3 11) were always the same and the apparent density and the slump diameter did not change much from one mix to another. The major differences regarded the more fluid consistence of the fresh mixes NM7501, NM7301, NMcast1, whose slump diameter reached around 19cm.

Table 3.3 11 Mix design, apparent density, consistence (slum diameter) of fresh natural hydraulic lime mortars without or with water-repellents

Mix name	additive			w/b	Density g/cm ³	Slump cm
	name	class	% by mass			
NMA	-	-	-	0.5	1.67±0.03	17.0±0.2
NM7500.5	Sitren p750	silane with amorphous silica as carrier	0.5	0.5	1.63±0.05	17.0±0.2
NM7501			1	0.5	1.54±0.04	19.0±0.2
NM7300.5	Sitren p730	Silane on CaCO ₃ carrier	0.5	0.5	1.74±0.09	18.0±0.2
NM7301			1	0.5	1.74±0.02	19.3±0.2
NMSil0.5	Silres A	silane with amorphous silica as carrier	0.5	0.5	1.74±0.02	18.0±0.3
NMSil1			1	0.5	1.52±0.05	17.5±0.2
NMcast0.5	Ca Stearate	metal soap	0.5	0.5	1.65±0.05	17.5±0.2
NMcast1			1	0.5	1.60±0.03	18.5±0.2
NMznst0.5	Zn stearate	metal soap	0.5	0.5	1.75±0.01	18.0±0.2
NMznst1			1	0.5	1.74±0.07	17.5±0.2
NMsoc0.5	Socal	Na Oleate on CaCO ₃ nanoparticles	0.5	0.5	1.65±0.08	16.5±0.2
NMsoc1			1	0.5	1.55±0.02	17.5±0.1

3.3.2.3 Properties of 28 days aged natural hydraulic lime mortars

FT-IR spectroscopy: characterization of natural hydraulic lime mortars after 28 days

Figure 3.3 5 shows the most interesting FT-IR ATR spectra of samples collected after 28 days of ageing from the different mortar mixes.

In the FT-IR spectrum of NMA it was possible to notice the presence of calcium carbonate (ν and σ -CO₃ absorptions at 1436 cm⁻¹ and at 875 cm⁻¹, respectively) and silicates (ν Si-O-Si absorptions 1098-1009 cm⁻¹). Only a low -OH absorption was observed around 3400 cm⁻¹, instead of the broad but stronger peak found for limestone cement mortars and for natural hydraulic lime pastes. Another missing absorption, in comparison to the natural hydraulic pastes at 28 days, was the -OH stretching of calcium hydroxide at 3640 cm⁻¹. However, it was possible to recognize the absorption at 950 cm⁻¹ due to hydrated compounds C-S-H. The hydration of mortars took place slowly (it should be remembered that the major silicates phase present is C₂S as seen for the NHL pastes) and silicate hydrates were formed together with calcium hydroxide, but the latter was fast carbonated.

The presence of different water repellents did not cause great differences. As already seen for the limestone cement mixtures, presence of calcium or zinc stearates was recognized thanks to the aliphatic $-CH$ stretchings at $2920-2850\text{ cm}^{-1}$. The other main difference noticed was a lower absorption at 950 cm^{-1} in NMsoc1 and NMcast1 samples in comparison to the other absorptions of the spectra, this lower absorption indicated a lower presence of C-S-H compounds, it might be that the presence of Socal® or calcium stearates decreased the hydration rate of the binder in the mortar, as already seen for NHLsoc1 and NHLcast1 in Chapter 3.2.

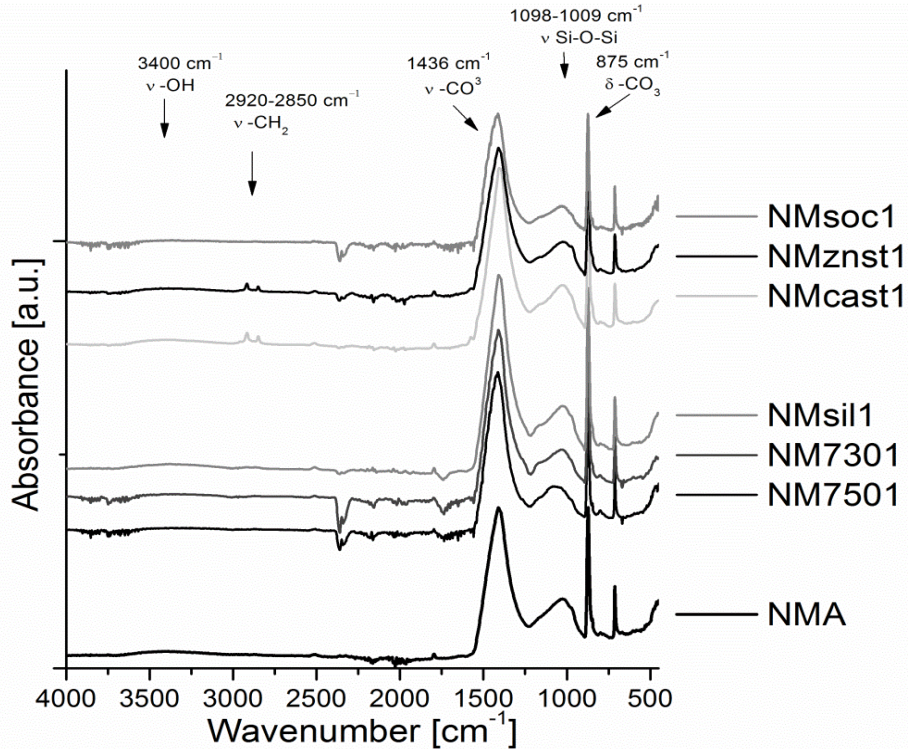


Figure 3.3 5 FT-IR ATR spectra of natural hydraulic lime mortars without (NMA) or with 1% of water-repellents, the spectra were collected on samples aged 28 days. On the right side the labels corresponding to each spectrum are reported.

Morphological and colour characterization

The natural hydraulic lime mortars prepared became a fine, nut-brown, smooth mortars after the hardening. The presence of different admixtures did not influence much the visual aspect of the mortars, as can be seen in some examples in Table 3.3 12, a smoother surface was observed for NMA.

Colorimetric measurements were done in order to register the colour values of the not-weathered mortars. The collected data (Table 3.3 13) showed that the colour was really homogeneous for the different mixes and no particular trends were found regarding the dosage used or the different nature of the water repellents.

Table 3.3 12 Images of different natural hydraulic mortars; above: macro photos (1:1 scale) ; below: digital optical microscope images OM collected with a Dino Lite (the scale bars indicates 2.0 mm)

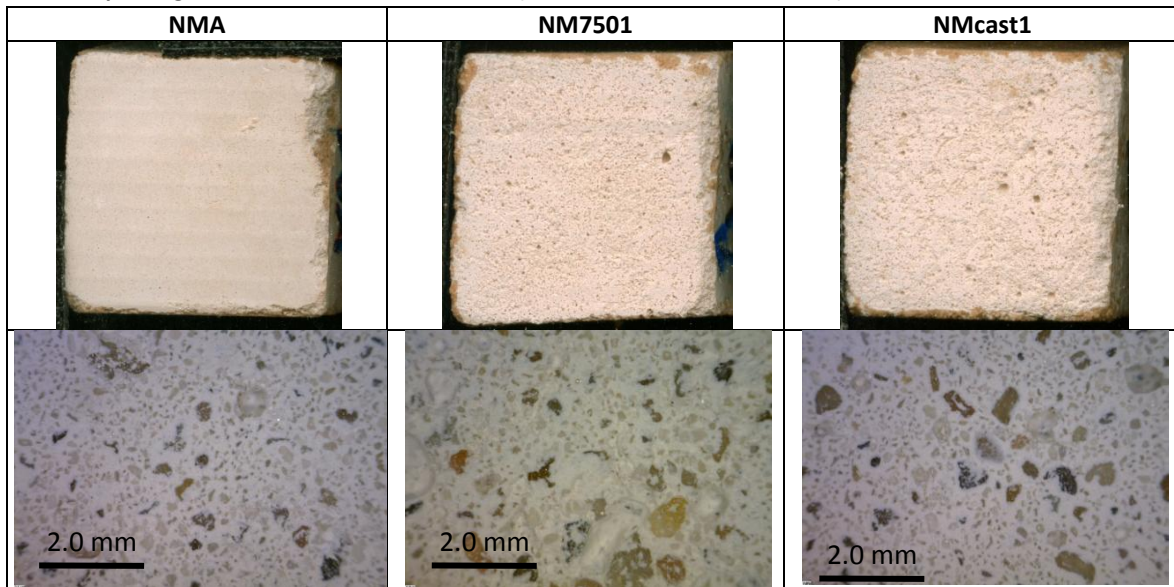
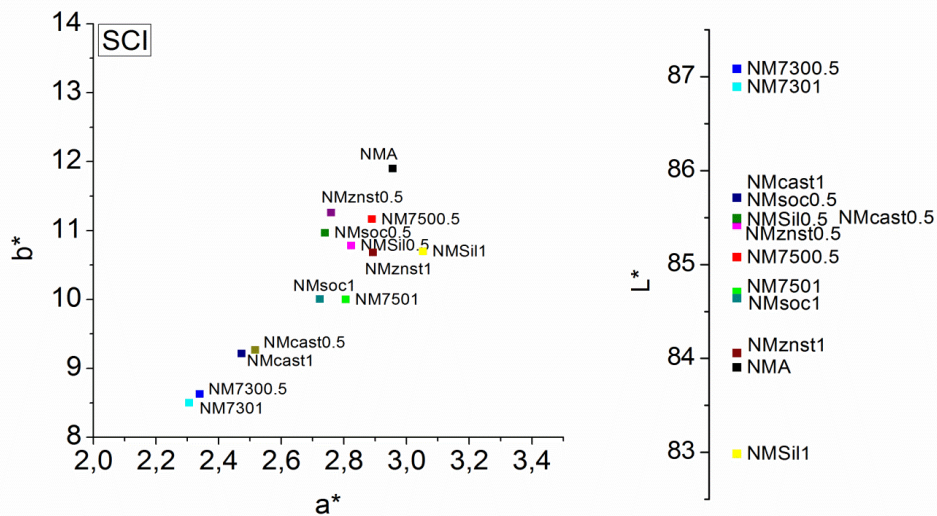


Table 3.3 13 Colorimetric data collected for natural hydraulic lime mortars. L*, a*, b* parameters regards the colour lightness, the red-green hue and the blue-yellow hue, respectively. Specular component included (SCI) or specular component excluded (SCE) is considered. Below the graph of the L*, a*, b* parameters is shown

	SCI			SCE		
	L*(D65)	a*(D65)	b*(D65)	L*(D65)	a*(D65)	b*(D65)
NMA	83.9±2.1	3.0±0.2	11.9±1.0	84.1±2.1	3.0±0.2	11.9±1.0
NM7500.5	85.1±0.0	2.9±0.1	11.2±0.9	85.2±0.0	2.9±0.1	11.1±0.9
NM7501	84.7±0.4	2.8±0.2	10.0±0.5	84.8±0.3	2.8±0.2	10.0±0.6
NM7300.5	87.1±0.4	2.3±0.1	8.6±0.3	87.2±0.4	2.4±0.1	8.6±0.2
NM7301	86.9±0.2	2.3±0.0	8.5±0.4	87.0±0.2	2.3±0.0	8.5±0.4
NMSil0.5	85.4±0.3	2.8±0.1	10.8±0.2	85.6±0.3	2.8±0.1	10.7±0.2
NMSil1	83.0±0.2	3.1±0.1	10.7±0.3	83.2±0.2	3.1±0.1	10.7±0.3
NMcast0.5	85.5±0.3	2.5±0.0	9.3±0.3	85.7±0.3	2.5±0.0	9.2±0.3
NMcast1	85.7±0.9	2.5±0.1	9.2±0.6	85.9±0.8	2.5±0.1	9.2±0.7
NMznst0.5	85.5±0.8	2.8±0.2	11.3±0.7	85.6±0.8	2.8±0.2	11.2±0.7
NMznst1	84.1±1.0	2.9±0.2	10.7±0.7	84.0±0.8	2.9±0.2	10.6±0.7
NMsoc0.5	85.5±0.4	2.7±0.1	11.0±0.5	85.7±0.3	2.8±0.1	10.9±0.5
NMsoc1	84.6±1.2	2.7±0.2	10.0±1.3	84.8±1.2	2.7±0.2	10.0±1.3



Density and porosity

Table 3.3 15 lists the density and porosity data of the natural hydraulic mortars hardened for 28 days. The most interesting differences observed are:

- The addition of different water repellents seemed always to cause the *decrease* of the apparent density in comparison to NMA. A correspondent decrease of the ultrasonic speed was also observed and the total porosity was in every case high, reaching 65% in NMznst0.5.
- Generally the apparent density tended to decrease with the admixtures dosages, except in NMznst mixtures.
- The MIP data did not always agree with the apparent density and total porosity data, and the total open porosity measured via MIP was in different case even higher than the total porosity. This discrepancy could be due to the sensitivity of the MIP methods¹³.
- The porosity distribution graphs reported in Table 3.3 14 show that NMA presented a porosity distribution centred on pores with radius around 1 μm , and that a similar distribution was found for NMcast0.5 and NMsoc. The addition of a silane/siloxane water repellents (NM750, NM730, NMsil) and NMcast1 resulted in a bimodal pore distribution, with a high percentage of large pores (1-10 μm). The addition of 1% of zinc stearate (NMznst1) caused the decrease of the porosity and a shift to lower pore radius.

Mechanical properties of natural hydraulic lime at 28 days of hydration

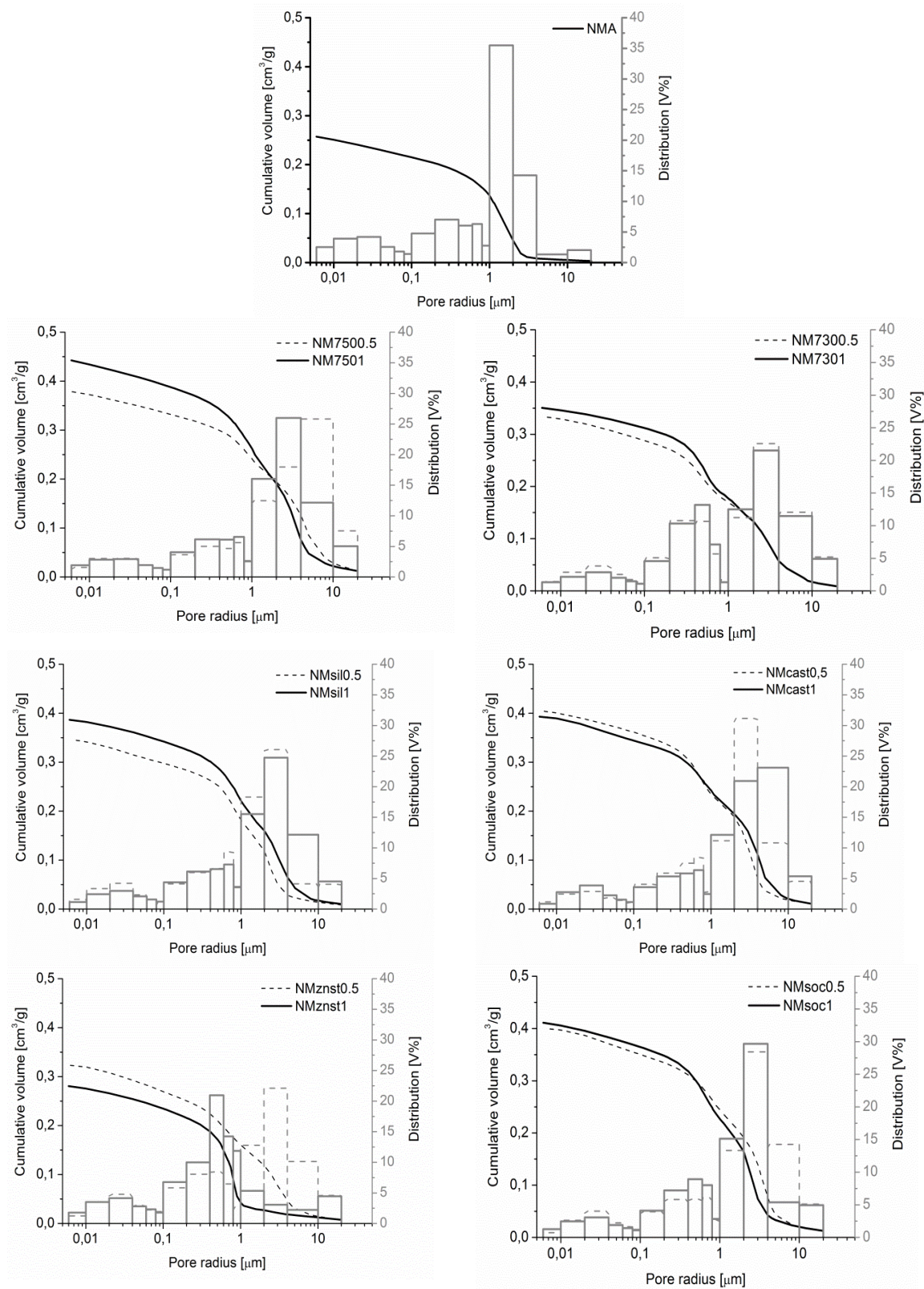
The mechanical properties were tested 16*4*4 cm specimens, for the compressive strength a pre load of 0.1 N, and a loading rate of 1N/s was used, for the flexural strength a preload of 20 N and a loading rate of 50N/s was chosen.

As can be seen in Table 3.3 16 and Figure 3.3 6, the compressive strength of NMA was around 1.32 MPa, while the flexural strength resulted 1.90MPa, these data agree quite well with the specification of the supplier which indicated a compressive strength after 28 days of 1.5 MPa.

- The addition of the different water repellents caused a drop of the compressive strength;
- when higher silane/siloxane dosage were used (1% by mass in comparison to 0.5%by mass) in NM750, NM730, NMsil the strength increase;
- when a stearate was introduced as in NMcast, Nmznst, Nmsoc the strength decrease, this behaviour could be due to the positive influence of the siloxanes on the hydration and the retarding effect of the stearates (as seen in Chapter 3.2).
- The flexural strength decreased with the increasing dosage for the siloxanes and increased for the stearates.
- The use of Sitren P750®, both at 0.5% and 1% (NM7500.5 and NM7501), and calcium stearates at 1% (NMcast1) caused the worse compressive resistance. These mixes were also characterised by low densities and high porosity, which might have influenced their mechanical resistance.

¹³ MIP measurements were performed on small bulk samples, it is not possible to measured all the open porosity (only pores with diameters $\geq 4\text{-}6\text{nm}$ can be measured), and the cylindrical pore model used for the calculation is not reflecting exactly the real pore structure in particular with high tortuosity or when bottle-necked pores are present (bibliografia manuale porosimetro)

Table 3.3 14 Distribution of the porosity and cumulative volume vs the pore radius of the different natural hydraulic lime mixes, the respective labels are reported on graphs legends



3.3 Chemical-physical properties of water-repellent mortars

Table 3.3 15 Structural and microstructure data of natural hydraulic lime mortars without (NMA) or with water repellents at 0.5% and 1% by mass (the average of three measurements with their standard deviation is reported).

	Real density (g/cm ³)	Bulk density (g/cm ³)	Bulk density MIP (g/cm ³)	Apparent density MIP (g/cm ³)	Total porosity (%)	Total open porosity MIP (%)	Total cumulative volume MIP(cm ³ /g)	Average pore radius MIP(micron)	Ultrasonic measurements (m/s)
NMA	2.74±0.09	1.53±0.03	1.43±0.01	2.71±0.02	44.3±0.1	47.3±0.5	0.34±0.01	3.4±0.5	1105±20
NM7500.5	2.74±0.09	1.46±0.02	0.36±0.02	2.12±0.01	46.6±0.1	52.0±0.8	0.38±0.01	4.8±0.5	1082±11
NM7501	2.74±0.09	1.18±0.02	1.11±0.05	2.22±0.02	56.8±0.1	50.0±0.4	0.45±0.01	3.2±0.5	1114±25
NM7300.5	2.74±0.09	1.50±0.04	1.39±0.01	2.62±0.01	45.3±0.1	46.9±0.1	0.34±0.01	3.4±0.5	1153±14
NM7301	2.74±0.09	1.32±0.01	1.56±0.01	3.48±0.01	52.0±0.1	55.2±0.1	0.35±0.01	3.4±0.5	1096±18
NMSi0.5	2.74±0.09	1.46±0.07	1.37±0.02	2.51±0.01	46.8±0.1	45.1±0.1	0.33±0.01	2.5±0.5	1080±22
NMSi1	2.74±0.09	1.18±0.03	1.29±0.03	2.60±0.03	57.0±0.1	50.3±0.9	0.39±0.01	3.3±0.5	1078±10
NMcast0.5	2.74±0.09	1.41±0.03	1.55±0.05	±3.99±0.05	48.5±0.1	61.2±0.5	0.40±0.01	4.0±0.5	1075±16
NMcast1	2.74±0.09	1.21±0.01	1.28±0.01	2.69±0.04	55.9±0.1	52.5±0.8	0.41±0.01	2.9±0.5	1105±6
NMznst0.5	2.74±0.09	0.95±0.70	1.33±0.08	2.34±0.07	65.2±0.1	43.3±0.7	0.33±0.01	3.2±0.5	1227±20
NMznst1	2.74±0.09	1.35±0.08	1.46±0.01	2.50±0.01	50.8±0.1	41.4±0.1	0.28±0.01	0.8±0.5	1278±11
NMsoc0.5	2.74±0.09	1.42±0.07	1.28±0.02	2.65±0.01	48.2±0.1	51.6±0.2	0.40±0.01	3.6±0.5	1029±17
NMsoc1	2.74±0.09	1.17±0.07	1.26±0.01	2.63±0.08	57.4±0.1	52.3±0.4	0.42±0.01	2.7±0.5	1048±5

Bulk density density =measured on the whole 4X4X4 cm specimens; Bulk density MIP= measured through MIP analysis; Apparent density MIP = density of the sample excluding the open porosity. evaluated via MIP; Total cumulative volume MIP(mm³/g)=volume of mercury intruded evaluated via MIP; Total open porosity MIP (%)= through MIP analysis only the open porosity is evaluated;

Table 3.3 16 Compressive and flexural strenght of natural hydraulic lime mortars with or without water repellents at 0.5% and 1% by mass. Average of three measurements with standard deviation.

Mortar mix	Compressive strenght			Flexural strenght
	σ_{max} (MPa)	E_{mod} tangential (MPa)	E_{mod} secant (MPa)	σ_{max} (MPa)
NMA	1.32±0.03	1.81±0.02	0.87±0.08	1.90±0.06
NM7500.5	0.34±0.19	0.02±0.02	0.23±0.02	2.88±0.14
NM7501	0.89±0.09	0.06±0.02	0.07±0.01	1.09±0.05
NM7300.5	0.41±0.18	0.04±0.03	0.74±0.05	3.47±0.04
NM7301	0.74±0.17	0.81±0.01	0.25±0.02	1.18±0.03
NMSil0.5	0.57±0.30	0.08±0.05	0.46±0.02	2.18±0.22
NMSil1	0.83±0.14	0.08±0.07	0.09±0.02	0.95±0.09
NMcast0.5	0.84±0.15	0.05±0.02	0.27±0.09	2.31±0.08
NMcast1	0.62±0.21	0.08±0.8	0.07±0.08	1.02±0.07
NMznst0.5	1.47±0.39	0.09±0.05	0.37±0.22	3.56±0.19
NMznst1	0.62±0.16	1.04±0.03	0.39±0.01	0.74±0.03
NMsoc0.5	1.06±0.11	0.04±0.03	0.35±0.16	2.23±0.06
NMsoc1	0.55±0.23	0.12±0.08	0.07±0.01	0.57±0.07

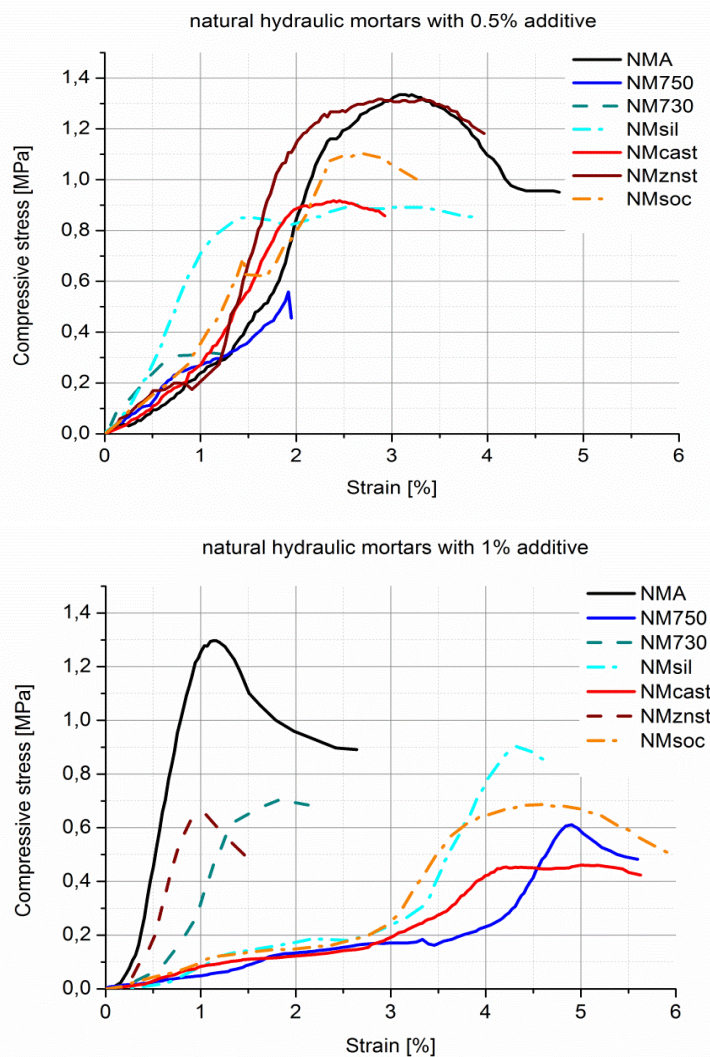


Figure 3.3 6 Graphs of the compressive stress of natural hydraulic lime mortars vs. their percentage strain, mixes with different water repellents at 0.5% (top), 1% (below)

Water vapour permeability of natural hydraulic lime mortars

The water vapour permeability of natural hydraulic lime specimens (see Figure 3.3 7 and the complete data reported in Table 3.3 18) was generally really low with μ (water vapour resistance) values around 3-4. The specimens structures allowed a complete and fast water vapour circulation inside the matrixes, which is very important for the compatibility of these kind of mortars with historical/traditional mortars¹⁴. High permeability could allow also a faster drying of wet specimens. The data were, therefore, positive.

The presence of the water repellents, which generally cause a porosity increase, resulted in even higher permeabilities and lower μ , in particular with higher dosages of water-repellent admixtures (except for NM7500.5 and NM7501). The use of silres A[®], calcium stearates and Social[®] allowed a high permeability.

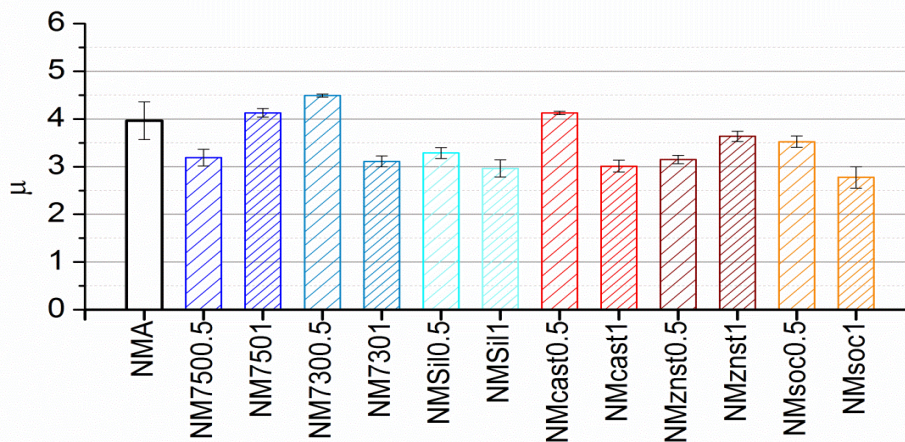


Figure 3.3 7 Histogram of the water vapour resistance μ values of the different natural hydraulic lime mortars. Average of three measurements with standard deviation as error bars.

Capillary water absorption and contact angle measurements of natural hydraulic lime mortars with water repellents

Figure 3.3 8 graphically shows the capillary water absorption coefficients of natural hydraulic lime mortars measured on the external surfaces and on inner cut-surfaces of the specimens, while Table 3.3 18 lists the same coefficients and the relative contact angle measured on the external surfaces.

The absorption was in every case higher than that for the limestone mortars, but also here it is evident the better water repellent effect given by the silane/siloxanes (NM7500.5, NM7501, NMSil0.5, NMSil1) and by zinc stearates (NMznst0.5, NMznst1). At least 1% of calcium stearates was required to obtain good water repellence (NMcast1).

The difference between the water absorption of the inner core and the absorption of the external surfaces was relevant, the high wettability of the inner core was evident also by observing the wetted cross sections of some specimens in Table 3.3 17. This behaviour might be explained by the presence of a more compact layer on the specimens surface due to a faster carbonation (as happens in NMA without admixtures), but probably it was due to the inhomogeneous distribution of the water repellents and by their tendencies to migrate to the surface in the fresh mixes.

¹⁴ Izaguirre, A. et al., 2010; Maravelaki-Kalaitzaki, P., et al. 2007; Biscontin, G., L. Falchi, 2011

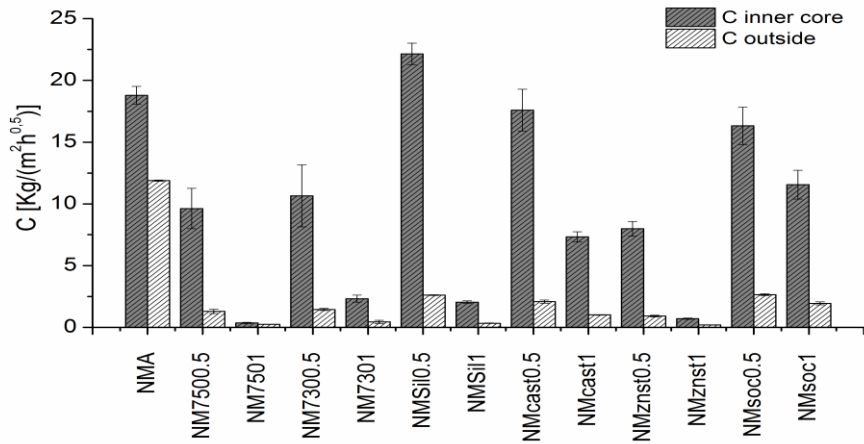


Figure 3.3 8 Histogram of the capillary water absorption coefficient of natural hydraulic lime specimens. Average of three measurements with standard deviation as error bars.

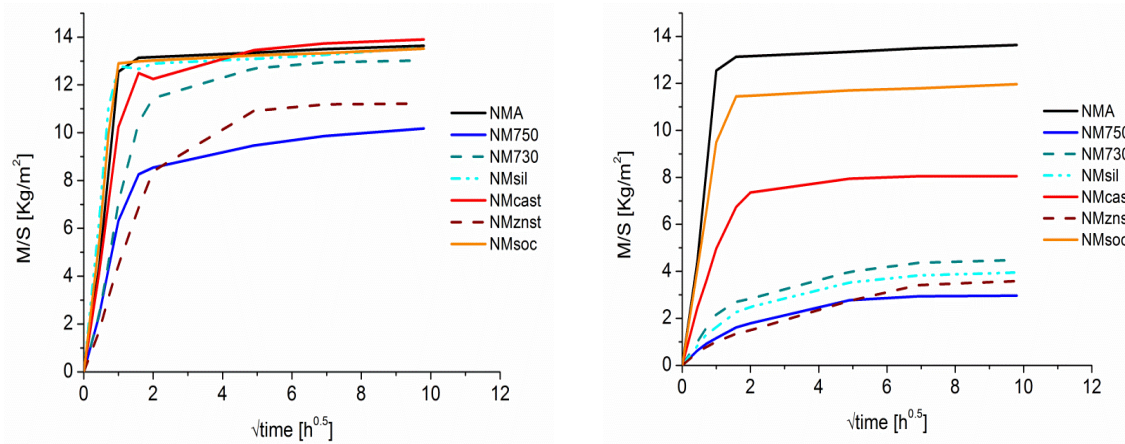





Figure 3.3 9 Capillary water absorption curves of the inner core of Inatural hydraulic lime mortars with or without water repellents at 0.5% (link), 1% (right)

Table 3.3 17 Pictures of wetted cross sections of natural hydraulic lime specimens.

<p>NMA(Macro, Scale 1:1) The specimen was completely wettable</p>	<p>NM750 (Macro, Scale 1:1) The inner core was wettable, the surface was water-repellent</p>	<p>NM730 (Macro, Scale 1:1) The core was wettable, the surface was partially wettable</p>
		

3.3 Chemical-physical properties of water-repellent mortars

Table 3.3 18 water vapour permeability expressed with following parameters: Permeability $\text{kg}/(\text{m}^2\cdot\text{s})$; WDD (wasserdampfdurchlässigkeit) $\text{g}/(\text{m}^2\cdot 24\text{h})$; water vapour resistance μ ; equivalent air layer sd of natural hydraulic lime mortars without (NMA) and with water repellents added at 0.5%, 1%, 1%. Water absorption coefficients of the inner core of the specimens and of the outside surfaces and contact angle measured on the specimens surfaces. Below: Histogram of the water absorption coefficients. The average of three measurements with their standard deviation is reported.

sample mix	Water vapour permeability				Capillary water absorption		Wettability
	Permeability ($\text{kg}/(\text{m}^2\cdot\text{s})$)	WDD ($\text{g}/(\text{m}^2\cdot 24\text{h})$)	μ	sd (m)	Inner core in contact with water C ($\text{kg}/(\text{m}^2\cdot\text{h}^{0.5})$)	Outside surface in contact with water C ($\text{kg}/(\text{m}^2\cdot\text{h}^{0.5})$)	Contac angle α ($^\circ$)
NMA	$2.16\cdot 10^{-6}\pm 0.09\cdot 10^{-6}$	187±39	4±1	0.079±0.016	18.6±0.73	11.9±0.73	W*
NM7500.5	$2.14\cdot 10^{-6}\pm 0.24\cdot 10^{-6}$	185±21	3.2±0.3	0.064±0.007	9.62±1.635	1.29±0.17	100±6
NM7501	$2.02\cdot 10^{-6}\pm 0.09\cdot 10^{-6}$	175±7	4.1±0.2	0.083±0.004	0.35±0.05	0.24±0.02	120±8
NM7300.5	$1.51\cdot 10^{-6}\pm 0.02\cdot 10^{-6}$	130±2	4.0±0.1	0.090±0.001	10.65±2.51	1.45±0.09	70±6
NM7301	$2.18\cdot 10^{-6}\pm 0.09\cdot 10^{-6}$	189±14	3.0±0.1	0.062±0.005	2.32±0.29	0.44±0.135	80±3
NMSil0.5	$2.06\cdot 10^{-6}\pm 0.09\cdot 10^{-6}$	178±12	3.3±0.2	0.066±0.005	22.15±0.87	2.61±0.035	W*
NMSil1	$2.33\cdot 10^{-6}\pm 0.28\cdot 10^{-6}$	201±24	3.0±0.1	0.059±0.007	2.04±0.11	0.33±0.025	125±4
NMcast0.5	$1.69\cdot 10^{-6}\pm 0.03\cdot 10^{-6}$	146±2	4.0±0.1	0.083±0.001	17.59±1.69	2.09±0.13	W*
NMcast1	$2.32\cdot 10^{-6}\pm 0.18\cdot 10^{-6}$	200±16	3.0±0.1	0.060±0.005	7.33±0.46	1.01±0.02	W*
NMznst0.5	$1.90\cdot 10^{-6}\pm 0.11\cdot 10^{-6}$	164±9	3.1±0.2	0.063±0.003	7.98±0.61	0.91±0.075	W*
NMznst1	$1.65\cdot 10^{-6}\pm 0.09\cdot 10^{-6}$	142±8	4.0±0.1	0.073±0.004	0.71±0.05	0.2±0.01	80±3
NMsoc0.5	$1.70\cdot 10^{-6}\pm 0.12\cdot 10^{-6}$	147±9	4.1±0.1	0.070±0.005	16.33±1.52	2.65±0.08	W*
NMsoc1	$2.19\cdot 10^{-6}\pm 0.38\cdot 10^{-6}$	189±33	3.0±0.1	0.056±0.009	11.56±1.17	1.94±0.12	W*

*W= completely wettable, it was not possible to measure the contact angle

3.3.3 POZZOLANA-LIME MORTARS WITH WATER REPELLENTS

3.3.3.2 Mix design, composition and properties of fresh mortars

Table 3.3 19 summarizes the composition, the density and the slump of the different fresh mortars made with pozzolana-lime binder.

The water/binder ratio was determined by measuring the slump diameter of the fresh mortars, and calibrated for each mortar mix in order to obtain a slump of 17 ± 2 cm. Therefore, it was fixed at 1.25 for the reference samples PMA. The correct w/b ratios ranged from 1.13 to 1.30 and it was possible to notice that the mix PMtes, with liquid silane, required the lowest content of liquid, while the mixes PM730, PMcasts, PMznst required a higher content of water to reach a good consistence. The density was consequently influenced by the w/b ratio but also by the different water-repellents. The use of silane/siloxanes supported on amorphous silica or the emulsion silane Tegosivin HE® (mixes PM7501, PMSil0.5, PMSil1, PMSil1.5, PMtes1) led to a lower density of the fresh slurries, while calcium stearates and zinc stearates (PMcast0.5,1,1.5 and PMznst0.5,1,1.5) did not cause a huge variation of the density of the fresh mortars.

Table 3.3 19 Mix names, composition, density and consistence (slump diameter) of fresh pozzolana-lime mortars

Mix name	additive			w/b	Density g/cm ³	Slump cm
	name	class	% by mass			
PMA	-	-	-	1.250	2.09±0.01	17.0±0.1
PM7501	Sitren p750	silane with amorphous silica as carrier	1	1.296	1.76±0.01	17.1±0.1
PM7301	Sitren p730	Silane on CaCO ₃ carrier	1	1.296	2.05±0.01	16.8±0.1
PMSil0.5	Silres A	silane with amorphous silica as carrier	0.5	1.301	1.91±0.01	18.3±0.1
PMSil1			1	1.196	1.89±0.01	17.2±0.1
PMSil1.5			1.5	1.246	1.86±0.01	17.5±0.1
PMtes1	Tegosivin HM	emulsion silane	1	1.139	1.92±0.01	18±0.1
PMcast0.5	Ca Stearate	metal soap	0.5	1.296	2.11±0.01	16.8±0.1
PMcast1			1	1.296	2.06±0.01	17.3±0.1
PMcast1.5			1.5	1.283	2.05±0.01	17.3±0.1
PMznst0.5	Zn stearate	metal soap	0.5	1.296	2.07±0.01	18±0.1
PMznst1			1	1.296	2.04±0.01	16.5±0.1
PMznst1.5			1.5	1.301	2.03±0.01	17±0.1

3.3.3.3 Properties of 28 days aged natural hydraulic lime mortars

FT-IR spectroscopy: characterization of pozzolana- lime mortars after 28 days

Thanks to FT-IR ATR spectroscopy it was possible to verify the absence of calcium hydroxide on the specimens surfaces (-OH stretching of Ca(OH)₂ should be at 3640 cm⁻¹) and to observe a large presence of calcium carbonates (ν -CO₃ absorption at 1436 cm⁻¹) instead.

Broad and intense peaks of silicates were detected too (Si-O-Si stretching at 1098-1009 cm⁻¹) mainly due to the presence of pozzolana.

As also seen in the study of pozzolana-lime pastes (Chapter 3.2), the presence of a sharp stretching absorption around 965 cm^{-1} was due to the formation of hydrated alumino-silicate compounds and was particularly visible in the FT-IR spectra of PM7501, PMtes1, PMsil1, PMcast1, indicating a faster hydration.

The aliphatic $-\text{CH}$ stretching absorptions of the stearates were also visible at $2920\text{--}2850\text{ cm}^{-1}$ in PMznst and PMcast.

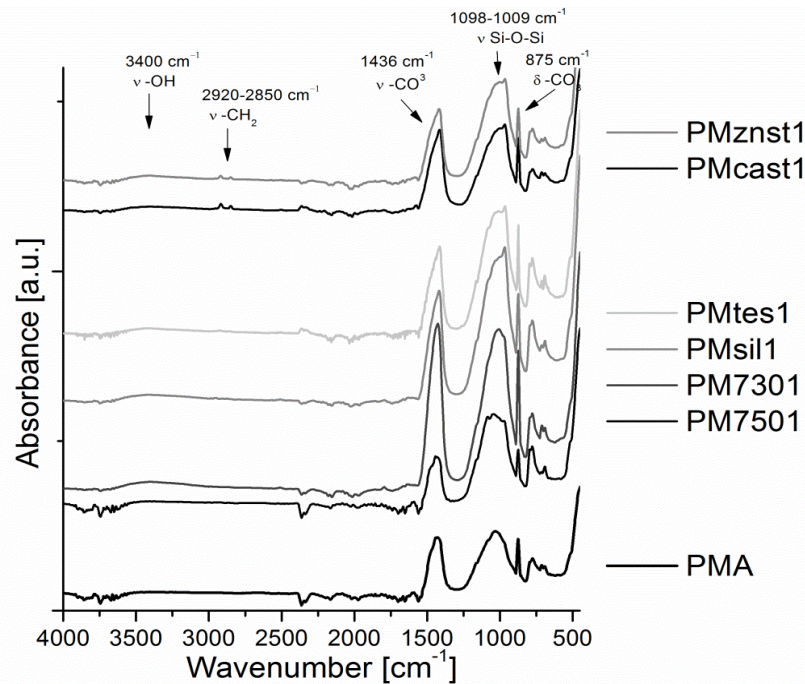





Figure 3.3 10 FT-IR ATR spectra of different pozzolana-lime mortars without (PMA) or with water repellents added at 1% by dry weight, the correspondent mix names are listed next to each spectrum

Morphological and colour characterization

Pozzolana- lime specimens (Table 3.3 20) were light grey with smooth surfaces, the aggregate grains were partially visible and some of the pastes showed a higher porosity (PMznst, PMtes). Colorimetric measurements done are reported in Table 3.3 21 and Figure 3.3 11, the different mortar mixes were characterised by similar colour and the $L^*a^*b^*$ parameters varied in a short range, the differences were quite negligible.

Table 3.3 20 Images of some significative pozzolana-lime mortars, macro photos (1:1 scale) and digital optical microscope images (the scale bars indicates 2.0 mm). The table continues on the following page

PMA	PM7501	PMznst1
Macro 1:1scale	Macro 1:1scale	Macro 1:1scale
		

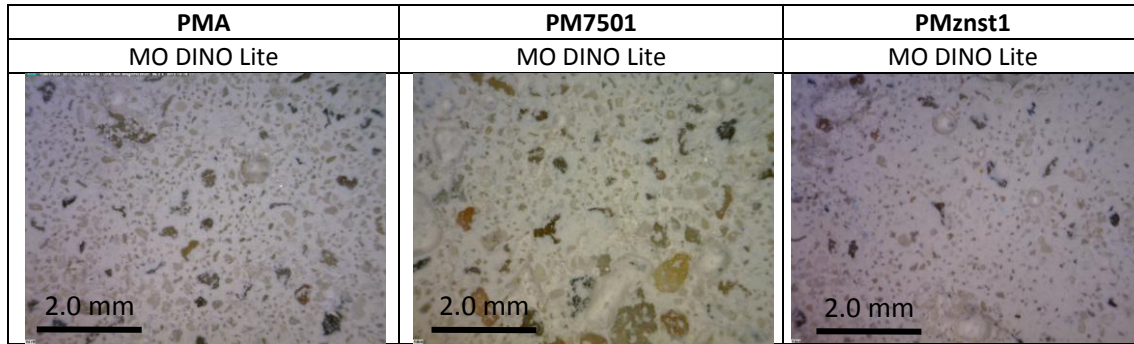


Table 3.3 21 Colorimetric data collected for pozzolana- lime mortars. L*, a*, b* parameters regard the colour lightness, the red-green hue and the blue-yellow hue, respectively. Specular component included (SCI) or specular component excluded (SCE) are considered.

	SCI			SCE		
	L*(D65)	a*(D65)	b*(D65)	L*(D65)	a*(D65)	b*(D65)
PMA	82.6±1.7	1.2±0.1	5.7±0.4	82.8±1.8	1.3±0.1	5.7±0.4
PM7501	84.6±0.3	1.0±0.4	5.0±0.5	84.7±0.3	1.0±0.4	5.0±0.5
PM7301	86.6±0.3	0.6±0.2	5.1±0.4	86.7±0.3	0.7±0.2	5.1±0.4
PMsil0.5	86.7±0.1	1.0±0.1	4.9±0.1	86.8±0.1	1.1±0.1	4.9±0.1
PMsil1	83.9±0.1	1.0±0.3	5.0±0.3	84.1±0.1	1.0±0.3	5.0±0.3
PMsil1.5	85.7±0.2	0.9±0.4	5.0±0.4	85.9±0.2	1.0±0.4	5.0±0.4
PMtes1	86.3±1.2	0.9±0.1	5.4±0.3	86.5±1.2	1.0±0.1	5.4±0.3
PMcast0.5	85.8±0.5	0.9±0.1	5.0±0.4	85.9±0.4	0.9±0.1	5.0±0.4
PMcast1	84.3±1.0	1.0±0.1	5.1±0.5	84.4±1.0	1.1±0.1	5.1±0.5
PMcast1.5	85.7±0.5	1.0±0.1	4.7±0.3	85.9±0.5	1.0±0.1	4.7±0.3
PMznst0.5	84.2±1.5	1.0±0.1	5.2±0.4	84.4±1.5	1.0±0.1	5.2±0.4
PMznst1	84.9±1.1	1.0±0.1	5.3±0.0	84.9±1.1	1.0±0.1	5.3±0.0
PMznst1.5	85.0±1.5	1.1±0.1	5.3±0.4	85.0±1.5	1.1±0.1	5.3±0.4

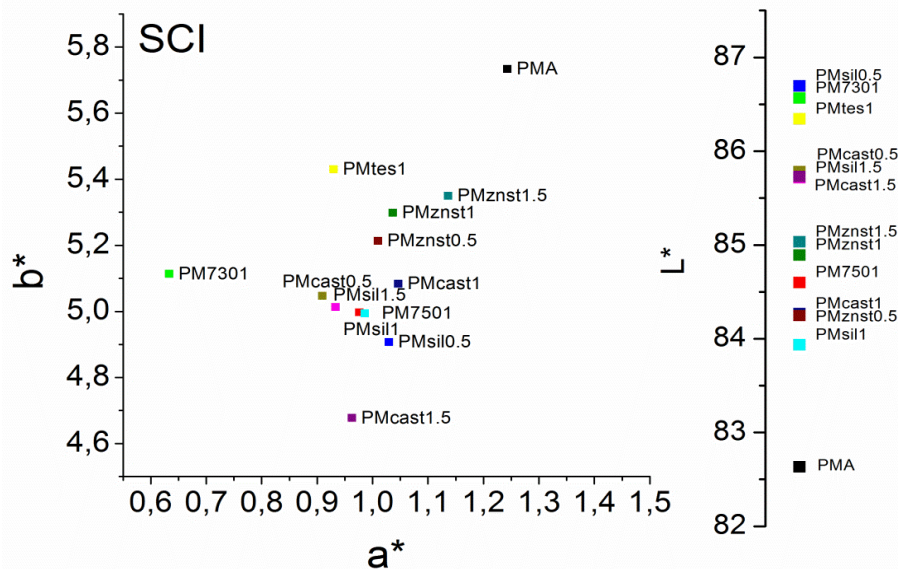


Figure 3.3 11 the graphs show the colorimetric parameters L*, a*, b* in the CIEL*a*b* space when the specular component is included (SCI).

Density and porosity of pozzolana-lime mortars with water repellents

By comparing the bulk densities data (Table 3.3 22) and the total porosity percentages, it was possible to observe that bulk density and total porosity were strongly influenced by the presence of water repellent additives:

- The reference mix PMA had the highest bulk density and a total porosity around 32%.
- The addition of silane/siloxanes (mixes PM7501, PM7301, PMSil0.5,1,1.5, PMtes1) caused the decrease of the density due to an increased porosity, in fact, values of the total porosity ranged from 37% (PMtes) to 45% (PM7501).
- The addition of stearates seemed, therefore, not to change drastically the porosity of the samples. PMcast0.5,1,1.5 and PMznst0.5,1,1.5 had similar densities and similar total porosity (33-34%) to PMA.
- the percentage of water-repellent did not strongly influence the bulk density.

The open porosity, measured via MIP, and the ultrasonic waves measurements agreed with the bulk density and total porosity data and showed similar trends.

The MIP analysis has the advantage of giving information about the open porosity, its distribution and the pore radius of the pores. In Table 3.3 23 the graphs of the distribution of the cumulative volume of mercury intruded versus the pores radius and the relative pore volume versus the pore radius are displayed. A bimodal distribution of the pores was observed for all mixes but three different distributions of the averages pore radius were observed:

- average pore radius around 0,1 μm and 9 μm for MPA, MP730, MPcast 1, 1.5;
- around 0,3-0,4 μm and 9 μm for PM7501, PMcast0.5, PMznst1, PMtes1;
- around 0,06 μm and 9 μm for PMSil0.5,1,1.5.

PM7501 presented an overall higher open porosity with a broader distribution of the pore radius in the region 0,5 μm -9 μm , while PMSil0.5,1,1.5 strongly differed from the other sample having thinner pores.

Mechanical properties of pozzolana- lime at 28 days of hydration

The maximum compressive strength of the reference mortar PMA (Table 3.3 24) was around 2 MPa and the flexural strength around 0,37 MPa, values that have been commonly observed in this kind of hydraulic lime mortars¹⁵.

The mechanical performance of the mortars were altered depending on which kind of additive was used (Table 3.3 24):

- the addition of the powder Silres A[®] and of calcium stearates led to a better compressive and flexural resistance (MPsil and MPcast mixes);
- the addition of the silane Sitren P750[®], P730[®] and the liquid silane Tegosivin[®] decreased the mechanical properties: the correspondent mixes PM7501, PM7301, PMtes1 reached the 50-60% of the compressive strength of PMA and from the 50% (Pmtes1) to 80% (PM7501) of the flexural strength.
- With the addition of Zinc stearate it was observed a dramatic loss of the compressive and flexural strength.
- in PMSil0.5,1,1.5 it was observed that the higher the percentage of the silane, the better the compressive strength. Adding calcium or zinc stearates, it was observed the opposite behaviour: the higher the percentage, the lower the compressive strength.

¹⁵ Moropoulou, et al., 2005; Izaguirre, A., J. Lanás, 2009

Table 3.3 22 Real density, apparent density and porosity data of mortars. The average of three measurements with their standard deviation is reported.

	Real density (g/cm ³)	Bulk density (g/cm ³)	Bulk density MIP (g/cm ³)	Apparent density MIP (g/cm ³)	Total porosity (%)	Total open porosity MIP (%)	Total cumulative volume MIP(cm ³ /g)	Average pore radius MIP(micron)	Ultrasonic measurements (m/s)
PMA	2.60±0.01	1.77±0.06	1.88±0.05	2.71±0.02	31.9±0.1	25.0±0.5	0.133±0.009	0.31±0.05	1205±25
PM7501	2.60±0.01	1.44±0.09	1.69±0.03	2.12±0.01	44.6±0.1	36.0±0.5	0.214±0.010	0.46±0.05	1160±10
PM7301	2.60±0.01	1.69±0.09	1.98±0.04	2.22±0.02	35.0±0.1	26.9±0.5	0.136±0.005	0.40±0.05	1180±35
PMsil0.5	2.60±0.01	1.55±0.09	1.95±0.05	2.62±0.01	40.4±0.1	27.5±0.5	0.148±0.004	0.15	1170±13
PMsil1	2.60±0.01	1.57±0.08	1.87±0.05	3.48±0.01	39.6±0.1	28.9±0.5	0.160±0.020	0.13±0.05	1150±18
PMsil1.5	2.60±0.01	1.56±0.01	1.90±0.08	2.51±0.01	40.0±0.1	27.9±0.5	0.149±0.005	0.18	1130±32
PMtes1	2.60±0.01	1.65±0.04	1.87±0.02	2.60±0.03	36.5±0.1	28.2±0.5	0.151±0.005	0.34±0.05	1008±10
PMcast0.5	2.60±0.01	1.74±0.06	1.64±0.05	±3.99±0.05	33.1±0.1	22.2±0.5	0.119±0.009	0.20	1075±16
PMcast1	2.60±0.01	1.73±0.05	1.94±0.01	2.69±0.04	33.5±0.1	24.9±0.5	0.128±0.009	0.27±0.05	1225±6
PMcast1.5	2.60±0.01	1.71±0.08	1.64±0.05	2.34±0.07	34.2±0.1	26.2±0.5	0.134±0.008	0.30	1227±20
PMznst0.5	2.60±0.01	1.72±0.06	-	2.50±0.01	33.8±0.1	-	-	-	1002±11
PMznst1	2.60±0.01	1.75±0.04	1.8±0.04	2.65±0.01	32.7±0.1	27.2±0.5	0.148±0.020	0.50±0.05	998±17
PMznst1.5	2.60±0.01	1.71±0.05	-	2.63±0.08	34.2±0.1	-	-	-	1000±5

Bulk density =measured on the whole 4X4X16 cm specimens; Bulk density MIP= measured through MIP analysis; Apparent density MIP= density of the sample excluding the open porosity. evaluated via MIP; Total cumulative volume MIP(mm³/g)=volume of mercury intruded evaluated via MIP; Total open porosity MIP (%)= through MIP analysis only the open porosity was evaluated

Table 3.3 23 Distribution of the porosity and cumulative volume vs the pore radius of the different pozzolana-lime mixes, the respective labels are reported on graphs legends

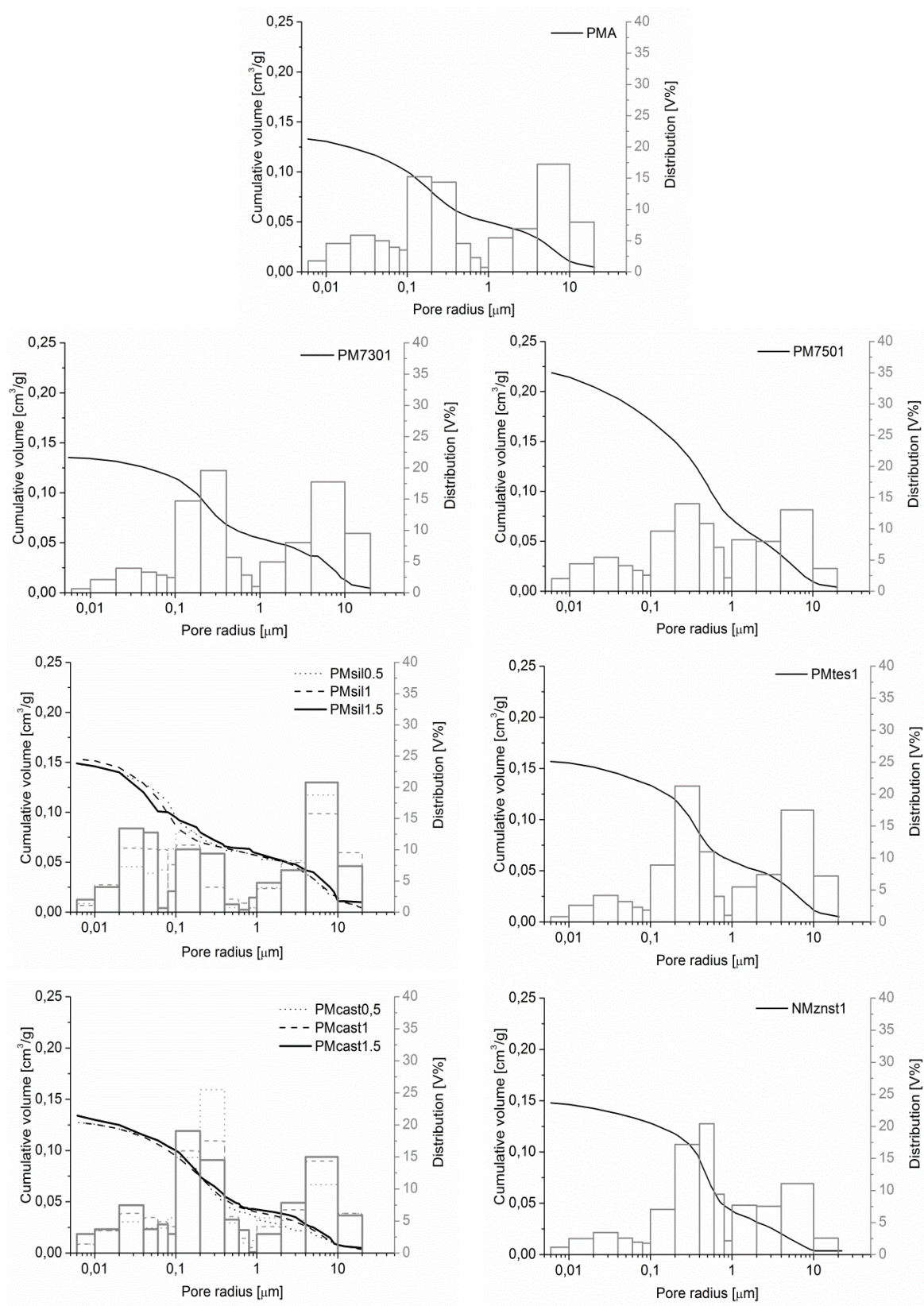


Table 3.3 24 Compressive and flexural strength of pozzolana-lime mortars without (NMA) or with water repellents at 0.5% and 1% by mass, the average of three measurements with their standard deviation is given.

Mortar mix	Compressive strenght			Flexural strenght
	σ_{max} (MPa)	E_{mod} tangential (MPa)	E_{mod} secant (MPa)	σ_{max} (MPa)
PMA	2.0±0.2	1.8±0.1	1.9±0.3	0.37±0.09
PM7501	1.07±0.05	1.32±1.07	0.8±0.2	0.32±0.02
PM7301	1.2±0.1	0.5±0.2	0.9±0.2	0.25±0.02
PMsil0.5	1.73±0.08	1.9±0.4	1.6±0.5	0.32±0.01
PMsil1	2.24±0.07	2.6±0.4	1.6±0.3	0.33±0.02
PMsil1.5	2.04±0.09	2.2±0.2	1.46±0.07	0.29±0.01
PMtes1	0.89±0.03	0.71±0.08	1.1±0.3	0.20±0.05
PMcast0.5	2.35±0.08	3.1±0.5	3.1±0.7	0.44±0.14
PMcast1	2.0±0.1	3.0±0.7	2.8±0.4	0.39±0.02
PMcast1.5	2.06±0.08	3.1±0.4	2.4±0.1	0.42±0.02
PMznst0.5	0.60±0.06	0.32±0.03	0.6±0.2	0.11±0.01
PMznst1	0.26±0.01	0.22±0.08	1.3±0.3	-
PMznst1.5	0.05±0.00	2.1±0.3	0.15±0.01	0.12±0.02

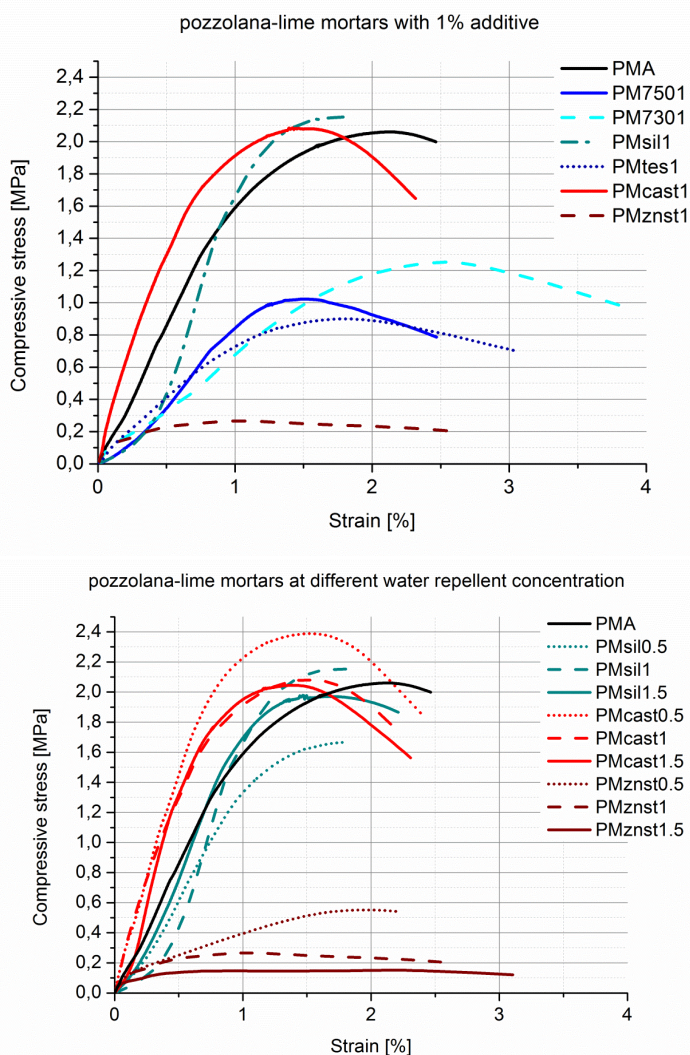


Figure 3.3 12 Graphs of the compressive stress of pozzolana-lime mortars vs. their percentage strain, mixes with different water repellents at 1% (above), and mixes with different percentages of water repellents added (0.5%, 1%, 1.5%) are shown (below).

Water vapour permeability of pozzolana-lime mortars

The obtained water vapour resistance μ is shown in Figure 3.3 13, while the water vapour permeability is listed in Table 3.3 26.

The reference mortar PMA had a μ of 11 ± 1 . For PM7501, PM7301, PMtes1 similar values were measured whereas for MPsil1, MPsil1.5, MPcast0.5, 1, 1.5 a higher μ were found. The addition of zinc stearates (PMznst0.5, 1, 1.5) caused a higher permeability and lower μ -values.

By increasing the percentage of additive used from 0,5% , 1% and 1,5% it was observed a reduction of the permeability for the mixes PMsil0.5, 1, 1.5 and for MPcast0.5, 1, 1.5, and an increase for PMznst0.5,1, 1.5.

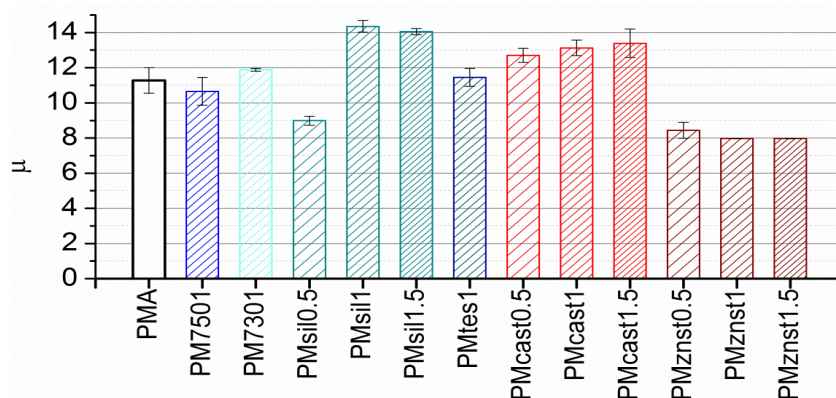


Figure 3.3 13 Histogram of the water vapour resistance μ values. Average of three measurements with standard deviation as error bars.

Capillary water absorption and contact angle measurements of pozzolana-lime mortars

The capillary water absorption coefficients are reported in Table 3.3 25 and Figure 3.3 15, together with the average contact angle of water drops on mortar surface. The collected data (Figure 3.3 15) and the observation of the water uptake curves allowed to divide the mixtures in three main groups:

- PMA and PM7301 had high capillary absorption coefficient C and a contact angle equal to zero: the presence of sitren P730® was not effective in assuring a good water-repellent effect.
- PMcast0.5 and PMcast1 can be considered as a separate group, here it was observed a water repellent effect. Though not so strong for low water-repellent concentration, this effect increased when higher percentages of calcium stearates were used, as in PMcast1, the same consideration can be made for PMznst0.5, 1, 1.5.
- The mixes PM7501, PMsil0.5, 1, 1.5, PMcast1.5, PMznst1, 1.5, PMtes1 formed a third group, where the water repellent effect was stronger. The absorption coefficients were really low and the contact angles measured, in any case more than 90° , indicate that the mortars surfaces were not wettable.

Regarding the differences of the water absorption measured on the inner or in the outer side, it was possible to observe that the capillary water absorption coefficients for the outer side were in any case lower. Huge differences, however, were seen in the following cases:



Figure 3.3 14 wettability behaviour of the inner core in comparison to the outer side layers in a PM7301 specimen

- PM7301 and PMcast0.5, 1 demonstrated better water repellent performances on the outer side;
- PMSil0.5 had a better water repellent behaviour in the inner core.
- PMznst0.5 showed a better water repellence on the outer side.

In general, the external layers were more compact, this fact can explain the differences obtained in most of the cases, nevertheless for the mortar mixes PM730, PMcast0.5, 1 it was observed a preferential wetting of the inner core not completely explainable only by a different porosity (Figure 3.3 14) and the hypothesis of a preferential migration of the additive to the mortar-air interface has to be taken into account.

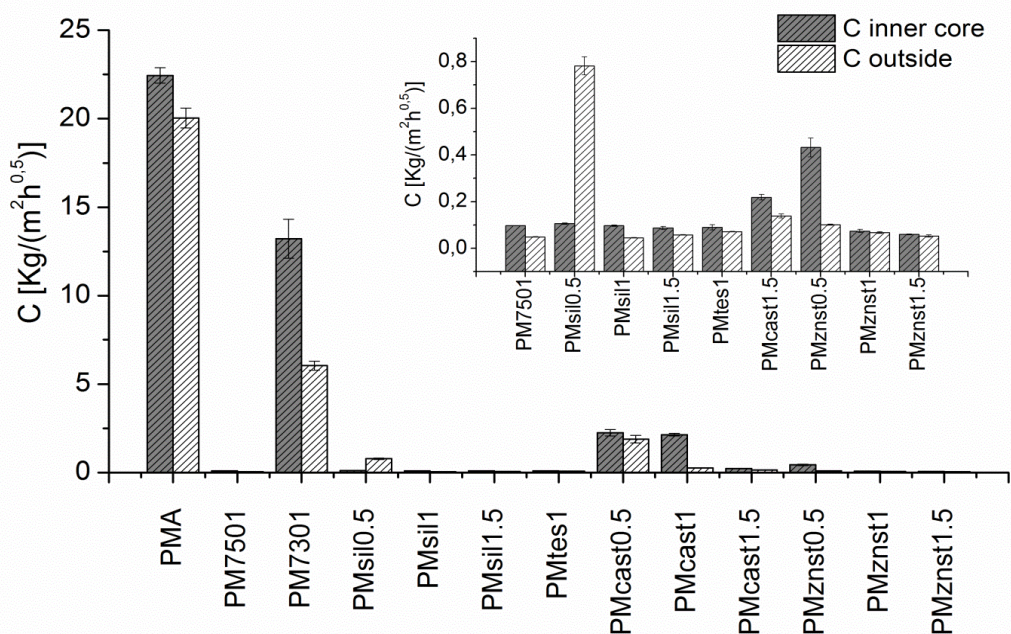
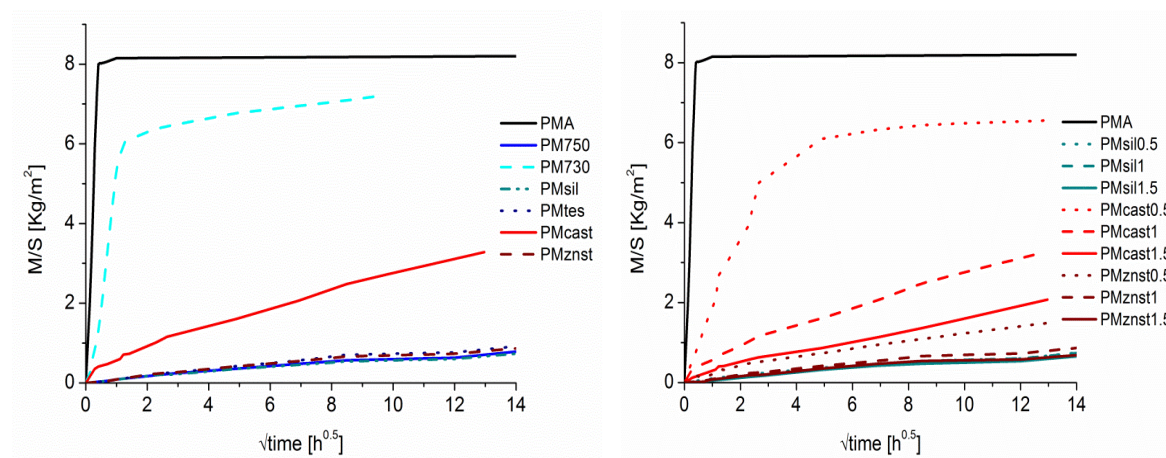


Figure 3.3 15 Histogram of the water absorption coefficient of the different mixes after several water absorption cycles. Average of three measurements with standard deviation as error bars.

Table 3.3 25 Capillary water absorption curves of the inner core of pozzolana-lime mortars without or with water repellents at 1% (link); with different water repellents percentages 0.5%, 1%, 1.5%.



3.3 Physico-chemical properties of mortars with water-repellents

Table 3.3 26 water vapour permeability expressed with following parameters: Permeability $\text{kg}/(\text{m}^2\cdot\text{s})$; WDD (wasserdampfdurchlässigkeit) $\text{g}/(\text{m}^2\cdot 24\text{h})$; water vapour resistance μ ; equivalent air layer sd of natural hydraulic lime mortars without (NMA) and with water repellents added at 0.5%, 1%, 1%. Capillary Water Absorption Coefficients and average Contact Angles. The average of three measurements with their standard deviation is reported.

sample mix	Water vapour permeability				Capillary water absorption		Wettability
	Permeability ($\text{kg}/(\text{m}^2\cdot\text{s})$)	WDD ($\text{g}/(\text{m}^2\cdot 24\text{h})$)	μ	sd (m)	Inner core in contact with water C ($\text{kg}/(\text{m}^2\cdot\text{h}^{0.5})$)	Outside surface in contact with water C ($\text{kg}/(\text{m}^2\cdot\text{h}^{0.5})$)	Contac angle θ ($^\circ$)
PMA	$6\cdot 10^{-7}\pm 1\cdot 10^{-7}$	53±9	11±1	0.35±0.07	22.4±0.9	20.0±1.1	W*
PM7501	$8.0\cdot 10^{-7}\pm 0.2\text{E-}07$	69±9	11±2	0.27±0.08	0.097±0.002	0.049±0.002	130±6
PM7301	$7.0\cdot 10^{-7}\pm 0.6\cdot 10^{-7}$	60±5	12±1	0.29±0.03	13.2±2.2	6.0±0.5	W*
PMsil0.5	$8.4\cdot 10^{-7}\pm 0.5\cdot 10^{-7}$	72±5	9±1	0.23±0.02	0.11±0.01	0.78±0.08	128±3
PMsil1	$5.6\cdot 10^{-7}\pm 0.7\cdot 10^{-7}$	48±6	14±1	0.38±0.05	0.10±0.01	0.045±0.003	130±2
PMsil1.5	$5.1\cdot 10^{-7}\pm 0.5\cdot 10^{-7}$	44±4	14±1	0.42±0.05	0.09±0.01	0.058±0.002	143±3
PMtes1	$6.5\cdot 10^{-7}\pm 0.7\cdot 10^{-7}$	56±6	11±1	0.32±0.05	0.09±0.02	0.071±0.002	126±8
PMcast0.5	$5.8\cdot 10^{-7}\pm 0.06\cdot 10^{-7}$	50±1	13±1	0.36±0.00	2.2±0.4	1.9±0.4	W*
PMcast1	$5.1\cdot 10^{-7}\pm 0.7\cdot 10^{-7}$	44±6	13±1	0.42±0.07	2.1±0.2	0.252±0.024	W*
PMcast1.5	$5.6\cdot 10^{-7}\pm 0.5\cdot 10^{-7}$	49±4	13±2	0.37±0.04	0.22±0.02	0.14±0.02	W*
PMznst0.5	$9.6\cdot 10^{-7}\pm 0.1\cdot 10^{-7}$	83±1	8±1	0.20±0.01	0.4±0.1	0.101±0.005	W*
PMznst1	$9.8\cdot 10^{-7}\pm 0.4\cdot 10^{-7}$	85±3	8±1	0.19±0.02	0.07±0.01	0.067±0.007	118±14
PMznst1.5	$9.8\cdot 10^{-7}\pm 0.4\cdot 10^{-7}$	85±3	8±1	0.19±0.02	0.06±0.00	0.05±0.01	126±6

W* = completely wettable, the contact angle was not measurable

3.4 Artificial weathering of mortar specimens

In this section the results of the study of artificial weathering of mortar specimens¹⁶ are presented, and separately discussed for each mortar system studied, i.e. limestone cement mortars, natural hydraulic mortars, pozzolana-lime mortars with or without water repellents added at 1% by dry mass.

As described in paragraph 2.2.3.1 a total of three sample for each mortar mix were subjected to the ageing, which consisted in 140 cycles of 5 hours and 45 minutes of UV-light exposure (UVA 290-400nm, 50°C) and 15 minutes of dousing with water at 15°C (conductance <25µs/cm, dosing rate 40Lmin⁻¹m⁻²). In order to isolate only one exposed surface and to avoid significant detachments of material which might have damage the climatic chamber, a layer of epoxy resin was brushed on the lateral surfaces¹⁷.

During the cycles, the samples were monitored (through naked eye observations) in order to detect failures and defects such cracks, scaling of the surfaces, material losses, detachments, peelings, delaminations. The effects of the ageing were further evaluated at the end of the cycles with optical microscope¹⁸, FT-IR-ATR analysis of the surfaces, colorimetric analysis, water absorption cycles, contact angle measurements.

This section reports the analyses done and the data obtained while the results will be further analyzed and discussed in Chapter 4. However, to shortly summarize the main results it was seen that:

- Limestone cement mortars did not show damages after the test, thanks to their higher mechanical strength;
- Natural hydraulic lime mortars demonstrated sufficient resistance to the weathering;
- Pozzolana-lime mortars admixed with silane/siloxanes showed better resistance in comparison to mortars admixed with stearates;
- All the mortars admixed with stearates became wettable and had higher water absorption coefficients at the end of the exposure.

3.4.1 ARTIFICIAL WEATHERING OF WATER-REPELLENT LIMESTONE CEMENT MORTARS

In Table 3.4 1 pictures of the specimens before and after the cycles are shown. As a consequence of the weathering the specimens cast using limestone cement as binder did not undergo significant decay processes. No evident cracks, crumbling, material losses or detachments were visible after the ageing.

In CMA, CMznst, CMvin a slight powdering of the surfaces was observed with a preferential leaching of the binder, the dark aggregates are therefore more visible at the end.

Also the observation with the digital optical microscope (Table 3.4 1) did not evidence other visible decay both under natural and UV-light. Even with microscope observation CMA and CMznst samples showed more visible dark aggregates and less light-coloured binder matrix.

¹⁶ See Chapter 2.2 casting procedure paragraph 2.2.3.1. Artificial ageing conditions

¹⁷ Chapter 2.1

¹⁸ Examination carried out using a Dino-light microscope

Colorimetric measurements of the weathered surfaces of limestone cement mortars with water repellents were performed according to the method described in Chapter 2¹. In Table 3.4 2 and Figure 3.4 1 the total colour variations, expressed as ΔE^* , are shown together with the variations of the three colorimetric values (L^* , a^* , b^*). The variations were calculated as differences between the value collected before the ageing (Chapter 3.3) and after the ageing. The colour variations were in every case low, ($\Delta E^* < 3$), in particular considering that mortars have rough and not homogeneous surfaces, difficult to measure. Negligible differences were found working with the specular component included (SCI) or excluded (SCE), only CM730 and CMznt 1 showed little differences. The samples after the weathering incremented the b^* component (yellowing) and darkened (decrement in L^*) due to a preferential dissolution of the lighter finer matrix, except CMA and CMznt which became brighter (increment in L^*).

FT-IR ATR spectra registered on samples collected from the specimens surfaces (Figure 3.4 2) showed that the complete carbonation of the surfaces occurred (1436 cm^{-1} , 875 cm^{-1}). The Si-O-Si stretching peak at 950 cm^{-1} of C-S-H was clearly visible in all the spectra collected except in CMznt samples. A complete maturation/hydration of the exposed surfaces took place during the ageing, thanks to the high temperatures reached during the UV exposure and the moisture during the dousing with water. The peaks related to the water repellents were concealed by the other absorptions and it was difficult to evaluate a possible degradation of the water repellents, but the complete absence of the aliphatic stretching at $2920\text{--}2850\text{ cm}^{-1}$ of CMcast and CMznt suggested the absence of the stearates on the mortar surfaces at the end of the exposure.

Capillary water absorption tests² were performed after the weathering cycles. The weathered surface of the specimens was put in contact with water and the value compared to the capillary absorption before the exposure. Table 3.4 3 reports the water absorption coefficients C ($\text{kg}/(\text{m}^2 \cdot \text{h}^{0.5})$) calculated. Consistent variations of the coefficient were observed in every case. The significant increase of the water absorption observed for CMA, CM7301, CMcast1, CMvin1 might be related, in particular for CMA, to a preferential erosion of the binder (observed with optical microscope) and to an increased surface porosity. In the other cases, together with the erosion of the binder, it might be possible that the water repellents were washed out or degraded. Before the exposure CM730, CMcast, CMvin had lower water absorption on the outer surfaces than in the inner core (Chapter 3.3) caused by a preferential disposition of the water repellents. Prolonged dousing with water of the surfaces might have caused the erosion of the surfaces and the water repellent wash-out.

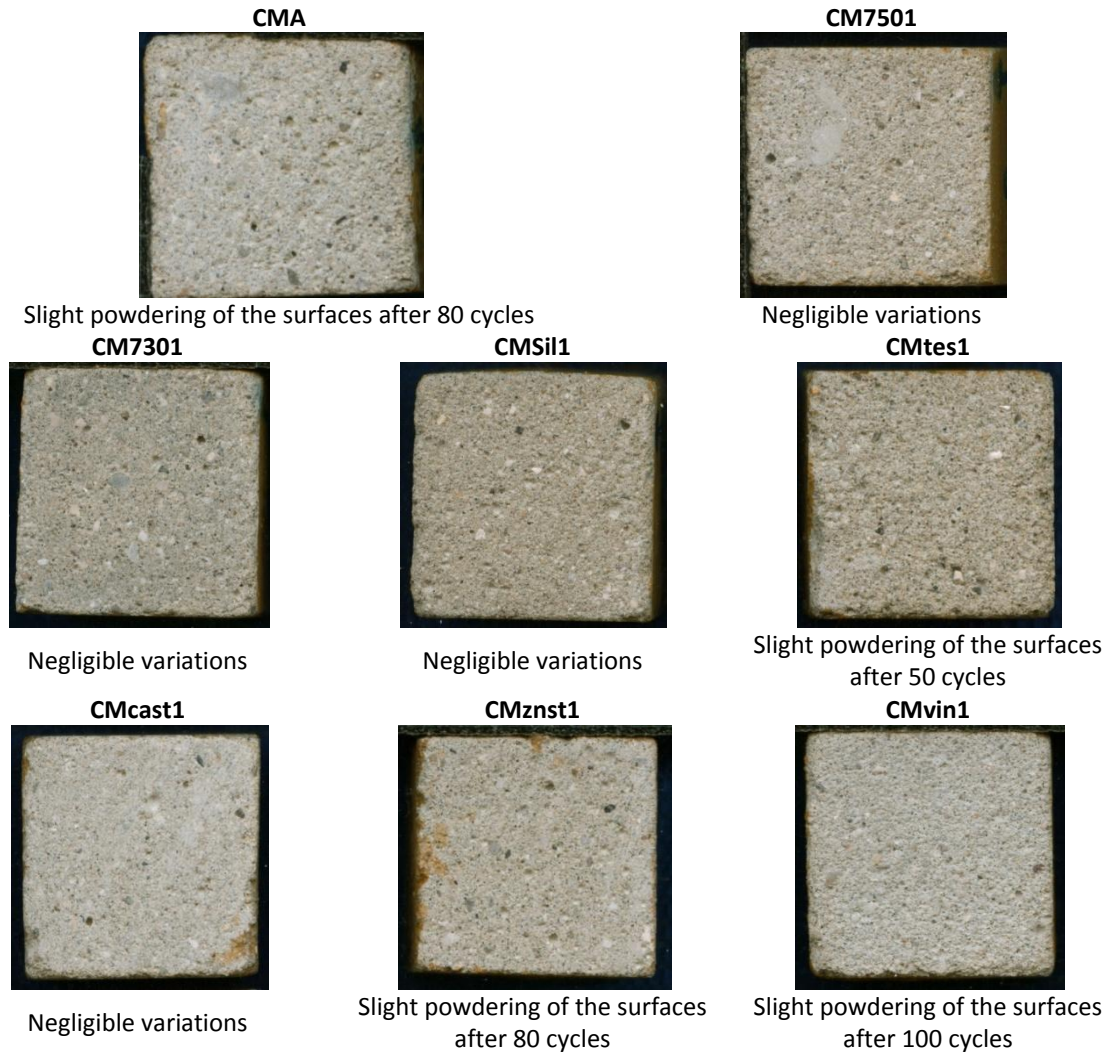
The UV-light and the temperature could have also caused a degradation of the organic part of the water repellents, in particular of the polymer Vinnapas® as suggested also by the degradation observed on Vinnapas® samples kept in oven (Chapter 3.1).

On the other side, the mortar mixtures CM7501, CMsil1, CMtes1, CMznt1 showed a decrease of the water absorption coefficient: the water-repellent effect was even enhanced. Probably the consecutive UV-light and dousing cycles with their high temperatures and high relative humidity, allowed the cement matrix to further hydrate and compact, while the water repellent admixtures were not washed out or degraded.

¹ Measurements were taken in 5 different areas of each samples. A set of 3 spectra was collected for each area so that, the final colorimetric values, came from an average of 9 acquisition. To overcome the problem of the non homogeneity of mortar surfaces the data were acquired with an illumination area of 11mm

² Tests performed on three cubic ($4 \times 4 \times 4\text{ cm}$) specimens for each mortar mix as described in Chapter 2.

Table 3.4 1 Above: Samples cast using limestone cement as binder, without or with water repellents added, after the artificial weathering (140 cycles; scale 1:1). Below: Light and UV-light microscopy examination of some of the specimens surface after the artificial weathering (225X scale bar= 0.4 mm)



Light and UV-light microscopy examination

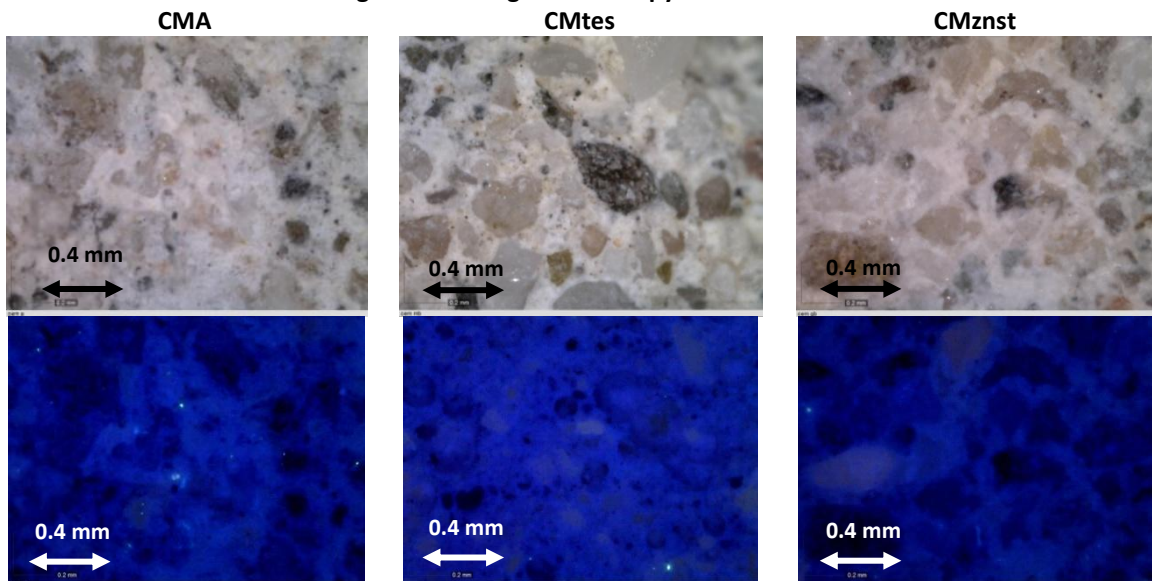


Table 3.4 2 The colour variations induced by the artificial weathering of the limestone cement mortars. The total colour variation (ΔE^*), the variation of Lightness (ΔL^*) and chromaticity coordinates (Δa^* , Δb^*) is shown. Data were calculated from values acquired both including and excluding the specular reflectance (SCI and SCE methods).

	SCI				SCE			
	ΔL^*	Δa^*	Δb^*	ΔE^*	ΔL^*	Δa^*	Δb^*	ΔE^*
CMA	-1,82±0.01	-0,27 ±0.02	0,03 ±0.01	1,84 ±0.01	-1,85 ±0.0 1	-0,23 ±0.02	0,19 ±0.01	1,88 ±0.01
CM7501	0,21±0.02	0,19 ±0.01	2,16 ±0.01	2,18 ±0.01	-0,84 ±0.02	0,21 ±0.01	2,19 ±0.01	2,36 ±0.01
CM7301	-3,12±0.04	0,0 1±0.01	1,22 ±0.01	3,35 ±0.01	-2,48 ±0.04	0,01 ±0.01	1,37 ±0.01	2,83 ±0.01
CMSil1	-1,92±1.02	0,11 ±0.08	3,08 ±0.05	3,63 ±0.05	-1,05 ±0.02	0,07 ±0.08	2,46 ±0.05	2,67 ±0.05
CMtes1	2,24±0.01	0,04 ±0.01	1,70 ±0.01	2,81 ±0.01	2,57 ±0.01	0,01 ±0.01	1,38 ±0.01	2,92 ±0.01
CMcast1	2,31±0.01	0,01 ±0.01	0,23 ±0.01	2,32 ±0.01	2,25 ±0.01	0,05 ±0.01	0,68 ±0.01	2,35 ±0.01
CMznst1	-1,55±0.01	0,15 ±0.01	1,09 ±0.01	1,90 ±0.01	-2,60 ±0.01	0,21 ±0.01	1,24 ±0.01	2,89 ±0.01
CMvin1	2,10±0.01	0,02 ±0.01	-0,88 ±0.01	2,27 ±0.01	1,98 ±0.01	0,05 ±0.01	-0,81 ±0.01	2,14 ±0.01

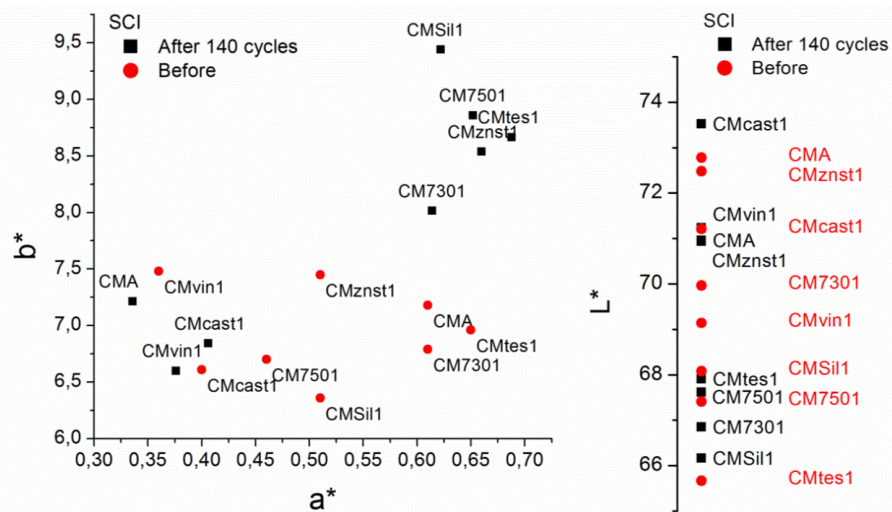


Figure 3.4 1 colorimetric measurements of limestone cement mortars before and after the weathering cycles

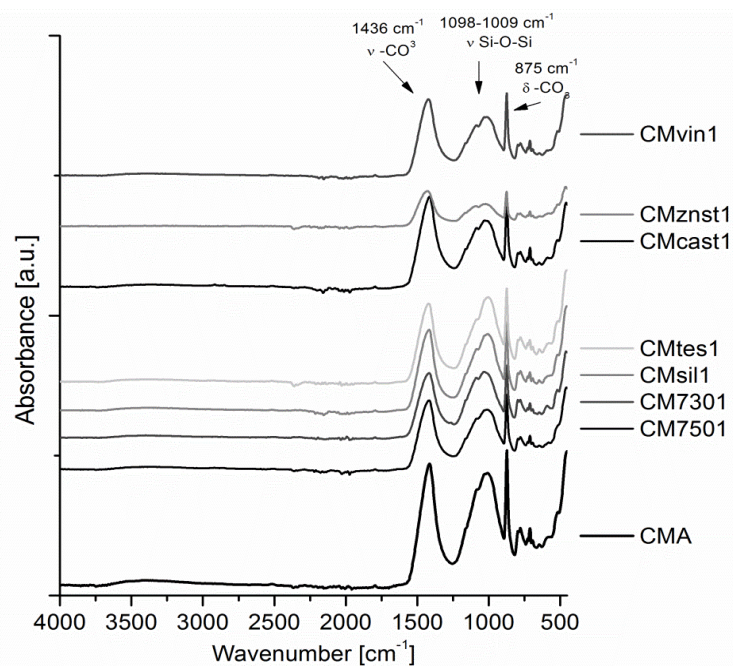
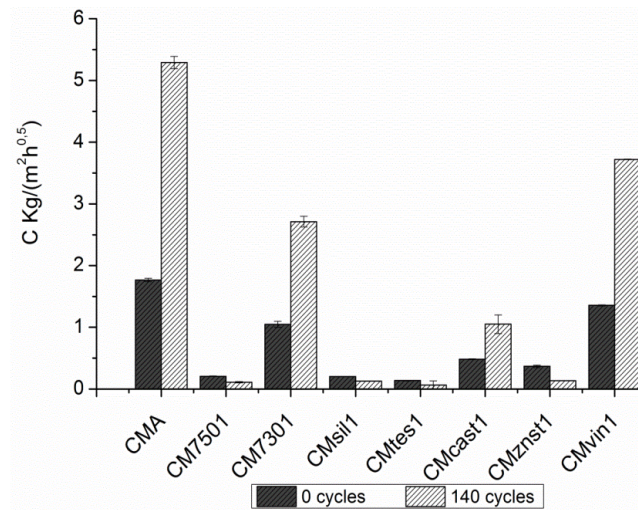


Figure 3.4 2 FT-IR ATR spectra of samples collected from the weathered surfaces of limestone cement mortars

Table 3.4 3 Capillary absorption coefficient of limestone cement mortars without or with water repellents at 1% by mass before and after artificial weathering. The capillary absorption of the outside was considered.

Mix names	Before	After 140 cycles
	kg/(m ² ·h ^{0.5})	kg/(m ² ·h ^{0.5})
CMA	0,77±0,02	5,29±0,10
CM7501	0,21±0,01	0,11±0,01
CM7301	1,05±0,04	2,71±0,08
CMSil1	0,20±0,01	0,13±0,01
CMtes1	0,14±0,01	0,06±0,07
CMcast1	0,48±0,01	1,05±0,10
CMznst1	0,37±0,02	0,13±0,06
CMvin1	1,35±0,01	3,72±0,01



3.4.1. ARTIFICIAL WEATHERING OF WATER-REPELLENT NATURAL HYDRAULIC LIME MORTARS

Table 3.4 4 summarizes the main variation detected during and after the cycles with naked eye and optical microscopy examinations.

Natural hydraulic lime mortars were more affected by the weathering cycles in comparison to limestone cement mortars. Detachment/peeling of the external epoxy layer due to a differential thermal expansion and different material cohesion were observed in several cases (NM750, NM730, NMsil), together with continuous crumbling and erosion of the surfaces. At the end of the test, NMA and NMznst had smoother surfaces; NMcast was only partially degraded; NM750, NM730, NMsil surfaces were consumed during the test.

The preferential dissolution/erosion of the binder in comparison to the aggregates in NM750, NM730, NMsil was observed by optical microscopy. Under the UV-light NMA, NMcast NMznst surfaces were homogeneously fluorescent thanks to the presence of a fine layer of binder on the surface, while the surfaces of NM750, NM730, NMsil were heterogeneous with brighter fluorescent area due to calcium carbonate aggregates which had been remained uncovered by the external binder layer.

Table 3.4 5 shows the colour variation assessed for natural hydraulic lime mortars after the ageing. The measurements were carried out according to the method previously described for limestone cement mortar samples. The colour of NMA remained quite stable during the test, while the other mortars yellowed (increment of b*), reddened (increment of a*) and assume a brighter colour (increase of L*). Negligible differences between SCI and SCE measurements were found.

FT-IR ATR analysis of the surfaces after the artificial weathering showed a high presence of calcium carbonates (1436 cm⁻¹, 875 cm⁻¹) and a low presence of silicates(900-1100 cm⁻¹). A

complete carbonation took place, as seen above for limestone cement mortars. On the contrary the aliphatic absorptions at $2920\text{-}2850\text{ cm}^{-1}$ of calcium and zinc stearates were here clearly detected, the total wash-out of the water repellent did not occur.

The capillary water absorption coefficient are displayed in Table 3.4 6. After the ageing, the water absorption increased in every case, except for NM7501. The increasing was probably due to the dissolution of the external, more compact, layer and to the subsequent increase of the surface roughness and porosity. The variation of the capillary coefficient of NMznst1 was particularly marked and cannot be explained only by the increased of surface roughness, however the presence of zinc stearates was observed with FT-IR analysis also after the test. We might suppose that a partial wash-out of the external layer and of the water repellent present within combined with the increasing of the porosity led to the higher water absorption. On the other hand, the silane/siloxane Sitren P750® was very effective and stable as water repellent in natural hydraulic lime systems.

Table 3.4 4 Samples prepared using natural hydraulic lime as binder, without or with water repellents added, before, during and after the artificial weathering (scale 1:1) .

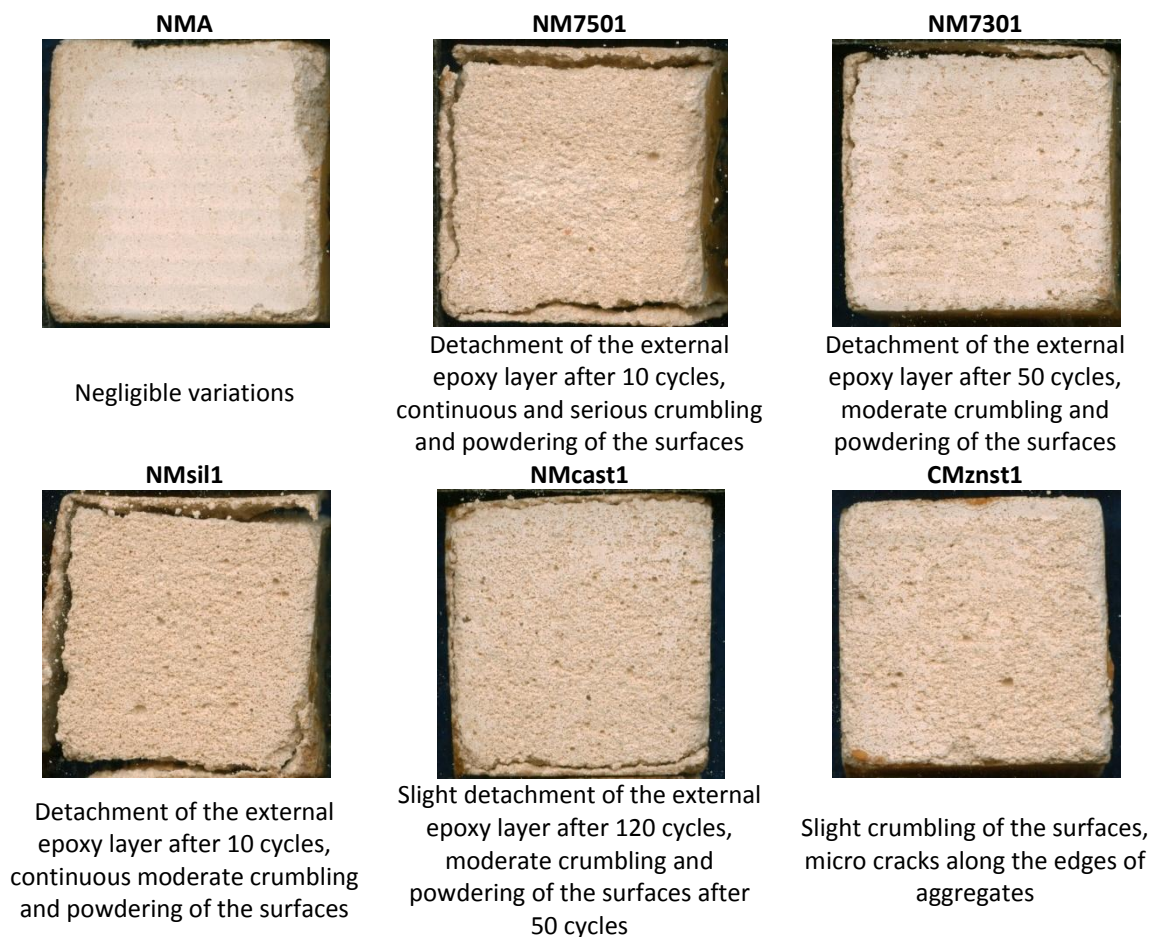
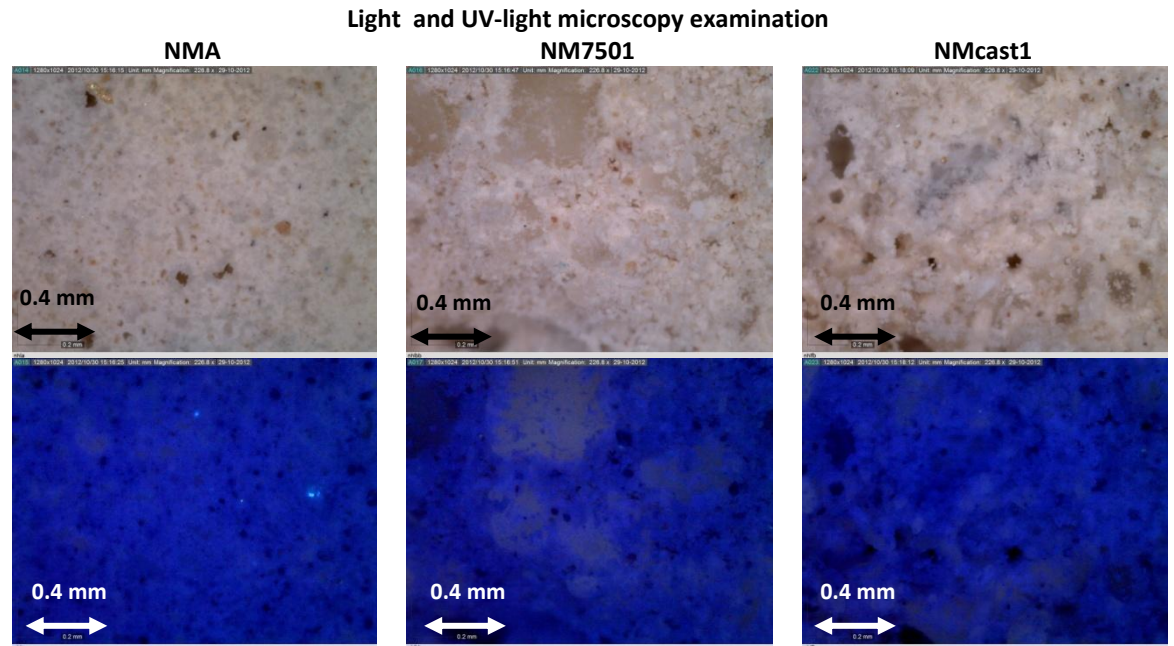


Table 3.4 5 Above: Light and UV-light microscopy examination of some of the specimen surfaces after the artificial weathering (225X, scale bar= 0.4 mm). Below: colour variations induced by the artificial weathering of the natural hydraulic lime mortars. The total colour variation (ΔE^*), the variation of Lightness (ΔL^*) and chromaticity coordinates (Δa^* , Δb^*) is shown with specular reflectance included or excluded (SCI and SCE methods).



Colour variations

	SCI				SCE			
	ΔL^*	Δa^*	Δb^*	ΔE	ΔL^*	Δa^*	Δb^*	ΔE
NMA	0,0±0,2	0,4±0,1	1,3±0,5	1,4±0,5	0,1±0,2	0,4±0,1	1,3±0,5	1,4±0,5
NM7501	4,5±1,0	-0,6±0,1	-2,8±0,4	5,4±1,1	4,5±1,1	-0,6±0,1	-2,8±0,4	5,3±1,2
NM7301	3,2±1,0	-0,6±0,2	-3,0±0,4	4,4±1,1	3,2±0,9	-0,6±0,2	-3,0±0,4	4,5±1,0
NMSil1	4,4±1,8	-0,7±0,1	-3,5±1,0	5,6±2,1	4,5±1,8	-0,7±0,1	-3,5±1,0	5,7±2,0
NMcast1	3,9±0,6	-0,8±0,0	-3,8±0,3	5,5±0,6	4,0±0,5	-0,8±0,0	-3,8±0,3	5,5±0,6
NMznst1	4,0±3,0	-0,2±0,0	-1,0±0,2	4,2±3,0	3,9±3,2	-0,2±0,1	-1,0±0,2	4,0±3,2

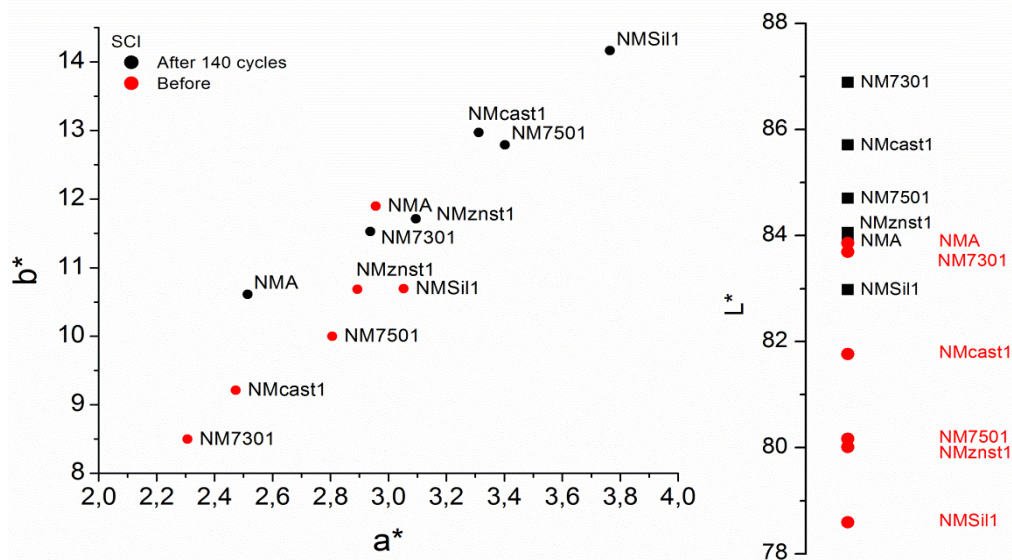


Figure 3.4 3 The colorimetric data acquired before (red dots) and after (black dots) the weathering are graphically shown at the end of the table.

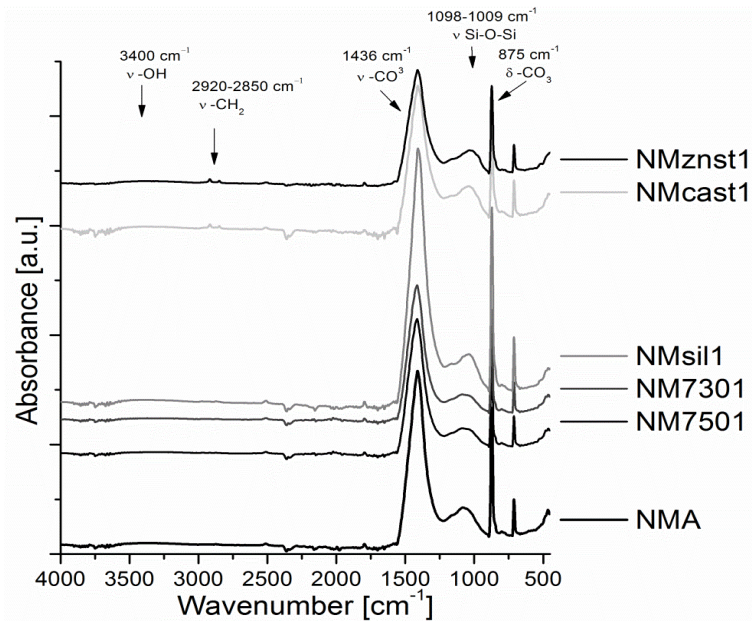
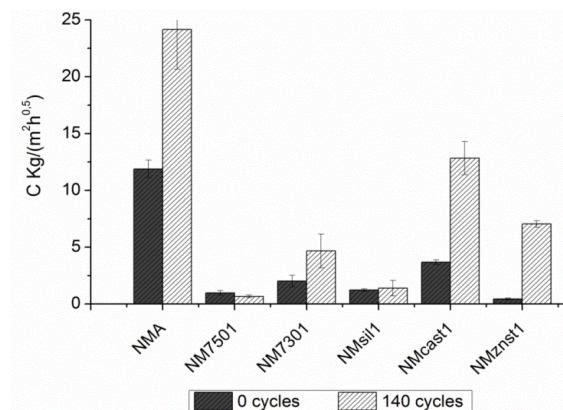


Figure 3.4 4 FT-IR ATR spectra of the surface of natural hydraulic lime mortars after the artificial weathering

Table 3.4 6 Capillary absorption coefficient of natural hydraulic lime mortars without or with water repellents at 1% by mass before and after artificial weathering. The capillary absorption of the outside was considered.

	Before C kg/(m ² ·h ^{0,5})	After 140 cycles C kg/(m ² ·h ^{0,5})
NMA	11,9±0,8	24,2±3,5
NM7501	0,98±0,19	0,67±0,12
NM7301	2,01±0,51	4,67±1,48
NMsil1	1,227±0,109	1,394±0,685
NMcast1	3,69±0,19	12,84±1,45
NMznst1	0,45±0,06	7,04±0,29



ARTIFICIAL WEATHERING OF POZZOLANA-LIME MORTAR Table 3.4 9 shows the surfaces of the specimens before and after the weathering test (140 cycles).

The reference mortar PMA began to show little cracks at the edges and detachments of the epoxy layer after 24 cycles, due to the different shrinkage behavior of the epoxy layer and the mortars as thermal changes occurred. Continuous crumbling/scaling of the surfaces was observed during the weathering test with a preferential removal of the binder, followed by loss of aggregates and powdering of surfaces.

The water-repellent mortars can be divided into two different groups on the basis of the weathering behavior:

- PMcast1, PMcast1.5, PMznst0.5,1,1.5 mixes (containing calcium stearates or zinc stearates) behaved like PMA specimens: cracks formation before the first 32-56 cycles and homogeneous powdering of the exposed surfaces, with serious mass losses for PMznst1, PMznst1.5 PMcast1.5. To higher stearates contents (1.0%; and 1.5%) corresponded worse damage.

- PM7501, PM7301, PMSil0.5, PMSil1, PMSil1.5, PMtes1 (admixed with silane/siloxanes) and PMcast0.5 (with calcium stearates at 0,5%) formed a second group with better resistance. Cracks at the edges occurred only for PMcast0.5 samples, while a slight crumbling and powdering was observed for PMcast0.5, PMSil1, PMSil1.5 only after 72 cycles.

Observation of the specimens surfaces with optical microscope after the test (some example are reported in Table 3.4 9) confirmed what it was seen with naked eye, i.e. the dissolution and preferential removal of the binder in particular in PMznst0.5, 1, 1.5. After the binder removal, the consequent powdering and loss of aggregates from the surfaces occurred .

Before the weathering test the colour did not differ much from one mixture to another, but the artificial weathering caused moderate colour variations (Table 3.4 9) with ΔE^* till 9.6 (PMcast1.5). PMznst0.5, 1, 1.5 and PMcast1.5 mixtures were seriously affected by the exposure with erosion/dissolution of the brighter external layer, rich in binder. The aggregates were no more covered by the brighter binder and remained exposed on the surface. This caused a colour change with the increment of the chromaticity coordinates a^* (red) and b^* (yellow) and the decrease of the Lightness L^* . Moderate variation were observed, instead, when the degradation was limited/less important as for PMA, P7501, PMSil1.

Carbonates and silicates were detected on the surfaces of the specimens after the weathering (Figure 3.4 5), no calcium hydroxide was observed: the external layer carbonated fast under the weathering conditions. The shift of the Si-O-Si stretching absorption to around 1010 cm^{-1} (related to the production of C-S-H) was observed in every sample after the exposure (see also Chapter 3.3.3): hydration of the binder took place thanks to the hot and moist/damp environment inside the climatic chamber during the weathering.

Despite the presence of cracks and the erosion of the surfaces the capillary water absorption coefficients of PMA, PM7301, PMSil0.5, PMznst1, PMznst 1.5 after the ageing test (Table 3.4 7). This could be due to a further hydration and carbonation of the samples, in particular of the exposed surfaces, which resulted in a denser matrix and in a lower open porosity and therefore a lower water uptake. PMtes1, PM7501, PMSil1, PMSil1.5 had almost stable water absorption coefficient. PMcast0.5, 1, 1.5 and PMznst0.5 were strongly affected from the weathering test: a higher water absorption was observed in particular for lower dosage of calcium stearates in the mixes.

Table 3.4 7 Capillary water absorption coefficients before and after artificial weathering, measured on the external surface.

Mix name	Before the ageing test $C\text{ kg}/(\text{m}^2 \cdot \text{h}^{0,5})$	After the ageing test $C\text{ kg}/(\text{m}^2 \cdot \text{h}^{0,5})$
PMA	20.0±1.1	15.1±1.0
PM7501	0.05±0.01	0.07±0.01
PM7301	6.0±0.5	5.41±0.09
PMSil0.5	0.78±0.08	0.06±0.01
PMSil1	0.05±0.01	0.07±0.01
PMSil1.5	0.06±0.01	0.07±0.01
PMtes1	0.07±0.01	0.08±0.01
PMcast0.5	1.9±0.4	3.9±1.1
PMcast1	0.25±0.02	1.1±0.4
PMcast1.5	0.14±0.02	0.21±0.03
PMznst0.5	0.10±0.01	1.0±0.3
PMznst1	0.07±0.01	0.06±0.01
PMznst1.5	0.05±0.01	0.04±0.01

Table 3.4 8 Samples prepared using natural hydraulic lime as binder, without or with water repellents added, before, during and after the artificial weathering (scale 3:4)










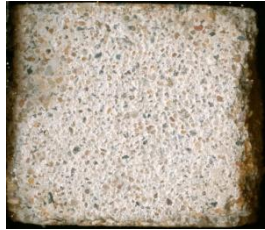


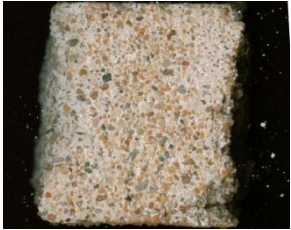
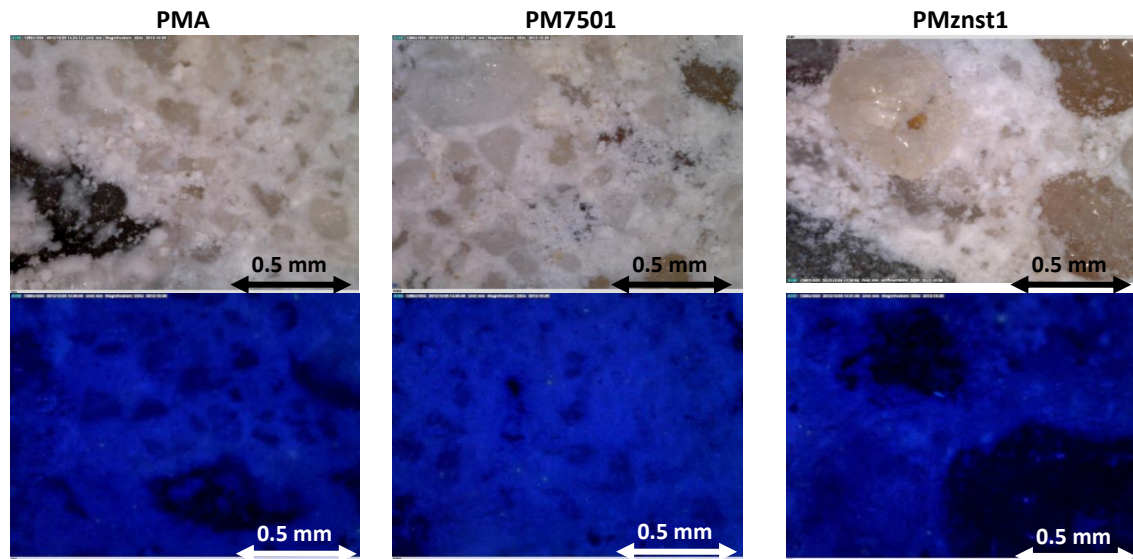
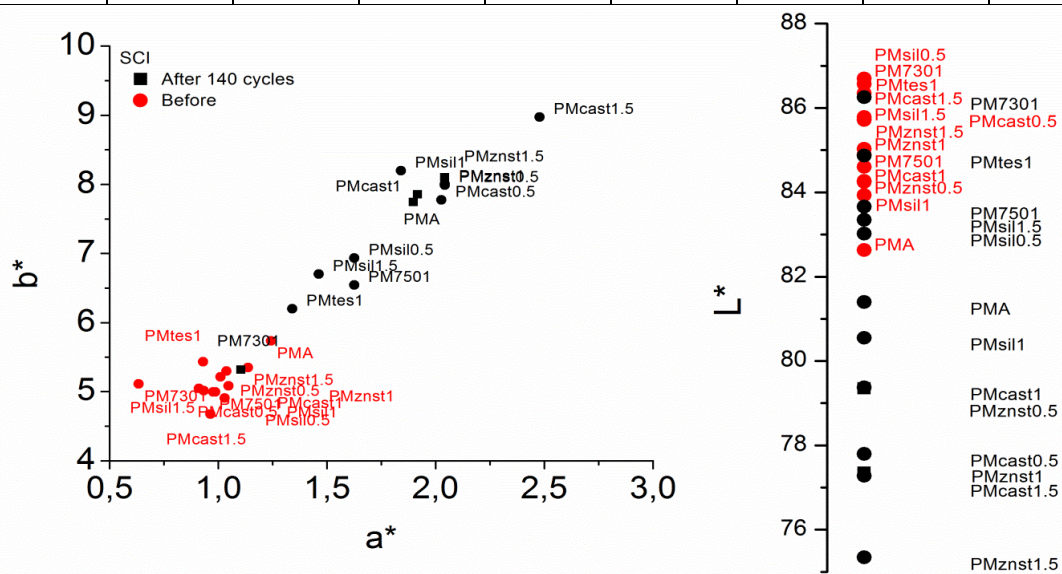
<p>PMA</p>  <p>First cracks after 24 cycles Continuous scaling/crumbling with loss of surface material Detachments and material losses at the edges</p>		
<p>PM7501</p>  <p>no cracks or crumbling No loss of material</p>	<p>PM7301</p>  <p>No cracks. Slight surface-erosion</p>	<p>PMtes1</p>  <p>No cracks. Slight scaling and crumbling</p>
<p>PMsil0.5</p>  <p>No cracks Slight scaling and crumbling</p>	<p>PMsil1</p>  <p>No cracks. Moderate scaling and flaking, loss of surface material</p>	<p>PMsil1.5</p>  <p>No cracks Slight powdering of the surface</p>
<p>PMcast0.5</p>  <p>Little cracks around the edges after 100 cycles. Slight erosion of the surface. Detachments and material losses</p>	<p>PMcast1</p>  <p>Cracks around the edges, detachment of the epoxy layer after 32 cycles. Erosion and powdering of the surface</p>	<p>PMcast1.5</p>  <p>Little cracks at the edges after 32 cycles. Serious erosion after 32-56 cycles. Rough and crumbled surface at the end of the test</p>
<p>PMznst0.5</p>  <p>Cracks after 16-24 cycles. Loss of surface material and detachments from the edges</p>	<p>PMznst1</p>  <p>Cracks after 32 cycles. Powdering of the surfaces after 56 cycles. Detachments</p>	<p>PMznst1.5</p>  <p>Serous cracks after 24 cycles. Serious crumbling, scaling, powdering of the surfaces.</p>

Table 3.4 9 Above: Light and UV-light microscopy examination of some of the specimen surfaces after the artificial weathering (225X, scale bar= 0.5 mm). Below: colour variations induced by the artificial weathering of the pozzolana- lime mortars. Values were acquired both with SCI and SCE methods.



	Colour variation							
	SCI				SCE			
	ΔL^*	Δa^*	Δb^*	ΔE	ΔL^*	Δa^*	Δb^*	ΔE
PMA	-1.2±0.4	-0.7±0.2	-2.0±0.1	2.4±0.5	-1.2±0.4	-0.7±0.2	-2.0±0.1	2.5±0.4
PM7501	-0.9±0.4	-0.6±0.2	-1.5±0.1	1.9±0.4	-0.9±0.4	-0.60.2	-1.5±0.1	1.9±0.4
PM7301	-0.3±0.6	-0.5±0.0	-0.2±0.1	0.6±0.6	-0.3±0.5	-0.5±0.1	-0.2±0.1	0.6±0.5
PMsil0.5	-3.7±1.8	-0.6±0.1	-2.0±0.9	4.2±2.0	-3.7±1.8	-0.6±-0.1	-2.0±0.9	4.2±2.0
PMsil1	-3.4±0.4	-0.9±0.2	-3.2±0.1	4.7±0.4	-3.4±0.4	-0.8±0.2	-3.2±0.1	4.7±0.4
PMsil1.5	-2.4±1.0	-0.5±0.3	-1.7±0.1	3.0±1.1	-2.4±1.0	-0.5±0.3	-1.7±0.1	3.0±1.0
PMtes1	-1.5±0.3	-0.4±0.0	-0.8±0.1	1.7±0.3	-1.6±0.3	-0.4±0.1	-0.8±0.1	1.8±0.3
PMcast0.5	-8.0±1.3	-1.1±0.1	-2.7±0.1	8.5±1.3	-7.7±0.9	-1.1±0.1	-2.7±0.1	8.2±0.9
PMcast1	-4.9±0.7	-0.9±0.1	-2.8±0.1	5.7±0.7	-5.1±1.0	-0.9±0.1	-2.8±0.1	5.8±1.0
PMcast1.5	-8.5±0.4	-1.5±0.5	-4.3±1.2	9.6±1.3	-8.5±0.3	-1.5±0.5	-4.3±1.2	9.6±1.3
PMznst0.5	-4.9±0.2	-1.0±0.2	-2.8±0.1	5.7±0.2	-4.9±0.1	-1.0±0.2	-2.8±0.1	5.7±0.2
PMznst1	-7.9±0.4	-1.0±0.0	-2.7±-0.3	8.3±0.5	-7.9±0.4	-1.1±0.1	-2.7±0.3	8.4±0.5
PMznst1.5	-9.0±0.1	-0.9±0.1	-2.8±0.1	8.58±0.0	-9.9±0.1	-1.3±0.1	-2.8±0.1	10.5±0.1



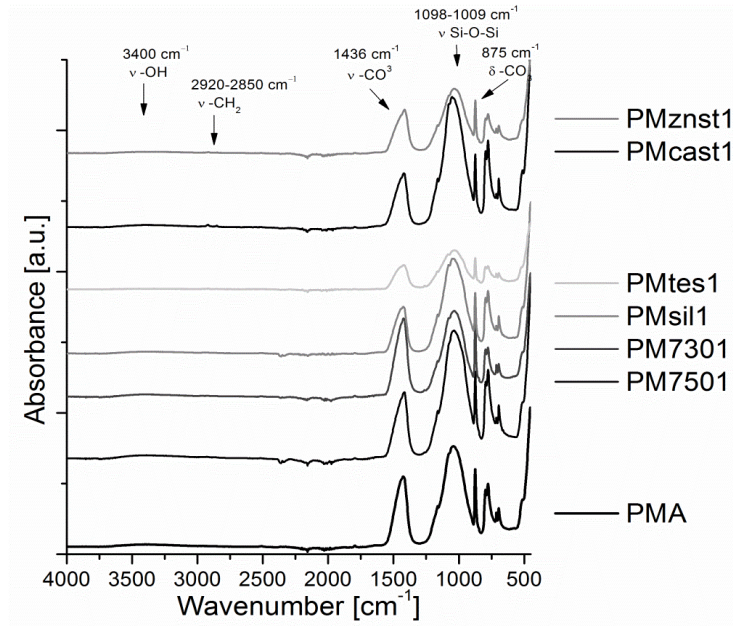


Figure 3.4 5 FT-IR ATR spectra of the surface of natural hydraulic lime mortars after the artificial weathering

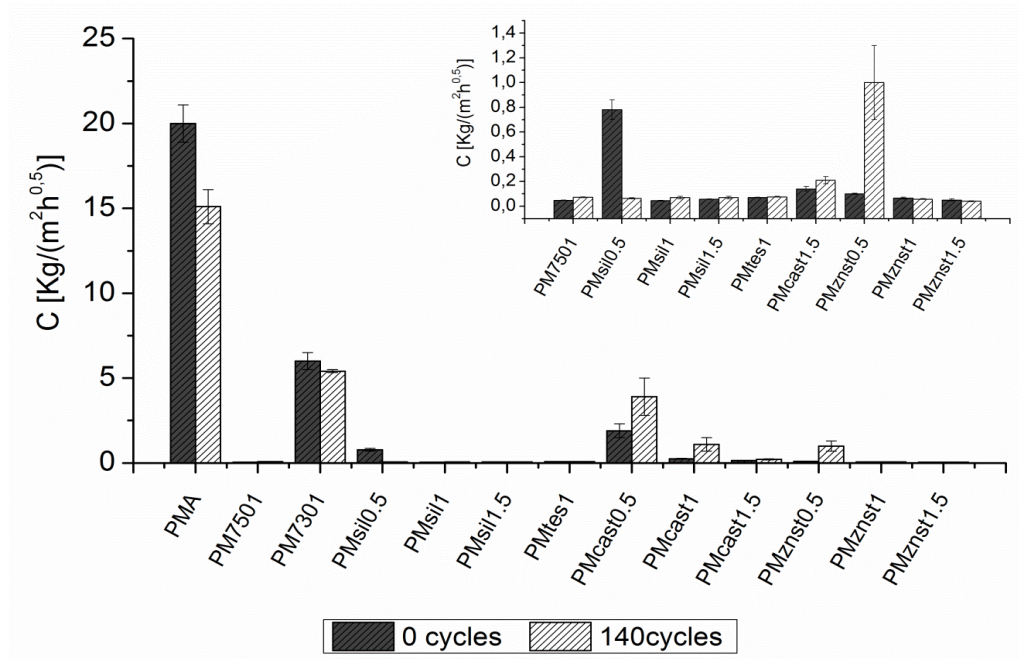


Figure 3.4 6 10 Capillary water absorption coefficients before and after artificial weathering

3.5. Resistance to salt crystallization

Salt weathering is a process of porous material disintegration that take place in a variety of environments and affects many kind of natural or artificial stone material. Mechanical action of salt crystallization processes can exert pressure capable of destroying even the most resistant stone³.

The purpose of this part of the study was to evaluate the effects of the exposure of water repellents mortars in saturate sodium solution under laboratory conditions (cycles of full immersion/drying), and to identify the consequent damages due to salt crystallization.

As described in Chapter 2 the different mortar mixtures were tested. Limestone cement mortars, natural hydraulic lime mortars, lime-pozzolan mortars with or without water-repellent admixtures aged for one years were considered, in order to have specimens with a completely hardened structure. The characterization was carried out during and after the cycles and extended with the microstructural analysis of the most performing/resistant mortar mixes.

Naked eye observations, colour measurements, evaluation of the microstructure with MIP analysis, capillary water absorption and compressive strength tests were performed at the end of the exposure, together with FT-IR and XRD analyses.

The technical results obtained are described in this section. Further discussion about the evaluation of the results and the correlation of the different data can be found in Chapter 4. However, the main results obtained after the exposure of mortar specimens to salt solutions indicated that:

- physical damages of the mortars occurred due to the crystallization pressure of the sodium sulphates;
- both the mechanical properties /internal cohesion of the matrixes and the water-repellent properties influenced the resistance;
- mortars with poor mechanical properties but with high water repellence showed good resistance to the exposure, because the penetration of the salt solution inside the pores was avoided and the salts did not crystallized inside the matrix;
- No chemical sulphate attack with formation of damaging salts as thaumasite or secondary ettringite was evidenced, even if a slight formation of gypsum inside limestone cement mortars was seen with XRD analyses.

³ Cardell, C. *et al.* 2003

3.5.1. SALT WEATHERING OF WATER-REPELLENT LIMESTONE CEMENT MORTARS

3.5.1.1. Resistance to salt crystallization and external appearance of water repellent limestone cement mortars after the exposure

The macroscopic observations during the salt weathering cycles allowed to verify the physical resistance to sodium sulphate crystallization of the mortars. and Table 3.5 1 and Table 3.5 2 shows the mortar specimens after the salt cycles and the weight variation during the test. Three different behaviour were observed during the cycles:

- CMA and CMvin0.5, 1 had a first mass increase due to the penetration and crystallization of sodium sulphate inside the mortar matrixes, followed by a continuous disaggregation of the external layer and decohesion of the samples with and a continuous loss of material.
- the specimens CM7501,1.5 , CMsil1, CMtes1,5 were almost unaffected, only a slight mass increase till 5 cycles followed by a slight mass loss was measured. Probably the penetration of the salt solution was inhibited and no crystallization occurred inside the mortar matrix.
- in CM7300.5,1,1.5, CMcast0.5,1,1.5, CMznst0.5,1,1.5 CM7500.5, CMsil1.5 mortars occurred a slight mass increase followed by serious mass losses (after 6-7 cycles). After 5-7 cycles the mass losses were due to a complete detachment of the external layer, with cracks and disaggregation of the internal matrix. This kind of decay might be due to a partial penetration of the solution inside the specimens and the formation of salt sub- efflorescences.

Table 3.5 1 allows to see the influence of the admixture dosage on the resistance to salts. Generally the higher the dosage of water repellent, the lower the water absorption, the better the resistance, except for CMsil1.5, CMcast1.5 and CMznst1.5 which showed worse resistance. This might depend on the mechanical strength of the specimens, we have seen in Chapter 3.3 that higher water repellent percentages led in CMcast1.5 and CMznst1.5 to lower mechanical performances due to the influence of the admixture on the hydration.

In order to better evaluate the physical changes of the salt cycles on the mortar surfaces, it was decided to perform observations with optical digital microscope under natural and UV light. Furthermore, SEM-EDX analysis of CMA, CM7501, CMcast1 were done¹. The most significant results are reported in Table 3.5 3.

After the test, CMA surfaces seemed free from salt crystals but disaggregated and the erosion of the binder was visible both at visual observation and with microscope observations. The continuous loss of external material prevented a thick deposition of salt crystals, which were removed together with the material detached. However, SEM observations allowed to observe the formation of salts crystals in the porosity and the EDX spectra of some point (see point b in Table 3.5 3) confirmed the presence of sodium and sulphur.

At the end of the test, CM7501,1.5, CMsil1 and CMtes1,5 presented a surface partially covered by salt crystals but compact. SEM observation of CM7501 allowed to observe the formation of long elongated prismatic crystals of sodium sulphate (thenardite)², as confirmed also by EDX analysis.

CMcast, CMznst, CM730 mixes were affected by the formation of sodium sulphate crystals on and behind the surfaces (visible with OM and SEM), causing the detachments observed during

¹ The samples were metallized with gold to reduce the charge effect

²Stoopes, G., *et. al.*, 2010, pp 447-448.

the test. Thick crust of salts together with needle like crystals were visible on the surfaces and at the interlayer between the detached material and the inner core of the specimens. Na and S were detected all over the surfaces of these samples.

A thick and compact salt crust was observed with OM over CMvin surfaces, even if the continuous loss of material from the external surfaces occurred during the cycles. CMvin' mixtures were characterised by high porosity: probably the salts were transported and deposited on the surfaces while the salt solution was evaporating.

The evaluation of the external appearance of the different mixes was concluded by performing colorimetric measurements of the exposed specimens (Table 3.5 4). SCI or SCE measurements did not differ much, the samples were not reflective, but higher standard deviation were found in comparison to the colour measurements done before the salt cycles due to the irregular and coarser surfaces.


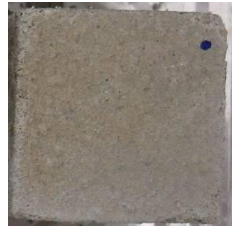
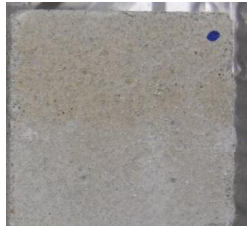






Important colorimetric variations were measured for CMcast0.5, CM7300.5,1,1.5, CMvin0.5 with yellowing, reddening and darkening of the colour (increase of a*,b* and decrease of L*), the samples were strongly affected by the salt weathering and the detachment of the external layer revealed the darker inner core. A similar but slightly lower variation was seen also in CMA, CMvin1,1.5 CMcast1.5 specimens. CMznst samples had an opposite trend with the decrease of a*,b* and the increase of L*, higher for higher water repellent dosages.

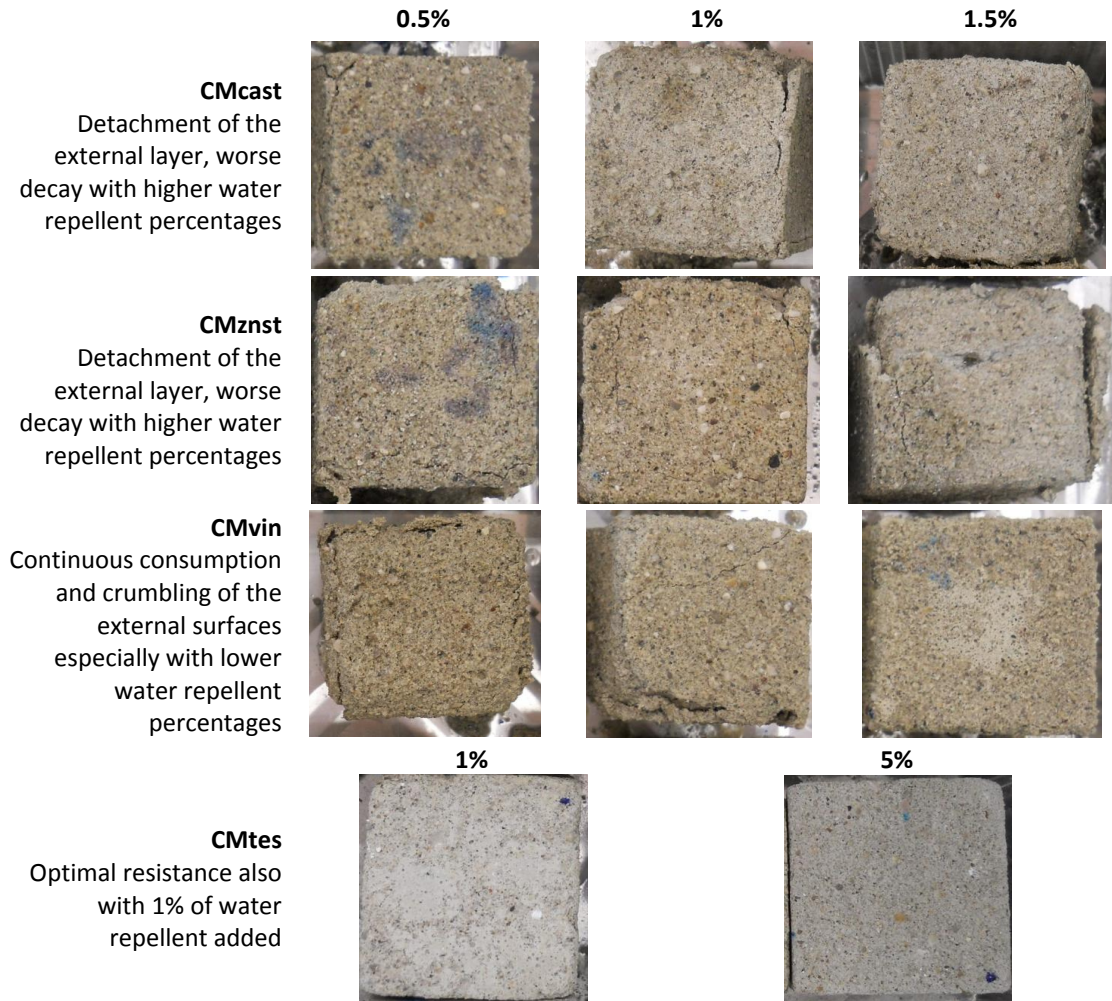
Table 3.5 1 Mortar samples after 10 salt cycles (scale 3:4). The table continues on the following page

CMA
Reference mix
Continuous consumption and
crumbling of the external surfaces



Specimens with water repellents at different concentration after 10 salt cycles

	0.5%	1%	1.5%
<p>CM750 Detachment of the external layer for low dosages, good resistance for higher dosages</p>			
<p>CM730 Serious detachment and crumbling of the external layers from the 3° cycle</p>			
<p>CMsil Detachment of the external layer with higher water repellent percentages. Optima behaviour: CMsil1</p>			



Mass losses during the cycles

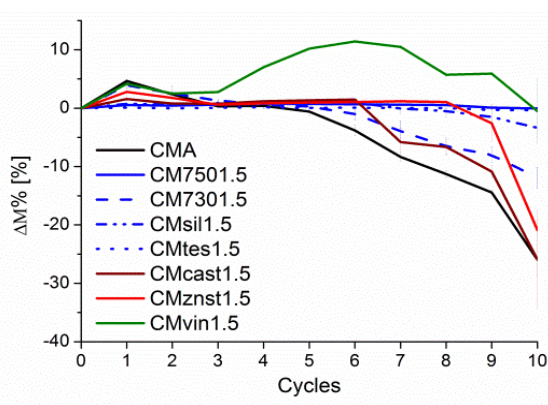
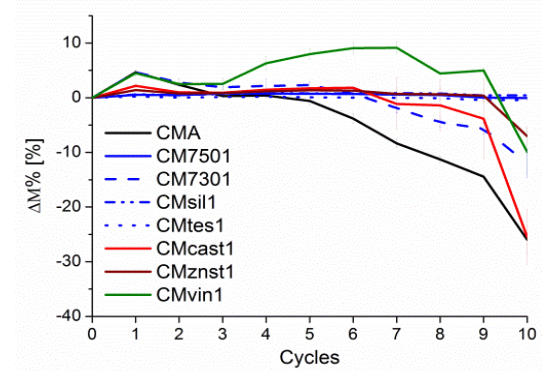
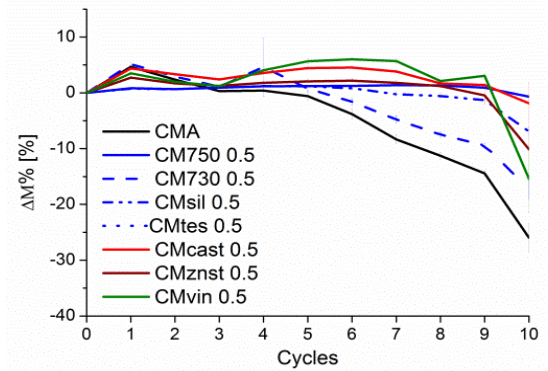
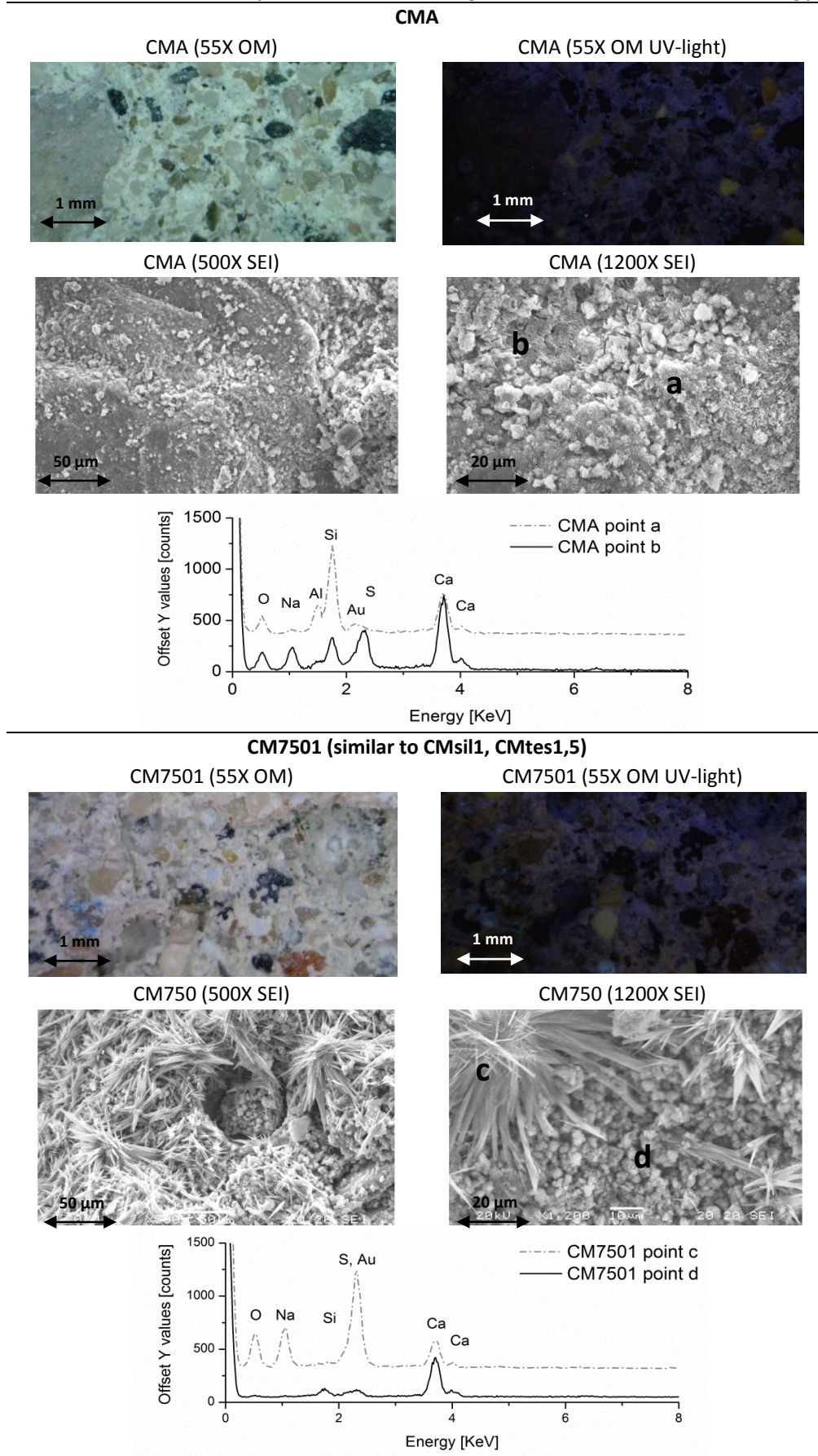


Table 3.5 2

Above: pictures of CMtes1, CMtes5 (scale 3:4).

Below: mass evolution of the specimens under ponding (relative mass change vs. time). From left to right specimens with 0.5%, 1%, 1.5% of water repellent added

Table 3.5 3 Optical microscope and SEM-EDX observations of mortar surfaces after the salt weathering test. EDX spectra were collected on the relative point marked on SEM images. The table continues on the following page.



CMcast1 (similar to CM730, CMznst, CMvin mixes)

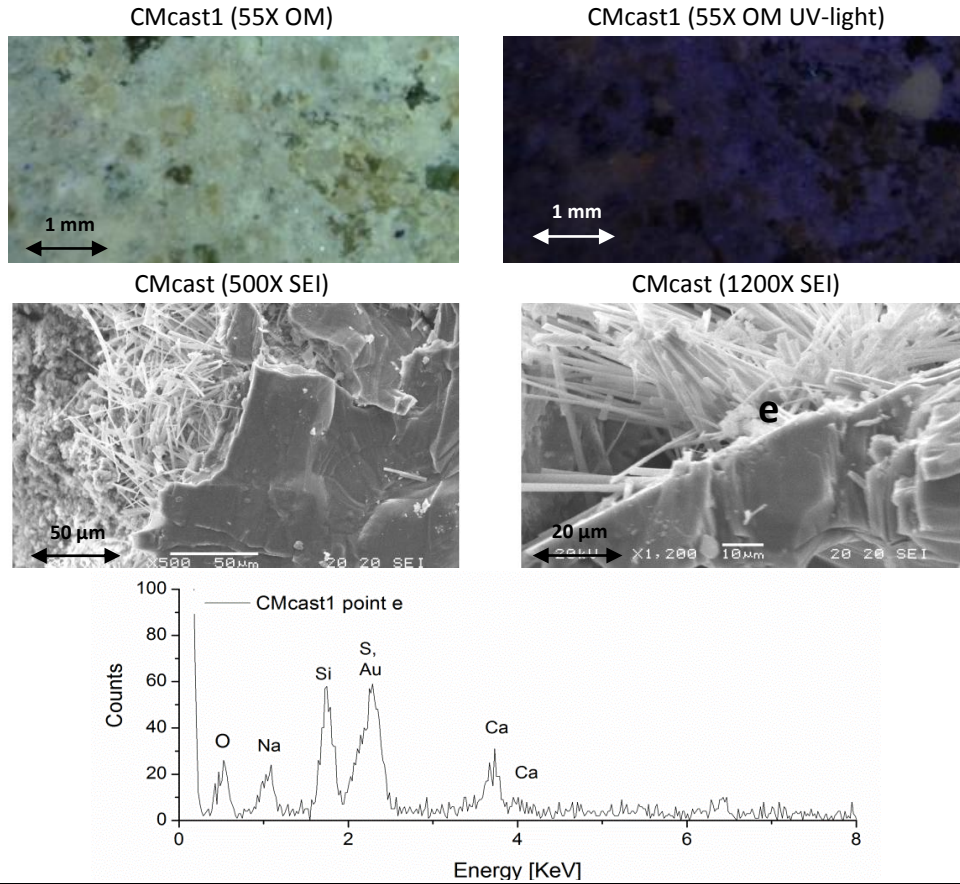
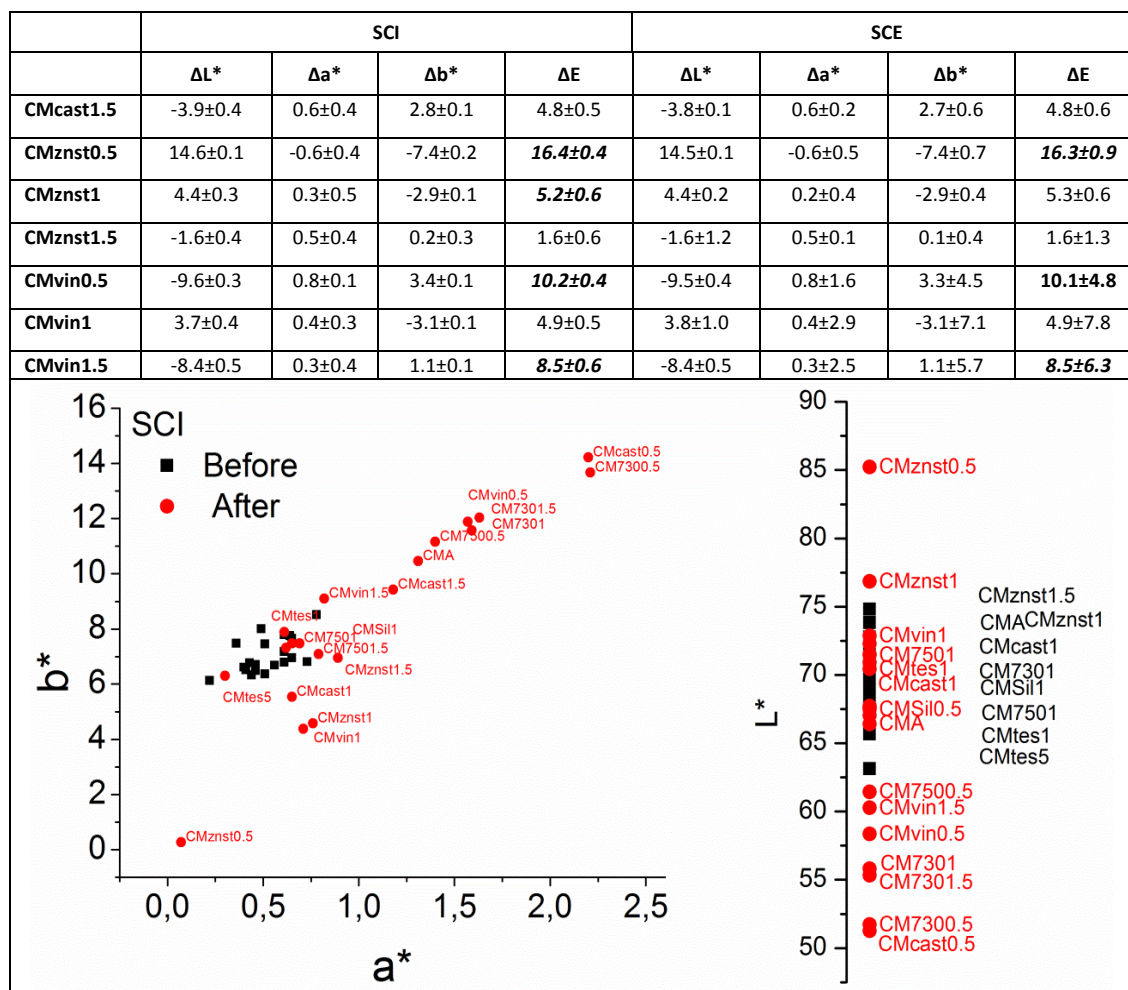


Table 3.5 4 Total colour variation ΔE , lightness ΔL^* and chromaticity Δa^* Δb^* variations of the specimens after the salt weathering test are shown, considering SCI or excluding SCE the specular component, the data resulted from the average of nine measurements. Bold font is used for those variations that, being higher than 5, are clearly discernible to naked eye examination. The graph reported below show the colour data of the specimens before and after the salt test. The table continues on the following page.

	SCI				SCE			
	ΔL^*	Δa^*	Δb^*	ΔE	ΔL^*	Δa^*	Δb^*	ΔE
CMA	-6.4±0.3	0.7±0.2	3.3±0.1	7.2±0.3	-6.1±1.8	0.7±1.2	3.3±2.7	6.9±3.5
CM7500.5	-13.4±3.3	0.7±1.3	4.4±0.4	14.1±3.6	-13.5±0.3	0.7±0.6	4.4±1.8	14.2±1.9
CM7501	4.0±0.5	0.2±0.1	0.6±0.2	4.1±0.6	4.1±0.3	0.2±1.6	0.6±3.0	4.1±3.4
CM7501.5	1.2±2.3	0.3±0.5	0.6±0.1	1.4±2.4	1.2±0.1	0.3±0.2	0.6±0.6	1.4±0.6
CM7300.5	-17.8±2.7	1.6±1.1	5.9±0.3	18.9±3.0	-17.7±0.1	1.6±0.5	5.8±0.7	18.7±0.9
CM7301	-14.7±1.6	1.0±0.8	4.8±0.4	15.4±1.8	-14.4±0.2	1.0±0.4	4.7±0.4	15.2±0.6
CM7301.5	-14.7±0.6	1.2±0.2	5.5±0.1	15.8±0.7	-14.6±1.2	1.2±0.1	5.4±0.4	15.6±1.3
CMSil0.5	0.0±1.4	0.0±0.3	-0.3±0.1	0.3±1.5	0.0±0.4	0.0±1.6	-0.3±4.5	0.3±4.8
CMSil1	-0.5±0.2	0.2±0.1	1.1±0.1	1.2±0.2	-0.5±1.0	0.2±2.9	1.1±7.1	1.2±7.8
CMSil1.5	2.9±2.9	0.2±1.1	1.0±0.1	3.1±3.1	2.7±0.5	0.2±2.5	1.0±5.7	2.9±6.3
CMtes1	4.8±0.6	0.0±0.2	0.9±0.1	4.9±0.6	4.8±1.5	0.0±1.5	0.9±3.7	4.9±4.2
CMtes5	3.9±2.3	0.1±1.1	0.2±0.1	3.9±2.5	3.9±1.8	0.1±1.2	0.2±2.7	3.9±3.5
CMcast0.5	-17.9±0.4	1.6±0.0	6.6±0.1	19.1±0.4	-17.8±0.3	1.5±0.6	6.5±1.8	19.0±1.9
CMcast1	-0.3±0.5	0.3±0.3	-1.1±0.2	1.1±0.6	-0.2±0.3	0.2±1.6	-1.1±3.0	1.1±3.4



3.5.1.2. Composition, microstructure and salt distribution in limestone cement mortars after the exposure

The chemical composition of the specimens was investigated with FT-IR spectroscopy. The FT-IR spectra of samples collected from the external layer of the specimens (0-0.5 mm) are reported in Figure 3.5 1.

The absence of the stretching absorption of the hydroxide group at 3640 cm^{-1} and the presence of the $-\text{CO}_3$ stretching at 1436 cm^{-1} alone was due to the complete carbonation of calcium hydroxide produced during the hydration reactions.

The silicates peaks in the $1100\text{-}1009 \text{ cm}^{-1}$ range were partially covered by the stretching absorption of the sulphate groups. Sodium sulphate presents a strong stretching absorption centred at 1120 cm^{-1} together with a sharp asymmetric bending absorption at 617 cm^{-1} . The presence of the sodium sulphate can, therefore, be easily investigate thanks to FT-IR analysis. In this case the spectra confirmed the previous observation regarding the sodium sulphate distribution on the different mortar surfaces (Figure 3.5 1). In fact, relative strong sulphate absorptions (in comparison to the other peak in the spectra) were observed for CMvin, CM730; medium absorptions for CM750, CMcast and CMznst; low absorptions for CMA and CMtes. Peaks related to the formation of other sulphate salts (such as epsomite) were not visible.

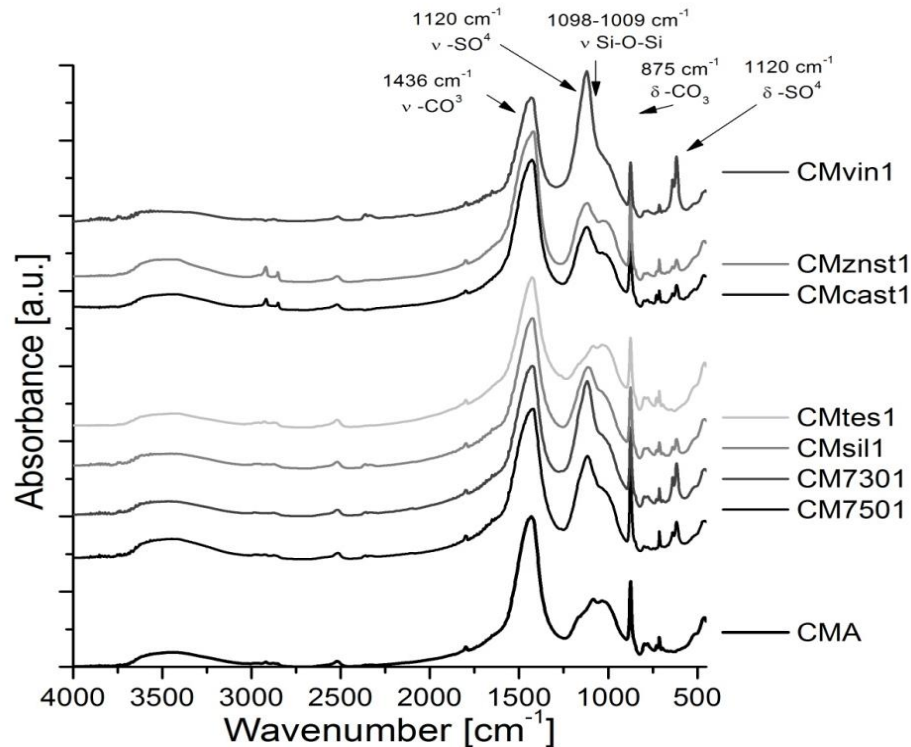


Figure 3.5 1 FT-IR analysis of the external layer of different mortar mixes added with 1% of water repellent

After the observation of the external damages caused by the salt weathering, the microstructure was further evaluated with MIP analysis on some significant cement mortar mixtures. The porosimetric analyses were performed on samples collected from the external layer (0- 0.8 mm from the surface) more affected by the weathering. The analyses were repeated on similar samples after a desalination process³. CMA, CM7501, CMsil1, CMcast1 mixes were considered representative of the different kind of degradation effects induced by the salt crystallization. Three samples for each mix were analysed and the results are reported in Table 3.5 5.

Considering the total open porosity of samples collected before and after the test and observing the graphs of the cumulative volume and the pore distribution vs. the pore radius, it was seen:

- a linear increase for CMA, and CM7501. CMA showed the increase of larger pores (6-10 μm) and the decrease of smaller pores (0.001- 1 μm);
- a porosity increase in CMsil1 after the salt test. CMsil porosity did not change much after the desalination, but the samples were very brittle and often broke during the measurements giving not completely reliable data;
- the decrease of the porosity after the test and a strong increase after the desalination for CMcast1. CM7501 and CMcast1 showed a decrease of pores in the range 1-10 μm , the increase in the range 0.1-1 μm and the decrease of smaller pores.

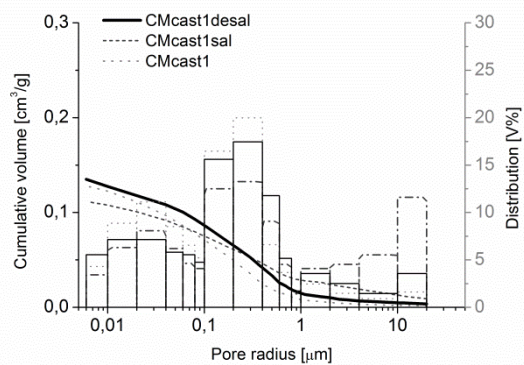
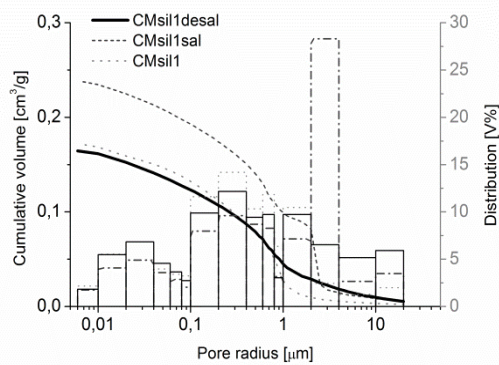
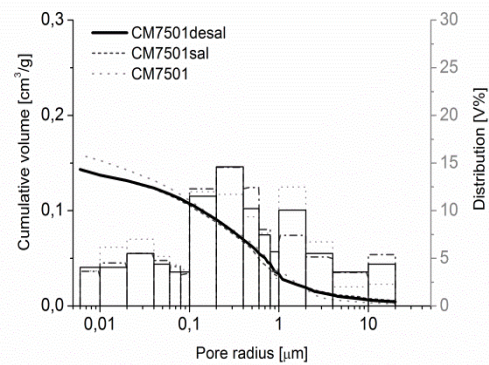
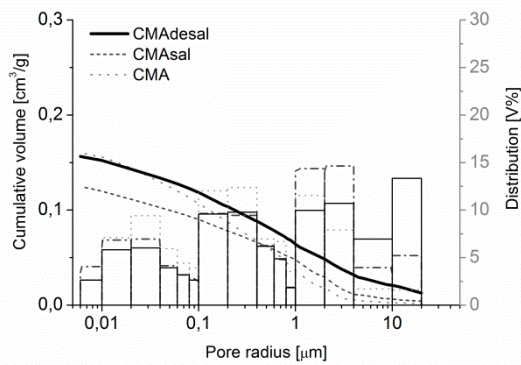
The salt weathering caused a porosity increase due to the crystallization pressure of salts of CMA, CM7501 and CMsil. In CMcast1 after the test the salts probably filled the pores and

³ The samples collected at 0-0.8mm from the surfaces were test directly after the weathering or put in deionised water to solubilise the salts till the conductivity of the solution reached values < 80 μs (average conductivity of water solution in contact with the specimens before the salt tests), after then the samples were dried in oven to constant weight and tested with MIP.

decreased the porosity, after the desalination the damaging effect of the salts crystallization on the microstructure was suggested by the porosity increase.

Table 3.5 5 Porosimetric analysis of CMA, CM7501, CMsil1 CMcast1 before salt cycles, after salt cycles, after desalination, the graphs of the cumulative volume and the pore distribution vs. the pore radius are reported below

		Bulk density MIP (g/cm ³)	Apparent density MIP (g/cm ³)	Total open porosity MIP (%)	Total cumulative volume MIP(cm ³ /g)	Average pore radius MIP(μm)
CMA	Before salt cycles	1.76±0.02	2.50±0.21	29.5±0.8	0,17±0,06	1.2±0.5
	After salt cycles	1,8±0.03	2,46±0.12	35,8±0.5	0,13±0.01	1,32±0.01
	After desalination	2,12±0.02	3,31±0.42	41,04±0.7	0,2±0.05	0,004±0.102
CM7501	Before salt cycles	1.79±0.01	2.51±0.02	28.9±0.7	0,16±0,04	1.1±0.2
	After salt cycles	1,94±0.01	2,89±0.08	32,94±1.2	0,17±0.04	0,004±0.002
	After desalination	1,89±0.05	2,9±0.18	36,92±0.8	0,18±0.06	0,004±0.300
CMsil1	Before salt cycles	1.74±0.01	2.49±0.10	30.3±0.4	0,17±0,03	0.8±0.1
	After salt cycles	1,94±0.04	3,98±0.81	51,15±0.5	0,26±0.02	0.1±0.5
	After desalination	1,85±0.08	3,45±0.05	36,34±0.1	0,2±0.03	0,04±0.01
CMcast1	Before salt cycles	1.92±0.04	2,71±0.07	28.7±4.2	0,15±0,02	1.4±1.0
	After salt cycles	2,03±0.02	2,77±0.04	26,68±0.9	0,13±0.04	0,004±0.012
	After desalination	2.00±0.05	2,88±0.01	31,12±0.7	0,16±0.01	0,003±0.500



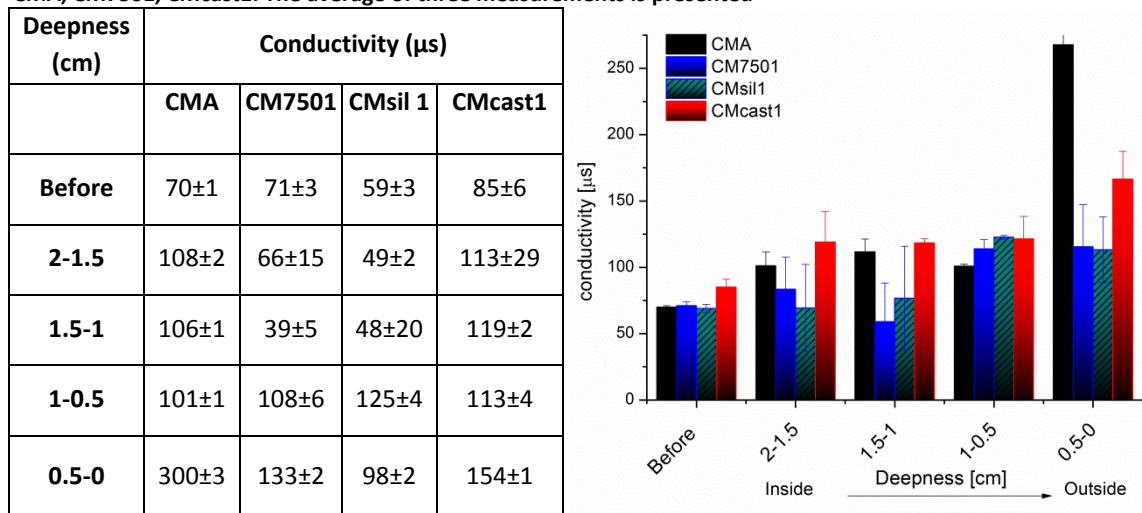
The evaluation of the salt distribution inside the whole specimens allowed to understand the different damages observed.

Unfortunately FT-IR measurements and SEM observations on the inner core did not produce interesting results, the salt concentration probably diminished fast and no acicular structure was seen with SEM or the FT-IR sulphate absorptions were fast overlaid by the silicates peaks under the first 0.5 mm. Therefore, it was chosen to consider the conductivity of samples⁴ collected at different depths to evaluate the total content of soluble salts. The conductivity was measured also before the salt cycles. The conductivity of cement mortars is usually affected by the presence of different ion due to the hydration reactions (for example formation of portlandite in fresh samples). In this research, however, specimens aged 1 year were used and this should assure a quite constant conductivity of the bulk. The results are presented in Table 3.5 6, the data refer to the average of three results for each sampling depth, a unique value is reported for the mixtures before the salt cycles because the conductivity was quite homogeneous at different depth.

- The conductivity before the salt cycles was around 70 μ s for each mix, slightly higher in CMcast1 samples.
- The conductivity strongly increased after the salt weathering in the external layers (0-1 cm) denoting a higher presence of soluble salts, in particular for CMA, CMcast1.
- The inner core (depths of 1-2 cm) of CM7501 and CMsil after the cycles had conductivities similar to the not-weathered samples, while the conductivity was higher for CMA and CMcast1.

The higher dosage of soluble salts inside CMA and CMcast1 samples should be related to a deeper penetration of the salt solution inside the matrix, while in CM7501 and CMsil1 the penetration depth is limited to the first centimetre.

Table 3.5 6 Dosage of soluble salts in samples collected at before and after the salt cycles at different depth from CMA, CM7501, CMcast1. The average of three measurements is presented



3.5.1.3. Capillary water absorption and compressive strength after the exposure

The effectiveness of the water-repellence and the possibility for water and water solution to penetrate inside the mortars after the salt weathering was evaluated with a capillary water

⁴ CNR- ICR NorMaL 13/83

absorption test⁵ (Table 3.5 7). The mortar mixes CMA, CM700.5, CMcast1, CMcast1.5, CMvin1.5 were seriously damaged during the salt cycles and it was not possible to manipulate and test them.

CMvin1 and CMcast0.5 increased their, already high, water absorption coefficients; while CM7501,1.5, CMsil0.5,1,1.5, CMtes1,5 (admixed with silanes/siloxanes) after the salt cycles had lower water absorptions than before. In the former cases the partial penetration of salt solution inside the samples and the crystallization of sodium sulphates in depth should have compromised the water- repellence effect of the admixed agents physically covering the wall pores and creating hydrophilic bridges. In the latter cases the salt solution was unable to penetrate in depth, but evaporation and condensation of the water might have contribute to a further hydration and compaction of the binder matrix, furthermore the formation of salt crystals and salt crusts on the surfaces (first 0-0.5 mm) could have caused the physical occlusion of the external open porosity (in particular of larger pores as described above for CM7501).

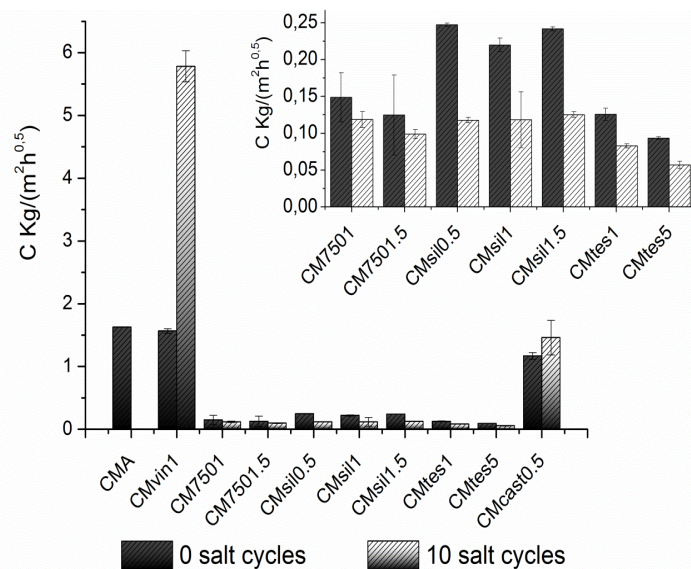
To further evaluate the damages caused by the crystallization of sodium sulphate compression strength tests were done on desalinates specimens. The specimens were desalinated through immersion into deionised water⁶ and then test as described in Chapter 2.

The compressive strength decreased after the salt weathering in every case (Table 3.5 8). CMA, CM700.5, CMcast1, CMcast1.5, CMvin1.5 were seriously damaged during the salt cycles and it was not even possible to test their compressive strength, because they were too brittle and they completely lost their cohesion. Also CMcast0.5 and CMvin1 lost quite completely their mechanical properties.

An almost linear relation was seen if it is considered the water-repellent dosage in CM7501 and CM7501.5, while an inverse proportion was observed in CMsil0.5,1,1.5 mixtures with a serious decrease of the compressive strength of CMsil1.5 in comparison to CMsil0.5.

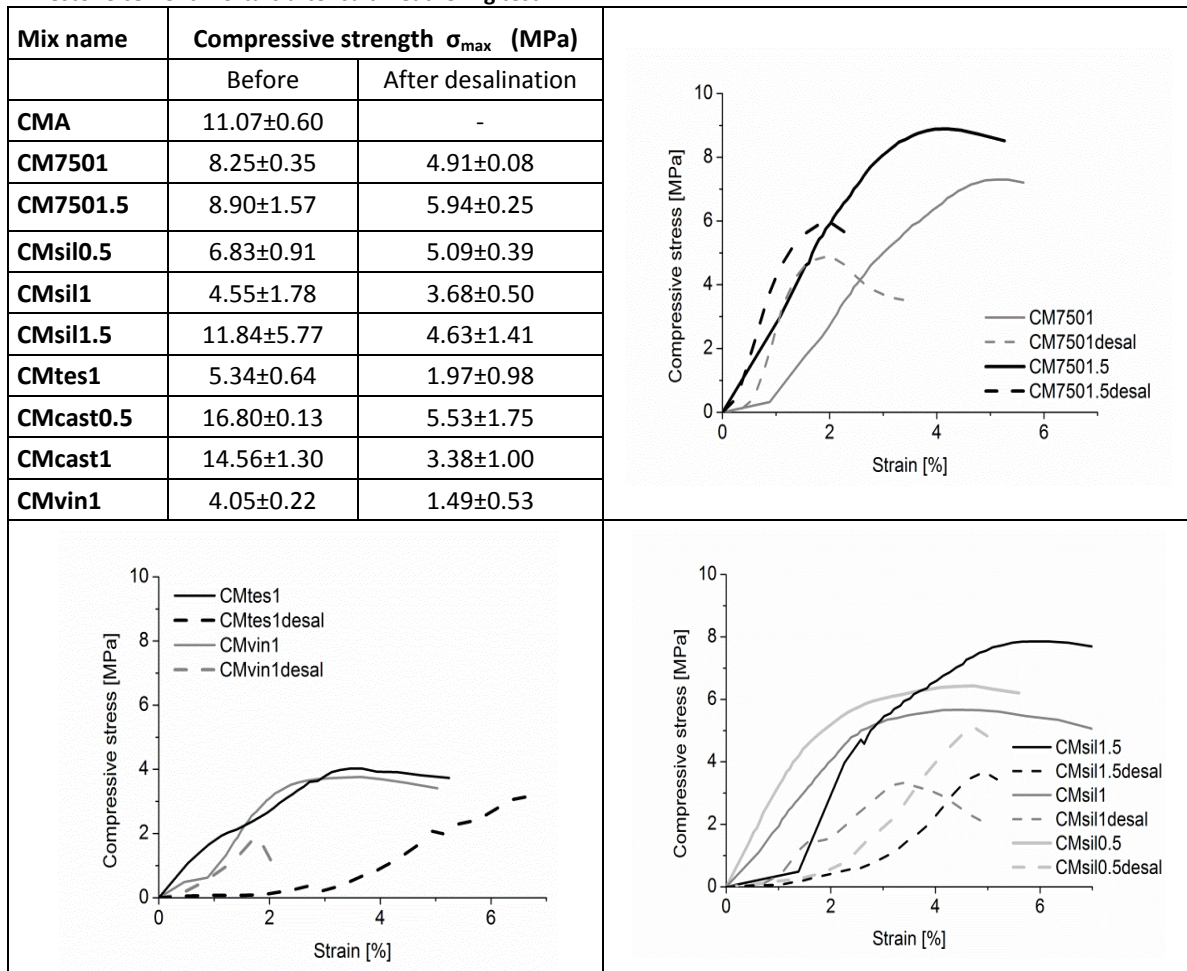
Table 3.5 7 Capillary water absorption coefficients of limestone cement mortars before and after the salt cycles. CMA, CM700.5, CMcast1, CMcast1.5, CMvin1.5 were seriously damaged during the salt cycles and the capillary water absorption was not test.

	Before salt cycles kg/(m ² ·h ^{0.5})	After 10 salt cycles kg/(m ² ·h ^{0.5})
CMA	1.63±0.01	--
CM7501	0.15±0.07	0.12±0.01
CM7501.5	0.12±0.08	0.10±0.01
CMsil0.5	0.25±0.01	0.12±0.01
CMsil1	0.22±0.01	0.12±0.07
CMsil1.5	0.24±0.01	0.13±0.01
CMtes1	0.13±0.01	0.08±0.001
CMtes5	0.09±0.001	0.06±0.001
CMcast0.5	1.17±0.05	1.46±0.28
CMvin1	1.57±0.04	5.78±0.25



⁵ EN 1015-18:1999 Methods of Test for Mortar for Masonry - Part 18

⁶ The specimens were put in deionised water to solubilise the salts till the conductivity of the solution reached values < 80 µs (average conductivity of water solution in contact with the specimens before the salt tests), after then the samples were dried in oven at 40°C to constant weight.

Table 3.5 8 compressive strength after salt cycles and curves of the compressive strength vs. the strain rate of limestone cement mortars after salt weathering test.

3.5.2. SALT WEATHERING OF WATER-REPELLENT NATURAL-HYDRAULIC-LIME MORTARS

3.5.2.1. Resistance to salt crystallization and external appearance of natural hydraulic lime mortars after the exposure

The hydraulic lime mortars underwent serious damages after three salt cycles, therefore the test was therefore stopped before the complete disaggregation of the specimens. Table 3.5 9 reports pictures of the specimens after the cycles and the mass variation during the test. Thanks to eye-naked visual inspection and to the evaluation of mass variation, it was possible to notice:

- a general disaggregation and decohesion of the specimens, more serious for lower dosages of water repellent admixtures (0.5%in comparison to 1% of water repellent added);
- the good resistance to salt crystallization of NM7501 and NM7301 in comparison to the other mixes;
- the formation of deep cracks in NM7300.5, NMsil0.5, NMsoc0.5;
- the exponential mass loss of NMA (without water-repellents), NMcast0.5,1, NMznst0.5,1, NMsoc0.5,1 (added with stearates) particularly serious after the 2° cycle;
- a continuous mass loss of NM7500.5,1 NM7300.5,1 NMsil0.5,1 (added with silanes/siloxanes) during the test.

The surfaces of the specimens were observed after the cycles also with optical microscope OM under normal and UV-light and with electron microscope SEM-EDX (Table 3.5 10). The images of the surfaces, which are not shown here, were similar to the surfaces of NMcast1.

The specimens loss material from the external layers at each cycles. At the end of the test no thick salt crusts were observed. Porous, coarse, brittle surfaces were seen instead.

The binder matrix was preferentially eroded and the aggregates remained exposed, except in NM7501, which was characterized by a smoother surface.

SEM observations allowed to recognize sparse crystals of mirabilite ($\text{Na}_2\text{SO}_4 \cdot 10\text{H}_2\text{O}$) as short rods in NMA.

NM7501 presented a surface free from sodium sulphate crystallization as also confirmed by EDX elemental analysis, which did not detected high concentration of sodium.

NMcast1 presented a more compact structure/matrix where the sodium sulphates acted as cementing phase and formed a layer on the surface. The crust of sodium sulphates on the surface of NMCast1 was confirmed by EDX analysis which evidenced a high presence of sodium and sulphur.

Colorimetric measurements of the specimens before and after the test are listed in Table 3.5 11 and shown below in Figure 3.5 2 Negligible differences were observed between SCI or SCE measurements, but high standard deviation were found in comparison to the colour measurements done before the salt cycles due to the irregular and coarser surfaces.

All samples, except NM7501, changed colour, strong colorimetric variations were measured after the salt weathering with ΔE values higher than 20. A general yellowing, reddening and darkening (increase of a^* , b^* and decrease of L^*) of the specimens was measured. Particular critical is the variation of mixes added with 0.5% of water repellents and NMsil1, NMcast1.

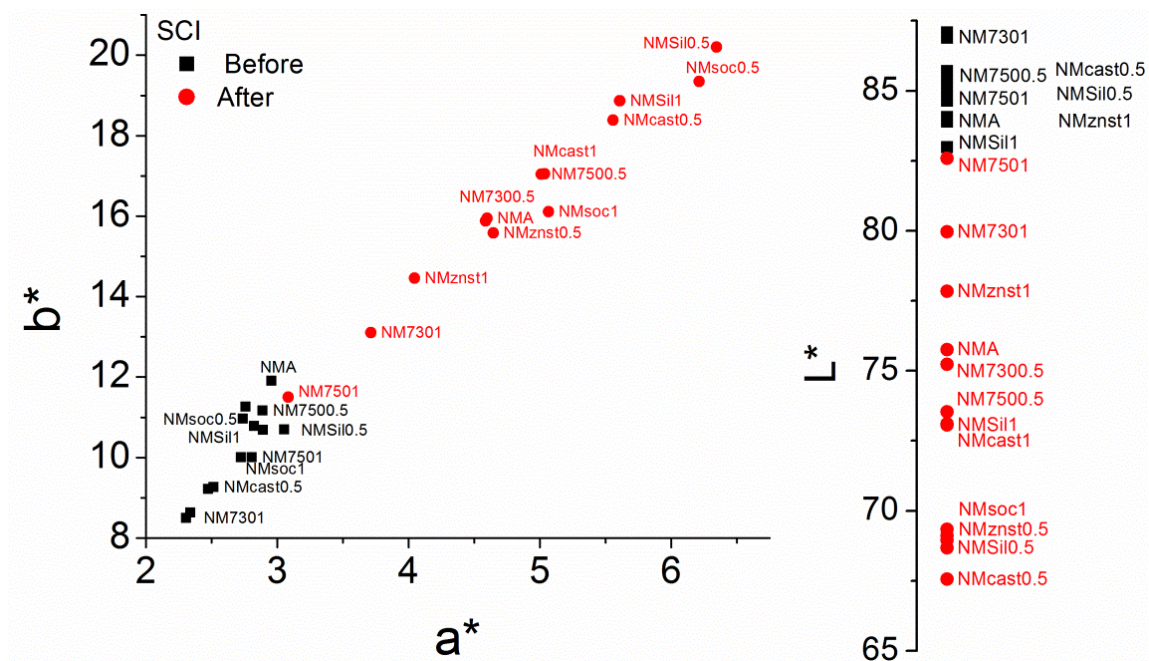


Figure 3.5 2 Lightness L^* and chromaticity a^* , b^* values of the specimens before and after the salt weathering test are shown (SCI values), the data resulted from the average of nine measurements.

Table 3.5.9 Above: pictures of natural hydraulic lime mixes after 3 salt cycles (scale 3:4) with 0.5% or 1% of water repellent added. Below: mass evolution of the specimens under ponding (relative mass change vs. time).

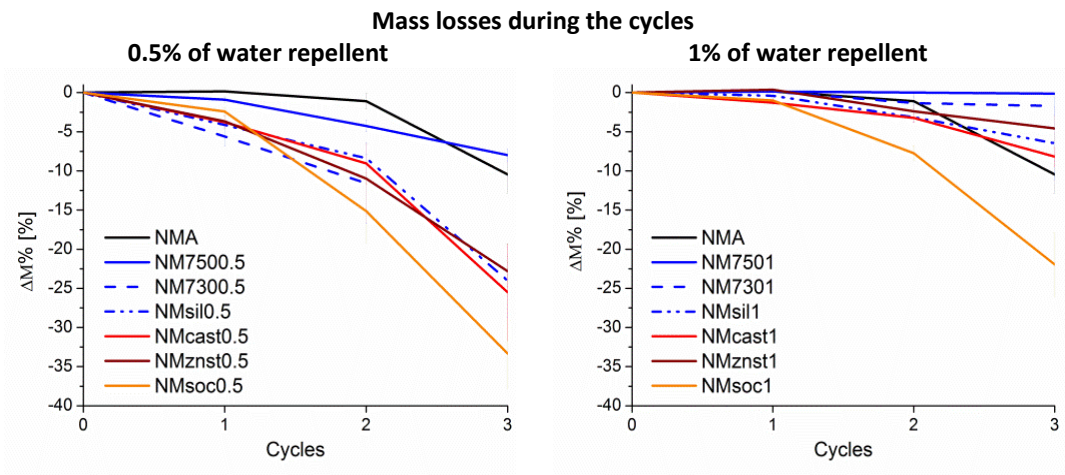
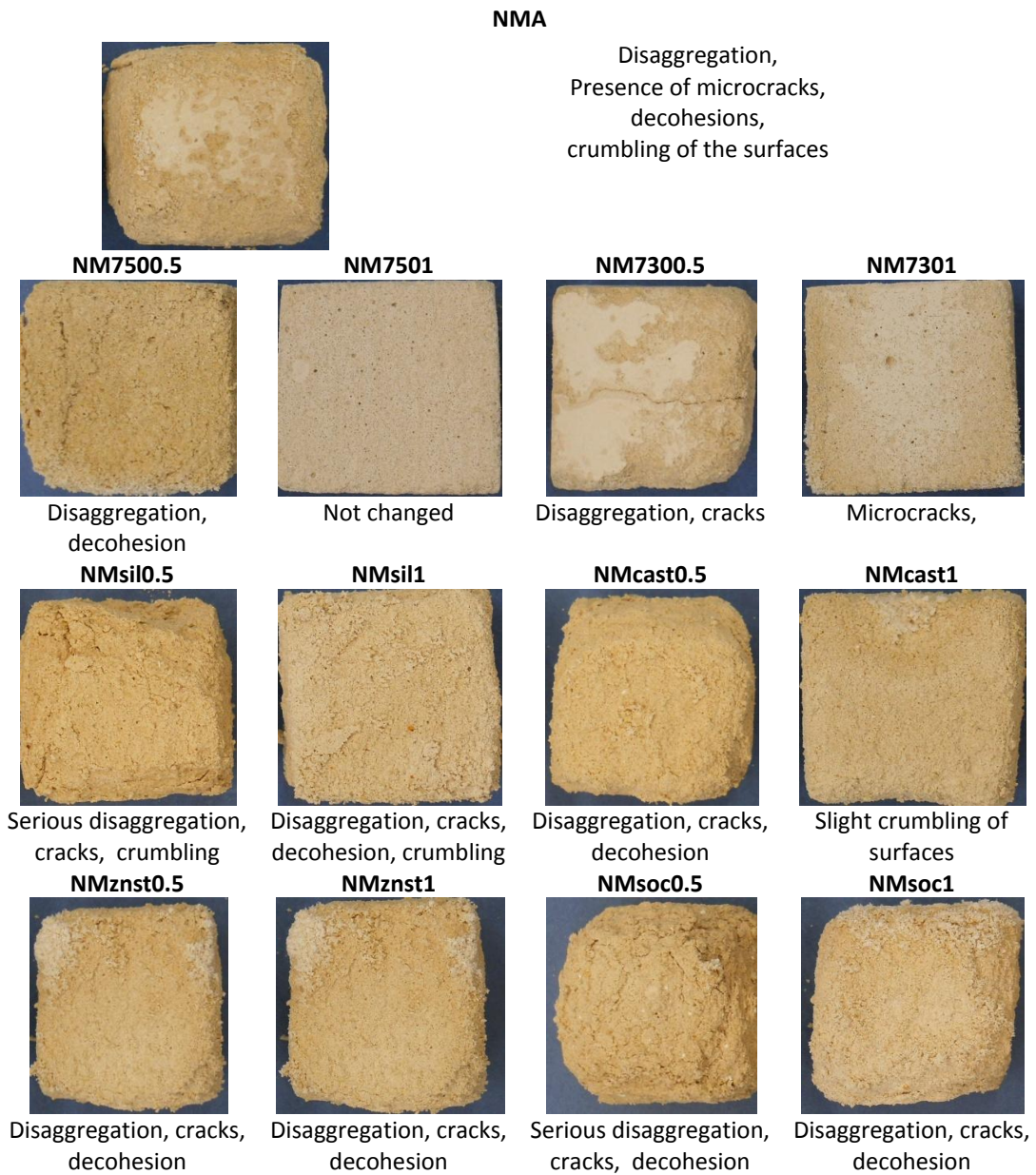
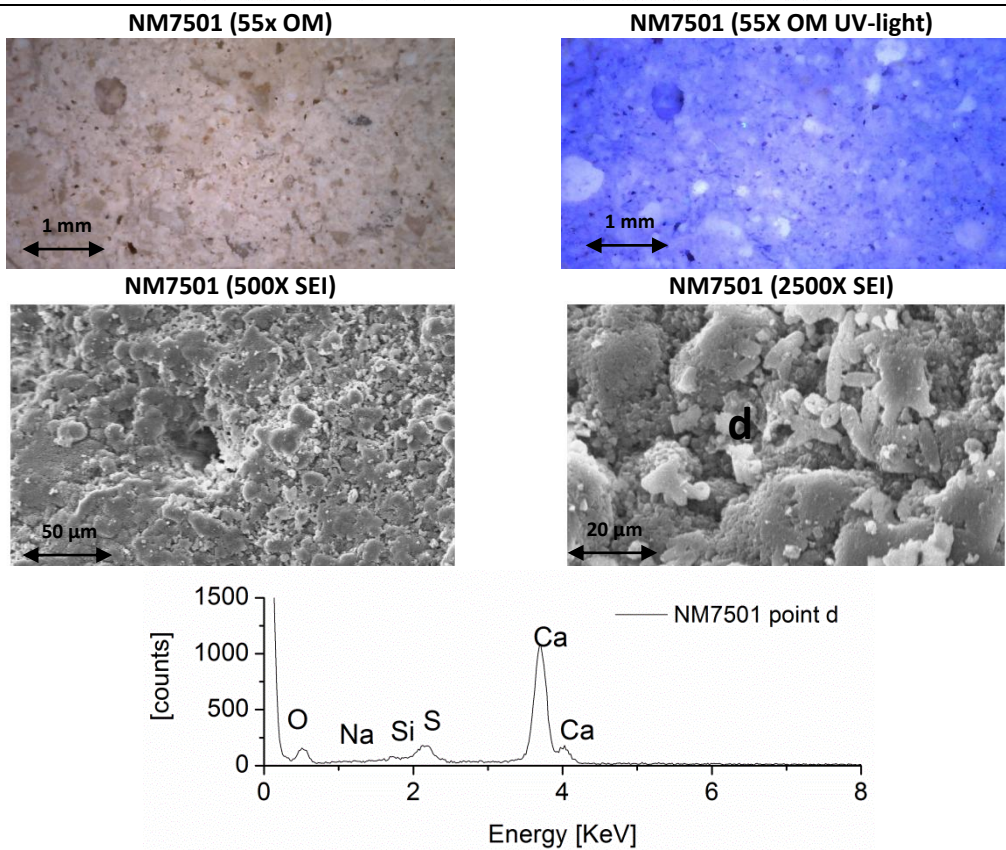
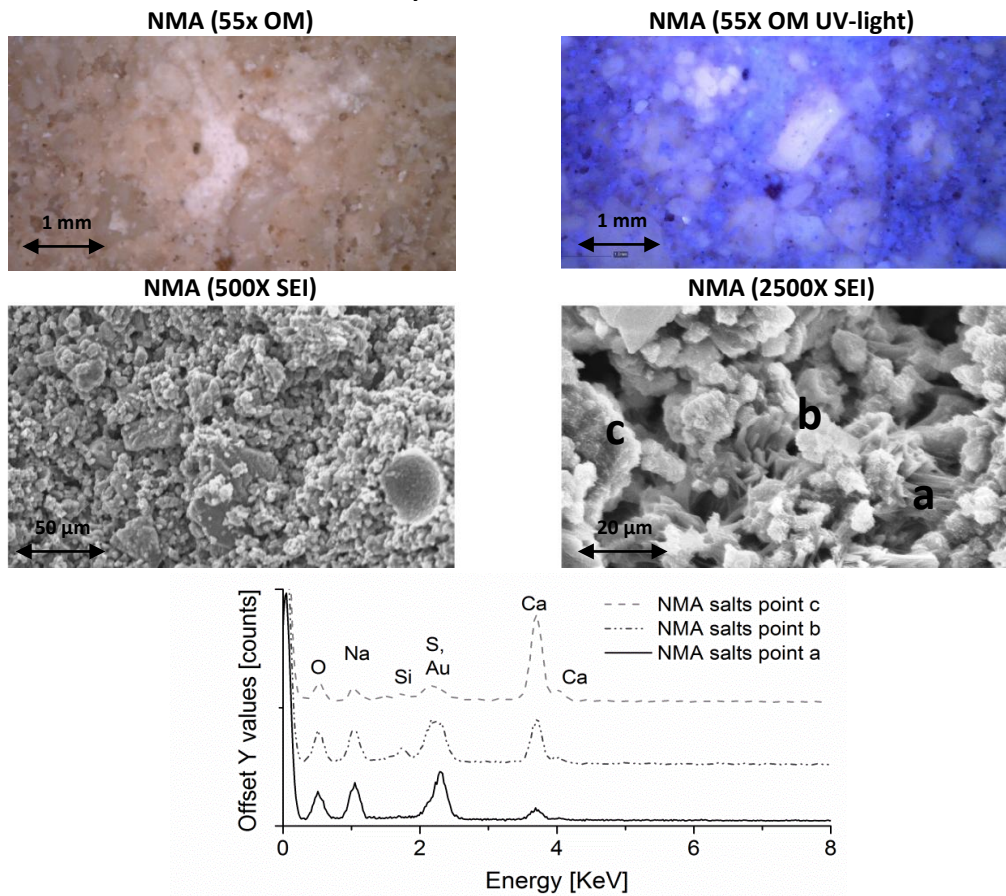


Table 3.5 10 Optical microscope and SEM-EDX observations of mortar surfaces after the salt weathering test. EDX spectra relative to the marked points on SEM images are shown. The table continues on the following page.

Surfaces of Natural hydraulic lime mortars after salt attack



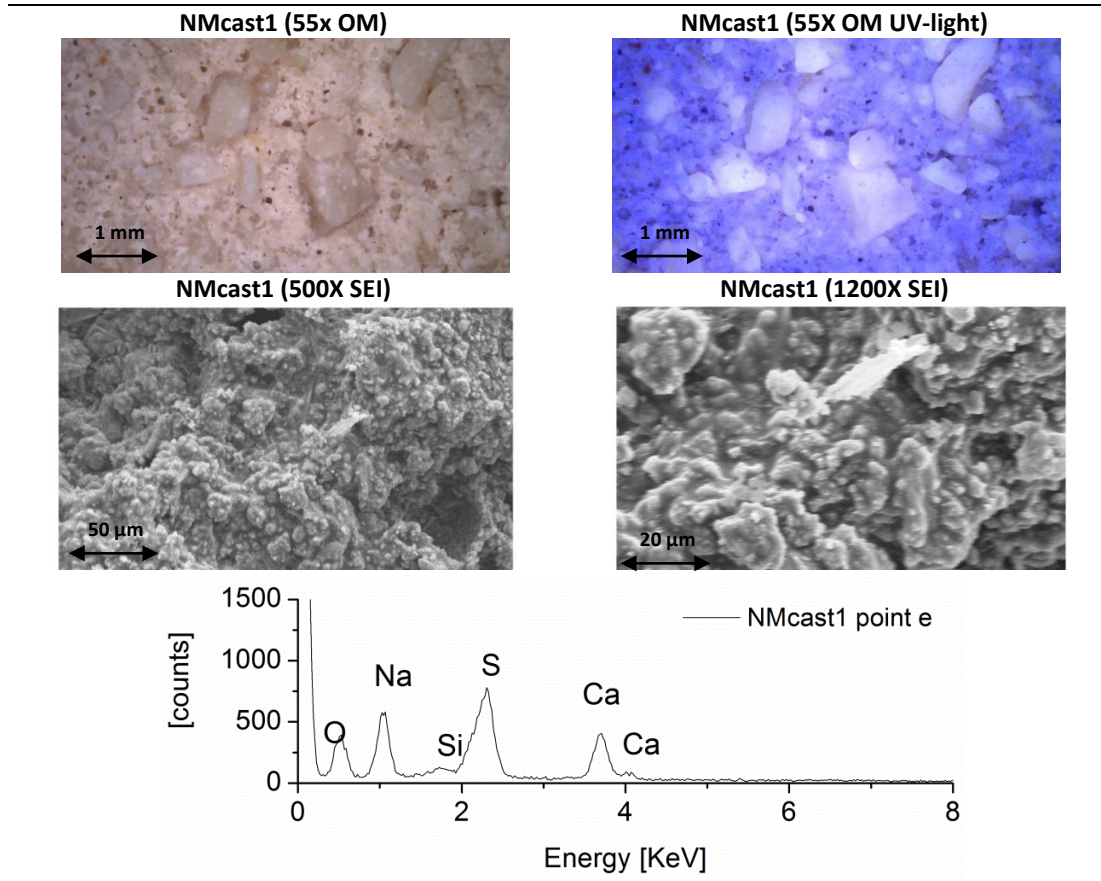


Table 3.5 11 Total colour variation ΔE , lightness ΔL^* and chromaticity Δa^* Δb^* variations of the specimens after the salt weathering test are shown, considering SCI or excluding SCE the specular component, the data resulted from the average of nine measurements and the standard deviation is reported as error. Bold font is used for those variations that, being higher than 5, are supposed to be clearly discernible to naked eye examination.

	SCI				SCE			
	ΔL^*	Δa^*	Δb^*	ΔE	ΔL^*	Δa^*	Δb^*	ΔE
NMA	-8.1±0.2	1.6±0.2	4.1±0.3	9.2±0.4	-8.2±0.2	1.6±0.2	4.0±0.3	9.2±0.4
NM7500.5	-11.6±4.8	2.1±1.3	5.9±3.3	13.1±5.9	-11.6±4.7	2.1±1.3	5.8±3.2	13.1±5.9
NM7501	-2.1±0.9	0.3±0.1	1.5±0.5	2.6±1.1	-2.1±1.0	0.3±0.1	1.5±0.5	2.6±1.1
NM730	-11.9±1.4	2.2±0.5	7.3±2.3	14.1±2.7	-11.8±1.4	2.2±0.5	7.2±2.3	14.0±2.7
NM7300.5	-6.9±4.2	1.4±1.1	4.6±2.7	8.4±5.2	-6.9±4.2	1.4±1.1	4.6±2.7	8.4±5.1
NMsil0.5	-16.7±3.1	3.5±0.8	9.4±1.6	19.5±3.5	-16.7±3.1	3.5±0.8	9.3±1.5	19.5±3.5
NMsil1	-9.9±2.6	2.6±0.3	8.2±0.6	13.1±2.7	-10.0±2.6	2.5±0.2	8.1±0.6	13.1±2.7
NMcast0.5	-17.9±3.0	3.0±0.3	9.1±1.4	20.3±3.3	-18.0±3.0	3.0±0.3	9.0±1.4	20.4±3.4
NMcast1	-12.6±2.2	2.6±0.1	7.8±0.2	15.1±2.2	-12.6±2.3	2.5±0.1	7.8±0.1	15.0±2.3
NMznst0.5	-16.4±7.4	1.9±1.1	4.3±2.9	17.0±8.0	-16.4±7.5	1.9±1.1	4.3±2.8	17.1±8.1
NMznst1	-6.2±0.5	1.2±0.2	3.8±0.6	7.4±0.8	-6.0±0.6	1.2±0.2	3.8±0.6	7.2±0.9
NMsoc0.5	-16.5±1.9	3.5±1.1	8.4±2.3	18.9±3.2	-16.5±1.9	3.4±1.1	8.3±2.3	18.8±3.2
NMsoc1	-15.3±5.2	2.3±0.1	6.1±0.9	16.6±5.3	-15.4±5.4	2.3±0.0	6.1±0.9	16.7±5.5

3.5.2.2. Composition, microstructure and salt distribution in natural hydraulic lime mortars after the exposure

The presence or absence of thick deposition of sodium sulphates on the surfaces was verified also by FT-IR analysis (Figure 3.5 3). Considering the FT-IR spectra registered on the different mixes was possible to notice higher presence of sulphates in NMA, NMznst, NMsoc samples. On the other hand, the spectra of mixes added with silane/siloxanes showed lower $-SO_4$ absorptions.

Regarding the other peaks visible, the presence of carbonates and silicates is confirmed by the absorptions at around 1436 cm^{-1} and 1000 cm^{-1} , respectively. The samples were completely carbonated during the analysis and $Ca(OH)_2$ was not detected.

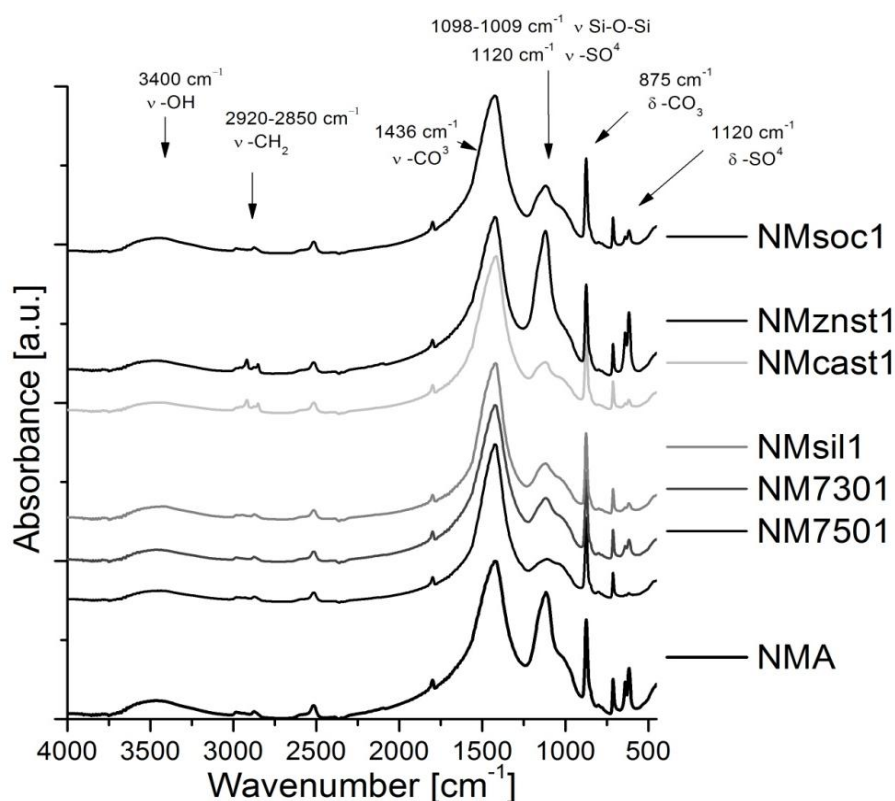


Figure 3.5 3 FT-IR spectra of natural hydraulic mortars after salt weathering.

Porosimetric analysis were performed on samples collected from the external parts of NMA, NM7501, NMsil1, NMcast1 specimens before, after the salt cycles and after the desalination of the specimens⁷ (sampling depth around 0-0.5 cm).

The results displayed in Table 3.5 12 evidenced a different behaviour of the mixes:

- NMA samples showed a slight decrease of the open porosity immediately after the salt cycles. This decrease (from 47% to 41%) should be due to the deposition/crystallization of salts inside their porous structure which clogged up the pores but exerted also a damaging crystallization pressure on the pore walls. In fact, after the desalination the total open porosity increased to 44%. In particular the salt crystallization caused the increase of pores with average radius

⁷ The samples collected at 0-0.8mm from the surfaces were test directly after the weathering or put in deionised water to solubilise the salts till the conductivity of the solution reached values $< 80\ \mu\text{s}$ (average conductivity of water solution in contact with the specimens before the salt tests), after then the samples were dried in oven to constant weight and tested with MIP. Three samples for each mix were analysed

around 1 μm and decrease of pores larger than 1 μm probably due to the deposition of salts and detached material inside the larger pores;

-NM7501 samples maintained a similar cumulative volume of mercury intruded, a slightly increased of the porosity, in particular pores around 1 μm increased after the cycles and more after the desalination process;

-NMsil1 increased the open porosity and the total cumulative volume during the tests, in this case the pores larger than 3-5 μm increased, and the smaller pores decreased, probably pores in the 0.1-1 μm range were enlarged under the crystallization pressure of the salts.

-NMcast1 maintained a similar total open porosity, with a slight decrease of the samples with salts. As seen in NMsil1 samples, also here the medium pore radius increased: pores with radius around 0.1-1 μm enlarged under the pressure of the crystals growth, as suggest the parallel increase of pores around 5-10 μm .

Analysis of the bulk of natural hydraulic lime mortars were performed in order to further evaluate the distribution of sulphate salts inside the specimens SEM-EDX. Images and EDX spectra of some significant samples are shown in Table 3.5 13.

The inner parts of NMA samples with salts (Table 3.5 13, above) had morphologies similar to NMA before the cycles. However, the EDX spectra collected on NMA, NM7501, NMcast1 samples (Table 3.5 13, below) underlined the difference between the elements on the external parts of the specimens (sampling depth: 0.0-0.5 cm, labelled as salts-surface) in comparison to the internal parts (sampling depth: 1.0-1.5 cm, labelled as salts-bulk). In NMA sodium and sulphur were detected only on the external layers; in NM7501 no sodium or sulphur were detected; in NMcast1 sodium and sulphur were both present on the external layer and in the bulk, even if in a lower percentage in the latter case. The samples admixed with 0.5% of water repellent and NMznst1 demonstrated in every case a behaviour similar to NMcast1, while the samples NMsil1 and NMsoc1 were similar to NMA.

The evaluation of the total content of soluble salts thanks to conductivity measurements⁸ was carried out on NMA, NM7501, NMsil1, NMcast1 by collecting samples at different depth: 0-0.5 cm, 0.5-1.0 cm, 1.0-1.5 cm, 1.5-2 cm, and comparing the results to the average conductivity of the specimens before the salts weathering.

The results listed in Table 3.5 14 evidenced that:

- The conductivity before the salt cycles was around 80-90 μs for each mix, slightly higher for NM7501 samples.
- The conductivity strongly increased after the salt weathering in the external layers (0-1.0 cm) denoting a higher presence of soluble salts, except for NM7501 samples.
- The inner core (1.0-2.0 cm) of NM7501 and NMsil after the cycles had conductivities similar to the not-weathered samples, while the conductivity was higher for NMA and NMcast1. A deeper penetration of the salt solution inside the matrixes of NMA and NMcast1 might be the cause of the higher conductivity.

The results agreed with the SEM-EDX analysis. It is shown that NM7501 and NMsil1 had a better resistance to salt weathering and to the penetration of salts solution.

⁸ CNR- ICR NorMaL 13/83

Table 3.5 12 Porosimetric analysis of NMA, NM7501, NMsil1 NMcast1 before salt cycles, after salt cycles, after desalination, the graphs of the cumulative volume and the pore distribution vs. the pore radius are reported below

		Bulk density MIP(g/cm ³)	Apparent density MIP (g/cm ³)	Total open porosity MIP (%)	Total cumulative volume MIP(cm ³ /g)	Average pore radius MIP(micron)
NMA	Before salt cycles	1.59±0.01	2.73±0.02	41.76±0.5	0.26±0.01	3.4±0.5
	After salt cycles	1.70±0.02	2.85±0.05	41.37±0.85	0.24±0.06	1.41±0.05
	After desalination	1.40±0.01	1.01±0.01	44.16±0.8	0.28±0.02	1.44±0.08
NM7501	Before salt cycles	1.11±0.05	2.22±0.02	50.0±0.4	0.45±0.01	3.2±0.5
	After salt cycles	1.37±0.04	3.16±0.26	57.45±2.32	0.46±0.09	3.14±0.93
	After desalination	1.28±0.05	2.65±0.01	53.20±4.0	0.43±0.20	2.86±0.16
NMsil1	Before salt cycles	1.29±0.03	2.60±0.03	50.3±0.9	0.39±0.01	3.3±0.5
	After salt cycles	1.40±0.08	3.46±0.10	61.13±2.18	0.45±0.07	2.16±0.05
	After desalination	1.30±0.07	3.13±0.16	58.37±0.4	0.45±0.01	3.96±0.78
NMcast1	Before salt cycles	1.28±0.01	2.69±0.04	52.5±0.8	0.41±0.01	2.9±0.5
	After salt cycles	1.45±0.11	3.10±0.22	51.93±1.07	0.37±0.02	3.51±0.80
	After desalination	1.33±0.04	2.57±0.05	51.62±0.9	0.42±0.07	4.90±0.12

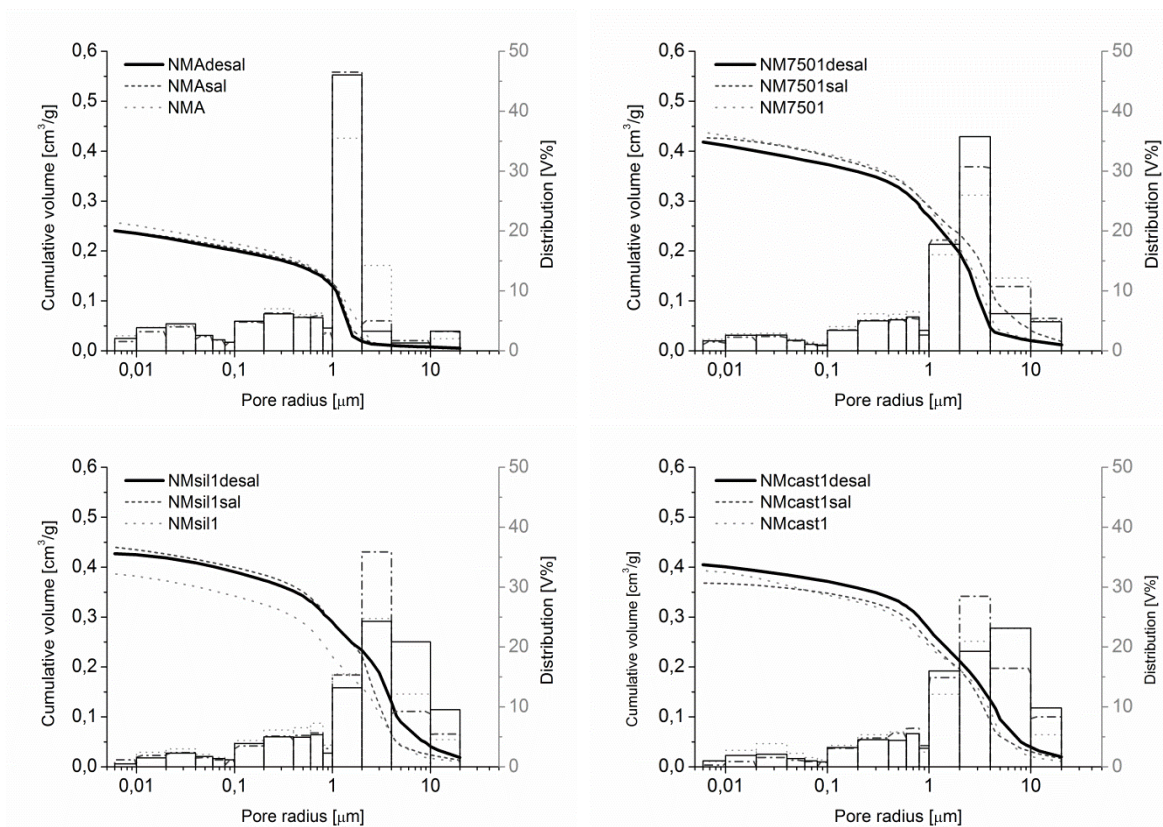
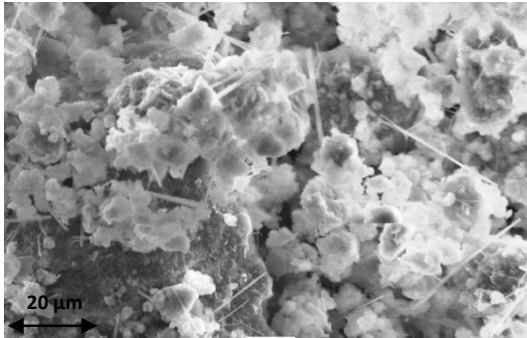
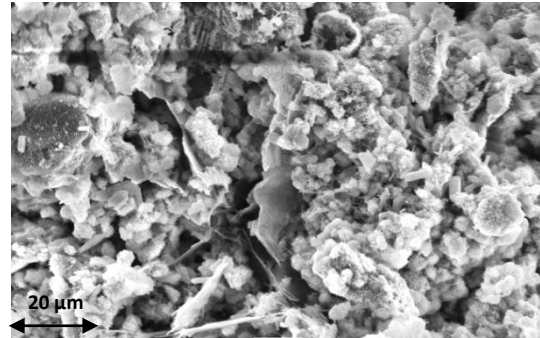


Table 3.5 13 Above: SEM images of NMA samples collected from the bulk (sampling depth: 1.0-1.5 cm). Below: EDX spectra of samples collected from NMA, NM7501, NMcast1 after the salt weathering.

NMA-bulk before salt weathering (SEI 1200X)



NMA-bulk after salt weathering (SEI 1200X)



EDX spectra of samples collected at different depth from NMA, NM7501, NMcast1 specimens after the salt weathering

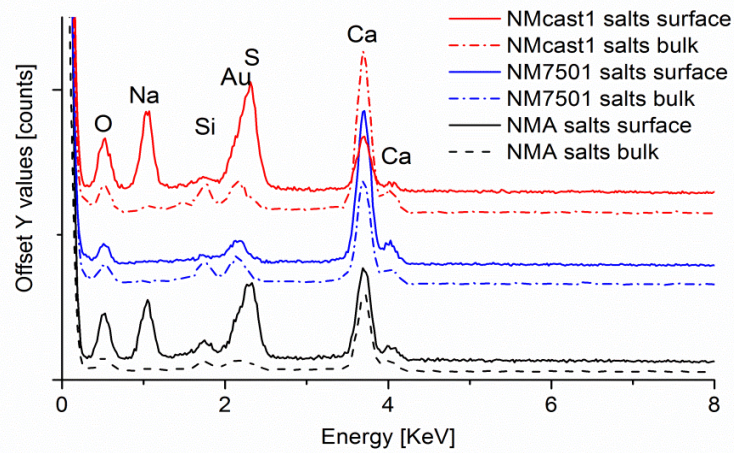
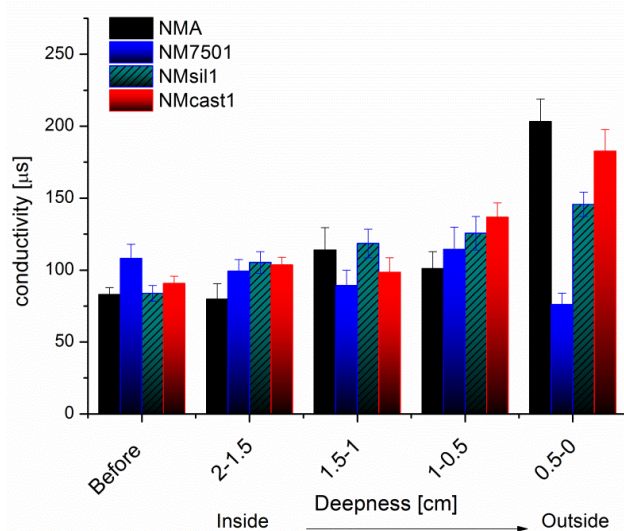


Table 3.5 14 Dosage of soluble salts in samples collected at before and after the salt cycles at different depth from NMA, NM7501, NMsil1, NMcast1. The average of three measurements is presented

Depth (cm)	Conductivity (μs)			
	NMA	NM7501	NMsil1	NMcast1
Before	83±5	108±10	84±5	91±5
2-1.5	80±11	99±8	105±7	104±5
1.5-1	114±16	89±11	119±10	98±10
1-0.5	101±12	114±16	126±12	137±10
0.5-0	203±16	76±8	146±8	183±15



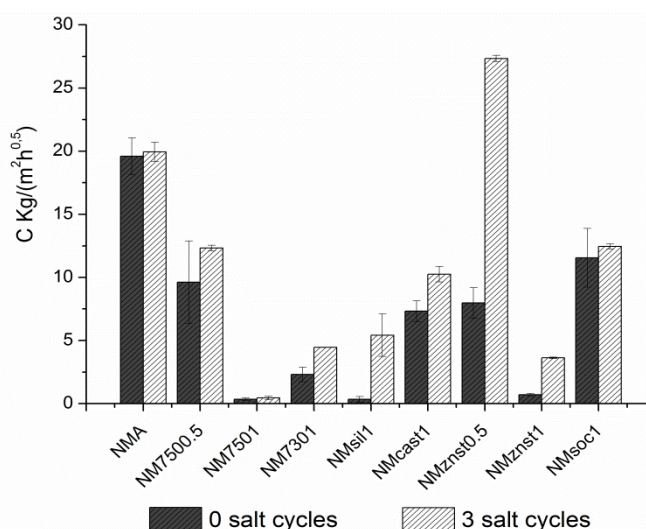
3.5.2.3. Capillary water absorption and compressive strength after the exposure

As can be seen from the data in Table 3.5 15, the capillary water absorption of the samples after the salt weathering increased in every case.

NMA was completely wettable since the beginning and the higher water absorption after the test might be due to the increased open porosity, which was, in turn, caused by the salts crystallization pressure on the pores walls. Mixes added with 0.5% of water repellents showed higher coefficients both before and after the salt cycles, a linear increase was observed for NM7500.5, NM7301. The increase of the water absorption coefficients was particularly high for NMznst0.5 also in comparison to NMznst1, NMcast1, NMsoc1 and also exceed the capillary coefficient of NMA, probably because NMznst0.5 specimens had higher open porosity. A good water repellence was maintained only by NM7501.

Table 3.5 15 Capillary water absorption coefficients of natural hydraulic lime mortars before and after the salt cycles. NM7300.5, NMcast0.5, NMsoc0.5 were seriously damaged during the salt cycles and the capillary water absorption was not test.

	Before salt cycles kg/(m ² ·h ^{0,5})	After 3 salt cycles kg/(m ² ·h ^{0,5})
NMA	19.60±0.46	19.95±0.76
NM7500.5	9.62±0.27	12.33±0.22
NM7501	0.35±0.10	0.45±0.13
NM7301	2.32±0.58	4.46±0.02
NMSil1	0.34±0.22	5.42±1.68
NMcast1	7.33±0.83	10.26±0.61
NMznst0.5	7.98±1.22	27.34±0.25
NMznst1	0.71±0.10	3.63±0.06
NMsoc1	11.56±2.33	12.46±0.20



The measurement of the compressive strength after the salt weathering represents another important parameter in order to evaluate the damages caused by the salt weathering. The specimens were desalinated before the test⁹.

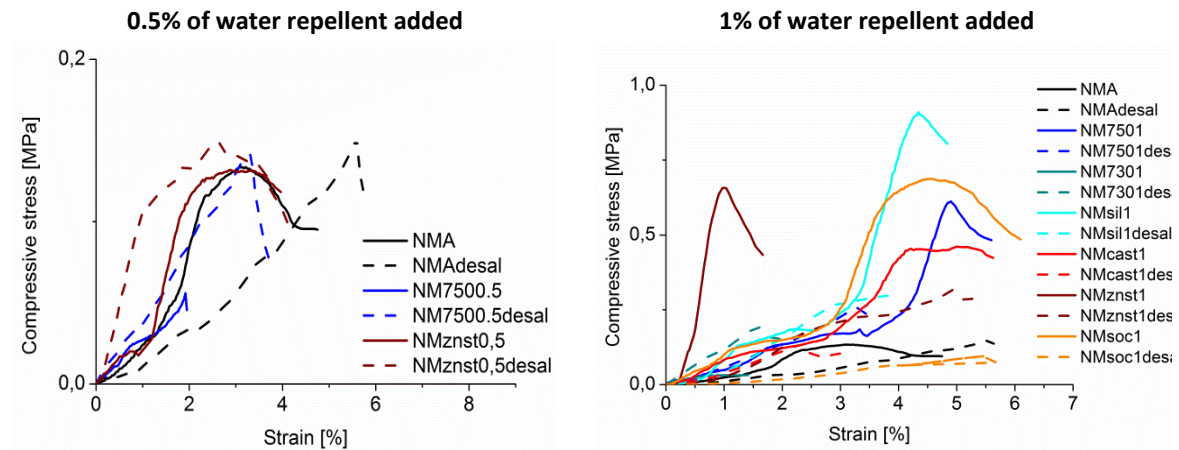
NM7300.5, NMSil0.5, NMsoc0.5 loss their cohesion during the salt cycles and it was not possible to test their compressive strength. We assume that their compressive strength was at the end of the test extremely low. By observing the graphs displayed below and the σ_{max} (Table 3.5 16, Table 3.5 17) it is interesting to notice that the mechanical strength did not changed much for mixes added with 0.5% of

Mortar mix	Compressive strenght σ_{max} (MPa)	
	Before salt cycles	After desalination
NMA	1.32±0.03	0,12±0,04
NM7500.5	0.34±0.19	0,12±0,02
NM7501	0.89±0.09	0,30±0,06
NM7301	0.74±0.17	0,24±0,06
NMSil1	0.83±0.14	0,21±0,12
NMcast1	0.62±0.21	0,12±0,02
NMznst0.5	1.47±0.39	0,16±0,01
NMznst1	0.62±0.16	0,27±0,07
NMsoc1	0.55±0.23	0,09±0,01

⁹ The specimens were put in deionised water to solubilise the salts till the conductivity of the solution reached values < 80 μ s (average conductivity of water solution in contact with the specimens before the salt tests), after then the samples were dried in oven to constant weight.

water repellent, even if serious damages of the surfaces was noticed (see above). Maybe the compressive strength was already low before the salt cycles and the salts might have been a slight strengthening action working as cement between the aggregates. The desalination process might have not completely removed these salts from the interstices inside the matrix, maintaining the strengthening effect. The mechanical strength seriously diminished, however, if samples added with 1% of water repellent were considered (Table 3.5 17 right) reaching unsatisfactory compressive strengths.

Table 3.5 17 Curves of the compressive strength vs. the strain rate of limestone cement mortars after salt weathering test.



3.5.3. SALT WEATHERING OF WATER-REPELLENT POZZOLANA-LIME MORTARS

3.5.3.1. Resistance to salt crystallization and external appearance of pozzolana-lime mortars after the exposure

The images of pozzolana-lime mortars after the evaluation of the resistance to salt crystallization are shown in Table 3.5 18, together with the mass variations of the specimens during the test.

Pozzolana-lime mortars with water repellents generally demonstrate a better resistance to salt crystallization in comparison to natural hydraulic mortars, therefore it was possible to perform 5 cycles of immersion in saturated sodium sulphate solution.

The salt cycles weathering highlighted that:

- PMA's specimens, without water-repellents, were unable to endure 5 cycles of immersion in salt solution, the specimens were seriously damaged after 3-4 cycles and completely destroyed during the fifth cycle. Serious loss of material during the cycles was measured.

- Specimens added with silane /siloxanes (PM7501, PMtes1, PMSil0.5,1,1.5) showed a better resistance to salt crystallization in comparison to the ones admixed with stearates (PMcast0.5,1,1.5 and PMznt1). A conspicuous material loss was measured for PM7301, PMznt1, PMcast0.5,1,1.5

- Higher water repellent percentages resulted in a better protection against the damages caused by the salt crystallization (see also the images of Sil0.5,1,1.5 and cast0.5,1,1.5 and the relative mass losses in Table 3.5 18.)

A more detailed observation of the surfaces of the specimens after the salt cycles was performed with optical microscope OM under normal and UV-light and with electron microscope SEM-EDX.

Table 3.5 19 summarizes three different kinds of observed features in the images of PMA, PM7501 and PMcast1:

-Deep macro- and micro- cracks and preferential erosion of the binders were observed for PMA, the binder matrix was brittle and granular. In correspondence of crystals interspersed inside the binder matrix, sodium and sulphur were detected by EDX.

-Homogenous surfaces with only slight erosion of the binder were observed in PM7501, sodium and sulphur were immediately detected under the exposed surfaces.

-Formation of salts efflorescences and erosion of the binder were observed in PMcast1, even if no sodium or sulphur were immediately detected under the exposed surfaces.

PMtes1, PMSil0.5,1,1.5 showed features similar to PM7501, while PMcast0.5, 1.5, PMznst1, PM7301 behaved like PMcast1.

Table 3.5 20 and Figure 3.5 4 shows the results of the colorimetric measurements. Pozzolana-lime mortars, as also observed in NM mortars, were characterized by coarse and not-homogeneous surfaces after the test, therefore high standard deviation of the data were found. The specular component was negligible in every case as it is demonstrated by the slight differences between SCI and SCE measurements. ΔE values exceeded in most cases 5, considered a threshold value, beyond which the colour variation is clearly discernible to naked eye examination. Specimens which demonstrated better resistance to salts crystallization, i.e. PM7501, PMSil0.5,1,1.5, PMtes, were less affected by high colour variations in comparison to PMcast0.5,1,1.5 or PMznst1. As for NM or CM mortars, a yellowing, reddening and darkening (increase of a^* , b^* and decrease of L^*) of the specimens occurred. Maybe the presence of hygroscopic salts caused the retention of moisture on the the surface of the specimens resulting in a "saturation-of-the colours-effect". It is often observed that a wet or damp mortar has a darker and saturated colour.

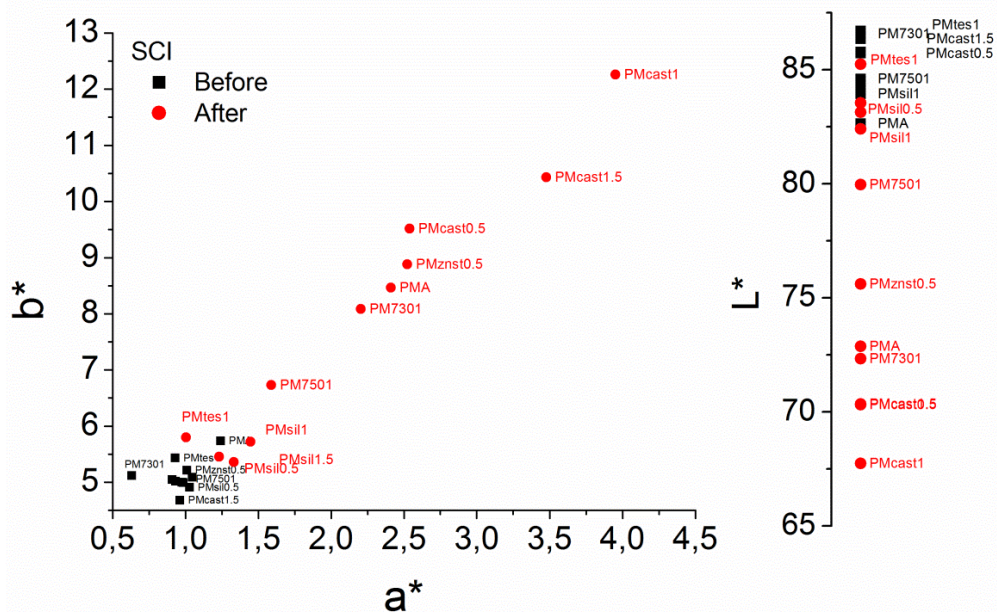
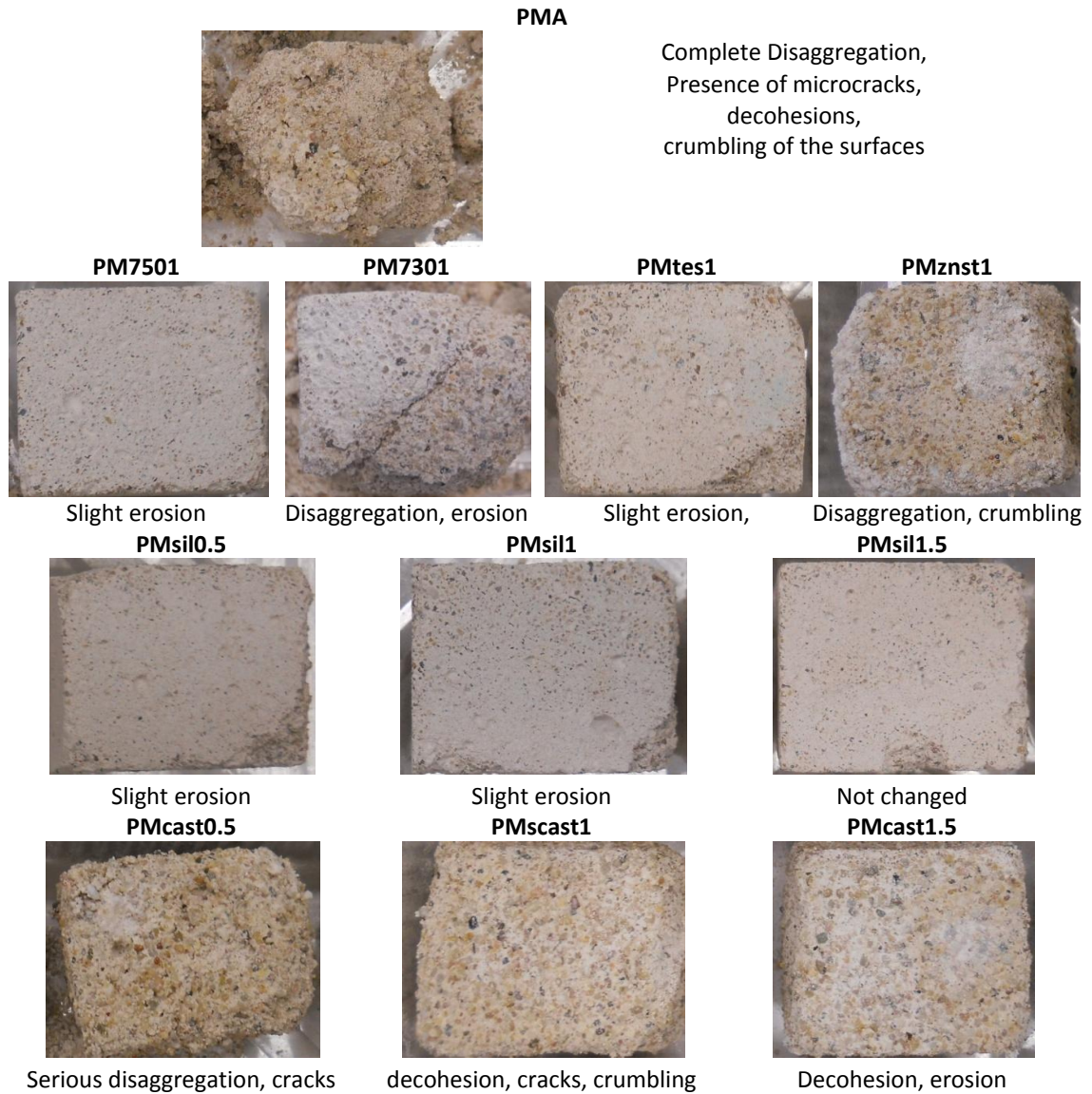


Figure 3.5 4 Lightness L^* and chromaticity a^* , b^* values of the specimens before and after the salt weathering test are shown (SCI values), the data resulted from the average of nine measurements.

Table 3.5 18 Above: pictures of pozzolana lime mixes after 5 salt cycles (scale 3:4). Below: mass evolution of the specimens under ponding (relative mass change vs. time).



Mass losses during the cycles

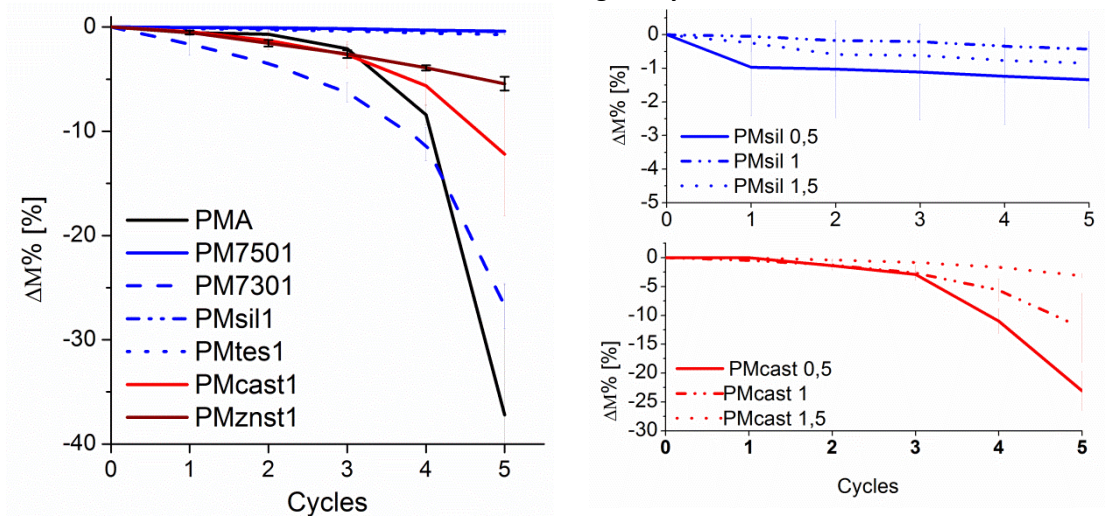
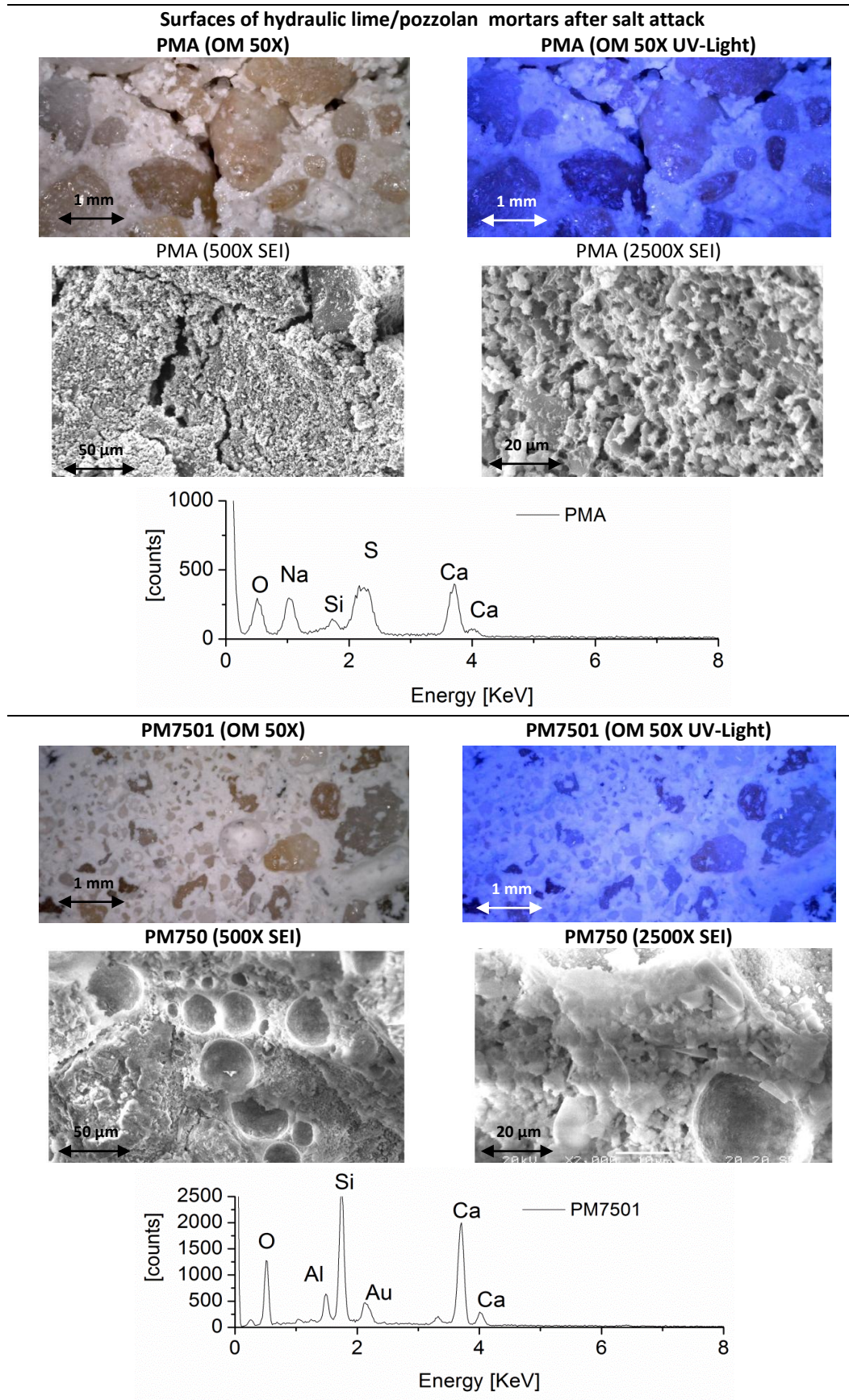


Table 3.5 19 Optical microscope and SEM-EDX observations of mortar surfaces after the salt weathering test. EDX spectra registered on samples collected under the surfaces (sampling depth: 0-0.5 cm). The table continues on the following page.



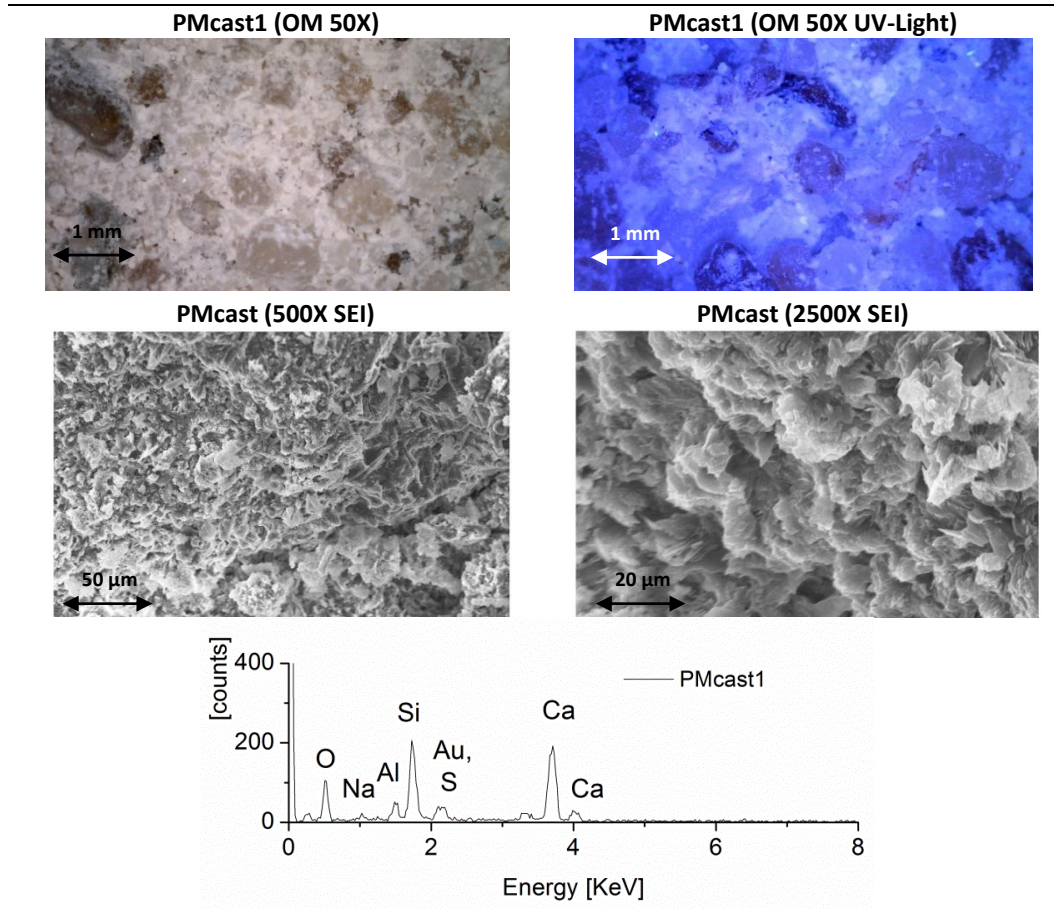


Table 3.5 20 Total colour variation ΔE , lightness ΔL^* and chromaticity Δa^* Δb^* variations of the specimens after the salt weathering test are shown, considering SCI or excluding SCE the specular component, the data resulted from the average of nine measurements with standard deviation. Bold font is used for those variations that, being higher than 5, are supposed to be clearly discernible to naked eye examination.

	SCI				SCE			
	ΔL^*	Δa^*	Δb^*	ΔE	Δa^*	Δb^*	ΔL^*	ΔE
PMA	-9.8±1.7	1.2±0.1	2.7±2.5	10.2±3.0	-9.8±1.8	1.2±1.0	2.7±0.4	10.2±2.1
PM7501	-4.6±0.3	0.6±0.4	1.7±1.7	5.0±1.8	-4.7±0.3	0.6±0.7	1.8±0.5	5.0±0.9
PM7301	-14.2±0.3	1.6±0.2	3.0±0.8	14.6±0.9	-14.3±0.3	1.6±0.5	3.0±0.4	14.7±0.7
PMsil0.5	-3.1±0.1	0.2±0.1	0.5±0.3	3.2±0.4	-3.2±0.1	0.2±0.1	0.6±0.1	3.2±0.2
PMsil1	-1.5±0.1	0.5±0.3	0.7±0.3	1.8±0.4	-1.6±0.1	0.5±0.1	0.7±0.3	1.8±0.3
PMsil1.5	-2.6±0.2	0.4±0.4	0.3±0.5	2.6±0.7	-2.6±0.2	0.4±0.1	0.4±0.4	2.7±0.5
PMtes1	-1.1±1.2	0.1±0.1	0.4±0.4	1.2±1.3	-1.1±1.2	0.1±0.3	0.4±0.3	1.2±1.3
PMcast0.5	-15.5±0.5	1.6±0.1	4.5±2.0	16.2±2.0	-15.6±0.4	1.6±1.3	4.5±0.4	16.3±1.4
PMcast1	-16.5±1.0	2.9±0.1	7.2±1.5	18.2±1.8	-16.6±1.0	2.9±0.7	7.1±0.5	18.3±1.3
PMcast1.5	-15.4±0.5	2.5±0.1	5.8±2.4	16.6±2.4	-15.4±0.5	2.5±0.8	5.7±0.3	16.6±1.0
PMznst1	-8.6±1.5	1.5±0.1	3.7±1.6	9.5±2.2	-8.6±1.5	1.5±0.5	3.7±0.4	9.5±1.6

3.5.3.2. Composition, microstructure and salt distribution in pozzolana-lime mortars after the exposure

FT-IR analysis reported in Figure 3.5 5 allowed to confirm the presence of high quantities of sulphates in PMcast1 and PMA surfaces (-SO_4 absorption at 1120 cm^{-1}), but also PMznst1, PMsil1 were not completely free by salts depositions.

In PMznst1 and PMtes1 was detected calcium hydroxide (-OH absorptions at 3640 cm^{-1}) not reacted during the hydration. In the other samples only carbonates and silicates were detected.

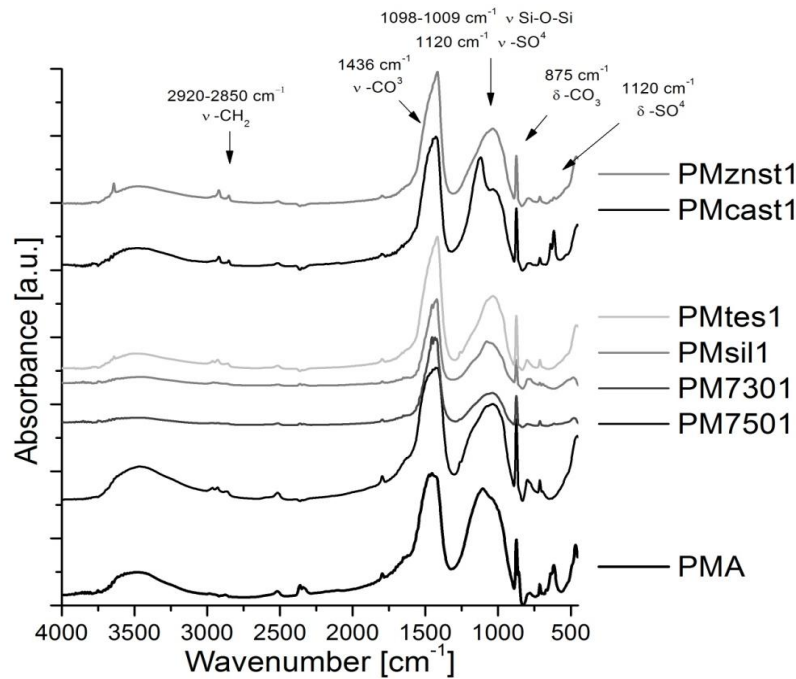


Figure 3.5 5 spectra of pozzolana-lime mortars after salt weathering.

MIP analysis were performed on samples collected from the external parts of PMA, PM7501, PMsil1, PMcast1 specimens before and after the salt cycles (sampling depth around 0-0.5 cm). It was not possible to test desalinated samples of pozzolana-lime mortars because they were too brittle and cracked during the analysis, giving unreliable results.

Table 3.5 21 reports the porosimetry results together with the graphs of the cumulative volume and of the pore size distribution.

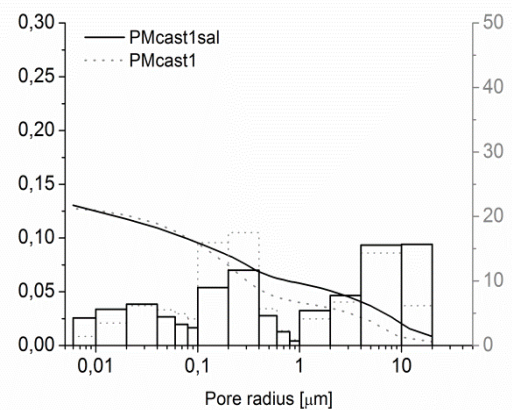
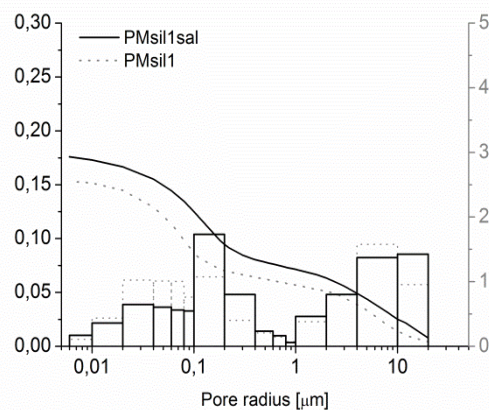
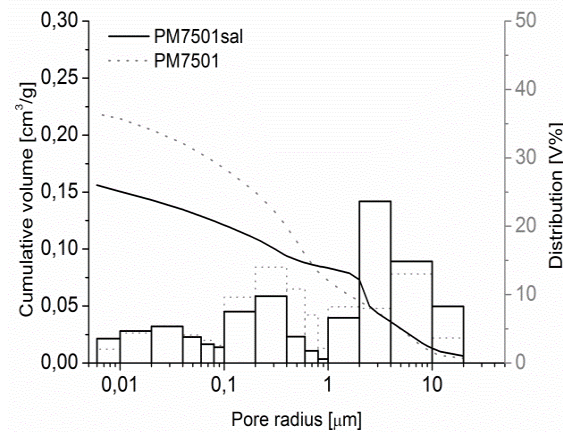
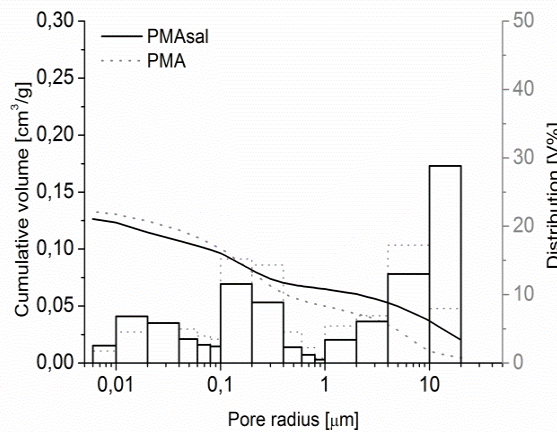
-PMA increased the total open porosity and pores with radius higher than $10\mu\text{m}$ after the cycles, the pressure exerted by the salts crystallization strongly affected the porous structure and the pore size.

-PM7501 and PMsil1 samples showed a general decrease of the porosity, and in particular of pores with radius around $0.1\text{-}1\mu\text{m}$, the formation of salts crystals and crusts on the surfaces might have partially occluded the pores.

-PMcast1 samples strongly increased their porosity, the reduction of pores around $0.1\text{-}1\mu\text{m}$ and the correspondent increase of pores bigger than $1\mu\text{m}$ should be linked to the damaging pressure exerted by the salts formation on the pore walls and their subsequent enlargement.

Table 3.5 21 Porosimetric analysis of NMA, NM7501, NMsil1 NMcast1 before salt cycles and after salt cycles, the graphs of the cumulative volume and the pore distribution vs. the pore radius are reported below

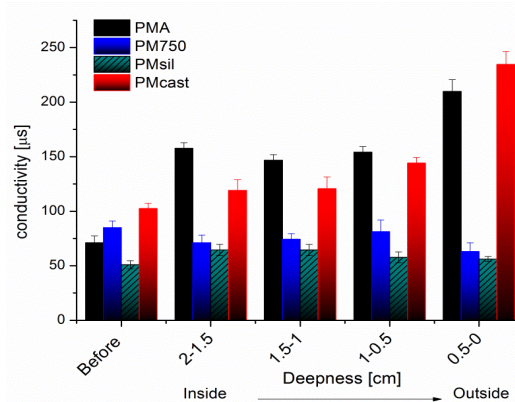
		Bulk density MIP (g/cm ³)	Apparent density MIP (g/cm ³)	Total open porosity MIP (%)	Total cumulative volume MIP(cm ³ /g)	Average pore radius MIP(μm)
PM A	Before salt cycles	1.88±0.05	2.71±0.02	25.0±0.5	0.13±0.01	0.31±0.05
	After salt cycles	2.23±0.08	2.88±0.04	29.36±0.07	0.14±0.08	0.001±0.05
PM 7501	Before salt cycles	1.69±0.03	2.12±0.01	36.0±0.5	0.21±0.01	0.46±0.05
	After salt cycles	1.78±0.05	2.43±0.02	29.3±0.7	0.17±0.02	2.17±0.05
PM sil1	Before salt cycles	1.87±0.05	3.48±0.01	28.9±0.5	0.16±0.02	0.13±0.05
	After salt cycles	1.46±0.01	1.88±0.02	25.7±0.8	0.18±0.01	18.21±0.05
PM cast	Before salt cycles	1.94±0.01	2.69±0.04	24.9±0.5	0.13±0.01	0.27±0.05
	After salt cycles	3.27±0.01	5.29±0.04	29.5±2.3	0.14±0.02	0.001±0.05



The performed conductivity measurements allowed to understand the salt distribution (Table 3.5 22). PMA and PMcast1 after salt crystallization showed higher conductivity, in particular in the outer part of the specimens (0.5-0 cm) reaching values of 200-250 μS/cm. The salts were, however, able to deeply penetrate inside the specimen cores (2.0-1.5 cm). On the other hand, PM7501 and PMSil1 did not show a dramatic increase of the conductivity after the salt cycles and the conductivity remained constant over the entire profile of the specimens.

Table 3.5 22 Dosage of soluble salts in samples collected before and after the salt cycles at different depth from NMA, NM7501, NMsil1, NMcast1. The average of three measurements is presented

Deepness (cm)	Conductivity ($\mu\text{s}/\text{cm}$)			
	PMA	PM7501	PMsil1	PMcast1
Before	71 \pm 6	85 \pm 6	51 \pm 4	102 \pm 5
2-1.5	158 \pm 5	71 \pm 7	64 \pm 5	119 \pm 10
1.5-1	147 \pm 5	74 \pm 5	64 \pm 5	121 \pm 11
1-0.5	154 \pm 5	81 \pm 11	58 \pm 5	144 \pm 5
0.5-0	210 \pm 11	63 \pm 8	56 \pm 2	235 \pm 12

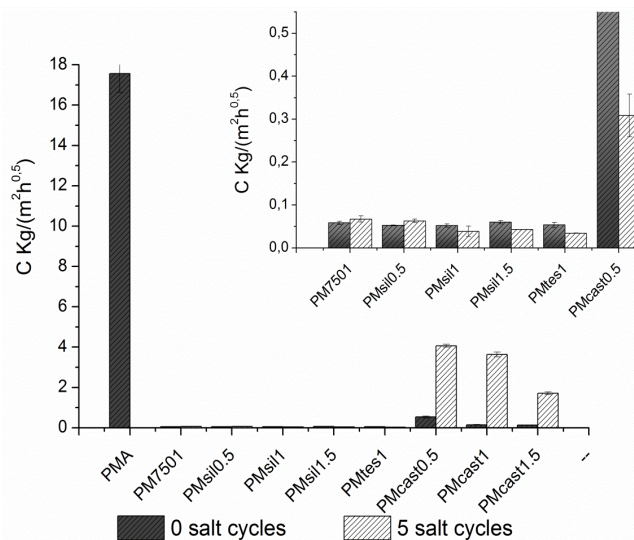


3.5.3.3. Capillary water absorption and compressive strength after the exposure

The water absorption coefficients after the cycles indicated that water absorptions of PM7501, PMsil0.5, 1, 1.5, PMtes, added with siloxanes remained low or even slightly decreased, due to a further hydration of the outer part of the specimens and a consequent decrease of the external open porosity (Table 3.5 23). PMcast mixtures had higher water absorption after the test in particular when lower percentages of calcium stearates were used. As observed in Chapter 3.3, calcium stearates disposed themselves on the outer part of the specimens, and it was observed a severe loss of material from this part in PMcast during the salt cycles. Probably, together with the material loss, the removal of the calcium stearates from the outer layer occurred and that caused a strong decrease of the water repellent properties. PMA, PM7301, PMznt1 specimens were completely disintegrated and it was not possible to test them.

Table 3.5 23 Capillary water absorption coefficients of natural hydraulic lime mortars before and after the salt cycles. NMcast0.5, NMsoc0.5 were seriously damaged during the salt cycles and not tested.

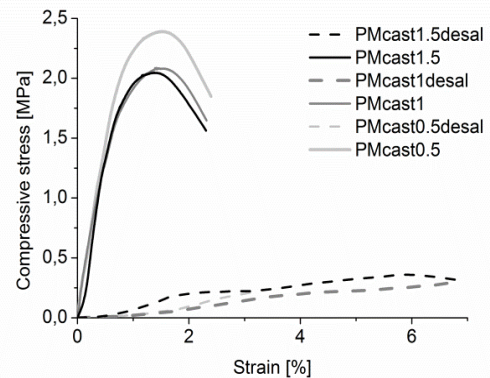
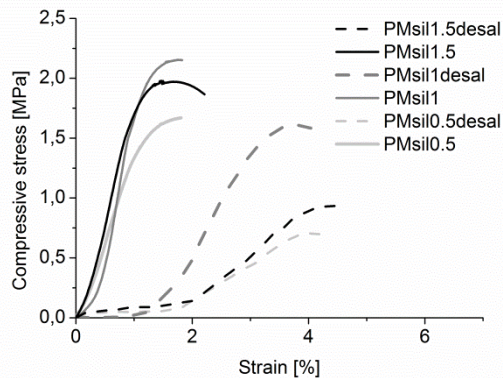
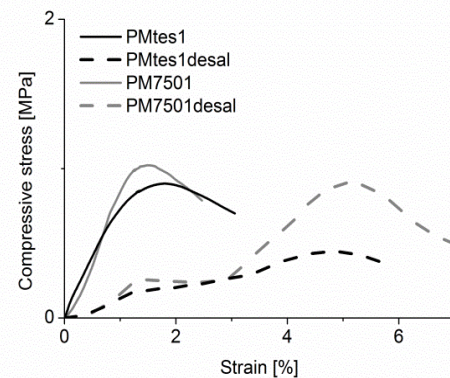
	CI before salt cycles	CI after 5 salt cycles
	$\text{kg}/(\text{m}^2 \cdot \text{h}^{0.5})$	$\text{kg}/(\text{m}^2 \cdot \text{h}^{0.5})$
PMA	17,561 \pm 0,920	-
PM7501	0,058 \pm 0,004	0,067 \pm 0,007
PMsil0.5	0,053 \pm 0,001	0,063 \pm 0,004
PMsil1	0,052 \pm 0,004	0,039 \pm 0,012
PMsil1.5	0,060 \pm 0,004	0,043 \pm 0,000
PMtes1	0,053 \pm 0,007	0,034 \pm 0,001
PMcast0.5	0,533 \pm 0,049	4,065 \pm 0,078
PMcast1	0,148 \pm 0,020	3,636 \pm 0,118
PMcast1.5	0,134 \pm 0,005	1,711 \pm 0,068



The compressive strength after the salt cycles and the desalination¹⁰ of the samples aid to evaluate the resistance to the salt crystallization. The results are shown in Table 3.5 24, it was not possible to measure PMA, PM7301, PMznst1 specimens, already disintegrated during the salt cycles. The σ_{\max} in every case decrease after the exposure to sodium sulphates solutions. The mechanical strength of specimens added with silane/siloxanes, such as PMtes, PM7501, PMsil0.5,1,1.5 did not decrease much in comparison to PMA or PMcast mixtures. PMcast mixtures almost completely lost their mechanical properties reaching σ_{\max} around 0.40 MPa.

Table 3.5 24 Curves of the compressive strength vs. the strain rate of limestone cement mortars after salt weathering test.

Mortar mix	Compressive strength σ_{\max} (MPa)	
	Before	After
PMA	2.0±0.2	-
PM7501	1.07±0.05	0.71±0.29
PMsil0.5	1.73±0.08	0.65±0.08
PMsil1	2.24±0.07	1.45±0.23
PMsil1.5	2.04±0.09	0.84±0.14
PMtes1	0.89±0.03	0.44±0.12
PMcast0.5	2.35±0.08	0.37±0.15
PMcast1	2.0±0.1	0.37±0.09
PMcast1.5	2.06±0.08	0.52±0.23



3.5.4. XRD ANALYSIS OF DIFFERENT MORTAR MIXES AFTER THE SALT WEATHERING

Besides the physical damages caused by the crystallization pressure of sodium sulphates salts on porous materials, the penetration of sulphate ions into hardened cement can lead to a physical-chemical degradation due to the formation of secondary sulphate bearing phases (see also Chapter 1).

Wet sulphate bearing environment might caused the loss of strength of concrete structures, due to the so-called "Sulfate Attack". This term defines a set of mineralogical changes with physical

¹⁰ The specimens were put in deionised water to solubilise the salts till the conductivity of the solution reached values $< 80 \mu\text{s}$ (average conductivity of water solution in contact with the specimens before the salt tests), after then the samples were dried in oven to constant weight.

effects, and it is generally attributed to the formation of secondary ettringite or Thaumasite from the interaction between sulphate and alumina-bearing phases in the cement¹¹. The exposure of lime mortars to SO₂ rich environment or to sulphates solution might cause the formation of calcium sulphates, in particular gypsum¹².

Some XRD analysis were therefore performed on CMA, NMA, PMA samples in order to understand if the formation of other dangerous salts occurred in consequence of the salt weathering. The mortars without water repellent were considered, because their high water absorption caused a deep penetration of the sodium sulphate solution and resulted in a prolonged contact between the minerals of the mortars and the ions of the solution.

The samples were collected in the first 0-1 cm, dried in oven at 40°C till constant weight and grinded. The pattern collected are displayed in Figure 3.5 6.

The XRD pattern of CMA after salt attack clearly showed the reflection peaks of thenardite and ettringite. However, ettringite was probably present as primary ettringite as already seen in the limestone cement pastes and in CMA samples collected after 28 days of hardening. A slight presence of gypsum was also found. Gypsum can form from portlandite and also from calcium in calcium carbonate and in C-S-H which becomes decalcified. The transformation of calcium carbonate in gypsum and a consequent washing out of this more soluble salts can seriously damage the mortar matrix. Furthermore, the decalcification of C-S-H, which is the main hydrate of cement matrix and stands for its cohesive property, might result in the softening of this phase.

The XRD patterns of NMA and PMA samples after the salt attack showed the presence of thenardite. The patterns did not show the presence of other damaging sulphates salts such as ettringite, thaumasite (which is formed only at low temperatures), gypsum.

The presence of a crystalline form of calcium silicate hydrate was found in PMA samples, and it confirmed that a pozzolanic reaction occurred.

The samples were dried in oven, therefore in the three mixtures only thenardite (Na₂SO₄) was found and not mirabilite (Na₂SO₄.10H₂O). In moist environments the thenardite might be transformed in mirabilite and this change in the crystalline structure might caused further damages due to the crystallization pressure. However, probably during the salt cycles, upon wetting with the salt solution, thenardite did not hydrate to form mirabilite but was dissolved¹³.

¹¹ Chabrelié, A., 2010

¹² Izaguirre, A., J. Lanás, J. Alvarez 2010

¹³ Rodríguez- Navarro C. et al. 2000

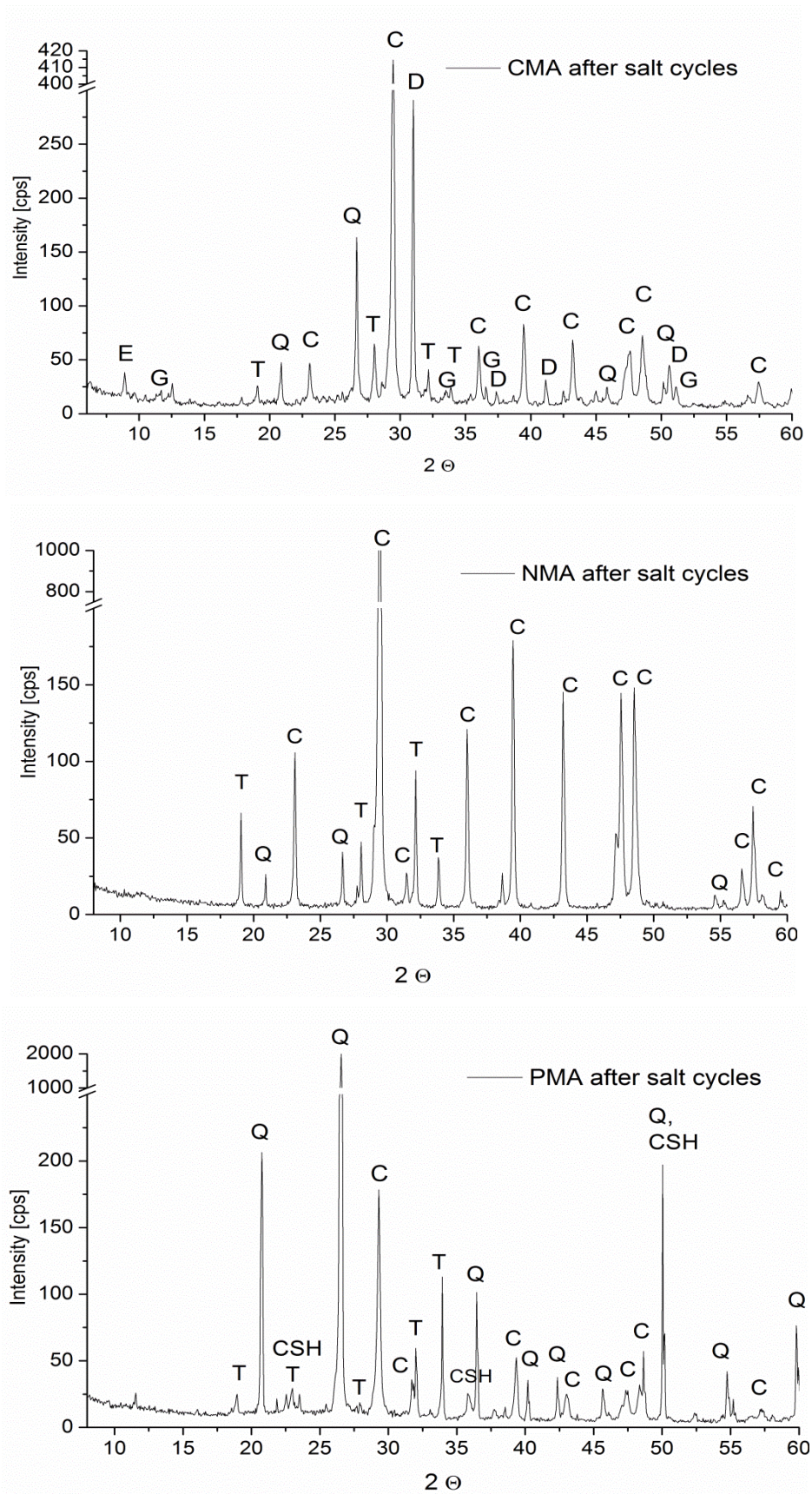


Figure 3.5 6 XRD patterns of samples of CMA, NMA, PMA after salt cycles. E= ettringite; T=thenardite; G= gypsum; C= calcite; D=dolomite; Q= quartz; CSH= calcium silicate hydrate

3.6. Water-repellent mortars applied on salty masonry

Some of the water-repellent mixtures, designed and studied in the previous chapters, were applied on small brick walls built *ad hoc* and previously treated with salt solutions. The aim of this part of the study was to create a model of salty masonry and to evaluate the behaviour of water-repellents mortars in that situation.

As explained in Chapter 2, the walls were made of traditional full bricks and they previously underwent capillary absorption of saturated salt solutions of sodium sulphates and sodium chloride (1:1 by dry weight of each salt) for almost one year to simulate an historical salty masonry of Venice.

The walls were left to dry and then the water repellent mortars were applied on the surfaces. After one month of hardening the walls were again subdued to capillary absorption of saturated salt solutions.

The applied mortar mixtures were chosen among those previously studied by considering the different binders, and the water-repellents admixtures which allowed a better protection on the basis of the test done (see chapter 3.3, 3.4, 3.5).

The chemical-physical characterization of the applied mortars and the evaluation of their behaviour after the exposure to rising salt solutions were done with direct visual observations, Mid IR thermography, capillary water absorption tube test, Schmidt Hammer PT sclerometer, colorimetric analyses, FT-IR spectroscopy, TG-DSC analyses, SEM observations, MIP porosimetry.

3.6.1. MORTAR MIXTURES

The applied mortar mixtures are described in Table 3.6 1. The mixtures were chosen in order to be representative of the different binders and of the different class of water-repellents studied. Therefore, one mixture added with stearates and one added with silane/siloxanes were considered. Among the mortar mixtures added with stearates or silanes, those ones which had shown better resistance to artificial weathering and to the action of sodium sulphates solutions in the previous studies (see Chapters 3.3, 3.4, 3.5) were applied on the brick walls. Furthermore mixtures without water-repellents were prepared.

The mortar mixtures were applied as a single layer and let hardened for 28 days at 20 ± 2 °C and at 70% HR. After then samples collected from the upper, medium and lower part of the walls were analysed to evaluate the properties of the hardened mortars.

The reservoirs underneath the walls were then filled with a saturated solution of sodium sulphate in order to expose the walls and the mortars to capillary rise of salt solution and to evaluate their behaviour. Visual observations and IR-thermograms of the walls were done.

After 28 days, other samples were collected from the walls and further analyses were performed in order to evaluate the effects of the exposure to capillary rise of saline solutions.

Table 3.6 1 Mortar mixtures prepared and applied on salty masonries and list of further abbreviations used in this chapter

Mix name	binder			Water-repellent admixture		
	type	class	% by mass	name	class	% by mass
WCMA	CEMIIB/L 32.5	Limestone cement	0.96	-	-	-
WCM7501				Sitren p750	silane with amorphous silica	1
WCMcast1				Ca Stearate	metal soap	1
WNMA	NHL3.5	Natural hydraulic lime	0.50	-	-	-
WNM7501				Sitren p750	Silane with amorphous silica as carrier	1
WNMcast				Ca Stearate	metal soap	1
WPMA	Pozzolana- calcium hydroxide 1:1 by dry weight	Pozzolana- lime	1.29	-	-	-
WPM7501				Sitren p750	silane with amorphous silica as carrier	1
WPMcast1				Ca Stearate	metal soap	1
Other Abbreviations used in this Chapter						
-A	Above; measurements performed/sample collected from the walls upper part (60-70cm from the floor)					
-M	Middle; measurements performed/sample collected from the walls middle part (45-55cm from the floor)					
-B	Below; measurements performed/sample collected from the walls lower part (25-35 cm from the floor)					

3.6.2. OBSERVATION DURING THE CAPILLARY RISE OF SALT SOLUTIONS

During the exposure of the walls to the capillary rise of sodium sulphate solution it was possible to observe the behaviour of the system wall/mortars.

Table 3.6 2 shows some of the more representative pictures and thermograms collected before and after the exposure:

- By considering the three mortars without water repellent admixtures, it was clearly visible that at the beginning the smooth and homogeneous surfaces of the mortars were almost dry and free from salt efflorescences. But, after one month of exposure, salt efflorescences appeared on the lower part of the wall, in particular near the corners and over the limestone cement. Also the thermograms indicated dishomogeneities of temperature in correspondence of the efflorescences. After the exposure, lower temperatures were detected on the lower part of the mortar layers, indicating the presence of moisture due to the capillary rise of the salt solution
- The limestone cement mortars with water repellent admixtures seemed free from visible salt efflorescences after the exposure, the salts were present only below the mortar layer and underneath it. The thermograms indicated homogeneous temperature all over the mortar layers, while lower temperature were detected immediately below them. This might indicate that the water-repellent mortars remained dry, and had lower

thermal conductivity. The mortar WCM750 showed however detachment from the walls in different points, maybe due to the formation of salt subefflorescences.

- The natural hydraulic lime mortars with water repellent showed salt efflorescences after the exposure and the thermograms were similar to those registered for the mortars without water repellents.
- The pozzolana-lime mortars with water repellents showed low adhesion to the wall and severe decohesions and exfoliation were seen after the exposure. Salt subefflorescences were visible underneath the detachments of the layers. However, the thermograms indicated homogeneous temperature over the mortars layer which were almost dry.

Also the colorimetric analysis of the exposed mortars aid to evaluate the extent of the damaging action of capillary rise of salt solution of the prepared mortars. Names and abbreviations listed in Table 3.6 1 were used.

Table 3.6 3 and Figure 3.6 1 summarize the collected data and allow to notice that higher colour variations were observed where salt efflorescences were more visible.

The lower part of the limestone cement without water repellents (WCMA-B) showed the higher colour variation, but sometimes also in the middle part of the mortar layer significant colour variation were seen, always due to the presence of salt efflorescences. WCMcast-M, WNMcast-B and WPMA-M, WPM750-B, WPMcast-M showed significant decrease of the L* parameters: a darkening of these area was observed, probably some spots remained moist due to the presence of salts underneath.




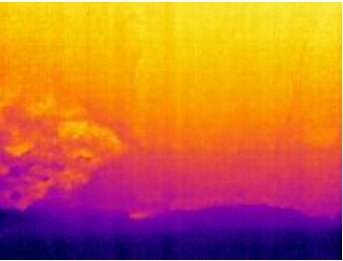

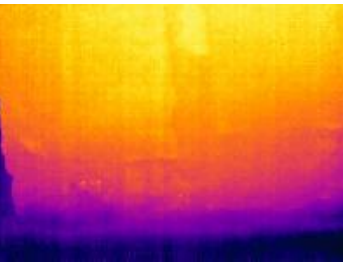

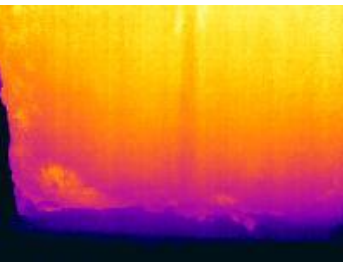

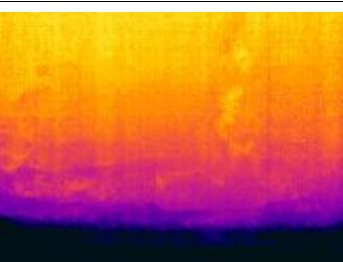

Table 3.6 2 Observation in visible light and IR- thermograms of the mortars applied on salty masonries before and after one month of exposure to capillary rise of salt solutions		
	Visible light	IR Thermograms (colour scale from 20 to 26°C)
Mortar mixtures without water repellent (in the pictures-link: WCMA, middle: WNMA, right: WPMA)		
Before the exposure		
After the exposure		
Limestone-cement mortars with water repellents (in both pictures-link:WCM750; right:WCMcast)		
After the exposure		
Natural hydraulic lime mortars with water repellents (in both pictures-link:WNM750; right:WNMcast)		
After the exposure		
Pozzolana-lime mortars with water repellents (in both pictures- link:WPM750; right: WPMcast)		
After the exposure		
<p>Scale rod of the Thermograms</p> <p>Blue 22°C  26°C White</p> <p>Linear colour scale</p>		

Table 3.6 3 Colorimetric variations collected for the mortar mixes before and after the exposure to capillary rise of sodium sulphate solutions, the L*, a*, b* parameters regarding the colour lightness, the red-green hue and the blue-yellow hue, respectively, are listed (illuminant D65). The measurements are reported with specular component included (SCI) or with specular component escluded (SCE). Each result is the average of nine measurements. -A (above) , -M (middle) , -B(below) indicates the height of the walls were the measurements were done. The higher variations noticed are highlighted in grey.

	SCI				SCE			
	$\Delta L^*(D65)$	$\Delta a^*(D65)$	$\Delta b^*(D65)$	ΔE	$\Delta L^*(D65)$	$\Delta a^*(D65)$	$\Delta b^*(D65)$	ΔE
WCMA-A	1.49±0.03	-0.04±0.47	-0.06±0.13	1.49±0.49	1.52±0.03	-0.05±0.50	-0.09±0.13	1.53±0.51
WCMA-M	-0.83±0.02	0.00±0.46	-0.15±0.05	0.85±0.46	-0.80±0.02	0.01±0.44	-0.20±0.05	0.83±0.45
WCMA-B	5.11±0.16	-0.24±0.91	-4.22±0.25	6.63±0.96	5.17±0.16	-0.26±0.88	-4.22±0.25	6.68±0.93
WCM750-A	0.91±0.05	-0.02±4.05	-0.47±0.05	1.02±4.05	0.92±0.05	-0.05±0.02	-0.45±0.05	1.03±0.08
WCM750-M	0.28±0.04	-0.04±0.90	-0.16±0.03	0.32±0.90	0.29±0.04	-0.04±1.34	-0.20±0.03	0.36±1.34
WCM750-B	-2.06±0.09	-0.03±1.87	-1.31±0.17	2.44±1.88	-2.05±0.09	-0.07±2.32	-1.32±0.18	2.43±2.33
WCMcast-A	0.83±0.05	-0.03±0.80	-0.16±0.15	0.84±0.82	0.83±0.05	-0.05±0.76	-0.16±0.15	0.85±0.78
WCMcast-M	-4.29±0.06	0.10±0.85	0.57±0.13	4.33±0.86	-4.27±0.06	0.09±0.84	0.57±0.13	4.31±0.85
WCMcast-B	-0.63±0.04	-0.05±1.19	-0.48±0.17	0.79±1.21	-0.62±0.04	-0.05±0.91	-0.46±0.17	0.77±0.93
WNMA-A	-0.40±0.02	0.14±0.12	0.38±0.09	0.57±0.15	-0.46±0.02	0.13±0.12	0.35±0.09	0.59±0.15
WNMA-M	-0.47±0.01	0.16±0.10	0.48±0.07	0.69±0.12	-0.43±0.01	0.16±0.10	0.45±0.08	0.65±0.12
WNMA-B	-0.90±0.02	0.10±0.08	0.45±0.05	1.01±0.09	-1.00±0.02	0.08±0.08	0.40±0.05	1.08±0.09
WNM750-A	-1.29±0.03	0.22±0.09	0.30±0.04	1.34±0.11	-1.28±0.03	0.21±0.09	0.29±0.04	1.33±0.10
WNM750-M	0.11±0.04	0.05±0.24	-0.37±0.16	0.39±0.29	0.14±0.04	0.05±0.23	-0.38±0.16	0.41±0.28
WNM750-B	-1.48±0.03	0.35±0.18	0.49±0.14	1.60±0.23	-1.45±0.03	0.35±0.18	0.47±0.14	1.56±0.23
WNMcast-A	0.65±0.01	-0.11±0.07	-0.51±0.06	0.83±0.09	0.65±0.01	-0.10±0.07	-0.50±0.06	0.83±0.09
WNMcast-M	-1.52±0.01	0.39±0.08	0.87±0.08	1.79±0.11	-1.42±0.02	0.38±0.08	0.86±0.07	1.70±0.11
WNMcast-B	-2.28±0.02	0.44±0.13	0.66±0.08	2.41±0.15	-2.17±0.02	0.43±0.13	0.65±0.08	2.31±0.15
WPMA-A	0.95±0.02	-0.17±0.08	-0.65±0.10	1.17±0.13	0.99±0.02	-0.17±0.08	-0.69±0.10	1.22±0.13
WPMA-M	-2.10±0.04	0.35±0.22	1.34±0.22	2.51±0.32	-2.14±0.04	0.33±0.22	1.30±0.22	2.52±0.32
WPMA-B	-1.26±0.05	0.23±0.34	0.67±0.31	1.45±0.46	-1.43±0.05	0.21±0.33	0.66±0.31	1.59±0.46
WPM750-A	0.64±0.04	-0.41±0.57	-0.46±0.22	0.89±0.61	0.64±0.04	-0.40±0.56	-0.44±0.22	0.88±0.61
WPM750-M	4.22±0.01	-0.28±0.14	-0.51±0.11	4.26±0.18	4.11±0.01	-0.28±0.14	-0.49±0.12	4.15±0.18
WPM750-B	-2.17±0.05	0.25±0.52	1.33±0.35	2.56±0.63	-2.18±0.04	0.25±0.51	1.33±0.35	2.56±0.62
WPMcast-A	-0.93±0.01	0.37±0.13	1.31±0.15	1.65±0.20	-0.60±0.01	0.36±0.14	1.34±0.14	1.51±0.20
WPMcast-B	-0.91±0.01	0.01±0.09	0.06±0.04	0.92±0.10	-0.95±0.01	0.02±0.09	0.05±0.04	0.95±0.10
WPMcast-M	-2.50±0.03	-0.63±0.96	-1.66±0.71	3.07±1.19	-2.43±0.03	-0.63±0.94	-1.61±0.70	2.98±1.17

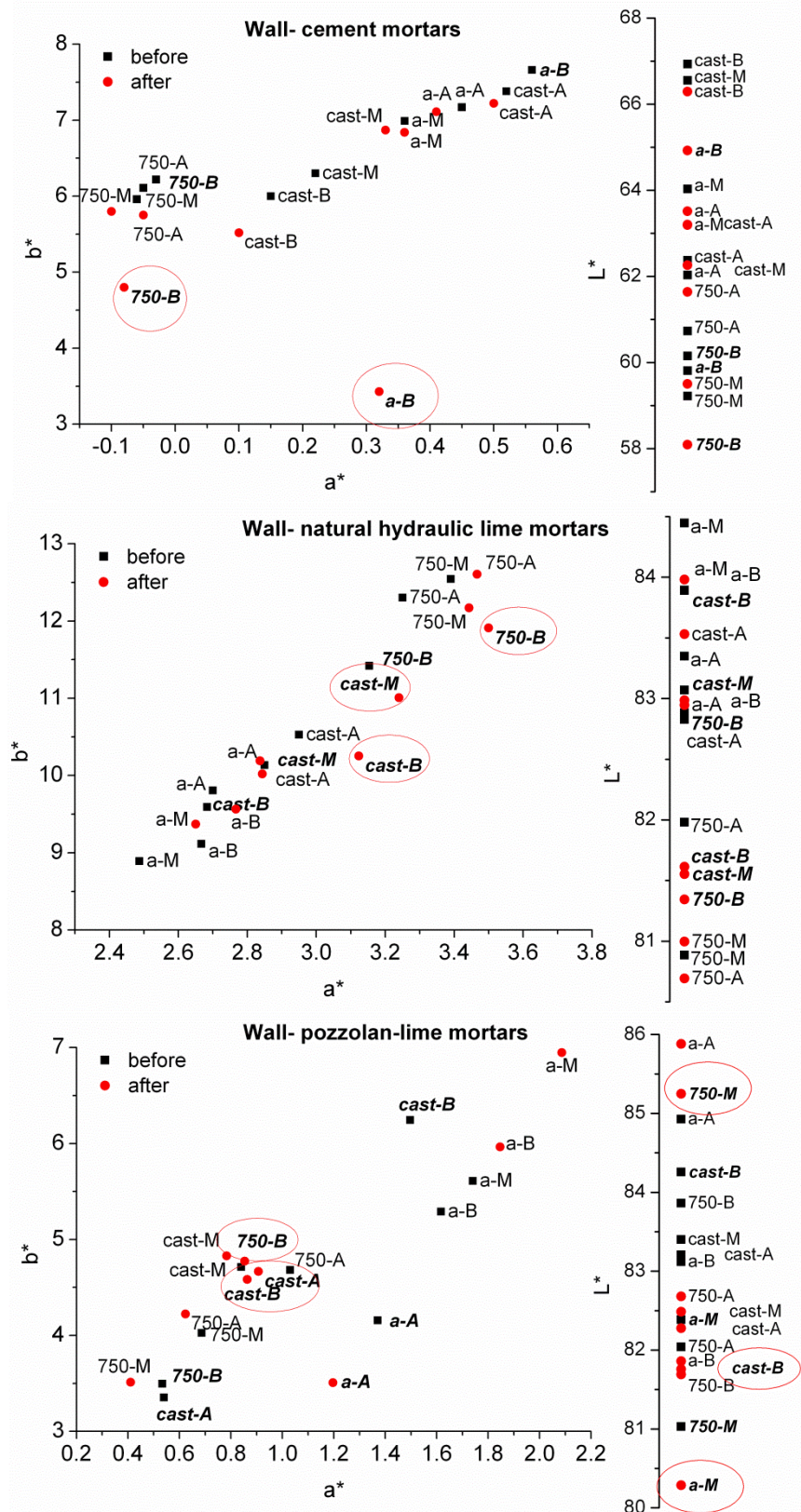


Figure 3.6 1 The graphs show the colorimetric parameters L^* , a^* , b^* in the CIEL*a*b* space when the specular component is included (SCI). From above to below: colorimetric parameters of limestone cement mortars, of the natural hydraulic lime mortars, and of pozzolana-lime mortars with or without water repellents applied on salty masonries. -A (above), -M (middle), -B (below) indicates the height of the walls where the measurements were done.

3.6.3. CHEMICAL-PHYSICAL PROPERTIES OF THE MORTARS BEFORE AND AFTER ONE MONTHS OF EXPOSURE TO CAPILLARY RISE OF SALT SOLUTION

3.6.3.1. Chemical composition

FT-IR and TG-DSC analyses together with SEM observations allowed to evaluate the composition of the mortars before and after the exposure. Table 3.6 4, Table 3.6 5 (see following pages, p. 194), Table 3.6 6 (p. 195) summarize the performed analyses and shown the most interesting results.

Before the exposure the same components seen for the mixtures described in Chapter 3.3 were observed: silicates and calcium carbonates were present and detected thanks to the FT-IR spectra (absorptions at $100\text{-}1100\text{ cm}^{-1}$ and 136 cm^{-1} , respectively) and thanks to TG-DSC analyses (mass losses at $50\text{-}200\text{ }^{\circ}\text{C}$ and at $650\text{-}800^{\circ}\text{C}$, respectively). The presence of calcium stearate as water repellent admixture was evidenced by the stretching absorption at $2920\text{-}2850\text{ cm}^{-1}$ in the FT-IR spectra and by the mass losses and endothermal peak at 470°C in the TG-DSC curves. No Calcium hydroxide was detected: a complete carbonation of the calcium hydroxide produced or present in the samples occurred already after 28 days of hardening, before the exposure to salt solution. SEM observations showed structures similar to the previously made mortars (see Chapter 3.3) with presence of hydrated C-S-H phases in particular in the limestone cement mortars.

After the exposure different samples were collected from the upper part of the walls (above -A) and from the lower part (below -B).

The FT-IR spectra showed that the hydration of the binders led to the formation of C-S-H, (absorptions at 950 cm^{-1}) in the limestone cement mortars and in natural hydraulic lime mortars, in particular in the lower part of the walls. Probably the higher moisture content of these areas allowed a faster hydration of the mortars. Also the spectra of the pozzolana-lime mixtures showed a moderate shift of the silicate peaks to lower wavenumbers, indicating the formation of hydrated aluminium-silicate phases. The absorptions at $1140\text{-}1100\text{ cm}^{-1}$ and at 620 cm^{-1} (stretching and bending of the S-O) pointed out the presence of sulphates, and were mostly visible in samples collected in the lower part of the walls (in particular: WCMA-B, WCM750-B, WCMcast-B, WNM750-B, WNMcast-B, WPMA-B).

TG-DSC analyses confirmed the results of the FT-IR spectroscopy, furthermore the DSC curves showed the presence of another reaction beside the decarbonation of calcium carbonate around $750\text{-}800^{\circ}\text{C}$, due to the melting of sodium chloride.

Table 3.6 4 Temperatures of transformation of the different compounds found in the mortars samples¹

Temperature $^{\circ}\text{C}$	Compound	Transformation
50-200	Silicates, alluminates, C-S-H,	Dehydration, loss of bound water
102	Sodium sulphate decahydrate	boiling
240	Sodium sulphate decahydrate	transformation to sodium sulphate
450-550	Calcium stearate	decomposition
480-620	Calcium hydroxide	dehydration
650-800	Calcium carbonate	decarbonation
800	Sodium chloride NaCl	melting

¹ MacKenzie R. C., 1970

SEM observation allowed to clearly see the presence of salt crystals and also of thick salt crusts in the samples collected in the lower parts of the mortars WCMa (limestone cement without water-repellents); WCM750, WCMcast; WNMcast. EDX elemental analysis (Figure 3.6 2) helped to understand the different present compound. Sodium, sulphur and chlorine were detected and due to the presence of sulphates and sodium chloride carried from the reservoirs through the bricks and inside the water-repellent mortars by the water.

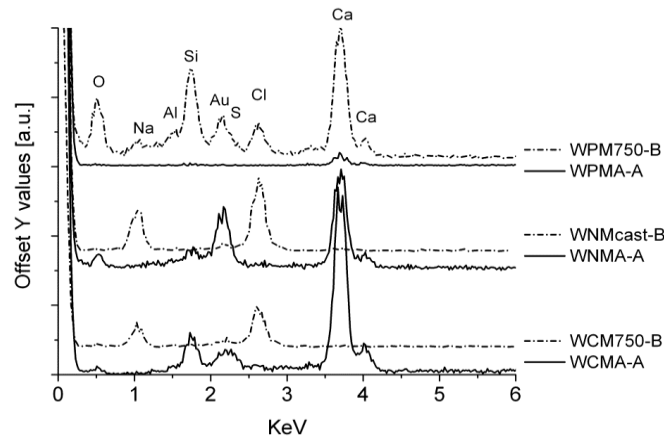


Figure 3.6 2 EDX spectra of mortar samples collected from the walls after one month of exposure to capillary rise of salt solutions.

3.6.3.2. Mechanical strength, capillary water absorption, microstructure and salt distribution

The mechanical properties and the capillary water absorption of the mortars were evaluated with specific tests² and gave precious informations about the behaviour of water repellent mortars applied on salty masonries (see Table 3.6 7 p.196). The measurements were performed: on the walls before applying the mortars, on the mortar layers after 28 days of hardening, on the mortars layers after another months of exposure to capillary rise of salt solutions.

Mechanical strength

The mechanical properties were investigated with a PT sclerometer, the values of the hammer rebound found are listed in Table 3.6 7 together with the correspondent theoretical mechanical strengths found following the indication of the manufacturer². Thanks to these measurements was possible to evaluate the mechanical strength of the walls, to compare the compressive strength of the different mortars and to find weak spots on the mortars layers.

The walls without the mortars showed a similar behaviour in the different areas with hammer rebound Φ around 35-40, which should correspond to compressive strength around 4.5-5 MPa. Limestone cement mortars after 28 days of hardening had hammer rebounds around 30. These values decrease after the salt exposure for the mortar WCM750 in the lower part of the wall and WCMcast in the medium part of the wall. Detachements of the mortar layers from the wall caused this decrease of the hammer rebounds.

Natural hydraulic lime mortars after 28 day of hardening showed hammer rebounds around 16-20, slightly lower for WNMA (without water repellents). After the salt exposure WNMA remained quite unchanged, while for the mortar WNM750 lower rebounds were registered on the upper part, where salt efflorescences appeared. WNMcast increased its strength on the

² See also Chapter 2.2.11 and 2.2.12

upper part (WNMcast-A) due to a further hardening of the mortar, but it decreased the strength on the lower part (WNMcast-B) where the mortar was damaged by the action of the salts.

WPMA, pozzolana-lime mortar without water-repellents, had hammer rebound around 25-30 after 28 days which slightly decreased after the exposure in the lower parts of the walls. The pozzolana-lime mortars with water-repellent admixtures showed also at 28 days lower hammer rebounds (25 for WPM750 and around 20 for WPMcast) probably due to a slower hydration and hardening of the binder in presence of the water repellents as observed in Chapters 3.2 and 3.3. After the exposure the hammer rebound and the mechanical strength of WPM750 and WPMcast dramatically drop, in particular in the lower part of the walls more exposed to the capillary rise.

Capillary water absorption

The capillary water absorption at low pressures was evaluated by following the indication of the RILEM Test Method II.4 water absorption tube test. The absorption degree GA after one hour and the graphs of the water absorbed versus time are shown in Table 3.6 7 p.196.

The mortars without water repellent admixtures absorbed in every case more water.

After the exposure to capillary rise of salt solutions the lower parts had always lower absorption: these areas were already moist due to the capillary rise from the reservoirs, therefore, did not absorb much water.

The limestone cement mortars and the natural hydraulic lime mortars admixed with calcium stearates (WCMcast and WNMcas) showed higher water absorption in comparison to the mixtures WCM750 and WNM750 at 28 days and absorbed more water, increasing their GA, after the exposure.

In particular for WCMcast the filtration of the water through little cracks and underneath the mortar layer was observed, the cracks and the detachments of the mortar from the walls caused the penetration of the water through the mortar and a water flow beneath the mortar layer and the wall.

WPMA showed similar capillary water absorption before and after the exposure, while the water absorption of WPM750 and WPMcast increased after the exposure. In WPMA the water was completely absorbed by the mortar, but in WPM750 and WPMcast beside the pure absorption the water penetrated underneath the mortars through little cracks.

The lower part of WPMcast (WPMcast-B) had lower water absorption/penetration through cracks because the mortars appeared more compact both before (28days of hardening) and after the exposure.

Microstructure

Mercury intrusion porosimetry, together with the SEM observation discussed above, allowed to further evaluate the microstructure of samples collected from the walls before and after the exposure, from the higher and the lower areas (see Table 3.6 8 and Table 3.6 9).

WCMA and WCMcast were characterized by a total open porosity around 30%, while the addition of sitren P750 (WCM750) caused the decrease of open porosity to 20%. The exposure caused an open porosity increasing in the lower part of the mortars WCMA and WCMcast. The pore distribution of the mortar before the exposure and of the upper part after the exposure were centred on pores around 1 μm , while the lower part after the exposure had a pore distribution centred on larger pores, around 10 μm .

Natural hydraulic mortars had open porosity around 35% before the exposure, and WNMA did not change after the exposure, also the distribution of pores did not change significantly. However, WNM750 and WNMcast increased their open porosity during the exposure and the pore distributions changed, shifting to higher pore radius (from 0.5-5 μm to over 10 μm).

The pozzolana lime mortar without water-repellents WPMA had open porosity around 23% and it maintained it and the overall pore distribution equal also after the exposure. WPMcast-B and WPMcast-A showed a porosity decrease after the exposure that might be due to the formation of thick salt crystals inside the pores or to a further hydration of the binder system.

The total open porosity increased after the exposure, it is probably due to the damaging action of the salt crystallization on the pore walls. The crystallization pressure might have induced the porosity increase. However the presence of salts inside the pores might cause also a reduction of the total open porosity clogging up the pores.

Salt distribution

The conductivity of samples collected on different areas of the walls allowed to indicate the distribution of soluble salts inside the walls. The obtained data should be considered as a general indication, because only the total content of soluble salts can be measured, and not each ion species.

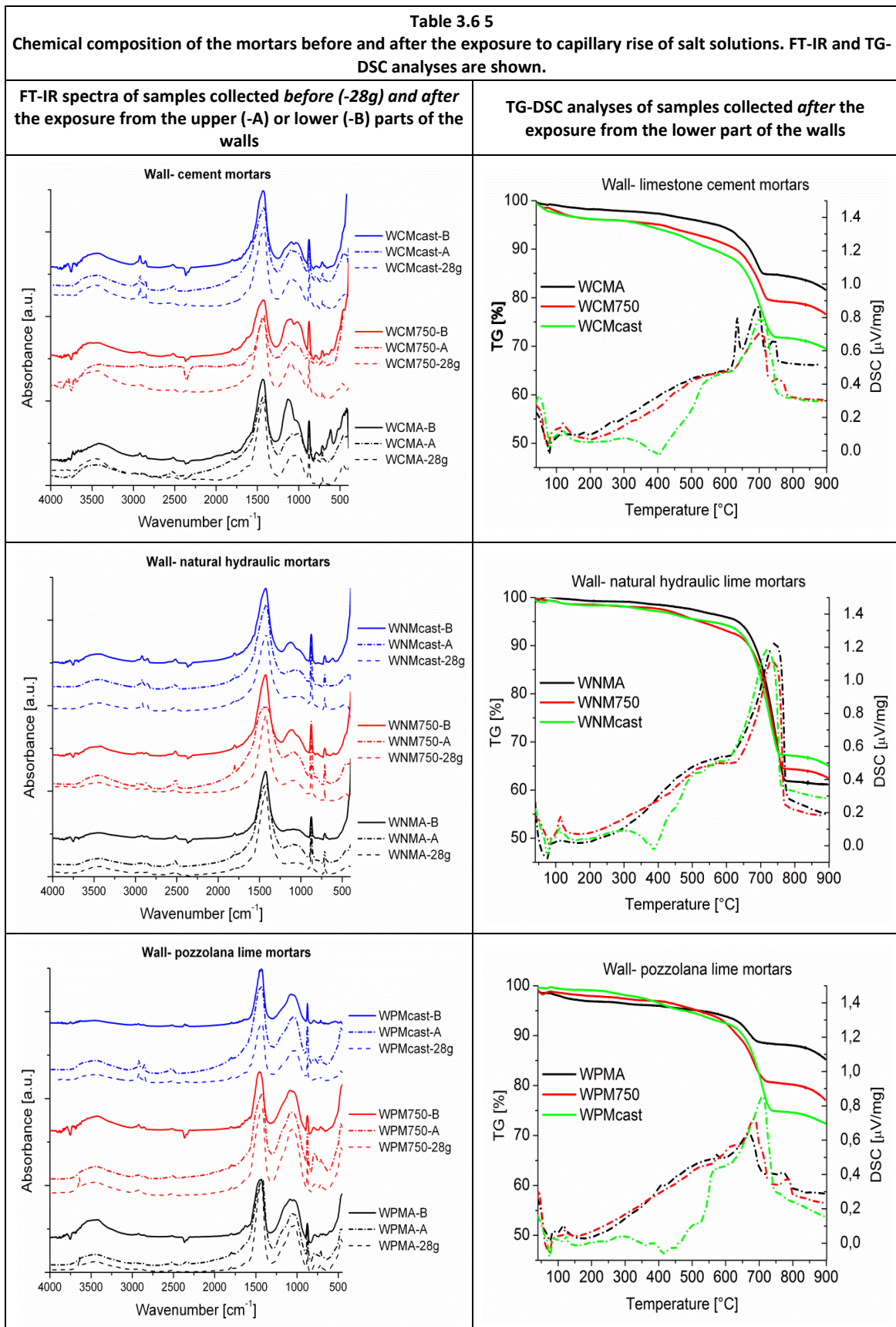
The conductivity of samples collected from the walls before applying the mortars was measured to indicate which areas had a higher concentration of salts since the beginning.

The limestone cement mortars had conductivity around 100-150 $\mu\text{s/cm}$ after 28 days, these high values were due to the presence of different ion species (in particular OH^- , Ca^{2+}) coming from the binder hydration. After the exposure, the conductivity of the lower areas increased, in particular in the case of WCMA. Probably WCM750 and WCMcast had lower increasing in conductivity because the salt solution was not able to be absorbed and to transport salt ions inside the mortar.

Natural hydraulic lime mortars showed a different behaviour. The conductivity was lower after 28 days (around 75 $\mu\text{s/cm}$) in comparison to the wall (around 100 $\mu\text{s/cm}$). After the exposure samples collected in the lower part of WCM750 and WCMcast (WCM750-B; WCMcast-B) had higher salt concentrations: in these areas salt efflorescences were visible also at naked eye observations. The admixtures did not assure a complete water-repellence and the water could flow through the mortars carrying the salts inside it.

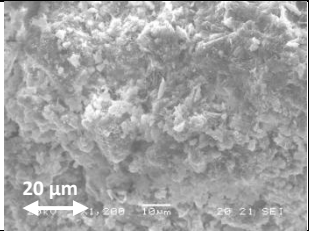
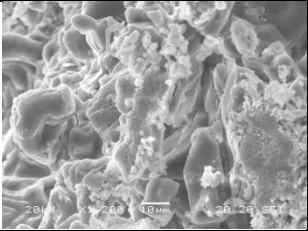
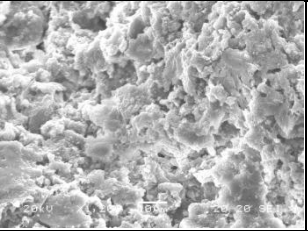
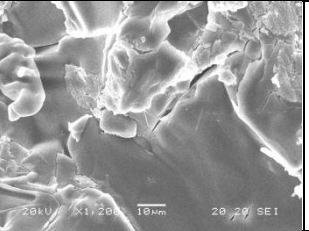
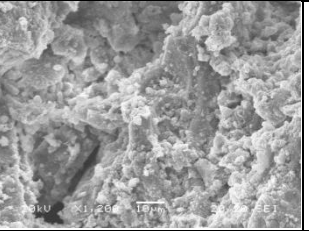
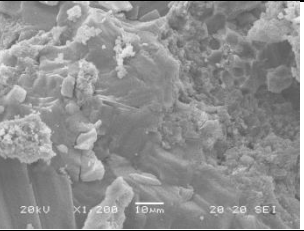
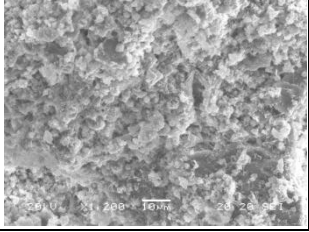
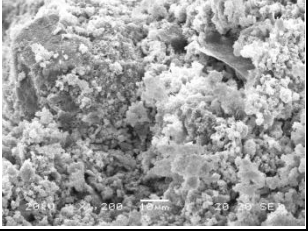
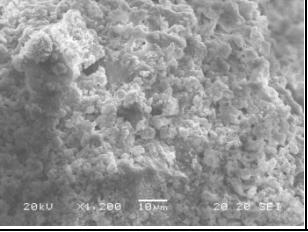
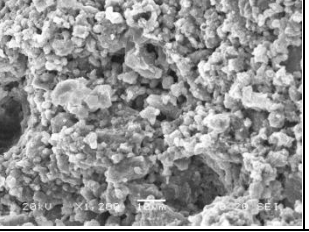
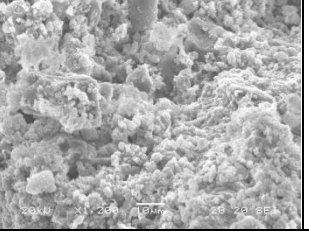
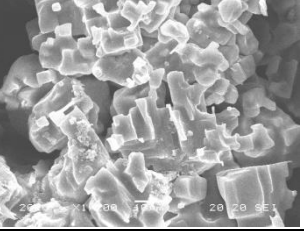
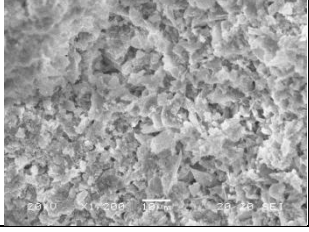
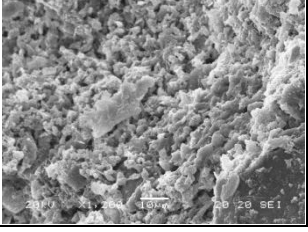
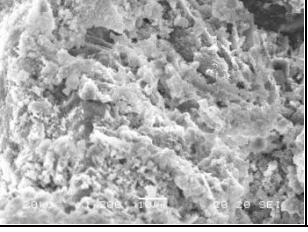
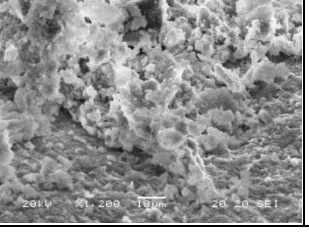
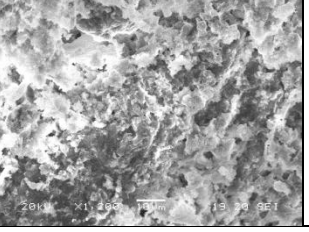
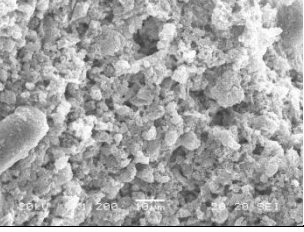
Also the pozzolana lime mortars had lower conductivity at 28 days in comparison to the wall. But after the exposure both WPMA-B and WPM750-B showed high conductivity due to a concentration of salts in these lower areas of the walls.

In presence of the water-repellents the conductivity is slightly lower for limestone cement mortars and natural hydraulic lime mortars, but higher for pozzolana-lime mortars. After 28 days (before the salt exposure) the conductivity should be mainly due to the presence of calcium hydroxide in the mortars. The delaying effect of the water repellent on the hydration reactions (see Chapter 3.2) might have caused a reduced production of $\text{Ca}(\text{OH})_2$ in WCM and WNM mortars and a reduced reaction of $\text{Ca}(\text{OH})_2$ with the pozzolana to form C-S-H in WPM mortars.



3.6 Water-repellent mortars on salty masonry

Table 3.6 6 SEM observation of the mortars applied on salty masonry after two month of exposure: samples collected from the upper part and the lower part of the walls (SEI 1200X)

Limestone cement mortars					
WCMA		WCM750		WCMcast	
above	below	above	below	above	below
					
Natural hydraulic lime mortars					
WNMA		WNM750		WNMcast	
above	below	above	below	above	below
					
Pozzolana –lime mortars					
WPMA		WPM750		WPMcast	
above	below	above	below	above	below
					

The scale rod indicates a length of 20 µm: ↔

Table 3.6 7 Mechanical and higric properties		Hammer rebound Φ sclerometer type PT			cube compressive strenght (theorical values) MPa			Water absorption GA ($\text{ml}\cdot\text{cm}^{-2}\cdot\text{h}^{-1}$)		Capillary water absorption versus time (tube method)
		wall	before	after	wall	before	after	before	after	
Wall-cement mortars	WCMA-A	34±5	31±5	30±5	3.5	3	2.8	0.53	0.61	
	WCMA-M	45±4	29±4	32±3	5	2.7	3.2	0.51	0.65	
	WCMA-B	40±4	29±2	31±2	4.5	2.7	3	0.61	0.40	
	WCM750-A	40±5	35±5	36±4	4.5	3.6	3.9	0.02	0.01	
	WCM750-M	34±6	32±3	32±3	3.5	3.2	3.2	0.03	0.02	
	WCM750-B	44±7	30±2	16±11	5	2.9	1	0.01	0.02	
	WCMcast-A	40±5	28±5	28±3	4.5	2.6	2.6	0.02	0.47	
	WCMcast-M	34±6	29±4	21±3	3.5	2.7	1.5	0.13	0.47	
	WCMcast-B	44±7	27±2	31±4	5	2.4	3	0.07	0.24	
Wall- Natural hydraulic lime mortars	WNMA-A	34±5	16±5	17±1	3.5	1	1.1	0.26	0.52	
	WNMA-M	45±4	17±3	16±2	5	1.1	1	0.22	0.63	
	WNMA-B	40±4	18±3	17±1	4.5	1.2	1.1	0.24	0.61	
	WNM750-A	39±5	26±5	22±2	4.3	2.2	1.6	0.02	0.12	
	WNM750-M	39±6	16±3	20±2	4.3	1	1.4	0.02	0.02	
	WNM750-B	41±5	20±4	21±2	4.6	1.4	1.5	0.02	0.01	
	WNMcast-A	39±5	20±5	24±4	4.3	1.4	2	0.11	0.14	
	WNMcast-M	39±6	20±3	20±2	4.3	1.4	1.4	0.28	0.28	
	WNMcast-B	41±5	22±4	18±2	4.6	1.6	1.2	0.46	0.20	
Wall- Pozzolana lime mortars	WPMA-A	34±5	21±5	24±2	3.5	1.5	2	0.67	0.70	
	WPMA-M	45±4	26±3	25±2	5	2.2	1.1	0.54	0.31	
	WPMA-B	40±4	33±3	28±4	4.5	3.4	2.5	0.37	0.54	
	WPM750-A	36±9	16±5	11±3	3.8	1	0.5	0.05	0.20	
	WPM750-M	33±5	25±5	13±7	3.4	2.1	0.6	0.37	0.01	
	WPM750-B	36±4	20±2	9±0	3.8	1.4	0.4	0.02	0.15	
	WPMcast-A	36±9	15±3	13±2	3.8	0.9	1.7	0.04	0.44	
	WPMcast-M	33±5	17±5	15±2	3.4	1.1	0.9	0.01	0.73	
	WPMcast-B	36±4	14±2	9±3	3.8	0.8	0.4	0.02	0.02	

3.6 Water-repellent mortars on salty masonry

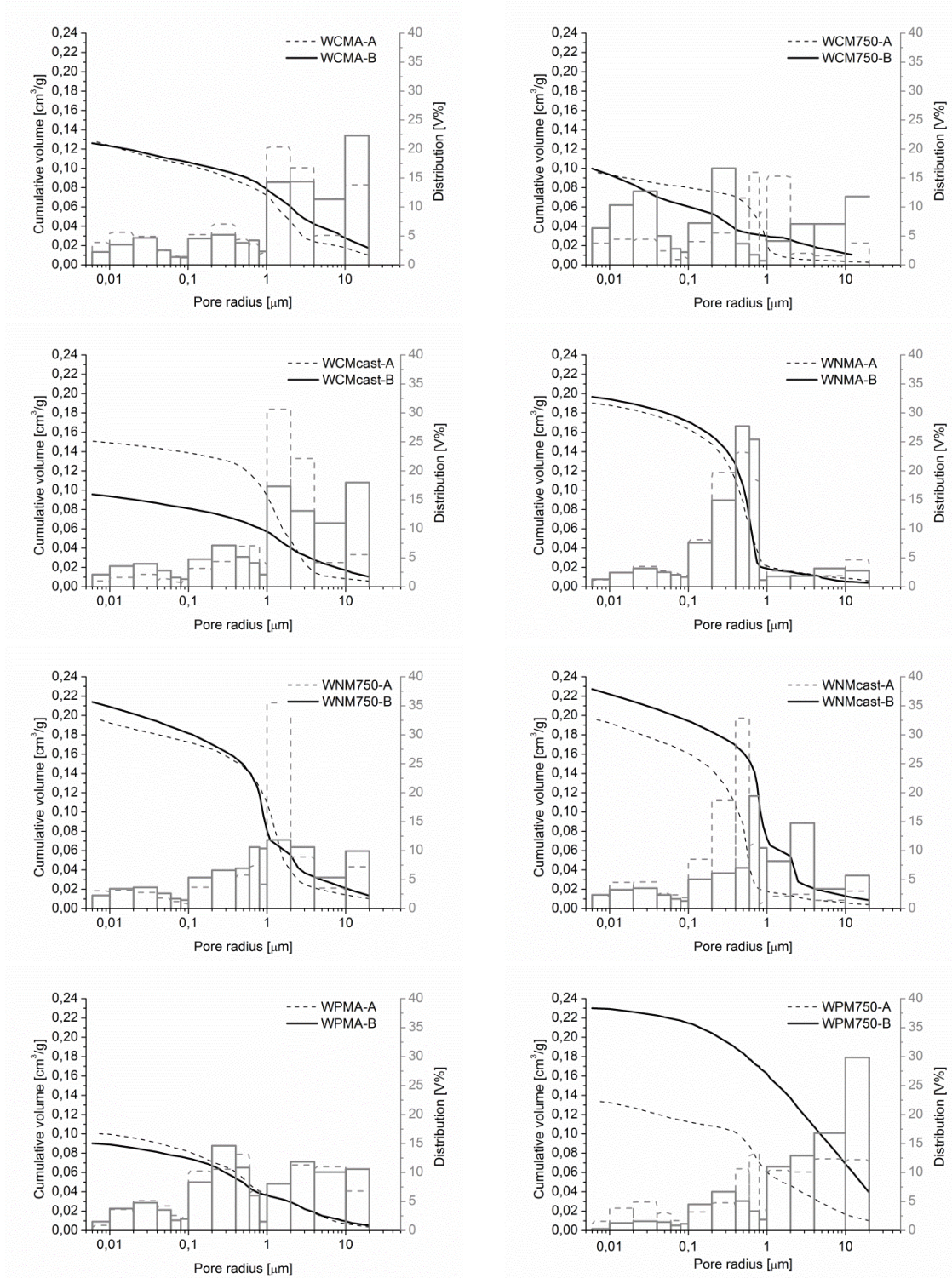
Table 3.6 8 Microstructural properties investigated through Mercury intrusion porosimeter and total content of soluble salts of samples collected from the mortars before and after the exposure. Each result is the average of three measurements. -A (above) , -M (middle) , -B(below) indicates the height of the walls were the measurements were done. The higher variations noticed are highlighted in grey.

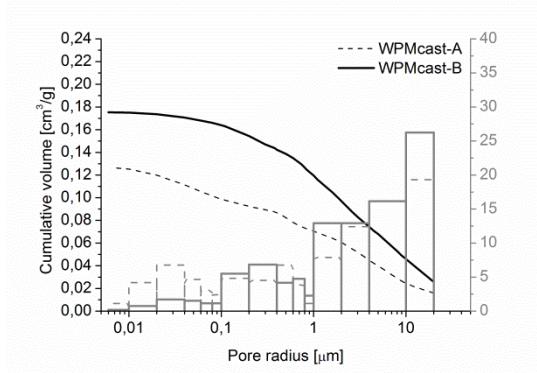
		MIP analyses										Total content of soluble salts		
		Total cumulative volume (mm ³ /g)		Bulk density (g/cm ³)		Apparent density (g/cm ³)		Total porosity (%)		Average pore radius (Micron)		Conductivity μ s/cm		
		before	after	before	after	before	after	before	after	before	after	wall	before	after
Wall-limestone cement mortars	WCMA-A	154	137	2.02	1.95	2.93	2.66	31	27	1.9	1.9	113±3	100±15	102±1
	WCMA-B	154	136	2.02	2.33	2.93	3.40	31	32	1.9	0.0	94±9	165±28	727±10
	WCM750-A	110	103	2.07	2.07	2.69	2.64	23	21	0.004	1.0	85±7	120±20	124±26
	WCM750-B	110	107	2.07	2.02	2.69	2.58	23	22	0.004	0.004	137±5	516±59	576±23
	WCMcast-A	177	155	1.87	1.95	2.79	2.79	33	30	1.3	1.4	85±7	148±49	264±4
	WCMcast-B	177	103	1.87	2.15	2.79	2.76	33	22	1.3	1.4	137±5	148±49	180±29
Wall- Natural hydraulic lime mortars	WNMA-A	194	197	1.86	1.85	2.91	2.91	36	36	0.4	0.6	113±3	76±3	56±4
	WNMA-B	194	206	1.86	1.75	2.91	2.73	36	36	0.4	0.6	94±9	76±3	71±1
	WNM750-A	218	204	1.66	1.82	2.59	2.88	36	37	1.3	1.3	120±5	57±1	73±2
	WNM750-B	218	223	1.66	1.79	2.59	3.01	36	40	1.3	0.9	82±1	57±1	882±4
	WNMcast-A	232	202	1.62	1.85	2.60	2.94	38	37	0.6	0.6	120±5	46±2	62±2
	WNMcast-B	232	237	1.62	1.74	2.60	2.95	38	41	0.6	0.8	82±1	46±2	399±16
Wall- pozzolana lime mortars	WPMA-A	111	105	2.09	2.18	2.72	2.83	23	23	0.5	0.6	113±3	55±6	47±1
	WPMA-B	111	97	2.09	2.21	2.72	2.81	23	21	0.5	0.004	94±9	55±6	682±13
	WPM750-A	211	145	1.76	2.53	2.81	3.99	37	37	0.004	0.004	61±1	74±1	61±3
	WPM750-B	128	236	2.06	1.90	2.81	3.45	26	45	0.004	8.1	159±5	74±1	597±10
	WPMcast-A	192	131	1.86	2.01	2.91	2.74	36	26	4.4	0.01	61±1	99±2	67±2
	WPMcast-B	137	118	1.98	1.92	2.71	2.48	27	23	0.004	0.004	159±5	99±2	95±15

Table 3.6 9

MIP analyses of mortars applied on salty masonries

The graphs illustrates the cumulative volume of mercury intruded and the pore distribution of samples collected after one months of exposure to capillary rise of saline solutions. The mixture name used were described above in Table 3.6 1, A=above, sample collected from the upper part of the wall; B=below, sample collected from the lower part of the wall. The graphs continues on the following page.





MIP analyses of mortars applied on salty masonries

Continues from the previous page-The graphs illustrates the cumulative volume of mercury intruded and the pore distribution of samples collected after one months of exposure to capillary rise of saline solutions. The mixture name used were described above in Table 3.6 1, A=above, sample collected from the upper part of the wall; B=below, sample collected from the lower part of the wall.

4 Discussion, conclusions and perspectives

The research have been divided into five main steps.

- Study of the hydration reaction of binder pastes admixed with water-repellents.
- Study of the chemical-physical properties of water repellent mortars and effectiveness of the water repellent admixtures in different mortar mixtures.
- Durability of water repellent mortars exposed to UV-light and rain.
- Resistance of water repellent mortars to salt crystallization.
- Study of water repellent mortars applied on salty masonries.

The data and the results of each step have been described by as many chapters in the previous section (chapter 3 Results).

In the present chapter the data are further analyzed, interconnected and discussed, using also statistical multivariate approaches. A discussion and summary of the main results is given for each step. The discussion goes on with the experimental application of statistic methods as tool to evidence the main results obtained.

The study ranged from the comprehension of the hydration mechanism to the evaluation of the behaviour in different situations and also when the mortars are applied in real cases on walls subjected to capillary rise of salt solutions.

The originality of the thesis is the complete study of water repellent mixtures, both from the chemical and the physical point of view. The parallel study of mortars made of different binders but admixed with same water-repellents allowed to investigate the influence of the water-repellents on the systems.

4.1 Discussing the results of Chapter 3.2: mechanisms of reaction of binders in presence of water-repellent admixtures

The chapter 3.2 regarded the hydration of binder pastes and the influence of water-repellent admixtures on it. In this paragraph, a summary of the reaction mechanism is given on the basis of the experimental evidences. The hydration mechanisms of the different binders alone and in presence of water-repellents are separately discussed considering also the vast literature published¹. The commonly used cement chemical nomenclature will be used, together with the usual chemical notation.

4.1.1 HYDRATION REACTIONS OF LIMESTONE CEMENT PASTES WITHOUT AND WITH WATER-REPELLENTS

Considering the results obtained from the different analytic techniques used, it turned out that the hydration mechanism of the limestone-cement pastes was different from the hydration reactions of an ordinary Portland cement OPC^{2,3}. Figure 4. 1 summarizes the tentative reaction mechanism of limestone cement pastes as obtained by the experimental results.

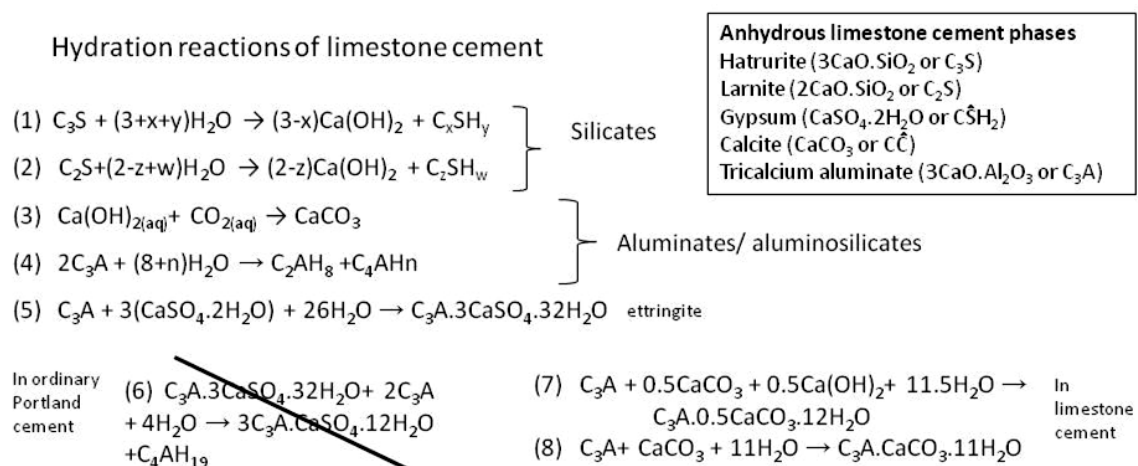


Figure 4. 1 Hypothesis of hydration mechanism of limestone cement pastes without water repellent (© L. Falchi 2013)

The principal phases founded in the anhydrous limestone cement studied were: hatrurite; larnite; gypsum; calcite; tricalcium aluminate.

During the hydration of the limestone cement paste without water-repellents the reactions (eq. 1) and (eq. 2) in Figure 4. 1 occurred, involving hatrurite and larnite and causing the formation of C-S-H and calcium hydroxide. XRD and TG-DSC data confirmed the consumption of C_3S and the formation of C-S-H and calcium hydroxide in the form of portlandite from early ages. The maximum production rate of calcium hydroxide and C-S-H was observed within the first 7 days, after that the production still went on slower. According to the SEM observations, the C-S-H precipitated on the clinker grain surfaces as poorly crystalline acicular structures (C-S-H type I),

¹ Collepardi, M. 1980; Lea, M., 1997; Taylor, H.F.W., 1997; Ramachandran, V.S., 1969

² Trezza, M.A, A.E Lavat, 2001; De Weerd, K. et al., 2011; Lothenbach, B., 2008; Tsvilis, S., et al., 1998; Hawkins, P., 2002; Odler, I. 2002

³ Collepardi, M. 1980; Lea, M., 1997; Taylor, H.F.W., 1997; Ramachandran, V.S., 1969

and was still visible also after 56 days. SEM observations allowed also to recognize portlandite with its typical hexagonal crystals. Even if the carbonation of calcium hydroxide was limited by the storage condition (pastes in closed vessels) the production of new calcite due to dissolved CO_2 in the liquid phase was not completely arrested.

In presence of calcium sulphates, tricalcium aluminates hydrated quickly forming calcium aluminate hydrates (eq. 4) and ettringite as the main hydration product (eq. 5). XRD analysis confirmed that gypsum was consumed in limestone cement pastes within 7 hours, while ettringite appeared and was recognized after 1 day. The formation of hexagonal platelets of C_4AHn was also observed. Ettringite and C_4AHn might have been present also as solid solution of both phases.

In ordinary Portland cements, when calcium sulphate is completely consumed, the ettringite starts to react with additional amounts of tricalcium aluminate, yielding calcium aluminate monosulphate hydrate (eq. 6). However, in presence of high percentages of calcium carbonate, as in limestone cements, the reaction (eq. 6) do not occur and carbonates phase are instead produced as described by equations 7 and 8 in Figure 4.1⁴. XRD measurements evidenced the formation of ettringite after 1 day, followed by the hemicarbonates after 7 days and their transformation into monocarbonates after 14 days. In the meanwhile the presence of ettringite remained constant and was detected till 5 months. Also Klemm and Adams⁵, working on similar system, found out that crystalline monocarbonate hydrate is slower to form than ettringite and that the most stable reaction phase would be ettringite, followed by monocarboaluminate and the monosulfoaluminate. Furthermore, SEM observation and FT-IR analysis (presence of a peak at 1600 cm^{-1}) showed that the transformation of hexagonal C_4AH_{19} into cubic C_3AH_6 did not occur also after 56 days.

The hydration reactions described above occurred in different stages. A pre-induction period began immediately upon contact of water with cement, with a rapid dissolution of ionic species into the liquid phase. First of all alkali sulphates and gypsum dissolved until saturation, contributing K^+ , Na^+ , Ca^{2+} , SO_4^{2-} ions. Tricalcium aluminate dissolved and reacted with Ca^{2+} and SO_4^{2-} ions present in the liquid phase and yielding ettringite. Also tricalcium silicate (C_3S) started to dissolve and hydrate and a layer of C-S-H phases precipitated at the cement particle surfaces. At this stage the fraction of C_3S hydrated remained low but the concentration of Ca^{2+} and OH^- in the liquid phase increased. After the pre-induction period, an induction (dormant) period was observed in the first three hours, when the hydration rates slowed down. The acceleration stage began after 5 hours and corresponded to: a faster hydration of C_3S ; the formation of C-S-H from C_2S ; the precipitation of crystalline portlandite from the supersaturated liquid phase. Isothermal calorimetry allowed to individuate the formation of aluminum-hemicarbonates and monocarbonates (visible from the 24h-48h with XRD) after 1 day. In the post acceleration period, C-S-H continued to be formed from C_3S and C_2S ; monocarbonates still formed, while ettringite remained stable.

The presence of *siloxanes water-repellents* influenced the hydration mechanism in different way, but always causing a slight hydration delay. When a siloxanes supported on inorganic carrier (Sitren P750®, Sitren P730®, Silres A®) was added the hydration reaction was slightly affect: less

⁴ Lothenbach, B., 2008; Tsvivilis, S., et al., 1998; Trezza, M.A, A.E Lavat, 2001

⁵ Klemm, W., L.D. Adams, 1990

$\text{Ca}(\text{OH})_2$ was present after 28 days, higher presence of hexagonal aluminates was seen and the hemicarbonatic phase remained stable for longer periods (except for CP730). When the liquid siloxane Tegosivin HE 328[®] was added the reaction rate decelerate: delayed precipitation of portlandite and diminished production of calcium hydroxide occurred.

The delay should mainly due to the hydrophobic nature of the admixtures which, disposing itself on the clinker grains, should be able to create a hydrophobic barrier to the water, delaying the hydration.

To better explain how this barrier could be formed we should consider the composition of the products used. According to the information given by the manufacturers⁶, the products were composed of organomodified siloxanes that contain dimethylsiloxy units $[\text{Me}_2\text{SiO}-]$ and different organic end groups⁷. The silicon-oxygen backbone of these compounds should give them affinity for the binder while their organic end groups impart a strong water repellency.

The adsorption of silane/siloxane on the surfaces of clinker grains might then occur:

- by electric interactions between the silicon oxygen backbone;
- by the formation of strong bonds due to a complete hydrolysis-condensation reaction between the alkoxy groups of these products and cement⁸.

In the powder products *Sitren P750[®]*, *Silres A[®]* and *Sitren P730[®]*, the siloxanes showed the tendency to slowly separate from the carriers in alkaline environment (see paragraph 3.1). Thereafter, the inorganic carrier grains might also participate to the hydration reactions. In fact, amorphous silica particles might enhance the cement hydration with a pozzolanic activity⁹, while fine calcium carbonate particles (present in *Sitren P730[®]*) can act as aggregation sites and filler between the grains of clinker or participate to the hydration reaction of C_3A and promote a faster formation of monocarboalluminates $\text{C}_4\text{A}\hat{\text{C}}\text{H}_{11}$ (see also reaction 7 and 8).

When *Sitren P750[®]*, *Silres A[®]* and *Sitren P730[®]* were added, the delaying effect of the hydrophobic silane/siloxanes layer on binder grains might have been partially balanced by the favourable effect of the little amount of amorphous silica or calcium carbonate on the hydration.

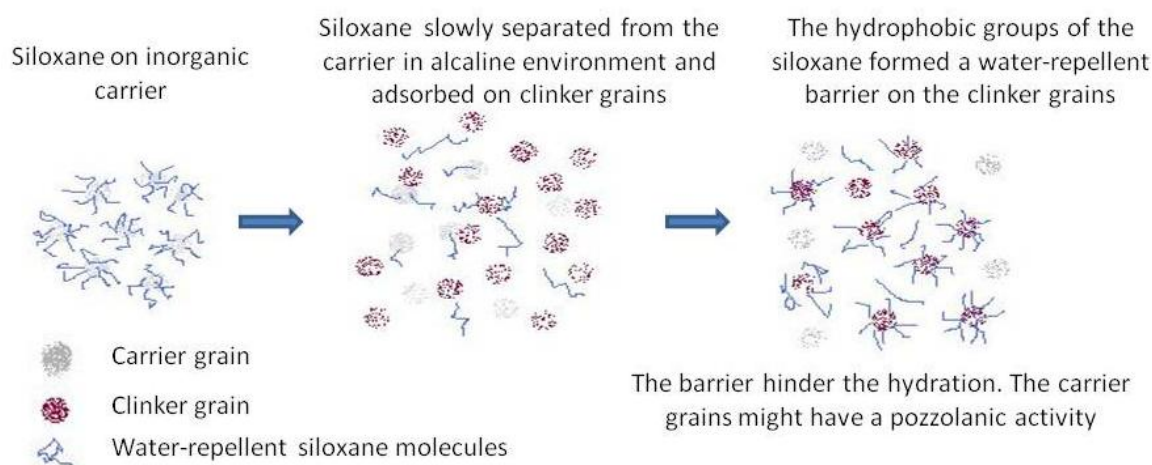


Figure 4. 2 Interaction of powder siloxane products on binder hydration (© L. Falchi 2013)

⁶ <http://www.construction-chemicals.com/product/construction-chemicals/Documents/elements-29-chemical-umbrella-for-buildings-2010.pdf>. See also Appendix 1.

⁷ Alkyltrialkoxysilanes such as isobutyltriethoxysilane, n-octyltriethoxysilane and iso-octyltriethoxysilanes are highly suitable for hydrophobization purposes and have been used in the products studied.

⁸ See also chapter 2 1.4.4.2. Silane /siloxanes

⁹ Mongkhon Narmluk, Toyoharu Nawa, 2011; Esteves, L. P, 2011; Schwarz, N., N. Neithalath, 2008

The addition of *calcium stearate* to limestone cement mixes decreased significantly the hydration rate. In particular, XRD and SEM results pointed out a higher formation of ettringite instead of hexagonal aluminates and TG-DSC measurements showed a delayed formation of Afm phases (monocarbonicaluminates). The principal explanation to this delay might be the adsorption of calcium stearate on clinker grains and on calcium carbonate. Ion exchange of calcium stearate with calcium carbonate or calcium present in the silicates allow the formation of an hydrophobic calcium stearate layer on the grain surfaces¹⁰. M. Song reports a complete analysis of the mechanism of stearates adsorption on calcium carbonate which consider that: "In aqueous solutions, stearate ions would react at the calcium carbonate surface as explained in Figure 4. 3 by equation (9), in addition can easily form calcium stearate precipitates following the equations (10) and (11). The surface layers could be composed of calcium ions, stearate ions, $\text{Ca}(\text{stearate})^+$ and complex precipitate". The hydrophobic layer resulting from this ionic change constitute a barrier for the normal hydration of the clinker phases. Probably the calcium stearates exchanged ions and covered preferentially the limestone particles, rendering them water repellent and preventing them to contribute to the reaction. This could explain the minor production of monocarbonates observed.

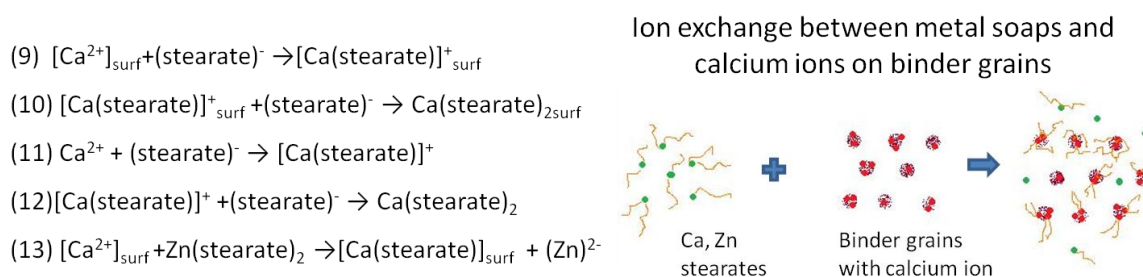
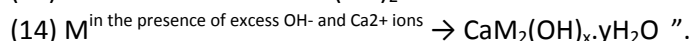
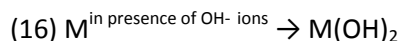


Figure 4. 3 Adsorption of metal soaps on binder grains (© L. Falchi 2013; equations from Lanzón, M., et al. 2011)

Marked delay in the hydration reaction rate was observed when *zinc stearates* were added: less formation of calcium hydroxide (observed thanks to XRD, TG-DSC, SEM), minor formation of CSH after 56 days (as indicated by FT-IR analysis) and a delayed acceleration stage (detected by isothermal calorimetry). In this case the hypothesis of a direct ion exchange mechanism between zinc stearate and calcium carbonate grain or calcium ions present in solution is proposed (Figure 4. 3 equation nr 13) and supported by the similar behaviour observed for zinc stearates in calcium hydroxide saturated solution (see chapter 3.1).

Furthermore, several studies underlines the delaying effect of zinc ions on the cement hydration¹¹. As Caroline Weeks¹² states, the delay is more likely attributed to: "the formation of calcium hydroxyl-zincate. This reaction consumes calcium and hydroxide ions from solution and delays the supersaturation and precipitation of calcium hydroxide and development of C-S-H gel. A generalised equation for the conversion of the retarding species, M, for example Zn, Pb or Sn, would therefore be:



Zinc ions can also substitute calcium in the crystal lattice of ettringite to variable extent¹³.

¹⁰ Song, M., et al. 2003; Wang, Z., et al., 2006; Lanzón, M., et al. 2011

¹¹ Chen, Q.Y., et al. 2007; Gineys, N., et al., 2010; Weeks, C. et al. 2008; Berger, S., et al., 2009

¹² Weeks, C. et al. 2008

¹³ Albino, V., et al. 1996

4.1.2 HYDRATION REACTIONS IN NATURAL HYDRAULIC LIME PASTES WITHOUT AND WITH WATER-REPELLENTS

Natural hydraulic lime had peculiar hydration reactions, in comparison to Portland cement, due to the presence of a high quantity of calcium hydroxide, calcium carbonate and dicalcium silicate C_2S , instead of tricalcium silicate C_3S .

Figure 4. 4 summarizes the reaction involved in the hydration of the natural hydraulic lime pastes.

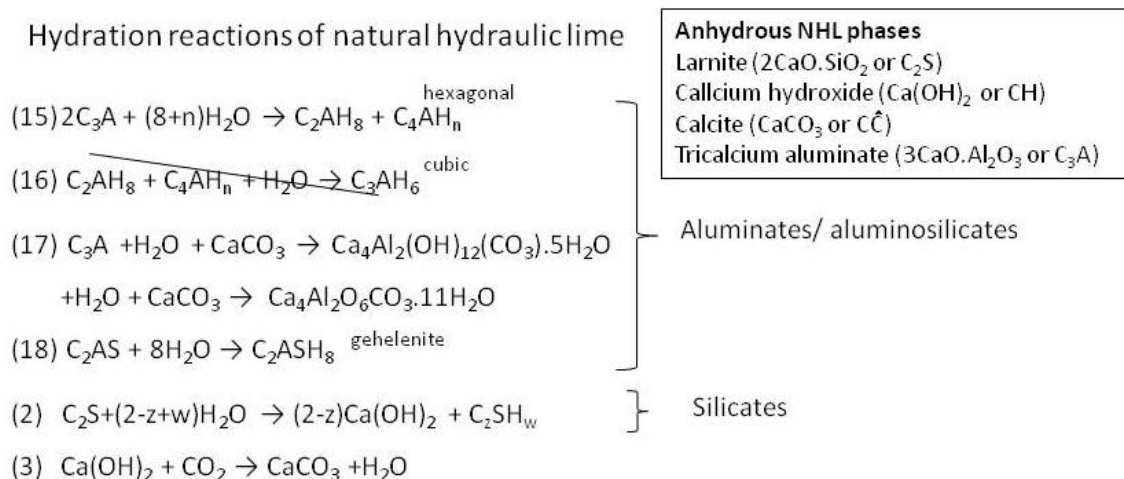


Figure 4. 4 Proposed mechanism of hydration of NHL pastes without water-repellent admixtures (© L. Falchi 2013; equations from Collepardi, M. 1980)

In the anhydrous natural hydraulic lime, a high presence of larnite C_2S , a minor presence of halite C_3S and tricalcium aluminates C_3A were confirmed by XRD measurement, together with the presence of a 32% of $CaCO_3$ and 10% of $Ca(OH)_2$ (TG-DSC measurements on the starting materials).

After the preparation of the pastes, the hydration reaction of larnite was slower in comparison of halite and the general hydration involved first of all the hydration of C_3A phases.

The absence of gypsum or other sulphates species allowed the formation of hexagonal aluminates from the hydration of tricalcium aluminate C_3A as described by reaction (15) in Figure 4. 4¹⁴. A further reaction of hexagonal C_4AH_n leading to the formation of cubic C_3AH_6 , see equation (16), was not observed with XRD or with SEM in this study probably because of the competitor reactions involving C_3A and calcium carbonate. XRD analysis showed, in fact, evidences of the formation of aluminium-carbonatic phases such as calcium aluminium hydroxide hydrate $Ca_4Al_2(OH)_{12}(CO_3) \cdot 5H_2O$ and calcium aluminium oxide carbonate hydrate $Ca_4Al_2O_6CO_3 \cdot 11H_2O$ (eq. 17). After 3 months were observed only hemicarbonatic phases and mono carbonatic phases. SEM observations in this first period showed the formation of a gel-like structure around the binder grains and of hexagonal crystals of $Ca(OH)_2$ and aluminates.

The slow hydration of C_2S led to the formation of hydrated silicates as described by equation 2, and acicular C-S-H structures around the binder grains after 28 and 56 days were visible thanks to SEM analysis. A minor presence of gehelenite hydrate C_2ASH_8 was also detected with XRD after 21 days arising from the hydration of C_2S in alumina rich solution (see equation 18).

¹⁴ Lea, M. 1997, p.260

The presence of *silane/siloxane water-repellents* did not seriously influenced the hydration reactions. No differences were observed in the evolution of the hydrate products with XRD analysis in NHL750 and NHL730, while in presence of silres A® (NHLsil) a prevalent formation of calcium-aluminium-hydroxide-carbonate-hydrate was observed. The FT-IR analysis showed, however, a fast formation of amorphous CSH (950 cm⁻¹ absorption) and after 28 days acicular structure of CSH were visible with SEM observation of NHL750 and NHLsil. TG-DSC measurements highlighted the formation of lower percentages of calcium hydroxide in comparison to NHLA, in particular for NHLsil and NHL750.

The general slight slowdown of the hydration reaction should be due to the presence of water repellent silane/siloxanes on the surface of binder grains. As in limestone cement pastes (see above), the alkaline environment should allowed the chemical reaction of the siloxane with the CSH phases and a partial coverage of the binder particles, while the presence of amorphous silica grains or calcium carbonate grains should promote a pozzolanic reaction, in particular after 7-14 days. The presence of a water repellent layer physically slowed down the hydration, while the pozzolanic activity of the carrier grain might accelerate it.

Calcium and zinc stearate caused a stronger slowdown of the hydration, with less CSH produced even after 28 days (SEM observations and FT-IR analysis) and lower amount of calcium hydroxide (TG-DSC analysis). XRD measurements detected a higher presence of gehlenite after 28 days. The influence on the hydration reaction is probably due to mechanisms similar to the ones proposed above for limestone cement. Also in NHL pastes the presence of stearate adsorbed on calcium carbonate grains can form an hydrophobic layer. This barrier delayed the hydration of the C₂S and the saturation of the solution with Ca²⁺ and OH⁻ ions and the consequent precipitation of portlandite.

4.1.3 HYDRATION REACTIONS IN HYDRAULIC POZZOLANA-LIME PASTES WITHOUT AND WITH WATER-REPELLENTS

Figure 4. 5 summarizes the proposed mechanism of hydration of pozzolana-lime pastes without water-repellent admixtures.

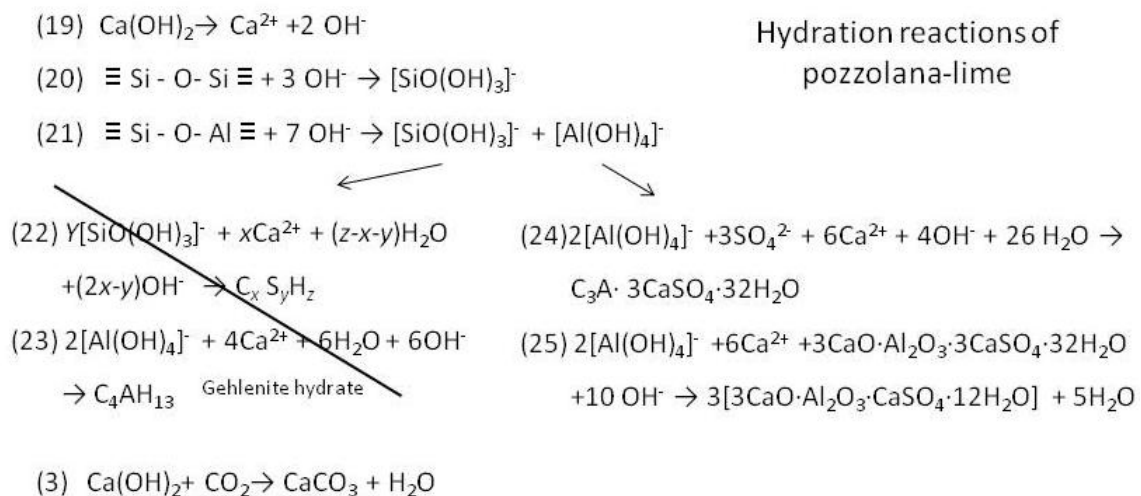


Figure 4. 5 Proposed mechanism for the hydration of pozzolana-lime pastes without water-repellent admixtures (© L. Falchi 2013)

The pozzolanic reaction proceeded from the mixing of calcium hydroxide with natural pozzolanas and water¹⁵. When water was added to the mix of lime and pozzolanas the calcium hydroxide dissolved and a basic solution (pH ~12,5 at 20°C) of calcium hydroxide was formed (see Figure 4. 1 eq. 19).

The cations Ca^{2+} , K^+ , Na^+ , etc. situated between the silicates and alluminates layers/chains were dissolved in the solution quickly, because of the basic pH and the presence of OH^- . Also the silicates and aluminosilicates networks were partially dissolved (eq. 20 and 21 in Figure 4. 5). This dissolved monosilicates and aluminates species were able to react with the Ca^{2+} ions in solution. Literature studies¹⁶ report that usually the reaction products is a poorly crystallized gel of calcium hydrosilicate C-S-H, gehlenite hydrate C_4ASH_8 and hydrogarnets $\text{C}_3\text{ASzH}_{6-2z}$, such as katoite $[\text{C}_3\text{A}(\text{S})_{3-x}(\text{H})_{2x}]$ (with $1.5 \leq x \leq 3$) (see eq. 22, 23). However, the experimental data collected suggested that only amorphous gel-like CSH was formed (recognized by FT-IR and SEM-EDX measurements), while C_4AH_{13} , hydrogarnets or other commonly found zeolites were not detected by XRD analysis. Instead of these aluminates phases, Aft and Afm carbonatic phases were recognized. Caijun Shi¹⁷ reported that if sulphates are present Aft phases ($[\text{Ca}_3(\text{Al,Fe})(\text{OH})_6 \cdot 12\text{H}_2\text{O}]_2 \cdot \text{X}_3 \cdot x\text{H}_2\text{O}$) forms first, but usually the sulphate content of natural pozzolan is low and the Aft transforms to Afm ($[\text{Ca}_2(\text{Al,Fe})(\text{OH})_6] \cdot \text{X} \cdot x\text{H}_2\text{O}$) (see eq. 24, 25).

In our case, the substitution of SO_3 with CO_3 occurred and led to the consequential formation/transformation of para-aluminumhydrocalcite $\text{CaAl}_2(\text{CO}_3)_2(\text{OH})_4 \cdot 6\text{H}_2\text{O}$, calcium aluminum oxide carbonate hydroxide hydrate $\text{Ca}_4\text{Al}_2\text{O}_6(\text{CO}_3)_{0.5}\text{OH} \cdot 11.5 \text{H}_2\text{O}$, calcium aluminum oxide carbonate hydrate $3\text{CaO} \cdot \text{Al}_2\text{O}_3 \cdot \text{CaCO}_3 \cdot 11\text{H}_2\text{O}$ after 1, 28, 140 days of hydration, respectively.

A higher concentration of Ca^{2+} was needed for the formation of aluminate hydrates, which were formed away from the pozzolana grains, while the silicates were formed on the surfaces of the grains. The dissolution of alumina-silicates glass determined the total reaction rate, because was the slowest step. After the precipitation of hydrated products on the outer surfaces of the pozzolana the reaction proceeded under diffusion control of OH^- and Ca^{2+} through the precipitated products and became a topochemical reaction.

The presence of *silane/siloxanes* supported on silica grains Sitren P750 caused an enhanced formation of gel-like C-S-H after 28 day and the formation of acicular structures of C-S-H type I after 84 days in HL750 (see SEM-EDX observation and FT-IR analysis). Probably the carrier grains had a pozzolanic effect similar to silica grains in cement pastes. This pozzolanic activity of the carrier enhanced the production of amorphous C-S-H instead of crystalline carbonate-aluminates.

However, the hydration of HLsil, with silres A[®], seemed delayed: FT-IR analysis did not show a high peak at 950 cm^{-1} due to C-S-H after 84 days (clearly visible in HL750), and lower TW and higher $\text{Ca}(\text{OH})_2$ contents were found with TG-DSC measurements. In this case Silres A[®] was probably adsorbed on the pozzolana surfaces creating an hydrophobic barrier which prevent a normal hydration.

The liquid silane Tegosivin allowed the production of coherent and compact gel-like C-S-H from the 28 days, but also a faster transformation of calcium aluminum oxide carbonate hydroxide

¹⁵ Shi Caijun, 2000

¹⁶ Donchev, I., 2010; Sepulcre-Aguilar, A., 2010; Gualtieri, A.F., 2006

¹⁷ Shi Caijun, 2000

hydrate $\text{Ca}_4\text{Al}_2\text{O}_6(\text{CO}_3)_{0.5}\text{OH}\cdot 11.5 \text{ H}_2\text{O}$ in calcium aluminum oxide carbonate hydrate $3\text{CaO}\cdot\text{Al}_2\text{O}_3\cdot\text{CaCO}_3\cdot 11\text{H}_2\text{O}$.

Pastes with Sitren P730®, supported on calcium carbonate grains, showed a fast formation of the latter compound ($3\text{CaO}\cdot\text{Al}_2\text{O}_3\cdot\text{CaCO}_3\cdot 11\text{H}_2\text{O}$) too, due to a higher availability of carbonates.

Calcium stearates and zinc stearates caused a delayed formation of calcium oxide carbonate hydrate, but the formation of carbonate phases was confirmed also by the double stretching absorptions at $1420\text{-}1450 \text{ cm}^{-1}$ in the FT-IR spectra. Gel-like C-S-H was detected with SEM only after 84 days (in HLA samples was present after 56 days). Also the FT-IR analyses confirmed a delayed production of C-S-H in HLznst pastes.

The delay was probably caused, as seen above for the other binders, by the ion exchange and adsorption of the long hydrophobic chains of stearates/palmitates on pozzolana and calcium hydroxide grains. In pozzolana-lime pastes, the dissolution of portlandite covered by hydrophobic stearates into the reaction solution might be prevented and the whole pozzolanic reaction proceeded slower.

4.2 Discussing the results of Chapter 3.3: Physico-chemical properties of mortars with water-repellents

The study of several chemical-physical properties of mortars with water-repellents allowed to evaluate the influence of different water repellent agents on distinct mortar systems such as limestone cement CM, natural hydraulic lime NM, pozzolana-lime PM.

The studied physical-chemical properties can be divided into three groups:

- Properties of the fresh mortars which might be related to the moment of the application of the mortar and give information on its workability;
- Physical and structural properties of the hardened mortars such as the density, porosity, microstructure, mechanical strength;
- Properties related to the behaviour of the hardened mortars in respect to water and water vapour such as water vapour permeability, capillary water absorption or surface wettability.

Several data were collected and it was tried to compare them by using different methods in order to find out possible common trends:

1. some physical properties have been directly compared with two-variables scatter plots;
2. a sort of “score” system for some of the most interesting variables was tentatively developed;
3. The correlation of the physical properties was further studied by multivariate statistic methods such as Principal component analysis (PCA).

The third point, i.e. the chemometric study of the physical properties of the mortars with PCA analysis, will be discussed in Chapter 4.6 Correlation of physical properties of water-repellent mortars: a multivariate approach at page 220.

Here, we would like to focus the attention to the first and second points, starting with the comparison of the properties studied thanks to two-variables scatter plots.

The two-variables scatter plots (Figure 4. 6) allowed to observe that the major differences which regarded the physical and structural properties of the hardened mortars were found between one mortar system to another. In fact, three different and separate groups can be observed plotting structural properties such as compressive strength versus total open porosity or ultrasonic measurements versus total open porosity. The structural characteristics of mortar mixtures with water repellents changed, therefore, primarily according to the mortar system. CMvin samples showed always a different behaviour and they were considered as a separate group.

It was also possible to observe a common trend inside each group: the mechanical properties or the ultrasonic measurements decreased with increasing porosity. However, the low R^2 found demonstrated that this correspondence was not completely linear and weak, in particular if NM (natural hydraulic lime) and PM (pozzolana-lime) groups were considered.

In a similar way the bulk density was correlated with the mechanical strength and the ultrasonic measurements.

The two-variables scatter plots (Figure 4. 6) of the permeability versus the total open porosity shows that a feeble correlation might be present allowing to distinguish a group formed by NM+CMvin from a CM+PM group, but no linear trends were found inside each group.

The capillary water absorption was not correlated with micro structural properties such as the total open porosity, but it depended more on the water-repellent used. Also the three groups NM, CM, PM, were not clearly separated.

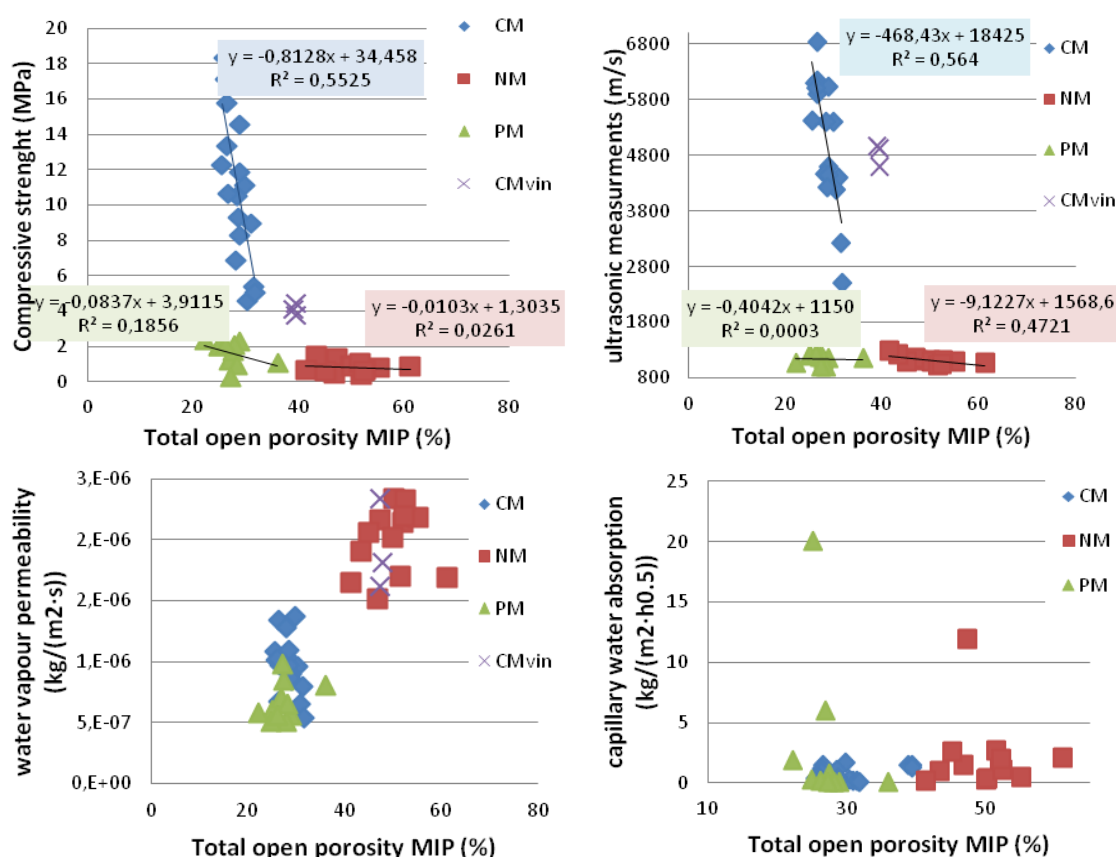


Figure 4. 6 From right to left and above to below. Relationship between: the compressive strenght and the total open porosity; ultrasonic measurements and total open porosity; water vapour permeability and total open porosity; capillary water absorption and total open porosity. CM= limestone cement mortars; NM=natural hydraulic lime mortars; PM= pozzolana-lime mortars; CMvin= limestone cement mortars admixed with Vinnapas 8031®.

In order to further summarize the results, it was tentatively developed a sort of “score” system for some of the most interesting variables, which is shown in Table 4. 1 and Table 4. 2: + indicating an high absolute values, - indicating low absolute values¹⁸. We took into account the results of the following test, chosen as meaningful¹⁹: the slump diameter to evaluate the consistence and workability of fresh mortars; the density and the open porosity of 28 days mortars to evaluate the structure; the compressive strength to evaluate the mechanical performances; the water vapour permeability; the capillary water absorption to evaluate the behaviour in presence of liquid water.

By observing Table 4. 2 and the results reported above, we can notice that the consistence of the fresh mortars is a property which depend on the added water-repellent and to the mortar system. The use of the silane/siloxanes caused a better consistence of the natural hydraulic lime and of the pozzolana-lime mortars, and a worse consistence of limestone cement mortars. The use of calcium stearates led to a better consistence of limestone cement mortars and natural hydraulic lime and to a worse consistence of the pozzolana-lime mortars. The use of zinc stearates caused quite always a worsening of the consistence properties.

It is not clear why the same admixtures caused a different consistence in different system. In the case of natural hydraulic lime mortars it should be considered that the formulation also contained plasticizers and the water repellents cannot influenced much the consistence of the fresh mortars. In the case of limestone cement mortars, it is possible that calcium stearates worked as plasticizers, while in the pozzolana-lime mortars the stearates might have interacted with the calcium hydroxide.

According to literature studies on OPC mortars or concrete, the bulk density, the open porosity and the mechanical strength are correlated properties, which mainly depend on the mortar structure. The correlation was observed also in this study:

- the bulk densities of limestone cement mortars and pozzolana-lime mortars are higher than the ones of natural hydraulic lime mortars;
- to the high bulk densities of the limestone cement mortars correspond low open porosities, high mechanical strengths; to the low bulk densities of the natural hydraulic lime correspond high open porosities, very low mechanical strengths, high water vapour permeabilities;
- to the high densities of the pozzolana-lime mortars correspond low open porosities but also low mechanical strengths. In particular the use of zinc stearates caused the worse mechanical strengths detected.

The mechanical properties depended on the bulk densities and on the hydration of the binder. Limestone cement mortars developed, in every case, high mechanical strengths in comparison to natural hydraulic lime mortars or pozzolana-lime mortars due to the formation of silicate hydrates and a strongly interlinked microstructure.

¹⁸ the complete legend is displayed after the table

¹⁹ As seen above with the two variables scatter plots the other results were linked to the ones proposed here (for example the ultrasonic measurements agree with the density measurements and open porosity) therefore were discussed above but not reported here.

The low mechanical strengths collected for natural hydraulic lime mortars and pozzolana-lime mortars added with zinc stearates were caused by a negative influence of the zinc stearates on the binders hydration. This negative influence was observed and extensively studied in Chapter 3.2 and confirmed by the FT-IR analysis on the 28 aged mortars in this Chapter. The delayed hydration was due probably to an ionic-exchange mechanism between zinc stearates and calcium hydroxide or calcium carbonate as explained in Chapter 3.2.

Silane/siloxanes admixtures can be divided into two groups on the basis of the physical properties of the relative mortars. Sitren P730[®] influenced less the densities, strengths, permeabilities in comparison to Sitren P750[®], Silres A[®], Tegosivin[®], but in every case no great changes were observed. The mechanical strengths of mortars added with siloxanes were proportional to the densities and porosities, therefore, we suppose that the siloxanes did not influence negatively the binders hydration (see also Chapter 3.2) but only the mortars structures (increased porosity). Sitren P750[®], Silres A[®], Tegosivin[®] acted as moderate air entraining agents, Sitren P730[®] as a moderate defoamer.

The organic polymer Vinnapas 8031[®] acted as strong air entraining agents and increased the flexibility of the mortar but not their compressive strength.

The behaviour of the mortars in respect to water (water vapour permeability and capillary water absorption) was independent to their structures, porosities or strengths, but strongly dependent to the water-repellent admixture.

It is possible to speak about a very good water repellents effect of the silanes/siloxanes Sitren P750[®], Silres A[®], tegosivin[®]. Good water repellence properties were observed when calcium or zinc stearates were used at higher dosages (1% and 1.5%). Higher water absorption and un-wettable surfaces were observed when Sitren P730[®], Vinnapas[®], Socal[®] were used, probably because the dosage of the active hydrophobizing principle was too low (the hydrophobic part of the silane/siloxanes or the apolar parts of the copolymer or the stearates attached to the calcium nanoparticles, respectively).

Table 4. 1 Legend of the score plot of Table 4. 2

The signs indicate the relative values of the results of each test, from higher to lower values, with the following order: +++ > ++ > + > +- > - > --.						
The correspondent values ranges for each physical properties considered are:						
	Consistence of fresh mortar Slump cm	Bulk Density g/cm ³	Open Porosity MIP %	Compressive strength MPa	Water vapour permeability μ	Capillary water absorption C (kg/(m ² ·h ^{0.5}))
+++	>22	>1.9	>48	>11	<4	>12
++	19-22	1.7-1.8	44-48	6-11	4-5	3-11
+	17-18	1.6-1.7	31-44	4-6	5-8	1.2-3
+-		1.4-1.5	28-31	1.3-4	8-14	0.8-1.2
-	16-17	1.3-1.4	26-28	0.8-1.3	14-16	0.8-0.4
--	<16	<1.2	<26	<0.8	>16	<0.4

Table 4. 2 Qualitative summary of the physical properties tested. The complete legend is reported below.

Mortar system	Mix name	Consistence of fresh mortar	Bulk Density	Open Porosity MIP	Mechanical strength	Water vapour permeability	Capillary water absorption
Limestone cement Mortars	CMA	+	+	+/-	++	+/-	+
	CM7500.5	-	++	+/-	++	+/-	--
	CM7501	-	+	+/-	++	-	--
	CM7501.5	-	+	+/-	++	--	--
	CM7300.5	-	++	-	++	+/-	+
	CM7301	+	++	-	+++	--	+
	CM7301.5	-	-	-	++	-	+
	CMSil0.5	-	+	+/-	+	+/-	--
	CMSil1	--	++	+/-	+	-	--
	CMSil1.5	--	+	+/-	++	-	--
	CMtes1	--	+	+	+	-	--
	CMtes5	+	+	+	+	--	--
	CMcast0.5	+	++	+/-	+++	+/-	+
	CMcast1	+	++	+/-	+++	-	+/-
	CMcast1.5	-	++	--	++	+/-	+/-
	CMznst0.5	--	++	-	+++	+/-	+
	CMznst1	--	++	-	+++	+/-	-
	CMznst1.5	--	+	+/-	++	+/-	-
CMvin0.5	++	-	+	+	++	+	
CMvin1	++	-	+	+	+	+	
CMvin1.5	++	-	+	+	+	+	
Natural hydraulic lime mortars	NMA	+	+/-	++	-	++	++
	NM7500.5	+	+/-	+++	-	+++	+/-
	NM7501	++	--	++	-	++	--
	NM7300.5	+	+/-	++	--	++	++
	NM7301	++	--	+++	-	+++	+/-
	NMSil0.5	+	-	++	--	++	+/-
	NMSil1	+	+/-	++	-	+++	--
	NMcast0.5	+	--	+++	-	++	+/-
	NMcast1	++	---	+++	--	+++	-
	NMznst0.5	+	--	+	-	+++	-
	NMznst1	-	-	+	--	++	--
	NMsoc0.5	-	-	++	-	++	++
	NMsoc1	+	--	++	--	+++	+
Pozzolana-lime mortars	PMA	+	++	-	+/-	+/-	+++
	PM7501	-	+/-	+	-	+/-	--
	PM7301	-	+	-	-	+/-	++
	PMsil0.5	++	+	+/-	+/-	+	--
	PMsil1	++	+	+/-	+/-	-	--
	PMsil1.5	++	+	+/-	+/-	-	--
	PMtes1	++	+	+/-	-	+/-	--
	PMcast0.5	-	++	--	+/-	-	+
	PMcast1	-	++	--	+/-	-	+/-
	PMcast1.5	-	++	-	+/-	-	-
	PMznst0.5	-	++	-	--	+/-	-
	PMznst1	-	++	-	--	+	--
	PMznst1.5	-	++	-	--	+	--

4.3 Discussing the results of Chapter 3.4: Artificial weathering of water-repellent mortars

The weathering test performed was an artificial accelerated weathering, it was developed by trying to reproduce a possible out-door exposure of the mortars. Therefore, two main factors have been taken into account: UV-light and rain.

The UV light was chosen in order to simulate the sunlight action; it is well known how the UV exposure of organic material induced an accelerating degradation which involves the break of chemical bonds and formation of free radicals²⁰. This degradation effect could also affect the water-repellent admixtures studied, diminishing their water-repellent performances and the water-repellent behaviour of the mortar mixtures, at least on the exposed surfaces.

On the other hand, the dousing water could have led to the washout of the water-repellent admixtures from the mortars surfaces.

The most damaging effect of the ageing test, was due to the succession of hot and cold temperatures, which entailed a mechanical stress of the material inducing cracks formation.

High humidity rates and hot temperatures could, otherwise, speed up the hydration reactions and the curing of the mortars, obtaining a strengthened matrix²¹.

Despite it is not possible to establish a direct comparison between this artificial test and an out-door natural ageing test or to give a lifetime prediction of the mortars, it is possible to calculate the total UV radiant exposure of the test. The test lasted 860 hours and 140 cycles were performed and the relative total UV radiant exposure H_e [$H_e = \int E_e dt$] calculated consisted of 130 MJ/m². The average UV radiant exposure in central Europe is estimated around 180 MJ/m² per year (under horizontal sample orientation and no shadowing). The Arpav agency and the ENEA report a minimum of average daily radiation of around 4-5 MJ/m² in December and over 20-23 MJ/m² in July and an average of 800-1000 mm of raining water per year on the Italian coast areas. The average temperature on the Padan Plain (North Italy) is 10-14°C per years with thermal excursion over than 20°C²².

By crossing the different data which have been obtained before and after the test it was possible to individuate some relationships between the physical properties and the resistance to the artificial weathering. In particular, low water-uptake together with higher mechanical properties determined a better weathering resistance of the mixtures. The mechanical properties were, in turn, determined by the binder used and by the physical-chemical influence of the different water-repellents²³.

Limestone cement mortars with and without water-repellents had high weathering resistance, thanks, probably, to a higher mechanical strength in comparison to natural hydraulic lime and pozzolana-lime mortars⁹. Between the different limestone cement mixtures it was possible, however, to distinguish different behaviours: CMsil1, CM7501, CMcast1, were not damaged by the weathering thanks to their good water-repellent properties (even if, their mechanical

²⁰ Mills, J.S., R. White, 1994 p.160-168; Martuscelli E., 2010; Y. Shashoua, 2008

²¹ Moropoulou, et al. 2005

²² Wypich, G. 2003; ARPAV, Quaderni per l'Ambiente Veneto. 2000; Petrarca, S. et al. ENEA, 2000

²³ As studied in Chapter 3.2, the water-repellents had both influence on the micro/macro structure (porosity, etc.) and/or the influence on the hydration reactions (delaying or speeding up the reactions).

properties were lower in comparison to the other limestone cements²⁴); also CM7301 demonstrated good resistance to the weathering (its capillary absorption was higher but it compensated with higher mechanical strength); slight powdering was observed for CMA, CMtes1, CMznst1, CMvin1 (their higher water absorption determined a worse weathering resistance).

Natural hydraulic lime mortars demonstrated good resistance to the artificial weathering. However, their different mechanical behaviour and their high shrinkage under temperature and humidity variations caused the detachment of the layer of epoxy resins brushed on the specimens sides. Regarding the differences between the different water repellents added, it was observed that: NMA and NM730 were resistant to the weathering thanks to a higher mechanical strength; NMznst1 and NMcast1 had higher water absorption at the end of the test, probably because the external layers, richer in water-repellent admixtures²⁵, were consumed and the internal core remained more exposed.

It was observed good resistance to the artificial weathering for *pozzolana-lime mortars* in different cases, even if lower mechanical properties were measured in comparison to limestone cement mortars (chapter 3.3). The weathering resistance of the pozzolana-lime mortars was different from one mixture to another and seemed to mainly depend on the water absorption of the specimens. PMsil0.5,1,1.5 demonstrated the better weathering resistance thanks to higher compressive strength and low water uptake. PM7501, PM7301, PMtes showed only negligible differences thanks to the low water absorption coefficients. PMA, PMCast0.5,1,1.5 and PMznst0.5 had high water absorption and did not resist to the weathering. PMznst1,1.5 mixtures had low water absorption but their mechanical properties were so poor that the weathering cycles caused serious damage to the surfaces. The specimens were brittle, and the FT-IR spectra showed how the formation of C-S-H was prevented by the water repellent. Zinc stearate had seriously influenced the hydration reaction of the binder by avoiding the formation of an interconnected and compact structure.

4.4 Discussing the results of Chapter 3.5: resistance of water repellent mortars to salt crystallization

Researchers have been routinely used sodium sulphate solutions to develop accelerated decay tests in order to simulate or reproduce decay conditions and damage to natural stone, concrete or other building materials and a normalized test, the EN 12370, was developed considering the resistance to sodium sulphates crystallization²⁶. Sodium sulphate is typically selected because it is very common in a wide range of locations and environments and because it is extremely destructive.

In the present study as well, it was possible to observe the damaging action of sodium sulphate and to verify that the principal damaging mechanism was due to the high degree of volume change of sodium sulphate when hydrated and, therefore, to its high crystallization pressure.

Generally speaking, the limestone cement mortars behaved better than the pozzolana-lime mortars and then the natural hydraulic lime mortars, enduring more salt cycles: the different

²⁴ See chapter 3.3

²⁵ See also the water absorption of NMznst1 and NMcast1 before the weathering test in Chapter 3.3

²⁶ Rodriguez- Navarro C. et al. 2000

microstructures (which determined a lower water uptake) and the higher mechanical strengths allowed a better resistance of the limestone cement mortars to the crystallization of salts.

When mixture made with the same binder but different water-repellent admixtures were considered, the resistance to salt crystallization was mainly due to:

- the possibility of the solution to enter inside the matrix, if there was not this possibility, e.g. the water repellence was high enough, no damages occurred;
- the mechanical resistance of the mortar mixture, if the solution was able to enter inside the porous structure, the mechanical strength and the internal cohesion of the specimens determined the resistance.

In particular, the silanes/ siloxanes supported on amorphous silica Sitren P750[®], Silres A[®] and the silane Tegosivin HE[®] allowed a complete water-repellence, a really low water absorption and good resistance to salt crystallization in every case. The stearates and the product Sitren P730[®] did not allow a complete and long-lasting protection. The product Vinnapas[®], acting as air-entraining agent and having high water absorption, was quite ineffective for the protection of the mortars against salt attack.

Moreover, when the water-repellence effect was low and the salt solution was able to enter in the porous structure through capillarity, also the microstructure of the specimens had to be taken into account. Materials with a large fraction of micropores (large surface area) have been noted as being more susceptible to sodium sulphate damage than macroporous materials²⁷. In pores of small radius (<1µm) the pressure in the solution filling the pore is reduced in comparison to the corresponding bulk solution due to the Laplace effect of curvature²⁸. The pressure reduction in small pores results in increased supersaturation of the sodium sulphate solution. The crystallization pressure is directly proportional to the supersaturation ratio according to Correns²⁹ (eq. 26). In our case a saturated sodium sulphate solution was used for the exposure and it is likely that, in the smaller pores, the supersaturation was easily established causing high crystallization pressures.

$$(26) \quad P = \frac{RT}{V_s} \ln \frac{C}{C_s}$$

Where V_s =molar volume of solid salt, C =concentration of the saline solution, C_s = solubility of salt at temperature T , R = gas constant.

The crystallization pressure can be linked directly to the pore radius considering the different approach of Everett, which is based on the properties of curved interfaces between the crystal and the solution (eq. 27). Furthermore, the crystal growth push the remaining solution generating an hydraulic pressure on the pore walls which can be expressed by the Darcy's law (eq. 28).

$$(27) \quad P_r = 2\gamma (1/r - 1/R)$$

where P_r = pressure by crystal growth; γ = surface tension of the salt; r and R = pore radius.

$$(28) \quad dV/dt = K A \Delta P/L$$

where dV/dt = volumetric flow rate; A = flow area perpendicular to L ; K = hydraulic conductivity; L = flow path length, ΔP = denotes the change of pressure at the hydraulic head.

²⁷ Schaffer, R.J., 1932

²⁸ Kashchiev, D., G.M. van Rosmalen, 1995.

²⁹ Correns C. W, 1949

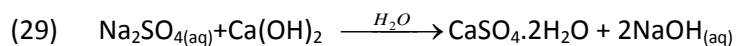
The anhydrous form of the sulphate, thenardite, should precipitate above 32.4 °C but in super saturation conditions (inside small pores) the precipitation of thenardite at temperatures lower than 32.5°C is favoured³⁰. According to Winkler and Wilhelm³¹, the precipitation of the thenardite could generate crystallization pressures even larger than the crystallization of mirabilite (Na₂SO₄·10H₂O) and thus more damage. Furthermore, the crystallization of thenardite might occur also at 20°C for heterogeneous nucleation of the salts over a defect (dust, fractures, scratches, etc.). Since thenardite tends to crystallize in particular in small pores (high supersaturation ratios) in comparison to mirabilite³², pressures enough to overcome the tensile strength of the porous material develop, resulting in building material breakdown.

No mirabilite, but only thenardite was found with XRD measurements in the samples studied. The thenardite might be due partially from the dehydration of mirabilite during the sample drying at 40°C before the XRD analysis, but suppose that also the crystallization of thenardite in supersaturation conditions (small pores) took place.

The damaging action of the crystallization of thenardite in small pores was evident in the mixtures of limestone cement mortar CMcast, CMznst (more than 50% of the total porosity constituted by pores smaller than 1µm) with disaggregation and scaling of the surfaces after 4-5 salt cycles, and in pozzolana-lime mixtures PMA, PMcast.

The damages caused by the crystallization pressure of sodium sulphates could be considered as a mainly physical process. However, among the processes that can generate a decrease in mechanical strength of building materials, the chemical reaction between the sulphate solutions and the material and the consequent formation of gypsum, monosulphoaluminate, ettringite, thaumasite, have been recognized for many years³³.

In the present research the movement of sulphates through the analyzed limestone cement mortars resulted in gypsum formation³⁴ (eq. 27), and in the softening of the binder matrix.



The formation of other sulphates was not confirmed by the analyses performed on other mortar mixtures. In the salt weathering conditions of the test, for short periods of time (the weathering lasted less than two months in total), no chemical reaction of the sodium sulphate solution with natural hydraulic lime mortars or with pozzolana-lime mortars was observed, dealing to the formation of ettringite, gypsum, thaumasite. Nevertheless, it cannot be excluded that prolonged salt weathering or even a prolonged contact of the sodium sulphates inside the mortars in favourable environmental conditions, such as with a high relative humidity HR%, might provoke the formation of other sulphates salts.

³⁰ Schaffer, R.J., 1932; Navarro, C. R. 2000

³¹ Winkler and Wilhelm, 1970

³² Benavente, D., et al. 2004

³³ Collepardi, M., 2003; Lawrence CD. 1995; Neville A. 2004; Tian, B., M.D. Cohen 2000; Patsikas, N., et al. 2012; Tesch, V., B. Middendorf, 2006

³⁴ A form of salt attack described by several authors, e.g. Brown, PW, S. Badger, 2000

4.5 Discussing the results of Chapter 3.6: Water-repellent mortars applied on salty masonry

The measurements and data collected in this part of the study were of particular interest to understand the behaviour of water-repellent mortars in real cases. The preparation of walls mock-ups as models of salty masonries allowed to evaluate the effectiveness and the suitability of the applied mortars in controlled lab conditions.

Different mortar systems based on limestone cement, natural hydraulic lime, pozzolana-lime binders and with or without calcium stearates or Sitren P750® as water repellent admixtures were applied on salty brick walls and exposed to capillary rise of salt solutions.

For each mixtures different behaviour were registered and investigated. Table 4. 3 summarizes the main results obtained on the samples collected from the lower part of the walls, which was more affected by the exposure.

Table 4. 3 Summary of the main results obtained on samples collected from the lower part of the mortars applied on salty masonry. The average of three measurements is given.

	Mix name	Capillary water absorption	Total cumulative volume	Bulk density	Hammer rebound Φ	conductivity	Colorimetric parameters		
		$ml \cdot cm^{-2} \cdot h^{-1}$	$mm^3 \cdot g^{-1}$	$g \cdot cm^{-3}$		$\mu s \cdot cm^{-1}$	L*	a*	b*
Before the exposure	WCM-B	0.61	154	2.02	29	165	59.81	0.56	7.66
	WCM750-B	0.01	110	2.07	30	516	60.15	-0.05	6.11
	WCMcast-B	0.07	177	1.87	27	148	66.93	0.15	6.00
	WNMA-B	0.24	194	1.86	18	76	64.92	0.32	3.43
	WNM750-B	0.02	218	1.66	20	57	58.09	-0.08	4.80
	WNMcast-B	0.46	232	1.62	22	46	66.29	0.10	5.52
	WPMA-B	0.37	111	2.09	33	55	83.89	2.67	9.12
	WPM750-B	0.02	128	2.06	20	74	82.83	3.15	11.42
	WPMcast-B	0.02	137	1.98	14	99	83.89	2.68	9.59
After the exposure	WCM-B s	0.40	136	2.33	31	727	82.99	2.77	9.56
	WCM750-B s	0.02	107	2.02	16	576	81.34	3.50	11.91
	WCMcast-B s	0.24	103	2.15	31	180	81.61	3.12	10.25
	WNMA-B s	0.61	206	1.75	17	71	83.12	1.62	5.29
	WNM750-B s	0.01	223	1.79	21	882	83.86	0.53	3.50
	WNMcast-B s	0.20	237	1.74	18	399	84.26	1.50	6.24
	WPMA-B s	0.54	97	2.21	28	682	81.86	1.85	5.96
	WPM750-B s	0.15	236	1.90	9	597	81.69	0.78	4.83
	WPMcast-B s	0.02	118	1.92	9	95	81.76	0.86	4.58

The limestone cement mortar without water repellents allowed the flow of water through the mortar and the transport of salts to the surfaces. This resulted in: formation of salt efflorescences, damages due to the crystallization of salts both outside and inside the porous matrix, higher water absorption from the outside³⁵, lower mechanical properties.

³⁵ e.g. in Venice, in outdoor environments sources of external water may be rains or high tide flooding.

The presence of Sitren P750® (siloxane) or calcium stearates in limestone cement mixtures caused a diminished adhesion of the mortars to the wall and a more difficult application. The high water-repellent effect prevented high water absorption from the outside, but blocked also the flow of water inside the mortar. This caused the formation of sub-efflorescences at the interface wall-mortars. The sub-efflorescences caused further decohesion of the mortar layers. Furthermore, the use of calcium stearates did not assure a long-lasting water-repellent effect to the external water because the formation of fine cracks (due to the decohesions and movements of the mortar layer) allowed the filtration of water. In presence of calcium stearates a lower compact matrix with lower mechanical properties was found, probably due to the delayed hydration of the binder.

The *natural hydraulic lime mortars* without or with water-repellent admixtures showed good resistance to the salt exposure. The mortar without water-repellents WNMA applied on wall had high capillary water absorption and the salt solution was free to penetrate inside. However, NM mortars were resistant to the crystallization pressure of salts thanks to their porosity distribution characterized by large pores (almost 25% of the open porosity were pores with radius $\geq 1 \mu\text{m}$). The water-repellent mortars had lower water uptake in comparison to WNMA but did not block completely the flow of water and salt efflorescences appeared in particular on the lower parts. The mixture added with siloxanes did not change its mechanical properties and the mixture added with calcium stearates enhanced it during the exposure. The water uptake of WNM750 at the end of the exposure was similar to WCM750 (with limestone cement) but did not show adhesion problems.

The *pozzolana-lime mortar* without water-repellent admixtures WPMA was strong and adherent to the wall, and the hardening process was fast with formation of calcium carbonate and C-S-H. However, WPMA slightly decreased its mechanical strength after the exposure. The mortar was completely wettable and the formation of salt efflorescences was soon enough clearly visible. The porosity did not change much during the exposure, indicating that the salts did not cause severe damage. The presence of water-repellent admixtures (both WPMcast and WPM750) caused serious delaying in the hydration of the binder resulting in a brittle mortar with low adhesion. The admixtures had high water-repellent effectiveness as low water uptakes were measured. The combination of low mechanical strength together with low water absorption which impeded the flow of water caused the formation of salt deposits/crystals beneath the mortar layers and the fall of entire pieces of mortars.

The application of water repellents mortars on salty masonries should take into account different problems due to the capillary rise of water and salt solutions inside the walls.

The mortars and their water-repellence should be calibrated in order to allow a good protection from the external water but avoiding the formation of salt sub-efflorescences.

First of all, the adhesion of the mortars to the walls have to be taken into account, then the influence of the water-repellents on the hardening. The free circulation of water vapour inside the system and the porosity of the materials are other important aspects, together with the capability of protecting the walls from the external water.

4.6 Correlation of physical properties of water-repellent mortars: a multivariate approach

Few statistical studies have been published aimed at the mortar characterization, and in particular regarding the grouping and classification of samples made comparing the chemical-physical properties. However, the published studies³⁶ had proved that the chemometric approach, and in particular the use of Principal Component Analysis, can be an useful tools in the study of building material properties and weathering conditions.

The prime purpose of the Principal Component analysis is to reduce the dimensionality of a multivariate data set and to simplify the interpretation by identifying a smaller number of variables which might summarize the larger set³⁷. The PCA may be then used to reduce the initial number of variables minimizing the loss of information.

In this work, multivariate statistics and in particular PCA analysis was used in the attempt to:

- Individuate if the water repellent mortars can be divided in distinct groups, depending on their physicochemical characteristics;
- evidenced differences due to the weathering processes, in particular on samples exposed to the action of salt solutions.

The statistical software STATISTICA 8.0 (Statsoft, Inc.) was used to elaborate the data: a first standardization of the data with an auto-scaling procedure allowed to overcome the lack of homogeneity due to different measurement units prior of the calculation.

4.6.1 PCA ANALYSIS OF WATER-REPELLENT MORTARS

Paragraph 4.2 already explained and discussed the results obtained studying the chemical-physical properties of the water repellent mortars. However, we have seen how complicated was to understand the relative importance of the different properties and to distinguish the different mortars on the basis of their behaviour and of their composition. Furthermore it was not completely clear the effect of the different water repellents on the mortars properties. Applying PCA analysis to the data, it was possible to simplify the interpretation and found out the more interesting relationship in an easier way.

The data were arranged into a matrix of 47 samples as objects (rows) by 9 properties as variables (columns) shown in Table 4. 4.

The physical variables examined for the PCA analysis were: the real density (RD), the bulk density (BD), the total porosity (TP), the total cumulative volume obtained with MIP analysis (TCV), the ultrasonic measurements (US), the compressive strength (CSV), the water vapour permeability (P), the capillary water absorption coefficient (C), and the contact angle (α).

After the autoscaling of the data and the calculation, the interpretation of the results was carried out looking at the loading plot, which gives information about the variables, and the score plot, which give information about the samples. The first three principal components

³⁶ Moropoulou, A., K. Polikreti, 2009; A. Moropoulou, K. Polikreti, A. Bakolas, P. Michailidis, 2003; L. Rampazzi, A. Pozzi, A. Sansonetti, L. Toniolo, B. Giussani, 2006; D.J. Bartholomew, 2010; Arizio, E, R. Piazza, W. R.L. Cairns, L. Appolonia, A. Botteon, 2013

³⁷ K.H. Esbensen, P. Geladi, Oxford 2009, Pages 211-226; F. Wang, Oxford 2009, Pages 1-7

found were considered, as their cumulative explained variance reached 87,12% (Table 4. 5). and the eigenvalue of the fourth component was lower than 1.

Table 4. 4 The table lists the properties and the samples used for the PCA analysis. The data are the results of three measurements on three homogeneous specimens.

Mix name	Real density	Bulk Density	Total porosity	Total cumulative volume MIP	Ultrasonic measurm ents	compressi ve strength	Water vapour permeability	Capillary water absorption	Contact angle
	RD	BD	TP	TCV	US	CS	P	C	a
	$g \cdot cm^{-3}$	$g \cdot cm^{-3}$	%	$mm^3 \cdot g^{-1}$	$m \cdot s^{-1}$	Mpa	$kg \cdot m^{-2} \cdot s^{-1}$	$Kg \cdot m^{-2} \cdot h^{-0.5}$	°
CMA	2.73	1.68	38.5	0.167	5397	11.07	1.37*10-6	1.64	0
CM7500.5	2.73	1.74	36.4	0.156	5397	10.51	1.03*10-6	0.06	89
CM7501	2.73	1.66	39.4	0.162	4594	8.25	0.84*10-6	0.18	98
CM7501.5	2.71	1.66	39.3	0.168	4398	8.90	0.65*10-6	0.16	113
CM7300.5	2.73	1.83	33.1	0.143	6129	10.61	0.97*10-6	1.47	35
CM7301	2.70	1.81	33.6	0.141	6821	15.76	0.67*10-6	1.13	61
CM7301.5	2.73	1.23	54.8	0.141	5899	13.31	1.34*10-6	0.81	86
CMSil0.5	2.75	1.69	38.1	0.155	4458	6.83	1.28*10-6	0.23	115
CMSil1	2.73	1.74	36.4	0.174	4172	4.55	0.96*10-6	0.21	108
CMSil1.5	2.74	1.61	41.0	0.157	4430	11.84	0.90*10-6	0.23	113
CMtes1	2.73	1.68	38.4	0.175	3224	5.34	0.79*10-6	0.11	118
CMtes5	2.75	1.63	40.5	0.171	2510	5.01	0.54*10-6	0.09	114
CMcast0.5	2.75	1.77	35.0	0.148	7008	16.81	0.97*10-6	1.04	65
CMcast1	2.73	1.78	34.7	0.149	6026	14.56	0.87*10-6	0.47	89
CMcast1.5	2.71	1.71	37.7	0.137	5423	12.23	1.08*10-6	0.38	86
CMznst0.5	2.73	1.73	36.6	0.136	6082	18.31	1.01*10-6	0.48	66
CMznst1	2.73	1.82	33.6	0.141	5996	17.08	1.02*10-6	0.34	80
CMznst1.5	2.72	1.65	39.5	0.161	4226	9.27	1.09*10-6	0.26	97
CMvin0.5	2.70	1.44	47.2	0.252	4949	4.05	2.33*10-6	1.47	49
CMvin1	2.73	1.44	47.2	0.255	4917	3.77	1.61*10-6	1.42	82
CMvin1.5	2.70	1.42	47.9	0.259	4593	4.40	1.81*10-6	1.23	74
NMA	2.74	1.53	44.3	0.341	1105	1.32	2.16*10-6	11.9	1
NM7500.5	2.72	1.46	46.6	0.380	1082	0.34	2.14*10-6	1.29	100
NM7501	2.74	1.18	56.8	0.451	1114	0.89	2.02*10-6	0.24	120
NM7300.5	2.74	1.50	45.3	0.340	1153	0.41	1.51*10-6	1.45	70
NM7301	2.73	1.32	52.1	0.351	1096	0.74	2.18*10-6	0.44	80
NMSil0.5	2.74	1.46	46.8	0.331	1080	0.57	2.06*10-6	2.61	1
NMSil1	2.71	1.18	57.0	0.391	1078	0.83	2.33*10-6	0.33	125
NMcast0.5	2.74	1.41	48.5	0.402	1075	0.84	1.69*10-6	2.09	0
NMcast1	2.74	1.21	55.9	0.411	1105	0.62	2.32*10-6	1.01	0
NMznst0.5	2.72	0.95	65.2	0.331	1227	1.47	1.90*10-6	0.91	0
NMznst1	2.74	1.35	50.8	0.281	1278	0.62	1.65*10-6	0.21	80
NMsoc0.5	2.75	1.42	48.2	0.401	1029	1.06	1.70*10-6	2.65	0
NMsoc1	2.74	1.17	57.4	0.420	1048	0.55	2.19*10-6	1.94	0
PMA	2.61	1.77	31.9	0.133	1205	2.01	0.60*10-6	20.01	0
PM7501	2.62	1.44	44.6	0.214	1160	1.07	0.80*10-6	0.05	130
PM7301	2.64	1.69	35.1	0.136	1180	1.21	0.71*10-6	6.01	0
PMsil0.5	2.61	1.55	40.4	0.148	1170	1.73	0.84*10-6	0.78	128
PMsil1	2.60	1.57	39.6	0.160	1150	2.24	0.56*10-6	0.05	130
PMsil1.5	2.58	1.56	40.1	0.149	1130	2.04	0.51*10-6	0.06	143
PMtes1	2.61	1.65	36.5	0.155	1008	0.89	0.65*10-6	0.07	126
PMcast0.5	2.59	1.74	33.1	0.119	1075	2.35	0.58*10-6	1.90	0
PMcast1	2.61	1.73	33.5	0.128	1225	2.01	0.51*10-6	0.25	2
PMcast1.5	2.60	1.71	34.2	0.134	1227	2.06	0.56*10-6	0.14	0
PMznst0.5	2.58	1.72	33.8	0.148	1002	0.61	0.96*10-6	0.10	0
PMznst1	2.63	1.75	32.7	0.148	998	0.26	0.98*10-6	0.08	118
PMznst1.5	2.61	1.71	34.2	0.148	1000	0.05	0.98*10-6	0.05	126

Variables

The loading plots in Figure 4. 7 and the coefficients of the components list in Table 4. 6 allowed to recognize the role of the different variables in the samples differentiation.

In particular the bulk density showed high positive weight on the first component, while the total porosity, the total cumulative volume and the water vapour permeability showed negative weights (therefore, anti-correlated to the bulk density).

This first component seemed to group the variables linked to the structure/microstructure of the sample and it was interesting to notice that also the water vapour permeability had an important weight on this component and that it was correlated with the porosity values (both TP and TCV). The good correlation between the total porosity TP and the cumulative volume TCV (relative only to the open porosity) confirmed that the close porosity remained constant in the different mortar mixtures as seen in Chapter 3.3.

The mechanical strength and the ultrasonic measurements were correlated and showed high negative weights on the second component.

The capillary water absorption (C) and the wettability (a) had high weights on the third components and were anti-correlated. Therefore, was possible to guess that the third components was related to the behaviour in presence of water.

We can summarize the results saying that: the first component was related to the mortars structure/microstructure, the second component was related to the mechanical properties, while the third component was related to the hygric behaviour.

Samples

The score plot of the first and second components (Figure 4. 8) showed a clear separation of the different mortars system (i.e. Limestone cement mortars, natural hydraulic lime mortars and pozzolana lime mortars). The comparison between the score plot and the loading plot helped to understand which variables contributed to the distinction of the systems.

The microstructural properties distinguished between i) the natural hydraulic mortars and ii) the limestone cement mortars with the pozzolana-lime mortars. The second component (characterized by high weights of CS and US) allowed to tell apart the limestone cement mortars and the pozzolana- lime mortars. The samples admixed with the polymer Vinnapas (CMvin0.5,1,1.5) formed a separate group with peculiar microstructural and mechanical properties, while the CM7301.5 remained alone.

The score plot of the first and third components (Figure 4. 8) did not clearly distinguish between the different mortars even if most of the pozzolana –lime mortars had higher values of the third component. The distinction from one mortars to the other was linked to the water-repellence of the mortars and was therefore possible to see that PCA, NMA, CMA (without water repellent) were located in the lower part of the graph, while samples admixed with Silres A® and Sitren P750® were located in the upper part. For each admixture the third component increased slightly with increasing dosage (e.g. CM7300.5, CM7301, CM7301.5).

The microstructure and the mechanical properties allowed to differentiate the mortars on the basis of the binder used. The third component (that explained 15.38% of the variance) allowed to distinguish the mortars on the basis of the water-repellent admixture and its effectiveness.

Table 4. 5 Variance explained by each principal component, subject marks data

Component	Variance explained		
	Eigenvalue	%	Cumulative %
1	4,22	46,85	46,85
2	2,24	24,89	71,74
3	1,38	15,38	87,12
4	0,53	5,87	92,99

Table 4. 6 Loading for the first three components.

Variables		1 st Component	2 nd Component	3 rd Component
RD	real density	-0,20	-0,56	-0,18
BD	bulk density	0,45	0,05	-0,15
TP	total porosity	-0,45	-0,15	0,11
TCV	total cumulative volume MIP	-0,46	-0,05	-0,04
US	ultrasonic measurements	0,25	-0,54	-0,16
CS	compressive strength	0,29	-0,49	-0,17
P	water vapour permeability	-0,43	-0,18	-0,13
C	capillary water absorption coefficient	-0,03	0,27	-0,64
a	contact angle	0,12	-0,15	0,67

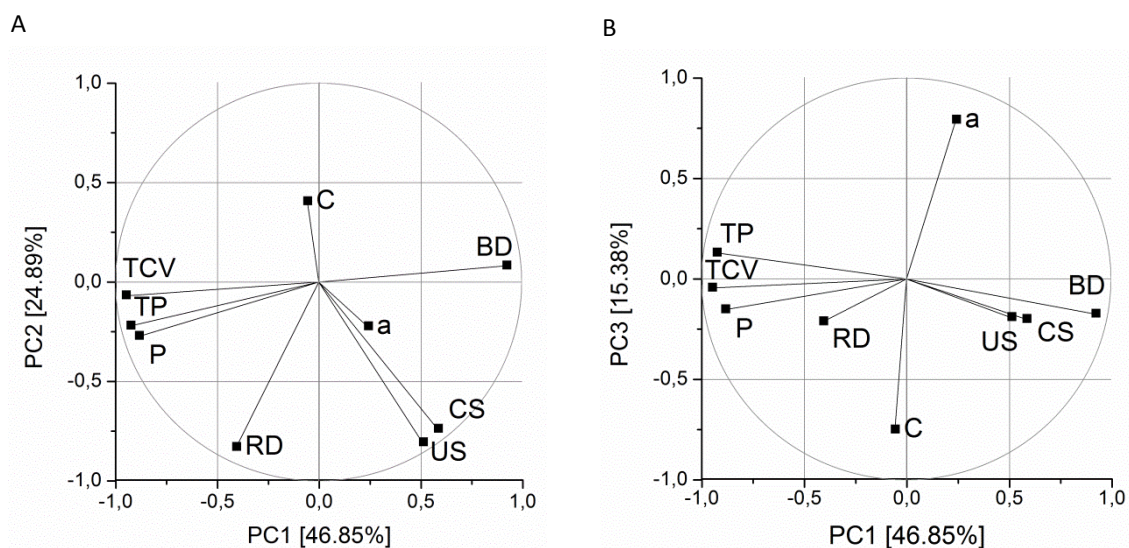


Figure 4. 7 PCA analysis of water repellent mortars, loading plots

A: plots of the first and second components.

B: plots of the first and third components.

Real density (RD), bulk density (BD), total porosity (TP), total cumulative volume obtained with MIP analysis (TCV), ultrasonic measurements (US), the compressive strength (CSV), water vapour permeability (P), capillary water absorption coefficient (C), contact angle (a).

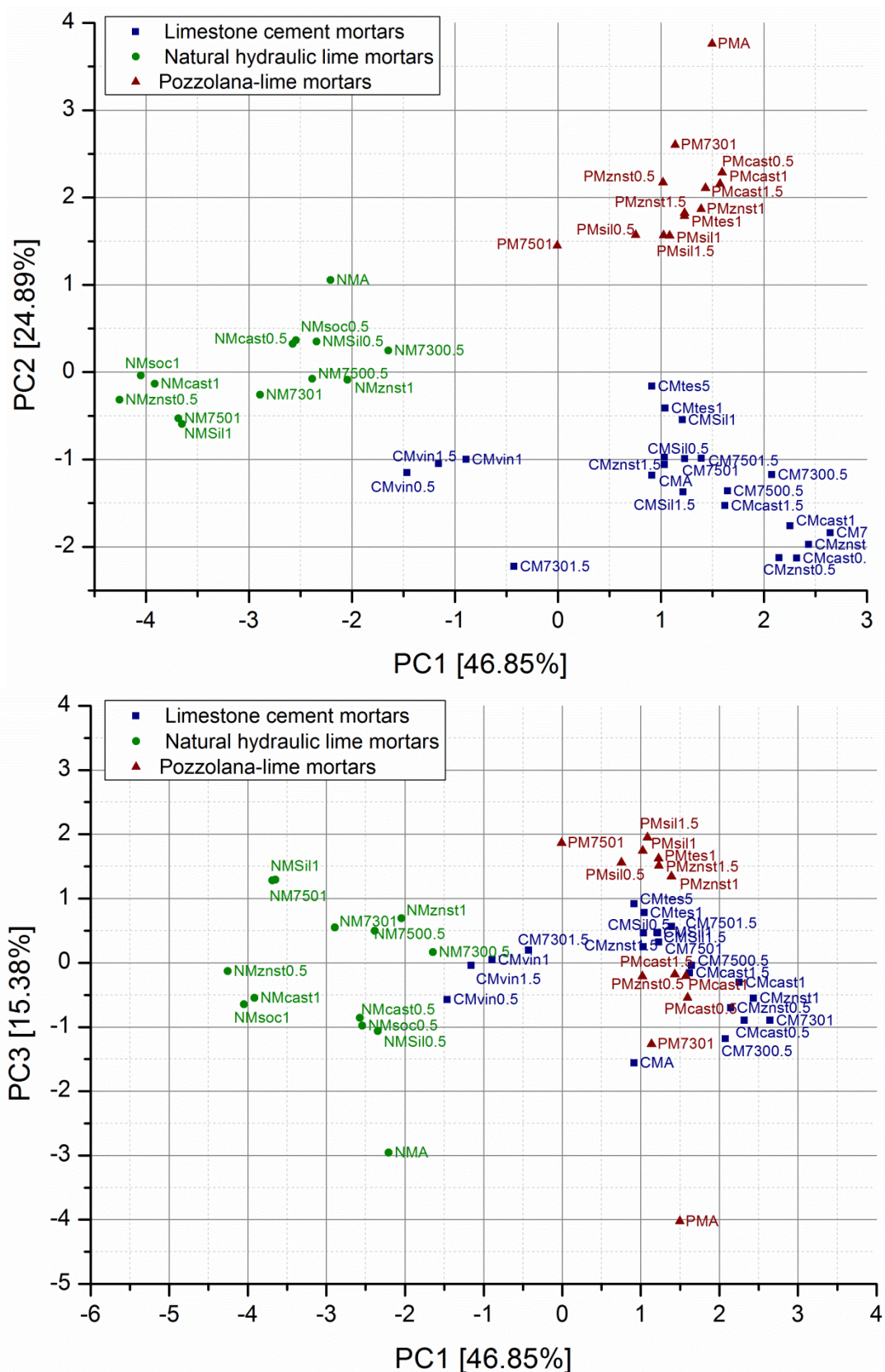


Figure 4. 8 PCA analysis of water repellent mortars. Above: score plot of the first and second components . Below: Score plot of the first and third components. CEM: limestone cement mortars; NM: natural hydraulic mortars; PM: pozzolana-lime mortars.

4.6.2 PCA ANALYSIS OF WATER-REPELLENT MORTARS BEFORE AND AFTER THE EXPOSURE TO THE ACTION OF SALINE SOLUTIONS

An attempt was made to analyse with Principal Component Analysis (PCA) also the data regarding the resistance of mortars to salt crystallization in order to evaluate the effectiveness and the durability of these materials in marine environment³⁸.

The data collected on the mortar mixtures CMA1, CM7501, CMsil1, CMcast1, NMA1, NM7501, NMsil1, NMcast1, PMA1, PM7501, PMsil1, PMcast1 (showed in Chapter 3.5) were considered. These mixtures were chosen because a complete study of the physical characteristics have been done including also MIP analyses.

Two separate PCA analyses were done to take two ‘snapshots’ of the situation before and after the test of resistance to salt crystallization.

The variables considered for the two analyses were:

- the total cumulative volume *TCV* measured via MIP in order to consider the open porosity of the samples;
- the compressive strength *CS* to evaluate the mechanical properties;
- the capillary water absorption *C*;
- the ionic conductivity *cond* of the samples on the outer part (0.0-0.5 cm depth);
- the ratio between the specimens mass before or after the test and the starting apparent volume (M/V_i). **This ratio correspond to the bulk density only for the specimens before the exposure, but it should be not confused, because for the samples after the test is different.** During the test the damages due to the exposure caused huge material losses. M/V_i was chosen as a parameter which allowed to consider the damaging effect of the test. **It is a “damage parameter” which consider the material loss due to the test**, higher values of M/V_i indicates lower mass loss and better resistance to the exposure.

Two matrices of 36 object by 5 variables were prepared considering the measurements done on three independent specimens for each mortar mixtures listed above. As a summary of the results Table 4. 7 lists the averages of the data obtained on the three independent specimens for each mixtures.

The two analyses were performed after the autoscaling of the data and compared.

The PCA analyses are henceforward referred as PCA-before and PCA-after, and the components are named $PC1_{\text{before}}$, $PC2_{\text{before}}$, $PC1_{\text{after}}$, $PC2_{\text{after}}$, etc.

The first two principal components explained together the 75.80% and the 76.93% of the total variance in PCA-before and in PCA-after, respectively (Table 4. 8) and were considered because theirs eigenvalues were higher than one.

³⁸ Immersion in saturated sodium sulphate solution and drying cycles of mortars, see also Chapter 3.5 and paragraph 4.4 above.

Variables

The loadings for the first two components on PCA-before (Table 4. 9) showed that CS and M/V_i had high positive weights on the first component PC1_{before}, while the TCV was anti-correlated (negative weight on PC1_{before}).

The capillary water absorption C had high positive weight in the PC2_{before}, while the conductivity cond had low weight. The PC2_{before} allowed to differentiate M/V_i and CS, which had positive and negative values, respectively.

The loadings for the first two components on PCA-after (Table 4. 8) showed a different situation in comparison to PCA-before. CS and the M/V_i had high positive weights on PC1_{after}, while C, cond and TCV had negative weights. It should be possible to guess that when the capillary water absorption were higher, the damages (M/V_i decrease) were higher and the compressive strength was lower. Higher C determined salt transport inside the mortars, lower mechanical strength, high material loss, and higher conductivity.

C and cond are correlated and had negative weights on PC2_{after}, while and TCV had positive weight on the same component. This suggests that, after the cycles, the water absorption was not correlate to the porosity (TCV), but to the specimens composition and in particular to the admixture used. Furthermore, high capillary absorptions allowed the salt solution to enter into the pores and the salts to crystallize inside, causing higher conductivity and chocking the pores (open porosity reduction).

It is interesting to notice that:

- in PCA-before M/V_i and CS were not correlated on PC2_{before}, but in PCA-after they were completely correlated both on PC1_{after} and in PC2_{after}.
- C and cond were not correlated on PC1_{before} and on PC2_{before}, but were correlated on PC1_{after} and in PC2_{after}.

Samples

The score plot of the first and second component of PCA-before in Figure 4. 10 showed a partial separation of the different mortar systems (i.e. natural hydraulic lime mortars NM from the limestone cement mortars CM and the pozzolana lime mortars PM) even if not so clear as the PCA analysis shown in the previous paragraph (4.6.1 PCA analysis of water-repellent mortars).

The two components PC1_{before} and PC2_{before} allowed to differentiate the objects on the basis of their structural properties (TCV, M/V_i, CS on PC1_{before}) and of the behaviour in presence of water (C on PC2_{before}). In particular, the projections of the mixtures on the PC1_{before} -PC2_{before} plot were located on the link due to high porosity, low compressive strength and high initial conductivity. The projections of NMAs and PMAs, without water repellents, were located on the higher part of the score plot due to high capillary water absorption.

The score plot of the first and second component of PCA-after in Figure 4. 11 showed a complex situation. The projections of the natural hydraulic lime mortars had low values of PC1_{after} and could be still recognized as a separate group (except NMAs samples), but the projections of the pozzolana-lime mortars and limestone cement mortars were overlapped.

It was seen that the mixtures without water repellents (NMA, PMA, CMA) had low values of both PC1_{after} and PC2_{after}, while the mortars added with siloxanes CMsil, CM750, PMsil, PM750 had high values of PC1_{after}. The mortars NM750 and NMsil had higher values of PC1_{after} only in

comparison to the other NM mixtures and had also high values on $PC2_{after}$ (high porosity but low water absorption and conductivity).

Before the exposure the structural and mechanical properties allowed to differentiate the objects on the basis of the binder used. The second component allowed to distinguish the mortars on the basis of the water-repellent admixture and its effectiveness.

After the exposure the first component allowed to differentiate the mixtures on the basis of their resistance to the salt crystallization. This resistance was no more dependent on the mortar binder, but on the water-repellent admixture used: higher resistance corresponded to the use of siloxanes.

This comparison of the two PCA analyses was useful to have a clear idea of the behaviour of the different mortar mixtures and how much they were affected by the exposure to salt solution. Few graphs were enough to summarize and visualize the data obtained. Furthermore, this analysis allowed to see the correlations between different variables and to understand which parameters were fundamental to evaluate the effects of the exposure. A complex comparison between chemical-physical, mechanical and effectiveness parameters (expressed by the variables) was done in a simple way.

Table 4. 7 The table is an example of the properties and the samples used for the PCA analysis, the data shown are the average of the data measured for three independent specimens for each mixture considered.

	Mix name	Total cumulative volume MIP	compressive strength	Capillary water absorption	Conductivity 0.5-1.0 cm depth	Mass/starting volume
		TCV	CS	C	cond	M/V _i
		$mm^3 \cdot g^{-1}$	Mpa	$Kg \cdot m^{-2} \cdot h^{-0.5}$	$\mu s \cdot cm^{-1}$	$g \cdot cm^{-3}$
Before the exposure	CMA	0.167	11.07	1.64	70	1.63
	CM7501	0.162	8.25	0.18	71	1.65
	CMSil1	0.174	4.55	0.21	69	1.62
	CMcast1	0.149	14.56	0.47	85	1.73
	NMA	0.340	1.32	11.90	83	1.53
	NM7501	0.450	0.89	0.24	108	1.18
	NMSil1	0.390	0.83	0.33	84	1.18
	NMcast1	0.410	0.62	1.01	91	1.21
	PMA	0.133	2.00	20.01	71	1.71
	PM7501	0.214	1.07	0.05	85	1.52
	PMsil1	0.160	2.24	0.05	51	1.60
	PMcast1	0.128	2.01	0.25	102	1.65
After the exposure	CMA	0.200	0.01	2.63	101	1.18
	CM7501	0.180	4.91	0.12	114	1.65
	CMSil1	0.200	3.68	0.12	120	1.63
	CMcast1	0.160	3.38	1.46	121	1.29
	NMA	0.280	0.12	19.95	101	1.37
	NM7501	0.430	0.30	0.45	114	1.18
	NMSil1	0.450	0.21	10.26	126	1.09
	NMcast1	0.420	0.12	3.63	137	1.11
	PMA	0.140	0.01	19.56	210	1.07
	PM7501	0.170	0.71	0.07	81	1.52
	PMsil1	0.180	1.45	0.04	58	1.59
	PMcast1	0.140	0.37	3.64	235	1.45

Table 4. 8 Variance explained by each principal component in the two PCA analyses

Variance explained						
	PCA-before			PCA-after		
Component	Eigenvalue	%	Cumulative %	Eigenvalue	%	Cumulative %
1	2.62	52.37	52.37	2.45	49.00	49.00
2	1.17	23.43	75.80	1.40	27.93	76.93
3	0.71	14.13	89.93	0.54	10.72	87.64

Table 4. 9 Loading for the first three components.

Variables	PCA-before		PCA-after	
	1 st Component	2 nd Component	1 st Component	2 nd Component
TCV total cumulative volume MIP	-0.93	0.00	-0.34	0.88
CS compressive strength	0.71	-0.39	0.83	-0.18
C Capillary water absorption coefficient	-0.20	0.88	-0.73	-0.34
cond Conductivity of the first 0.5-1.0 cm	-0.60	-0.45	-0.59	-0.65
M/V_i Degradation parameter	0.92	0.20	0.87	-0.22

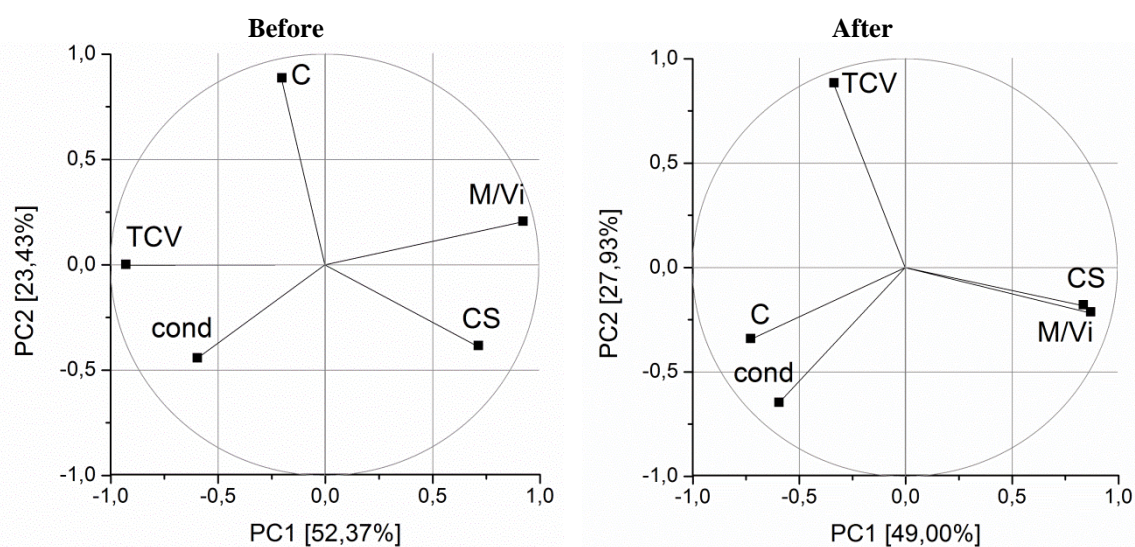


Figure 4. 9 loading plot of the first and second components of PCA-before (left) and PCA-after (right). TCV= Total cumulative volume obtained with MIP analysis, CS= compressive strength, C= capillary water absorption coefficient, Cond= conductivity measured on samples collected at a depth of 0.5-1 cm (cond), M/V_i= mass/ starting volume.

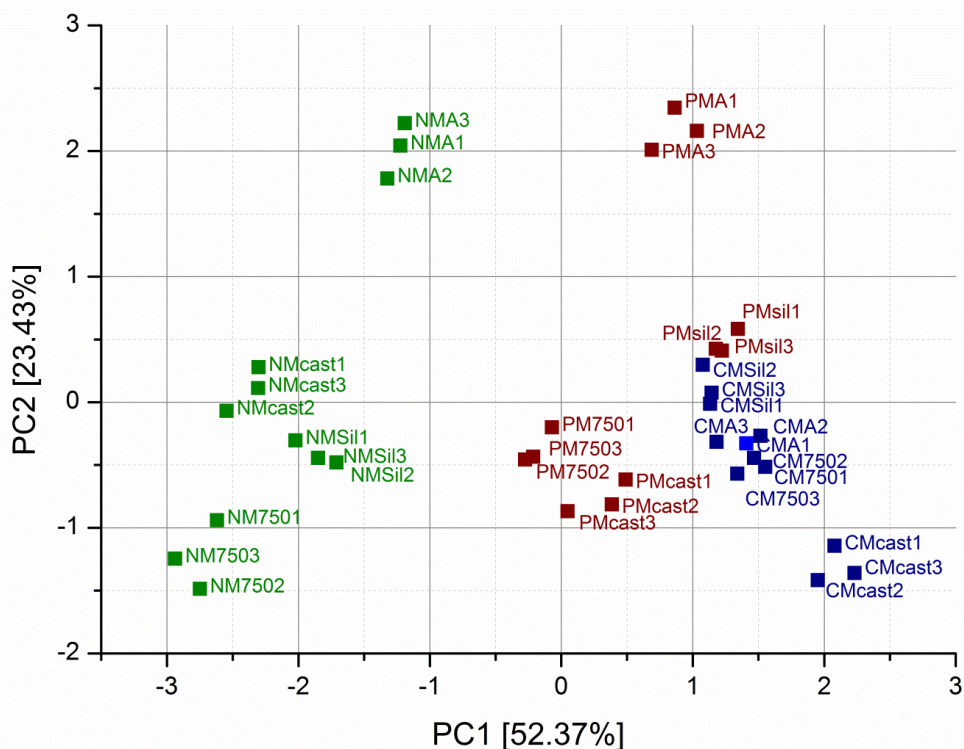


Figure 4. 10 Score plot of the first and second component of PCA-Before. Green: natural hydraulic lime mortars NM; Red: Pozzolana-lime mortars PMA; Blue=limestone cement mortars CM. A=without admixtures; cast= with calcium stearates 1%; 750= with siloxane Sitren P750 1%.

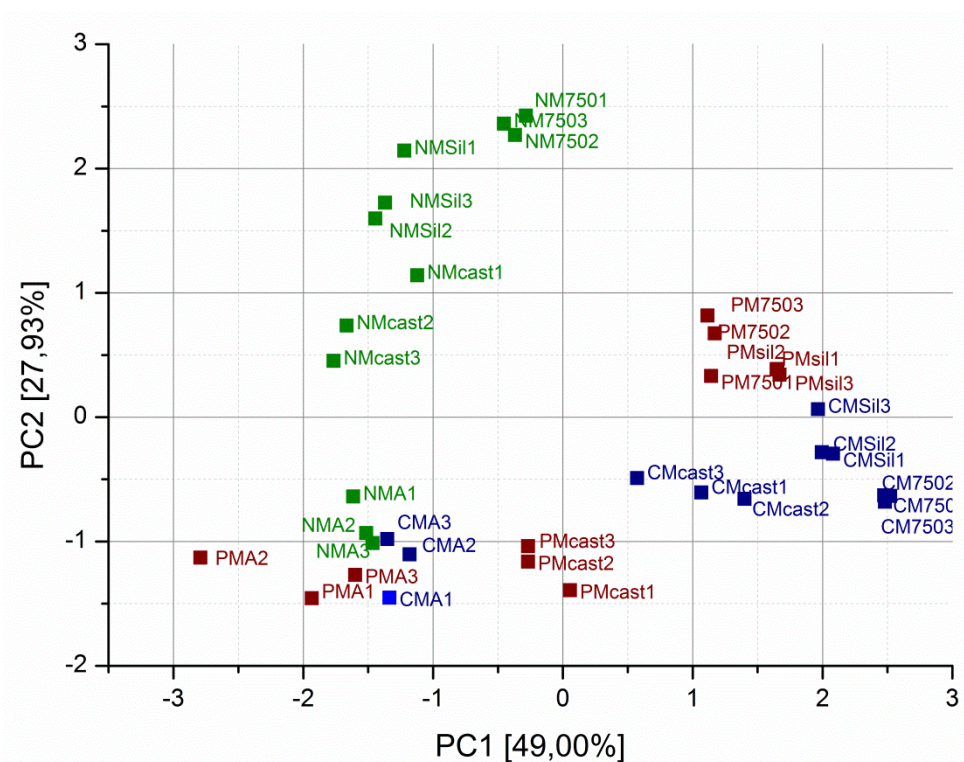


Figure 4. 11 Score plot of the first and second component of PCA-After. Green: natural hydraulic lime mortars NM; Red: Pozzolana-lime mortars PMA; Blue=limestone cement mortars CM. A=without admixtures; cast= with calcium stearates 1%; 750= with siloxane Sitren P750 1%. The lines showed the three zone described in the main text.

4.7 Conclusions

This research work addressed an important problem in the maintenance and restoration fields of the architectural surfaces: the protection against the damages caused by the action of water.

The building materials decay due to the action of water is a well-known and serious problem. Several studies, solutions, and products have been carried out and developed in order to find suitable materials, able to resist and protect from the action of water. Among them, particular attention have been given to the design and production of water-repellent external layers, such as protective treatments applied by impregnation on the buildings surfaces and integral water-repellent mortars used as renders.

The present research started from two main needs: i) the need of further information on integral water-repellent mortars as protection system; ii) the need of developing sustainable and compatible building materials.

- i. The use of hydrophobic admixtures to obtain water-repellent mortars, grout and renders have been recently investigated by considering the effectiveness of the use of metal soaps and siloxanes in cement mortars and in lime mortars from the physical point of view. Poor attention was instead directed to the effect of these admixtures from the chemical point of view. In particular the influence of water repellents on the binders hydration, and the influence of the presence of salts on water-repellent mortar systems have been less studied. For these reasons a chemical-physical approach to the study of integral water-repellent mortars was chosen, ranging from the study of their hydration/hardening, to the study of their properties once hardened, to the evaluation of the effectiveness of the admixtures in different environmental conditions.
- ii. In the last years, a new sensibility has been growing regarding the use of more sustainable materials, with the necessity of developing building materials compatible with the historical buildings. This first consideration led to the choice, in the present research, to study water-repellent mortars based on binders such as pozzolana-lime (hydraulic binder product with lower energies and compatible with historical mortars), natural hydraulic lime (which requires lower production temperatures and energy), limestone cement (i.e. a cement substituted by a 30% of limestone which saves the use of Portland cement), instead of Portland cement type I.

The methods and tests developed allowed to face the problem and to obtain a vast knowledge. Particularly useful have been the step by step process going from 1) the study of the chemical influence of the admixtures on the binder hydration, 2) the study of the microstructure and physical properties of water repellent mortars, 3) the study of mortars undergoing different environmental stress and exposures and 4) the evaluation of the behaviour of the water repellent mortars applied as renders on salty masonries. Furthermore, tools as the PCA analysis helped to summarize and compare the data obtained.

4.7.1 MAIN RESULTS

The study of the influence of the admixtures on the hydration reaction allowed to found out that metal soaps such as calcium and zinc stearates were able to exchange the metal ions with all the binders under exam and to strongly delay the hydration reactions.

Siloxane admixtures behaved as air-entraining agents lowering the density of the binder pastes and of the mortars but they slightly influenced the formation of hydration products, and in some cases even enhanced them.

The other admixtures studied (such as Vinnapas®) influenced the microstructure and delayed the hydration to a lesser extent than the mortars admixed with stearates.

Both the metal soaps and the siloxanes were effective in reducing the water uptake, even if the zinc and calcium stearates influenced the mechanical properties of the mortars, and pozzolana-lime mortars with stearates had low mechanical strength due to the influence of the stearates on the binder hydration.

The effectiveness of mortars admixed with the siloxane emulsion Tegosivin HE® and the siloxane on silica carrier Sitren P750® and Silres A® remained good enough also after the exposure under UV-light, douse with water, and in presence of saturated salt solutions. The mixes made with these siloxane admixtures showed better resistance to salt crystallization and to the action of water in comparison to the non admixed mortars, thanks to their reduced water absorption.

The metal soaps did not allowed a resistance comparable to the siloxanes to the salt crystallization, and the mortars admixed with metal soaps showed, almost in every case, an enhanced water uptake after the exposure, due probably to the wash-out and degradation of the water-repellent.

The water-repellent mortars applied as renders on salty masonry subjected to rising damp of salts solutions behaved in a different way.

The limestone cement mortars without water-repellent admixtures were strongly damaged by the absorption of salt solution from the wall which caused exfoliations, disaggregation of the mortar matrix and salt efflorescences. The natural hydraulic lime and the pozzolana-lime mortars without water-repellents showed a better resistance.

The limestone and natural hydraulic lime mortars with calcium stearates and Sitren P750® showed enough resistance to the crystallization of salt solutions, but the correspondent wall/render systems were not resistant. Damages due to the salt transport inside the system occurred according to the following mechanism:

1. The moisture transports the salts present inside the brick wall to the wall/render interface.
2. The liquid salt solution cannot cross the render, which is water repellent.
3. The water evaporates and the water vapour can cross the render, thanks to the high water vapour permeability of the mortars, while the salts precipitates from the supersaturated liquid solution forming sub-efflorescences.
4. The water-repellent mortars tended to be separated bodily from the bricks, due to the formation of salt sub-efflorescences beneath the render layer.

The pozzolana-lime mortars with water-repellent suffered even worse damages because the water-repellent admixtures influenced negatively the hydration, preventing the pozzolanic reaction and leading to brittle and cracked mortars. Beside the formation of sub-efflorescences, the exfoliation of the render layer occurred when the salt solution filters through cracks.

4.8 Perspectives

This research work and its results open to different perspectives of research and development of new materials.

- The results regarding the influence of the different water-repellent admixtures on the binders hydration lead to rethink the current use of water-repellent admixtures and to propose further research aimed at the study and synthesis of new kind of water-repellent admixtures, with less influence on the hydration processes.
- The results of the exposure tests showed that the commonly used laboratory test regarding the resistance to the salt crystallization might be limited when the mortars have to be developed for a particular application (e.g. as render in salty masonries). More complex tests considering systems similar to real system (as the salty masonry test developed in this research) and field applications should be deeply investigated.
- The results also highlighted the necessity of deeper and further study of salty masonry/water-repellent render systems and, in particular, the need to define suitable mix designs in order to obtain durable solutions.
- A larger use of non invasive analytical techniques, such as conductivity measurements, ultrasonic measurements, Hammer tests, IR thermography to monitor the damages and the decay of the mortars in on-field condition would be desirable.
- The statistical approach to the study of the mortar properties and characterization should be enhanced. In particular PCA analysis demonstrated to be a useful tool in order to study the properties of mortars subjected to different kind of degradation processes.

References

- Aberlee, T., P. Emmenegger, F. Vallee.** New Approaches to Increase Water Resistance of Gypsum Based Building Materials. Proceedings of the conference "Drymix Mortar Yearbook 2010". 2010
- Adediran Mesubi, M.** An infrared study of zinc, cadmium, and lead salts of some fatty acids. *Journal of Molecular Structure*. Vol. 81: 1–2. 1982. Pages 61-71
- AITEC, RELAZIONE ANNUALE 2010.** Associazione Italiana Tecnico Economica Cemento, G. Scalia – Roma. 2011
- AITEC, RELAZIONE ANNUALE 2011.** Associazione Italiana Tecnico Economica Cemento, G. Scalia – Roma. 2011
- A.T. Albayrak, M. Yasar, M. A. Gurkaynak, I. Gurgey.** Investigation of the effects of fatty acids on the compressive strength of the concrete and the grindability of the cement. *Cement and Concrete Research*. Vol. 35. 2005. Pages 400–404
- Albino, V., R. Cioffi, M. Marroccoli, L. Santoro.** Potential application of ettringite generating systems for hazardous waste stabilization. *Journal of Hazardous Materials*, Vol. 51: 1–3. 1996. Pages 241-252
- Allen, G., J. Allen, N. Elton, M. Farey, S. Holmes, P. Livesey.** Hydraulic lime mortar for stone, brick, block and masonry, Donhead ed., Shaftesbury. 2003
- Amoroso, G., V. Fassina.** Stone Decay and Conservation: Atmospheric Pollution, Cleaning, Consolidation and Protection, Elsevier Science Ltd, London. 1983
- Arkles, B.** Tailoring Surfaces with Silanes. *Chemtech*. Vol. 7. 1977
- Armani, E.** Intonaci a Venezia, l'evoluzione storica delle superfici intonacate. *Primo Inventario degli intonaci e delle decorazioni esterne dell'architettura veneziana, Ricerche di storia dell'arte*. Vol. 24. 1984
- Arnold, A.** Rising damp and saline minerals. In Proceedings of "Deterioration and preservation of Stone Objects, Fourth International Congress", July 7-9, Louisville. 1982. Pages 11-28
- Arizio, E., R. Piazza, W. R.L. Cairns, L. Appolonia, A. Botteon.** Statistical analysis on ancient mortars: A case study of the Balivi Tower in Aosta (Italy), *Construction and Building Materials*, Vol. 47. 2013. Pages 1309-1316
- ARPAV AA.VV.** La caratterizzazione climatica della Regione Veneto. ARPAV, *Quaderni per l'Ambiente Veneto*. Venice. 2000
- AA.VV.** L'intonaco: storia, cultura, tecnologia, *Atti del Convegno Scienza e Beni Culturali*. Libreria Progetto editore, Padova. 1985
- Bakolas, A., G. Biscontin, A. Moropoulou, E. Zendri.** Salt impact on brickwork along the canals of Venice. *Materials and Structures*. Vol. 29. 1996. Pages 47-55
- Banfill, P., M. Frias.** Rheology and conduction calorimetry of cement modified with calcined paper sludge, *Cement and Concrete Research*, Vol. 37: 2. 2007. Pages 184-190
- F. Barreca, C.R. Fichera.** Use of olive stone as an additive in cement lime mortar to improve thermal insulation. *Energy and Buildings*. Vol. 62. 2013. Pages 507–513
- Bellamy, L.J.** The Infra-red Spectra of Complex Molecules, 3rd ed., Chapter 20. Chapman and Hall, London. 1975.
- Benavente, D., M.A. Garcia del Cura, J. Garcia-Guinea, S. Sanchez-Moral, S. Ordóñez.** Role of pore structure in salt crystallization in unsaturated porous stone. *Journal of crystal growth*, Vol. 260. 2004. Pages 532-544
- Bensted J.** Seventh International Congress on the Chemistry of Cement, vol. II, Paris. 1980. Pages 1–6

- Berger, S., C. Cau Dit Coumes, P. Le Bescop, D. Damidot.** Hydration of calcium sulfoaluminate cement by a $ZnCl_2$ solution: Investigation at early age. *Cement and Concrete Research*. Vol. 39:12. 2009. Pages 1180-1187
- Biscontin, G., L. Falchi et al.** Dispersione acriliche nanometriche e silici colloidali acquose per il consolidamento dei materiali porosi. In "Scienza e Beni Culturali". Ed. Arcadia Ricerche, Venezia. 2011. Pages 387-400
- Biscontin G., F. Izzo, E. Rinaldi.** Il sistema delle fondazioni lignee a Venezia, valutazione del comportamento chimico-fisico e microbiologico. CORILA, Venezia. 2009
- Biscontin, G.** L'azione chimico-fisica dell'acqua di mare sulle murature di sponda a Venezia, in "I muri di sponda, problemi e tecniche di manutenzione delle sponde dei rii" *Quaderni INSULA*, Venezia. Vol.9. 2001. Pages 79-88
- Biscontin, G.; Cattalini, L.** "Venice regained", *Chemistry in Britain*, Vol.16:7. 1980. Pages 360-364
- Biscontin, G.; Fassina, V.; Lazzarini, L.; Mazzon, R.** "Studio dell'umidità ascendente, delle caratteristiche fisiche delle murature di Palazzo Badoer e prove di desalinificazione" (Study of rising damp, of physical characteristics of the walls of Palazzo Badoer and desalting tests) *Proc. Of the Symposium*, Cini Foundation, Oct. 22-23. 1979
- Brien, J. V., K.C. Mahboub.** Influence of polymer type on adhesion performance of a blended cement mortar, *International Journal of Adhesion and Adhesives*. Vol. 43. 2013. Pages 7-13
- Brown, P.W., S. Badger.** The distribution of bound sulfate and chlorides in concrete subjected to mixed $NaCl$, $MgSO_4$, Na_2SO_4 attack. *Cement and Concrete Research*. Vol. 30. 2000. Pages 1535-1542
- Callebaut, K., J. Elsen, K. Van Balen, W. Viaene.** Nineteenth century hydraulic restoration mortars in the Saint Michael's Church (Leuven, Belgium) Natural hydraulic lime or cement?, *Cement and Concrete Research*. Vol. 31. 2001. Pages 397-403
- Cappitelli, F., P. Principi, R. Pedrazzani, L. Toniolo, C. Sorlini.** Bacterial and fungal deterioration of the Milan Cathedral marble treated with protective synthetic resins. *Science of The Total Environment*, Vol. 385: 1-3. 2007. Pages 172-181
- Cardell, C., F. Delalieux, K. Roumpopoulos, A. Moropoulou, F. Auger, R. Van Grieken.** Salt induced decay in calcareous stone monuments and buildings in a marine environment in SW France, *Construction and Building Materials*, Vol. 17. 2003. Pages 165-179
- Carretti, E., L. Dei.** Physicochemical characterization of acrylic polymeric resins coating porous materials of artistic interest, *Progress in Organic Coatings*, Vol. 49:3. 2004. Pages 282-289
- Chabrelie, A.** Mechanisms of degradation of concrete by external sulphate ions under laboratory and field conditions, Ph.D Thesis Material Science and Engineering, Ecole Polytechnique Federale de Lausanne, supervisor prof. K. Scrivener. 2010
- Chen, Q.Y., C.D. Hills, M. Tyrer, I. Slipper, H.G. Shen, A. Brough.** Characterisation of products of tricalcium silicate hydration in the presence of heavy metals, *Journal of Hazardous Materials*, Vol. 147: 3. 2007. Pages 817-825
- Collepardi, M.** *Scienza e tecnologia del calcestruzzo*. Hoepli, Milano. 1980
- Collepardi M.** A state of the art review on delayed ettringite attack on concrete, *Cement Concrete Composites*, Vol. 25:4-5. 2003. Pages 401-407
- Collepardi, M.** *Diagnosi del degrado e restauro delle strutture in C.A.*, seconda edizione. Enco, Treviso. 2010
- Correns, C. W.** Growth and dissolution of crystals under linear pressure, *Discussion of the Faraday Society*, Vol. 5. 1949. Pages 267-271
- Crispim, C.A., P.M. Gaylarde, C.C. Gaylarde.** Algal and cyanobacterial biofilms on calcareous historic buildings, *Current Microbiology*, Vol.46. 2003. Pages 79-82

- De Weerd, K., M. Ben Haha, G. Le Saout, K.O. Kjellsen, H. Justnes, B. Lothenbach.** Hydration mechanisms of ternary Portland cements containing limestone powder and fly ash, *Cement and Concrete Research*, Vol. 41: 3. 2011. Pages 279-291
- Deschner, F., F. Winnefeld, B. Lothenbach, S. Seufert, P. Schwesig, S. Ditrach, F. Goetz-Neunhoeffler, J. Neubauer.** Hydration of Portland cement with high replacement by siliceous fly ash, *Cement and Concrete Research*, Vol. 42: 10. 2012. Pages 1389-1400
- Donchev, I., J. Ninov, I. Doykov, N. Petrova, L. Dimova.** On the formation of cement phases in the course of interaction of Kaolinite with Portlandite, *Journal of the University of Chemical Technology and Metallurgy*, Vol. 45: 4. 2010,. Pages 391-396
- O' Dowd, C., M. Smith, I. Consterdine, J. Lowe.** Marine aerosol, sea-salt and the marine sulphur cycle: a short review, *Atmospheric environment*, Vol 31: 1 . 1997. Pages 73-80
- Driussi, G.; Valle, A.; Biscontin, G.** Porosity and soluble salts as decay parameters of stone materials, Vth international congress on deterioration and conservation of stone. Proceedings, Lausanne. 25-27 September, 1985
- Ellison, P.T.** Hydraulic lime mortars, Thesis (M.S: in Historic preservation). University of Pennsylvania, USA. 1998.
- Elsen, J, K. Van Balen, G. Mertens.** Hydraulicity in Historic lime mortars, a review, in *Historic Mortars*, J. Válek, J. J. Hughes, C. Groot Editors RILEM, London. 2012. Pages 125-140
- Esbensen, K.H., P. Geladi.** Principal Component Analysis: Concept, Geometrical Interpretation, Mathematical Background, Algorithms, History, Practice, In: Editors-in-Chief: Stephen D. Brown, Romà Tauler, and Beata Walczak, Editor(s)-in-Chief, *Comprehensive Chemometrics*, Elsevier, Oxford. 2009. Pages 211-226
- Esteves, L. P.** On the hydration of water-entrained cement–silica systems: Combined SEM, XRD and thermal analysis in cement pastes, *Thermochimica Acta*, Vol. 518: 1–2, 10. 2011. Pages 27-35
- European Environment Agency.** EEA. Report No 05/2008. Greenhouse gas emission trends and projections in Europe, 2008.
- Everett, D.H.** The Thermodynamics of Frost Damage to Porous Solids, *Transactions of the Faraday Society*, Vol. 57. 1961. Pages 1541-1551
- Fassina, V., M. Favaro, A. Naccari, M. Pigo.** Evaluation of compatibilità and durability of a hydraulic lime-based plaster applied on brick masonry of hystorical buildings affected by rising damp phenomena, *Journal of Cultural Heritage*, Vol. 3. 2002. Pages 45-51
- Fitzner, B., R. Snethlage.** Über Zusammenhänge zwischen Salzkristallisationsdruck und Porenradienverteilung, *GP News Letter*, Vol.3. 1982. Pages 13-24
- Fraay, A.L.A., J.M. Bijen, Y.M. Dehaan.** The reaction of fly ash in concrete — a critical examination, *Cement and concrete research*, Vol. 19. 1989. Pages 235–246
- Gaylarde, C.C., P.M. Gaylarde.** A comparative study of the major microbial biomass of biofilms on exteriors of buildings in Europe and Latin America, *International Biodeterioration and Biodegradation*, Vol. 55. 2005. Pages 131–139
- García del Cura, P. G.** Petrographical analysis of calcium aluminate cement mortars: Scanning electron microscopy and transmitted light microscopy. *Cement and Concrete Research*, Vol.29:12. 1999. Pages 1881-1885
- Garnier, P., P. Gregoire.** Polymorphism of crystalline phases of calcium stearate, *Journal of materials science*, Vol. 23. 1988. Pages 3225-3231
- Gibbons, P.** Pozzolans for lime mortars. *The Conservation and Repair of Ecclesiastical Buildings*. UK: Taylor von Cathedral Communications, 1997.
- Gineys, N., G. Aouad, D. Damidot.** Managing trace elements in Portland cement—Part I: Interactions between cement paste and heavy metals added during mixing as soluble salts, *Cement and Concrete Composites*, Vol. 32: 8. 2010. Pages 563-570

- Gönen, M. et al.** Zinc Stearate Production by Precipitation and Fusion Processes. *Industrial and Engineering Chemical research*, Vol. 44. 2005. Pages 1627-1633
- Gönen, M. , S. Öztürk, D. Balköse, S. Okur, S. Ülkü.** Preparation and Characterization of Calcium Stearate Powders and Films Prepared by Precipitation and Langmuir-Blodgett Techniques. *Industrial and Engineering Chemical research*, Vol. 49: 4. 2010. Pages 1732-1736
- Grinzato, E., P.G. Bison, S. Marinetti.** Monitoring of ancient buildings by the thermal method. *Journal of Cultural Heritage*, Vol. 3:1. 2002. Pages 21–29
- Grinzato, E., C. Bressan, S. Marinetti, P.G. Bison, C. Bonacina.** Monitoring of the scrovegni chapel by IR thermography: Giotto at infrared, *Journal of Infrared Physical Technology*, Vol. 43:3–5. 2002. Pages 165–169
- Grinzato, E., C. Bressan, F. Peron, P. Romagnoni, A.G. Stevan.** Indoor climatic conditions of ancient buildings by numerical simulation and thermographic measurements. *Thermosense XXII^o, SPIE*, Vol. 4020. 2000. Pages. 314–323.
- Gualtieri, A.F. A. Viani, C. Montanari.** Quantitative phase analysis of hydraulic limes using Rietveld method. *Cement and Concrete research*, Vol. 36. 2006. Pages 401-406
- Gulotta, D., S. Goidanich, C. Tedeschi, T. G. Nijland, L. Toniolo.** Commercial NHL-containing mortars for the preservation of historical architecture. Part 1: Compositional and mechanical characterisation, *Construction and Building Materials*, Vol. 38. 2013. Pages 31-42
- Habert, G. , N. Choupay, J.M. Montel, D. Guillame, G. Escadeillas.** Effects of the secondary minerals of the natural pozzolans on their pozzolanic activity, *Cement and concrete research*, Vol. 38. 2008. Pages 963-975
- Hall, C., W.D. Hoff.** Water transport in brick, stone and concrete. Taylor and Francis, New York. 2002
- Hawkins, P., P. Tennis, R. Detwiler.** The use of Limestone in Portland Cement, A State-of-the-Art Review, Portland Cement Association EB227, USA, 2002, ISBN: 0-89312-229-7
- Houvenaghel, J. Carmeliet.** Dynamic Contact Angles, Wettability and Capillary Suction of Hydrophobic Porous Materials. Proceeding of "Hydrophobe III Surface Technology with Water Repellen Agents. 2001, Pages 191-200.
- Itul, A.** Interactions entre organo-silanes et ciment, Conséquences sur l'hydratation et les propriétés mécanique, Master thesis of Chemical physics, Bourgogne University 2010. Pages 74 ss.
- Izaguirre, A., J. Lanas.** Effect of water-repellent admixtures on the behaviour of aerial lime based-mortars. *Cement and Concrete Research*, Vol. 39. 2009. pages 1095-1104
- Izaguirre, A., J. Lanas, J. Alvarez.** Ageing of lime mortars with admixtures: Durability and strength assesment. *Cement and Concrete Research*. 2010, Vol. 40, p 1081-1095
- Jakobsmeier, L.** Reaktivität und Wechselwirkungen siliciumorganischer Verbindungen in einer CaSO₄.2H₂O- Matrix", Ph.D Thesis in Chemical Sciences Technischen Universität München, Advisor prof. G. Morteani. München, Germany , 2000.
- Johansson, A.** Impregnation of Concrete Structures, Licentiate Thesis in Structural design and Bridges. Stockholm, Sweden , 2006. ISSN 1103-4270.
- Kakali, G. et al.** Hydration products of C₃A, C₃S and Portland cement in the presence of CaCO₃. *Cement and Concrete Research*, Vol. 30. 2000. Pages 1073-1077
- M.A. Kargol, et al.,** Influence of blended cements on the performance of water repellent agents. Proceedings of the Conference Hydrophobe VI, 2011
- Karoglou, M., A. Bakolas, N. Kouloumbi, A. Moropoulou.** Reverse engineering methodology for studying historic buildings coatings: The case study of the Hellenic Parliament neoclassical building, *Progress in Organic Coatings*, Vol. 72: 1–2. 2011. Pages 202-209
- Kashchiev, D., G.M. van Rosmalen.** Effect of pressure on nucleation in bulk solution and solutions in pore and droplets, *Journal of Colloid Interface Science*, Vol. 169. 1995. Pages 214-219
- Klemm, W., L.D. Adams.** An investigation on the formation of carboaluminates. Carbonate addition to

- cement, American society for Testing and Materials, Philadelphia. 1990. Pages 60-72
- Lanas, J., P. Bernal, M.A. Bello, A. Galindo.** Mechanical properties of natural hydraulic lime-based mortars, *Cement and Concrete Research*, Vol. 34:12. 2004, Pages 2191-2201
- Lanzón, M., A. Garrido, P.A. García-Ruiz.** Stabilization of sodium oleate as calcium oleate in cement-based mortars made with limestone fillers, *Construction and Building Materials*, Vol. 25: 2. 2011, Pages 1001-1008
- Lanzón M., P.A. Garcia Ruiz.** Effectiveness and durability evaluation of rendering mortars made with metallic soaps and powdered silicone. *Construction and Building Materials*, Vol. 22. 2008. Pages 2308-2315
- Lanzon M, Garcia-Ruiz PA.** Evaluation of capillary water absorption in rendering mortars, made with powdered waterproofing additives. *Construction and Building Materials*, Vol. 23. 2009. Pages 3287-3291
- Lawrence CD.** Mortar expansion due to delayed ettringite formation. Effects of curing period and temperature. *Cement and Concrete Research*, Vol. 25:4. 1995. Pages 903–914
- Lazzarini, L, M.L. Tabasso.** Il restauro della pietra. s.l. : CEDAM, 1986.
- Lea, M.** Chemistry of Cement and Concrete. 4th ed. Ed Peter C Hewlett, London. 1997
- Li, W., F.H. Wittman, R. Jiang, T. Zhao, R. Wolfseher.** Metal soaps for the production of integral Water repellent Concrete, In *Borelli E. Fassina V. editors proceedings of Hydrophobe VI, 6th international conference on water repellent treatment of building materials*, Freiburg: Aedificatio Publisher. 2011. Pages 145-154
- Liebig, E.** Gebrannte Tonminerale und Trassmehle als puzzolanische Komponenten in Kalkmörteln. Karlsruhe University, Germany : Thesis, Advisor Prof Dr E. Althaus, 1997.
- Litvan, G.G.** Freeze-thaw durability of porous building materials. *ASTM Special Technical Publication*. Vol. 691. 1980. Pages 455-463
- Lothenbach, B., G. Le Saout, E. Gallucci, K. Scrivener.** Influence of limestone on the hydration of Portland cements, *Cement and Concrete Research*, Vol. 38:6 2008. Pages 848-860
- Lubelli, B., R.PJ. van Hees, C. J.W.P. Groot.** The role of sea salts in the occurrence of different damage mechanisms and decay patterns on brick masonry, *Construction and Building materials*, Vol. 18. 2004. Pages 119-124
- Mackenzie, R. C.** Differential Thermal Analysis, Academic Press. Inc. London, 1970
- Maranhao, F.L., V.M John.**
The influence of silicone based Water Repellents as Admixtures on the Rheological properties of Cement Slurry. In *Proceedings of Hydrophobe V*, Brussels, Belgium, 2008.
- Maravelaki-Kalaitzaki, P., I. Karastasios, A. Bakolas, V. Kilikoglou.** Hydraulic lime mortars with siloxane for water proofing historic masonry. *Cement and Concrete research*, Vol. 37. 2007. Pages 238-290
- Marengo, E., M.C. Gennaro, D. Giacosa, C. Abrigo, G. Saini, M.T. Avignone.** How chemometrics can helpfully assist in evaluating environmental data. Lagoon water. *Analitica chemical acta*, Vol. 317. 1995. Pages 53-63
- Martionola, G. et.al.** Modified ECC by means of Internal Impregnation. *Journal of advanced Concrete technology*, Vol. 2: 2. 2004. Pages 207-212.
- Martuscelli E.** The chemistry of degradation and conservation of plastic artefacts of pre-synthetic “era” based on natural or artificial polymers. Ed. Paideia Firenze, Florence. 2010
- McInnes, L.M., P.K. Quinn.** Gravimetric analyses, ionic composition, and associated water mass of the marine aerosol, *Atmospheric Environment*, Vol. 30: 6, Pages 869-884 1996
- Mesubi, M.A.** An infrared study of zinc, cadmium, and lead salts of some fatty acids, *Journal of molecular structure*, Vol. 81. 1982. Pages 61-71.

- Micheletti, C., S. Gottardo, A. Critto, S. Chiarato, A. Marcomini.** Environmental quality of transitional waters: The lagoon of Venice case study, *Environment International*, Vol. 37: 1. 2011. Pages 31-41
- Milanesi, C., F. Baldi, S. Borin, L. Brusetti, F. Ciampolini, F. Iacopini, M. Cresti.** Deterioration of medieval painting in the chapel of the Holy Nail, Siena (Italy) partially treated with Paraloid B72, *International Biodeterioration & Biodegradation*, Vol. 63: 7. 2009, Pages 844-850
- Mills, J. S, R. White.** The Organic Chemistry of Museum Objects, Second Edition; Elsevier Science Ltd, Oxford. 1994
- Mittal, K.L. editor.** Contact angle, Wettability and Adhesion, Volume 3, Boston. 2003
- Molero Armenta, M., I. Segura, M. Hernandez, M.A. Garcia Izquierdo, J. Anaya.**
Ultrasonic characterization of cementitious materials using frequency-dependent velocity and attenuation, NDTCE'09, Non-Destructive Testing in Civil Engineering, Nantes, France, June 30th – July 3rd, 2009
- Mongkhon Narmluk, Toyoharu Nawa .** Effect of fly ash on the kinetics of Portland cement hydration at different curing temperatures, *Cement and Concrete Research*, Vol. 41: 6. 2011. Pages 579-589
- Moreira, A. P. D. et al.** Monitoring of calcium stearate formation by thermogravimetry. *Journal of thermal analysis and calorimetry*, Vol. 97. 2009. Pages 647–652
- Moropoulou, A., K. C. Labropoulos, E.T. Delegou, M. Karoglou, A. Bakolas.** Non-destructive techniques as a tool for the protection of built cultural heritage. *Construction and Building Materials*, In Press, Corrected Proof, Available online 11 April 2013
- Moropoulou, A. Bakolas, P. Moundoulas, E. Aggelakopoulou, S. Anagnostopoulou.** Strength development and lime reaction in mortars for repairing historic masonries. *Cement and Concrete Research*, Vol. 27: 2. 2005. Pages 289-294
- Moropoulou, A., K. Polikreti, A. Bakolas, P. Michailidis.** Correlation of physicochemical and mechanical properties of historical mortars and classification by multivariate statistics, *Cement and Concrete Research*, Vol.33: 6. 2003. Pages 891-898
- Musumarra, G., M. Stella, M. Matteini, M. Rizzi,** Multiariate characterization, using the SIMCA method, of mortars from two frescoes in Chiaravalle Abbey, *Thermochimica Acta*, Vol. 269–270. 1995. Pages 797-807
- Myung-Geun Song, Jong-Yun Kim, Jong-Duk Kim.** Effect of sodium stearate and calcium ion on dispersion properties of precipitated calcium carbonate suspensions, *Colloids and Surfaces A: Physicochemical and Engineering Aspects*, Vol. 229: 1–3. 2003. Pages 75-83
- Neville A.** The confused world of sulfate attack on concrete, *Cement and Concrete Research*, Vol. 34:8. 2004. Pages 1275–1296
- Odler, I.** Special Inorganic Cements, London, 2000
- F. Pacheco, et al.** Some consideration about the use of lime-cement mortars for building conservation purposes in Portugal: A reprehensible option or a lesser evil? *Construction and Building Materials*, Vol. 30. 2012. Pages 488-494.
- Pajares, I., S Martínez-Ramírez, M.T Blanco-Varela,** Evolution of ettringite in presence of carbonate, and silicate ions, *Cement and Concrete Composites*, Vol. 25:8. 2003. Pages 861-865
- Patsikas, N., N. Katsiotis, P. Pipilikaki, D. Papageorgiou, E. Chaniotakis, M. Beazi-Katsioti,** Durability of mortars of white cement against sulfate attack in elevated temperatures, *Construction and Building Materials*, Vol.36. 2012. Pages 1082-1089
- Pellizzon Birelli, M.** Characterisation and Reactivity of silicatic systems found in historic hydraulic binders, Ph. D. Thesis in chemical science 16th cycle, supervisor prof. Guido Biscontin, Ca' Foscari University of Venice A.A. 2002-2003
- Petrarca, S. et al.** La radiazione solare globale al suolo in Italia, valori medi mensili stimati sulle immagini del satellite Meteosat, anni 1998-1999 e media 1994-1999. ENEA, Roma. 2000
- Piana, M., E.Danzi.** The Catalogue of Venetian external Plasters: Medieval Plasters. 2002. Pages 65-71.

- Potgieter-Vermaak, S.S., J.H. Potgieter, A. Worobiec, R. van Grieken, L. Marjanovic, S. Moeketsi.** Fingerprinting of South African ordinary Portland cements, cement blends and mortars for identification purposes — Discrimination with starplots and PCA, *Cement and Concrete Research*, Vol. 37:6. 2007. Pages 834-843
- Quadrelli, M., F. Koenig, M. Roos, S. Stadtmueller, B Weyershausen.** New powdery water repellents for dry mortar applications, More than a durable protection, in Drymix Mortar yearbook 2007. Pages 34-43
- Ramachandran, V.S.,** Applications of Differential thermal analysis in Cement Chemistry, New York. 1969
- Ramachandran, V.S.** Thermal analyses of cement components hydrated in the presence of calcium carbonate, *Thermochimica Acta*, Vol. 127. 1988. Pages 385-394
- Ramachandran, V. S.** Concrete Admixtures Handbook, 2nd Ed.: Properties, Science and Technology. Publisher W. Andrew, New Jersey. 1997
- Ramachandran, V. S.** Thermal analysis of construction materials, New York. 2003
- Ramachandran, V.S., Ralph M. Paroli, J. J. Beaudoin, A. H. Delgado.** Handbook of thermal analysis of construction materials, Norwich, New York. 2002
- Ramli, M., A. A. Tabassi,** Effects of polymer modification on the permeability of cement mortars under different curing conditions: A correlational study that includes pore distributions, water absorption and compressive strength, *Construction and Building Materials*, Vol. 28: 1. 2012. Pages 561-570
- Rampazzi, L., A. Pozzi, A. Sansonetti, L. Toniolo, B. Giussani.** A chemometric approach to the characterisation of historical mortars, *Cement and Concrete Research*, Vol. 36: 6. 2006. Pages 1108-1114
- Riethmayer, S.A.** Die metall seifen als Hydrophobierungsmittel. SÖFW. 1961. Pages 3-6.
- Rodriguez- Navarro C., E. Doehne, E. Sebastian.** How does sodium sulfate crystallize? Implications for the decay and testing of building materials, *Cement and Concrete research*, Vol. 30. 2000. Pages 1527-1534
- Rossi-Manaresi, R., A. Tucci.** Pore structure and the disruptive or cementing effect of salt crystallization in various types of stone, *Studies in Conservation*, Vol. 36. 1991. Pages 53-58
- Roos, M. et al.** Evolution of Silicone based Water Repellents for Modern Building Protection. *Proceedings of the Conference Hydrophobe V, Water repellent treatment of Building materials.* Aedificatio Publisher, 2008.
- Sabbioni, C. , A. Bonazza, G. Zappia.** Damage on hydraulic mortars: the Venice Arsenal. *Journal of Cultural Heritage*, Vol. 3: 1. 2002. pages 83-88
- Sabbioni, C. et al.** Atmospheric deterioration of ancient and modern hydraulic mortars. *Atmospheric Environment*, Vol. 35. 2001. Pages 539-548.
- Sandrolini, F. et al.** Ethyl silicate for surface treatment of concrete – Part I: Pozzolanic effect of ethyl silicate. *Cement and Concrete Composites*, Vol, 34: 3. 2012, Pages 306-312
- Sarkar, S., S. Mahadevan, J.C.L. Meeussen, H. van der Sloot, D.S. Kosson.** Numerical simulation of cementitious materials degradation under external sulfate attack, *Cement and Concrete Composites*, Vol. 32: 3. 2010. Pages 241-252
- Schaffer, R.J.** The weathering of natural building stones, DSIR, Buiding research station Special Report No. 18, Stationary Office, London 1932
- Scherer, G.W.** Stress from crystallization of salt in pores, 9th International Congress on Deterioration and Conservation of Stone, Venice, 19-24 June 2000
- Schwarz, N., N. Neithalath.** Influence of a fine glass powder on cement hydration: Comparison to fly ash and modeling the degree of hydration, *Cement and Concrete Research*, Vol.38: 4. 2008. Pages 429-436
- L. Scueremans, et al.** Durability of hydrophobic agents in a marine environment. proceeding of the conference Hydrophobe V Water Repellent Treatment of Building materials. Aedificatio publishers. 2007. Pages 1-11.

- Schueremans, L., Ö.Cizer, E. Janssens, G. Serré, K. Van Balen**, Characterization of repair mortars for the assessment of their compatibility in restoration projects: Research and practice, *Construction and Building Materials*, Vol.25: 12. 2011. Pages 4338-4350
- Sepulcre-Aguilar, A. F.H. Olivares**. Assesment of phase formation in lime based mortars with added metakaolin, portland cement and sepiolite, for grouting of hystoric masonry. *Cement and Concrete research*, Vol. 40:1. 2010. Pages 66-76.
- Shayan, A., R. Diggins, I. Ivanusec**. Effectiveness of fly ash in preventing deleterious expansion due to alkali-aggregate reaction in normal and steam-cured concrete. *Cement and Concrete Research* , Vol. 26. 1996. pages 153–164
- Sha, W., G.B Pereira**, Differential scanning calorimetry study of ordinary Portland cement paste containing metakaolin and theoretical approach of metakaolin activity. *Cement and Concrete Composites*, Vol. 23:6. 2001. Pages 455-461
- Shashoua Y**. Conservation of plastics, material science, degradation and preservation, Editor ElsevierLtd, Slovenia. 2008
- Shi, C., R. L. Day**. Pozzolanic reaction in the presence of chemical activators Part II. Reaction products and mechanism, *Cement and Concrete research* , Vol. 30. 2000. Pages 607-613
- Singh, M., M. Garg**. Reactive pozzolana from Indian clays- their use in cement mortars, *Cement and Concrete Research*. 2004. Pages 1903-1907
- Snellings, R., G. Mertens, J. Elsen**. Calorimetric evolution of the early pozzolanic reaction of natural zeolites. *Journal of therma analysis and calorimetry*, Vol.101. 2010. Pages 97–105
- Song M.-G. and Kim J.-Y. and Kim J.-D**. Effect of sodium stearate and calcium ion on dispersion properties of precipitated calcium carbonate suspensions, *Colloids and Surfaces A:Physicochemical and Engineering Aspects*, Vol. 229:1. 2003. Pages 75-83
- T. Stambolov, J.R.J. Van Aspered de Boer**. The deterioration and conservation of porous building Materials in Monuments: A Litterature Review. *International Center for the study of the preservation and restoration of cultural property*. 1972.
- Stoopes, G., V. Marcellino, F. Mees**. Interpretation of Micromorphological Features of Soils and Regoliths, Elsevier, Netherlands. 2010. Pages 447-448
- Struble, L., J.Godfrey**. How sustainable is concrete? *International Workshop on Sustainable Development and Concrete Technolog*, Beijing 2004
- Stewart, J.D., A. Henry** . Practical Building Conservation: Mortars Plasters and Renders, English Heritage 2011
- Taylor, H.F.W**. Cement Chemistry, 2 edition Academic press London, 1997
- Tavukçuoğlu, A., A. Düzgüneş, E.N. Caner-Saltık, Ş. Demirci** . Use of IR thermography for the assessment of surface-water drainage problems in a historical building, Ağzıkarahan (Aksaray), *Turkey, NDT & E International*, Vol. 38: 5. 2005. Pages 402-410
- Tesch, V. , B. Middendorf**, Occurrence of thaumasite in gypsum lime mortars for restoration, *Cement and Concrete Research*, Vol. 36:8. 2006. Pages 1516-1522
- Tian, B., M.D. Cohen**. Does gypsum formation during sulphate attack on concrete, lead to expansion?, *Cement and Concrete Research*, Vol. 30:1. 2000. Pages 117–123
- Torii, K., M. Kawamura**. Effects of fly ash and silica fume on the resistance of mortar to sulfuric acid and sulfate attack. *Cement and Concrete Research*, Vol. 24. 1994. Pages 361–370
- Torraca, G**. Porous building materials- Materials science for architectural conservation, ICCROM, Rome, 1981
- Trezza, M.A, A.E Lavat**, Analysis of the system $3\text{CaO}\cdot\text{Al}_2\text{O}_3\text{--CaSO}_4\cdot 2\text{H}_2\text{O--CaCO}_3\text{--H}_2\text{O}$ by FT-IR spectroscopy, *Cement and Concrete Research*, Vol. 31: 6. 2001. Pages 869-872

- Tsivilis, S. E Chaniotakis, G Kakali, G Batis.** An analysis of the properties of Portland limestone cements and concrete, *Cement and Concrete Composites*, Vol.24:3–4. 2002. Pages 371-378
- Tsivilis, S., G. Kakali, E. Chaniotakis, A. Souvaridou.** A study on the hydration reaction of Portland limestone cement by means of TG, *Journal of thermal analysis*, Vol.52. 1998. Pages 863-870
- Tsivilis, S., J. Tsantilas, G. Kakali, E. Chaniotakis, A. Sakellariou,** The permeability of Portland limestone cement concrete, *Cement and Concrete Research*, Vol. 33: 9. 2003. Pages 1465-1471
- United Nations Environment Programme – UNEP.** Buildings and Climate Change: Status, Challenges and Opportunities, 978-92-807-2795-1 Sustainable Buildings and Construction Initiative (2007)
- Valor, A., E. Reguera, E. Torres-García, S. Mendoza, F. Sanchez-Sinencio,** Thermal decomposition of the calcium salts of several carboxylic acids, *Thermochimica Acta*, Vol. 389: 1–2. 2002, Pages 133-139
- Van Gemert, D., L. Czarnecki, M. Maultzsch, H. Schorn, A. Beeldens, P.Łukowski, E. Knapen.** Cement concrete and concrete–polymer composites: Two merging worlds: A report from 11th ICPC Congress in Berlin, 2004, *Cement and Concrete Composites*, Vol. 27: 9–10. 2005. Pages 926-933
- Varas, M.J., M. Alvarez de Buergo, R. Fort,** Natural cement as the precursor of Portland cement: methodology for its identification, *Cement and concrete research* Vol., 35:11. 2005. Pages 2055–2065
- Veniale, F., M. Setti, C. Rodriguez-Navarro, S. Lodola, W. Palestra, A. Busetto.** Thaumassite as decay product of cement mortar in brick masonry of a church near Venice, *Cement and concrete composites*, Vol. 25. 2003. Pages 1123-1129
- Verhoef, L.G.W.** Water-AParadox, the prerequisite of Life but the Cause of Decay. Proceedings of the conference Hydrophobe III Surface technology with Water Repellent Agents. Aedificatio Publisher, 2001. pages. 21-36.
- Marco Vitruvio Pollione,** *De Architettura, liber V.* 15 B.C
- Wang F.** Factor Analysis and Principal-Components Analysis, In: Editors-in-Chief: Rob Kitchin and Nigel Thrift, Editor(s)-in-Chief, *International Encyclopedia of Human Geography*, Elsevier, Oxford. 2009. Pages 1-7
- Wang K.** Proceedings of the International Workshop on Sustainable Development and Concrete Technology, Workshop held in Beijing 2004, 2004 Iowa State University ISBN 0-9652310-7-0
- Wagner, H.B.** Polymer-modified hydraulic cements, *Industrial and Engineering Chemistry Product Research and Development* , Vol. 4:3. 1965. Pages 191–196
- Wang, Z., C. Wang, Y. Sheng , Hari-Bala, X. Zhao, J. Zhao.** Synthesis of hydrophobic CaCO₃ nanoparticles. *Materials Letters*, Vol.60. 2006. Pages 854–7
- Weeks, C., R. J. Hand, J. H. Sharp.** Retardation of cement hydration caused by heavy metals present in ISF slag used as aggregate, *Cement and Concrete Composites*, Vol. 30:10. 2008. Pages 970-978
- Wendler, E., A.E: Charola.** Water and its Interaction with Porous Inorganic Building Materials. *Proceedings of the Conference " Hydrophobe V, Water repellent treatment of building materials"*. Aedificatio Publisher. 2008. Pages 57-74.
- Winkler, E.M., E.J. Wilhelm,** Salt burst by hydration pressures in architectural stone in urban atmosphere, *Geological Society of America Bulletin*, Vol. 81. 1970. Pages 567-572
- Winkler E.M.** Stone: properties, durability in man’s environments, Wien. 1975
- Wittmann, F.H., R. Jang, R. Wolfseher, T. Zhao.** Application of natural products to make integral water repellent concrete, In Borelli E. Fassina V. editors proceedings of Hydrophobe VI, 6th international conference on water repellent treatment of building materials, Freiburg: Aedificatio Publisher 2011,. Pages 117-124
- Witucki, G. L.** A Silane Primer: Chemistry and Applications of Alkoxy Silanes . 57th Annual Meeting of the Federation of Societies for Coatings Technology, on October 21,1992, in Chicago, In *Issue of the JOURNAL OF COATINGS TECHNOLOGY*. Vol. 65: 882. 1992

Wypich, G. Handbook of Material Weathering, 3rd Edition. Toronto- New York : Chem Tech Publishing. 2003

Ylmén, R., L. Wadsö, I. Panas. Insights into early hydration of Portland limestone cement from infrared spectroscopy and isothermal calorimetry, *Cement and Concrete Research*, Vol. 40: 10. 2010. Pages 1541-1546

Zhao, T., Wittman, F.H, R. Jiang, W. Li. Application of silane-based compounds for the production of integral water repellent concrete, In Borelli E. Fassina V. editors proceedings of Hydrophobe VI, 6th international conference on water repellent treatment of building materials, Freiburg: Aedificatio Publisher 2011. Pages 137-144

Zhang, P., FH. Wittmann, Tj Zhao. Observation and quantification of water penetration into strain Hardening Cement-based Composites (SHCC) with multiple cracks by means of neutron radiography”, *Nuclear Instruments and Methods in Physic Research A*, Vol. 260. 2010. Pages 414-420

NORMATIVE REFERENCES

ASTM C91-03a, Standard specification for masonry cement. s.l. : West Conshohocken, PA.

ASTM C150-02 Standard specification for Portland cement. West Conshohoken PA.

EN 196-1:2005 Methods of testing cement - Part 1: Determination of strength. European Committee for Standardization.

EN 196-3 Methods of testing cement. Determination of setting time and soundness. European Committee for Standardization.

EN 197-1:2011 European standard , Cement- Part 1. Composition, specification and conformity criteria for common cements.

EN 413-1:2011 Masonry cement - Part 1: Composition, specifications and conformity criteria 2011

EN 459-1:1996, EN 459-2:1996, EN 459-3:1996 . Building lime. Part1: Definitions specifications and conformity

EN 998-1:2003. Specification for mortar for masonry.-Part 1: rendering and plastering mortar. European Committee for Standardization.

EN 1015-2 Methods of test for mortars for masonry- Bulk sampling of mortars and preparation of test mortars

EN 12370 Natural stone test methods-Determination of resistance to salt crystallization

EN 1015-3 Determination of Consistence of fresh mortars (by flow table). European Committee for Standardization.

EN 1015-6:2007 methods of test for mortar for masonry - part 6: determination of bulk density of fresh mortar. European Committee for Standardization.

EN1015-11 Methods of test for mortars for masonry- Determination of flexural and compressive strength of hardened mortar

EN 1015-18:1999 Methods of Test for Mortar for Masonry - Part 18: Determination of Water Absorption Coefficient due to Capillary Action of hardened Rendering Mortar. European Committee for Standardization.

EN 1015-19 Methods of Test for Mortar for Masonry - Part 19: Determination of Water Vapour Permeability of hardened Rendering and Plastering Mortars

EN 12370 Natural Stone Test Methods - Determination of Resistance to Salt Crystallisation. European Committee for Standardization.

EN 12390-3:2009 Testing hardened concrete. Compressive strength of test specimens. European Committee for Standardization.

EN 12390-5:2009 Testing hardened concrete. Flexural strength of test specimens. European Committee for Standardization.

EN 13687 Products and systems for the protection and repair of concrete structures- Test Methods- determination of thermal compatibility- Part2 Thunder-shower cycling (thermal shock)

CNR-ICR NorMaL 4/80 Distribuzione del Volume dei Pori in Funzione del loro Diametro (Italian normative on stone material-Distribution of pores volume vs. their diameter). Commissione Beni Culturali UNI NorMaL

CNR- ICR NorMaL 13/83 Dosaggio dei sali solubili totali mediante misure di conducibilità (Italian normative on stone material- Determination of the content of soluble salts with conductivity measurements)

CNR-ICR NorMaL 33/89 Misura dell'angolo di contatto (Italian normative on stone material-Contact angle measurement). Commissione Beni Culturali UNI NorMaL

CNR-ICR NorMaL 43/93 Misure colorimetriche di superfici opache (Italian normative on stone material- colorimetric measurements of opaque surfaces). Commissione Beni Culturali UNI NorMaL

CNR-ICR NorMaL 44/93 Assorbimento d'acqua a bassa pressione (Italian normative on stone material- watecapillary water absorption at low pressure). Commissione Beni Culturali UNI NorMaL

DIN 52615 Testing of thermal insulating materials; Determination of water vapour permeability of construction and insulating materials

SO 9869 Thermal Insulation – Building Elements – In-situ Measurement of Thermal Resistance and Thermal Transmittance International Organization for Standardization (1994)

RILEM Test Method II.4 water absorption tube test

UNI8941: 1987 Coloured surface- Colorimetry, Principles, colour measurement, calculation of colour differences

WEB REFERENCES

VIMAK BIO.

supplier website www.villagacalce.it (accessed 19-08-2013)

S&B μ -SILICA B.

<http://aci-lebanon.com/Modules/News/Attachments/S&B-SILICA-an-engineered-mineral-based-SCM-for-durable-concrete.pdf> (accessed 19-08-2013)

Degussa-Evonik silane /siloxanes.

<http://www.construction-chemicals.com/product/construction-chemicals/en/downloads/pages/default.aspx>; (accessed 19-08-2013)

[<http://www.construction-chemicals.com/product/construction-chemicals/Documents/Keeping-moisture-at-bay.pdf>]; (accessed 19-08-2013)

<http://www.construction-chemicals.com/product/construction-chemicals/Documents/drymix-conference-yearbook-2007.pdf>; (accessed 19-08-2013)

<http://www.construction-chemicals.com/product/construction-chemicals/Documents/elements-29-chemical-umbrella-for-buildings-2010.pdf>] (accessed 19-08-2013)

Metal soaps.

http://www.baerlocher.com/fileadmin/media/0.5_Service/0.5.1_brochures/0.5.1.3_product_brochures/metallic_stearates.pdf

Socal.

<http://www.solvaychemicals.com/SiteCollectionDocuments/PCC/Performance.pdf>

Thermography.

http://www.flir.com/uploadedFiles/Thermography_APAC/Products/Product_Literture/B400_Datasheet%20APAC.pdf

Ultrasonic measurements

<http://www.controls-group.com/ita/calcestruzzo-testing-equipment/ultrasonic-pulse-velocity-testers.php>

Others

www.forumcalce.it (accessed 29-08-2013)

ACI CT-13-ACI concrete terminology,

ACI standard (American Concrete Institute), 2013

http://www.concrete.org/Technical/CCT/ACI_Concrete_Terminology.pdf (accessed 29-08-2013)

WBCSD. Cement Sustainability Initiative: Cement Industry Energy and CO₂ Performance “Getting the Numbers Right,” Geneva and Washington DC: World Business Council on Sustainable Development.

〈<http://www.wbcd.org/DocRoot/IV5ZFD9dESJoSb3h7kxM/csi-gnrreport-withlabel.pdf>〉 ; 2009.
(accessed 29-08-2013)

Publications and conference activity

Falchi, L., U. Müller, P. Fontana, F. C. Izzo, E. Zendri, *Influence and Effectiveness of Water-Repellent Admixtures on Pozzolana-Lime Mortars for Restoration Application*, *Construction and Building Materials*, 2013 DOI 10.1016/j.conbuildmat.2013.08.030 (in press)

Falchi, L., Balliana, E., F. C. Izzo, L. Agostinetto, E. Zendri, *Distribution of nanosilica dispersions in Lecce stone*. *Science at Ca' Foscari*, nr 1, 2013, pp. 35-42 DOI: 10.7361/SciCF-441.

Falchi, L., M. Sgobbi, M. Piovesan, E. Balliana, E. Zendri, *Stucco Forte in Venice between the 16th and 17th Centuries: The Case Study of Addolorata Chapel Stuccoes in San Pantalon's Church*. *Procedia Chemistry*, Volume 8, 2013, Pages 92-99, ISSN 1876-6196, 10.1016/j.proche.2013.03.013.

Falchi, L., E. Balliana, F. C. Izzo, E. Zendri, G. Biscontin. *Mass hydrophobized lime cement mortar as tool for preventive conservation*. *Proceedings XIII Congresso nazionale di chimica dell'ambiente e dei beni culturali. Dall'emergenza alla sostenibilità: il contributo della Chimica*, Taranto, 10-14 Settembre 2012

Falchi L., Balliana E., Agostinetto L., Izzo F.C., Biscontin G., Zendri E. *Nanosilica-based consolidants distribution in a carbonatic matrix*. *Proceedings NICOM4- Nanotechnology in Construction 4th International Symposium, Agios Nikolaos, Crete, Greece, 20-22/05/ 2012*

Izzo, F. C., L. Falchi, E. Zendri, G. Biscontin. *A study on materials and painting techniques of 1930s Italian mural paintings: two cases by Mario Sironi and Edmondo Bacci in Venice*. *Proceedings Modern and contemporary Mural Painting*, Valencia, 4-5/05/2012 (in press)

Zendri, E., E. Balliana, F.C. Izzo, M. Melchiorre Di Crescenzo, L. Falchi, M. Sgobbi, G. Biscontin *The choice of parameters for the monitoring and the maintenance of architectural stone surfaces*. *Proceedings Euromed2012, 4th International Conference, Progress in Cultural Heritage Preservation*, Lemesos, Cyprus, 29 Ott-3 Nov 2012, pp. 331-336, ISBN 9781907132414

E.Zendri, M.Melchiorre Di Crescenzo, F.C.Izzo, E.Balliana, G.Biscontin, M.Sgobbi, L.Falchi. *Aerosol art: a preliminary survey of the spray paints, La conservazione del patrimonio architettonico all'aperto*, Marghera Venezia, Edizioni Arcadia Ricerche 2012, pp. 313-323, ISBN 9788895409160

G. Biscontin, U. Dainese, G. Driussi, L. Falchi, M. Mazzari, R. Nicoletti. *Dispersioni acriliche nanometriche e silici colloidali acquose per il consolidamento di materiali porosi*, *Scienza e Beni Culturali*, Venezia, Arcadia Ricerche, 2011, pp. 387-400 ISBN 9788895409153

E.Zendri, E.Balliana, F.C.Izzo, M.Melchiorre Di Crescenzo, L.Falchi, G.Biscontin, M.Sgobbi. *The monitoring of architectural stone surface treatments: choice of the parameters and their threshold limit values*. *Proceedings Conference on preventive conservation of architectural heritage*, Nanjing, UNESCO Asia-Pacific World Heritage Training and research, Nanjing, 29-30/10/2011, China, pp. 123-130

Posters and oral presentations:

F. Izzo, E. Zendri, E. Balliana, L. Falchi, G. Biscontin, S. Fuso, M. Piccolo, *The conservation of a big Canvas painting cycle: Giulio Aristide Sartorio and The poem of Human Life (1907) at Ca' Pesaro, Venice*. Symposium Issues in Contemporary Oil Paint, Amersfoort 28/29 March 2013 (short paper and poster)

F.C. Izzo, G. Biscontin, E. Zendri, E. Balliana, L. Falchi, A. Moropoulou, A. Kostanti, J.A. Cassar, R. De Angelis. Il coinvolgimento dei giovani nella cultura e nella valorizzazione dei siti archeologici: proposta di un metodo innovativo. *Scienza e Beni Culturali*, Venezia, Arcadia Ricerche, 2013, pp. 1253-1259, ISSN 2039-9790; ISBN 978-88-95409-17-7 (short paper and poster)

Zendri, E., L. Falchi, E. Balliana, F. Caterina Izzo, G. Biscontin. *Effectiveness of nanosilica dispersions as consolidants for porous architectural surfaces*. XIII Congresso nazionale di chimica dell'ambiente e dei beni culturali. Dall'emergenza alla sostenibilità: il contributo della Chimica, Taranto, 10-14 Settembre 2012 (Abstract and oral presentation)

E. Zendri, L. Falchi, F.C. Izzo, M. Sgobbi, E. Balliana, Chemical characterization of stuccoes from the addolorata chapel in St. Pantalon church in Venice, XIII Congresso nazionale di chimica dell'ambiente e dei beni culturali. Dall'emergenza alla sostenibilità: il contributo della Chimica, Taranto, 10-14 Settembre 2012 Taranto, 10-14 Settembre 2012 (poster)

F. C. Izzo, E. Zendri, F. Pinton, E. Balliana, L. Falchi. Comportamento di film pittorici dell'arte moderna e contemporanea in ambiente indoor", proceedings XIV CONGRESSO NAZIONALE DI CHIMICA DELL'AMBIENTE E DEI BENI CULTURALI "La chimica nella società sostenibile", Rimini, 2-5 giugno 2013 (Abstract and oral presentation)

E. Balliana, E. De Zordi, E. Zendri, L. Falchi, F. C. Izzo. Studio della morfologia e della composizione dei depositi su superfici lapidee in area portuale ed aeroportuale a Venezia. Proceedings XIV CONGRESSO NAZIONALE DI CHIMICA DELL'AMBIENTE E DEI BENI CULTURALI "La chimica nella società sostenibile", Rimini, 2-5 giugno 2013 (Abstract and oral presentation)

Appendix

Materials information

LIMESTONE CEMENT¹

The limestone cement used is a CEM IIB/L 32.5R supplied by Cementirossi conform to the European norms EN 197-1:2000/A1:2004/A3:2007.

VIMAK BIO²

VIMAK BIO is a dry-mix, machine applied plaster composed of calcium-silicate aggregate with a granulometric curve of 0-1.2 mm and natural hydraulic lime (NHL 3.5). It is used to attain brown (base) coats with high levels of gas permeability, elasticity and adhesiveness.

Technical characteristics

- Compressive strength: CSI category
- Adhesion: 0.4 N/mm²
- Fire resistance: Class A1
- Water vapour permeability: $\mu \leq 8$
- Thermal conductance: 0.54 W/mK
- Bulk density: 1330 Kg/m³
- Granulometry: 0-1.2 mm

S&B μ -SILICA B³

Is an ultrafine amorphous aluminosilicate, suitable to be used as pozzolanic additive in concrete. A tailored-made SCM product, used as durability enhancer in concrete under harsh conditions was made with volcanic glass of Milos (Greece). It has pozzolanic properties ("natural pozzolan") and consists essentially of SiO₂ and Al₂O₃, cumulatively at least 85% by mass.

Physical characteristics

- Surface area (N₂-BET): >3 m²/g
- Loose Bulk Density : 400 ± 100 kg/m³
- Specific Gravity : 2300 ± 100 kg/m³
- Moisture: 3% max
- Granulometry: +45 μ m : 2% max.; +15 μ m : 10 % max.; -2 μ m : 20 % max.; Mean size: 6 μ m

¹ Information from the supplier site <http://www.cementirossi.it/it/new/default.htm> (accessed 19-08-2013)

² The information come from the supplier website www.villagacalce.it (accessed 19-08-2013) and from the Technical Data sheet

³ Information from the technical data sheet and from the presentation at the webpage <http://aci-lebanon.com/Modules/News/Attachments/S&B-SILICA-an-engineered-mineral-based-SCM-for-durable-concrete.pdf> (accessed 19-08-2013)

SITREN P750⁴

SITREN[®] P 750 is a highly efficient water repellent based on modified silanes/siloxanes in powder form. SITREN[®] P 750 may be used in a variety of cementitious drymix applications where the application of conventional liquid water repellents is not feasible or desired, e. g.: tile grouts, plasters, renders, sealing slurries. As well as excellent water repellence and beading SITREN[®] P 750 provides: long term performance; improved soil release properties; good free-flow behavior; low dust formation.

Physical Properties

Appearance white powder

Active content: approx. 50 %

Carrier: Inorganic.

SITREN[®] P 750 is added to the other powdery components and mixed until a homogenous formulation is obtained. The dosage may vary from 0.2 – 0.5 % (referred to dry material) depending on the application.

SITREN[®] P 730⁴

is a powdered water repellent based on organo-siloxanes, which can be used in those applications where the use of conventional liquid water repellents is not possible or desired, e. g. admixture for cement based formulations such as dry mortars and renders and fillers for tile joints. The dosage may vary from 0.2 – 1.0 % (referred to dry material) depending on the intended use.

Physical Properties

Appearance: white powder

Active content: approx. 20 %

Carrier: inorganic

TEGOSIVIN[®] HE 328⁴

Is an emulsion concentrate based on reactive siloxanes. It is especially designed for the impregnation and efflorescence control of manufactured concrete products and particularly suitable for the hydrophobization of neutral substrates, natural stones and aged concrete. The active material are organomodified siloxanes and silanes.

SILRES BS POWDER A⁵

SILRES[®] BS POWDER A is a highly efficient silicone water-repellent additive in powder form for enhancing the water repellency and water resistance of cementitious construction material mixes, e.g. premixed plasters, joint mortars and powder paints. Properly formulated products exhibit: low water absorption coefficients; excellent droplet effect; low soiling tendency; durability.

SILRES[®] BS POWDER A can be used in both dry powder and liquid systems. To produce non load-bearing precast concrete products or mineral construction material mixes such as premixed plasters, joint mortars or powder paints SILRES[®] BS POWDER A should be mixed with the other dry materials using suitable equipment. Very good water repellency and durability can be achieved with 0.1 - 0.5% based on the dry

⁴ Information and technical data sheet at : <http://www.construction-chemicals.com/product/construction-chemicals/en/products/drymix-applications/water-repellents/Pages/default.aspx?pfcat=997&antiloop=handled>; <http://www.construction-chemicals.com/product/construction-chemicals/en/products/concrete-protection/water-repellents-for-concrete-admixtures/pages>; <http://www.construction-chemicals.com/product/construction-chemicals/Documents/Keeping-moisture-at-bay.pdf>; (accessed 19-08-2013); <http://www.construction-chemicals.com/product/construction-chemicals/Documents/drymix-conference-yearbook-2007.pdf>; (accessed 19-08-2013); <http://www.construction-chemicals.com/product/construction-chemicals/Documents/elements-29-chemical-umbrella-for-buildings-2010.pdf>] (accessed 19-08-2013)

⁵ http://www.wacker.com/cms/en/products-markets/brands_3/silres/silres-bs/silres-bs.jsp;
http://sdb.wacker.com/pf/e/result/report.jsp?P_LANGU=E&P_SYS=2&P_SSN=41344&P_REP=00000000000000000002&P_RES=149030&P_SPEC=R

weight. After sufficient water has been added, the earth-moist or liquid material can be mixed by hand or machine.

General characteristics

Appearance: white powder

Active substance: approx. 50 %

Bulk density: approx. 500 kg/m³

VINNAPAS 8031 H⁶

VINNAPAS[®] 8031 H (VINNAPAS[®] RI 551 Z) is a terpolymer powder of ethylene, vinyl laurate and vinyl chloride that is dispersible in water. Compounds modified with VINNAPAS[®] 8031 H (VINNAPAS[®] RI 551 Z) exhibit improved adhesion, flexural strength in bending, deformability and abrasion resistance, are easier to process and provide long and lasting water repellency on alkaline building materials and significantly reduced water absorption. VINNAPAS[®] 8031 H (VINNAPAS[®] RI 551 Z) contains a fine mineral filler as an antiblocking agent. It is free of solvents, plasticizers and film-forming agents. It has no effect on rheological properties and is a hydrophobizing powder in the lower Tg range.

For the production of ready-mixed powders, such as dry mortars, adhesives and troweling compounds, blend VINNAPAS[®] 8031 H (VINNAPAS[®] RI 551 Z) with the other dry ingredients in appropriate equipment.

General characteristics

Solids content: 98 - 100 %

Ash Content: 11 - 15 %

Bulk density: 400 - 500 kg/m³

Appearance: Visual white - light beige

Protective colloid / emulsifier system: Polyvinyl alcohol

Particle size: Max. 2 % over 400 µm

Predominant particle size redispersion: 0,3 - 9 µm

Minimum film forming temperature: 0 °C

Film properties of the redispersion: cloudy, flexible

SOCAL U1S2⁷

Socal U1S2 is an ultrafine surface treated precipitated calcium carbonate. It is a very fine, white and odourless powder with unique crystal size and shape. The use of Socal U1S2 gives excellent rheological properties like anti-slump behaviour and good control over yield value and viscosity. It is used in a huge variety of different sealants, adhesives, plastisols and printing inks.

General characteristics

Coating content: Solvay Method (MTS005) 24 – 36 g/kg

Loss on drying: Solvay Method (MTS015) ≤ 6 g/kg

Mean particle diameter (dp): Solvay Method (MTS001) 0.07 – 0.13 µm

Residue on sieve (45 µm): Solvay Method (MTS022) ≤ 250 ppm

Yield value: Solvay Method (MTS010) 90 – 250 Pa and ambient conditions.

Crystal structure: Calcite Rhombohedral

Crystal shape: Cubic

Appearance: White powder

Density: 2.71 g/cm³

Free flowing density: 350 g/L

Specific surface area: 16 m²/g

⁶http://sdb.wacker.com/pf/e/result/report.jsp?P_LANGU=E&P_SYS=2&P_SSN=41346&P_REP=000000000000000000004&P_RES=149052&P_SPEC=R

⁷<http://www.solvaychemicals.com/SiteCollectionDocuments/PCC/Solvay%20PCC%20Applications.pdf>;
<http://www.solvaychemicals.com/SiteCollectionDocuments/PCC/Performance.pdf>

Estratto per riassunto della tesi di dottorato

L'estratto (max. 1000 battute) deve essere redatto sia in lingua italiana che in lingua inglese e nella lingua straniera eventualmente indicata dal Collegio dei docenti.

L'estratto va firmato e rilegato come ultimo foglio della tesi.

Studente: Laura Falchi matricola: 955842

Dottorato: SCIENZE CHIMICHE

Ciclo: XXVI

Titolo della tesi : Study of innovative water repellent systems for the preservation and restoration of artificial stone materials

Studio di nuovi sistemi idrorepellenti per il risanamento e il recupero di materiali lapidei artificiali

Abstract:

Il lavoro di tesi riguarda lo studio di malte idrorepellenti preparate con l'utilizzo di additivi idrofobizzanti per la protezione, la manutenzione e il recupero delle superfici architettoniche storiche e civili. Questo studio considera in particolare i processi di degrado causati dalla presenza di acqua (per azione diretta o come mezzo di trasporto di inquinanti e sali solubili) sui materiali dell'edilizia e valuta la durabilità di malte idrorepellenti in varie condizioni ambientali. Lo studio ha considerato l'influenza di diversi additivi idrorepellenti sull'idratazione di alcuni leganti e la resistenza all'azione di degrado fisico conseguente la cristallizzazione di Sali o l'esposizione a radiazioni UV e alla pioggia. Alcuni impasti sono stati applicati su modelli di murature sottoposti a risalita capillare di soluzioni saline. Lo sviluppo della ricerca ha previsto il ricorso a numerose tecniche analitiche (FT-IR, TG-DSC, SEM-EDX, XRD, MIP), test normati e analisi non invasive.

The thesis deals with the study and development of water repellent mortars, made with water-repellent admixtures, suitable for the protection, maintenance and restoration of historical and civil buildings. This study deals with the damage processes due to the action of water (both as direct action and or as carrier of pollutants and soluble salts) on the building materials and evaluates the durability of water-repellent mortars in different environmental conditions. The study considers the interactions of different water repellent admixtures on the hydration reactions of some binders and the resistance to the physical degradation due to the crystallization of soluble salts or the exposure to UV light and rain. Some mixes were applied also on salty masonries. Different analytical techniques (FT-IR, TG-DSC, SEM-EDX, XRD), test according to the european normative, porosimetric ultrasonic measurements and IR- thermography were used.

Parole chiave (da scegliere max 5): idrorepellenti, stearati, silossani, malte, restauro

Keywords: water repellents, stearates, siloxanes, mortars, restoration

Firma dello studente
